University of Nottingham

Institute of Engineering Surveying and Space Geodesy

Strategies for long–term monitoring of tide gauges using GPS

by

Felix Norman Teferle

Dipl.-Ing., Vienna University of Technology, 1996

Thesis submitted to the University of Nottingham

for the degree of Doctor of Philosophy

May 2003

ABSTRACT

Changes in mean sea (MSL) level recorded relative to tide gauge benchmarks (TGBM) are corrupted by vertical land movements. Accurate estimates of changes in absolute sea level, require these MSL records to be corrected for ground level changes at tide gauge sites. For more than a decade, the Global Positioning System (GPS) has been used to determine positions of TGBMs and to monitor their position changes, i.e. station velocities, over time in the International Terrestrial Reference System (ITRS). This was initially carried out by episodic GPS campaigns and later on by continuous GPS (CGPS) or a combination of both.

Highly accurate realizations of the ITRS, satellite orbits and models for the mitigation of systematic effects currently enable the determination of station positions using GPS at the centimetre or even millimetre level. It is however argued that accurate long–term estimates of changes in the vertical component at the 1 mm/yr level cannot be achieved, making intercomparisons between GPS estimates and other techniques necessary.

Daily processing and analysis of continuous GPS networks requires automated procedures. The modifications and improvements to the existing procedures at the IESSG are described. The newly developed tools include the monitoring and quality control of daily archived GPS observations and of processing results. A special focus is on the coordinate time series analysis and methodologies used to obtain the best possible estimates of vertical station velocities and associated uncertainties.

The coordinate time series of 21 CGPS stations in the UK and France are analysed. Eight of these stations are co–located with tide gauges. The effects of two processing strategies and two realizations of the ITRS on the coordinate time series are investigated. Filtered coordinate time series are obtained by application of a regional filtering technique. Station velocity estimates are obtained by fitting a model including a linear and annual term, and offsets to the unfiltered and filtered coordinate time series. Realistic uncertainties for these velocities are obtained from the application of two empirical methods which account for coloured noise in the coordinate time series. Results from these are

compared to the Maximum Likelihood Estimation (MLE), which allows for more rigorous and accurate, simultaneous estimation of the model parameters and their uncertainties. Strategies for coordinate time series analysis on a daily or monthly, and annual or bi–annual basis are defined.

At two CGPS stations the dual–CGPS station concept is tested and compared to the single baseline analysis and the application of an adaptive filter. An empirical method to obtain coordinate time series specific filter parameters is described. This investigation shows that reliable relative vertical station velocity estimates can be obtained after much shorter observation spans than absolute vertical station velocity estimates. The availability of dual–CGPS station pairs allows a simplified processing strategy and a multitude of coordinate time series analysis methods, all contributing to a better understanding of the variations in the positions of CGPS stations.

Vertical station velocity estimates for the unfiltered and filtered coordinate time series and different analysis strategies are compared for 17 of the CGPS stations and show disagreements of up to 2 mm/yr. At the eight CGPS stations co–located with or close to tide gauges alternative estimates of vertical land/crustal movements from absolute gravimetry, geological information and glacial isostatic adjustment models are compared to the GPS estimates, and it is suggested that the latter are systematically offset. An alignment procedure is demonstrated, correcting the vertical station velocity estimates of all 17 CGPS stations for this offset. The correlation of the geology–aligned vertical station velocity estimates and the MSL records from eight tide gauges suggests changes in absolute sea level of approximately +1 mm/yr around the UK.

ACKNOWLEDGMENTS

I am grateful for the supervision of Alan Dodson and Richard Bingley and their continuous support and encouragement throughout my work. I thank them for their time spent during our many discussions and for creating an environment where I could develop my ideas. A very special thank you to Richard Bingley who also laboured for many hours reading, correcting and commenting on the manuscript for this thesis.

I would also like to thank both my examiners Trevor Baker and Gethin Roberts for their time and effort. I hope they found some aspects interesting at times.

I owe many special thanks to Simon Williams for all his advice in countless discussions and emails on noise, offsets and coordinate time series analysis. I am especially indebted for his and Hadley Johnson's Maltlab M–files and Simon's collection of C programs to carry out the MLE.

Many thanks to David Lavallée for his discussions on periodic signals and a copy of his Ph.D. thesis, Spiros Pagiatakis for his Least Squares Spectral Analysis software, and Dave Thomas for the spectral analyser and the Horn antenna used in Aberdeen. For preprints of papers, coordinate time series results and figures, many thanks to Jan Johansson, Maria Mareyen, Jason Lowe, Zivony Malkin, Ambrus Kenyeres and Ben Horton.

At the IESSG I would like to thank many friends, in particular, Xiaolin Meng for all our discussions on least squares, adaptive filtering and Ping Pong, Sam Waugh and Theo Veneboer for being around and for their contributions to the tide gauge monitoring projects, Caroline Noakes for running the *General Inquiries Office* with me, and David Park for always putting a smile on all our faces. At this stage I would also like to mention Norman Bonnor for inviting me to the Institute to do a Ph.D. in the first place.

Furthermore, thanks should also go to former colleagues Nigel Penna and Simon Booth for their contributions during the initial phase of my work, David Russell for his help with the site–investigations in Aberdeen and Andy *Roo* Evans for all the *fun* during the time Hazel and I stayed at his house. Thanks also to Andy Nesbitt and Kenny Gibson for their help and participation in the episodic GPS campaigns.

The UK GPS data were taken from the British Isles GPS archive Facility (BIGF) (`www.bigf.ac.uk`) operated by the IESSG and funded by the Natural Environment Research Council (NERC). Furthermore, without the voluntary contributions from the many people involved in the IERS and IGS, this Ph.D. would not have been achievable. The author has used the Generic Mapping Tools (GMT) (Wessel and Smith, 1995, 1998) throughout his thesis.

Most of my thank yous should go to my very special and lovely wife Hazel, who supported me throughout my Ph.D. and without whom it would have not been possible. Not only was her patience tested on numerous occasions, but she also sacrificed many evenings, weekends and holidays. Thanks should also go to my parents–in–law, Rosalind and David, who have served me well during the last few months of my Ph.D., cooking, cleaning and DIYing.

DEDICATION

Für meine Eltern Anne und Felix und meine liebe Frau Hazel.

ACRONYMS AND ABBREVIATIONS

ANTEX	Antenna Independent Exchange Format
BIFROST	Baseline Inferences for Fennoscandian Rebound Observations, Sea Level, and Tectonics
DORIS	Doppler Orbitography by Radiopositioning Integrated on Satellite
EOSS	European sea–level observing system
EOSI	Earth Observation Science Initiative
EPN	EUREF Permanent GPS Network
EUVN97	European Vertical Reference Network
GIA	Glacial Isostatic Adjustment
GLOSS	Global Sea Level Observing System
IAPSO	International Association for Physical Sciences of the Ocean
IERS	International Earth Rotation Service
IESSG	Institute of Engineering Surveying and Space Geodesy
IGS	International GPS Service
IGS TIGA PP	IGS Tide Gauge Benchmark Monitoring Pilot Project
IPCC	Intergovernmental Panel on Climate Change
JPL	Jet Propulsion Laboratory
LGM	Last Glacial Maximum
MLE	Maximum Likelihood Estimation
MSL	Mean Sea Level
NERC	Natural Environment Research Council
OTL	Ocean Tide Loading
POL	Proudman Oceanographic Laboratory
PSMSL	Permanent Service for Mean Sea Level
RINEX	Receiver Independent Exchange Format
RLR	Revised Local Reference
SBL	Special Bureau for Loading
SCIGN	Southern California Integrated GPS Network
SET	Solid Earth Tides
SINEX	Solution Independent Exchange Format
SOPAC	Sripps Orbit and Permanent Array Center
TGBM	Tide Gauge Benchmark
TZD	Tropospheric Zenith Delay
UNAVCO	University Navstar Consortium
VLBI	Very Long Baseline Interferometry

Contents

List of Figures

List of Tables

Chapter 1

Introduction

Global sea level rise is a direct consequence of mostly thermal expansion of sea water caused by the global warming and the melting of mountain glaciers (Houghton et al., 2001; Hulme et al., 2002). Working Group 1 of the Intergovernmental Panel on Climate Change (IPCC) made predictions of changes in average sea level over the period 1990 to 2100 in the range of 0.09 to 0.88 m, with a central value of 0.48 m. Rising sea levels lead to increased erosion of beaches due to increased loss of sediment, increased submergence of marshes and other low–lying lands, increased salinity of estuaries and aquifers, raised coastal water tables and exacerbated coastal flooding and storm damage (Leatherman, 2001; Brown, 2001). Furthermore, higher sea levels can lead to an increased incidence of extreme high water levels during storm surges and to an increased frequency of storm surges (e.g. Flather and Williams, 2000; Flather, 2001; Flather et al., 2001; Gregory, 2001; Price et al., 2001; Lowe et al., 2002).

The change in global sea level is not expected to be the same all over the world. This is partly due to the fact that more heat is taken up and stored in some oceans than others and changes in ocean circulation will occur (Gregory, 2001). Although the variations in global sea level change due to these effects are substantial, the interaction of ice sheets, sea level and the solid Earth over geological time scales are far more important (Houghton et al., 2001; Hulme et al., 2002). Over large areas the melting of the ice sheets during the last deglaciation prompted vertical land movements due to the Earth's viscous response to

changes in the surface load of ice and water and by the concomitant redistribution of mass within the Earth and oceans. These large scale adjustments in addition to more localized sediment consolidations partly due to anthropogenic effects, e.g. groundwater extraction, cause the majority of vertical land movements observed in the UK (Shennan, 1989; Hulme et al., 2002; Shennan and Horton, 2002).

Since 50% of the global population currently occupy coastal zones, the socio–economic and environmental effects of global sea level rise are far-reaching (e.g. Howarth and Monahan, 1996; Nicholls and Small, 2002). Most at risk are poorer nations with densely populated coastal areas. For a 1 metre sea level rise, Bangladesh and Indonesia are projected to lose 15 and 40% of their land surfaces respectively, while several island nations, e.g. the republic of Maldives, Kiribati, the Marshal Islands, Tokelau, Tuvalu, and the Torres Straits Islands, will be completely submerged (Howarth and Monahan, 1996). A recent study showed that the value of the assets at risk due to flooding and coastal erosion in England and Wales is approximately £214 billion and about 6 million people live in areas at risk (Samuels and Burgess, 2001; Deakin et al., 2001).

Furthermore, the results from the Coastal Defence Vulnerability 2075 (CDV2075) project (Sutherland and Wolf, 2001) showed that a considerable increase in overtopping of coastal defences can be expected over the next century. Sea level rise is the main factor determining changes in this vulnerability, although coastal steepening, a reduction of the intertidal width, has also been shown to be very important. The study suggested that it was not sufficient to increase heights of sea defences by amounts equivalent to sea level rise if coastal steepening occurs. It is straight forward to see that local or regional ground level changes will also affect the projected heights of sea defences required in the future. From this it is clear that in order to arrive at a reliable future sea level scenario, it is necessary to combine information on changes in mean sea level, tidal regime, land level, and surges. The main thrust of the author's research has been focused on obtaining information on changes in ground level in the UK through the use of high precision GPS for monitoring vertical land movements.

Since the early 1990s geodesy with GPS has been continually and significantly improved in precision and accuracy. The reasons for this are manifold but can be attributed to

improvements in instrumentation, e.g. receiver, antenna and satellite technology, the establishment and densification of the global International GPS Service (IGS) tracking network (Beutler, 1996a), which prompted improvements in the computation of satellite orbits and tracking station positions, and improvements in analysis models, i.e. mitigation of systematic biases (e.g. Lavallée, 2000; Nikolaidis, 2002; Herring, 2003). Additionally, the global reference frame in which high precision GPS station coordinates are determined has been continuously improved, benefiting from the increasing number of IGS tracking stations and the development of more rigorous combination methods of data from different geodetic observing systems by the International Earth Rotation Service (IERS) (e.g. Boucher and Altamimi, 1996; Sillard et al., 1998; Sillard and Boucher, 2001).

The reported achievable scatter in daily GPS coordinate solutions is currently at the 1 to 3 and 3 to 5 millimetres level for the North and East components, and at the 7 to 10 millimetres level for the vertical component, e.g. Zhang et al. (1997); Zumberge et al. (1997); Bock et al. (2000); Lavallée (2000); Zerbini et al. (2001); Johansson et al. (2002) and Nikolaidis (2002). The lower precision in the vertical component can be attributed to the fact that many systematic errors and biases have their largest effect on the vertical component which is already weakened by the geometry of the satellites to receiver configuration, i.e. the fact that satellites are all above a specific station. The precision and accuracy currently achievable for the vertical component is limited by errors in satellite orbits and the reference frame, that propagate via the use of the IERS or IGS products into the coordinate solutions of regional GPS networks, and by biases related to the signal propagation and local station motions. Whereas certain errors and biases cannot be mitigated when relying on external products, it is possible to reduce the effect of others through the choice of adequate models.

Using these freely available, high quality IGS and IERS products, the author has carried out a detailed investigation on the use of continuous GPS (CGPS) for the long–term monitoring of vertical land movements at tide gauge sites at the 1 mm/yr level. This poses several logistical challenges, e.g. the handling of the continuous data, the automation of all required processing steps to arrive at time series of daily coordinate solutions for each station, the introduction of automated checking and reporting facilities, and the automated analysis of the daily coordinate time series. Besides the development of many

of the required automated procedures, the author has also developed and tested a number of strategies for the analysis of coordinate time series for the computation of vertical land movement estimates from CGPS. The dual–CGPS station concept as an observation strategy has also been tested for two station–pairs in the UK and compared to the single baseline analysis and an adaptive filtering method. As a result of this research, for the first time it has been possible to make meaningful comparisons of vertical land movement estimates for the UK based on alternative evidence with those from CGPS.

Chapter 2 introduces sea level in an absolute and relative sense and discusses how estimates of sea level change are derived from tide gauge measurements. The process of glacial isostatic adjustment (GIA) is introduced and briefly discussed. Mean sea level (MSL) records and various estimates of vertical land and crustal movements for selected tide gauge sites in the UK and France are presented. At this stage the author would like to define the terms vertical land and crustal movements in more detail. GIA models predict vertical crustal movements which do not include motions due to tectonic and seismological activities, compaction and settlements due to natural or anthropogenic origins and local engineering type effects. The term vertical land movements however describes the sum of all movements. In this respect, the geological information presented in this thesis can be considered to be estimates of vertical land movements. Similarly, unless the station is adequately connected to the Earth's crust, vertical station velocity estimates from absolute gravimetry (AG) or GPS must also be considered to be estimates of vertical land movements.

Issues related to the use of CGPS for the monitoring of vertical land movements at the 1 mm/yr level are discussed in Chapter 3. This includes details of several meetings, national and international projects and initiatives, all with the aim of precisely geo–referencing tide gauge benchmarks (TGBM) in a global reference system. The International Terrestrial Reference System (ITRS), as the only system currently believed to allow the accurate computation of vertical station velocity estimates, is introduced and discussed. A discussion of systematic errors and biases and their mitigation then follows.

The contributions of the author to the automated procedures used for GPS processing, coordinate time series analysis and quality control are described in Chapter 4. The auto-

mated GPS processing has been carried out using the Institute of Engineering Surveying and Space Geodesy (IESSG) GPS Analysis Software (GAS) in combination with a set of procedures that allow routine processing without any user intervention.

Chapter 5 introduces the UK CGPS data set analysed by the author. After each station has been introduced, this Chapter focuses on the quality indicators for GPS observations that can be obtained prior to any GPS processing. Suggestions for the active quality control of GPS data archives using TEQC (Estey and Meertens, 1999) in combination with the available RINEX (**R**eceiver **IN**dependent **EX**change (Gurtner and Mader, 1990)) format observation files are given. Site-specific investigations at several CGPS stations are then presented.

The analysis of the CGPS network carried out by the author is discussed in Chapter 6. This starts with a discussion of the two GPS processing strategies applied and the differences in the station velocity estimates obtained by using two recent ITRS realizations. This chapter then goes on to introduce the concepts of periodic signals and coordinate offsets, and their effects on station velocity estimates, regional filtering and noise analysis. Following this, the results shown in Chapter 6 include those of the standard and improved coordinate time series analyses. The latter include the analyses for both unfiltered and filtered ITRS2000 coordinate time series, each arriving at three independent estimates for station velocities. These were obtained by estimating the model parameters for a linear trend, annual signal and coordinate offsets, with separate computation of white and flicker noise amplitudes using two empirical methods, and by simultaneous estimation of all model parameters including the noise amplitudes using maximum likelihood estimation (MLE) with either fractional and integer spectral indices.

Chapter 7 then introduces the dual–CGPS station concept and compares this new monitoring tool to the single baseline analysis and an adaptive filtering method, using synthetic coordinate time series. For the adaptive filter, an empirical method to optimize the parameters is introduced and a set of coordinate time series specific filter parameters are obtained.

In Chapter 8 the results obtained by the author are compared with those from alternative analyses. The coordinate time series and station velocity estimates for several stations

are compared to those of two IGS Analysis Centers, the official ITRF2000 analysis and the results in Panafidina and Malkin (2001). The absolute and relative vertical station velocity estimates are compared to vertical land movement estimates from absolute gravimetry and geological information, and to vertical crustal movement estimates predicted from GIA models. Finally, an alignment method is introduced using either vertical land movement estimates from absolute gravimetry or geology in order to obtain reference frame independent vertical station velocity estimates from CGPS measurements.

Chapter 2

Sea Level and Vertical Land Movements

2.1 Introduction

This chapter will briefly introduce the concepts of sea level in an absolute and relative sense and how estimates of sea level change are derived from measurements obtained using tide gauges. The process of glacial isostatic adjustment will be discussed as a global phenomenon affecting present–day tide gauge observations. After the introduction of these general topics, mean sea level records and estimates of vertical land movements for selected tide gauge sites in the UK and France will be analysed in order to show the importance of delivering a strategy for the long–term monitoring of these movements at tide gauge sites.

2.2 Sea Level and its Measurement

Sea level is a highly variable, gravitationally self–consistent surface which has and still is undergoing large temporal and spatial changes. Over the past 500 hundred million years, large scale shifts in the global ocean basin geometry, due to the dynamics of the Earth's tectonic plates, forced changes in the level of the sea of up to 600 m (Lambeck and

Chappell, 2001). During the Quaternary[1], the main contributor to sea level changes was the periodic exchange of mass between ice sheets and oceans, with sea level lowstands at times of glaciation events and sea level highstands at times of interglacial periods (Lambeck and Chappell, 2001). The effects of the last deglaciation event which started 21,000 years ago, are still noticeable on a global scale. Due to the collapse of the large continental ice sheets, sea level rose by 120 m on average, and although deglaciation was finished 6,000 years ago, the Earth's delayed visco–elastic response to the redistribution of mass on its surface, still affects sea level in areas formerly covered by ice sheets (Peltier, 1998; Lambeck et al., 1998a; Peltier, 1999; Lambeck and Chappell, 2001; Shennan et al., 2002), and in areas far from these (Mitrovica and Davis, 1995; Milne and Mitrovica, 1998; Milne, 2002). This phenomena is commonly known as *glacial isostatic adjustment* (GIA) or *post–glacial rebound* and will be discussed in §2.3.

Evidence for sea level changes in the late Holocene[2] can often be obtained from raised or submerged shorelines, indicated by, e.g. fossil coral reefs above their present growth positions or submerged in situ tree stumps. Geological evidence of sea level change can also be based on peats and sediments found in shallow elevated basins that at some time where in contact with the sea and have since been isolated as sea level has fallen or the land has risen (Shennan, 1989; Shennan et al., 2002). Furthermore, transitions from freshwater to marine deposits and microfossils give an indication of marine flooding or a fall in sea level, if the transition sequence is reversed (Lambeck and Chappell, 2001). Timing of these sea level indicators can generally be carried out using, e.g. radiocarbon dating methods, and if sequential *age–height pairs* exist for a particular site, these can be approximated by *sea level curves*. Douglas et al. (2001) reported that global data bases hold over 500 late Holocene sea level curves and thousands of dated sea level indicators. Examples of the analysis of these geological sea level indicators and of sea level curves can be found in, Shennan (1989); Lambeck (1993, 1997); Lambeck et al. (1998a); Lambeck (1998); Peltier (1998); Firth and Stewart (2000); Shennan et al. (2000); Bennike et al. (2002); Peltier et al. (2002) and Shennan and Horton (2002).

[1] approximately 1.8 million years until present

[2] the last 10,000 years to present

For the period of the last 2,000 years, changes in sea level have also been inferred from archaeological findings in coastal areas. Archaeological data have two advantages over geological information in that dating of e.g. pottery can be carried out very precisely for the classical cultures in the Mediterranean and Mesoamerica, and the relationship between the evidence and mean sea level, mainly through structures from ancient ports, can also be drawn fairly precisely (Kearney, 2001). Along the coast of the Mediterranean Sea, it has been possible to obtain estimates of changes in sea level in the recent history based on around 335 archaeological sites (Zerbini et al., 1996).

Sea level variations on more recent time scales, i.e. the well documented secular sea level change of the twentieth century or oscillations with decadal, interannual, annual, and even shorter character, are mainly due to climate, meteorology and tide–driven effects. Detailed measurement of these has only been possible at coastal locations since the development of tide gauges in the nineteenth century. For a general discussion of sea level rise and its implications, the reader is referred to, e.g. Douglas et al. (2001). For information on recent investigations into the temporal variability of sea level in the North Sea and Baltic Sea, the North Atlantic and the tropical Pacific, the reader is referred to Plag and Tsimplis (1999), Kuhn et al. (2001), and Merrifield et al. (1999), respectively.

Over the last two centuries, sea level has been measured using various types of tide gauges (TG), basically consisting of a float inside a stilling well, to filter out the effects of waves. However, modern tide gauge technology also employs pressure sensors or acoustic transducers to determine the height of the water column above the measuring unit (Pugh, 1987). Observations of instantaneous, sea level obtained by tide gauges, are averaged over a monthly or yearly time span in order to filter out higher frequency effects due to e.g. tides and surges. Such mean sea level (MSL) records have been the basis for investigations into recent changes in sea level and its variation and, along with satellite altimetry, still continue to take an important part in related research.

Changes in sea level derived from tide gauge MSL records are, however, biased by low frequency variations at the interannual or interdecadal scale, whose amplitudes are larger than the underlying trend, and hence only long records can be used. Although the data bank of the Permanent Service for Mean Sea Level (PSMSL) (see §2.2.1) contains

MSL records from over 1,800 globally distributed tide gauges, only about 100 of these have reliable records of 60 or more years (Baker, 1993). Furthermore, the geographical distribution of these tide gauges is biased towards the northern hemisphere with a high density of the longest MSL records being from high quality tide gauges in Europe and the USA. This lack of long MSL records for the southern hemisphere complicates the determination of changes in global sea level (Douglas and Peltier, 2002).

Tide gauge measurements are referenced to a local tide gauge benchmark (TGBM), which is situated nearby either in solid rock or a solid structure, e.g. a pier or quay. In order to obtain a history of consistent MSL records over long time scales, i.e. decades or centuries, despite repairs or replacements of the tide gauge or changes in tide gauge technology, the TGBM should be fixed with respect to a local network of benchmarks. If changes to this network or the tide gauge itself have been documented, then it is possible to include its MSL record in the *Revised Local Reference* (RLR) data set of the PSMSL.

Tide gauge measurements are inherently ambiguous as from tide gauge MSL records alone, it is not possible to distinguish between sea level changes or vertical land movements at the tide gauge site. Hence, tide gauges measure changes in sea level relative to the local surface of the solid Earth, i.e. *relative* sea level. In order to monitor changes in global sea level using tide gauge MSL records, these must be corrected for vertical land movements. For the purpose of this thesis, changes in relative sea level corrected for vertical land movements will be referred to as changes in *absolute* sea level. Other definitions, e.g. changes in geocentric sea level, refer the sea surface to the origin of the reference frame in which, e.g. satellite altimeter measurements were carried out (Blewitt and Clarke, 2003).

Early estimates of changes in absolute sea level were based on only a few MSL records from a set of global tide gauges far from areas assumed to be affected by the GIA process or to be tectonically active. Advances in modelling the visco–elastic rebound of the Earth's crust, then enabled predictions of vertical crustal movements at tide gauge sites in order to de–contaminate their MSL records (Woodworth, 1997). However, besides, these geologically induced effects, MSL records may also be contaminated by localized vertical movements due to sediment loading and compaction, oil or water extraction or local stability problems associated with the structure supporting the tide gauge. For example,

the pumping of oil, water and gas, coupled with natural changes is causing subsidence of the US Gulf Coast at the rate of tens of centimetres per year (Schenewerk et al., 1999). Subsidence rates of up to 1 cm/yr have also been observed in Port Adelaide and its Outer Harbour area in Southern Australia, which have been associated with increasing urban and industrial utilization and groundwater withdrawal (Harvey et al., 2002). Additionally, Baker (1993) stated that several authors had pointed out that estimates of changes in absolute sea level may be biased, since subsidence is more common than uplift in oceanic and coastal areas.

Integrated and sustainable coastal development, e.g. flood and coastal defence construction or harbour developments, require accurate estimates of changes in relative sea level. Future predictions of these however, depend on climate models and estimates of vertical land movements. Estimates of changes in absolute sea level are required to fine–tune climate models by testing their ability to re-produce changes in absolute sea level over the past century as a measure of their overall capability in predicting future climate (Baker, 1993). As a result, both changes in relative and absolute sea level are required in order to assess the impact of climate change on a global and local scale (Plag, 1998).

Other research areas that require estimates of changes in absolute sea level are ocean circulation studies. Changes in ocean circulation can be determined from changes in the geostrophic flow between islands or over straits (Baker, 1993). In order to identify long–term changes in this flow between a pair of tide gauges, vertical land movements must be closely monitored. Satellite altimeters, e.g. TOPEX/-POSEIDON, which are capable of measuring changes in geocentric sea level, require calibration of their altimeter range errors. This is basically carried out by comparison of the altimetric sea surface height information with adjacent tide gauge sea level data located within the same reference frame as the altimeter (Neilan et al., 1997; Dong et al., 2002a; Douglas et al., 2001).

Figure 2.1 shows a schematic diagram of a typical tide gauge configuration to measure changes in absolute sea level. The tide gauge is connected to the TGBM and additional benchmarks by spirit levelling. One of the benchmarks is also co–located with a Global Positioning System (GPS) monitoring station. The use of GPS at tide gauge sites, as

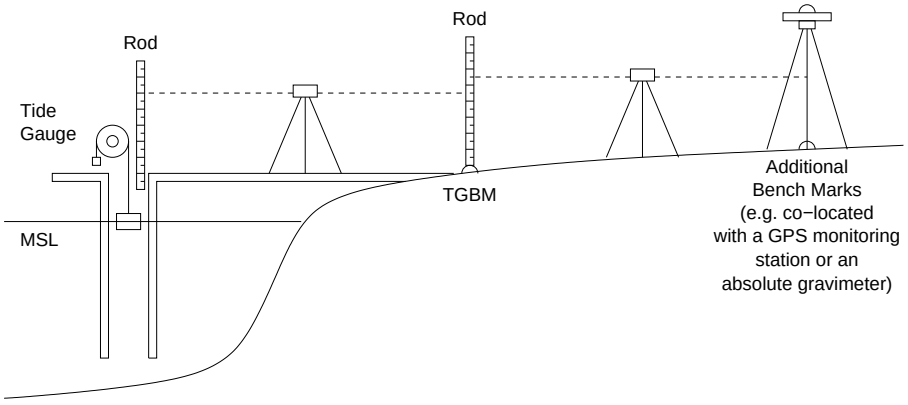

Figure 2.1: Schematic diagram of a tide gauge to measure changes in *absolute* sea level (modified from Baker (1993)).

pictured in Figure 2.1, has been the theme of several workshops and meetings (§3.2.1) and will be the main topic explored in this thesis.

From the above discussion it is clear that accurate estimates of changes in absolute sea level are of great importance and that although estimates of vertical land movements can be obtained from GIA models, measurement of actual changes in the tide gauge position using an independent method, such as GPS, is necessary. Estimates of vertical land movements from GPS can then be used directly or estimates of vertical crustal movements from GPS can be used as constraints in order to improve modeling of the GIA process (Milne et al., 2001; Johansson et al., 2002; Park et al., 2002).

2.2.1 The Permanent Service for Mean Sea Level (PSMSL)

The Permanent Service for Mean Sea Level (PSMSL) is one of a number of Services grouped within the Federation of Astronomical and Geophysical Data Analysis Services. Since 1993, the PSMSL has taken over the responsibility for the collection, publication, analysis and interpretation of sea level data from the global network of approximately 1,800 tide gauges (PSMSL, 2002a). In February 2001, the database of the PSMSL contained over 47,000 station–years of monthly and annual mean values of sea level from this global station network.

The *Revised Local Reference* (RLR) dataset of the PSMSL contains those tide gauge records, for which time series analysis of sea level changes can be carried out. The RLR data base contains those records for which the full benchmark history is available. All analyses of secular changes in absolute sea level during the last century have been performed on the basis of this data set using tide gauges with long MSL records.

The RLR MSL trends for the tide gauge network in the UK and the tide gauge in Brest, France, used in this thesis where obtained from the PSMSL web site (PSMSL, 2002b).

2.2.2 The Global Sea Level Observing System (GLOSS)

The Global Sea Level Observing System (GLOSS) is an international programme coordinated by the Intergovernmental Oceanographic Commission aimed at the establishment of high quality global and regional sea level networks (GLOSS, 2002). It was initiated to provide an approximately evenly–distributed sampling of global coastal sea level variations, as there was a higher density of tide gauges in the northern hemisphere.

The main component of GLOSS is the *Global Core Network* of sea level stations around the world for long–term climate change and oceanographic sea level monitoring. Other components include the GLOSS *Long Term Trends*, the GLOSS *Altimeter Calibration*, and the GLOSS *Ocean Circulation* set of tide gauges, of which some but not all are included in the Core Network.

It is important to mention at this place that GLOSS Long Term Trend tide gauges are priority locations for the installation of continuous GPS stations to monitor vertical land movements (GLOSS, 2002).

2.3 Glacial Isostatic Adjustment (GIA)

Glacial isostatic adjustment (GIA) or post–glacial rebound, is the ongoing visco–elastic response of the solid Earth to changes in ice–mass loading that occurred during the late

Pleistocene[3] cycles of glaciation and deglaciation. It involves changes in the Earth's shape, i.e. horizontal and vertical crustal deformations, changes in absolute sea level, changes in the gravitational field and changes in polar motion and Earth rotation (e.g. Mitrovica and Peltier, 1989; Peltier, 1998; Mitrovica et al., 2001; Milne, 2002).

The last deglaciation event of the current ice–age began at the Last Glacial Maximum (LGM) approximately 21,000 years ago and deglaciation was essentially complete by 6,000 years ago (Peltier, 1999). Prior to this present Holocene epoch of Earth history, the planet experienced 9 cycles of glaciation and deglaciation over a time span of approximately 900,000 years, each glaciation phase lasting approximately 90,000 years interspersed by a deglaciation phase of approximately 10,000 years.

During times of glaciation, snow would be converted into ice under its own weight and ice sheet thickness would reach up to 4 km prior to the onset of the deglaciation period (Peltier, 1999). In the northern hemisphere, North America and Northwestern Europe experienced the most significant glaciation processes with ice sheets covering Canada, Greenland, Iceland, Fennoscandia, Siberia and the British Isles. In the southern hemisphere, ice sheets covered the regions of West Antarctica and Western Patagonia. During the last deglaciation, which involved melting of the continental ice sheets in the northern hemisphere, except the one in Greenland (there is little detail known about the deglaciation of the ice sheets in the southern hemisphere), sea level rose by approximately 120 m on average as meltwater returned to the ocean basins. This meltwater return caused spatially varying changes in relative sea level because of the deformation of the Earth's surface under the ice and water load and the changing gravitational potential (Milne and Mitrovica, 1998; Peltier, 1999; Lambeck and Chappell, 2001; Douglas and Peltier, 2002; Milne, 2002).

Since the LGM in the late Pleistocene, the strongest post–glacial rebound has occurred in the deglaciated regions, which can be identified by falling relative sea levels, such as in Fennoscandia (e.g. Lambeck et al., 1998a) and Northeastern Canada (e.g. Milne et al., 1999). Surrounding these regions, are areas of rising relative sea levels, which are

[3]The Pleistocene is the geological time period of approximately 1.8 million to 10,000 years before present.

controlled by the collapse of the feature known as the *post–glacial forebulge* (Douglas and Peltier, 2002). During the glaciation period, mantle material beneath the loaded region is displaced outward forming the post–glacial forebulge around the loaded region. When the ice sheets disintegrate, the unbalanced gravitational force induces a return flow of material that drives the GIA process in the previously ice–covered area and also collapses the forebulge. This results in sea level signatures where, after an initial rapid rise, relative sea level continues to rise slowly once deglaciation is completed, as observed e.g. for Chesapeake Bay (Douglas and Peltier, 2002) or Southern England (Shennan, 1989; Lambeck and Chappell, 2001).

Over the last 25 years, numerical modelling of the glacial isostatic adjustment process has been successfully implemented by several research groups in North America, Europe and Australia. Most numerical GIA predictions have been based on a spherically symmetric (Maxwell[4]) visco–elastic Earth model to a load composed of a model of late Pleistocene ice–cover and a gravitationally self–consistent ocean load (Milne et al., 2001; Douglas and Peltier, 2002). The radial visco–elastic structure of the Earth is then fixed to a reference Earth model, i.e. the Preliminary Reference Earth Model (PREM) model (Dziewonski and Anderson, 1981), which is based on seismic observations. The only parameter of the model left, is the molecular viscosity of the planetary mantle, which can be inferred by fitting the model to geological, geophysical or astronomical data.

Peltier and Jiang (1996) derived detailed models of the radial viscosity structure of a spherically symmetrical Earth mantle by formal inversion of dated relative sea level curves and data related to the rotational response of the Earth to the glaciation–deglaciation cycle of the late Pleistocene ice age. In several other studies (Lambeck et al., 1998a; Marotta and Sabadini, 2002; Milne et al., 2001; Park et al., 2002), however, this viscosity structure has been modelled as a simple three–layer model defined by the thickness of an elastic lithosphere and uniform upper and lower mantle viscosities, respectively, where the boundary between the viscous layers coincides with the seismic discontinuity at a depth of approximately 670 km.

[4] A Maxwell visco-elastic model is used to describe a material that behaves elastically on a short time scale and viscously on a long time scale if a constant stress is applied.

By solving iteratively for the *sea level equation*, as outlined by e.g. Peltier (1998) or Milne (2002), predictions of the time–dependent separation between sea level and the surface of the solid Earth can be obtained. Employing the ICE–4G model to describe the space and time–dependence of the ice sheet thickness during the LGM and the following deglaciation phase, with the VM2 viscosity model (Peltier and Jiang, 1996), Peltier (1999) and (Peltier et al., 2002) showed excellent agreement between predicted sea level curves and geological sea level curves for the US East coast and the British Isles for the last 10,000 years.

In recent years, numerical models have been shown to be able to adequately describe the geophysical processes involved in modelling post–glacial rebound. By using additional observations as constraints, e.g. geological sea level records (Johnston and Lambeck, 2000; Lambeck et al., 1998a; Lambeck, 1998; Shennan et al., 2002), absolute gravity measurements (Lambert et al., 2001), modern tide gauge records (Davis et al., 1999; Lambeck et al., 1998b), or GPS derived estimates of 3–dimensional crustal movements (Milne et al., 2001; Park et al., 2002), GIA models can be tested and properties of Earth rheology or a wide range of processes related to the internal dynamics of the climate system inferred.

2.4 Mean Sea Level and Vertical Land Movements observed in the UK

In the previous two sections the concepts of tide gauge MSL records, for the analysis of secular sea level change, and the GIA process, as one of the main processes that induce vertical crustal movements, have been introduced. It was concluded that it is generally not possible to derive changes in absolute sea level based on tide gauge measurements alone and that vertical land movements at such sites need to be known.

The GIA process was identified as being able to contaminate estimates of the secular change in absolute sea level on a global scale and described as the only such process that can be adequately modelled and predicted. However, besides the GIA process a number of geological or engineering type processes do cause vertical land movements of varying

spatial extent, ranging from continental, regional and even local scale subsidence or uplift. Additionally, these processes do not operate in isolation, but will interact with each other possibly producing vertical land movements of a very complex character (Booth, 2000).

The UK was one of the first nations world wide to start recording sea level in a consistent way and, in fact, Sheerness was the site of the first automated tide gauge to commence operation in 1834. Besides the RLR MSL record for the tide gauge in Sheerness, several other long records exist for the sites in Aberdeen, North Shields, Liverpool and Newlyn, which have been of great importance in previous research (e.g. Thompson, 1980; Mitrovica and Davis, 1995; Woodworth, 1999; Woodworth et al., 1999; Peltier, 2001b; Tamisiea et al., 2001). The UK currently operates a network of 44 *Class A* tide gauges, funded primarily for flood warning purposes but all operated to the required standards for sea level research (Woodworth et al., 1999).

Global sea level rise has been estimated to be in the range of 1 to 2.5 mm/yr over the last century with a *best central value* of 1.8 mm/yr (Houghton et al., 2001). The long MSL records obtained from UK tide gauges have been shown by Woodworth et al. (1999) to be consistent with the bottom range of the IPCC estimates and with those from northwest Europe. Furthermore, Woodworth et al. (1999) stated that the spatial pattern of these long–term changes is consistent with the pattern of vertical land movements obtained from Holocene geological information (Shennan, 1989; Shennan and Woodworth, 1992), with subsidence rates of up to 2 mm/yr reported for south–eastern England and uplift due to glacial isostatic adjustment of 1 to 2 mm/yr for central Scotland.

In order to briefly discuss MSL around the British Isles and its interaction with predicted or observed vertical land movements, the author has obtained annual MSL data and long–term secular trends for a set of UK tide gauges and the tide gauge in Brest, France, from the RLR data set of the PSMSL data base (PSMSL, 2002b). The tide gauge sites of interest are those near or co–located with continuous GPS (CGPS) stations (Chapter 3).

Figure 2.2 shows the annual MSL data of the RLR data set for selected tide gauges co–located with or close to CGPS stations in the UK and for Brest in France. All time series have been offset to arbitrary heights for comparison. Clearly visible are the interannual and annual variations in all MSL records, which generally are at the decimetre level. In some

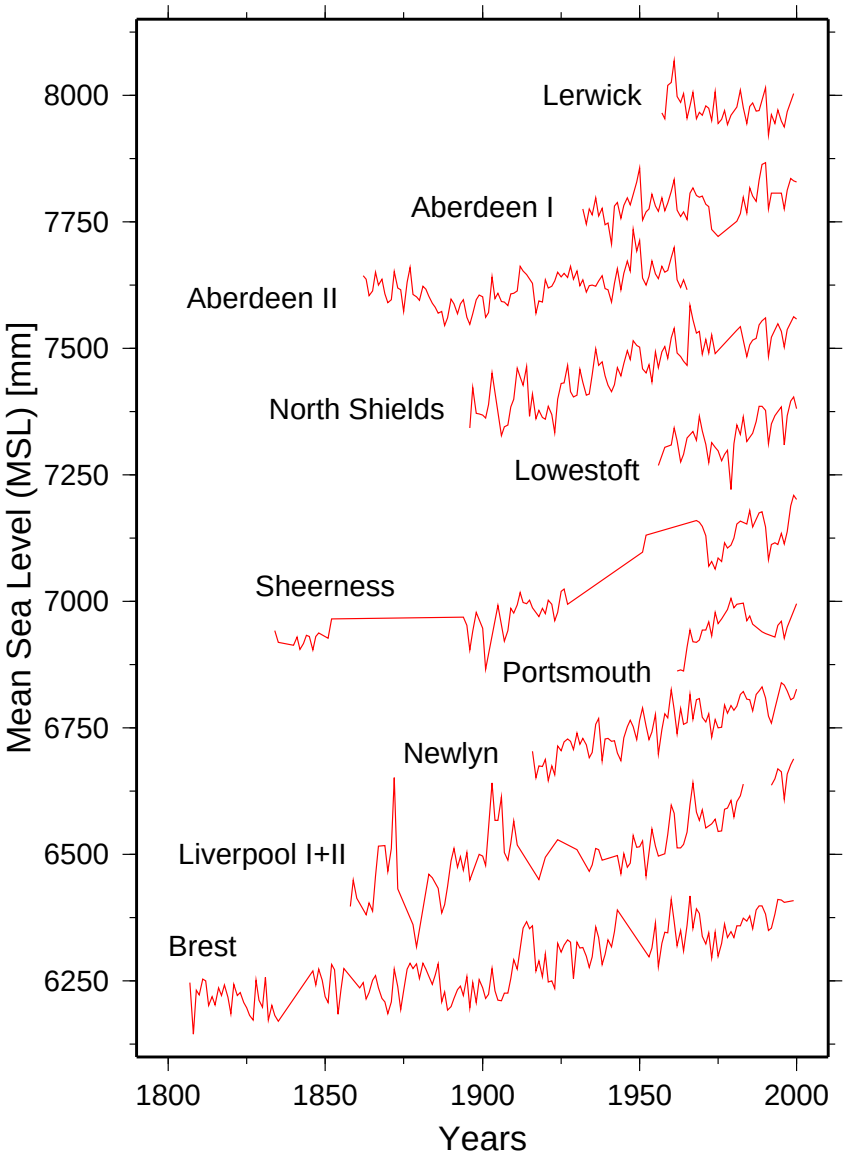

Figure 2.2: Annual mean sea level (MSL) records from the Revised Local Reference (RLR) data set in the Permanent Service for Mean Sea Level (PSMSL) data base for selected tide gauges co–located with or close to continuous GPS (CGPS) stations in the UK and France. Note: MSL records shown are offset for demonstration purposes.

records it is possible to identify similar features due to regionally coherent oceanographic sea level variations (Woodworth et al., 1999), e.g. Lerwick, Aberdeen and North Shields, located in the Shetland Isles and on the east coasts of Scotland and Northern England, respectively, and Newlyn and Brest. Furthermore, the MSL record for the most northern station in Lerwick shows a negative trend and, although positive, the trend in both MSL records for Aberdeen seems to be less positive than for sites to the south of Aberdeen.

Table 2.1 shows the MSL trends for the tide gauge sites of interest. The table lists the station name and their coordinates in longitude and latitude, the number of years used to compute the MSL trend (only complete years, i.e. which contain data for all 12 months, have been used), the start and end years of the observation time span, the MSL trend and its standard error. It should be noted at this stage that for the tide gauges in Aberdeen and Liverpool, the information shown is with respect to their composite records. Woodworth et al. (1999) also obtained improved estimates of the MSL trend for the stations at North Shields and Sheerness, which are also included in Table 2.1 instead of the MSL trends from the RLR data set. The composite records, are all of 70 years or more in length. However, it should be noted that although it is recommended that only MSL records of 60 years or more should be used for analysis, Table 2.1 also contains MSL trends for much shorter records.

From a first inspection of the MSL trends, it is possible to see that the majority of them are in the range of 1 to 2 mm/yr, with only Lerwick exhibiting a negative trend. Furthermore, it is evident from this table that the trends estimated clearly depend upon the location and the time span used for their computations. Based on this, it is possible to state that one needs typically 30 years of data in order to determine a secular sea level trend with a standard error of less than 0.5 mm/yr (Woodworth et al., 1999).

It is possible to compute an estimate for the vertical land movement at tide gauge sites based on the global average change in absolute sea level and the computed MSL trend, as has previously been demonstrated (Zerbini et al., 1996; Plag et al., 1998b). The rate of change in the vertical land movements r_{VLM} at a particular tide gauge site can be

Table 2.1: MSL trends for tide gauges in the British Isles and Brest, France based on Revised Local Reference (RLR) information in the Permanent Service for Mean Sea Level (PSMSL) data base (PSMSL, 2002b) and the analysis of the composite records for tide gauges in Aberdeen and Liverpool (Woodworth et al., 1999).

Tide Gauge Site	Longitude	Latitude	Years	Observation Time Span	MSL Trend [mm/yr]
LERWICK	01 08 W	60 09 N	36	1957 - 1997	-1.03±0.38
ABERDEEN[a]	02 05 W	57 09 N		1901 - 1999	0.69±0.11
NORTH SHIELDS[b]	01 26 W	55 00 N		1901 - 1999	1.87±0.14
LOWESTOFT	01 45 E	52 28 N	37	1956 - 1999	1.98±0.46
SHEERNESS[c]	00 45 E	51 27 N		1901 - 1999	2.14±0.15
PORTSMOUTH	01 07 W	50 48 N	29	1962 - 1997	1.30±0.56
NEWLYN	05 33 W	50 06 N	83	1916 - 1999	1.66±0.11
LIVERPOOL[d]	03 00 W	53 24 N		1901 - 1999	1.39±0.15
BREST	04 30 W	48 23 N	166	1807 - 1999	0.97±0.05

[a] composite record (Woodworth et al., 1999)
[b] (Woodworth et al., 1999)
[c] (Woodworth et al., 1999)
[d] composite record (Woodworth et al., 1999)

estimated from the rate of change in the MSL r_{MSL} and the global average change in absolute sea level r_{ASL} using following relation

$$r_{VLM} = -(r_{MSL} - r_{ASL}) \tag{2.1}$$

Despite 1.8 mm/yr being the best central value determined by Houghton et al. (2001) for the global average change in absolute sea level, the computations carried out by the author were based on a value of 1.5 mm/yr. This was based on the fact that when the MSL trends were corrected for vertical crustal movements due to GIA (Peltier, 2001a), an average change in absolute sea level of approximately 1.5 mm/yr is obtained for this particular set of tide gauges.

Besides the MSL trends, it is also possible to compile estimates of vertical land or crustal movements from different sources for the tide gauge sites of interest. Based on the ICE–4G (VM2) model, Peltier (2001a) computed radial GIA corrections to be applied to the MSL records of a global set of tide gauges. Using these corrections for tide gauge sites in the British Isles and Northern Europe, the author has produced a contour–plot (Figure 2.3)

of the predicted vertical crustal movements in the UK due to this process. Although, this figure does not truly show the predicted GIA signal of uplift and subsidence, the pattern displayed is representative in showing the main uplift zone in the Scottish Highlands and the areas of subsidence in southern England. For comparison, Figure A.1 in Appendix A shows the predicted vertical crustal movements reproduced from Figure 2 in Scherneck et al. (2002a), which were based on a slightly different GIA model (Milne et al., 2001).

A different source of estimates for vertical land movements are the geological sea level indices and relative sea level curves introduced in §2.2. Extensive research in this area has been summarized in the works of Shennan (1989); Shennan and Woodworth (1992) and Shennan and Horton (2002). A discussion on uplift/subsidence rates for the UK and North Sea regions can also be found in Woodworth et al. (1999). A reproduction of Figure 6 in Shennan and Horton (2002) is shown in Figure A.2 in Appendix A. The recently published results of Shennan and Horton (2002) are based on the analysis of more than 1000 radiocarbon dated sea level index points. In contrast to Shennan (1989), the ages of these data were calibrated, corrected for sediment compaction and for the east coast of England, corrected for changes in the tidal range. The changes in the tidal regime resulted from large scale changes in paleogeography and were modelled using high–resolution models of the coast line (Shennan and Horton, 2002).

From AG measurements carried out at UK tide gauge sites by the Proudman Oceanographic Laboratory (POL), it is also possible to derive estimates for vertical land movements. In the period since 1995, several AG campaigns took place at the three tide gauge sites of Newlyn, Aberdeen and Lerwick. In all three cases, the AG measurements were not directly carried out at the tide gauge itself, but within several kilometres distance and on stable ground. For a detailed description of absolute gravimetry the reader is referred to e.g. Vanìček and Krakiwsky (1986); Torge (2001). The results used in this study are those described in (Williams et al., 2001) and those for the latest AG measurements in 2002.

Recently, initial results from an attempt to derive vertical land movements from differences of satellite altimeter and tide gauge sea level measurements were published (Nerem and Mitchum, 2002). For 114 global tide gauge sites estimates of vertical land movements were obtained, however a comparison with these and estimates from other space geodetic

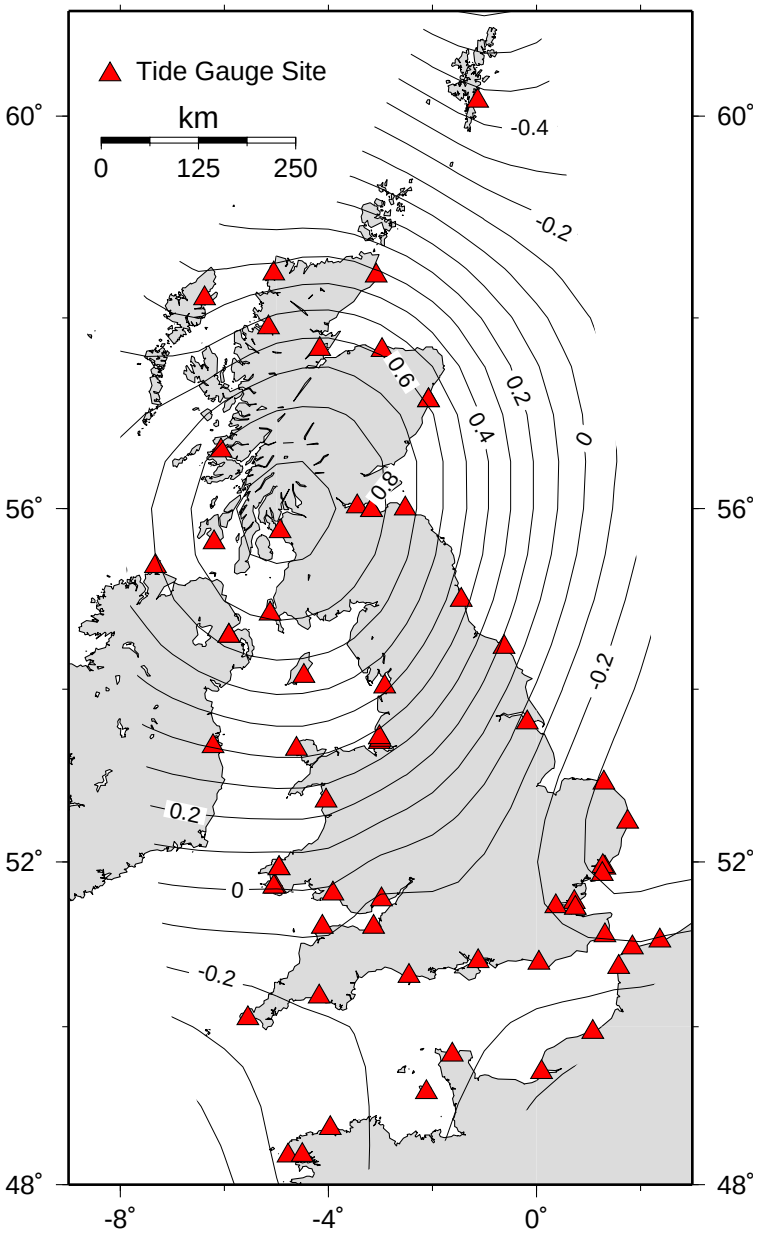

Figure 2.3: Estimated rates of current vertical crustal movements in mm/yr for the UK based on predicted glacial isostatic adjustment (GIA) corrections. Corrections have been provided by Peltier (2001a) and are based on the ICE–4G (VM2) model. Contours have been generated from the corrections for northern European and British Isles tide gauge sites using the Generic Mapping Tools (GMT) modules `surface` and `grdcontour` (Wessel and Smith, 1998).

techniques, e.g. DORIS (Doppler Orbitography by Radiopositioning Integrated on Satellite) and GPS, revealed little correlation. For completeness, the author has also included estimates of vertical land movements for Newlyn and Lerwick based on the analysis of Nerem and Mitchum (2002).

In order to allow a better comparison of these estimates of vertical land and crustal movements for the UK, Table 2.2 summarizes the values obtained from the different sources discussed above. Based on Table 2.1 and 2.2 it is now possible to discuss the general pattern of changes in sea level and vertical land movements for tide gauge sites in the British Isles.

In Table 2.1 the MSL trend for the tide gauge at Lerwick shows a relative sea level fall of -1.03 $\pm$ 0.38 mm/yr. This would indicate a significant uplift of 2.53 mm/yr for this site based on an absolute sea level rise of 1.5 mm/yr. It is however believed that due to the proximity of the Shetland Islands to the continental shelf, changes in relative sea level in this area seem anomalous (Baker, 2003a). This is confirmed by the vertical crustal movements predicted by both GIA models and the movements based on the AG measurements shown in Table 2.2. Interestingly, the subsidence at Lerwick suggested by the GIA model predictions, is typical for a station situated on the glacial forebulge, lying between the late Pleistocene Scottish and Fennoscandian ice sheets.

For Aberdeen, the MSL trend in Table 2.1 was derived from the composite record of the two MSL records for Aberdeen in the RLR data set of the PSMSL data base (see Figure 2.2). Woodworth et al. (1999) reported a systematic difference of 14 mm between the two sets of levels, which has been determined from their period of overlap. By adding this offset to the record of Aberdeen II, a composite record for Aberdeen was constructed, making it one of the longest MSL records in the UK. Table 2.1 shows a change in relative sea level for the composite record of Aberdeen of +0.69 $\pm$ 0.11 mm/yr over the period from 1901 up to 1996, which is relatively smaller than for the other tide gauges. The MSL record of Aberdeen clearly shows a trend affected by the GIA process. This is confirmed by the values shown in Table 2.2 with all evidence suggesting an uplift of 0.6 to 0.9 mm/yr, with the exception of the GIA predicted values in Scherneck et al. (2002a) and the current estimate from the AG measurements.

Table 2.2: Vertical land/crustal movements for selected tide gauge sites in the UK and France equipped with continuous GPS (CGPS) stations or which are close to a CGPS station, based on: MSL trends from Table 2.1 combined with an estimate of absolute sea level rise of 1.5 mm/yr (Eq. 2.1); predictions from glacial isostatic adjustment (GIA) models, with precise values from Peltier (2001a) and approximate values from Figure 2 in Scherneck et al. (2002a); estimates from geological information (Woodworth et al., 1999; Shennan and Horton, 2002); current and previous (in parenthesis) estimates from absolute gravity (AG) measurements (Williams et al., 2001), and satellite altimetry (Nerem and Mitchum, 2002). The associated statistical uncertainties are given were available.

Tide Gauge Site	-(MSL-1.5) (Eq. 2.1) [mm/yr]	GIA[a] Signal [mm/yr]	GIA[b] Signal [mm/yr]	Geology[c] [mm/yr]	AG[d] [mm/yr]		Satellite Altimetry[e] [mm/yr]
LERWICK	2.53	−0.47	−1.50		-0.7 ± 1.6		−1.9
ABERDEEN	0.81	0.60	2.00	0.69 ± n.d.	1.8 ± 1.9	(0.9)	
NORTH SHIELDS	−0.37	0.44	2.00	0.17 ± 0.06			
LOWESTOFT	−0.48	−0.35	−0.25	-0.61 ± 0.17			
SHEERNESS	−0.64	−0.24	−0.30	-0.74 ± 0.13			
PORTSMOUTH	0.20	−0.14	−0.30	-0.58 ± 0.03			
NEWLYN	−0.16	−0.25	−0.40	-1.12 ± 0.21	1.5 ± 0.7	(1.0)	2.9
LIVERPOOL	0.11	0.36	1.00	-0.21 ± 0.03			
BREST	0.53	−0.26	−0.49	-0.2[f]			

[a] (Peltier, 2001a)
[b] (Scherneck et al., 2002a)
[c] (Shennan and Horton, 2002)
[d] (Williams et al., 2001)
[e] (Nerem and Mitchum, 2002)
[f] Woodworth et al. (1999)

Another long MSL record is available for the tide gauge in North Shields. A similar MSL trend as shown in Table 2.1 was computed by Sanli and Blewitt (2001). They determined the relative sea level trend for the tide gauge in North Shields by simultaneously estimating statistically significant tidal components and obtained a value of +1.82 ± 0.06 mm/yr for a tidal record of 103 years in length. They also carried out a series of levelling campaigns over 3.5 years which suggested that the tide gauge had risen by about +0.8 ± 0.2 mm/yr relative to a benchmark situated on solid rock over this period. Recent levelling however suggested that the uplift of 0.8 mm/yr between the benchmark and the tide gauge may have been over estimated by a factor of two (Clarke, 2003). There is a clear discrepancy

between the MSL record, the GIA models and the geological evidence. Along with the local levelling, these results all suggest that the tide gauge itself may be experiencing a combination of movements acting over different time scales, e.g. subsidence due to mining activities over the last 100 years (Shennan, 1989) with more recent engineering movements of the pier structure (Sanli and Blewitt, 2001).

A shorter MSL record held in the RLR data base is for the tide gauge at Lowestoft with 37 years of observations. For this site, Table 2.2 shows a good agreement between the estimates of vertical land movements and the predicted vertical crustal movements in the range from approximately -0.6 to -0.3 mm/yr, which confirm the MSL trend in Table 2.1.

With 73 years of RLR data, the MSL record for the tide gauge in Sheerness is one of the longest in the UK. However this record contains large gaps and shows large differences to nearby stations in the Thames Estuary, e.g. Southend (not pictured in Figure 2.2), which suggests the need for further checks on site selection or data quality (Woodworth et al., 1999). Although all estimates for vertical land movements agree on subsidence, there is a discrepancy between the GIA models (predicted subsidence in the range between 0.2 to 0.3 mm/yr) and those derived from the MSL trend and geological data (estimated subsidence in the range between 0.6 to 0.7 mm/yr).

Although the record for the tide gauge at Portsmouth has reached an observation period of 30 years, it is described as not a good record for analysis. There have been doubts about the stability of the tide gauge during the 1960s to 1970s, although, recent trend analyses show values more like those expected from geological evidence (Woodworth et al., 1999). Recently, a new quay side has been developed housing the new tide gauge at Portsmouth. From Figures 2.3, A.1 and A.2 it can be seen that the regions in the south of England are generally subsiding, affecting the MSL record for Portsmouth and other tide gauge sites in this area.

The long record of MSL measurements for the Newlyn tide gauge was begun in 1915 in order to provide a MSL datum for the levelling of Britain (Araújo et al., 2001). The MSL record for Newlyn in Figure 2.2 shows no large data gaps and the interannual variability is relatively small compared to other records. Table 2.1 shows a trend of $+1.66 \pm 0.11$ mm/yr, which is similar to the trend of $+1.78 \pm 0.13$ mm/yr obtained from an intensive MSL

analysis carried out by Araújo et al. (2001). Based on geological information, Shennan (1989) gave a rate of vertical land movements in the range of -0.1 to -1.4 mm/yr for the south west of England. In order to be consistent with other MSL records and geologically derived subsidence rates, e.g. Brest in France, a value of -0.7 mm/yr for the site at Newlyn seemed more favorable (Woodworth et al., 1999). Table 2.2 shows the latest estimates for Newlyn based on geological information to be -1.12 $\pm$ 0.21 mm/yr. The computed and both the GIA predicted vertical movements shown in Table 2.2 show an average subsidence rate of 0.27 mm/yr, which is smaller than the above geology–derived estimates. To the contrary, the AG measurements at this tide gauge site show an uplift of 1.5 $\pm$ 0.7 mm/yr (1.0 mm/yr in Williams et al. (2001)) and the satellite altimetry derived estimates an uplift of nearly 3 mm/yr. Clearly, the latter estimate seems rather unrealistic and indicates problems with the current methodology of deriving estimates for vertical land movements using satellite altimetry data.

Liverpool has one of the longest histories of sea level recording in the UK. The MSL record shown in Figure 2.2 is a composite record of the Georges and Princes Pier records covering a timespan from 1853 to 1983 and the Gladstone Dock record from 1991 onwards. For the period of 1901 to 1996, Woodworth et al. (1999) gave an estimate for the trend of the composite record of +1.39 $\pm$ 0.19 mm/yr as shown in Table 2.1. In some respects, Liverpool is similar to North Shields in terms of the discrepancies between the GIA models and the geological information, which may also suggest that a combination of geophysical, geological and engineering effects are taking place at this site.

The MSL time series for Brest in Figure 2.2 is the longest of the figure and dates back to 1807. Woodworth et al. (1999) investigated the relative MSL trend between Newlyn and Brest and concluded that the trend for Brest was approximately 0.5 mm/yr less than that of Newlyn during the twentieth century. From geological information, they obtained a long–term subsidence rate for Brest of 0.2 mm/yr, which is, although poorly constrained by the geology, similar to the predictions obtained from both GIA models. As France lies beyond the immediate area covered by the ice sheets of the last glaciation of northern Europe, the crustal response to the removal of the ice is expected to be subsidence as mantle material flows towards the area of maximum rebound (Lambeck, 1997).

The vertical land movements discussed above for the selection of UK tide gauges and the tide gauge in Brest, France, have been plotted against latitude in Figure 2.4. The large differences in the estimates for the tide gauge site at Lerwick are clearly visible. The other sites have varying levels of agreement which support the suggestion that the computed movements are based on a combination of uplift and/or subsidence taking place at each site due to a combination of geophysical, geological and engineering movements.

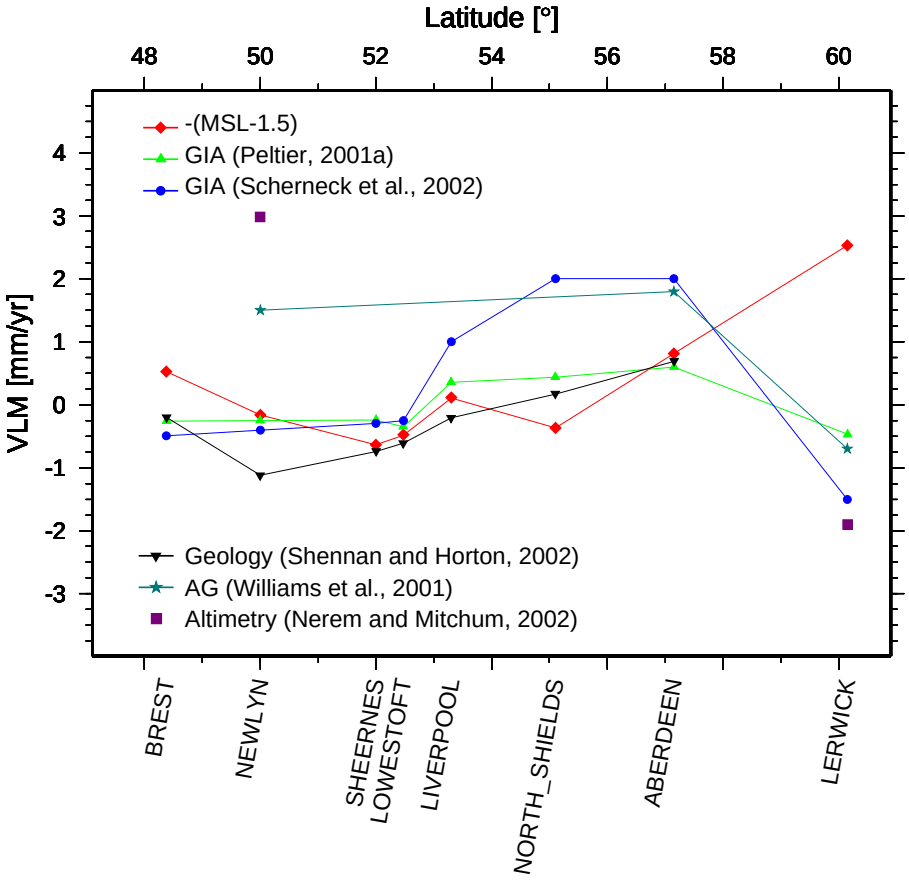

Figure 2.4: Vertical land/crustal movements for selected tide gauge sites in the UK and France equipped with continuous GPS (CGPS) stations or which are close to a CGPS station, based on: MSL trends from Table 2.1 combined with an estimate of absolute sea level rise of 1.5 mm/yr (Eq. 2.1); predictions from glacial isostatic adjustment (GIA) models, with precise values from Peltier (2001a) and approximate values from Figure 2 in Scherneck et al. (2002a); estimates from geological information (Woodworth et al., 1999; Shennan and Horton, 2002); estimates from absolute gravity (AG) measurements (Williams et al., 2001), and satellite altimetry (Nerem and Mitchum, 2002).

2.5 Summary

In this chapter the basic concepts of sea level and its measurement have been introduced. The topic of GIA was also discussed in order to recognize its importance as a geophysical process capable of affecting estimates of changes in absolute and relative sea level. It is the only such process that introduces vertical land movements that can be predicted by numerical models. However, due to the variety of geological or engineering type processes that may cause uplift or subsidence at one site, it is often difficult to analyse this complex pattern of land movements. It is therefore clear that in order to derive accurate estimates of changes in absolute sea level, vertical land movements at tide gauge sites have to be determined in an independent way.

The last section of this chapter discussed the MSL records available from the RLR data set of the PSMSL data base and those obtained from various publications. Estimates of vertical land/crustal movements based on MSL trends, with an assumed change in absolute sea level of 1.5 mm/yr, two GIA models, geological information, AG and satellite altimetry measurements were presented. From the differences in the estimates of vertical land/crustal movements there are clear indicators for local effects that cannot be attributed to GIA induced movements and hence, a long–term monitoring strategy to determine vertical land movements at tide gauge sites is required.

Chapter 3

The Global Positioning System (GPS) for Monitoring Tide Gauge Sites

3.1 Introduction

This Chapter gives a historic overview of the application of GPS to the monitoring of vertical land movements at tide gauge sites. It summarizes the early GPS campaigns in the UK and Europe, which were carried out following the recommendations of several international working groups concerned with this topic. Several systematic biases and errors still limit the achievable absolute accuracy in the vertical coordinate component. Some issues with direct relevance to this work will be discussed in short in this Chapter, however for a general description of the GPS and its systematic biases and errors the reader is referred to several texts on this subject, such as Hofmann-Wellenhof et al. (1993); Leick (1995), and Kaplan (1996).

3.2 Historical and Current Initiatives

This section briefly introduces the international meetings at which topics related to the monitoring of vertical land movements at tide gauge sites were discussed. Following this, an overview of the tide gauge monitoring projects carried out in the UK and Europe is given. Two recent international initiatives dealing with this issue on a global and European scale, i.e. the IGS Tide Gauge Benchmark Monitoring Pilot Project (IGS TIGA–PP) and the European Sea Level Service (ESEAS) Project are introduced.

3.2.1 International Tide Gauge Monitoring Meetings

Over the last century, tide gauge records have been the main source of data on changes in sea level. However, tide gauges cannot distinguish between changes in absolute sea level and vertical movements of the land at the tide gauge sites. In August 1989 an *ad hoc committee* of the the International Association for Physical Sciences of the Ocean (IAPSO) Commission on Mean Sea Level and Tides met at the Woods Hole Oceanographic Institute, USA, to discuss available geodetic technologies that would enable the separation of these movements from the tide gauge records. The committee's conclusions were summarized in the first *Carter Report* (Carter et al., 1989) and among the recommendations it was suggested that TGBMs should be connected to a global reference system, i.e. the International Terrestrial Reference System (ITRS) and monitored through episodic GPS (EGPS) campaigns, with simultaneous measurements made at GPS stations close to TGBMs and fundamental International Terrestrial Reference Frame (ITRF) stations.

In December 1993 the second workshop of the *IAPSO committtee* to study geodetic fixing of TGBMs, took place at Deacon Laboratory, UK, and culminated in the second *Carter Report* (Carter, 1994). Due to significant advances in GPS technology, which showed in cheaper and more reliable GPS receivers, the completion of the GPS satellite constellation, the establishment of the International GPS Service (IGS); and the first experiences of geodynamic monitoring using GPS (Dixon, 1991; Larson and Agnew, 1991; Larson et al., 1991; Feigl et al., 1993), the committee concluded that in order to achieve the minimum accuracy needed of 1 to 2 mm/yr over 5 year intervals and 0.3 to 0.5 mm/yr

over intervals of a few decades CGPS should be used. Hence, it was recommended that CGPS stations should be established at about 100 tide gauge sites world–wide to form a core network of a global absolute sea level monitoring system. It was further concluded that regional densification of this core network should be carried out, through EGPS or the use of additional CGPS stations (Carter, 1994).

In succession of the two *Carter Reports* followed the technical report of the IGS/PSMSL Workshop on Methods for Monitoring Sea Level, held at the Jet Propulsion Laboratory (JPL), California, in March 1997, entitled "GPS and Tide Gauge Benchmark Monitoring and Altimeter Calibration" (Neilan et al., 1997). One recommendation of this third meeting was to set up a technical working group to define recommended standards and specifications for operating CGPS at tide gauge sites. These standards would cover the suggestions for making measurements for precise ties, e.g. between the GPS reference point and the TGBM or local reference networks, the data handling of the survey tie information, site stability and monumentation aspects, observing methods and strategies and the acquisition of complementary information on vertical coastal movements and mass redistribution by AG and ancillary measurements, e.g. meteorology and other environmental data (Neilan et al., 1997).

A fourth meeting on this topic was held in Toulouse, France in May 1999. An international working group was initiated on "How to Operate GPS at Tide Gauge Sites" with the emphasis on CGPS rather than EGPS measurements (PSMSL, 2002a). This working group has become known as the CGPS@TG Working Group.

In October 1999 a survey was carried out to establish the number of globally distributed CGPS stations already existing or planned for the near future within the vicinity (<10 km) of tide gauges. The latest list of global CGPS@TG sites can be found on `http://www.sonel.org/stations/cgps/surv_update.html` (Wöppelmann et al., 2002). Furthermore, the CGPS@TG Working Group established a web–site dealing with the technical issues and recommendations related to the installation of CGPS@TG stations (see `http://imina.soest.hawaii.edu/cgps_tg` or (Bevis et al., 2002)). In a follow up meeting held in Hawaii in April 2001, an IGS pilot project on the topic of GPS at tide gauges was proposed (§3.2.4).

3.2.2 The UKGAUGE and EUROGAUGE Projects

Following the recommendations of the first *Carter Report* the then Ministry of Agriculture Fisheries and Food (MAFF), through the long term commission with the Proudman Oceanographic Laboratory (POL), initiated a project for monitoring vertical land movements at selected sites of the UK Tide Gauge Network (see also `http://www.pol.ac.uk/tgi`) using GPS. This first POL/IESSG project, *UKGAUGE I*, involved nine tide gauge sites in the UK observed during three EGPS campaigns from 1991 to 1993 (Ashkenazi et al., 1993, 1994, 1998).

The *EUROGAUGE* project, funded by the European Commission and initiated in 1992, involved two GPS campaigns at a selection of sixteen tide gauge sites along the European Atlantic Coast and in the Mediterranean (Ashkenazi, 1995). The results from the two independent measurement campaigns indicated that accuracies better than 10 mm in plan and height were achieved in this project. For further details the reader is referred to (Chang et al., 1996).

In 1995, MAFF/POL initiated the second UK wide tide gauge monitoring project, *UKGAUGE II*, which involved a network of sixteen tide gauge sites and three further EGPS campaigns in 1995 and 1996 (Beamson, 1995). All together nine EGPS campaigns were carried out by the IESSG and POL from 1991 to 1996, through the UKGAUGE I, EUROGAUGE, and UKGAUGE II projects. For an in depth description of the projects the reader is referred to Ashkenazi et al. (1997).

EGPS measurements at these initial 16 tide gauge sites have since then been continued in 1999, 2002 and 2003 as part of the UKGAUGE III and IV projects. Furthermore, since the commencement of these projects, seven EGPS sites have been upgraded with CGPS stations directly at the tide gauge (Bingley et al., 2000a,b, 2001a,b).

During this time, similar projects were being carried out in other countries and regions, the Sea Level Fluctuations in the Mediterranean: interactions with climate processes and vertical crustal movements (SELF) projects (Zerbini, 1994, 1996; Zerbini et al., 1996; Zerbini, 1997; Becker et al., 2002); and the tide gauge monitoring initiative in the

Chesapeake Bay, USA (Nerem et al., 1997; Schenewerk et al., 1999). A comprehensive list of related projects in Europe can also be found in Plag et al. (1998a).

3.2.3 European Commission COST Action 40 and ESEAS

Besides the international meetings described in §3.2.1 and the national and regional tide gauge monitoring initiatives described in §3.2.2, and after a proposal by Baker et al. (1997), a lot of effort to coordinate activities in this area has recently taken place on a European scale.

One European Commission funded action was the European co–operation in the field of scientific and technical research (COST) Action 40: European sea–level observing system (EOSS) (Plag et al., 2000). This set out to coordinate various European sea-level activities and to publish recommendations related to height reference systems and fixing TGBMs, MSL determination, sea surface topography, tidal models and storm surge warning, and storage and exchange of data.

One of the major results of COST Action 40 was the establishment of the European Sea Level Service (ESEAS). Since September 2001 a Governing Board, Technical Committee and Central Bureau have been formed to facilitate the establishment of ESEAS. Following calls for participation, more than 150 tide gauges from 18 countries were proposed as ESEAS observing sites. This includes all 44 tide gauges in the UK National Tide Gauge Network, with the IESSG submitting a proposal to contribute date from the CGPS@TG stations at Newlyn (and Camborne), Portsmouth, Sheerness, Lowestoft, Liverpool, North Shields (and Morpeth) and Aberdeen. More information on ESEAS can be found on the official website: `http://www.eseas.org`.

3.2.4 The IGS TIGA Pilot Project

In June 2001, the IGS called for participation for the GPS Tide Gauge Benchmark Monitoring (TIGA) Pilot Project (PP) (Schöne, 2001). The project's main goals include the establishment, maintenance and expansion of a global CGPS@TG network and to further promote more CGPS stations to be established in the southern hemisphere. The

project also aims at creating links to other space geodetic sites, e.g. DORIS, Satellite Laser Ranging (SLR), and Very Long Baseline Interferometry (VLBI), and to AG sites, which may contribute to vertical motion determination. A set of minimum technical standards is to be agreed and recommended for all sensors, i.e. GPS, tide gauge and other ancillary systems, levelling ties between benchmarks and their documentation (Schöne, 2001).

It is also suggested that a contribution to the procedures in which the IGS realizes a global reference frame is made, focussing on improving the vertical component. This has been recently identified as being one of the major limiting factors in improving vertical station velocities (Herring, 2001; Kierulf et al., 2001). The TIGA–PP proposal also suggests two processing streams, one with a latency of up to one year and a second one with a much reduced latency, in order to arrive both at the highest quality coordinates and velocities for all CGPS@TG stations and to support operational activities that do not tolerate large delays.

The IESSG has submitted an application to contribute data from the CGPS@TG stations at Newlyn, Sheerness, North Shields (and Morpeth) to this international initiative.

3.3 A Global Reference System for Vertical Monitoring

As mentioned previously, the coordinates and changes in coordinates of a TGBM must be referenced to a global reference system in order to derive changes in absolute sea level at any tide gauge site around the world. The surface of the Earth does not in itself provide an ideal reference system for this purpose, as the crust undergoes constant changes in time. However, for geodetic measurements, terrestrial reference systems can be defined by a set of orthogonal axes, a reference ellipsoid, a gravity model and a geoid. Normally the axes are defined with their origin at the centre of mass (CM) of the Earth system (includes the solid Earth, oceans and the atmosphere), i.e. the geocentre, and a specific orientation and scale. The realization of a reference system is by means of a reference frame, which is defined by the positions of stations, i.e. the station coordinates, fixed to the Earth's crust at a defined reference epoch and the linear rate of change in their positions, i.e. the station velocities (e.g. Bock, 1996).

The usefulness of the reference frame for the computation of highly accurate vertical station velocities from GPS coordinate time series, depends on its ability to describe changes in coordinates over time. In time, station coordinates are degraded by spurious movement of the station with respect to the reference frame, internal deformations of the reference frame and during updates of the reference frame. Currently the only global reference system potentially capable of delivering the required positioning accuracy and the long–term stability is the International Terrestrial Reference System.

3.3.1 International Terrestrial Reference System

The International Terrestrial Reference System (ITRS) is a very accurate geodetic reference system, comprising a set of right–handed orthogonal axes, whose origin is defined at the CM, whose axes are orientated to be consistent with those of the Bureau International de l'Heure (BIH) at epoch 1984.0, and whose unit of length is the metre. The axes are fixed to the Earth's crust such that there is no residual global rotation of the system with respect to the crust (McCarthy, 1996). The ITRS is maintained by the International Earth Rotation Service (IERS). Realizations of the ITRS are produced by the IERS under the name International Terrestrial Reference Frame (ITRF).

3.3.2 International Terrestrial Reference Frame

The first realization was the ITRF88 (Boucher et al., 1996). Since then, the IERS has published ITRS realizations on a nearly annual basis sustaining continuous improvements and enhancements. For a detailed progress on these realizations and the developments in the computational methodology, see Boucher et al. (1993, 1994, 1996); Boucher and Altamimi (1996); Boucher et al. (1998); Sillard et al. (1998); Boucher et al. (1999); Altamimi and Boucher (1999); Altamimi et al. (2001) and Sillard and Boucher (2001).

The ITRF is realized through the cartesian coordinates and linear velocities of a global set of monitoring stations equipped with various space geodetic observing techniques, such as VLBI, SLR, Lunar Laser Ranging (LLR), GPS, and DORIS (Altamimi et al., 2002). Additionally the frame also depends on the surveyed tie vectors that relate these co–located

systems at a subset of ITRF sites, as without these ties, each observing technique would realize individual terrestrial frames (Altamimi et al., 2001). The complimentarity of these independent techniques requires an integrated approach to achieve the highest accuracy and consistency. The current methodology is based on simultaneously combining station positions and velocities, and surveyed tie vectors using full–covariance information provided in **S**olution **IN**dependent **EX**change (SINEX) format files for each single observing technique (Altamimi et al., 2002).

Each of the space techniques has certain strengths and weaknesses for the determination of the reference frame parameters; VLBI uniquely defines accurate Earth orientation in an inertial frame, but the station positions remain relative (Angermann et al., 2002). Thus, VLBI does not contribute to the determination of the geocentre. The direct range measurements of SLR/LLR instruments allow for absolute positioning with respect to the geocentre and accurate determination of the Earth scale (Altamimi et al., 2002; Angermann et al., 2002; Pavlis, 2002). Although GPS has not been included in the determination of the scale or origin definition, it makes a large contribution in terms of the velocity field.

The most recent realization of the ITRS, i.e. the ITRF2000, is the most extensive and accurate terrestrial reference frame so far (Altamimi et al., 2001) and includes positions and velocities for about 800 stations located at about 500 sites. Its scale definition is based on a weighted average of VLBI and SLR results and its origin was derived from SLR measurements (Altamimi et al., 2001; Pavlis, 2002).

Pavlis (2002) reported the ITRF2000 scale to be stable to approximately 1 part–per–billion (ppb). The long–term stability, evaluated over 10 years, is estimated to be better than 4 mm in origin and better than 0.5 ppb in scale, however this is equivalent to a shift in station heights of approximately 3 mm (Altamimi et al., 2002). Furthermore, the ITRF2000 analysis standard deviation for the vertical velocities of the IGS cumulative solution is about 3 mm/yr, as estimated for a set of 158 stations excluding some poorer stations (Ferland, 2001).

The orientation of the ITRF2000 has been aligned with its preceding realization, ITRF97, however, there are reports of discrepancies between different realizations, which

can also affect the velocity estimates of stations on the Earth's surface. (Lavallée, 2000) reported a significant 2 mm/yr difference in the Z component translation rate between IRTF97 and preceding realizations. A similar magnitude of disagreement of the ITRF97 was reported with respect to the reference frame used by satellite altimeters. However, this 2 mm/yr drift is reported to have been removed in the ITRF2000, as its frame origin was determined using SLR results (Ries et al., 2001).

The IGS produces its own ITRS2000 realization by aligning its cumulative solutions to ITRF2000. So far this has been carried out using a network of 54 IGS reference sites, however it was recently proposed to increase this number to 83 sites (Heflin, 2003). This is primarily carried out in order to improve the internal stability and consistency of the weekly product alignment. The IGS realization of the ITRF2000 is termed IGS00.

Ferland (2001) and Heflin et al. (2002) reported of better agreement between the components of the IGS00 and the ITRF2000 itself, than those obtained for IGS97 and the ITRF97. Furthermore, Ferland (2002) stated that the analysis of the residuals between IGS00 and ITRF2000 showed a position RMS of about 1 mm and 3 mm and a velocity RMS of 2 mm/yr and 5 mm/yr for horizontal and vertical coordinate components respectively.

3.4 GPS Systematic Biases and Errors limiting Accuracies in the Vertical Component

It is commonly known that most GPS systematic biases and errors have the potential of corrupting, especially, the vertical coordinate component if not mitigated appropriately. Even under the assumption that all error sources could be perfectly modelled, the vertical coordinate component would still be the least accurate as satellites are only observed above the horizon. Additionally, many factors contributing to the bias in the vertical component are highly correlated, making modelling and mitigation of these difficult.

Santerre (1991), Shardlow (1994); Beamson (1995) and Penna (1997) deal with systematic biases and errors in GPS observations in great detail and the reader is referred to their work for a more complete discussion. Here only a brief overview will be given with

an emphasis on how those error sources may affect global reference frame definition and what are the implications of these systematic effects on regional GPS analyses, such as the one carried out by the author.

3.4.1 Reference Frame, Geocentre Motion, Satellite Orbits and GPS Scale

For height measurements, the most important quantities of the system are the origin and the scale, as both directly affect the distance between the CM and the station on the Earth's surface (Herring, 2001; Kierulf et al., 2001). Modern terrestrial reference frames are based on measurements of various space geodetic systems, mostly using Earth orbiting satellites. Due to the gravitational forces, satellites rotate about the instantaneous CM of the entire Earth system and not the geocentre used by the reference system, which is in fact the centre of the polyhedron created by the globally distributed stations, i.e. the centre of figure (CF). Although there is no known physical process that can sustain a long–term velocity of this CF with respect to the CM (Argus et al., 1999), there are apparent variations of the CF, i.e. geocentre motions, with respect to the CM on timescales ranging from diurnal to interseasonal frequencies (Chen et al., 1999; Crétaux et al., 2002; Pavlis, 2002; Dong et al., 2003). Currently, even the most comprehensive and accurate reference frame, i.e. ITRF2000 (§3.3.2), does not model this effect and only a linear evolution of the CF is assumed in the computation of the frame (Altamimi et al., 2001). Although, this allows for good long–term stability of the ITRF2000, as reported by Altamimi et al. (2002), the realization of an accurate origin of the reference frame in the short term is dependent on the appropriate modelling of known and anticipated motions in the CM of the Earth. As these *geocentre variations* are to a large percentage due to the astronomical driven tidal variations, models can be included a priori in the computation of the frame (Pavlis, 2002; Dong et al., 2003). Additional geocentre variations have been attributed to global mass re–distribution processes within the Earth system (e.g. van Dam and Wahr, 1987; van Dam et al., 1994, 1997; Blewitt et al., 2001; Mangiarotti et al., 2001; Dong et al., 2002b) and are more difficult to model. In general, to provide more accurate terrestrial reference systems for height measurements, a full understanding of these variations is required.

On a global scale unmodelled geocentre variations move the whole reference frame primarily introducing a seasonal term with amplitudes of 3 to 5 mm (Chen et al., 1999). For regional network analyses, using different subsets of the ITRF global network will introduce different relative seasonal terms with amplitudes of up to 1 cm (Dong et al., 2002b).

Besides the effect on station coordinates and the reference frame, unmodelled geocentre variations are manifested in temporal changes of the degree one terms of the geopotential model used in the precise orbit determination process. In addition to geocentre variations, episodic mass transport causes momentum changes with concomitant variations in the orientation of the terrestrial inertia axes. Such deficiencies in modelling orbital dynamics or the dynamics of Earth rotation feed back into the reference frame realization.

The realization of the reference frame through a set of station positions at a related reference epoch and constant station velocities for the entire data time span in itself introduces systematic biases into the ITRF solutions. Stations that are located close to plate boundaries might be affected by transient effects, e.g. the IGS station in Fairbanks, Alaska, was recently displaced due to an earthquake, resulting in the exclusion of the station from reference frame computations, introducing a change in the reference frame definition. Such episodic or time dependent motions cannot be modelled correctly by linear velocities. Furthermore, the accuracy of the space techniques has increased significantly over the last decade, so that the older data might decrease the accuracy of the newly computed reference frame solutions. Finally, a large number of stations are occupied with different systems, which might produce systematic effects in the time series that feed into reference frame computations. This effect is of particular importance with respect to mis–modelled antenna phase centre variations (§3.4.3) and tropospheric delay estimates (§3.4.2).

Another source of error in GPS coordinate estimates stem from biases in the applied precise ephemeris. From a purely geometric point of view in that GPS measurements are basically distance measurements between a station and a GPS satellite, it is clear that errors in the GPS satellite orbits will directly affect coordinate estimates of that station. Beutler (1996b) argued that the propagation in the errors $\mathbf{dr}$ of the satellite coordinates

into errors **db** in the coordinate components of a baseline of length b can be described using following rule:

$$\left|\frac{\mathbf{db}}{b}\right| = \left|\frac{\mathbf{dr}}{r}\right| \tag{3.1}$$

with r being the mean distance between the station and the satellite. Using Eq. 3.1 with an accuracy of the IGS final ephermis of 5 cm, it is easy to see that for a baseline of 1000 km will lead to approximately 2 mm error in the station coordinates. Due to the fact that the largest orbit errors are expected to be in the along track component, which leads to tilting of the station network, station heights are affected most (Rothacher, 2002).

Although it is assumed that when using IGS final ephemeris, errors in satellite orbits have a minimal effect on station coordinates, changes in the reference frame of the orbits introduce steps in the derived coordinate time series, affecting station velocity estimates. Fortunately, this can be mitigated by using an appropriate GPS processing strategy (§6.2.1).

It should also be mentioned that by introducing station coordinate constraints in regional networks, the coordinates are required to be very accurate and consistent with the reference frame of the satellite orbits. Fixing sites with erroneous height will lead to scaling of the network and to a common height bias (Rothacher, 2002).

As was mentioned above, accurate vertical station velocity estimates from GPS coordinate time series depend also on the long–term stability of the scale of the GPS. Herring (2001) showed that based on 10 years of GPS measurements the GPS scale may be changing by as much as 0.5 ppb/yr, which is equivalent to 3 mm/yr changes in the vertical coordinate component. This change in scale has to a large degree been attributed to effects of GPS satellite phase center modelling and the evolution of the GPS constellation from Block I, to Block II, IIA and currently Block IIR generations of satellites (Marquis, 2001). Heflin et al. (2002) attributes the apparent scale also to residuals in the tropospheric delay estimates.

Besides the influence of the GPS scale, Kierulf et al. (2001) showed that the achievable accuracy in height is also dependent on the elevation of a satellite. The combined effect of a change in the GPS scale and the elevation dependency can be demonstrated using

Figure 3.1, showing the simplified geometric relation between a ground based station and a satellite (Kierulf et al., 2001).

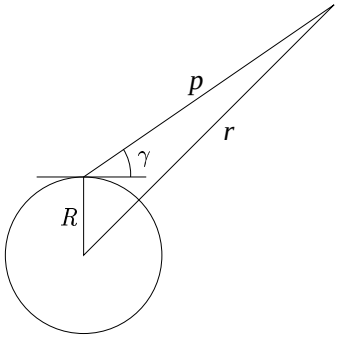

Figure 3.1: Simplified geometric relationship between a ground based station and a satellite (Kierulf et al., 2001).

As can be seen from Figure 3.1, the geometric relationship between a satellite at geocentric distance r and a surface station at geocentric distance R can be described using following equation (Kierulf et al., 2001)

$$r^2 = R^2 + p^2 - 2pR\cos(\gamma + \pi/2) \tag{3.2}$$

with p being the distance between station and satellite, and γ being the elevation angle of the satellite as viewed from the station. A scale error ϵ can now be introduced with $r = r_0(1 + \epsilon)$, where r_0 is the geocentric distance of the satellite not affected by the scale error. Equation 3.2 can now be extended by the scale error and re–written to solve for the geocentric distance to the station so that (Kierulf et al., 2001)

$$R = -p\sin\gamma + \sqrt{(r_0(1+\epsilon))^2 - p^2\cos^2\gamma}. \tag{3.3}$$

The distance p is then determined as a function of r_0, R_0 and γ, with R_0 being the geocentric distance of the station not affected by the scale error. Hence, the apparent vertical displacement $\delta h = R - R_0$ is a function of the scale error ϵ and the satellite elevation angle γ, i.e. $\delta h = \delta h(\epsilon, \gamma)$ (Kierulf et al., 2001).

Kierulf et al. (2001) showed that a scale error of 0.1 ppb/yr introduces a vertical displacement of 2 mm/yr for satellites at elevation angle greater than 30° and more than 5 mm/yr for satellites lower than 15°. This is of particular importance for GPS stations in high–latitude areas, as the number of low–elevation satellites in view will be larger.

3.4.2 Atmospheric Biases

GPS signals are affected by refraction and signal bending on their path through the atmosphere, which need to be mitigated correctly in the analysis. If not accounted for, they will propagate directly into the station coordinate estimates and displacements of centimetre level can occur, especially in the vertical coordinate component. Atmospheric biases affect the range between satellite and receiver antennas, thus they introduce scale errors into the measurements.

Atmospheric biases are generally described in terms of the delay occurring in the ionizing or neutral segments of the atmosphere, i.e. ionospheric and tropospheric delay. The characteristics of GPS signal propagation through the atmosphere and appropriate delay models have extensively been described in numerous GPS textbooks (Hofmann-Wellenhof et al., 1993; Seeber, 1993; Langley, 1996) and further investigated with respect to GAS (§4.2) by Shardlow (1994); Hubbard (1995) and Baker (1998).

Ionospheric Delay

The ionosphere covers the upper section of the Earth's atmosphere and reaches from approximately 50 to in between 1000 and 2000 km (Langley, 1996). It is a dispersive medium for electromagnetic waves at GPS frequencies, which means that the refractive index of a signal is dependent on the signal's frequency. This characteristic can be used in the analysis of dual–frequency GPS observations to largely reduce the effect of the ionospheric delay on GPS measurements by creating the ionospherically free linear combination (L0 in GAS) of the two carrier signals L1 and L2 such that L0 $\approx$ 2.545L1 - 1.984L2 (Booth, 2000). This ionospherically free observable forms the main observable in the current analysis of the UK CGPS network discussed in this thesis.

GPS signals propagating through the ionosphere may also be affected by rapid changes in the number of electrons along the signal path, such that it becomes difficult for a GPS receiver to keep track of the carrier phase because of variations in its amplitude and phase. These short term variations (1 to 15 sec) are commonly known as ionospheric scintillation. In cases where the receiver completely loses lock on a satellite signal, a phase discontinuity

or cycle slip occurs. These cycle slips must be *repaired* before carrier phase measurements after the slip can be used in the analysis. The amount of ionospheric activity depends on the number of sunspots which follow a 11–year cycle. The period since the last minimum in the number of sunspots in May 1996 coincides roughly with the establishment of the CGPS stations in the UK. It is therefore not surprising that days of high ionospheric activity and days on which observation sessions could not be cleaned for cycle slips seem to be correlated (§5.3).

Tropospheric Delay

The neutral atmosphere extends from the Earth's surface to approximately 50 km above it and is a non-dispersive medium, i.e. the refractive index is independent of the signal frequency. Tropospheric delay models estimate the tropospheric zenith delay (TZD) (Shardlow, 1994), which is the delay at 90° from the horizon, i.e. the zenith. At sea level, values for the TZD can reach magnitudes of up to 2.3 or 2.6 m (Langley, 1996). The TZD can be separated into a *hyrostatic* and a *wet* component, so that the total delay $\Delta L(\gamma)$ at elevation γ can be written as

$$\Delta L(\gamma) = \Delta L_h^z \cdot m_h(\gamma) + \Delta L_w^z \cdot m_w(\gamma) \tag{3.4}$$

with ΔL_h^z and ΔL_w^z being the hydrostatic and wet zenith delay respectively and $m_h(\gamma)$ and $m_w(\gamma)$ the hydrostatic and wet mapping functions respectively (Niell, 1996). The mapping functions are required since satellites appear in elevation angles between 0 and 90° from a GPS station and take into account that signals at lower elevation angles will have travelled longer through the atmosphere and hence will have experienced a larger delay (Dodson et al., 1996). In this analysis the broadly used mapping function by Niell (1996) has been applied, with a set of coefficients for both the hydrostatic and wet components. The mathematical form is the same for both delays, but differs in the coefficients a, b and c. Therefore the mapping functions have the form

$$m(\gamma) = \frac{1 + \dfrac{a}{1 + \dfrac{b}{1+c}}}{sin(\gamma) + \dfrac{a}{sin(\gamma) + \dfrac{b}{sin(\gamma)+c}}} + \delta m_h \tag{3.5}$$

with δm_h being applied in order to account for the height dependence of the hydrostatic component. This height correction does not apply to wet delay mapping, since the distribution of atmospheric water vapour is not predictable from station heights (Niell, 1996).

In Eq. 3.4 the hydrostatic contribution accounts for approximately 90% of the total delay and can be modelled by assuming the atmosphere to be in a state of hydrostatic equilibrium (Langley, 1996). The wet tropospheric delay is a function of the water vapour content along the path of the electromagnetic signal and is highly variable both spatially and temporally and is therefore more difficult to mitigate. Although, Eq. 3.4 suggests that both delay components can be estimated, this is in practice very difficult, as both components have a similar dependence on the elevation angle. It is however possible, to solve for the total or a residual wet zenith delay, i.e. after the hydrostatic component is modelled, by introducing an extra unknown in the GPS least–squares parameters estimation process. Time correlation and variability of the tropospheric delay can additionally be accounted for by means of a stochastic process (Baker, 1998).

The tropospheric delay is the hardest bias to mitigate in order to arrive at highly accurate daily height estimates. The TZD estimates tend to be highly correlated with other biases affecting the vertical component, e.g. ocean tide loading (Baker, 1998; Dodson et al., 1999; Dragert et al., 2000) or antenna phase centre variations (Kaniuth and Stuber, 2002; Rothacher, 2002). Improper modelling of the tropospheric delay will produce a scale error in the analysis. Within the global networks of the IGS, a residual bias in the tropospheric delay may lead to biases in the reference frame and satellite orbits. By using these products in regional network analyses, such biases manifest themselves in the estimated parameters. The seasonal character of the troposphere is primarily described by the wet tropospheric component. Therefore, residual tropospheric delay biases may be responsible for some of the annual signals observed in coordinate time series (Dong et al., 2002b).

3.4.3 Antenna Issues

The observed range between a receiver antenna and the transmitting satellite antenna is the distance between the electrical phase centres of both antennas. However, the geometric antenna centres of both the transmitting and receiving antennas and their electrical phase centres do not coincide, and can differ for receiver antennas by centimetres and for satellite antennas by up to one metre (Mader and Czopek, 2001). The offset between the geometric antenna centre and the electrical phase centre of the receiver antenna can be described using a constant and varying component. The constant offset arises from the difference between the mean phase centre and an antenna reference point (ARP), whereas the variable offset depends on the elevation angle, azimuth and intensity of the incoming signal and differs for L1, L2 and the ionospherically free linear combination (Schupler and Clark, 1991; Rothacher et al., 1995).

For transmitting satellite antennas, the offset between the electrical phase centre and the geometric reference point has been assumed to be constant for a specific satellite block type. The IGS therefore uses offsets for Block I, II, IIA and IIR, which are referenced to the centre of mass of the GPS satellite. Currently there are no elevation–dependent antenna phase centre variations applied for satellite antennas. Mader and Czopek (2001) however showed that the IGS satellite phase centre offsets differ significantly from offsets determined during a satellite antenna phase centre offset calibration carried out on a Block IIA satellite antenna.

Receiver antenna phase centres also vary between different antenna types, but are consistent between antennas of the same model. For high precision geodetic choke ring antennas using the Dorne Margolin antenna element, the antenna phase pattern was shown to have hardly any azimuthal phase centre variations (Wübbena et al., 2000). For short baselines, this means that by using identical antennas and orientating them in the same direction, the effect of antenna phase centre variations can be mitigated. If baselines are longer, and satellites do not appear in the same elevation angle anymore, then the bias does not difference out and antenna phase centre models must be applied.

If antenna types are mixed, then Rothacher (2002) stated that even with application of antenna phase centre models, there would be no guarantee of sub–centimetre height determinations, especially for longer baselines, where the ionospherically free linear combination is used, and where tropospheric delay parameters are estimated. Furthermore, Rothacher (2002) concluded that if precise height determination was the objective, the same equipment (antenna, receiver, monument, etc.) should be used at all stations and any changes to the equipment avoided.

There are currently three different methodologies in use for antenna phase centre calibrations, which can be grouped into *absolute* and *relative* calibration procedures (Rothacher and Mader, 2002).

The first method for absolute calibrations of GPS antenna phase centre variations was reported by Schupler and Clark (1991). This method involves measurements in an anechoic chamber[1] where the antenna to be tested is mounted on a positioner, which enables rotations around two independent axes and shifts in three directions. A transmitting antenna is kept fixed, while the receiving antenna is rotated through zenith angles from -90° to +90° in various azimuths.

In relative antenna phase centre calibrations the phase centre variations of a *test* antenna are determined with respect to a reference antenna over a small baseline (<10 m) (Mader and MacKay, 1996). The antenna phase centre variations of the reference antenna are assumed as known, and if known absolutely, absolute antenna phase centre variations for the test antenna can be derived.

In recent years, an in field automatic absolute antenna phase centre calibration method was developed by Wübbena et al. (1998). In this case, the antenna to be calibrated is mounted onto a precisely calibrated robot, which rotates the antenna around a fixed point, i.e. the nominal phase centre. By carrying out the experiments over two siderial days the multipath effect, which is a problem of the relative field calibration, can be largely reduced. Furthermore, the antenna elevation mask is dynamically adjusted depending on the inclination of the antenna in order to guarantee an elevation mask of 18°, further

[1] An anechoic chamber is a room of which all interior surfaces are lined with radio frequency absorbent material

improving the multipath situation. As this procedure is carried out fully automatically, the antenna can be rotated and inclined into several thousand precise positions, resulting in a high resolution and precise phase centre variation model (Wübbena et al., 2000).

By investigating the geometric relation between the satellite and receiver antenna elevation–dependent phase centre variations, Rothacher and Mader (2002) found that these phase centre variations were not separable. The elevation–dependent phase centre pattern of the receiver antenna may thus be interpreted as a phase centre pattern of the satellite antenna and vice versa. They concluded that this was the reason for the inconsistencies seen between the absolute receiver antenna phase patterns determined in the anechoic chambers and the relative phase patterns. The analysis of global IGS data and different phase centre patterns recently obtained for Block II/IIA and Block IIR satellites, in combination with absolute phase centre variations from anechoic chamber and in–field absolute calibrations showed that a large part of the change of scale in the GPS, as reported by Herring (2001); Wübbena et al. (2000); Heflin et al. (2002) and Herring (2002), was due to the mis–modelling of antenna phase centre variations. Based on this, Rothacher and Mader (2002) suggested that the IGS should adopt these recently determined satellite antenna offsets (Mader and Czopek, 2001), together with the consistent satellite antenna phase centre variations (Rothacher and Mader, 2002) and the absolute receiver antenna phase centre variations determined by Wübbena et al. (2000), in order to produce a more consistent ephemeris.

Recently, Rothacher (2003) announced the availability of a test set of absolute antenna phase centre offsets and phase centre variations for receivers and satellites. The satellite antenna phase centre variations have to be used together with the absolute receiver antenna phase centre variations in order to avoid scaling of the GPS results. However, to date these have not been applied in the generation of IGS products.

In order to protect GPS antennas at remote sites from snow and ice accumulations or weathering, antennas can be equipped with radar domes; covers that are *transparent* at GPS frequencies. However, there is evidence that radomes affect the incoming GPS signals and directly bias station coordinate estimates. For local networks, the effect does not exceed the several millimeter level, however for regional networks, the effect increases

remarkably as soon as local troposphere parameters are to be estimated in the adjustment (Kaniuth and Stuber, 2002). The resulting height errors have been reported to be as large as 3 cm for a cut–off elevation angle of 10° and tend to increase with increasing cut–off angle. Furthermore, the error depends on the antenna and radome type and there are suggestions for a dependence on the local antenna environment. Although it has been reported that the addition of a radome does not affect phase and amplitude patterns noticeably (Schupler and Clark, 2001), a systematic lowering of the mean phase centre position by 2 to 3 mm is observed, and visually confirmed by the height time series shown in Johansson et al. (2002). If both antennas are fitted with identical radomes, it can be assumed that the effect cancels completely on short baselines and partly on longer baselines (Braun et al., 1997; Kaniuth and Stuber, 2002; Schupler and Clark, 2001).

3.4.4 Earth Tides and Loading Effects

Surface stations undergo motions due to deformations of the Earth's crust on sub–daily to annual time scales. These effects need careful attention and using IERS Standards (McCarthy, 1996), some can be estimated accurately. A brief description of these loading effects follows.

Solid Earth Tides

The visco–elastic surface of the Earth undergoes periodic deformations due to the gravitational attractive forces of the planets in our solar system, predominantly the Sun and the Earth's moon. These deformations can reach through a range of over 40 cm at low latitudes in just little over 6 hours, so that both horizontal and vertical coordinates of a station vary with time (Baker, 1984). In order to determine highly precise station coordinates, corrections for these periodic deformations must be applied such that the final coordinate estimates represent those of the mean position that a station occupies (Penna, 1997). This is especially true for longer baselines as the solid Earth tides (SET) will not difference away as with shorter baselines.

Additionally, there is also one particular long–period tidal deformation, i.e. the *permanent* tide (Poutanen et al., 1996), which cannot, because of its permanent character, be separated in any unique way from the *background* shape of the Earth's crust. It is therefore important to state whether station coordinate estimates have been corrected for SET and whether the final coordinate estimates include the permanent tide, or whether it has been eliminated and coordinate estimates refer to the *non–tidal* crust. Although the non–tidal crust is a physically meaningless surface with all SET effects removed, ITRF station coordinates and the final IGS precise ephemerides are both referred to it (McCarthy, 2000).

Ocean Tide Loading

Besides the tidal deformation of the solid Earth, i.e. solid Earth tides, ocean tides cause a periodic surface mass loading of the Earth, which causes further tidal deformations of the solid Earth. These ocean tide loading (OTL) deformations can affect both horizontal and vertical coordinate components and can cause perturbations in precise geodetic observations, as shown and described in detail by Baker et al. (1995) and Curtis (1996). The displacements observed are dependent of time and location and are a combination of semi–diurnal, diurnal and long–term tidal constituents. Curtis (1996) gives a description of each of the 11 known constituents M_2, S_2, N_2, K_2, K_1, O_1, P_1, Q_1, M_f, M_m and S_{sa}. The principal lunar tidal harmonic M_2 can cause a periodic vertical displacement of up to 4.5 cm in the south west of the UK every 12 hours (Baker et al., 1995). Especially episodic GPS measurements are affected by OTL deformations as these can be aliased into the longer–period deformations investigated. It is therefore necessary to correct GPS observations for OTL effects (Baker et al., 1995; Beamson, 1995). Even for CGPS data the effect may not average out completely and residual biases may propagate into tropospheric delay estimates. Reasons for residual OTL effects may be attributed to some longer wavelength loading harmonics or the M_2 and K_2 constituents whose periods of 12.42 and 11.97 hours, respectively, differ from the 12 hours half day cycle related to the processing of daily data as 24 hour RINEX format observation files.

There are a number of OTL models for which corrections are available from the OTL provider at the Onsala Space Observatory (see `http://www.oso.chalmers.se/~loading`) (Scherneck and Bos, 2001). Several models have recently been compared (Scherneck et al., 2002a; Bos et al., 2002; Baker and Bos, 2003; Boy et al., 2003), however for the application of monitoring tide gauge benchmarks, it is recommended that models which have been tuned to fit tide gauge data, should be applied (Curtis, 1996).

Due to the fact that OTL deformations have mainly short spatial correlation on the order of hundreds of kilometres, station displacement due to OTL are applied at the GPS processing stage. Furthermore, in order to avoid systematic biases in satellite orbits and derived station estimates, models for site displacement should be applied at the stage of orbit computation, with compatible models applied in any regional analysis (Scherneck et al., 2000). However, to date IGS do not apply OTL when generating products including ephemerides and station coordinates.

Atmospheric Pressure Loading

Atmospheric pressure loading (APL) is the effect of pressure induced deformations of the Earth's crust and sea surface. The effect is of very long wavelength (1000 – 2000 km) nature and is associated with the passage of pressure systems. The observed loading signals are largest at higher latitudes, where pressure variations are greatest causing surface displacements with magnitudes of up to 3 cm for the vertical coordinate component (Rabbel and Zschau, 1985; van Dam and Wahr, 1987; van Dam et al., 1994). These large surface displacements are induced by pressure systems with periods of several days, however, there is also an annual component with amplitudes between 0.5 to 3 mm (van Dam et al., 2002).

Due to its long wavelength character, it can be assumed that the effect on short GPS baselines, i.e. a few hundred kilometres, can be neglected. However, if baseline lengths reach magnitudes of the extent of the loading displacements, they must be accounted for in the GPS analysis. As with OTL, GPS orbits may introduce regional perturbations since APL is not applied at the stage of orbit computations (Johansson et al., 2002).

In fact, the IERS conventions (McCarthy, 1996) currently do not give comprehensive recommendations for treating the full range of loading signals (van Dam et al., 2002).

Hydrological Loading

Similar to the loading effects described above, hydrological loading is the elastic deformation of the Earth's crust due to the water mass stored in continents, subjected to the seasonal and long term variability in the hydrological cycle. The main contributors are changes in groundwater storage, soil moisture and snow coverage (Mangiarotti et al., 2001; van Dam et al., 2001), which can cause vertical deformations of 15 mm or more over large regions of the globe, with maximum deformations of up to 30 mm in some regions. Contrary to APL, hydrological loading amplitudes are largest at annual periods (van Dam et al., 2002). Unfortunately, there are large uncertainties in all available hydrological models used to compute site displacements. The IERS Special Bureau for Loading (SBL) has recently been established to investigate these uncertainties.

In principle, most of the water storage induced variability would average out after a few years of continuous GPS monitoring. However, due to long term variability in the water mass load, it is believed that some residual linear trend would remain in height time series, which would decrease as the length of the time series increases (van Dam et al., 2001).

Storm Surge Loading

Previous loading effects have been predominantly periodic in their signatures, with semi–diurnal to annual periods. As with OTL, the redistribution of the water mass due to storm surges causes deformations of the Earth's crust, which may be detectable using space geodetic methods, especially using CGPS at tide gauge sites.

Storm surges are pronounced increases in water level due to strong wind set–up and the inverted barometer effect under the low pressure area near the centre of a storm (Forrester, 1983). This can be exaggerated, if the storm depression travels over the water surface and a long surface wave travels with it such as to direct this wave up on the shore. The North

Sea is a perfect arena for storm surges; after being generated by winds over the shelf north and northwest of Scotland and by pressure gradients traveling from the deep Atlantic to the shallow shelf waters, surges propagate southwards into the North Sea. These events last for typically 12 to 48 hours and the associated, predicted vertical displacements at sites along the east coast of England are about 20 mm (Baker, 2003b).

3.5 Summary

Several international meetings at which the monitoring of TGBMs was discussed have been introduced. A brief overview of the tide gauge monitoring projects carried out in the UK and along the European Atlantic coast was given. This was followed by a description of two current initiatives related to the topic of monitoring vertical land movements at tide gauge sites, i.e. EOSS COST Action 40 and its evolution into ESEAS, and on a global scale, the IGS TIGA PP.

The ITRS as the most accurate global reference system and the only system available to partly delivering the needed absolute accuracy for monitoring vertical land movements at the 1 mm/yr level, was introduced. Its current realization, the ITRF2000, was described with its long–term stability of 4 mm in origin and 0.05 ppb in scale, and its relation to the previous realization, the ITRF97, and the IGS realization of the ITRS2000, i.e. the IGS00, used for all IGS products, was discussed.

The importance of the origin and scale of the reference system were highlighted as these directly affect the vertical coordinate component (Herring, 2001; Kierulf et al., 2001).

The definition of the CM and the CF was given and geocentre variations as the motions of the CF with respect to the CM have been explained. Although the reported long–term stability of the origin of the ITRF2000 is in excellent agreement with CM (Dong et al., 2003) the short–term stability is compromised due to the apparent geocentre motions, i.e. the origin of the ITRF2000 follows the CF.

Geocentre variations have been attributed to global mass–redistributions on different time scales. Those due to astronomically driven tidal variations, which form the dominant

component, can be anticipated and modelled. Additional variations, due to purely episodic mass transports, cause additional variations of the CF with respect to the CM, affecting satellite and Earth dynamics, which affect satellite orbit determinations.

Additionally the effect of orbit errors on GPS baseline was reviewed and systematic biases in GPS observations due to atmospheric delay, antenna phase centre variations and different loading deformations were discussed.

From this discussion it is clear that station height estimates are biased by the reference frame, satellite orbits and errors which are highly correlated and therefore extremely difficult to separate. Among the latter are systematic effects due to tropospheric delay and antenna phase centre variations acting together with any unmodelled loading effects. Any mis–modelling of one bias will affect the mitigation of the others and vice versa. For local networks, these errors are spatially correlated, e.g. similar signal scattering at similar monuments (Johansson et al., 2002), and may result in local reference frame biases. Furthermore, tight constraints on a priori parameter estimates, such as for satellite ephemeris, satellite clock variations, or site positions, especially if correlated, may introduce biases into the frame. Site–specific errors, associated with multipath or antenna phase centre variations, may also indirectly manifest themselves as reference frame errors. If the source of correlated noise could be determined and eliminated, then Johansson et al. (2002) state that this would enable an improvement of the velocity uncertainties from GPS for regional networks up to 50%.

Some biases are a by–product of the global analysis affecting the ITRF and precise ephemeris. Not accounting for geocentre variations and non–secular station motions, biases both the reference frame and precise satellite orbits. Other biases are a by–product of the fact that regional networks are subjected to different relative seasonal movements than global networks. Hence, determination of the seasonal terms at global ITRF stations will greatly improve the stability and accuracy of the ITRF reference frame (Dong et al., 2002b) and reduce the dependency of derived estimates of station coordinates and velocities on the local frame.

On a global scale, in order to improve the computation of the reference frame and satellite orbits, corrections for the anticipated geocentre variations need to be applied (Pavlis,

2002). Scherneck et al. (2000); Herring (2001); Dong et al. (2002b); Johansson et al. (2002) and Dong et al. (2003) recommended that the ITRF requires non–secular components in the station motion model to better define the terrestrial system. Furthermore, in order to remove the observed GPS scale instability, the new absolute antenna phase centre variation models need to be used consistently for satellites and receiver antennas.

On a local scale, in order to minimize the effects due to antenna phase centre variations, Rothacher (2002) suggested using identical equipment if possible at all stations and to avoid changes of it. Furthermore, for national or regional GPS networks, it is recommended to apply the consistent absolute phase centre variation models. However, with these and with other models, the crucial point is that assumptions and methods applied by users of the system need to be consistent with the satellite orbits provided by the IGS.

It can therefore be concluded that neither the ITRS with its current realization, ITRF2000, nor the IGS final ephemeris currently support the objective of determining vertical station coordinates at the 1 mm/yr absolute accuracy. Estimating vertical station velocities at this level remains a challenge. It is hoped that efforts to improve reference systems and orbits with respect to the vertical coordinate component by ESEAS and the IGS TIGA PP will be successful. Under these circumstances, for the scope of this thesis, the ability of comparing the estimated vertical station velocities from GPS with the alternative evidence of vertical land/crustal movements introduced in Chapter 2 becomes very important as a possible mean to quantify the reference frame bias in this analysis and to validate the obtained velocities. In Chapter 8 a detailed comparison of the vertical station velocity estimates obtained by the author and those from the alternative evidence is carried out.

Chapter 4

Automated GPS Processing and Analysis

4.1 Introduction

Processing of continuous GPS observations can effectively only be carried out using some kind of automated procedures, which need little or no user intervention in order to arrive at the final products, e.g. daily station coordinate solutions. All main scientific GPS software packages, i.e. the GIPSY–OASIS II Software (Zumberge et al., 1997), the GAMIT–GLOBK Software (King and Bock, 2000) or the Bernese GPS Software (Hugentobler et al., 2001), allow for automation in some way. Therefore, much effort was invested at the Institute of Engineering Surveying and Space Geodesy by Penna (1997), Booth (2000) and the author of this thesis, to automate GPS processing with the in–house GPS Analysis Software (GAS) package (§4.2).

Due to the modular structure of GAS, it was possible to automate the GPS processing using UNIX Korn shell (Rosenblatt, 1993) scripts, denoted by Booth (2000) as automated procedures *Mark 1*, *Mark 2*, and *Mark 3*. Based on the Mark 3 automated procedures, the author has derived several improved versions (3.1, 3.2 and 3.3) of the initial scripts. With the development of additional automated procedures for preparatory processing, daily processing and GPS coordinate time series analysis, a fully automated configuration

for the daily processing, analysis and quality control of the UK 25 CGPS station network has been achieved.

A large improvement in the automation process was due to the introduction of Perl (Practical Extraction and Report Language) scripts by the author. Perl was initially designed as a 'glue' language on the UNIX operating system (or any of its variants), but is now available for numerous other systems (Wall et al., 1996). The fact that it is easily possible to run UNIX shell scripts, FORTRAN or C programs from within Perl scripts has enabled a close integration between the already existing 'Mark 3' automated procedures and the newly developed Perl scripts.

This Chapter will start with a brief introduction to the GPS Analysis Software (GAS), before concentrating on the developments made by the author during the last four years. Automated GPS processing with GAS and the development of automated procedures Version 3.1, 3.2 and 3.3 are described in detail. This is followed by a discussion of the daily processing scripts Versions 1.0 and 2.0, which have been developed around the automated procedures. The final part of this Chapter will describe the automated coordinate time series analysis procedures.

4.2 The IESSG GPS Analysis Software (GAS)

All results shown in this thesis have been produced by the author using the IESSG GPS Analysis Software (GAS) (Stewart et al., 2002). The GAS package has been under development at the IESSG since the mid 1980's with major contributions by M. P. Stewart, G. H. Ffoulkes–Jones, W. Y. Ochieng, P. J. Shardlow and N. T. Penna. It is a collection of seven independent FORTRAN 77 processing modules, each designed to undertake a separate part of the GPS data processing load. Shardlow (1994), Beamson (1995), Penna (1997), and Baker (1998) describe these processing modules and their systematic bias mitigation capabilities in great detail, hence the reader is referred to their work.

Each GAS processing module is executed at the UNIX command line and requires a module specific control file located in the current directory. This control file includes all processing parameters needed by the GAS processing module in order to carry out its task successfully.

GPS processing with GAS is divided into four processing stages, i.e. pre–processing, cycle–slip detection and correction, network–processing and post–processing (Booth, 2000). However, due to the fact that both pre–processing and cycle slip detection and correction are carried out by the same set of automated procedures, the author prefers to define three GAS processing stages with the first two phases of Booth's definition denoted as the GAS Pre–Processing stage and the latter two as the GAS Network–Processing and GAS Post–Processing stages.

4.2.1 GAS Pre–Processing Stage

GPS receivers store observations in a manufacturer specific binary file format. In order to exchange and process data of several different GPS receiver types, each observation file must be converted to a standardized file format, i.e. the RINEX format.

The main GAS processing module PANIC (Program for the Adjustment of Networks by Interferometric Carrier Phase), requires all GPS data to be in Nottingham 2 (NOTT2) format observation files, hence at the GAS Pre–Processing stage, RINEX format observation files are converted to NOTT2 format observation files. This initial file format change is carried out using the GAS processing module FILTER, which also detects and corrects large cycle slips and enables the removal of any unwanted epochs of observations. The module can also be used to split the 24–hour session of the RINEX format observation files into four 6–hour sessions, as required by PANIC.

Prior to the GAS Network–Processing stage, all cycle slips must be detected and corrected in the NOTT2 format observation files. During this process, one station is assumed to be cycle slip free and is therefore denoted as a *base* station. Cycle slip detection and correction is then carried out by the GAS processing modules PANIC, FILTER and SLIPCOR, between the base station and all other stations in a network,

each station pair defining a GPS baseline. In cycle slip detection mode, PANIC estimates cycle slips by monitoring the change in the double difference residuals from epoch to epoch for each baseline, i.e. the triple difference (Hofmann-Wellenhof et al., 1993). This is an iterative process, which involves detecting smaller and smaller cycle slips on each iteration. Although this process is highly successful, as will be shown in §5.3, the wide lane triple difference residuals for long baselines are often noisy due to un–mitigated ionospheric effects. This makes it difficult to always detect every cycle slip, particularly when there are jumps in the triple differences, induced by noisy observations. In these cases, FILTER is used to remove epochs of observations with large residuals.

During a cycle slip detection run, PANIC writes information on detected cycle slips into a *slip* file, which gives an estimate of the σ_0 of the residuals for each frequency processed. Once the σ_0 is below a certain threshold, the cycle slips in the NOTT2 format observation files can be corrected by using the slip files in combination with the GAS processing module SLIPCOR. In this research, the threshold for the σ_0 on the ionospherically free observable was set to 10 mm, however a maximum σ_0 of up to 20 mm (Shardlow, 1994) was accepted in some cases, when the automated procedures could not detect and correct all cycle slips successfully.

As a result of the GAS Pre-Processing stage, a set of four 6–hour session, cycle slip free NOTT2 format observation files are obtained for each station on each day, which can be fed into the following GAS Network–Processing stage.

4.2.2 GAS Network–Processing Stage

In the GAS Network–Processing Stage, the previously *cleaned* observation files are used to compute the least–squares adjustment solution for a network of GPS stations. In GPS network processing mode, the GAS processing module PANIC has a number of options for the mitigation of systematic biases, including models for solid Earth tides (§3.4.4), ocean tide loading (§3.4.4), antenna phase centre variations (§3.4.3) and tropospheric delay (§3.4.2).

The mitigation of solid Earth tides and ocean tide loading in the GAS processing module PANIC are implemented according to the IERS 1992 Standards (McCarthy, 1992). The antenna phase centre options are based on the IGS_01.PCV relative values, which were first released in June 1996 (Rothacher and Mader, 1996) and are updated periodically. PANIC also offers a wide range of options to mitigate or model the tropospheric delay (Shardlow, 1994; Baker, 1998). The strategy applied in this research, is to estimate the total zenithal tropospheric delay (TZD) after the effect of the hydrostatic atmospheric was modelled using the Saastamoinen model (Saastamoinen, 1973). For both, the wet and hydrostatic components the appropriate Niell mapping functions (Niell, 1996) were used (see 6.2.1). For a more detailed description of the computational operations of PANIC, the reader is referred to Penna (1997).

During the year 2000, the GAS processing module PANIC was modified to enable exporting of solutions and associated variance–covariance information in the SINEX format. This is the standardized file format used by the IGS to exchange weekly solutions of the IGS Analysis Centres and Associated Analysis Centres, which was initially suggested by Blewitt et al. (1994) and is detailed in IGSCB (2000).

In the least–squares adjustment estimation process of the GAS processing module PANIC, the four 6–hour observation sessions are combined in order to produce one *daily* solution. This solution consists of a set of independent GPS baseline vectors and their associated variance–covariance information for the whole processing session.

4.2.3 GAS Post–Processing Stage

The GAS Post–Processing stage is carried out by two GAS processing modules, i.e. CARNET and REPDIF. The GAS processing module CARNET is a general least–squares adjustment program, which can handle a wide variety of geodetic observations. The GPS baseline vectors and their variance–covariance information output from PANIC are used as input to the CARNET adjustment process, in order to produce a weighted mean set of station coordinate estimates and associated standard errors in a specific reference frame. In this way, it is possible to *stack*, e.g. daily, solutions to produce a weighted weekly solution similar to the weekly solutions of the EUREF network (Bruyninx et al., 2001,

2002) or the global IGS network (Davies and Blewitt, 2000), and/or to express station coordinates from multiple epochs in a common frame.

The evaluation of the quality of the sets of coordinates computed by the GAS processing modules PANIC and CARNET can then be carried out using REPDIF. REPDIF enables the computation of station coordinate or GPS baseline vector repeatabilities, e.g. daily solutions with respect to a weekly solution or with respect to a *truth*. It can therefore be used to identify any poor daily solutions.

4.3 Preparatory Processing Procedures

Although, the automated procedures denoted as *Mark 3* in §4.4 had reached a high level of automation for the processing of continuous and episodic GPS data, they assume that certain additional input files are readily available in the correct location at the time of execution. Among these files are the GAS ancillary file and the GAS ocean tide loading file. GAS ancillary files are only valid for a period of 40 days, therefore new files have to be created periodically using the GAS processing module MKGAF. The formation of the GAS ocean tide loading file, can be a cumbersome task if many stations are involved. Besides this, at the start of the authors research, there was no comprehensive processing data archive with all RINEX format observation files, IGS ephemeris, GAS ancillary file and GAS ocean tide loading file automatically updated in a *ready–to–use* condition.

This section briefly introduces the software developments carried out by the author, which provide the environment required by the automated procedures described in §4.4 and 4.5.

4.3.1 Processing Data Archive `procarch`

In order to consolidate all of the data required for automated GPS processing using GAS, the *Processing Data Archive* `procarch` was created. In `procarch`, data from the different archives on workstation `ukcogr` are combined into one archive using daily directories in the form of `yyddd`, with `yy` identifying the year and `ddd` the day–of–year. Among

these data are the GPS RINEX format observation files of the EOSI archive `eosi`, which consists of all CGPS@TG stations in the UK, the CGPS stations at UK Meteorological Office (Met Office) (MO) sites, the IGS stations at the National Physical Laboratory and at Herstmonceux, and the CGPS stations at Morpeth and the IESSG. Furthermore, `procarch` includes IGS data and products from the `igseur` archive, which contains RINEX format observation files from a number of European IGS stations and the broadcast, IGS rapid and IGS final precise ephemerides. As outlined in §4.3.2, the GAS ancillary files are also added to `procarch` on a daily basis.

Initially the `procarch` archive was situated on workstation `ukcogr`, however due to the accumulated data volume it was moved to the new workstation `monix`, where the Perl script `updateprocarch.pl` carries out the data transfer described above. Besides this, `updateprocarch.pl` is also designed to check global IGS data servers for any IGS data or products missing when the file transfer from the `igseur` archive is attempted.

A significant improvement to previous scripts that simply collected all daily files into the `procarch` archive, is a reporting function within `updateprocarch.pl`. Each execution of `updateprocarch.pl` updates the *data content* reports in `procarch`. These reports are organized according to different archive categories on workstation `ukcogr`, i.e. *eosi, igs* and *ephem*. Additionally, there are separate data content reports for RINEX format observation files of episodic GPS stations occupied in the 1999 and the 2002 GPS campaigns. All `procarch` data content reports generated up to 30 April 2002 can be found under the directory tree `/Procarch_Reports` on the CD–Rom included.

Figure 4.1 illustrates the daily tasks carried out by the Perl script `updateprocarch.pl` on workstation `monix`. Although the GAS ancillary files are not transferred by this script, their data flow into `procarch` is included in the figure. The Perl script `updateprocarch.pl` and its control file `updateprocarch.ctl` are included in the directory tree under directory `/Software_Developments` on the CD–Rom.

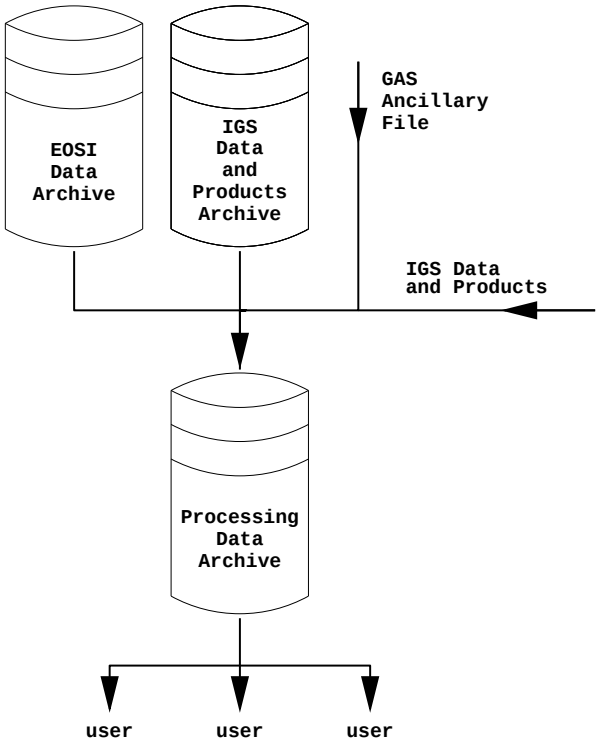

Figure 4.1: Data flow for Processing Data Archive `procarch` on workstation `monix`.

4.3.2 GAS Ancillary Files

The GAS processing module PANIC is able to correct for systematic biases in the GPS observations, e.g. solid Earth tides or ocean tide loading effects (§4.2.2). If models to mitigate these effects are included in the PANIC least–squares estimation, which is normally the case, then a daily GAS ancillary file (GAF) is required. This file is created using the GAS processing module MKGAF (Stewart et al., 2002) which uses three input files containing Earth Rotation and Polar Motion values (BIH–file), Planetary Ephemerides and the current offset between Universal Time Coordinated (UTC) and International Atomic Time (TAI)[1]. The last file only changes every one to two years and the latter two files are effectively in the correct format for use with MKGAF. However, the Earth Rotation and Polar Motion values are published by the IERS in its Bulletin B on a monthly basis, and the final Earth orientation parameters in the Bulletin B have a delay of 2 months. This

[1]TAI is a continuous time scale, i.e. it does not synchronize with the solar day (universal time), as opposed to UTC, which is kept to be within 0.9 s of universal time by the IERS through the introduction of leap seconds (Hofmann-Wellenhof et al., 1993).

means that preliminary GAFs have to be created, in order to carry out GPS processing within one month of the epoch of observations. These preliminary GAFs are then updated for archiving once the final Earth orientation parameters are available.

This task has been automated by the author through the introduction of two Perl scripts, i.e. `updatebih.pl` and `updategaf.pl`, both using the UNIX `cron` utility. The Perl script `updatebih.pl` is automatically executed on a monthly basis, normally on day 8, in the `igseur` user environment on workstation `ukcogr`. It performs the Bulletin B file download from the IERS using the FTP (File Transfer Protocol), extracts final and preliminary Earth Rotation and Polar Motion values and adds them to the current BIH–file, the file format needed for input into the GAS processing module MKGAF.

Preliminary Earth Rotation and Polar Motion values in the BIH–file, can be identified by an appended 'p' to each line. The newly created BIH–file is then archived for general use at the IESSG on workstation `ukcogr` in `/raid/archive/igseur/iers`.

Similarly to the preliminary values in the BIH–file, the GAFs can be identified by either 'f' or 'p' included in their file names. GAFs are generated by the Perl script `updategaf.pl` in the `procarch` user environment on workstation `ukcogr` on a daily basis. The script prepares the control file for MKGAF and invokes the execution of the module. Furthermore, it checks, whether the BIH–file has been updated since the last execution of `updategaf.pl` and whether recently generated preliminary GAFs can now be replaced by final ones. The GAFs are then archived in the processing data archive `procarch` (§4.3.1) on workstation `monix` for general use.

Both Perl scripts `updatebih.pl` and `updategaf.pl` and example control files, identified by their extension `.ctl`, can be found in the directory `/Software_Developments` on the CD–Rom included.

4.3.3 GAS Ocean Tide Loading File

In order to correct for the systematic station displacements due to ocean tide loading (OTL) (§3.4.4) during GPS network processing, a GAS ocean tide loading File (GOF) (Stewart et al., 2002) needs to be created containing amplitudes and phases for up to

eleven ocean tide constituents for each station in the network analysed. Initially in 1999, when the author commenced his research at the IESSG, these parameters were obtained from the Proudman Oceanographic Laboratory and manually inserted into the GOF. However, with the availability of parameters from different OTL models and the need to use such models in a wider range of networks as part of the IESSG's research, manual generation and editing of the GOF seemed inefficient.

During 2001, the Onsala Space Observatory started to offer an internet based service to obtain OTL displacement parameters for 11 different ocean tide models (Scherneck and Bos, 2001). By submitting an email address and either geocentric or geodetic station coordinates to the web form, an email is generated by the web site containing the ocean tide loading displacement parameters requested. The content of this email can then be copied into a text file and submitted to the Perl script `otl2gas.pl`, which converts the file into the GOF Format.

The Perl script `otl2gas.pl` and its control file `otl2gas.ctl` with some sample files are included in the directory tree under directory `/Software_Developments` on the CD–ROM.

Through the use of the web service and the Perl script developed by the author, it is a simple task to update the GOF whenever a new CGPS station is introduced into the network or to create a new GOF for a complete network of stations for any new project.

4.4 Automated GPS Processing with GAS

Due to the modular structure of GAS, consisting of seven independent processing modules, it was possible to develop procedures for automated processing. Prior to automation, these GAS processing modules were operated manually, by initially creating and editing the module specific control files and then invoking their execution on the command line. Furthermore, after successful execution of each module, output and solution files had to be viewed, and often results were dependent on subjective user decisions, especially during cycle slip cleaning. This process involved iterative editing of control files and processing of larger data sets would quickly become cumbersome if not impossible.

In 1997, therefore, the IESSG started the development of automated procedures, consisting of a collection of UNIX shell scripts and shell functions and some auxiliary C programs. The initial automated procedures, basically used control file templates, which could be stream edited using the UNIX `sed` command in order to obtain the final control file. Further developments lead to three distinct sets of automated procedures, denoted by Booth (2000) as *Mark 1, Mark 2* and *Mark 3*. The main improvements in the three sets were associated with the refinement of the GAS pre–processing stage, especially cycle slip detection and correction was improved, and in increasing the overall flexibility of the procedures. This lead to the fact that the percentage of *cleaned* data increased from around 60 to over 90% for the Mark 3 compared to the Mark 1 automated procedures (Booth, 2000).

The Mark 3 automated procedures were related to the three GAS processing stages, to allow every stage to be carried out independently if required. Further refinements of the UNIX scripts and some new auxiliary programs also allowed easier modifications to the network solution or the post–processing procedures, e.g. different systematic bias mitigation or the use of different reference frames. The first improvement to the Mark 3 automated procedures carried out by the author was the introduction of the Modified Julian Date (MJD) (Hofmann-Wellenhof et al., 1993) as the integer count variable in the top level UNIX shell script (denoted as 'UNIX `.now`' script in Figure 5.16 of Booth (2000)). Previously, the count variable was the Julian Day (JD), which limited the automated processing to remain within one year. By switching to MJD, which represents time evolution as a continuously increasing integer, incremented by one for each processing day, it was possible to engage in process runs that would cover several years, which became absolutely vital as observation periods got longer.

At this stage the Mark 3 automated procedures had reached a level in which the pre–processing, the network–processing and the post–processing stages could be reliably carried out in a fully automatic mode. However, if all data were to be automatically processed each day without any user intervention, some further modifications to the automated procedures were necessary in order to facilitate the monitoring and reporting of results for each day.

Before the fully automated daily processing scripts are described in detail in §4.5, the author would like to highlight some of the changes and improvements made to the initial Mark 3 automated procedures during the course of his research, which led to Versions 3.1, 3.2 and 3.3.

4.4.1 Automated Procedures Version 3.1

The automated procedures Version 3.1 are based on the Mark 3 automated procedures described in detail by Booth (2000). The developments involved, were mainly necessary because of changes to the processing data archive and the requirement to optimize the disk storage required for the results of the processing. In this respect, it was necessary to be more restrictive as to whether files were to be removed rather than just compressed in the daily processing directory structure. A close look was also taken at UNIX warnings and error messages sent to the UNIX standard error, which are normally shown on the screen display. Once processing runs were invoked using the UNIX `cron` utility without user interaction, this proved to be essential, as every warning or error message sent to the UNIX standard error was now re–directed into an email, sent to the user who owned the process. In order to reduce unnecessary messages and therefore cluttering of the display during process runs, more 'if–then–else' clauses were introduced and command arguments using UNIX wildcards, e.g. '*' in file names, were replaced with commands using precise references, e.g. giving the complete file name.

All automated procedures associated with GAS can be attributed to four levels of scripts. At the top level is a UNIX Korn shell script with extension `.now`. Generally, this script defines the processing environment using variables for directory path definitions and the processing time span. This can be invoked either manually or automatically using the UNIX `cron` utility. The top level UNIX shell script then invokes a GAS D shell script, which can be identified by the file extension `*.dates`. This GAS D shell script checks the processing time span specified for plausibility and carries out the processing loop over each day specified by the time span in the UNIX `.now` shell script. Within the GAS D shell script, the GPS stations to be processed are also defined. Due to memory limitations in the GAS processing module PANIC, the network–processing stage can currently only

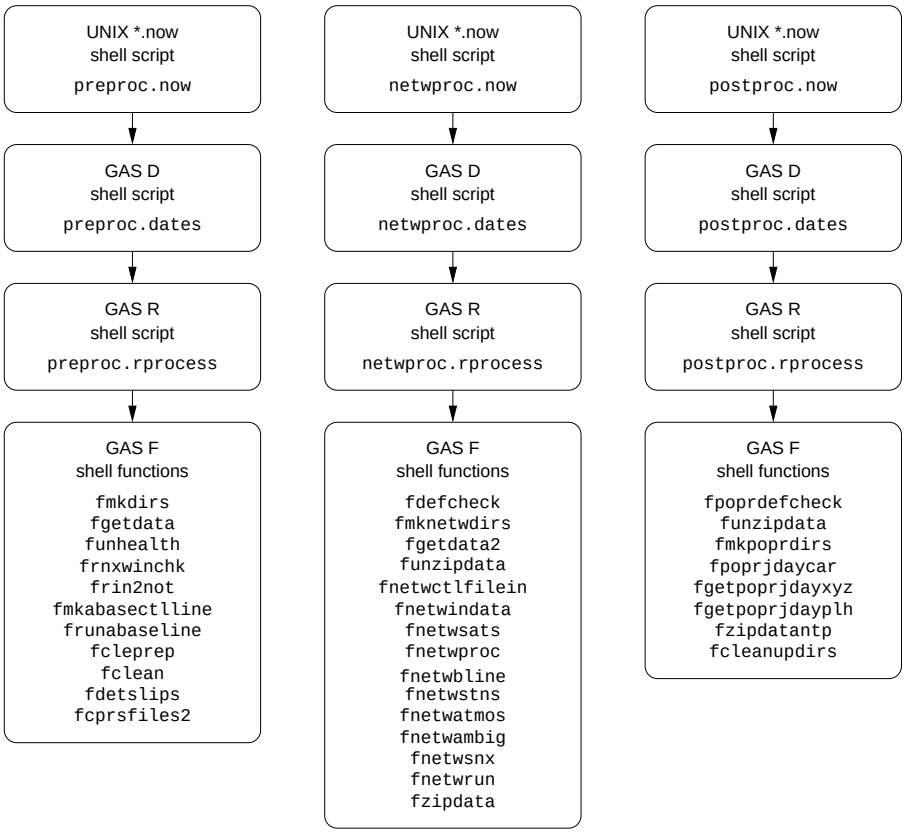

Figure 4.2: Automated Procedures for GPS Processing with GAS (Version 3.1).

process a maximum of nine baselines simultaneously, which means that the CGPS network analysed in this study, had to be split into a series of sub–networks of ten stations each.

The GAS D shell script then calls the GAS R shell script, which is the third level script and is identified by the file extension `.rprocess`. A GAS R shell script contains a series of user–defined variables, which mainly define the GPS processing options depending on the processing stage. The GAS R shell script then calls a series of GAS F shell functions, which are effectively the fourth level scripts. The GAS F shell functions basically carry out the tasks for a processing stage. GAS F shell functions can easily be identified by their filename, which starts with the character 'f'. The GAS F shell functions use template files that are stream edited and concatenated to produce specific control files for each GAS processing module. An overview of all shell scripts and functions is shown in Figure 4.2. The figure lists filenames for the pre–, the network– and the post–processing stages of the automated procedures Version 3.1.

In preparation for an automated processing run, the shell scripts, shell functions and template files have to be arranged in a *project* directory containing following directory structure:

```
# ls
preproc             netwproc             postproc             netwinfo
preprocscripts      netwprocscripts      postprocscripts
preproctemps        netwproctemps        postproctemps
```

where the level one, two and three GAS shell scripts for each processing stage are in the `preproc`, `netwproc` and `postproc` directories respectively. GAS F shell functions are placed in directories with names ending `-scripts` and template files in the directories with names ending `-temps`. An additional directory `netwinfo` is needed for the automated procedures, which contains the GOF, a file assigning the correct antenna phase centre models, and reference frame specific coordinate files, for all stations in the project.

After the general structure for the automated procedures has been described, it is now possible to explain the different stages and their changes since Version 3.0 in more detail.

Pre–Processing Stage

The pre–processing stage is invoked using the top level UNIX shell script `preproc.now`. This script will execute the GAS D shell script `preproc.dates`, which will call the GAS R shell script `preproc.rprocess` for each day according to the time span defined by the user in `preproc.now`. The GAS R shell script will then call each GAS F shell function of the pre–processing stage as listed with their file names in Figure 4.2.

The first GAS F shell function to be called is `mkdirs`, which creates the daily directory structure needed for any GAS processing run. Using the GAS F shell function `getdata`, the necessary RINEX format observation files, the IGS precise ephemeris and the daily GAF (§4.3.2) are obtained from the processing data archive. In 1999, this data archive was located on workstation `ukcogr` and was called `tgarch`. It used a directory structure (`/wwww/yyddd/`) based on the 4–character designator for the GPS week (wwww), the last two digits of the current calendar year (yy) and the 3–character designator for the day–

of–year (ddd), e.g. for week 1016, year 1999 and day–of–year 92, the directory would look like `/1016/99092`.

Mark 3 of the automated procedures used the UNIX remote copy command `rcp` to obtain all necessary daily files from the `tgarch` archive on workstation `ukcogr`. The new processing data archive `procarch` was based on a different directory structure, not including the GPS week in the path definition for the daily directories. As the automated procedures were modified to copy the daily observation and ephemeris files from this archive, changes had to be applied to the GAS F shell function `getdata`. When the processing data archive `procarch` was moved to the new workstation `monix` in 2001, changes to the GAS shell scripts were again necessary.

After the RINEX format observation files, the IGS ephemeris files for the previous, the current and the following day, and the daily GAF are copied to the correct processing directories, the GAS F shell function `unhealth` determines if any satellites observed in the RINEX format observation files are missing in the IGS ephemeris and which satellites are not common to all three IGS ephemeris files, in order to declare them to be unhealthy (Booth, 2000). The output of `unhealth` is a block of unhealthy satellites, which is used by the GAS F shell function `rin2not` at a later stage during the creation of the control file of the GAS processing module FILTER.

At the next step, the RINEX format observation files are checked for errors. The GAS F shell function `rnxwinchk` removes any RINEX format observation files that do not contain any raw GPS observations, i.e. an empty file or one which simply contains the header (Booth, 2000).

As mentioned above, the GAS F shell function `rin2not` prepares the FILTER control file. FILTER is used to split the 24–hour RINEX format observation files into four 6–hour files in the NOTT2 observation file format. At this stage, *known* station coordinates are inserted into the NOTT2 format observation file headers based on the FILTER ancillary file `filter.anc` located in directory `netwinfo`.

The GAS F shell functions `mkabasectline` and `runabaseline` determine a set of base satellites, normally three satellites for each of the six hour observation sessions. The

satellites giving the greatest average elevation angle over the session and which are visible from each station for the greatest period are selected as input for the base satellite block in the PANIC control file. The control file itself, is then created in the next step by the GAS F shell function `cleprep` (Booth, 2000) which stream edits a number of template files in order to produce a PANIC control file.

Using the NOTT2 format observation files, the GAS F shell functions `clean` and `detslips` now carry out the cycle slip detection and correction. The GAS F shell function `clean` invokes the GAS processing modules PANIC, FILTER and SLIPCOR, using function `detslips` and the auxiliary C program SCANRES. SCANRES scans the carrier phase residuals file, created by PANIC in cycle slip detection mode, for periods of *noisy* double difference observations. If such a period for a specific satellite is identified, then SCANRES produces a temporary FILTER control file, which can be used by FILTER to remove this satellite specific period of noisy data. Again the reader is referred to Booth (2000) for a detailed description of this key step in the automated procedures for the GAS pre–processing stage.

All the procedures mentioned above create and use temporary files, which are not needed in the coming processing stages or can easily be re–created. To ensure efficient hard disk usage, files have to be removed or compressed. This is now carried out by the largely modified GAS F shell function `cprsfiles2`. This improved version of function `cprsfiles`, uses fewer UNIX wildcards, e.g. '*', in file names and directory paths, and carries out more file checks using if–then–clauses. As a result, the new GAS F shell function `cprsfiles2` is far more selective with respect to which files are being removed, rather than compressed.

Network–Processing Stage

The network–processing stage is invoked using the top level UNIX shell script `netwproc.now`. This script will execute the GAS D shell script `netwproc.dates`, which will call the GAS R shell script `netwproc.rprocess` for each day according to the time span defined by the user in `netwproc.now`. The GAS R shell script calls each GAS F shell function of the network–processing stage as listed by their file names in Figure 4.2.

The changes from Mark 3 to Version 3.1 of the automated procedures for the network–processing stage, are mainly related to the GAS F shell functions `getdata2` and `zipdata`. As with the automated procedures for the pre–processing stage, this was due to changes in the processing data archives and a more restrictive policy with respect to which files were to be kept. Apart from that, modifications to the GAS processing module PANIC, which enabled the output of SINEX format solution files (§4.2.2) drove changes to the GAS F shell function `netwrun`, and the introduction of the new function `netwsnx` and the auxiliary Perl script `compepoch.pl`.

The first GAS F shell function to be invoked by the GAS R shell script `netwproc.rprocess` is `defcheck`. This function checks user–defined variables in the GAS R shell script and although very unlikely, terminates the execution, if any errors in the definitions occurred. The GAS F shell function `mknetwdirs` then creates the network solution directory, before the IGS ephemeris of the previous, current and following days and the GAF for the current day are copied from the processing data archive by the GAS F shell function `getdata2`. A modification in function `getdata2` of the automated procedures Version 3.1 was made, in that no RINEX format observation files are copied, as these are not needed in the network–processing stage. Before the data can be used in the processing, the GAS F shell function `unzipdata` uncompresses the NOTT2 format observation files, produced by the pre–processing stage.

In the next step, the PANIC default control file and the PANIC control file are then created by stream editing and concatenating a number of template files. This is carried out by the GAS F shell functions `netwctlfilein`, `netwindata`, `netwsats`, `netwproc`, `netwbline`, `netwstns`, `netwatmos`, `netwambig`, and `netwsnx`. For a detailed description of these functions, except for `netwsnx`, the reader is referred to Booth (2000). After the GAS processing module PANIC was modified to export SINEX format solution files, a new GAS F shell function had to be developed which would create the SINEX block in the PANIC control file. This also involved the computation of the epoch of the solution, thus an additional script was required. Using the auxiliary Perl script `compepoch.pl`, which is called by GAS F shell function `netwsnx`, this simple computation is carried out and the correct reference epoch is included in the SINEX block in the PANIC control file. The

GAS F shell function `netwrun` then executes PANIC and renames output files for further use.

Since Version 3.1, the tropospheric scale factor output files (Stewart et al., 2002) and the newly generated SINEX format solution files have been archived. In order to resemble file naming conventions of the IGS as much as possible, the author decided to use the RINEX format file naming convention (Gurtner and Mader, 1990), using the character 't' as observation type indicator for the tropospheric scale factors in the file extension. The SINEX format solution file name should resemble IGS or EUREF weekly SINEX solution file names. Therefore, a 3–character SINEX solution designator was introduced in the GAS R shell script `netwproc.rprocess`. The SINEX file name is then a combination of this 3–character word, the GPS week, the day–of–week and the extension `*.snx`[2].

By declaring user–defined variables in the GAS R shell script `netwproc.rprocess`, it is possible to select GPS network processing strategies (Booth, 2000). For the analysis of the GPS observations in this research, the standard processing strategy included the mitigation of solid Earth tides (§3.4.4), ocean tide loading (§3.4.4), antenna phase centre variations (§3.4.3), and tropospheric delay (§3.4.2). These remained unchanged throughout the complete time span of available CGPS data. In all instances, the IGS final precise ephemeris was held fixed, and the a priori coordinates of any IGS stations were computed in the same realization of the ITRS as the satellite ephemeris, i.e. the ITRF94, ITRF96, ITRF97, or ITRF2000 (§3.3.2), and motioned to the observation epoch. The consistent use of common reference frames for station coordinates and satellite ephemeris is necessary in order to avoid offsets in the coordinate time series at epochs when the reference frame was updated (§3.4.1).

The GAS processing module PANIC can process a maximum of ten stations simultaneously. For convenience, the base station for pre–processing was chosen to be the CGPS station at the IESSG, as it lies centrally to all of stations analysed. In addition, four IGS stations have been used in all of the networks analysed by the author. In all cases, this has meant that the network has been divided into a series of sub–networks (with

[2]e.g. for the sub–network cluster 1, the designator could be declared to be c_1, and with GPS week 0998, day–of–week 5, the complete file name would be `c_109985.snx`

the IESG station and the four IGS stations included in each sub–network) and the GAS network–processing stage being carried out for each sub–network separately.

The network solution results consist of the daily GPS baseline vectors and their associated variance–covariance information. These are obtained in the form of PANIC network solution files and the SINEX format solution files. The availability of both files allows for two different analysis approaches in the following post–processing stage, in that the PANIC network solution files can be used as input to the GAS module CARNET and the SINEX format solution files as input to the Bernese GPS Software modules SNXNEQ and ADDNEQ (Hugentobler et al., 2001).

In the final step of the network–processing stage, the GAS F shell function `zipdata` compresses all of the cleaned NOTT2 format observation files and the various solution files.

Post–Processing Stage

The post–processing stage is invoked using the top level UNIX shell script `postproc.now`. This script will execute the GAS D shell script `postproc.dates`, which will call the GAS R shell script `postproc.rprocess` for each day according to the time span defined by the user in `postproc.now`. The GAS R shell script calls each GAS F shell function of the post–processing stage as listed by their file names in Figure 4.2.

Overall, the main difference between the Mark 3 and Version 3.1 of the automated procedures for the post–processing stage is the implementation of two different processing modes, i.e. the *single network* and the *network combination* mode. Due to limitations in the GAS processing module PANIC, the increasing UK CGPS network had to be divided into an increasing number of sub–networks, with a combined solution only achieved at the post–processing stage. In single network mode, the automated procedures carry out processing using GPS baseline vectors of a single sub–network. In network combination mode, all GPS baseline vectors of all sub–networks are used to compute a solution for the combined network.

Switching between the two processing modes is achieved by specifying the number of networks to be processed in the shell script `postproc.now`. If this variable is set for one network, then a network name must be specified in the GAS R shell script `postproc.rprocess`. For more than one network, names for all sub–network must be declared in the GAS R shell script instead.

The post–processing stage of the automated procedures Version 3.1 can only be carried out on a daily basis. Thus it is not possible to produce weighted weekly solutions or repeatabilities using CARNET and REPDIF, as with the Mark 3 automated procedures. Although, the original GAS F shell functions of the Mark 3 automated procedures are still included in Version 3.1, they were not modified with respect to the introduction of the network combination mode.

During a monitoring period of several years, the reference frame in which the precise ephemeris are computed can be updated several times. These changes in the reference frame would cause discontinuities in any coordinate time series based purely on solutions obtained at the network–processing stage. It becomes difficult, therefore, to base any further analysis on these time series, unless they are transformed to a common frame. The GAS R shell script `postproc.rprocess` also provides the possibility of expressing the daily coordinate solutions in a common reference frame.

The first GAS F shell function to be called by `postproc.rprocess` is `poprdefcheck`. This function carries out checks on the user definitions in the GAS R shell script. With the introduction of the network combination mode, `poprdefcheck` required some extra check routines included. The next two functions executed, un–compress the PANIC network solution files and the cleaned NOTT2 format observation files, and create the post–processing directory. This is carried out by the GAS F shell functions `unzipdata` and `mkpoprdirs`, respectively.

The GAS F shell function `poprjdaycar` then creates the CARNET control file by stream editing CARNET template files and concatenating them into the final format. This process involves extracting the station coordinates from the header section of the cleaned NOTT2 format observation files to form a CARNET input file holding approximate coordinates for all stations. For stations that are to be held fixed in order to introduce

the common reference frame, coordinates and velocities are taken from reference frame dependent ancillary coordinate files in the directory `netwinfo` (Booth, 2000), and station coordinates at the epoch of the observations are inserted into the CARNET control file.

After CARNET has been executed by the shell function `poprjdaycar`, the cartesian and geodetic coordinates for each GPS station are extracted from the post–processing solution file and archived using the GAS F shell functions `getpoprjdayxyz` and `getpoprjdayplh` respectively. Both shell functions create a coordinate time series file for each station by adding the daily coordinate solutions to the end of the coordinate files (Booth, 2000). These functions remained essentially the same in Version 3.1 as in the Mark 3 automated procedures.

In the last step of the post–processing stage the GAS F shell functions `zipdatantp` compresses all archived files, and the GAS F shell function `cleanupdirs` removes any unnecessary files.

4.4.2 Automated Procedures Version 3.2

The automated procedures Version 3.2 are based on automated procedures Version 3.1 described in §4.4.1. They were initially developed by the author in September 2001, when automated processing was split onto several UNIX/Linux workstations. In the period from 1999 to 2001, processing was only carried out on workstation `geodix` copying the required IGS precise ephemeris and RINEX format observation files from the processing data archives `tgarch` and, later, `procarch` (§4.3.1) on workstation `ukcogr`. With the establishment of the new workstation `monix` in 2001, the processing data archive `procarch` was moved from workstation `ukcogr` to workstation `monix`.

At this time, the new processing results archive `procres` was introduced in order to remove the daily processing directories from the project directory. Besides the directories containing the shell scripts, shell functions and template files, the number of daily directories in the project directory had reached well over 1000, making it inefficient. Initially, `procres` was created on workstation `geodix`, but was then moved to workstation `monix` in order to separate processing from archiving workstations. This configuration was enabled

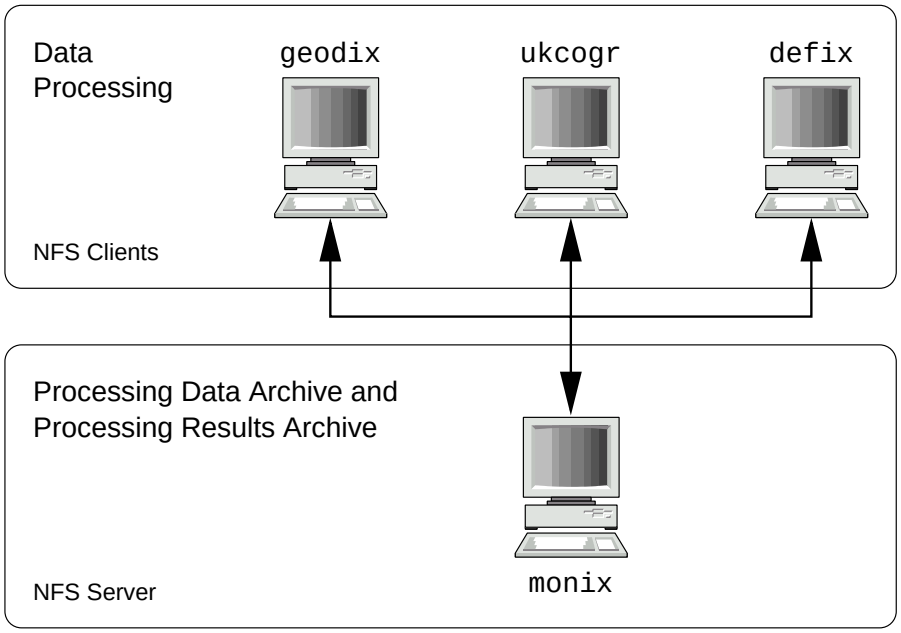

Figure 4.3: Workstation configuration at the IESSG using automated procedures Versions 3.2 and 3.3 during re–analysis of the UK 25 CGPS station data set in the period 2001/2002.

by running workstation `monix` as a NFS server, sharing its archive directories with a number of specified NFS client workstations. By configuring workstations `geodix`, `ukcogr` and `defix` as NFS clients, automated GPS processing could be carried out on all three workstations simultaneously. This approach was necessary, as it was decided to re–analyse the complete processing data archive in `procarch` spanning the period from 1997 to 2002, and extend the CGPS network from 13 to 25 stations. Figure 4.3 shows the workstation configuration at the IESSG during the re–analysis of the UK 25 CGPS station data set.

With the creation of the NFS server–client workstation configuration, it was now also possible to establish a directory `finalcoords` on workstation `monix`, which contained the final coordinate time series files for different post–processing runs. Each time post–processing was carried out using different process settings, e.g. a reference frame, a directory was created in the project directory on the processing workstation. In order to de–clutter this directory and to have all coordinate time series in one area, the automated procedures Version 3.2 account for these changes.

The idea behind the development of the automated procedures Version 3.2 was to create a temporary daily directory structure on each of the workstations which carry out data processing, and to transfer observation files and results files from and to the archiving workstation `monix`. This NFS server–client workstation configuration required changes to the automated procedures Version 3.1, mainly related to data transfer issues, i.e. the copying of observation files or results files from a previous processing stage into the temporary directory structure on the current processing workstation. Additional functions were also necessary in order to push the results of the current processing stage back onto the archiving workstation and to allow the removal of the temporary daily directory structure on the processing workstations.

In principle, the automated procedures Version 3.2 are comparable to those of Version 3.1, in that a processing run is invoked using the top level UNIX Korn shell scripts with extension `.now`. As in Version 3.1, these scripts define the processing environment using variables for directory path definitions and the processing time span. The top level UNIX shell scripts then invoke the GAS D shell scripts, the second level, which can be identified by their extension `*.dates`. These GAS D scripts check the processing time span specified for plausibility and carry out the processing loop over each day specified by the time span in the level one shell scripts.

Similar to Version 3.1, the GAS D shell scripts of Version 3.2 then call the GAS R shell scripts, which define the third level of scripts. The GAS R shell scripts then call the GAS F shell functions, which are the bottom level scripts. Figure 4.4 lists the filenames for all four levels of the pre–, the network– and the post–processing stages of the automated procedures Version 3.2.

Pre–Processing Stage

As in Version 3.1 (§4.4.1) of the automated procedures, the pre–processing stage is invoked using the top level UNIX shell script `preproc.now`. This shell script will execute the GAS D shell script `preproc.dates`, which will call the GAS R shell script `preproc.rprocess` for each day according to the time span defined by the user. The

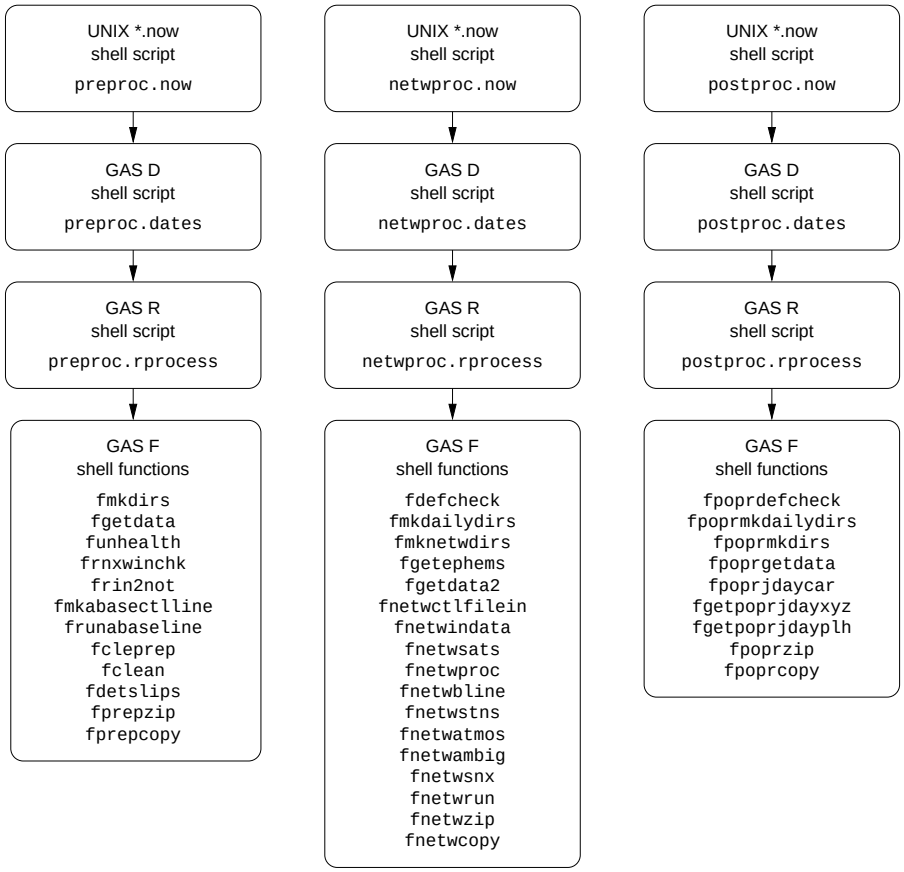

Figure 4.4: Automated Procedures for GPS Processing with GAS (Version 3.2).

GAS R shell script then calls each GAS F shell function of the pre–processing stage as listed by their file names in Figure 4.4.

The GAS F shell functions for the pre–processing stage are essentially the same as in Version 3.1. Modifications were made in the GAS F shell function `getdata` to account for the NFS server–client workstation configuration between archiving and processing workstations. Furthermore, the GAS F shell function `rin2not`, which creates the FILTER control file was modified due to problems occurring during cycle slip detection of the first session of the first day of the GPS week. It was noticed by the author that the automated procedures sometimes failed to detect and correct cycle slips in this session. The GAS processing module PANIC would report a large cycle slip within this time period and would crash thereafter. By removing the GPS observations of the first 15 to 20 minutes however, the procedures were able to clean these data. It was therefore decided, to implement the

removal of the first 15 minutes for the first day of the GPS week, as a standard approach within this research.

Slight changes were carried out on the GAS F shell function `cprsfiles2` of Version 3.1 (§4.4.1), which removes and compresses observation and processing files after the pre–processing stage. In order to make its file name conform with other shell function names of the procedures Version 3.2, it was also renamed to `prepzip`.

The introduction of designated workstations for automated processing and archiving of GPS data, required a GAS F shell function that would push the temporary created daily directory structure on the processing workstations `geodix`, `ukcogr` and `defix` onto the archiving workstation `monix`. This was accomplished, by introducing the new shell function `prepcopy`, which transfers amongst others, the cleaned NOTT2 format observation files and the session and baseline dependent processing files to the archive `procres`.

Network–Processing Stage

As in Version 3.1 (§4.4.1) of the automated procedures, the network–processing stage is invoked using the top level UNIX shell script `netwproc.now`. This script will execute the GAS D shell script `netwproc.dates`, which will call the GAS R shell script `netwproc.rprocess` for each day to be processed. The GAS R shell script will then call each GAS F shell function of the network–processing stage as listed by their names in Figure 4.4.

As with the pre–processing for Version 3.2, the modifications necessary to the network–processing of Version 3.1 were mainly related to the separation of the workstations according to their main tasks. Besides that, path definitions had to be modified in several procedures in order to account for the new processing results archive `procres` being on workstation `monix`.

Since December 2001, the IGS produces its ephemeris products in the new realization of the ITRS, the ITRF2000 (Weber, 2001). This required an update of the GAS R shell script `netwproc.rprocess` to accommodate this new reference frame.

After the slightly modified GAS F shell function `defcheck` has checked the user–definitions, the new GAS F shell function `mkdailydirs` checks whether a daily directory structure for the current processing day already exists on this processing workstation and if not, creates it. GAS F shell functions `getephems` and `getdata2` were both modified in order to incorporate the transfer of the precise ephemeris, the GAF and the cleaned NOTT2 format observation files to the processing workstation using the NFS server-client workstation configuration. The GAS F shell function `getdata2` also copies GPS baseline dependent files, i.e. the `bsatfile.out` containing the base satellites for each baseline to be used in the PANIC adjustment (Booth, 2000).

At this stage, the PANIC control file and the PANIC default control file are created using a number of GAS F shell functions, this is essentially carried out in the same way as described for the automated procedures Version 3.1 (§4.4.1).

Finally, after the GAS processing module PANIC has been executed and a network solution has been obtained, the network solution files are compressed using the GAS F shell function `netwzip`, which varies slightly from the GAS F shell function `zipdata` in Version 3.1. The new GAS F shell function `netwcopy`, then copies the complete network processing directory to the processing archive `procres` on workstation `monix`.

Post–Processing Stage

The post–processing stage of the automated procedures Version 3.2 is invoked as in Version 3.1 (§4.4.1) using the top level UNIX shell script `postproc.now`. This script will execute the GAS D shell script `postproc.dates`, which will call the GAS R shell script `postproc.rprocess` for each processing day. The GAS R shell script will then call each GAS F shell function of the post–processing stage as listed by their file names in Figure 4.4.

As with the pre– and network–processing procedures for Version 3.2, the modifications necessary to the automated procedures of Version 3.1 were mainly related to the separation into processing and archiving workstations. Path definitions in several shell scripts and

functions had to be amended in order to accommodate the introduction of the two archives `procres` and `finalcoords` on workstation `monix`.

The large number of CGPS stations in the re–analysis of the data set caused problems with the baseline definition, which is carried out during the execution of GAS D shell script `postproc.dates`. This affected in particular, the network combination mode (§4.4.1) of the post–processing procedures. Here, the auxiliary C program DEFBLNS (Booth, 2000) is used to generate a temporary file containing the number of all GPS baselines to be processed and a list of the associated CGPS station names. DEFBLNS is an independent module, which receives its input parameters as UNIX command line arguments handed over at invocation. This list however, can only contain a limited number of elements and since the baseline vectors of all 25 CGPS stations are to be combined in one network, the argument list was too long for the UNIX shell. In the new approach it was decided to hand over the networks themselves rather than the individual stations. Using the newly developed auxiliary Perl script `netwdefblns.pl` the problem was solved. `netwdefblns.pl` reads a list of arguments from the command line which must include the root and project directories, the GPS week, the base station and the list of networks. The command to execute Perl script `netwdefblns.pl` may look like:

```
# netwdefblns.pl /usr2/people/tgproc3 tgcogrs 1024 iesg cls1 cls2 cls3
```

with `/usr2/people/tgproc3` and `tgcogrs` defining the paths to the root and project directories, `1024` being the GPS week, `iesg` being the 4–character base station name, and `cls1`, `cls2`, and `cls3` being the networks to be combined. In order to produce a list of GPS baselines from the list of networks handed over, `netwdefblns.pl` requires the network definition file, which will be introduced later in §4.5.2.

As with the GAS R shell shell script `netwproc.rprocess` of the automated procedures Version 3.2, the GAS R shell script `postproc.rprocess` also needed modifications with respect to the change of the reference frame of the IGS precise ephemeris to ITRF2000 in December 2001.

The first GAS F shell function to be called by shell script `postproc.rprocess` is `poprdefcheck`. There were few changes in this version of the GAS F shell function

compared to its previous version. A check for the existence of the newly introduced coordinate time series directory `finalcoords` on workstation `monix` was added.

An additional GAS F shell function was needed that would check for the existence of the daily directory structure on the processing workstations and create the directory tree if needed. This new shell function `poprmkdailydirs` would be called before `poprmkdirs`, which is a modified version of shell function `mkpoprdirs` of the procedures Version 3.1 (§4.4.1).

The GAS F shell functions `getdata` needed minor changes in order to provide the PANIC network solution files and the cleaned NOTT2 format observation files using the NFS server–client configuration. This new version of the shell function also un–compresses the copied files so the shell function `unzipdata` of Version 3.1 was no longer required.

The GAS F shell function `poprjdaycar` did not require any modifications from previous version, however functions `getpoprjdayxyz` and `getpoprjdayplh`, which extract the cartesian and geodetic coordinates from the CARNET solution files, needed updating with respect to the new coordinate time series archive directory `finalcoords` on workstation `monix`.

After the CARNET execution, the GAS F shell function `poprzip` compresses the post–processing directory. This file was based on `zipdatantp` of the previous version of the automated procedures. The final GAS F shell function to be called during the post–processing stage is the new shell function `poprcopy`. It pushes the post–processing directory into archive `procres` onto workstation `monix`.

4.4.3 Automated Procedures Version 3.3

The automated procedures Version 3.3 are not to be considered an improvement to the procedures of Version 3.2 (§4.4.2). Like the procedures of Version 3.2, they are based on the automated procedures Version 3.1 (§4.4.1), and were also developed by the author in September 2001, when automated processing was split onto several workstations.

This parallel development was prompted by the NFS server–client workstation configuration shown in Figure 4.3. The idea behind the automated procedures Version 3.3 was to run the different processing stages on the NFS client workstations, however, not using a temporary, locally created daily directory structure as in Version 3.2, but to directly access the daily directory structure in the processing results archive `procres` on the NFS server `monix`. At that time, it was regarded as a disadvantage of the procedures of Version 3.2 that data had to be transferred from and to the archiving and processing workstations at every processing stage and that temporary directory structures had to be created and removed.

However, as the GAS processing module PANIC creates large temporary files (> 100 Mb) in the network directories during the least–squares adjustment process, accessing a network directory directly causes large amounts of data to be shifted over the computer network. Experience showed that this actually slowed the processing time considerably. Furthermore, tests by the author showed that for the current configuration, file operations on a remote workstation take more processing time than copying the file to a local directory and carrying out identical operations locally. This effect is magnified when considering that if all GAS processing stages were carried out sequentially, e.g. if the processing was carried out on a daily basis, fewer file transfer operations between the workstations would be necessary as more and more data would already be available within the local directory structure on the processing workstation. Therefore, although large amounts of data were processed using Version 3.3 during the re–analysis of the UK 25 CGPS station data set, the new automated daily processing procedures, which were developed in June 2002 (§4.5.2), were based on the automated procedures Version 3.2 rather than 3.3.

4.5 Automated Daily Processing with GAS

In the previous section, the automated procedures Versions 3.1 (§4.4.1), 3.2 (§4.4.2), and 3.3 (§4.4.3) were introduced. Each version was described as a collection of UNIX Korn shell scripts and associated functions with some auxiliary C programs and Perl scripts.

The automated procedures for all versions are separated into the three GAS processing stages for pre–, network–, and post–processing, all of which can be executed independently.

Booth (2000) demonstrated how, by using the UNIX `cron` utility and the GAS processing module MKGASCMD (Stewart et al., 2002), it was possible to execute the automated procedures without user interaction at a given time on a daily basis. Although, he was able to achieve excellent results with the Mark 3 automated procedures, these contain few tools that enable reporting on the individual processing stages and results. For a small network of five CGPS stations and over a limited period of time, it might be possible to carry out checks on progress manually, by checking the result files of each processing stage on a daily basis. However, for larger networks this will obviously become more difficult as the number of files increases and more and more data is added. Therefore, if daily processing was to be carried out fully automated over many years, some standard means for reporting on the processing in a summarized manner had to be developed.

The initial CGPS network analysed by the author consisted of 13 stations. From §4.4 it is clear that the automated procedures of the pre–processing stage have to be executed for each GPS baseline. This involved editing of the GAS D shell script `preproc.dates` twelve times. Furthermore, if using the automated procedures for network–processing, a network of 13 stations would have to be divided into two sub–networks, of which each would require a separate execution of the procedures. Prior to each invocation, the GAS D and GAS R shell scripts `netwproc.dates` and `netwproc.rprocess` would need to be edited to incorporate the correct CGPS stations associated with each sub–network and the correct sub–network designations. With the introduction of even more CGPS stations to be analysed, additional sub–networks would have to be defined, each requiring its own network–processing stage.

The final processing result for each processing day are the coordinates and their standard errors for each CGPS station, as a result of one combined network adjustment. Therefore, as described in §4.4, the GPS baseline vectors, which have been obtained from all individual sub–network solutions are combined using the GAS processing module CARNET at the post–processing stage. Due to the fact that identical GPS observations of several stations are introduced to all sub–networks, the standard errors related to those

stations are too optimistic in the combined solution. A simple method to re–scale the affected error information to the level of stations introduced only once was developed by the author. However, this requires that the post–processing stage is carried out for each sub–network individually. Then in another step, average daily standard errors can be computed for each station affected based on each sub–network. These *corrected* daily standard errors can then be included in the final corrected coordinate time series files.

For several individual executions of the automated procedures of the post–processing stage, `postproc.now`, `postproc.dates` and `postproc.rprocess` would require editing. The number of networks in shell script `postproc.now` defines whether post–processing is carried out in single network or network combination mode (§4.4.1). The GAS D shell script `postproc.dates` requires the names of the corresponding network or sub–networks in order to define all possible GPS baselines per definition, and the GAS R shell script `postproc.rprocess` needs the names and post–processing names of the affected network or sub–networks.

None of these additional tasks, be it a quality control or reporting mechanism, or the management of multiple executions of any single processing stage, are carried out by the automated procedures described in §4.4. Using the advantages of the scripting language Perl over the UNIX Korn shell scripts, the author developed the daily processing Perl script described in detail below. This script wraps around the existing automated procedures and adds the missing functionalities. The scripting language Perl seemed perfect for this task, as it enabled easy communication between the already existing software and the newly developed scripts. The main Perl script has been termed `dailyproc.pl`, and can be invoked either manually or using the UNIX `cron` utility. Processing parameters necessary for the execution of the Perl script are defined in a control file, e.g. `dailyproc.ctl`, similar to a GAS processing module control file. An outline of the processing tasks carried out during a standard `dailyproc.pl` execution is shown in Figure 4.5. Included are also suggestions by the author for reporting and summarizing of results at each processing stage, of which some have already been implemented in the Perl scripts described below.

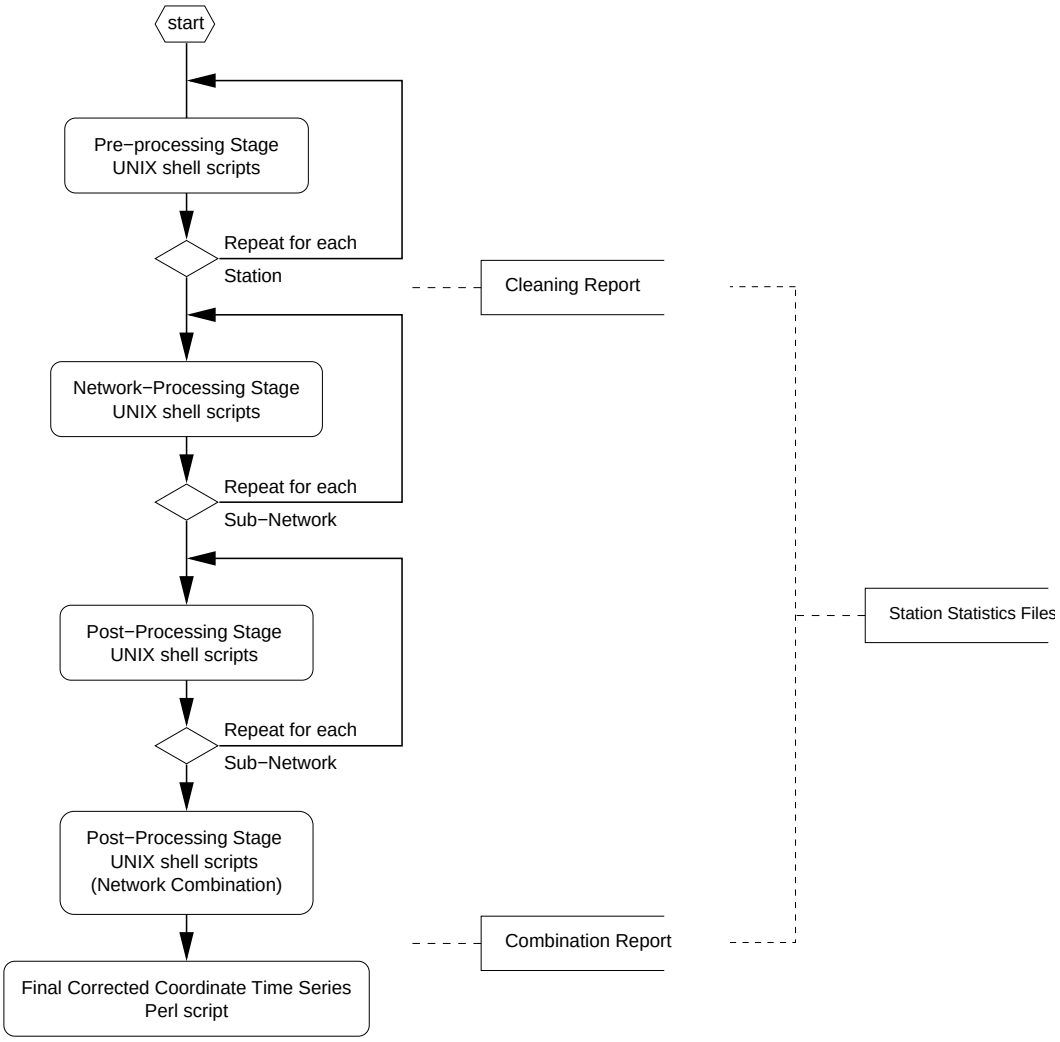

Figure 4.5: Outline of tasks carried out by the Daily Processing Script Version 1.0 for automated daily processing with GAS.

4.5.1 Daily Processing Script Version 1.0

In Summer 2000, fully automated daily processing started using Version 1.0 of the Perl script `dailyproc.pl` and the control file `dailyproc.ctl` in connection with the automated procedures Version 3.1 (§4.4.1). Using the UNIX `cron` utility, the execution of the Perl script was invoked automatically every morning, carrying out all three GAS processing stages. Processing was carried out on a daily basis on data, approximately 30 days back from the current calendar day, allowing extra time for problems in the data flow to be solved prior to processing.

In the first step of the execution of `dailyproc.pl`, the script reads the processing dependent parameters from the control file and carries out general checks on directory path definitions. The Perl script also checks for all UNIX `.now`, GAS D and GAS R shell script template files in the directory `dailyproctemps`, which will be used to create the final shell script for each GAS processing stage using the Perl stream editor, similar to the UNIX `sed` command used by the automated procedures themselves.

If the GAS pre–processing stage is to be carried out, then `dailyproc.pl` creates a loop over all stations specified in the control file. This involves creating the `preproc.now` shell script and the `preproc.rprocess` from the template files for the specific day to be processed. The GAS D shell script `preproc.dates` then needs to be modified after each station–specific pre–processing run.

In Version 1.0 of the daily processing script, after the pre–processing stage has been completed for each station, a *cleaning* report is generated. The Perl script checks for the availability of a cleaned NOTT2 format observation file and if found, reads the σ_0 of the residuals for the ionospherically free observable from the associated slip file. If there is no cleaned NOTT2 format observation file for a particular station, then it is investigated whether `procarch` on workstation `monix` contains a RINEX format observation file for this station on this day. Depending on the outcome of these checks, a different set of characters are written to the cleaning report file enabling the identification of the problem.

The second part of the quality control occurs after the cycle slip cleaning stage, with the generation of a file for each station holding some statistical information, e.g. the total

theoretical number of days and sessions for which data could have been available, actual numbers of available RINEX and NOTT2 format observation files, total number of cleaned days and sessions, total number of sessions that have not been cleaned, the sum of all σ_0, and the average σ_0 obtained after the data was cleaned for cycle slips. These files have been denoted as *station statistics files*.

If specified in the control file `dailyproc.ctl`, the next stage to be carried out by the Perl script `dailyproc.pl`, is the GAS network–processing stage. As mentioned above, this involves executing the automated procedures for each sub–network separately. Using Version 1.0 of the `dailyproc.pl` script, this was performed for a two sub–network configuration. In order to execute the automated procedures for each network, the GAS D shell script `netwproc.dates` is automatically edited prior to execution.

The next step to be carried out by the daily processing script is the post–processing stage. It was already mentioned that this requires several executions in single network mode in order to post–process each sub–network. After this is completed, all GPS baseline vectors are combined using the network combination mode of the automated procedures. By selecting the post–processing option in the control file `dailyproc.ctl`, the Perl script uses template files for creating the `postproc.now`, the `postproc.dates` and the `postproc.rprocess` for each sub–network. This involves, stream editing the day to be processed and the number of networks in `postproc.now`, a list of stations for the baseline definition in `postproc.dates` and the names and post–processing names for each network in `postproc.rprocess`. The latter two require modifications after each processing run, as the variables specified are network dependent. Prior to the network combination run of the automated procedures, `postproc.now` is modified by `dailyproc.pl` to contain the correct number of sub–networks to be combined, the GAS D shell script `postproc.dates` is edited to contain a list of all possible stations to be expected by the scripts, and the GAS R shell script is modified with the correct sub–network names, and post–processing name.

Once all runs of the GAS post–processing stage have been completed, a *combination report* is compiled by the Perl script `dailyproc.pl`. The first check carried out is on the final CARNET solution file of the combined network adjustment. Then the number

of cleaned NOTT2 format observation files is established and whether at least one file per station is available for the current processing day. Based on this information, the number of stations, which have been used in several sub–networks is known. Now the overall a–posteriori σ_0 of the least–squares adjustment process is read from the CARNET summary file. Using the standard errors for each coordinate component of each station listed in this file, the 3–dimensional radial errors for each station can be computed. For stations, which have been used in several sub–networks, the coordinate standard errors of the CARNET solution file of each sub–network are averaged, before the radial error is computed. At this stage, the combination report can be compiled containing the overall a–posteriori σ of the CARNET least–squares adjustment process and the 3–dimensional radial errors for each station. If for any station no radial error was computed, i.e. there was no record for this station in the CARNET solution file, then `dailyproc.pl` checks for a RINEX format observation file in `procarch` and depending on the result, a different set of characters is written to the report. Thus by reading this report, it is possible to evaluate, whether a coordinate solution has been obtained for a specific station on a specific day, or whether there was a problem, either due to a missing RINEX format observation file or a computational problem. Using this report together with the cleaning report produced after the GAS pre–processing stage, it is possible to quickly check, whether a `dailyproc.pl` run for a specific calendar day was successful.

At the end of the post–processing stage, the station statistics files are updated with the new total number of daily coordinate solutions and with the last day for which post–processing has been carried out.

If selected in the control file, the error information of those stations included in several sub–networks can be corrected and final coordinate time series for each station can be produced. To do this, `dailyproc.pl` first determines which stations have been used in more than one sub–network, by checking the CARNET solution files of the GAS post–processing stage. During this process the associated standard errors for the cartesian and geographic coordinates are obtained from each sub–network and once all CARNET solution files have been read, average coordinate standard errors for each station are computed. These corrected coordinate standard errors are then written to the new final

coordinate time series files. The coordinate standard errors of stations included only once or which have been fixed in the post–processing stage are not modified.

The last step in the Perl script `dailyproc.pl` is to update the control file with the new date information. If any of the three processing stages or the standard error correction is carried out by the Perl script, then the date of last execution for this stage is incremented by one. This enables `dailyproc.pl` to determine for which day processing is to be carried out on the next automatic invocation.

4.5.2 Daily Processing Script Version 2.0

The inclusion of twelve additional CGPS stations during the re–analysis of the UK 25 CGPS station data set in the period from October 2001 to June 2002, meant that the complete network had to be divided into six rather than just two sub–networks. Furthermore, the introduction of the NFS server–client workstation configuration (Figure 4.3), drove the development of the automated procedures Version 3.2 (§4.4.2). Both of these factors required an overhaul of the Perl script `dailyproc.pl` and a review of the format of its control file `dailyproc.ctl`, in order to make the script independent of network size and to account for any possible future developments.

In June 2002, Version 2.0 of the daily processing script `dailyproc.pl` and its control file were developed. The new script was based on the automated procedures Version 3.2 as opposed to Version 3.3, due to the problems outlined in §4.4.3. In general, the new Perl script carries out the same tasks as the previous version, and its structure has remained much the same as that shown in Figure 4.5. Figure 4.6 shows an outline of the processing tasks carried out by the daily processing script Version 2.0.

In order to carry out automated daily processing using the new Perl script `dailyproc.pl` Version 2.0 and Version 3.2 of the automated procedures, a project directory, containing the following sub–directories must be created in the user environment on one of the processing workstations.

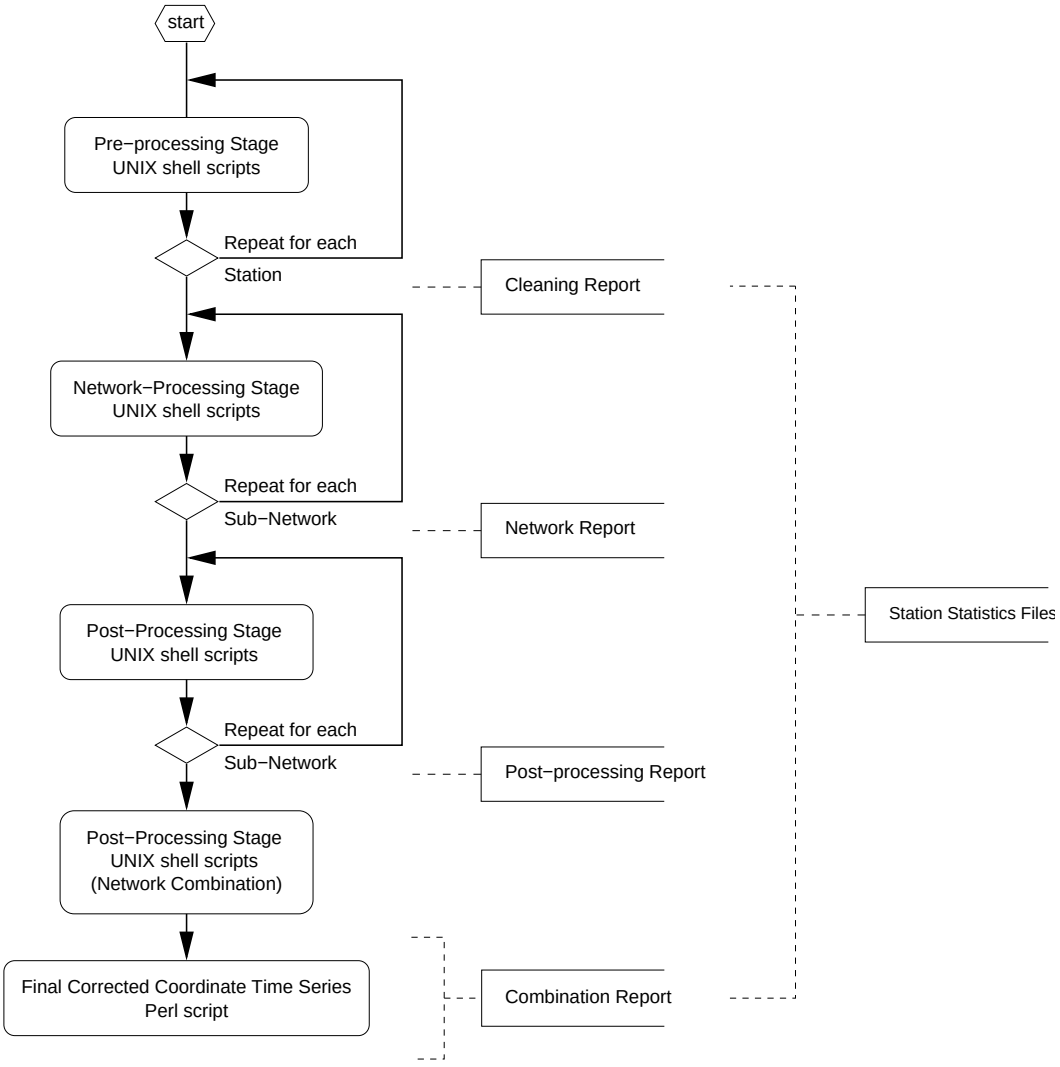

Figure 4.6: Outline of tasks carried out by the Daily Processing Script Version 2.0 for automated daily processing with GAS.

```
# ls
dailyproc       netwproc          postproc          preproc
dailyproctemps  netwprocscripts   postprocscripts   preprocscripts
netwinfo        netwproctemps     postproctemps     preproctemps
```

Directory `dailyproc` contains the Perl script and its control file. The directory `dailyproctemps` contains all template files for the UNIX `.now`, the GAS D and the GAS R shell scripts used directly by the Perl script `dailyproc.pl`. The importance of the remaining directories was described in detail in §4.4, however it should be pointed out that with this new directory structure the scripts for the pre–, the network– and post–processing stages are created by the daily processing Perl script.

Similar to Version 1.0 of the Perl script `dailyproc.pl`, the execution of Version 2.0 is carried out automatically using the UNIX `cron` utility. The first task the script carries out, is to read the specified control file, which holds the processing parameters for the `dailyproc.pl` execution. In order to accommodate for the increased number of stations and thus the need for more sub–networks, these are not defined in the control file anymore. Instead, the user is required to specify a *network definition file* in `dailyproc.ctl` and the file must be located in the directory `netwinfo`. This network definition file contains information on the network names, the network post–processing designations and a 3–character definition for the network–specific SINEX format solution files. Also included is the date[3] on which the sub–network is to be processed the first time. At the moment the script assumes that once a sub–network is established it will always be included in the analysis thereafter. This will need some modifications in order to be more flexible, e.g. the use of episodic or quasi–continuous GPS stations will create the need for more sub–networks for which processing is started and stopped. Besides these four parameters, the network definition file must also contain a list of all CGPS stations attributed to a specific sub–network, excluding the base station. An example network definition file as used currently for automated daily processing with GAS is given below.

[3] in Modified Julian Days (MJD)

```
NETW POPR_NAME SNX_NAME NETW_START SUB_NETW_STATIONS (without base station)
================================================================================
cls1 c1kovw    c_1      50567      kosg,onsa,vill,wtzr,lerw,camb,shee,sunb,bark
cls2 c2kovw    c_2      50567      kosg,onsa,vill,wtzr,lerw,camb,hers,abyw,hems
cls3 c3kovw    c_3      51074      kosg,onsa,vill,wtzr,lerw,camb,newl,aber,live
cls4 c4kovw    c_4      51222      kosg,onsa,vill,wtzr,lerw,camb,lowe,morp,nstg
cls5 c5kovw    c_5      51274      kosg,onsa,vill,wtzr,lerw,camb,brst,dunk,hurn
cls6 c6kovw    c_6      51772      kosg,onsa,vill,wtzr,lerw,camb,pers,port,npld
```

Besides the network definition file, the control file `dailyproc.ctl` also contains parameters for the names of a *station times file* and a *station categories files*, both of which must be located in the directory `netwinfo`. The station times file contains the MJD of the first observation day of each station. If a station was abandoned during the processing period, e.g. Hemsby, then the last MJD must be included too, alternatively the string '99999' will tell the Perl script `dailyproc.pl` that the station is still active. At the moment of writing, the station times file only allows start and stop times for one *active* period to be specified. This will need some modifications in order to be able to include episodic and quasi–continuous GPS stations in the automated daily processing. The top section of the currently used station times file is shown below, the complete file can be found on the CD–Rom in the directory `/Software_Developments/Daily_Processing_Scripts_V2/netwinfo`.

```
SITE  STARTMJD ENDMJD
=====================
aber  51074    99999
abyw  50913    99999
bark  50567    99999
 *      *        *
 *      *        *
```

In order to be able to make the cleaning report introduced in Version 1.0 of the Perl script `dailyproc.pl` clearer, the cleaning reports of Version 2.0 have been divided according to the station categories assigned to each station in the station categories file. The top section of the currently used station categories file is shown below, the complete file can be found on the CD–Rom in the directory `/Software_Developments/Daily_Processing_Scripts_V2/netwinfo`.

```
SITE  CATEGORY
==============
aber  TG
abyw  MO
bark  OTHER
 *      *
 *      *
```

After the control file is read a series of directory path checks is carried out. Also the existence of the network definition, station times and station categories files in the directory `netwinfo` is evaluated. If any necessary template files for creating the UNIX `.now`, the GAS D or the GAS R files are missing in the directory `dailyproctemps` the process is stopped. However, once the processing environment is correctly set up by the user, definition errors are very unlikely.

The following GAS pre–processing stage is carried out in the same manner as in Perl script `dailyproc.pl` Version 1.0. However, a cleaning report for each station category is generated based on the assignment of each station in the station categories file. Currently, stations are separated into four different categories depending on the site, e.g. tide gauge sites (TG), IGS tracking sites (IGS), Met Office sites (MO) and any other sites (OTHER). Stations sponsored by the Environment Agency, by the University of Newcastle or the IESSG have been attributed to category OTHER, if they do not fall into any other category. Another modification to `dailyproc.pl` with respect to the cleaning reports is that a new report is started at the beginning of each calendar year, which should improve readability. The cleaning reports can be found on the CD-Rom in the directory `/GPS_Processing_Reports/Preprocessing_Stage`.

The network–processing stage is carried out much in the same way as in Version 1.0 of the Perl script `dailyproc.pl`. Due to the fact that the current CGPS network is divided into six sub–networks, a rigorous method for monitoring the results of this stage had to be introduced. Version 1.0 did not have a routine quality control tool for the network–processing stage. However, by obtaining the a–posteriori σ_0 for each PANIC least–squares adjustment process from the PANIC network solution files and writing them into a *network report* (Figure 4.6), it is possible, to quickly evaluate the results of the adjustment process

for each sub–network. The annual network reports have been compiled on the CD-Rom in the directory `/GPS_Processing_Reports/Networkprocessing_Stage`

The post–processing stage of the Perl script `dailyproc.pl` Version 2.0 is generally carried out in the same manner as in Version 1.0. First, the automated procedures are executed for each sub–network as defined by the network definition file. Then in a second stage, the network combination is carried out by including GPS baselines of all networks in the CARNET least–squares adjustment. If the post–processing stage for each sub–network has already been carried out, Version 2.0 of the Perl script `dailyproc.pl` allows to only execute the combination run if necessary. This feature was introduced as a result of the re–analysis in 2001/2002, where each GAS processing stage was carried out for the whole data set prior to attempting the next stage.

Version 2.0 of Perl script `dailyproc.pl` also carries out the correction of the standard errors in the combined network for stations which have been used in several sub–networks. Some technical improvements in the Perl script have also been made, in order to allow any number of sub–networks to be processed.

The updated Perl scripts `dailyproc.pl` also provide, a report of the a–posteriori σ_0 for each sub–network, denoted as a *post–processing report*. This report is based on the a–posteriori σ_0 of the CARNET solution files for each individual network. The post–processing reports then contain the σ_0 for all six networks for each day processed for one calendar year. If no CARNET solution file is found for a specific sub–network, then the space is left empty in the report. Using this report, post–processing problems can quickly be identified by the user.

Furthermore, to check the overall solution of the network combination, a combination report is formatted. In Version 2.0 of the daily processing script this report has also been divided into individual reports depending on station categories and checks both the CARNET solution files and the final coordinate time series files. A list of stations with a solution for a specific day is established from the CARNET solution file of the network combination and their correct standard errors are read from the coordinate time series files. Again, the 3–dimensional radial error for each station is computed and entered into the report. However, this list of stations is also compared with the list of active stations

from the station times file and and if a station is missing in the CARNET solution file, Perl script `dailyproc.pl` assigns a different set of characters as an indication for a problem. In addition, due to the possibility of expressing the final coordinate solutions in different reference frames, the combination reports created by Version 2.0 of the daily processing script are frame dependent. Examples of the post–processing and combination reports created by `dailyproc.pl` for the time span from 1997 to 2002 can be found on the CD–Rom in the directory `/GPS_Processing_Reports/Postprocessing_Stage`.

As an additional feature, email reporting has been implemented in Version 2.0 of the daily processing script. At the moment, an email is automatically generated containing the start and stop times of each GAS processing stage. From experience it is known, how long each processing stage takes on average to be carried out successfully. A shorter than usual processing time period in the email, will then indicate that something during the process has failed.

Based on the quality control reports implemented in Version 2.0 of the Perl script `dailyproc.pl`, it is possible to generate histograms, similar to other CGPS analyses e.g. Hurst (2000), such as histograms of station coordinate repeatabilities. Using histograms of the σ_0 of the ionospherically free residuals collected in the cleaning report, it is possible to investigate the long–term data quality of each CGPS station in the analysis, thus separating better stations from bad ones. These station specific histograms for the UK 25 CGPS station data set can be found in §5.3. An interesting aspect of the cleaning reports was identified, when sessions reported to be not cleanable, were correlated with periods of high ionospheric activities. Particularly for the CGPS station Lerwick, a good correlation between the inability of the scripts to clean the GPS observations for cycle slips and large K indices can be observed. The K index gives a local measure of geomagnetic activity of the ionosphere (§3.4.2) relative to a quiet day for a specific site (Dodson et al., 2001b).

In a similar manner, histograms of the sub–network dependent a–posteriori σ_0, can give an indication for the quality of each adjustment computation and also identification of possible long–term variations. Similar graphs can also be generated for the two processing reports of the post–processing stage as a final quality check. This has not yet been

implemented by the author, however, will be suggested for further improving the daily processing script.

4.6 Automated Coordinate Time Series Analysis

In the previous sections automated GPS processing using GAS in combination with automated procedures and the daily processing script was introduced. As a result of this, coordinate time series for both cartesian and geodetic coordinates have been obtained for each station in the UK 25 CGPS station network. This section will now discuss the next stage in which the coordinate time series are analysed in an automated way using two Perl scripts developed by the author. These scripts incorporate many modules of the Generic Mapping Tools (GMT) (Wessel and Smith, 1995, 1998) in order to generate graphs of the results in a fully automated manner.

The main Perl script of the *analysis stage* is the analysis script `analysis.pl`. Similar to the GAS processing modules or the daily processing script, it obtains its execution settings from the control file `analysis.ctl`. The main tasks carried out by the analysis script are outlined in Figure 4.7. The script `analysis.pl` uses a number of internal and external (separate files with extension `*.pm`) Perl subroutines, which will not be discussed any further as this would be beyond the scope of this thesis. All files are, however, included on the CD–Rom in directory `/Software_Developments/Automated_Analysis_Procedures`.

The first step after the invocation of `analysis.pl` is to read the control file and check whether the user definitions, e.g. directory definitions or required files, are existent and in the correct location. In a second step, the cartesian and geodetic coordinate time series files, created and corrected during network combination are scanned for multiple entries for a specific day. During automated GPS processing it is however, very unlikely that days have several entries in these files. In the Mark 3 automated procedures (Booth, 2000), outlier detection was implemented at the post–processing stage and was carried out by supplying a manually created and edited outlier file. This was based on the fact that the Mark 3 automated procedures produced weekly solutions which were used to define outliers. The post–processing stage would then be repeated and the procedures would

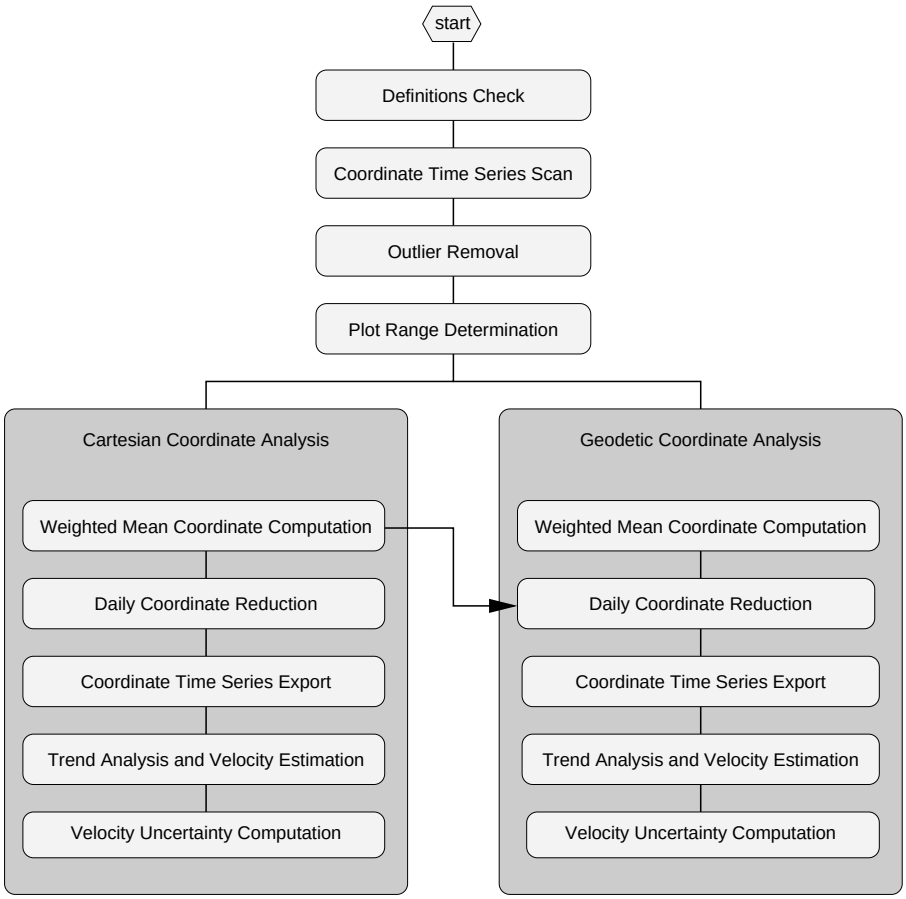

Figure 4.7: Outline of tasks carried out by the Automated Coordinate Time Series Analysis Script `analysis.pl`.

not copy days listed in the outlier file into the coordinate time series files. As weekly solutions are no longer computed in Versions 3.1 and 3.2, outlier detection and removal is now implemented at the analysis stage.

In the analysis script outlier detection and removal is carried out by fitting a linear regression model (see Eq. E.1 in Appendix E) to the *raw* coordinate time series, based on weighted least–squares. The weights w_i are derived from the daily coordinate standard errors σ_i from the CARNET solution files and the mean standard error σ_{mean} for each coordinate component for each station such that

$$w_i = \frac{\sigma_{mean}^2}{\sigma_i^2} \tag{4.1}$$

The daily coordinate estimates are then differenced from this linear model, to form residual coordinate time series or *detrended* coordinate time series. The weighted root mean square (WRMS) (Eq. D.2 in Appendix D) of the coordinate residual is then computed and any residual that is found to be greater than three times the WRMS is defined as an outlier. These daily coordinates are then removed from the coordinate time series (Wdowinski et al., 1997; Teferle, 2000; Johansson et al., 2002). This way, after fitting a linear regression model to the raw coordinate time series (with outliers removed), a *revised* linear velocity estimate is obtained. The now detrended and *cleaned* coordinate residual time series can then be further analysed.

Besides the analysis of the coordinate time series, the Perl script `analysis.pl` also produces a series of different figures, showing the time series of the cartesian or geodetic coordinate components either individually, combined for one station or combined for a set of stations. In order to carry this out, the script needs to determine the earliest start and latest end times, i.e. the *plot range*, for all graphs. This plot range is identical for all generated figures to allow for comparisons between the different stations.

From this point onwards, the user defines whether the analysis script `analysis.pl` carries out the analysis based on cartesian only or on both cartesian and geodetic coordinate time series. At the moment the script cannot carry out the analysis of the geodetic coordinate time series on its own as will be described later on.

After the previously *cleaned* coordinate time series have been read from their files, weighted mean coordinates and variances for the complete observation time span are computed for each station. These mean coordinates are then used to reduce the coordinate time series prior to the trend analysis. In order to further analyse the coordinate time series using GMT (Wessel and Smith, 1998) or Matlab©, these time series are exported separately for each component and station to files, containing either the MJD and the coordinate component, the MJD, coordinate component and the associated weight, or the MJD, the coordinate component and the re–scaled standard errors. Following this, the trend analysis is carried out using the GMT module `trend1d` and the Perl subroutine `lstrendfit`, based on the FORTRAN subroutine `fit` (Press et al., 1992), obtaining two independent estimates for the linear rate of change of the coordinates, i.e. the *station*

velocity. In the final step uncertainties for the station velocity estimates can now be computed using Eq. H.12 along with Eqs. H.19 and H.20 (Zhang et al., 1997; Mao et al., 1999). These five steps are shown in Figure 4.7 as weighted mean coordinate computation, daily coordinate reduction, coordinate time series export, trend analysis and velocity estimation, and velocity uncertainty computation.

Although, the analysis steps of the cartesian and geodetic coordinate time series are very similar, the coordinate reduction of latitude and longitude requires projection into North and East coordinate components for interpretation. This additional step requires the cartesian coordinate time series files in order to compute the weighted mean cartesian coordinates for each station which are used in the projection.

Each stage of the coordinate time series analysis is carried out for each station separately. As mentioned, `analysis.pl` is capable of producing several different graphs showing the results of these analysis runs. Figures showing the coordinate time series either for one coordinate component or one station are generated during these processing loops. Those figures showing the coordinate time series for several stations are created after completion of the analysis runs for either cartesian or geodetic coordinates.

The analysis script `analysis.pl` is also capable of carrying out parts of the dual–CGPS station analysis which will be discussed in detail in Chapter 7. However, further development of these initial routines was only carried out on Matlab© and therefore this functionality has not been included in Figure 4.7.

In Teferle et al. (2002a) the application of a *common mode bias* filtering technique to the coordinate time series of UK CGPS stations was discussed. In Chapter 6 of this thesis this regional filtering technique is applied to the current coordinate time series. Although the common mode bias estimation has been implemented by the author in the Perl script `ion.pl`, it has not yet been included in the automated analysis script. Perl script `ion.pl` estimates the common mode bias on a daily basis for both cartesian and geodetic coordinate components. The user can specify which stations the bias estimation is based upon in order to exclude contributions from stations with known problems as discussed in §5.3.3. Besides estimating the common mode bias, `ion.pl` can also carry out numerous other tasks which partly require some user interaction, e.g. spectral analysis of

the coordinate time series using the GMT module `spectrum1d` based on a Fast Fourier Transform or the FORTRAN program LSSA (Pagiatakis, 1999) using a least–squares spectrum analysis algorithm.

Besides Perl scripts `analysis.pl` and `ion.pl`, the author has during his research developed numerous Matlab© M–files to carry out most of the analysis discussed in Chapters 6, 7 and 8. A discussion of these in detail would go beyond the scope of this thesis, however a selection of these files has been included on the CD–ROM in directory `/Software_Developments/Matlab_M-files`.

Additionally, the author has obtained the `cats_MLE` C routines from Simon Williams, which have been used to carry out most of the noise analysis using the Maximum Likelihood Estimation (MLE) (Eq. H.7 in Appendix H).

4.7 Summary

This Chapter has discussed the software developments carried out by the author during his research since 1999. After a brief introduction of GAS, the preparatory processing procedures for the comprehensive processing data archive `procarch`, the GAF's and GOF's were described. Following this, details of improvements to the automated procedures (Versions 3.1, 3.2 and 3.3) and the development of a daily processing script (Version 1.0 and 2.0), which now enable automated daily processing with GAS, were given. This includes details of the newly developed reporting tools, i.e. the cleaning, network, post–processing and combination report, which were introduced to help in the quality assurance of the increasing amount of GPS data being processed as part of the UK 25 CGPS station network. Finally, the newly developed scripts and tools for the estimation of station velocities and their uncertainties, and the further analysis of coordinate time series were described.

Chapter 5

The UK CGPS Data Set

5.1 Introduction

In Chapter 3, the use of GPS to monitor vertical land movements at tide gauge sites has been introduced. Initially, this was carried out using EGPS campaigns, with stations occupied simultaneously at selected UK tide gauge sites and a number of European fiducial sites part of the evolving IGS network (Beutler, 1996a; Beamson, 1995). Prompted by advances in GPS, several EGPS stations have since been *upgraded* to CGPS stations, i.e. CGPS@TG stations (Teferle, 2000; Bingley et al., 2001a). Although the author has actively participated in further EGPS campaigns in 1999 and 2002, this thesis only deals with the CGPS stations.

This Chapter will introduce the UK CGPS stations for which data in the form of RINEX format observation files are held at the British Isles GPS archive Facility (BIGF) (`http://www.bigf.ac.uk/` (Dodson et al., 2000)) located at the IESSG. It is shown, how the quality of the data for each CGPS station is investigated at the archiving stage and after the initial stages of GPS processing, i.e. pre–processing stage (§4.2.1).

Special site investigations were carried out at four stations for which the author identified problems in the quality of the observations. These were by no means fully comprehensive site investigations, more an initial attempt to identify the source for the degradation in the CGPS observations. As is shown, several other stations may also have multipath

or interference problems, however, further investigations at these are beyond the scope of this work and are recommended for future work.

5.2 The CGPS Stations

As mentioned in §3.2.1 the use of CGPS@TG stations was initially recommended by Carter (1994). It was then suggested to establish CGPS stations at a global network of core tide gauges sites, which would be further densified using EGPS campaigns. Following these recommendations, the IESSG and POL have so far installed seven CGPS@TG stations throughout the UK in the period from March 1997 until September 2001.

For the installation of the CGPS@TG stations the main criteria was to include the sites with the longest tide gauge MSL records. Additional aspects, e.g. national flood defence requirements also influenced the decision of where the CGPS stations were to be placed. A CGPS station basically consists of a GPS antenna, a geodetic monument and a continuously operating GPS receiver, connected to a modem and telephone line for remote access. Once a tide gauge site was selected, a suitable location for the GPS antenna had to be identified. Suitable sites for tide gauge measurements are often far from optimal for GPS measurements, as will be demonstrated later (see §5.3.3), but the requirement was for the GPS antenna to be as close as possible to the tide gauge, i.e. within a few metres of the tide gauge itself, and still in a location suitable for GPS. In order to attach the GPS antenna to a stable structure and to define a geodetic reference mark for the CGPS station, site–specific monumentation was manufactured and mounted in each chosen location. The continuously operating GPS receiver also requires secure housing with restricted access, mains power and access to a telephone line. However, by locating the antenna and monument as close as possible to the tide gauge, the receiver could be housed in the same building as the tide gauge.

The seven CGPS@TG stations that have been established are situated near the tide gauges at Sheerness, Aberdeen, Newlyn, Liverpool, Lowestoft, North Shields and Portsmouth. In March 1997 the first of these CGPS@TG stations became operational at Sheerness. A stainless steel bracket, which is attached to the concrete roof of the

single–storey, brick tide gauge building, holds the GPS antenna. The building is located in the Sheerness docks area on a small pier, with piled foundations. The second CGPS@TG station was established in Aberdeen and became operational in September 1998. At this site, a 4 m high carbon fibre pole, with stainless steel ends, holds the GPS antenna. The pole is located adjacent to the tide gauge building and attached directly to the concrete pier. This pier is situated in the busy harbour area of Aberdeen. The third CGPS@TG station was set up at Newlyn and like Aberdeen also became operational in September 1998. At this site, the GPS antenna is mounted on a 3 m high carbon fibre pole, with stainless steel ends, which is attached to a lighthouse observation platform, 5 m above the base of the tide gauge building, which is located on a *well–founded* pier. A fourth CGPS@TG station was installed at Liverpool tide gauge in February 1999. At this site, a stainless steel bracket, which is attached to a 3 m high concrete wall, located on the same pier as the tide gauge building, holds the GPS antenna. The Lowestoft CGPS@TG station also became operational in February 1999. At this site, the GPS antenna is mounted on a 1 m high carbon fibre pole, with stainless steel ends, which is attached to a stainless steel bracket fastened to the side of a two–storey brick building. This building is located adjacent to the tide gauge building, which is close to the sea entrance to the docks. In May 2001 the CGPS@TG station in North Shields became operational. In this case, it was possible to directly use the antenna mount which had already been in place for the EGPS measurements in 1999 (Bingley et al., 2001a). The GPS antenna sits on a 4 m aluminium pole which pierces the roof of the tide gauge building and is bolted to the concrete floor. The tide gauge building itself is positioned on the quayside. Finally, in September 2001, the last CGPS@TG site was established in the Portsmouth Royal Naval Base. There, the tide gauge is situated on a recently constructed quay with piled foundations, which is adjacent to the old quay on which the newly constructed single–storey brick building that houses part of the tide gauge instrumentation is located. As it was not feasible to place the GPS antenna close to the quayside, it was fixed to the wall beneath the apex of the building using a steel bracket. Due to the antenna's proximity to the Historic Naval Base, the radome had to be painted black. Whether this will have an effect on the GPS observations cannot completely be excluded.

Another tide gauge of interest for this research is situated in Brest in France. The French Institut Géographique National (IGN) established a CGPS@TG station there in 1998. The CGPS station is part of the EUREF Permanent GPS Network (EPN) and daily RINEX format observation files can be obtained freely from the IGN FTP–site. The antenna is set on a metallic pillar approximately 1 m above a hemispheric bronze bolt, which is cemented into a terrace which is built directly onto metamorphic bedrock (Nicolon, 2002). From the analysis of the coordinate time series of the CGPS@TG station in Brest it is hoped to get a picture of the cross–channel differences in vertical land movements in order to compare the tide gauge records of Newlyn and Brest. Also of interest are the large OTL displacements at Brest(§3.4.4), which are comparable to the ones observed across the Channel in Southwest England. For comparison with other analyses, the improved EUREF (European Reference System) weekly time series *for geokinematics* for BRST obtained from the EPN website (`http://www.epncb.oma.be`) is included as Figure B.1 in Appendix B.

Besides the CGPS@TG stations described above, a number of other CGPS stations were established in the UK during the period of March 1997 to September 2001, of which it was planned that their monumentation would allow scientific investigations into recent vertical land movements of the UK.

One of these CGPS stations, at approximately 100 km distance from the North Sea, is at Nottingham and is owned by the IESSG. This station was established in April 1997 and the antenna is mounted using a stainless steel rod, bolted onto the wall on the top of the turret. It is hoped that although the building only stems from the mid–nineties and may still undergo some settlement, that the turret, which is founded on the underlying sandstone, would provide a stable location for high precision CGPS measurements. For the current CGPS network analysis carried out by the author, this station is used as the base station (4.2) from which all GPS baseline vectors to the other CGPS stations are formed.

Simultaneous with the commencement of the CGPS station at the IESSG, two additional CGPS stations were established along the River Thames. These two and the above mentioned CGPS@TG station at Sheerness formed a network of reference stations for the

monitoring of regional ground level changes in the Thames Estuary and Greater London (Booth, 2000). The GPS antenna at Sunbury Yard is mounted onto a carbon–fibre pole with stainless steel ends, which in turn is mounted, using a stainless steel bracket, to the wall of a two–storey brick building which is built on alluvial deposits of the Thames River, comprising of silt, clay and peat overlying sub–alluvial gravel, which in turn rests on London Clay (Booth, 2000). The second CGPS station is situated on the roof of the West Tower of the Barking Barrier and is mounted using a stainless steel bracket. The barrier is operated by the Environment Agency (EA) and protects the inner city of London from flooding due to storm surges pushing up the Thames Estuary. The foundations of the barrier are piled down to Upper Chalk and therefore should exhibit a high degree of stability (Booth, 2000).

In Chapter 7, the *dual–CGPS* station concept is introduced, consisting of two CGPS stations relatively close by. At Newlyn and Lowestoft tide gauge sites, it has been possible to test this approach using other CGPS stations established near to these sites. These stations are part of a network established by the UK Meteorological Office (Met Office), primarily for the estimation of integrated water vapour (Baker, 1998). Four CGPS stations were installed at radiosonde sites, shortly before the establishment of the initial CGPS@TG stations and a further three CGPS stations were installed in 2000 and 2001. All seven GPS antennas were mounted on 1.8 m high carbon fibre poles, with stainless steel ends. These poles were then attached to sub–surface concrete blocks that reach 2 m deep into the ground. Of these seven CGPS stations, one is located at Camborne, which is about 20 km away from Newlyn, and one was located at Hemsby, which is about 24 km away from Lowestoft. Therefore the CGPS stations at Camborne and Newlyn and the CGPS stations at Hemsby and Lowestoft form the station pairs according to the dual–CGPS concept. Unfortunately in Spring 2001, the Met Office site at Hemsby was abandoned and hence the operation of the CGPS station stopped. A third CGPS station of the Met Office is located on the Shetland Islands. This CGPS station is about 5 km from the tide gauge at Lerwick, were an EGPS station exists. Another Met Office CGPS station is in Aberystwyth, which is the only CGPS station situated in Wales that has been analysed in this research. The CGPS stations at the Met Office sites at Dunkeswell, Hurn and Pershore have been established over the last two years with Pershore now using the GPS receiver

and antenna from the abandoned CGPS station at Hemsby. All three CGPS stations are situated inland with Pershore being the furthest from the coast at approximately 40 km from the upper Bristol Channel and over 130 km from the Irish Sea. Dunkeswell is south west of Taunton and about 40 km inland of both the Bristol Channel and the English Channel. The CGPS station at Hurn is at Bournemouth Airport which is just 8 km from the English south coast.

The longest CGPS station operational in the UK is the IGS station at the National Environment Research Council (NERC) Space Geodesy Facility at Herstmonceux Castle. The site at Herstmonceux has a state-of-the-art satellite laser ranging (SLR) station and in 1992 a CGPS station was established in the grounds of the castle a few metres from the SLR system (Wood, 2000). From a British Geological Survey map (BGS, 1979) showing the solid geology, it can be seen that the area around Herstmonceux can be attributed to Lower Cretaceus[1] Hastings Beds. A reconnaissance by the British Geological Survey at the Herstmonceux facilities in 1997, suggests that the area of the grounds is covered by Tunbridge Wells Sand and is just south of a (non–active) fault passing the site in north easterly direction. SLR data from Herstmonceux are used by the IERS in the realization of the ITRF (§3.3.2). Furthermore, GPS station coordinates and velocities are computed as part of the analysis of the EUREF and IGS networks. The improved EUREF weekly time series for geokinematics, the global JPL coordinate time series and the global SOPAC (Scripps Orbit and Permanent Array Center) coordinate time series for HERS are given in Figures B.2, B.3, and B.4 in Appendix B, respectively.

Station coordinates and velocities in the ITRS are also available for a second IGS station, which has been operational at the National Physical Laboratory (NPL) in Teddington, Greater London since 2000. Here, the GPS antenna is mounted in the north east corner of the liftshaft of a building. NPL uses the CGPS data mainly for time transfer applications (Shemar, 2001). For NPLD, the improved EUREF weekly time series for geokinematics and the global JPL coordinate time series are included in Appendix B, i.e. Figures B.5 and B.6 respectively.

[1] Geological time period between approximately 140 to 98 million years before present.

The Department of Geomatics of the University of Newcastle has been operating a GPS station in Morpeth since 1996 (Blewitt et al., 1997). The GPS antenna is directly placed on top a single quarried rock, i.e. a *menhir*, which weighs 4.5 t, is 2.4 m high and 1.5 m wide at the base. Due to its trapezoidial shape it converges to about 0.7 m at the top. The menhir was placed in a 2.4 m deep hole extending about 0.4 m into the sandstone bedrock (King, 2002) so that its top is flush with the ground. It was believed that this would reduce local environmental effects, such as multipath. Whether this assumption holds will be examined in this analysis. During the period of writing this thesis, MORP was established as the third UK based IGS station, however, currently only data from September 2002 onwards has been analysed in the EUREF and IGS analyses. For convenience, this development has not been reflected in this thesis and the CGPS station at Morpeth remains assigned to station category OTHER (see §4.5.2).

Figure 5.1 shows the 21 CGPS stations introduced above of which data is held in BIGF. The continuously operating GPS receivers use a 5° elevation mask, store the raw GPS data at 30 seconds recording interval and, depending on CGPS station in either 1–hour or 24–hour data files. For the CGPS stations that are operated by the IESSG, these files are then downloaded automatically either hourly or on a daily basis via standard telephone lines and the data is converted into RINEX format observation files and archived. A detailed description of these procedures can be found in Booth (2000). Table 5.1 shows the 4–char Station IDs for each CGPS station archived and analysed. Further indicated are which stations are co–located with tide gauges, the ownership of the GPS equipment and information on the automated data transfer.

Table 5.2 shows the start dates for the CGPS station data holdings in the data processing archive `procarch` (§4.3.1). The dates are listed in years plus day–of–year (DOY) and in GPS week plus the day of the week (DOW). The table also states the total observation length (TOL) in years.

A more detailed description of the data holdings in the data processing archive `procarch` (§4.3.1) is included on the CD–Rom in directory `Procarch_Reports`, which contains the content files for each station category and year.

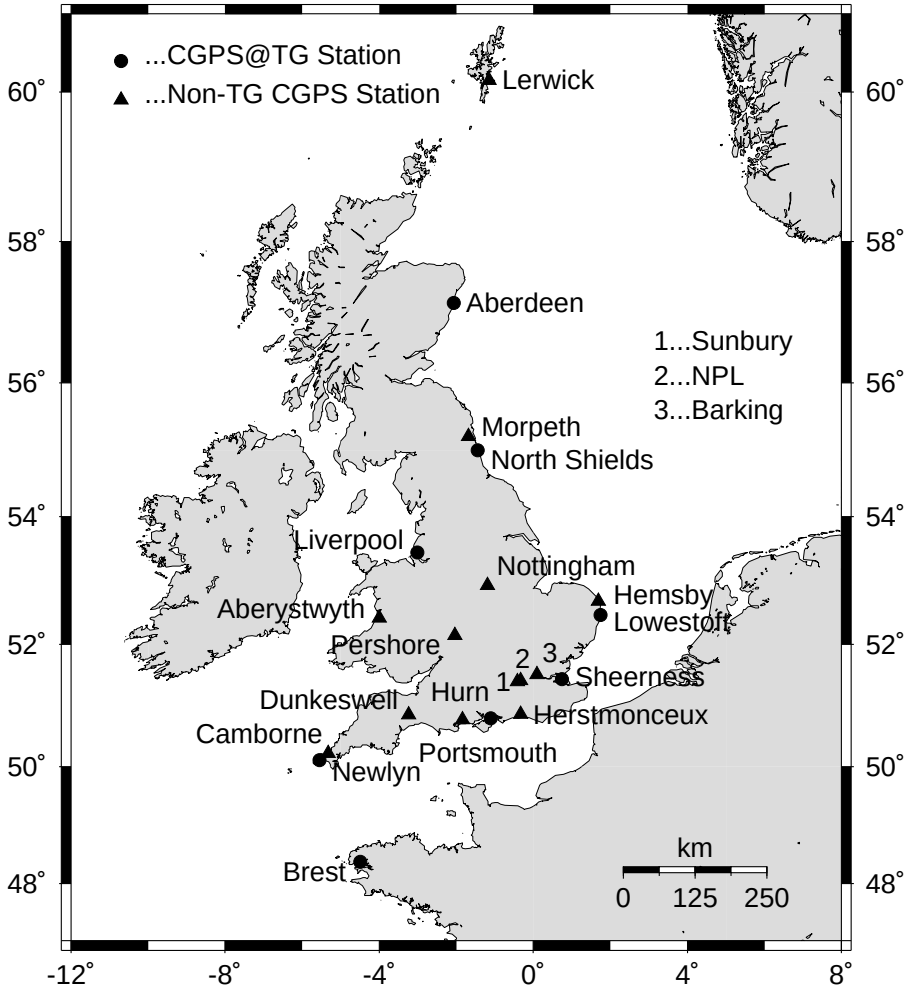

Figure 5.1: Continuous GPS (CGPS) network analysed up to 31 May 2002

Table 5.1: Summary for the continuous GPS (CGPS) stations archived and analysed for vertical land movements. Also shown are the agencies owning the stations and the mode in which the data is currently transferred to the archive.

Station Location	Station ID	@TG	Owner	Data Transfer
Sheerness	SHEE	•	EA[a]	daily (telephone)
Aberdeen	ABER	•	IESSG[b]/ POL[c]/ DEFRA[d]	hourly (telephone)
Newlyn	NEWL	•	DEFRA	hourly (telephone)
Liverpool	LIVE	•	DEFRA	hourly (telephone)
Lowestoft	LOWE	•	DEFRA	hourly (telephone)
North Shields	NSTG	•	NCL[e]/ DEFRA	hourly (telephone)
Portsmouth	PMTG	•	DEFRA	hourly (telephone)
Brest	BRST	•	IGN[f]	daily (FTP)
Nottingham	IESG		IESSG	hourly (telephone)
Sunbury Yard	SUNB		EA	daily (telephone)
Barking Barrier	BARK		EA	daily (telephone)
Camborne	CAMB		MO[g]	hourly (telephone)
Aberystwyth	ABYW		MO	hourly (telephone)
Lerwick	LERW		MO	hourly (telephone)
Hemsby	HEMS		MO	N/A
Dunkeswell	DUNK		MO	hourly (FTP)
Hurn	HURN		MO	hourly (FTP)
Pershore	PERS		MO	hourly (FTP)
Herstmonceux	HERS		NSGF[h]	daily (FTP)
Teddington	NPLD		NPL[i]	daily (FTP)
Morpeth	MORP		NCL	daily (FTP)

[a] Environment Agency (EA)
[b] Institute of Engineering Surveying and Space Geodesy (IESSG)
[c] Proudman Oceanographic Laboratory (POL)
[d] Department for Environment, Food and Rural Affairs (DEFRA)
[e] Department of Geomatics, University of Newcastle (NCL)
[f] Institut Géographique National (IGN)
[g] UK Meteorological Office (MO)
[h] National Space Geodesy Facility (NSGF)
[i] National Physical Laboratory (NPL)

Table 5.2: CGPS station start dates, data holdings and total observation length (TOL) within data processing archive `procarch` (§4.3.1). Date information is shown in year, day–of–year (DOY), GPS week, and day–of–week (DOW).

Station Location	Station ID	Year	DOY	GPS Week	DOW	TOL (Years)
Sheerness	SHEE	1997	085	0898	3	5.2
Aberdeen	ABER	1998	261	0975	5	3.7
Newlyn	NEWL	1998	273	0977	3	3.7
Liverpool	LIVE	1999	035	0995	4	3.3
Lowestoft	LOWE	1999	044	0996	6	3.3
North Shields	NSTG	2001	135	1114	2	1.0[a]
Portsmouth	PMTG	2001	268	1132	2	0.7
Brest	BRST	1999	096	1004	2	3.2
Nottingham	IESG	1997	117	0903	0	5.1
Sunbury Yard	SUNB	1997	098	0900	2	5.1
Barking Barrier	BARK	1997	115	0902	5	5.1
Camborne	CAMB	1998	099	0952	4	4.1
Aberystwyth	ABYW	1998	100	0952	5	4.1
Lerwick	LERW	1998	108	0953	6	4.1
Hemsby	HEMS	1998	100	0952	5	2.8[b]
Dunkeswell	DUNK	2000	036	1047	6	2.3
Hurn	HURN	2000	257	1079	3	1.7
Pershore	PERS	2001	129	1113	3	1.1
Herstmonceux	HERS	1997	119	0903	2	5.1
Teddington	NPLD	2000	229	1075	3	1.8
Morpeth	MORP	1996	305	0877	4	5.6

[a] Excluding episodic and quasi–continuous GPS data from 1998–2000

[b] Ended on 2001 JD 026, Week 1098 DOW 5

5.3 Quality of the CGPS observations

In Chapter 3 the author argued that monitoring of vertical land movements at the 1 mm/yr level using GPS remains a challenge that cannot easily be achieved at the moment. One strategy in support of this aim is to collect and analyse any additional site–specific information from which conclusions with respect to e.g. station motion may be drawn. An integral part of this task is associated with checking and monitoring the quality of the GPS observations collected at each station on a daily basis. As has already been mentioned in Chapter 4, the author has included several reporting mechanisms in the automated procedures. Here, the author has developed further tools to carry out the quality check at two levels. Firstly, at the archiving stage; this is carried out without any GPS processing and uses only the archived RINEX format observation files and the broadcast ephemeris. Secondly, after the pre–processing stage (§4.2.1); by investigating the distribution of the σ_0 of the residuals of the ionospherically free observable. Below follows a brief description on how the author has achieved both tasks.

5.3.1 Quality–checking at the archiving stage

In Chapter 4 the Processing Data Archive `procarch` was introduced and discussed. It is this archive that holds the RINEX format observation files for all stations analysed by the author. The automated procedures, which update the contents of the archive on a daily basis was discussed in §4.3.1. Additionally to the management of the data flow, it is important that the quality of the data in the daily RINEX format observations file are routinely checked.

Since 1996, the University Navstar Consortium (UNAVCO) located in Boulder, Colorado, has developed TEQC (**t**ranslate, **e**dit and **q**uality **c**heck), the multi–purpose toolkit for GPS/GLONASS data (Estey and Meertens, 1999). This tool is now widely used in the community and allows for a quick and easy check of the quality of GPS/GLONASS data. The IGS uses TEQC in this *QC mode* to carry out quality–checks on all archived data (`http://igscb.jpl.nasa.gov/network/list.html`) based on the TEQC summary files which are then also archived. From these files, several important parameters can

be extracted, which can be monitored and thus give evidence of the quality of the raw GPS data. A similar but simpler method, which has been implemented by the author to monitor the CGPS data quality in the Processing Data Archive `procarch` at the IESSG, is described.

The TEQC QC mode allows to process static and kinematic dual–frequency GPS and GLONASS data and can be invoked from the command line on numerous different platforms, e.g. Unix or Windows, allowing a fully automated quality check (Estey and Meertens, 1999). A result of the QC–run is a TEQC summary file or S–file, from which it is possible to extract several parameters describing the quality of the GPS data in the supplied RINEX format observation file. If a RINEX format navigation file or the broadcast ephemeris are included in the execution of TEQC, then the TEQC summary file also includes satellite and satellite elevation dependent quality statistics. Furthermore, TEQC is capable of computing the total number of possible observations for a specific site. Besides this, several parameters from those S–files have been identified as important statistics for monitoring the quality of the GPS data captured at any one site.

The time line window length (below denoted as time window length) is computed from the time of start of window and the time of end of window, i.e. the start and end times of the data contained in the RINEX format observation file. During normal operation, this should be a value close to 24 hours for daily RINEX format observation files. The S–files also contain the total number of satellites for which observations have been found in the RINEX format observation files and the number of complete observations above an elevation of 10°. By inclusion of the RINEX format navigation file or the broadcast ephemeris, TEQC is capable of computing the number of possible observations above the elevation of 10° for a particular station and day. Monitoring of these parameters on a daily basis therefore allows identification of problems at sites, which may show in a reduced number of observations while the total number of tracked satellites or possible observations remain unchanged. Using a 30 second data recording interval over a 24 hour period, will, depending on the elevation mask, result in approximately 20,000 or more observations. Two important statistics obtained from TEQC are the RMS values of the detrended estimates of the P–code multipath on the two GPS carrier signals L1 and L2 (Estey and Meertens, 1999). Monitoring changes in these RMS MP1 and MP2

values allows to identify small changes in the multipath or generally the electromagnetic environment of the antenna. Another statistic used to monitor the quality of the raw GPS data, is the ratio of the number of slips due to rapid changes in the ionospheric advance or changes in the multipath estimates above an elevation of 10°, with the number of complete observations above an elevation of 10°. For convenience, these ratios can be scaled by 1000 in order to arrive of values between 0 to 10.

Using TEQC in QC mode, the 25 CGPS station network has been quality–checked in automated mode for data archived from 1997 to present. This network included all of the UK stations described in §5.2 and the four IGS stations Kootwijk (KOSG), Onsala (ONSA), Wettzell (WTZR) and Villafranca (VILL), which have been used by the author in this analysis to define the reference frame (§4.2.3).

Figure 5.2 shows the *Daily TEQC Summary Plot* for CGPS@TG station ABER. The figure contains the station name, the receiver and antenna types copied from the RINEX format observation files, the last plot day and the date and time at which the figure has been created. In the top window, Figure 5.2 shows the time window length in hours, the second window shows the number of satellites (Max Sats), for which observations have been found and the number of complete observations above an elevation of 10°. The third window then contains the daily RMS MP1 and MP2 values and the bottom window the ratio of the number of slips, multiplied by 1000 and divided by the number of observations. This window may also include vertical lines indicating documented changes of the antenna and receiver configurations according to the IGS site information log files.

From Figure 5.2 it can be seen that the time window length indicates that there are no real problems with obtaining the full 24–hour observation files on a daily basis. From the total number of complete observations in window two and the RMS MP1 and MP2 statistics in window three, a jump in early 2001 is evident. Special site investigations, discussed below in §5.3.3, revealed that this site was affected by radio frequency (RF) interference prior to April 2001. As the RF interference problem was resolved, the number of complete observations increased and the RMS MP1 and MP2 values decreased to the level generally observed for this type of receiver and antenna (`http://igscb.jpl.nasa.gov/network/dataplots.html`). Interestingly, from the bottom window it is indicated

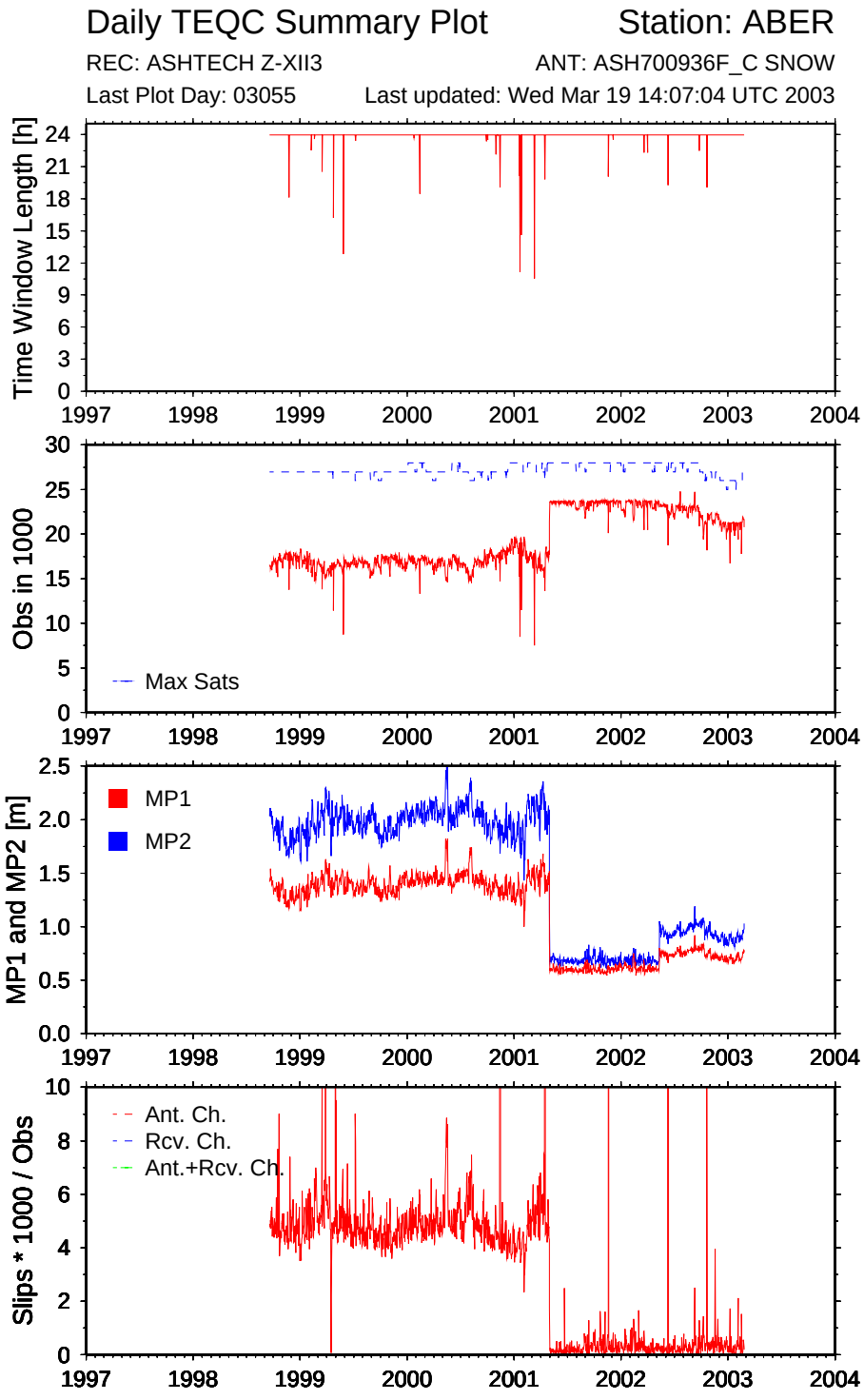

Figure 5.2: Daily TEQC Summary Plot for ABER. Station–specific antenna (Ant. Ch.), receiver (Rcv. Ch.), or antenna and receiver (Ant.+Rcv. Ch.) changes are shown as vertical dashed lines in the bottom frame if applicable.

that there was approximately one slip for every 100 observations for the period up to early 2001. Since early 2002, there is unfortunately the suggestion of another step in the RMS MP1 and MP2 statistics. Based on this, the author suggests this to be investigated.

The Daily TEQC Summary Plots for ABYW, MORP and NSTG have been included as Figures C.1, C.2 and C.3 in Appendix C, as these are referred to during the site specific investigations carried out at these stations (see §5.3.3). All other Daily TEQC Summary Plots can be found on the CD-ROM in directory `/Daily_TEQC_Summary_Plots`.

5.3.2 Quality–checking after the pre–processing stage

In Chapter 4 the automated procedures for GPS processing with GAS were introduced. The procedures can basically be divided into three stages, i.e. the pre–, network–, and post–processing stage. On a daily basis, each stage is carried out sequentially and is managed by the daily processing script `dailyproc.pl` (§4.5). As the script runs through the three stages, mechanisms were introduced to produce reports that summarize the results of each stage. Hence, by checking these reports, it is possible to assess whether a day of GPS processing was successful or not.

A good indication of whether the pre–processing stage, which carries out cycle slip detection and correction on a baseline per baseline basis, was successful, are the σ_0 of the carrier phase residuals. These are given for L1 and L2 and for the carrier phase linear combinations of L0 (ionospherically free) and L3 (wide lane) (Stewart et al., 2002). As discussed in §4.5, a report of the pre–processing stage is formed by retrieving the σ_0 of the L0 residuals from the station dependent slip files for each cleaned session and day. These cleaning reports have been arranged according to the classification of the CGPS stations, e.g. CGPS@TG stations, IGS stations, stations owned by the Met Office (MO) and other (OTHER) stations.

The results of the σ_0 of the L0 residuals can be summarized in histograms showing the frequency in % of an incident that a L0 σ_0 falls into a certain bin with a width of 0.5 mm. Figure 5.3 shows the histograms for the CGPS@TG stations ABER, BRST, LIVE, LOWE, NEWL, NSTG, PMTG and SHEE analysed up to 31 May 2002. Each figure contains the

histogram of the σ_0 for the specified CGPS station and an average histogram, based on the σ_0 of the L0 residuals of all stations in the network (excluding ABER and NSTG). It can be seen that the quality of the CGPS observations for NSTG is compromised. A more detailed description of the problems observed at this station and problems with radio frequency (RF) interference at ABER follows in §5.3.3.

Most histograms in Figure 5.3 show the mode for σ_0 in the range of 6 to 7.5 mm, which resembles the graph for the average histogram. The histogram for BRST seems to fit this average histogram the best, most σ_0 values for this station are in the range of 6 to 7 mm and the graph follows the average for σ_0 up to 10 mm. The modes obtained for LIVE, LOWE, NEWL and PMTG are at 6.5, 6.5, 7 and 5.5 mm respectively, showing that the data of PMTG can be cleaned more efficiently. This is good news with respect to worries that the black radome (local site specifications required the radome to be black) might affect the GPS observations. For SHEE, the histogram is a little different, with values spread over the whole range from 6 to 10 mm, maybe indicating that the data quality achieved at this station is slightly less than average. From the Daily TEQC Summary Plot for SHEE included on the CD-ROM it can be seen that for the initial observation period during 1997, the RMS statistics of the MP1 and MP2 values were raised. Although these values abruptly improved in November 1997, their magnitudes remain larger than those for comparable stations.

Figure 5.4 shows the histograms of the σ_0 of the L0 residuals for the IGS stations HERS, KOSG, NPLD, ONSA, VILL, and WTZR. Each graph shows the histogram of an individual station compared to the average histogram. From Figure 5.4 it can be seen that the data for HERS and WTZR have been cleaned to an average level with ONSA and NPLD being slightly better and KOSG and VILL being slightly worse than the average.

The histograms of the seven CGPS stations at the Met Office (MO) sites, i.e. ABYW, CAMB, DUNK, HEMS, HURN, LERW, and PERS are shown in Figure 5.5. Again, the individual histograms are compared to the average histogram. From this comparison, it can be seen that the quality of the GPS observations at ABYW is degraded. For a closer inspection of the circumstances that lead to the bad data quality see §5.3.3. For all other Met Office CGPS stations the σ_0 of the L0 residuals are better than average. At this point

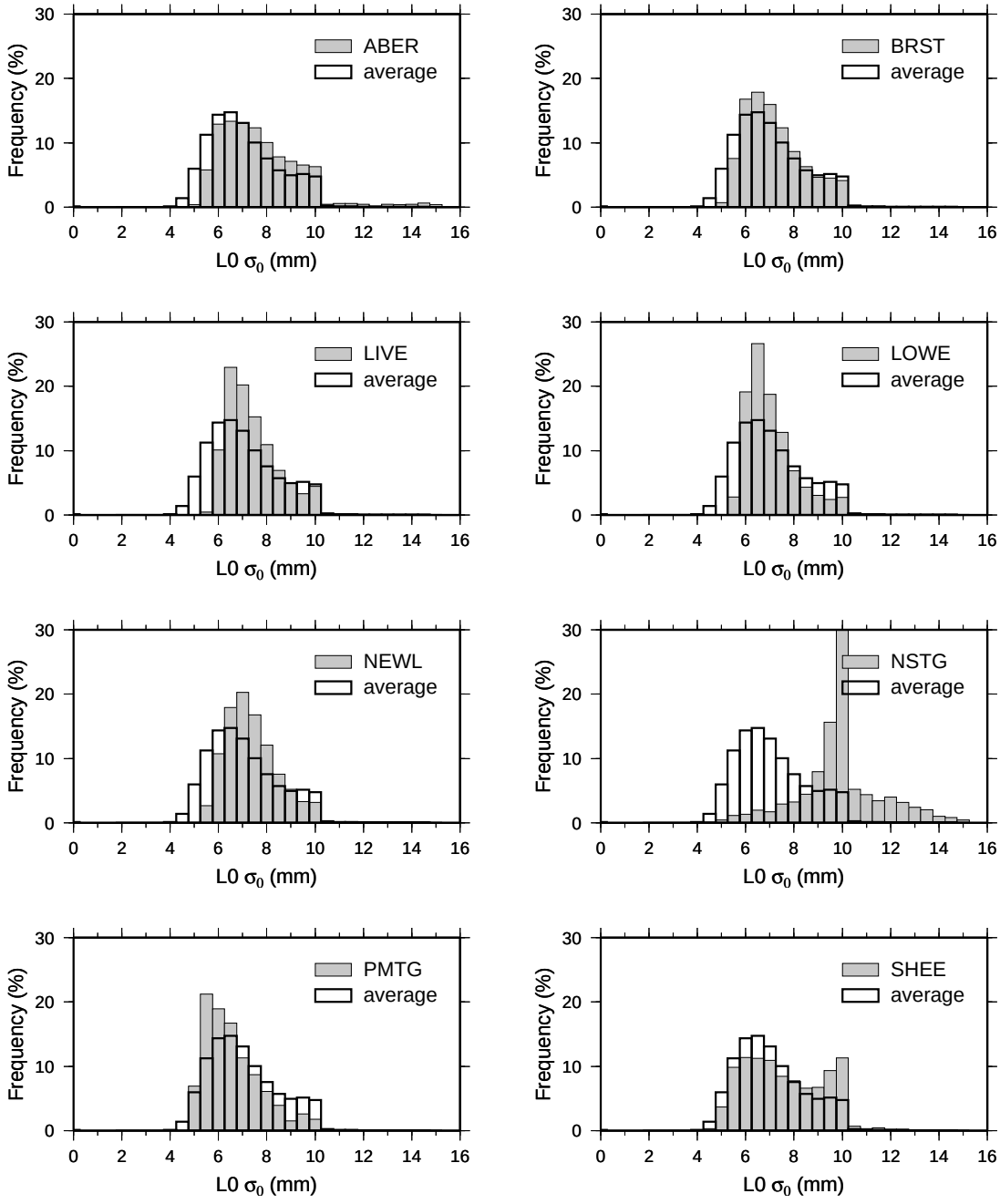

Figure 5.3: Frequency of the σ_0 of the L0 residuals for the CGPS@TG stations analysed until 31 May 2002.

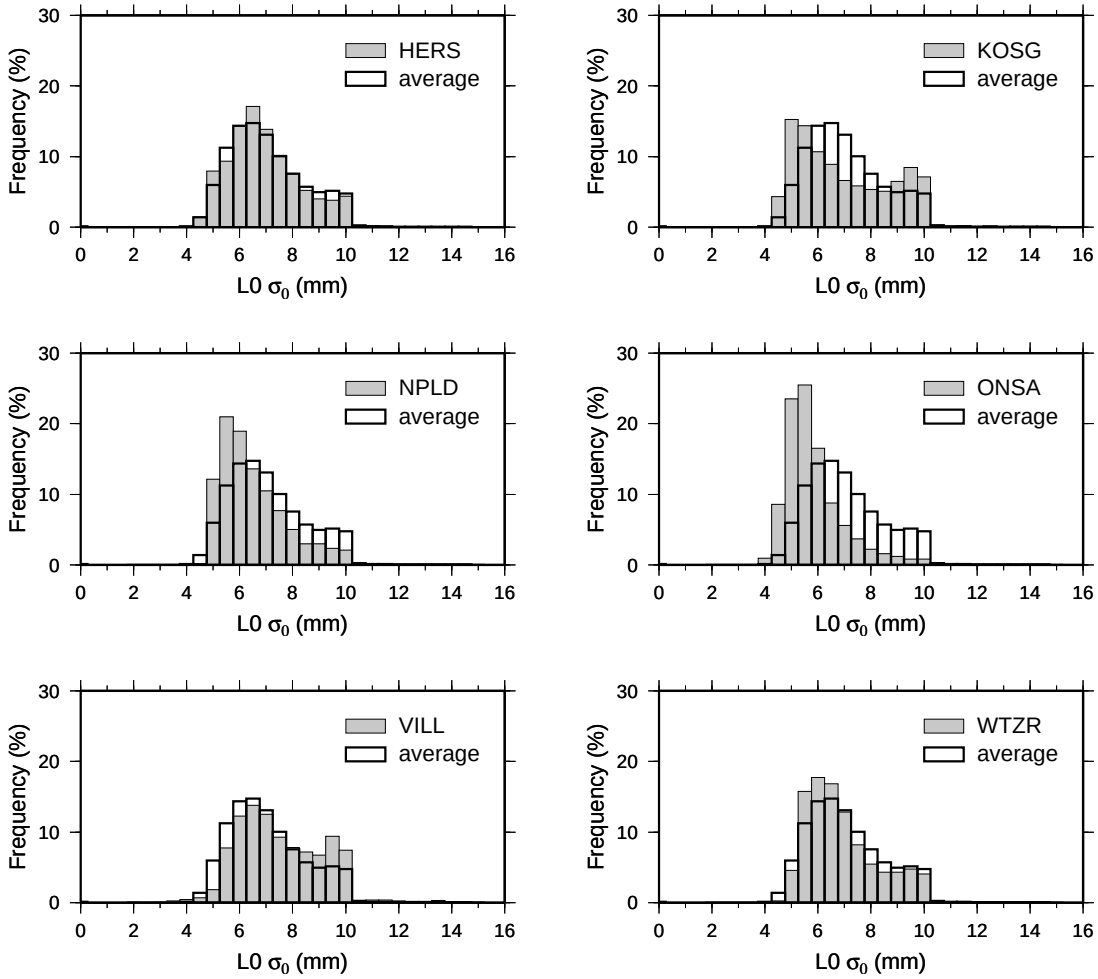

Figure 5.4: Frequency of the σ_0 of the L0 residuals for the IGS tracking stations analysed until 31 May 2002.

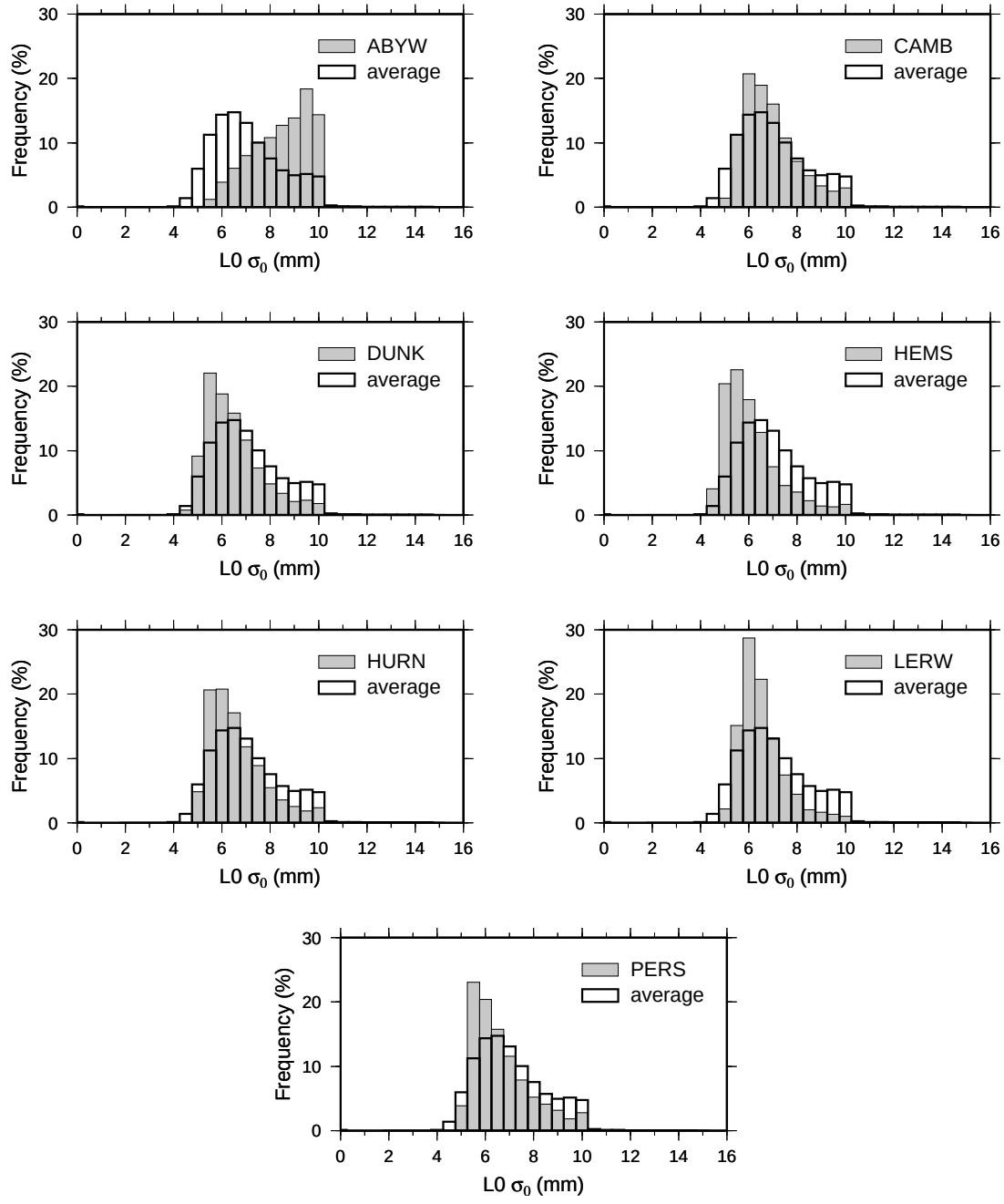

Figure 5.5: Frequency of the σ_0 of the L0 residuals for the UK Met Office CGPS stations analysed until 31 May 2002.

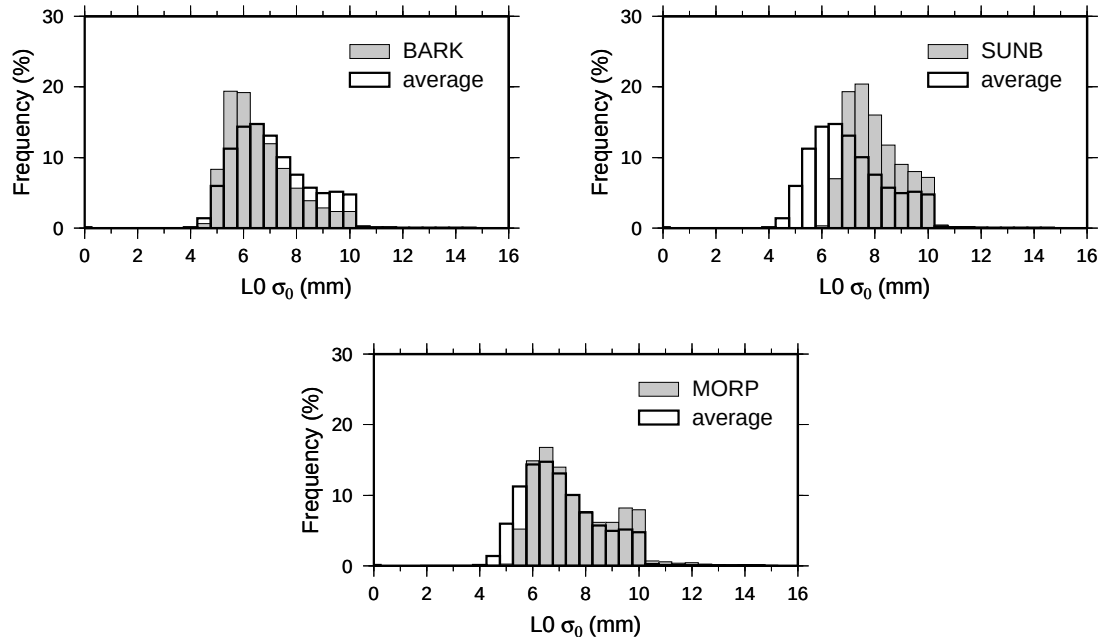

Figure 5.6: Frequency of the σ_0 of the L0 residuals for CGPS stations belonging to category *OTHER* analysed until 31 May 2002.

it should be noted that these sites are all situated in an *open* environment with few or no obstructions above the antenna horizon and the GPS antenna mounted 1.8 m above the ground (§5.2).

The histograms of the other CGPS stations BARK, SUNB, and MORP are shown in Figure 5.6. Although BARK seems to be cleaned more efficiently than the average, SUNB and MORP do show a slightly worse distribution. The GPS antenna at Sunbury is located just above the apex of the roof of a two–storey brick building (§5.2) close to a telecommunications tower. The degradation effect observed at Morpeth may be attributed to the fact that the GPS antenna is mounted just above ground level and GPS signals may be obstructed by a wooden fence (§5.3.3).

Besides the cleaning reports, which show the σ_0 of the L0 residuals, a summary file for each CGPS station is produced containing station dependent statistics (§4.5). These station statistics files have been included on the CD–Rom and can be found in station specific directories under the directory tree `/GPS_Processing_Reports/Preprocessing_Stage`. A summary of the station statistics is shown in Table 5.3. The table shows the

Table 5.3: Statistics for daily CGPS observations cleaned until 31 May 2002.

Station ID	ANOADRD	ANOSFRD	TNODC	[%]	TNOSC	[%]	Mean σ_0 [mm]
IESG	1835	7340	1835	100.0	7337	100.0	
SHEE	1795	7180	1771	98.7	7012	97.7	7.62
ABER	1348	5392	1333	98.9	4335	80.4	7.72
NEWL	1308	5232	1302	99.5	5157	98.6	7.37
BRST	908	3632	882	97.1	3324	91.5	7.19
LIVE	1207	4828	1200	99.4	4752	98.4	7.39
LOWE	1200	4800	1193	99.4	4730	98.5	7.04
NSTG	584	2336	563	96.4	1795	76.8	9.89
PMTG	220	880	218	99.1	839	95.3	6.60
KOSG	1834	7338	1799	98.1	6988	95.2	6.99
ONSA	1802	7208	1770	98.2	6973	96.7	5.83
VILL	1757	7028	1702	96.9	6367	90.6	7.55
WTZR	1848	7392	1817	98.3	7019	95.0	6.92
HERS	1580	6320	1555	98.4	6101	96.5	6.97
NPLD	621	2484	620	99.8	2439	98.2	6.51
CAMB	1499	5996	1486	99.1	5748	95.9	6.91
ABYW	1453	5812	1445	99.4	5659	97.4	8.44
HEMS	1017	4068	1009	99.2	3990	98.1	6.11
LERW	1496	5984	1486	99.3	5774	96.5	6.55
DUNK	770	3080	766	99.5	2962	96.2	6.49
HURN	469	1876	467	99.6	1776	94.7	6.62
PERS	376	1504	375	99.7	1472	97.9	6.65
SUNB	1792	7168	1767	98.6	6983	97.4	8.03
BARK	1693	6772	1668	98.5	6578	97.1	6.61
MORP	904	3616	860	95.1	3000	83.0	7.59

actual number of available daily RINEX data (ANOADRD) files, the actual number of sessions from RINEX data (ANOSFRD), when the daily files are separated into four 6–hour sessions, the total number of days cleaned (TNODC), which is the total number of days for which at least one 6–hour session was cleaned, the total number of 6–hour sessions cleaned (TNOSC), and the mean σ_0 of the L0 residuals from the sessional slip files.

For most stations the total number of days cleaned is above 98% and the total number of sessions cleaned is above 95%. This discrepancy in the percentage for days and sessions cleaned arises from the fact that theoretically only one session per day needs to be cleaned in order for a day to be classed as cleaned. Table 5.3 suggests that only five of the

twenty four CGPS stations show lower than average data quality. The lowest percentage for the TNOSC are shown for ABER and NSTG with 80.4 and 76.8%, respectively. The circumstances, which lead to the poor results for both stations will be discussed in detail in §5.3.3. The statistics for BRST show that only 91.5% of all sessions were cleaned effectively. This cannot be explained at the moment. Although, the histogram in Figure 5.3 does not indicate any problems at this site, the statistics do point to difficulties in the cycle slip detection and correction phase. During the period from 1999 to 2002, several problems at this station were reported which lead to the exclusion of data from BRST in the EUREF analysis (EPNCB, 2002a). From the cleaning reports for CGPS@TG stations, it can be seen that for several instances, the processing scripts could not clean data from this station prior to or after periods excluded from the EUREF analysis. Another station with bad performance is MORP. Although the station has been in operation since late 1996, it has only recently been made a CGPS station with a designated receiver. From the table it can be seen that for the ANOADRD of 904, the TNODC and TNOSC were 95.1 and 83.0% respectively. At this stage it needs to be mentioned that these statistics have been affected by the large number of days for which less than 24 hours of data are available due to the fact that the receiver was temporarily removed.

One way to investigate the σ_0 of the L0 residuals further, is to plot the mean σ_0 of all cleaned sessions for each station against the distance from the base station, i.e. the baseline length. This should help to identify whether there is a correlation between the magnitude of the L0 residuals and the baseline length, but also whether GPS observations to stations with similar baseline lengths are noisier at CGPS@TG stations that are near to the coast. Figure 5.7 shows the mean L0 σ_0 over all cleaned sessions for CGPS@TG stations, IGS tracking stations, Met Office and other CGPS stations against the length of each baseline. Most baselines have a length of only a few hundred kilometres, only baselines to the IGS stations on the European continent reach 1000 or more kilometres. From Figure 5.7 it may be concluded that with the exception of NSTG and ABYW, as a group, CGPS@TG stations are slightly noisier than Met Office stations.

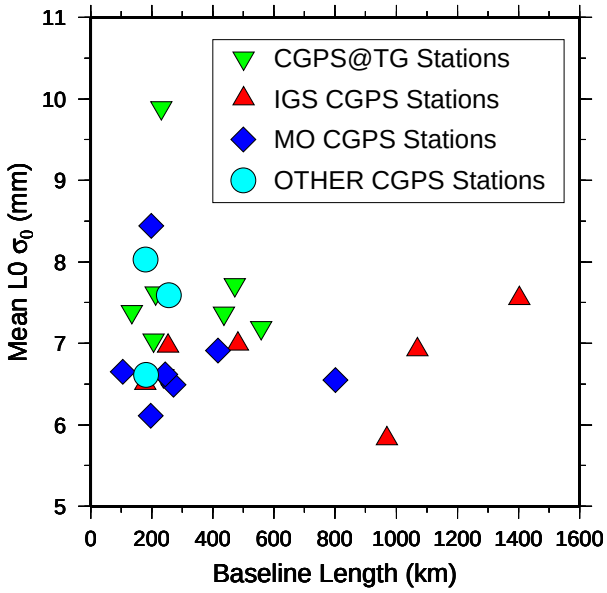

Figure 5.7: Mean σ_0 of L0 residuals against baseline length.

5.3.3 Special Site Investigations

As mentioned in Section 5.3 the CGPS@TG stations ABER (prior to 30 April 2001) and NSTG showed poorer performance when compared with other CGPS@TG stations in the UK, as evident from the Daily TEQC Summary Plots, the station statistics files and the σ_0 in the cleaning reports. Further investigations were, therefore, carried out at both CGPS stations in order to identify the causes for these degradations.

Based on the results for the standard ITRS2000 coordinate time series (see §6.3.1), the author decided to also carry out some initial tests in order to investigate the problems at ABYW and MORP.

CGPS@TG station ABER

From the initial results for the coordinate time series for ABER in late 1999, it was obvious that the site was exposed to radio frequency (RF) interference of some kind. However, a detailed investigation into the source of the observed interference was only carried out in late 2000 and early 2001.

RF interference can seriously affect signal tracking in GPS receivers and numerous authors have investigated these effects and the susceptibility of GPS receivers to RF interference, especially on continuous GPS installations and in aviation (e.g. Johnson and Erlandson, 1995; Nisner and Owen, 1995; Butch, 1997; Sang and Kubik, 1997; Haddrell and Khawaja, 1998; Borza and Fejes, 1999; Jaksic, 2001; Butch, 2002; Clynch et al., 2003; Forssell and Olsen, 2003).

Basically, interference on GPS signals can be attributed to three different sources. Firstly, in–band RF interference, which includes harmonics, spurious and intermodulation products falling in the nominal GPS band segments of 1565–1586 MHz. Secondly, out–of–band RF interference, which is due to powerful signals near the nominal GPS bands strong enough to overcome the receiver's passive RF filtering, and thirdly physical interference. Physical interference includes multipath, shadowing, terrain masking and other interference caused by the physical environment (Johnson and Erlandson, 1995).

When the CGPS@TG station was established in Aberdeen in 1998, it was not obvious that this site was affected by RF interference and only during the initial analysis of coordinate time series in 1999 (Teferle, 2000), was it noticed that the day–to–day scatter of the coordinate time series for station ABER was comparably larger than that for other CGPS@TG stations in the UK.

The Aberdeen Port Authority requires current tide gauge measurements on its survey vessel in order to carry out hydrographic surveys within the harbour area. These tidal measurements are constantly transmitted via a radio link from the tide gauge building to the vessel. Although the radio transmitter is a widely used standard radio transmitter with a frequency of 460 MHz and a nominal transmitting power of 0.5 Watts at the radio antenna, it was suspected that this was the source of the RF interference at the GPS antenna, due to its proximity. The transmitting radio antenna is situated on a lamp pole adjacent to the back of the tide gauge building approximately 5 m away from the CGPS choke ring antenna. Furthermore, although the CGPS antenna is approximately 0.7 m above the roof of the building, it is approximately 1 m below the radio antenna.

The apparent RF interference at the CGPS antenna at ABER revealed itself through the fact that observations were missing from the RINEX observation format files for epochs

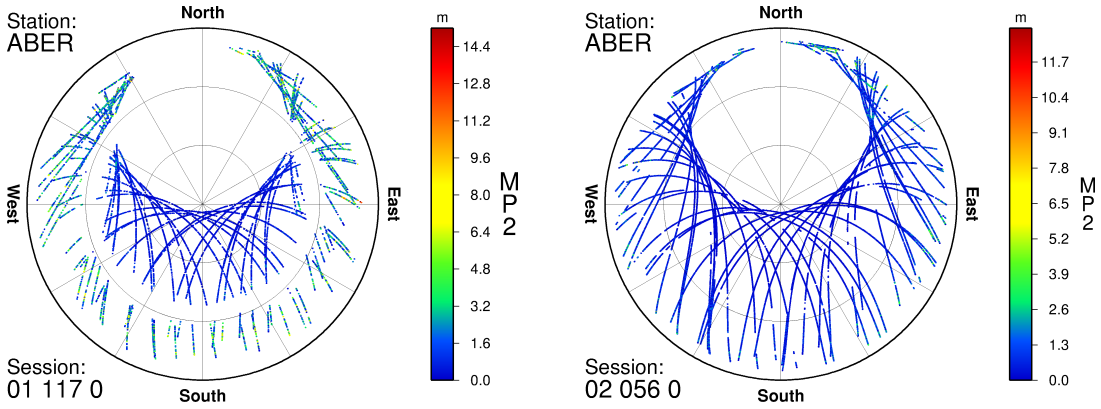

(a) with RF interference

(b) without RF interference

Figure 5.8: Skyplots of the estimated P–Code multipath on L2 (MP2) for ABER for 27 April 2001 and 25 February 2002 (i.e. with and without RF interference)

when satellites were passing through an elevation of approximately 30 to 40°. Figure 5.8a shows a skyplot of the P–code multipath on L2 (MP2) computed using TEQC (Estey and Meertens, 1999) for ABER for the 27 April 2001. Clearly visible is the elevation band where the GPS receiver could not track the GPS signals due to interference. By comparison, Figure 5.8b shows the skyplot of MP2 values for a day in 2002 after the source of interference was removed. Using the MP1 and MP2 values from TEQC has proven to be very efficient in identifying possible problems at this GPS site (see Figure 5.2). Based on the experience of the author with using Ashtech Z–XII receivers, the expected RMS statistics for the MP1 and MP2 values should be between 0.5 and 0.6 m for good CGPS stations. As was shown in Figure 5.2 this was not the case for the period prior to April 2001.

In order to clearly identify the source of the experienced RF interference at the CGPS@TG station in Aberdeen, observations with a Hewlett Packard Spectrum Analyser 8591E and a wide–bandpass Horn antenna, both borrowed from the School of Electrical and Electronic Engineering at the University of Nottingham, were carried out in early 2001. Similar instrumentation was previously used for RF interference investigations at GPS sites in Hungary as described by Borza and Fejes (1999). Figure 5.9 shows the wide–bandpass Horn antenna, which is specified to allow detection of signals of frequencies up

Figure 5.9: Wide–bandpass Horn antenna on quayside in front of tide gauge building in Aberdeen Harbour

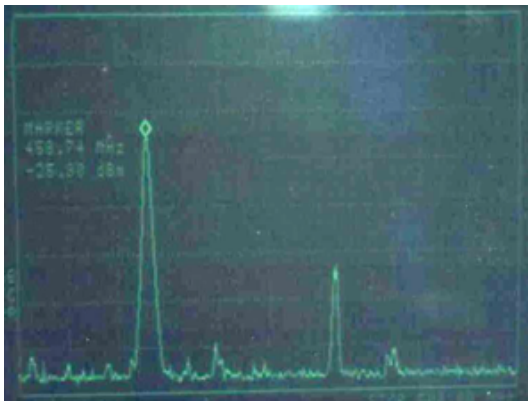

Figure 5.10: Radio frequency (RF) signal spectrum displayed by spectrum analyser at the CGPS@TG station in Aberdeen Harbour

to 2 GHz and Figure 5.10 shows a view of the display of the spectrum analyser, which can detect frequencies in the range from 9 kHz to 1.9 GHz.

No pre-amplifier was used in connection with the Horn antenna. The antenna pattern of the Horn antenna is furthermore directional so that the azimuth of arriving radio signals can be determined. The Horn antenna was set up on the roof of the tide gauge building beside the CGPS antenna, at which the RF interference was to be investigated. Then the antenna was stepwise turned horizontally and any significant peaks were noted. The main peaks displayed on the spectrum analyser remained the same across the horizon, however varied in signal strength. The dominant frequency in all directions was at 460 MHz, the frequency of the nearby radio transmitter. At a bearing of approximately 300°, the direction in which the radio transmitter appears from the CGPS antenna, the amplitude of this signal reached its largest level of -8.7 dBm. In other bearings, the amplitude was always below this value, but still dominated the spectrum. It was therefore assumed that the observed RF interference is out–of–band and purely caused by the power level of the locally transmitted radio signal.

Tests with additional GPS receivers and antennas set up on the roof of the tide gauge building showed that raising the GPS antenna above the level of the transmitting radio antenna reduced if not completely removed, the RF interference. Based on these

conclusions, the Aberdeen Port Authority was informed and it was planned to raise the GPS antenna of the CGPS@TG station. However, at the same time a service of the radio antenna was carried out, as it was noticed that the data transfer success rate of the radio link dropped from about 99 to 90% (personal communication with the Hydrographic Surveyor of the Aberdeen Port Authority). After the serviced antenna was re–installed on 29 April 2001, a quality test of the GPS data collected at ABER showed no signs of RF interference.

Interestingly, similar problems have recently been reported by Clynch et al. (2003) for Moss Landing Harbour, California. A defective pre–amplifier in a commercially available television antenna exhibited unintended oscillations, which jammed the GPS signals received at the local differential GPS reference station and an area of approximately 1 km out at sea.

It must therefore be assumed that the radio transmitter at the tide gauge in Aberdeen created similar unintended oscillations at frequencies harmful for GPS, i.e. in–band–interference, rather than the initially suspected out–of–band interference.

Following the servicing of the radio antenna in Aberdeen, a re–analysis of the cleaning reports and the station statistic file for ABER were carried out based on data before and after 30 April 2001. Evidence for a degradation of the GPS signal is clearly visible when comparing the histograms of the σ_0 of the L0 residuals for ABER before and after 30 April 2001 (Figure 5.11). Furthermore, Table 5.4 shows the statistics for ABER until 31 May 2002, separated into periods before and after 30 April 2001. The degradation by RF interference until that day is obvious from the increase of the percentages for the TNOSC from 72.0 to 98.2% and the decrease in the mean σ_0 from 8.16 to 6.95 mm.

Table 5.4: Statistics for daily CGPS observations for station ABER cleaned until 31 May 2002.

Period	ANOADRD	ANOSFRD	TNODC		TNOSC		Mean σ_0
				[%]		[%]	[mm]
before 30 April 2001	952	3808	935	98.2	2743	72.0	8.16
after 30 April 2001	396	1584	395	99.7	1556	98.2	6.95

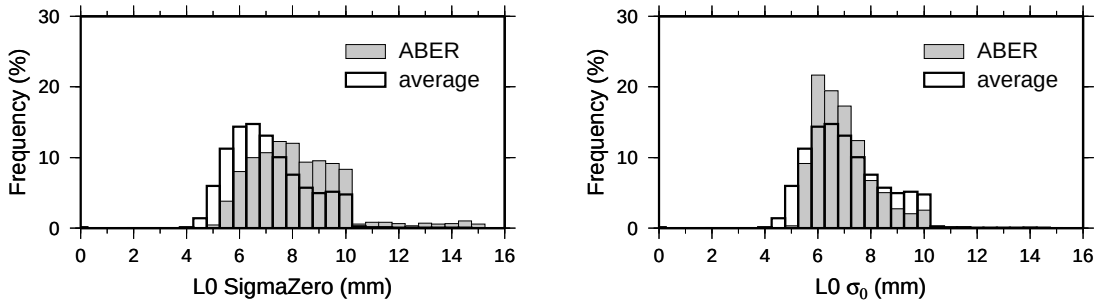

(a) Before 30 April 2001 (b) After 30 April 2001

Figure 5.11: Frequency of the σ_0 of the L0 residuals for ABER before and after 30 April 2001.

CGPS@TG station NSTG

GPS observations have been carried out at North Shields tide gauge by the Department of Geomatics at the University of Newcastle since 1998 in a quasi–continuous (Bevis et al., 1997) manner, with additional EGPS campaigns carried out by the IESSG in 1999. Since May 2001 the CGPS@TG station NSTG went on–line and data is now archived on a daily basis in the BIGF at the IESSG.

When analysing the GPS data for years 2000 and 2001 in the course of this research, it was noticed that the automated cleaning scripts had problems correcting cycle slips from the GPS observations and only a small number of sessions could be cleaned successfully. After some modifications were made to the code of the GAS processing module `filter`, it was possible to obtain a higher number of successfully cleaned sessions for the years 2000 and 2001. However, the problem was not completely resolved.

From investigations using TEQC and the Daily TEQC Summary Plot for NSTG shown in Figure C.3 in Appendix C, it was further discovered that GPS observations collected at the tide gauge in North Shields in December 1999 were of a high quality when compared to those collected from February 2000 onwards. Figure 5.12 shows skyplots of MP2 values for NSTG for 9 December 1999 and for 12 February 2000. Gaps in the MP2 tracks for each satellite for 12 February 2000 are clearly visible, when compared to the skyplot for 9 December 1999. These gaps are an indication of missing data in the RINEX observation format file for these epochs, as no MP2 value was computed by TEQC. However, both

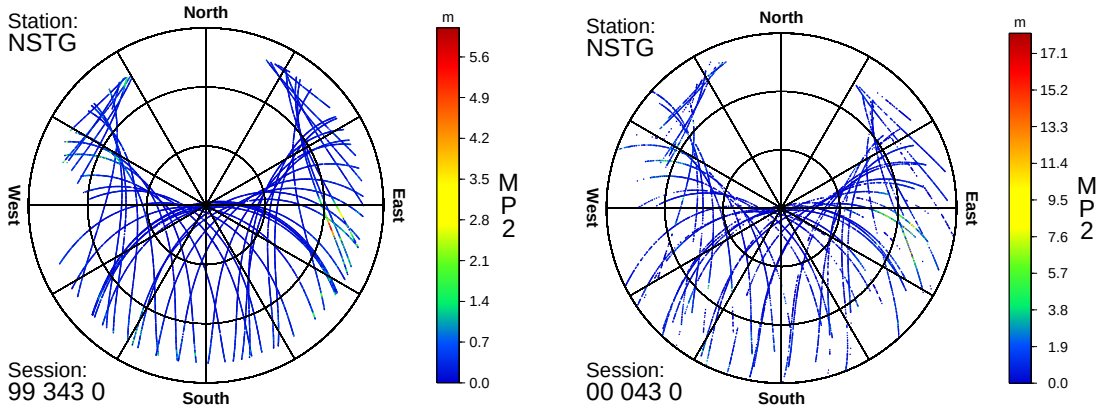

(a) 9 December 1999 (b) 12 February 2000

Figure 5.12: Skyplots of the estimated P–Code multipath on L2 (MP2) for NSTG for 9 December 1999 and 12 February 2000

graphs indicate that the GPS signals are obstructed from being received at the GPS antenna in a westerly direction as there are no MP2 values for this area on both skyplots. Furthermore, based on the MP2 estimates in both graphs, two areas of high multipath can be identified, independent of the quality of the GPS observations on both days. One area that is suggested to be affected is in a north–westerly direction from the CGPS antenna and can be identified by the change in colour of the MP2 values. The second high multipath area is in an easterly direction from the GPS antenna. When comparing the skyplots for both days, it can be seen that the range for the MP2 values also differs, i.e. 0 to approximately 6 m and 0 to approximately 17 m for the 9 December 1999 and the 12 February 2000 respectively.

Based on this, it was decided on 12 March 2002 to initially change the GPS antenna at the station in order to try to identify the source of the problem. The antenna swap proved to be unsuccessful, so the GPS receiver itself was changed on 4 April 2002. At the same time the old antenna was re–installed at the point. Initial tests with TEQC showed that the data quality was now comparable with other CGPS@TG stations. However, the magnitude of the MP2 values remains at a slightly higher than normal level due to the apparent multipath effects at this site. During April/May 2002 the CGPS receiver suspected to be faulty was repaired and was re–installed on 17 May 2002. After the analysis of the cleaning reports and the station statistics file for NSTG, it was, much to

Table 5.5: Statistics for daily CGPS observations for station NSTG until 31 May 2002.

Period	ANOADRD	ANOSFRD	TNODC		TNOSC		Mean σ_0
				[%]		[%]	[mm]
before 5 April 2002	529	2116	508	96.0	1611	76.1	9.72
5 April to 17 May 2002	42	168	42	100.0	147	87.5	11.46
after 17 May 2002	13	52	13	100.0	37	71.2	11.07

the disappointment of everybody involved, discovered that the problem with the CGPS receiver persisted (see Figure C.3 in Appendix C).

Table 5.5 summarizes the statistics for NSTG for the period prior to and since the recent investigations. Clearly indicated by the increase in the percentages for the TNOSC of 76.1 and 87.5% respectively, for the periods before 4 April 2002 and from 5 April to 17 May 2002, is the effect of the temporarily installed GPS receiver. Although the CGPS receiver of NSTG has been serviced by the manufacturer during April/May 2002, after its re–installation at the tide gauge, the percentage of the TNOSC dropped to 71.2%, a value comparable with the one prior to the investigations. An interesting fact however, can be seen in the increase of the mean σ_0 of the L0 residuals from 9.72 to 11.46 and 11.07 mm for the periods before, during re–placement and after the re–installation of the CGPS receiver at NSTG respectively, which will require further investigations. For now, it can only be concluded that due to the apparent multipath at North Shields, the older CGPS receiver cannot track satellites when their GPS signals are severely affected by multipath, whereas the more modern receiver, which was installed as a replacement between 5 April and 17 May 2002, seemed to continuously track satellites in view.

Although, these findings point to some problems with the receiver operating at NSTG, the jump in the RMS statistics for the RMS MP1 and MP2 values shown in Figure C.3 in Appendix C between December 1999 and February 2000 remains unexplained. In order to improve the results for the coordinate time series and the estimated station velocities, local interference investigations at NSTG are highly recommended for future work.

Met Office CGPS station ABYW

As outlined in §5.2, ABYW was established by the Met Office for the estimation of integrated water vapour (Baker, 1998) in 1998. From the histogram of the L0 σ_0 and the day–to–day scatter in the coordinate time series (§6.3.1) for this station, it is clear that the quality of the GPS data collected at ABYW is compromised. Using TEQC (Estey and Meertens, 1999), it was possible to investigate the pattern of the degradation observed in order to identify the source for this interference. Figure 5.13 shows skyplots of the estimated P–code multipath on L1 and L2 (MP1 and MP2) for ABYW for the 10 April 2002.

As can be seen from this figure, the MP1 and MP2 values are larger for the GPS signals to the north of the antenna, possibly indicating the direction of the source of the problem. As the GPS antenna is situated just south of the 110×110 m antenna array of the NERC Mesosphere–Stratosphere–Troposphere (MST) radar profiler (Met Office, 2002), it may be suggested as the source for the observed signal degradation.

The wind profiler is a 160 kW 46.5 MHz pulsed Doppler radar and is used for studies of atmospheric winds, waves and turbulence. Figure 5.14 shows the GPS antenna with the MST wind profiler in the background.

From Figure C.1 in Appendix C showing the Daily TEQC Summary Plot for ABYW it can clearly be seen that there seem to be no major problems with the data transfer or the number of complete observations. Even the RMS MP1 and MP2 values are only slightly larger than for comparable sites. Interestingly, there is a periodic pattern in the RMS MP1 and MP2 time series, which cannot be explained by the author at the moment, and which has not been found to that extent in any other station analysed. It is assumed by the author that the observed signal degradation is linked to the effect creating the periodicities in the estimated P–code multipath. This means that in order to identify the nature of the signal degradation, further investigations at ABYW are required.

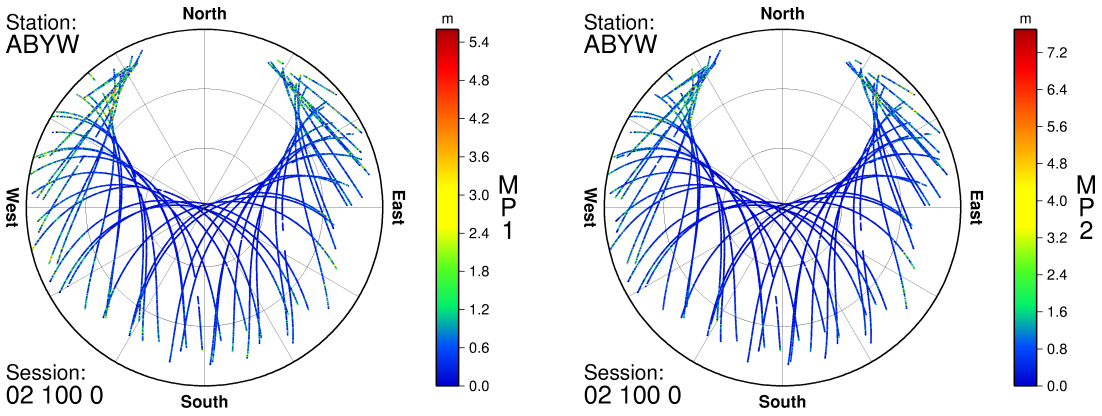

Figure 5.13: Skyplots of the estimated P–Code multipath on L1 (MP1) and L2 (MP2) for ABYW for 10 April 2002

Figure 5.14: GPS antenna at ABYW with antenna array of the NERC MST radar profiler in the background (Courtesy of the Met Office)

CGPS station MORP

From Figure 5.6 only, showing the distribution of the σ_0 of the residuals of the ionospherically free observable, there is little indication that there may be a problem at MORP. This view is however changed when inspecting the Daily TEQC Summary Plot for MORP given as Figure C.2 in Appendix C. Firstly, there seem to have been many days, which have less than 24 hours of data. It could be argued that this was due to the fact that the station was only operated sporadically and that there are many days were the receiver was switched off. From Figure C.2 it is however also shown that both RMS MP1 and MP2 values are slightly raised at the 0.8 m level and that there are a large number of cycle slips during 2000. Although, the ratio of slips per observations has visibly improved since operations started again in 2001, it is clear that the data observed at this site is degraded when compared with other stations.

As MORP is located in an open environment, RF interference as observed for ABER can be excluded as possible source for the signal degradation. It was therefore believed that the proximity of the antenna to the ground may have introduced multipath or some other signal scattering effect. However, recent events have showed that this assumption was incorrect. King (2003) reported of the introduction of a line amplifier, improving the signal to noise ratio at the GPS receiver. This change at MORP coincides with an abrupt change in the RMS MP1 and MP2 values in December 2002 in Figure C.2 in Appendix C. It is clearly visible that for the period since December 2002, the RMS MP1 and MP2 values have been around 0.5 m, close to the expected level using this receiver type.

This difference in the MP1 values before the introduction of the line amplifier and after can also be demonstrated using Figure 5.15. The figure shows the skyplots of MP1 values for MORP for 27 October 2002 and 30 December 2002. Gaps indicate epochs at which no MP1 values were computed due to the receiver not being able to track the GPS signals.

Clearly visible from Figure 5.15 are the differences in the tracking capability of the receiver due to the improved signal to noise ratio using the line amplifier. Especially at low elevations when the signal to noise ratio is normally the worst, the improvement for 30 January 2003 when compared with 27 October 2002 is evident.

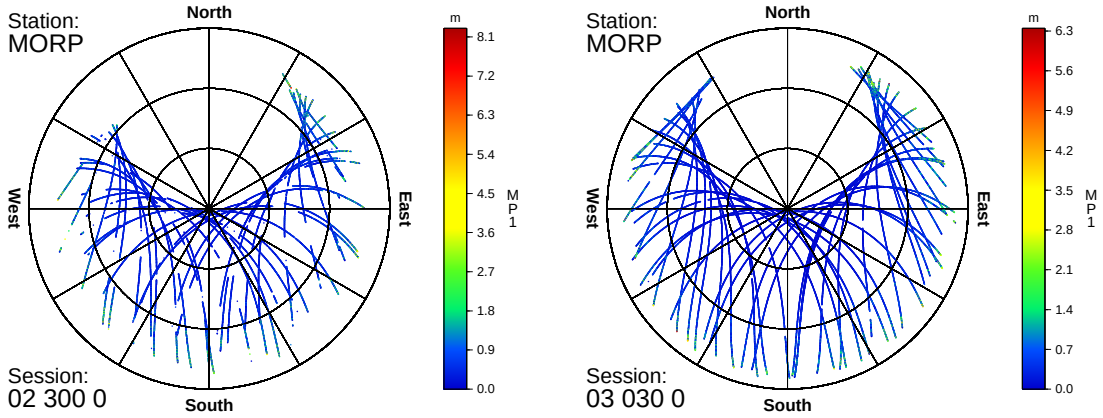

(a) 27 October 2002 (b) 30 January 2003

Figure 5.15: Skyplots of the estimated P–Code multipath on L1 (MP1) for MORP for 27 October 2002 and 30 December 2002

Although, the author has only used GPS data up to 31 May 2002 in his analysis, the improvement in the data quality for MORP will be of benefit for any future analysis in the sense of the envisaged sustainable geodetic monitoring approach (Blewitt et al., 1997).

5.4 Summary

This Chapter has introduced the UK CGPS data set available to the author for analysis. The data set includes 25 CGPS stations in the UK and Europe, with eight being co–located with tide gauges, and observation time spans ranging from 0.7 to 5.6 years with most stations having more than 4 years of observations. Some technical aspects of the installation of CGPS@TG stations have been discussed and all stations have been briefly introduced.

Using TEQC, the author has investigated several parameters useful for monitoring the quality of the raw data in the RINEX format observation files. This method does not require any GPS processing and can be carried out in automated mode on a daily basis for a GPS data archive such as BIGF. A second quality check is based on the σ_0 of the residuals of the ionospherically free observable after cycle slips have been detected and removed, i.e. the pre–processing stage (§4.2.1). Statistics for each CGPS station derived from the pre–processing stage have been presented.

Based on the findings from both quality–checks, and the standard ITRS2000 coordinate time series in Chapter 6, the author has carried out some special site investigations at ABER, NSTG, ABYW and MORP. These identified RF interference at ABER to be responsible for the signal degradation observed until April 2001. For NSTG, no final conclusion as to the source of the bad data has been made, although it is suspected that local multipath effects may be responsible for observed problems. No conclusions have been possible for ABYW, although there is the suggestion of possible interference with a wind profiler operated by the Met Office. For MORP, the inclusion of a line amplifier seemed to have solved the problems experienced, with the improved signal to noise ratio of the GPS signals at the receiver helping the tracking of satellites at low elevations.

Chapter 6

Analysis of the Continuous GPS Network

6.1 Introduction

Chapter 6 details the coordinate time series analysis strategies applied by the author to the 25 CGPS station network introduced in Chapter 5. The results obtained are discussed and several sets of vertical station velocities and uncertainties are derived for further analysis.

Standard coordinate time series obtained using automated coordinate time series analysis (§4.6) are investigated for two different GPS processing strategies and reference frames. Firstly, the effect of constraining one IGS station to its epochal coordinates during the GPS processing stage is discussed and secondly, standard coordinate time series computed based on two ITRS realizations, ITRF97 and ITRF2000, are compared.

Improved coordinate time series, which enable the estimation of more *realistic* station velocities and associated uncertainties are then discussed. These require the modelling of periodic signals and the identification of possible offsets in the coordinate time series. Using a regional filtering technique, the improved coordinate time series have then been filtered by removing a daily common mode bias.

The unfiltered and filtered improved coordinate time series have then been analysed in order to identify their noise characteristics. Using maximum likelihood estimation (MLE) the model parameters for a linear and annual term, the magnitudes of any coordinate offsets, the amplitudes for white and coloured noise and the spectral index have been estimated simultaneously for each coordinate time series.

6.2 Concepts and Methodologies

This section will introduce the concepts and methodologies applied in this part of the authors research. It will discuss the two GPS processing strategies used and investigate the reference frame dependency of the results. In order to arrive at improved coordinate time series, several station–dependent systematic effects, e.g. periodic signals, coordinate offsets and coloured noise, need to be accounted for in the coordinate time series analysis. Furthermore, the coordinate time series can then be filtered, to reduce global and regional systematic effects.

6.2.1 GPS Processing Strategies

In Chapter 4 the GPS processing stages using GAS and the procedures for automated processing were introduced. Using these, a 13 CGPS station data set was processed and analysed on a daily basis, using data up to September 2001. During the re–analysis of the data set archived in the processing data archive `procarch` (§4.3.1), this 13 CGPS station network was extended to a total of 25 CGPS stations, including additional data for several IGS stations for the period of 1997 to 1998. Both analyses differ slightly in the applied processing strategies, which have been denoted as *Strategy 1* and *Strategy 2* in this thesis.

For Strategy 1, the data for nine UK CGPS stations were processed along with data from four IGS stations in Europe, used as fiducial stations. The nine UK CGPS stations used were: Aberdeen (ABER), Camborne (CAMB), Hemsby (HEMS), IESSG (IESG), Lerwick (LERW), Newlyn (NEWL), Liverpool (LIVE), Lowestoft (LOWE) and Sheerness (SHEE) (see Tables 5.1 and 5.2 for information on station categories and data availability). The IGS stations used for this analysis were Kootwijk (KOSG), over the complete

timespan, Onsala (ONSA), Wettzell (WTZR), and Villafranca (VILL), for a limited time span from 13 September 1998 onwards.

As a result of the daily GPS processing, a series of *loosely constrained* daily GPS network solutions were obtained for the period up to 25 September 2001. In these solutions the final IGS precise ephemeris was held fixed and the coordinates for KOSG were *tightly constrained*. The coordinates of KOSG were taken from the same ITRF realization as the IGS precise ephemeris. In each case, the coordinates of KOSG were motioned to the observation epoch using the station velocity given in the appropriate ITRF realization. All of these loosely constrained daily GPS network solutions were computed using the ionospherically free double difference observable with integer ambiguities free and systematic error models for solid Earth tides (§3.4.4), ocean tide loading (§3.4.4) and antenna phase centre variations (§3.4.3). For the modelling of the hydrostatic zenith tropospheric delay, the Saastamoinen model (Saastamoinen, 1973) with the Niell dry mapping function (Niell, 1996) was used. The wet zenith tropospheric delay was then modelled as a random walk process (§3.4.2) with a process noise of $0.4\,\mathrm{cm}/\sqrt{hr}$, and mapped to the appropriate station to satellite elevation angle using the Niell wet mapping function, as previously described in Teferle et al. (2002a). Due to the application of the random walk process, it was not possible to fix the ambiguities to integers within GAS (Penna, 1997). Not fixing ambiguities to integer values has been reported to increase the formal errors by between 20 to 30% (Johansson et al., 2002). However, with a focus on the height component it was decided to accept the possible worsening of the solution caused by not fixing ambiguities in favour of the improvement in the height obtained from the refined tropospheric modelling.

In order to form coordinate time series for each station, the baseline vectors and associated variance-covariance information, obtained from each loosely constrained daily GPS network solution, are transformed to a common reference frame. To do this, in 1997 and partly 1998, the IGS station at KOSG was tightly constrained to its ITRF97 coordinates, motioned to the observation epoch. However, from 13 September 1998 onwards, a network of four European IGS stations, consisting of ONSA, KOSG, WTZR and VILL, was used in this transformation, with each station tightly constrained to its ITRF97 coordinates, motioned to the observation epoch. Hence, for each of the nine

UK CGPS stations, continuous daily coordinate time series were obtained in the ITRS97 (Teferle, 2000).

Panafidina and Malkin (2001) and Malkin and Voinov (2001) reported that the official EUREF weekly coordinate time series contain jumps and systematic seasonal errors, especially in the height component. It was reported that these systematic errors may have been caused by distortions of the reference frame caused by errors in the modelling of the movement of fiducial stations, if more than one fiducial station is used with tight constraints. Errors in the velocities of fiducial stations, e.g. peculiar station motion, local displacements or equipment changes, would result in errors distributed over the whole processed network. Furthermore, these distortions increase towards the edges of the network, especially if fiducial stations are concentrated near the centre of the network (Panafidina and Malkin, 2001). Their results from a re–analysis of selected EUREF stations showed that solutions based on a *non–fiducial* strategy (Blewitt et al., 1992; Heflin et al., 1992; Rius et al., 1995; Park et al., 2002) were most likely to be free of seasonal signals. In addition it was noted that, this non–fiducial strategy would also enable the EUREF weekly solutions to be transformed to any reference frame and re–transformed to another one using a much simpler procedure than that needed for removing constraints (Mareyen and Becker, 2000).

With the re–analysis of the 25 CGPS station network, including stations Aberystwyth (ABYW), Barking Barrier (BARK), Brest (BRST), Dunkeswell (DUNK), Herstmonceaux (HERS), Hurn (HURN), Morpeth (MORP), National Physical Laboratory (NPLD), North Shields (NSTG), Pershore (PERS), Portsmouth (PMTG), and Sunbury (SUNB), this non–fiducial strategy, was introduced such that no IGS stations were constrained at the network processing stage. This is referred to as Strategy 2 in this thesis.

The second major difference between Strategies 1 and 2, was that additional data for the IGS stations ONSA, WTZR and VILL for the period prior to 13 September 1998, were obtained in order not to change the processing configuration throughout the total observation period, thus reducing the possibility of offsets in the coordinate time series (see §6.2.4) for Strategy 2. Introducing the additional IGS station data also removed the need for the re–scaling of the daily standard errors prior to 13 September 1998 (§4.6).

With the introduction of Strategy 2 at the start of the re–analysis of the 25 CGPS station data set, the ocean tide loading (OTL) (§3.4.4) model was also updated, to the more recent FES99 (Lefèvre et al., 2001) as opposed to the FES94.1 (Le Provost et al., 1994). The OTL parameters for the FES99 model were obtained from Scherneck and Bos (2001) (see §4.3.3). With the introduction of the new model, it was also decided by the author to include modelling of the effect on the horizontal coordinate components, which was not carried out in Strategy 1.

6.2.2 Reference Frame Selection

At the post–processing stage, the non–fiducial daily GPS network solutions obtained using Strategy 2 are transformed to a common global reference frame (§3.3.2). As new realizations of the ITRS become available, e.g. ITRF94, ITRF96, ITRF97, ITRF2000, it is regarded as advantageous to use the latest realization, which can normally be assumed to be an improvement in absolute accuracy, as more data has been included in its computation, and the estimation methodology improved. During the period of the author's research, the ITRS realization ITRF2000 was published and on 2 December 2001 the IGS00 reference frame, which is aligned to ITRF2000 to within 2 mm, was adopted as the official reference frame for IGS products. The IGS uses this frame in order to ensure better internal consistency among the time series of the IGS products (Craymer and Piraszewski, 2002; Ferland, 2002). It was therefore decided, to base the coordinate time series of the re–analysed 25 CGPS station data set on both ITRF97 and ITRF2000, in order to evaluate the impact of the change in the global reference frame on the station velocities obtained for the CGPS network analysed.

Lavallée (2000) reported a 2 mm/yr error in the definition of the ITRF97 velocity origin and recommended that the ITRF origin be realized using geodetic means rather than the NNR NUVEL–1A definition (§3.3.2). This geophysical model does not fulfill the no net rotation condition of the reference frame with respect to the Earth's lithosphere, as it provides geological motions averaged over the past 3 million years, rather than present–day plate motions (Lavallée, 2000; Angermann et al., 2001). Furthermore, it only includes the rigid plates and not the plate boundary deformation areas. Angermann et al. (2002)

reported of a difference between ITRF97 and ITRF2000 in the definition of the frame origin of less than 1 cm for the translation in x and y and about 2 cm for z at the reference epoch 1997.0, with a rate difference of 2 mm/yr. The accuracy of the published ITRF2000 station coordinates and velocities are therefore believed to be about 2 to 5 mm and 1 to 2 mm/yr for the best stations. Obviously, due to the uncertainty in the velocity determination, coordinate errors will grow as the positions are extrapolated from the reference epoch (Willis and Morel, 2002).

6.2.3 Periodic Signals

Many of the biases and effects introduced in §3.4, potentially manifest themselves in GPS coordinate time series as cyclic signals with frequencies ranging from semi–diurnal to interannual or even decadal periods. Periodic signals in coordinate time series have been shown to affect the estimated station coordinate velocities (Blewitt and Lavallée, 2002) (see §6.3.1). As will be shown, many of the time series analysed in this thesis, contain significant variations with annual or nearly annual frequencies. Similar repeating signals in coordinate time series have also been reported, by e.g. Chen et al. (1996); Dixon and Mao (1997); Scherneck et al. (1998); Calais (1999); Mao et al. (1999); Braitenberg et al. (2001); Heki (2001); Kenyeres et al. (2001); Poutanen et al. (2001); Zerbini et al. (2001); Johansson et al. (2002); Kleijer (2002) and Vespe et al. (2002). In fact Herring and Springer (2002) stated that nearly all IGS stations show annual height variations.

Wdowinski et al. (1997) removed a *common mode bias* (§6.2.5) from their coordinate time series, thus indirectly removing the annual signal common to all sites. This approach has previously also been applied by the author to a set of UK CGPS stations (Teferle et al., 2002a). Mao et al. (1999) analysed a global data set and removed an annual sinusoidal signal in order to investigate the low–frequency content of their coordinate time series. A more complex approach was used by Scherneck et al. (1998) and Scherneck et al. (2002b) in that annual, semi–annual, ter–annual and quarter–annual sine and cosine terms were fitted to the coordinate time series, modelling the variations more closely to absorb some climatic influences, e.g. snow and ice depositions on the antenna or the radome (Jaldehag et al., 1996).

A long–term periodic signal of large amplitude with a period of about 450 days was reported by Calais (1999). Due to the fact that this period is not seasonal and that the signal was larger in the east–west component, he concluded that it was possibly due to errors in the reference frame, satellite orbit or Earth orientation. The source of the *common mode bias* was also attributed to this group of effects in Wdowinski et al. (1997). Scherneck et al. (1998) stated that long–term effects with annually repeating character may arise from residual perturbations due to the basic repeat cycle of the GPS satellite constellation. Herring and Springer (2002) stated that from comparison of GPS and VLBI coordinate time series, some part of the annual signals seen in GPS coordinate time series may be artefacts (possibly induced by orbit modelling errors that have annual modulation due to the orbital period of GPS satellites).

Poutanen et al. (2001) investigated periodic variations in the GPS baseline time series of the Finnish permanent GPS network (FinnRef) for periods from one day to one year. They concluded that some of these periodicities can be connected to physical loading effects (§3.4.4). Recently, Dong et al. (2002b) listed the contributions of geophysical sources and model errors to the observed annual vertical variations in global GPS station positions. For information, their findings are re–produced here in Table 6.1.

Dixon and Mao (1997) stated that errors in station velocities due to an annually repeating signal were minimal at integer years. This was shown to be false by Blewitt and Lavallée (2002). Based on a detailed review of this topic by Lavallée (2000), it can be concluded that the effect of annual variations on station velocities is smallest at *integer–plus–half* year observation spans and that coordinate time series of less than 2.5 years should not be analysed for geodetic interpretation. Furthermore, estimating the parameters describing a cyclic component simultaneously with a linear regression, using a least–squares model, can result in highly correlated parameters and was not recommended for coordinate time series shorter than 2.5 years. For a more detailed summary of their findings and the equations used by the author to compute the *velocity bias* or the associated velocity uncertainty, the reader is referred to Appendix F.

Modelling of an annual term along with a linear trend has been carried out for the improved coordinate time series (§6.3.3) and the noise analysis using MLE (§6.2.6). How-

Table 6.1: Contributions of geophysical sources and model errors to the observed annual vertical variations in station positions (Dong et al., 2002b)

Sources	Range of Effects
Pole Tide	approx. 4 mm
Ocean Tide	approx. 0.1 mm
Atmospheric Mass	approx. 4 mm
Non–tidal ocean mass	2–3 mm
Snow mass	3–5 mm
Soil moisture	2–7 mm
Bedrock thermal expansion	approx. 0.5 mm
Errors in orbit, phase centre and troposphere models	No quantitative results yet
Error in the network adjustment (network dependent)	approx. 0.7 mm
Differences from different software	some stations 5–7 mm

ever, following Lavallée (2000) the author did not attempt to analyse any of the coordinate time series for UK CGPS stations with time spans of less than 2.5 years.

6.2.4 Coordinate Offsets

Discontinuities in coordinate time series are generally termed coordinate offsets. Such offsets can be known or unknown in their magnitudes, the epochs at which they occurred and their causes. Except in the case of earthquakes, offsets in coordinate time series are generally undesirable and until recently, their effect on station velocities and uncertainties had not been investigated in detail (Williams, 2002).

The most obvious reason for coordinate offsets is due to movements of the CGPS stations. Earthquakes, are a common source for offsets in coordinate time series in seismically active areas, such as Japan, the USA or southern Europe, e.g. Feigl et al. (1993); Sagiya et al. (1995); Hudnut et al. (1996); Miyazaki et al. (1996); Bock et al. (1997); Langbein and Johnson (1997); Wdowinski et al. (1997); Hurst et al. (2000); Li et al. (2000), and Nikolaidis (2002). It is normally possible to correlate coordinate offsets with such events and hence the exact time of an offset can be established. However, besides these crustal movements, there is a range of other events that have been reported to cause coordinate offsets.

One of the most common causes for artificial offsets in GPS coordinate time series is due to changes of the GPS antenna or receiver configuration. Alterations at the antenna, removing and replacing the antenna temporarily or adding or removing a radome, can introduce coordinate offsets, e.g. Braun et al. (1997); Scherneck et al. (1998); Árnadóttir et al. (2000); Emardson et al. (2000); Schupler and Clark (2001); Bruyninx et al. (2002); Johansson et al. (2002); Kaniuth and Stuber (2002), and Vespe et al. (2002). Changes in the immediate environment can also introduce coordinate offsets. The most prominent offset in the EUREF weekly coordinate time series for HERS was observed in March/April 1999 and was attributed to partial GPS signal obstructions (Takacs and Bruyninx, 2001). More recently, Dong et al. (2002b) reported that the trimming of a tree to less than half height close to a GPS antenna caused an offset of 1 and 4 cm in the horizontal and vertical coordinate components, respectively. Ice or snow accumulation on antenna radomes have also been reported to cause jumps in the height time series of the SWEPOS network at the centimetre level (Jaldehag et al., 1996; Scherneck et al., 1998; Johansson et al., 2002). Additionally, vandalism at unsecure sites or errors in log files can also introduce or lead to discontinuities in coordinate time series (Williams, 2002). Some of these offsets may have small magnitudes and may therefore remain undetected, as it is often difficult to accurately correlate them with any specific event. Williams (2002) shows percentages of offsets with unknown causes of up to 66% for various published data sets and concludes that for these data there is on average one offset every nine years.

Careful logging of any changes at CGPS sites may help the identification of offsets. Therefore, the IGS and EUREF have made great efforts in documenting receiver and antenna changes at their CGPS stations in a consistent and appropriate way. Such *IGS Site Information Forms* are available for each IGS or EUREF station from any of the IGS or EUREF analysis centres. Such forms have been obtained from the IGN ftp site (`ftp://igs.ensg.ign.fr/pub/igscb/station/log/`) for stations BRST, HERS, KOSG, NPLD, ONSA, VILL and WTZR. At the IESSG, similar site information forms, are maintained for all of the UK CGPS stations analysed by the author. All recent site information forms, including those of the IGS and EUREF stations, are contained on the CD–Rom in directory `/Site_Information_Forms`.

Table 6.2: Antenna and receiver changes for UK CGPS stations in the period from March 1997 to May 2002

Site	Date	MJD	Detail
ABER	30–04–01	52029	RF interference resolved
HERS	21–03–99	51258	New signal obstruction (Takacs and Bruyninx, 2001)
	08–08–01	52129	Antenna re–mounted
IESG	09–03–98	50881	Antenna re–mounted
MORP	03–03–00	51606	Receiver changed
	12–03–02	52345	Antenna changed
	15–04–02	52379	Receiver changed
	20–05–02	52414	Receiver changed
NSTG	30–08–98	51055	Antenna and receiver changed
	04–12–99	51516	Antenna and receiver changed
	12–02–00	51586	Antenna and receiver changed
	09–05–01	52038	Antenna and receiver changed
	12–06–01	52073	Antenna changed
	13–03–02	52346	Antenna changed
	05–04–02	52369	Antenna and receiver changed
	18–05–02	52412	Receiver changed

From the site information forms of the UK CGPS stations, it can be seen that for most stations no receiver hardware, antenna or radome changes were reported for the observation period since 1997. For many sites, the only entry on the form was a receiver firmware upgrade in August 1999, which at this stage is believed to have not introduced any offsets. A summary of all other identified events that could cause a coordinate offset at a particular CGPS station can be found in Table 6.2. This table lists the dates, the Modified Julian Days (MJD) and the details of the changes documented in the site information forms.

Although, no physical change to the antenna at ABER was reported, it was assumed that due to the observed RF interference (§5.3.3) prior to 30 April 2001 the coordinate time series may have been offset. It was therefore decided, to test for a discontinuity in the coordinate time series for ABER on this date. The largest offset in all coordinate time series analysed is apparent at HERS on 21 March 1999, as shown in Figure 6.4 in §6.3.1 on page 168. This offset has already been mentioned and was reported to be due to a newly

introduced obstruction in the sky view of the GPS antenna. From the IGS site information form for HERS, it can be seen that on 18 June 2001 the antenna was mounted on an 8 m high, open lattice, cross–braced steel mast, but had to be sent away for repair after it was discovered that the antenna was faulty. When it was returned on 8 August 2001, it was re–mounted on the same mast. Hence, this date will also be used in this analysis for the estimation of coordinate offsets. For IESG, the site information forms state that on 9 March 1998 the GPS antenna was temporarily removed to enable spirit levelling of the survey marker on the turret of the IESSG as part of the EUVN97 GPS campaign (Ineichen et al., 1999). According to experiences by Scherneck et al. (1998) and Johansson et al. (2002) in the BIFROST project, it is very likely that this will have introduced a coordinate offset even though the antenna was re–mounted and orientated with uttermost care. Johansson et al. (2002) reported that offsets have been estimated every time antennas were removed and replaced for local stability surveys of their monuments. Changes of up to 10 mm in the estimated height have been attributed to tiny changes in the antenna orientation. At NSTG and MORP several changes have taken place. However, some details have unfortunately not been recorded and assumptions on the receiver or antenna configuration have had to be made. Some of the entries for NSTG can be associated with the recent investigations into the receiver problems at that site (§5.3.3).

Due to the network processing strategy applied in this research, i.e. the processing of the CGPS stations as radial baselines with respect to IESG, it may be assumed that discontinuities in the coordinates of the European IGS stations would definitely affect the results for CGPS station IESG, and possibly affect the results for all other stations in the network. Therefore, the author has compiled a list of antenna and receiver configuration changes for these IGS stations as documented in their IGS site information forms. Table 6.3 lists the date, the Modified Julian Day (MJD) and the details of the changes for the IGS stations KOSG, ONSA, VILL, and WTZR up to 31 May 2002.

Although the antenna and receiver configuration changes indicated in this table pose a possible source for discontinuities in the coordinate time series of these IGS stations, it is not possible to visibly identify them by inspecting the EUREF weekly coordinate time series obtained from `http://www.epncb.oma.be/series_sm.html`. Kenyeres (2002) reported that apart from the antenna and receiver change at ONSA on 2 February 1999,

Table 6.3: Antenna and receiver changes for European IGS stations used to define the reference frame in this analysis (KOSG, ONSA, VILL and WTZR) from March 1997 to May 2002

Site	Date	MJD	Detail
KOSG	01–Mar–99	51238	Receiver changed
KOSG	14–Jul–99	51373	Receiver changed
KOSG	24–Nov–00	51872	Receiver changed
KOSG	27–Nov–00	51875	Receiver changed
ONSA	02–Feb–99	51211	Receiver and antenna changed
VILL	29–May–01	52058	Receiver changed
WTZR			None reported

all offsets in Table 6.3 were small or undetectable and hence were not included in the EUREF analysis. The offset in the height time series for ONSA on 2 February 1999 was estimated to be about 11 ± 2 mm (Kenyeres, 2002).

In order to investigate the coordinate time series of the UK CGPS stations for any unknown coordinate offsets, a change detection algorithm (CDA) was used to scan the residual coordinate time series for any changes (see Appendix G). The algorithm assumes the coordinate time series to be a sequence of independent random observations with a certain standard deviation. By comparing the means computed for the coordinate time series prior to and after the investigated epoch, an unknown coordinate offset at this epoch can be estimated using a threshold value based on the standard deviation of the total sequence. Williams (2002) investigated the effectiveness of this algorithm and concluded that best results would be obtained in the middle of coordinate time series as the detection threshold was much lower. Based on simulated time series, he concluded that in order for the CDA to correctly estimate the epoch of an offset at the 95 or 99% significance levels, the discontinuity needed to be four or eight times the threshold value of the coordinate time series. Although, it is easier for the CDA to detect the correct offset epoch in the middle of the coordinate time series, this is the worst position in terms of the velocity uncertainty associated with the offset (Williams, 2002).

The Student's t–test (Eq. D.4 in Appendix D) allows for comparison of the means of two normally distributed data sets with the same variance. This test can be used to investigate, whether there is a statistically significant difference in the means for a period

before and after a suspected coordinate offset. Tests into whether a model including a parameter for a specific coordinate offset fitted to the coordinate time series, is statistically better than a model not including the offset can be carried out by means of the F–test (Eq. D.5 in Appendix D).

Using the documented epochs for possible coordinate offsets given in Tables 6.2 and 6.3, and those detected by the CDA, in connection with both statistical tests, the aim was to establish a list of epochs at which coordinate offsets should be estimated in the final analysis strategy.

6.2.5 Regional Filtering

Coordinate time series derived from daily solutions in regional GPS networks have previously been shown to contain large spatial correlations. Penna (1997) observed correlations in the measurements obtained at UK episodic GPS stations of up to 500 km. Calais (1999) showed that the coordinate time series of three CGPS stations in the Alps were highly correlated and Herring (1999) reported spatial correlations in the order of 60 to 70% for two IGS stations in Australia separated by 300 km. Spatial correlations in BIFROST have been reported to be in the order of 1000 km (Johansson et al., 2002). The characteristic of these correlations suggests a common source for this systematic effect, which has been attributed to reference frame or satellite orbit type biases (Wdowinski et al., 1997; Calais, 1999; Mao et al., 1999; Herring et al., 2002). It is believed that this *common mode bias* affects GPS observations in regional networks in a similar manner, e.g. by use of a common set of satellites in all regional stations, thus introducing the observed spatial correlations.

Several methods for a *spatial filter* in order to reduce the amount of correlation can be found in the literature. The method of *stacking* the daily residual was first introduced by Wdowinski et al. (1997). The coordinate time series of the then Southern California Permanent Geodetic GPS Array (PGGA) (now Southern California Integrated GPS Network (SCIGN) see `http://www.scign.org`) were filtered using this approach and it was possible to improve the signal–to–noise ratio in the data. The reduced RMS scatter of the coordinate time series provided much higher resolution for detecting transient signals on a site–by–site basis without having to fix the position of any site in the regional network.

This method has previously also been applied by the author to the preliminary height time series of a network of CGPS stations in the UK (Teferle et al., 2002a). A different method for reducing the global scale systematic bias in coordinate time series was presented by Herring et al. (2002). This approach is based on a local frame realization using stations in a 1200 × 1800 km region in the Tien Shan, Central Asia. In this study, the local frame was matched onto a frame based on Eurasian sites by rotation and translation. This reference frame was in turn defined by minimizing the velocities of these stable Eurasian sites Herring et al. (2002). The application of a local reference frame definition in order to remove the common mode bias from the GPS coordinate time series of a regional network has also been applied in the analyses of the SCIGN carried out by JPL (Hurst, 2000, 2001).

Using the *stacking method* (Wdowinski et al., 1997), the common mode bias can be computed as the mean of the coordinate residuals for a selection of stations on a particular day. Here it is important to note that Wdowinski et al. (1997) did not detrend the height time series prior to computing the common mode bias, as they were within their uncertainties. They also applied the algorithm separately for periods before and after an earthquake, and stations that were suspected of experiencing gradual displacements after the event, were not included in the stacking of the daily position components.

In this analysis, the author has applied an updated method for computing the common mode bias. Coordinate offsets, as determined in §6.3.3, have been used to correct for any changes in the coordinate time series and two sets of residual coordinate time series have then been generated, i.e. a trended and a detrended one. Based on the coordinate residuals $v_{i,s}$ of each station s for each day $i = 1, \ldots, N$ and the standard errors $\sigma_{i,s}$ of the coordinates, the following equation has been applied to estimate a common mode bias ϵ_i for each day (Nikolaidis, 2002):

$$\epsilon_i = \begin{cases} 0 & : \quad S_i(t_i) < 3 \\ \frac{\sum_{s=1}^{S_i} v_{i,s}/\sigma_{i,s}^2}{\sum_{s=1}^{S_i} 1/\sigma_{i,s}^2} & : \quad S_i(t_i) \geq 3 \end{cases} \tag{6.1}$$

with S_i being the number of available CGPS stations in the network per day. If $S_i < 3$, then no common mode bias was computed. In a second step, the daily, coordinate specific,

common mode biases are then subtracted from the raw coordinate time series y_i of all stations so that a spatially filtered coordinate time series $\tilde{y}_i$ is derived according to

$$\tilde{y}_i = y_i - \epsilon_i \tag{6.2}$$

These filtered coordinate time series then allow the estimation of the best fitting model parameters using least–squares. A new RMS statistic of the residual coordinate time series obtained at this stage can be computed and compared to the RMS statistic of the residual coordinate time series based on the unfiltered data. The amount of change in the RMS scatter can then be expressed in percent of improvement using the following ratio

$$\%\text{Improvement} = \frac{\text{RMS}_{unflt} - \text{RMS}_{flt}}{\text{RMS}_{unflt}}. \tag{6.3}$$

When computing the common mode bias using this method, several issues have been identified by the author. First, the reduction in the RMS scatter and hence the improvement of the signal–to–noise ratio is favourable, however care must be taken in order not to introduce signals into individual coordinate time series by inclusion of stations with abnormal behavior in the common mode computation. This may be carried out by selecting a number of *representative* stations in the regional network on which the common mode computation can be based. Nikolaidis (2002) applied this strategy in the analysis of the SCIGN network, where in order to maintain a consistent setup for the analysis, eight fiducial stations were defined, which have been observed throughout an eleven year period. In Teferle et al. (2002a), the author excluded ABER from the computation of the common mode bias due to the RF interference (see §5.3.3) at that site. Since the re–analysis, additional CGPS stations have been introduced suggesting a need for a more detailed investigation into which of the UK CGPS stations should be included in the stacking process.

A series of thirteen tests were carried out by the author in order to define a set of CGPS stations to be used for the regular computation of the common mode bias. These tests are summarized in Table 6.4. In all thirteen tests carried out, the detrended residual

Table 6.4: Common mode bias tests for the UK CGPS station network. () indicate that only this coordinate component has been excluded in the stacking process.

Test	Horizontal Components	Height Component	Stations included in the stacking process
1	detrended	trended	all stations included
2	detrended	detrended	all stations included
3	detrended	trended	all except for ABER[a], ABYW[b], MORP, and NSTG[c]
4	detrended	detrended	as for Test 3
5	detrended	trended	all except for ABER, ABYW, BARK(H), BRST(E,H), DUNK(E), LERW(E,H), LIVE(N,E), MORP, NSTG, SHEE(N) and SUNB(E)
6	detrended	detrended	as for Test 5
7	detrended	trended	all except for ABER[a], ABYW, BARK(H), LERW(H), MORP, NSTG, SHEE(N) and SUNB(E)
8	detrended	detrended	as for Test 7
9	trend and annual signals removed		all stations included
10	detrended	trended	ABYW, CAMB, HEMS, LERW, DUNK, HURN, PERS, and IESG
11	detrended	detrended	as for Test 10
12	detrended	trended	BRST, CAMB, NEWL
13	detrended	detrended	as for Test 12

[a] before 30 April 2001 (see §5.3.3)
[b] see §5.3.3
[c] see §5.3.3

coordinate time series for the horizontal components were used, however for the height component the detrended residual height time series were only used in six cases.

In general, the estimation of the common mode bias is assumed to be better if more stations are included in its computation (Wdowinski et al., 1997). Therefore, all stations were included in the initial tests 1 and 2. In tests 3 and 4, four CGPS stations ABER (prior to 30 April 2001), ABYW, MORP and NSTG were excluded from the stacking process, as all have already been identified to be affected by RF interference, multipath or other receiver problems (see §5.3.3 and §6.3.1). In tests 5 and 6, all stations with annual amplitudes > 3 mm were also excluded as these were assumed to be due to local effects

rather than the common mode bias. In tests 7 and 8, only the initial four CGPS stations plus those showing amplitudes larger than two times the standard deviation σ_a of the mean amplitude of the annual signals computed in §6.2.3 were excluded. Test 9 differs from previous tests in that the residual coordinate time series were computed using a model consisting of a linear and annual term and parameters for coordinate offsets. Whereas these tests tried to use as many stations as possible, tests 10 to 13 used a selection of stations only. In accordance with Nikolaidis (2002), tests 10 and 11 investigated whether a common mode bias representative for all UK CGPS stations could be based on a few stations covering the whole network. As the CGPS stations of the Met Office present themselves as possibly being of higher quality than the CGPS@TG stations (§5.3 and §6.3.1), the author decided to test whether it was possible to base the stacking algorithm on the Met Office and IESG CGPS stations only, purposely excluding the noisier CGPS@TG stations. The final set of tests was only based on the coordinate time series for stations BRST, CAMB and NEWL. As mentioned, these stations are situated in an area with large OTL effects, which have not been modeled correctly as was discovered by the author in the GPS processing (see §6.3.1). Clearly, it cannot be expected that a common mode bias for the whole of network based on these three stations can be computed, however, in this case the emphasis was on whether it was possible to *correct* the coordinate time series for these stations for the mis–modelling of OTL.

6.2.6 Noise Analysis

In this thesis, the author assumes the reader to be familiar with the concepts and terminology of white and coloured noise. An introduction to this topic can be found in Appendix H.

It was initially expected that CGPS measurements would improve estimates of station coordinate velocities uncertainties by a factor of $1/\sqrt{N}$, with N being the number of measurements, when compared to episodic GPS measurements. These expectations and the assumption that daily variations in the GPS coordinate solutions are purely random, are now widely accepted as unrealistic. Besides, random or *white* (time–independent) noise, errors have also been characterized as *coloured* (time–correlated) noise. Whereas white

noise can be greatly reduced by increasing the number of measurements and averaging, coloured noise is not or to a far lesser degree reduced by these measures. Several analyses, e.g. Johnson and Agnew (1995); King et al. (1995); Zhang et al. (1997); Calais (1999); Mao et al. (1999); Johnson and Agnew (2000); Lavallée (2000); Nikolaidis (2002) and Williams et al. (2003), have shown that CGPS coordinate time series contain coloured noise. The general conclusion being that if coloured noise is not accounted for, station velocity uncertainties may be underestimated by an order of magnitude.

Two special cases of coloured noise with integer spectral indices have previously been discussed: random walk and flicker noise. Flicker noise, or $1/f$ noise, has been observed as fluctuations in e.g. the frequency of quartz crystal oscillators, average seasonal temperature, annual amount of rainfall or the rate of traffic flow (Keshner, 1982). Spurious motions of the geodetic monument, with respect to the underlying Earth's crust, have been identified to follow a random walk process (Johnson and Agnew, 1995; Langbein and Johnson, 1997). Using 2.5 years of CGPS data from an 8 km baseline across the Hayward fault in California, King et al. (1995) were not able to detect such random walk noise in their baseline time series. However, the detectability of random walk noise depends on the length of the time series, the sampling frequency, and the relative amplitudes of the other noise components. By investigating the baseline time series between the two CGPS stations at the Piñon Flat Observatory separated by only 50 m, thus reducing the amount of white noise to a tenth of the amount normally observed in coordinate time series, Johnson and Agnew (2000) did find that these well monumented sites do show a random walk process at low frequencies, but could not confirm this for the vertical component.

It is inherently important to understand the time–correlated noise content of coordinate time series in order to obtain realistic station velocity uncertainties. Zhang et al. (1997) analysed the CGPS measurements of 10 stations in southern California with only 1.6 years of data, Mao et al. (1999) assessed the noise characteristics in the time series of 23 globally distributed CGPS stations with 3 years of data and Calais (1999) performed a similar analysis on three CGPS stations in the Western Alps with 2.5 years of data. Lavallée (2000) then compared their results with those obtained from 4 years of global weekly GPS solutions for 66 stations. In all these analyses, the stochastic model best describing the data was found to be a combination of white plus flicker noise. Following this, the most

comprehensive noise analysis of CGPS data so far, was carried out for an 11 year period, for a total of 877 global and regional CGPS coordinate time series from 377 individual sites in seven different GPS solutions (Williams et al., 2003). They concluded that indeed for global GPS solutions the combination of white plus flicker noise is the most suitable stochastic model for all three coordinate components. For regional GPS solutions however, especially when spatial correlations were reduced using the regional filtering technique, it seemed that at different sites and networks different noise sources dominated, including residual common mode noise (white plus flicker noise), monument instabilities (random walk noise) and localized deformation due to changes in the groundwater table (unknown power–law noise plus annually repeating signals) (Williams et al., 2003). Furthermore, a latitude dependency of both white and flicker noise amplitudes was identified with amplitudes being largest close to the equator and amplitudes in general being noisier in the southern hemisphere than the northern hemisphere.

For CGPS coordinate time series in particular, Mao et al. (1999) concluded that mis–modelled satellite orbits, other reference frame effects, mis–modelled atmospheric effects, mis–modelled antenna phase centre variations, which may vary with satellite elevation, and local environmental factors can be regarded as sources for large amounts of coloured noise. It is further believed that the contribution of these effects to the noise spectrum of the CGPS coordinate time series dominates over the effect of monument motion. Calais (1999) also suggested that temporal correlations observed in the CGPS coordinate time series are not due to site–specific noise such as monument motion, multipath, or antenna phase centre variations, but rather to noise sources common to all sites. This assumption is confirmed by the results shown in Williams et al. (2003) who stated that even the observed equatorial noise bulge may only partly be of tropospheric origin but also due to the reference frame via propagation.

Several methods for investigating the noise characteristics of the coordinate time series of UK CGPS stations were available to the author. These included the spectral analysis using the periodogram by Scargle (1982) (Eq. H.2 in Appendix H), two empirical methods by Mao et al. (1999) and Williams (2003a) (Eq. H.12, and Eqs. H.13 and H.14 respectively, both in Appendix H) and the most accurate and precise method using maximum likelihood estimation (MLE) (Eq. H.7 in Appendix H).

As outlined in Appendix H, the use of the periodogram (Eq. H.2) rather than the commonly applied Fast Fourier Transform (FFT) ensures the correct computation of the power spectrum for unevenly sampled data. Although, for most stations analysed, data gaps only extend from one to several days, as indicated by the high percentages of over 98% for the total number of days cleaned for most stations in Table 5.3, there are a number of sites with longer periods of missing data. Hence, the use of a FFT, which requires evenly spaced data to estimate the power spectrum of the coordinate time series may lead to spurious bulges of power at low frequencies (Press et al., 1992), thus affecting the estimation of coloured noise and in severe cases, making it even impossible to detect any. Filling large gaps has been shown to be problematic, as many interpolation methods perform poorly (Press et al., 1992).

By fitting a line in the form of Eq. H.5 to the power spectrum in the log–log space, an estimate of the spectral index κ of a power–law process (Eq. H.1 in Appendix H) can be computed. This has previously been carried out in a simple manner by Zhang et al. (1997), who concluded that this method would underestimate the spectral index, especially if the higher frequency range is dominated by white noise. Therefore, Mao et al. (1999) fitted a more sophisticated curve to the log–log power spectra, modelling both coloured noise in the low frequency range and white noise in the higher frequency band. Mao et al. (1999), however, reported of convergence problems of this model fit when an annual signal was removed from the coordinate time series prior to estimating the power spectra and had to resort to not removing the annual term before computing the spectral indices. In this thesis, the author follows a different approach in that a line is only fitted to the low frequency band of the power spectrum rather than the whole frequency range investigated (Calais, 1999; Lavallée, 2000; Nikolaidis, 2002). This has the advantage that there are no convergence problems if a known annual signal has been removed, and also that the estimated spectral index is not affected by the power in the higher frequency band.

Both Mao et al. (1999) and Williams (2003a) derived simple methods to determine the amplitudes of white and flicker noise. Mao et al. (1999) based their method on simple linear correlations of the WRMS statistic and the noise amplitudes (Eq. H.12 in Appendix H). Williams (2003a) derived a comparable method from the equivalence of the RMS statistic and the power spectrum (Eq. H.13 in Appendix H). Although not exact, these empirical

methods allow the computation of more realistic station velocity uncertainties, Eq. H.19 and H.20 in Appendix H, without carrying out a spectral analysis or the time consuming MLE.

As mentioned, the MLE can be regarded as the most accurate and precise method to analyse the noise characteristics of coordinate time series (Langbein and Johnson, 1997; Zhang et al., 1997; Mao et al., 1999; Williams, 2003a). Using the MLE, it is possible to simultaneously estimate the noise amplitudes for several stochastic models and the parameters of, e.g. a linear trend, periodic signals and coordinate offsets. The initial algorithm (Langbein and Johnson, 1997; Zhang et al., 1997; Mao et al., 1999) was based on the assumption that the noise content is either classical white (WN) or a combination of white plus flicker (WN+FN) or white plus random walk (WN+RWN) noise, i.e. both cases with integer spectral indices (see Appendix H). The main reason for choosing these specific models was that at the time of these studies, the general form for the covariance matrix, describing the noise properties based on power–law noise (Eq. H.1 in Appendix H), was not known (Williams, 2003b). The exact covariance matrix for random walk noise was shown in Langbein and Johnson (1997) while an approximation for the flicker noise covariance matrix was shown in Zhang et al. (1997). Recently, Williams (2003a) derived a general form for a power–law covariance matrix (Eqs. H.8 and H.9 in Appendix H), which now allows the MLE to also estimate the spectral index. As no assumption on the a–priori noise model is made, the MLE determines the fractional spectral index best describing the noise characteristics of the coordinate time series.

Although, the MLE with fractional spectral indices, i.e. fitting a white plus power–law (WN+PLN) noise model, has the advantage that no a–priori noise model selection is required, the MLE with integer spectral indices is much faster as either a combination of WN+FN or of WN+RWN is assumed (Williams, 2003a). However, this is achieved by disregarding the fact that the spectral index of the coordinate time series is most likely not an integer value.

To test which of the noise models best fits the data, Zhang et al. (1997) applied the maximum–log–likelihood ratio test statistic (Kendall and Stuart, 1979)

$$\begin{aligned}\Lambda &= \frac{\max \text{likelihood } 1}{\max \text{likelihood } 2} \\ &= \exp[(\text{max–log–likelihood } 1) - (\text{max–log–likelihood } 2)]\end{aligned} \tag{6.4}$$

Assuming the null hypothesis that the white noise only model best fits the data, it is possible to test whether the null hypothesis can be rejected in favour of the alternative hypothesis that any of the combined white and coloured noise models describe the data more appropriately. From tests on synthetic coordinate time series, Zhang et al. (1997) concluded that the maximum–log–likelihood test statistic was a reliable and powerful test to identify the correct model. They stated that if the Λ–statistic equals 1.0, then this would imply that the log–likelihood values from the null and alternative hypotheses were identical and in case $\Lambda << 1$ that the alternative hypothesis was to be favoured.

By evaluating the above mentioned methods of spectral analysis, the MLE and the two empirical methods presented by Mao et al. (1999) and Williams (2003a), to estimate the spectral index and the amplitudes of white and coloured noise, the author aimed to get an insight into the stochastic characteristics of the coordinate time series of the UK CGPS stations and the comparability between the different methods described.

6.3 Results

In the previous section the concepts of periodic signals, coordinate offsets, regional filtering and noise characterization have been introduced. Following these concepts, the results obtained by the author for the 25 CGPS station network are now presented in terms of the standard and improved coordinate time series and noise analysis.

6.3.1 Standard Coordinate Time Series

The standard coordinate time series for the UK CGPS stations have been analysed using automated coordinate time series analysis (§4.6). The analysis was carried out based on

both the ITRF97 and ITRF2000 reference frame realizations. Both sets of coordinate time series were obtained from the re–analysis of data up to 31 May 2002, using the non–fiducial strategy (i.e. Strategy 2 in §6.2.1). At this stage, only a linear regression with no annual term (Eq. E.1 in Appendix E) is fitted to the data. Furthermore, the automated routines do not allow for the estimation of coordinate offsets in the time series and no regional filtering is carried out during the analysis. From this perspective, the standard coordinate time series are believed to be helpful in monitoring the daily GPS network results, the quality of each CGPS station and the continuity with regards to coordinate offsets. However, although the standard coordinate time series are not to be used for any geophysical interpretations, they are useful for investigating the GPS processing strategies (§6.2.1) and to evaluate the effects of reference frame selection (§6.2.2).

Figures 6.1 to 6.4 show the standard coordinate time series computed in the ITRS2000 arranged according to the four CGPS station categories outlined in Chapter 5. Each plot contains the time series for each coordinate component, and the WRMS (Eq. D.2 in Appendix D) about the best fitting line (estimated using Eq. E.1 in Appendix E). If the coordinate time series are longer than approximately 2.5 years, then the plot also contains an estimate of the station velocity and its associated uncertainty computed using Eq. H.12, H.19 and H.20 in Appendix H (i.e. a WN+FN model). The standard coordinate time series computed in the ITRS97 are shown in Figures J.1 to J.4 in Appendix J.

Figure 6.1 shows the standard ITRS2000 coordinate time series obtained for the CGPS@TG stations investigated. The figure is arranged to show the coordinate time series according to the observation time span, with the longest time series at the top of the figure. From a first inspection, it can be seen that there are large differences in the amount of day–to–day scatter of the daily GPS coordinates. Furthermore, it is not possible to identify a common periodic signal in the height component, however there are apparent annual variations in the coordinate components of several stations. Due to their individual characteristics, it can be argued that these variations are real and not artefacts of some kind. Interestingly, all three stations obviously affected, i.e. the North component of SHEE and the North and East components of both NEWL and LIVE, are all situated on piers that are assumed to be stable. Also clearly identifiable is the apparent improvement in the day–to–day scatter of the coordinate time series for ABER, which coincides with

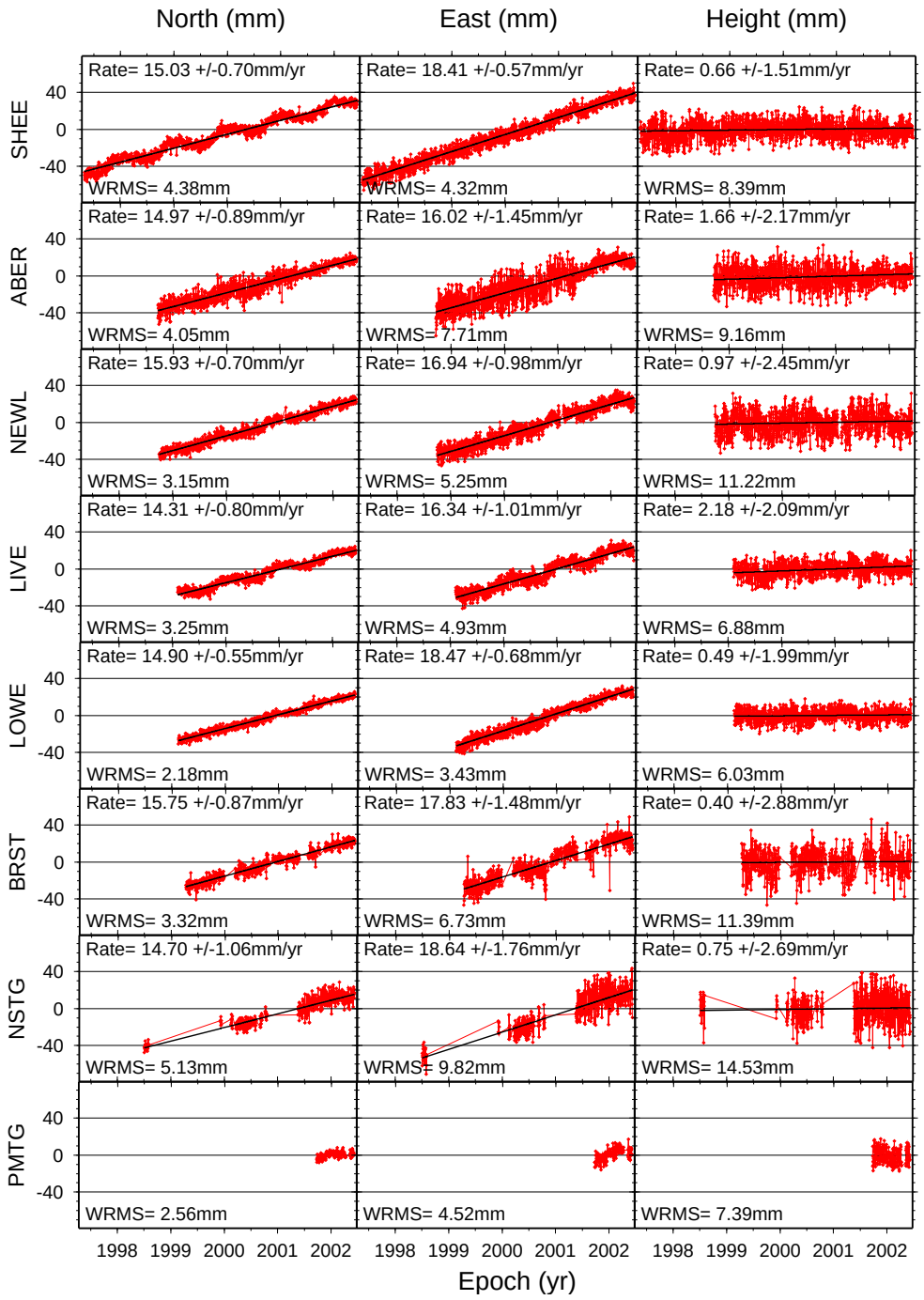

Figure 6.1: Standard ITRS2000 coordinate time series for CGPS@TG stations, based on Strategy 2 and using data up to 31 May 2002.

the removal of the RF interference at this site in April 2001 (§5.3.3). A similar day–to–day scatter in the height time series, observed for ABER, can be seen for NEWL. There is no apparent RF interference at this site to explain this level of scatter, however that station is situated in a region largely affected by OTL (§3.4.4). In this area, the M_2 ocean tide constituent has one of the largest amplitudes in the world of approximately 4.5 cm (Baker et al., 1995).

Both LIVE and LOWE seem to be the *cleanest* in the CGPS@TG station category. This is visibly evident when comparing the coordinate time series for both stations with the others and is further supported by their smaller WRMS statistic. The coordinate time series for BRST are again noisier than those for LIVE or LOWE. Similar to NEWL, with its position across the English Channel, BRST is also in an area of large OTL effects. However, there are also two large gaps in the coordinate time series for BRST, due to receiver failures (Maillard, 2000; Nicolon, 2000a,b,c, 2001). For completeness, the NSTG coordinate time series plots also contain the solutions for periods prior to May 2001, when the station became continuously operating. Although, there are large data gaps in the coordinate time series for NSTG, and the continuous part of the coordinate time series is only about one year in length, the linear model is shown and the station velocities are given. As described in §5.3.3, the station is still under investigation as to why the data quality is compromised. Due to the shortness of the coordinate time series, no station velocities are shown for PMTG, however, the WRMS statistic suggests that there are no problems at this site so far.

Figure 6.2 shows the coordinate time series obtained for the seven CGPS stations located at Met Office sites. Again, the longer coordinate time series have been arranged at the top of the figure. Although, the top four CGPS stations; CAMB, ABYW, HEMS and LERW, were established within several days in 1998, the Met Office site at Hemsby was abandoned in Spring 2001 hence the abrupt end in the coordinate time series for HEMS (§5.2). Stations DUNK, HURN and PERS were established by the Met Office more recently, with station PERS now operating the GPS receiver and antenna from HEMS (§5.2). The coordinate time series for HURN and PERS are still shorter than the required minimum length of 2.5 years, hence no rates are shown for these. From a first inspection it seems that all stations are of similar quality. Although it is possible to make

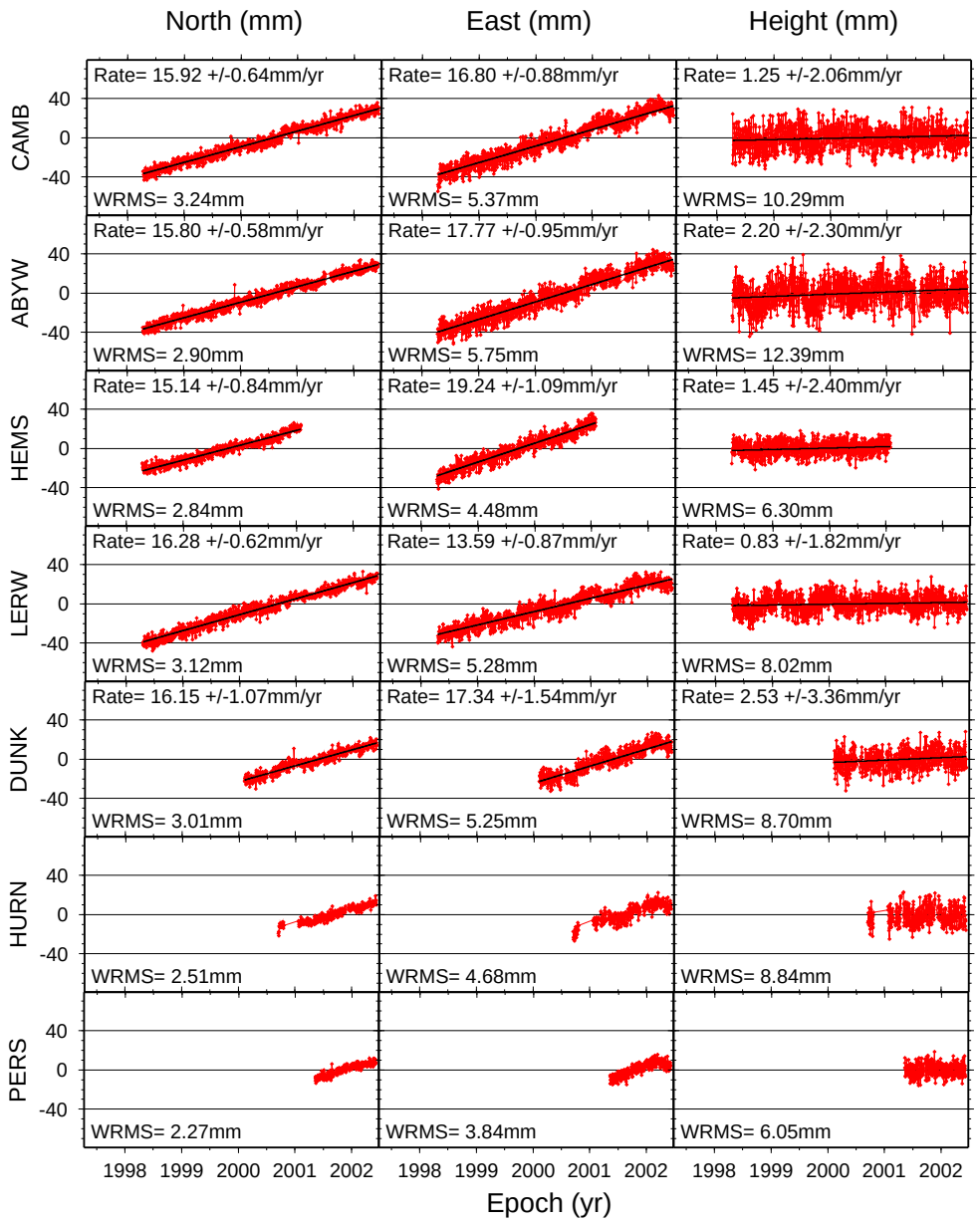

Figure 6.2: Standard ITRS2000 coordinate time series for UK Met Office CGPS stations, based on Strategy 2 and using data up to 31 May 2002.

out annual signals in the North coordinate components, their amplitudes seem only at the sub–millimetre or millimetre level. For the longer East time series of CAMB, ABYW and LERW, there is however the suggestion of annual variations with larger amplitudes starting from late 2000. This signal may also be identified in the East time series of HURN. Also the height time series seem to contain annual signals with amplitudes of several millimetres. This signal is very pronounced for LERW prior to approximately half way through 2000. A similar signal could also be hidden in the height time series for CAMB and ABYW. Both stations seem to have a larger day–to–day scatter than the rest. From Figure 6.2 it can be seen that the WRMS statistic for their height time series is greater than 10 mm, compared to values below 9 mm for the rest. Interestingly, the WRMS for the height time series of CAMB is at a similar magnitude as for NEWL and BRST. Due to the fact that all three sites are in a region with large OTL effects, it could be argued that this is due to a problem in the GPS processing software or deficiencies in the OTL model. The former argument is supported by the results for NEWL and CAMB based on the comparison of the two processing strategies which follows below.

The differences between Strategies 1 and 2 have been described in §6.2.1. In connection with these, three changes to the strategy were identified that could have affected the results in this manner. Firstly, in Strategy 2, the more recent FES99 OTL model was applied rather than the older FES94.1 model. However, it seems unlikely that this would cause a decrease in the precision of the results, as it was reported that based on tests on all FES models, the FES99 was identified as a significant improvement on previous models both in the deep ocean and along coasts (Lefèvre et al., 2001). Bos et al. (2002) tested eight OTL model including FES94.1 and FES99 in the Nordic seas and compared them to tidal gravity observations. Their tests also revealed that the FES99 model gave superior results compared to the FES94.1 and overall the best fit. Scherneck et al. (2002a) compared the maximum differences between eleven different tide models including the FES94.1 and FES99 and found the differences to be minimal for the stations tested. If the recent model was less accurate, one would expect the model to be less effective in modelling the observed signal at each station, which in turn would increase the WRMS of the coordinate time series obtained for each station. As can be seen from Table J.2 in Appendix J this is not the case. The argument could however be based on the fact that this effect has

by far the largest impact on stations in the south west, and that is exactly were the degradation in the coordinate time series has been observed. It was also mentioned that with the application of the more recent FES99 OTL model in the re–analysis, the effect was modeled in both the horizontal and vertical components rather than just in the vertical. As can be seen from Table J.2 in Appendix J for both stations the WRMS statistic of the height time series worsened for Strategy 2 when compared to Strategy 1 although, for the other stations (except for ABER), the WRMS statistic improved. This also holds true for the other coordinate components as shown in Table J.2.

The third argument to explain the increase in the day–to–day scatter in the coordinate time series for NEWL and CAMB could be based on the other difference between Strategies 1 and 2, i.e. the constraints applied to station coordinates at the network processing stage. These station constraints were initially applied in support of the estimation of the total tropospheric zenith delay (§3.4.2). By constraining station coordinates at the network processing stage, it was possible to obtain better estimates of integrated water vapour when compared with radiosonde observations (Baker, 1998). However, as will be shown below, this strategy introduces artificial seasonal variations, which then need to be accounted for. If no constraints at the network processing stage means noisier daily coordinate solutions, then this would affect all stations and not just NEWL and CAMB and possibly BRST.

As discussed in §5.3.3, the degraded coordinate time series for ABYW in Figure 6.2 are at this stage assumed to be affected by interference or multipath due to the close by antenna array of the wind profiler operated at the Met Office site in Aberystwyth. From the results for CGPS stations HEMS, LERW, DUNK, HURN and PERS in this figure, it can be seen that there are no signs of any problems at these sites and it is hoped that data from these sites will support the investigations into vertical land movements. With overall average WRMS statistics for the coordinate time series of the Met Office CGPS stations of 2.8, 5.0 and 8.7 mm for the North, East and height components respectively, the results from §5.3 are confirmed, in that GPS observations at the Met Office sites are among the best quality for the UK CGPS stations analysed.

The four longest coordinate time series in the UK have been obtained for the CGPS stations; IESG, BARK, SUNB and MORP, although the site MORP has many data gaps. As pointed out in Chapter 4, IESG is used as base station in both GPS processing strategies. From Figure 6.3 it can be seen that the coordinate time series for this site is amongst those with the smallest WRMS statistics in all three coordinate components. There are visible periodic signals with approximately annual frequency in the coordinate time series of both BARK and SUNB, especially in the height component for BARK and the East component for SUNB. In both cases, it is suggested that these are true variations as they are not visible or to a lesser degree visible in the other coordinate time series discussed. From §5.2 it is known that the GPS antenna for BARK is situated on top of the Barking Barrier in London. The foundations of the barrier are piled down to Upper Chalk suggesting a good connection to the Earth's crust. The observed height variations with annual character may therefore be due to thermal expansion of the concrete and steel structure. The GPS antenna at SUNB is mounted on a two–storey brick building located on alluvial deposits of the Thames River. The observed motion is mainly in an east–westerly direction and may suggest real ground movements due to some local hydrological processes. An interesting station from the point of its monumentation, as described in §5.2, is MORP. From the station statistics (§5.3), it was suggested that there were some difficulties cleaning the GPS data for MORP, which leads to a slightly larger σ_0 of the L0 residuals than average, and is most likely due to the tracking problems associated with low–elevation satellites (§5.3.3). Furthermore, due to the large data gaps, it is not possible to clearly identify a periodic signal contained in the coordinate time series. Due to these factors, the given station velocities may not be as reliable as suggested by their uncertainties. The WRMS of over 10 mm for the height time series confirms that the observed signal degradation must be a localized effect, i.e. the signal tracking problem which was identified recently.

The coordinate time series of the two UK based IGS stations; HERS and NPLD, are shown in Figure 6.4. From this figure it can be seen that there are several position changes in the coordinate time series for HERS. The most prominent change shown is for March/April 1999. This is due to the introduction of a significant signal obstruction between azimuths 270° and 340° and a low elevation of ($< 20°$) (Takacs and Bruyninx,

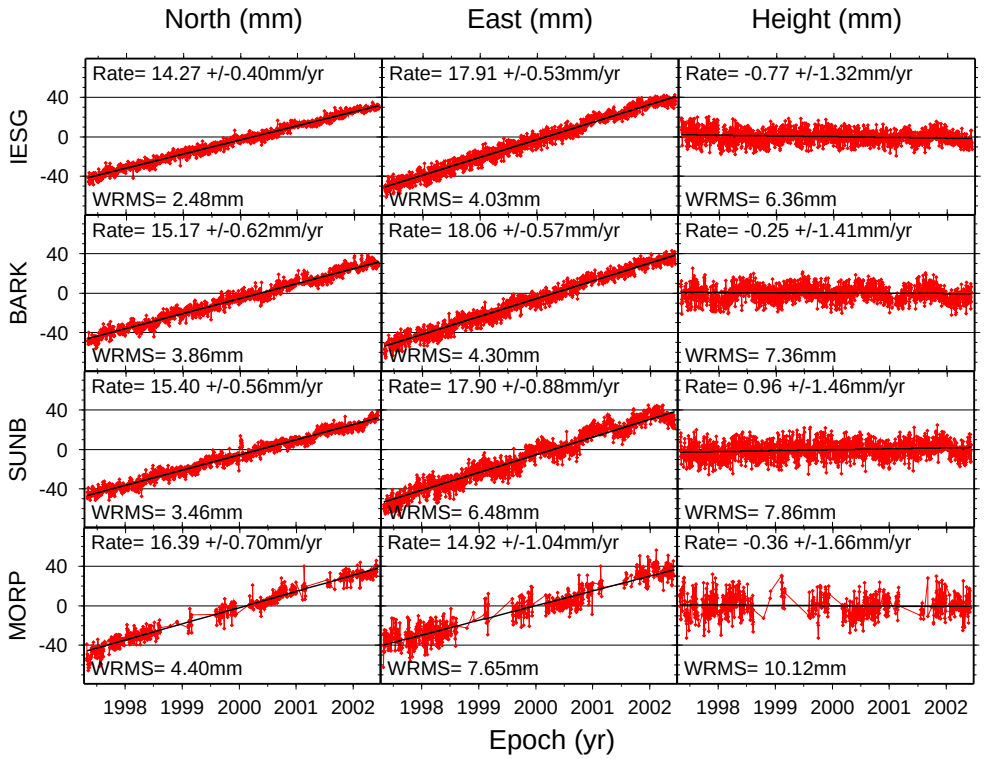

Figure 6.3: Standard ITRS2000 coordinate time series for CGPS stations belonging to category *OTHER*, based on Strategy 2 and using data up to 31 May 2002.

2001). As can be seen in the coordinate time series for HERS, there are several other position jumps apparent, which can be correlated with changes to the GPS receiver or antenna configuration as stated in the IGS site information form for HERS (Wood, 2000). Similar position changes can also be seen in the existing coordinate time series for HERS shown in Figures B.2, B.3 and B.4 in Appendix B. It is clear from this that the station velocities shown in Figure 6.4 cannot be assumed to be correct as there is currently no means to account for these *offsets* in the automated coordinate time series analysis. This topic will be discussed in more detail in §6.3.3.

From the coordinate time series and the day–to–day scatter of NPLD shown in Figure 6.4 it can be assumed that there is no degradation of the GPS signals observed at this site.

Table 6.5 summarizes the results presented for the standard coordinate time series in the ITRS2000. The table shows the WRMS (Eq. D.2 in Appendix D) about the best

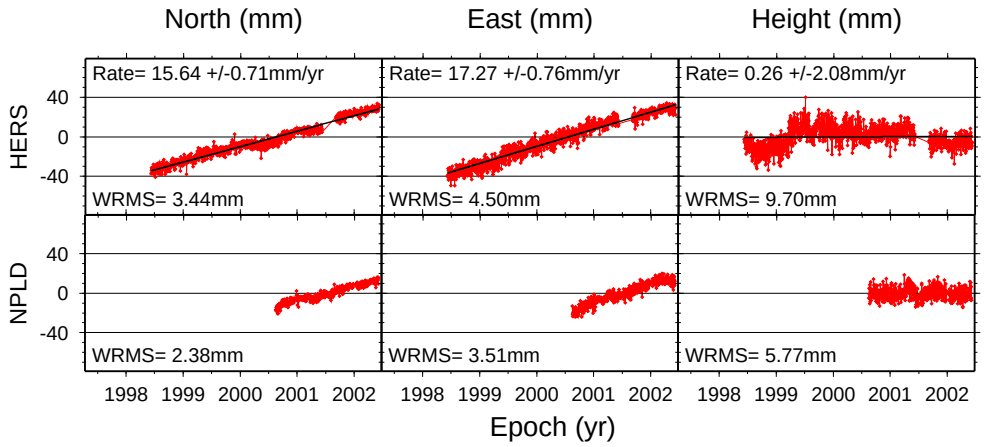

Figure 6.4: Standard ITRS2000 coordinate time series for the UK based IGS stations, based on Strategy 2 and using data up to 31 May 2002.

fitting line (Eq. E.1 in Appendix E) for each coordinate component, the station velocity and the associated uncertainties computed using Eqs. H.12 along with H.19 and H.20 in Appendix H (i.e. a WN+FN model). Also included in Table 6.5 are the average WRMS over all categories and coordinate components, calculated for all stations excluding the four stations which have been identified as degraded by interference or multipath, i.e. ABER, ABYW, NSTG and MORP. Table J.1 in Appendix J show the results obtained for the standard coordinate time series in ITRS97.

From a first inspection of Table 6.5 it can be seen that excluding the CGPS stations with interference or multipath problems (ABER, ABYW, NSTG and MORP), those in the south west of England and France (CAMB, NEWL and BRST) and HERS, the WRMS statistics for the height component are in the range of 6 to 9 mm.

In §5.3 it was suggested that, based on the σ_0 of the L0 residuals after the cycle slip detection and correction stage, the CGPS@TG stations seemed slightly noisier than the Met Office CGPS stations, which are in general situated in an open environment with no or little obstructions. This can be further investigated by computing the mean WRMS for each CGPS station category and coordinate component based on the WRMS statistics shown in this table. Excluding the WRMS statistic for ABER and NSTG, the average WRMS for the CGPS@TG stations can be computed to be 3.1, 4.9 and 8.6 mm

Table 6.5: Summary of the standard ITRS2000 coordinate time series results, based on Strategy 2 and using data up to 31 May 2002.

Site	North Component		East Component		Height Component	
	WRMS [mm]	Velocity [mm/yr]	WRMS [mm]	Velocity [mm/yr]	WRMS [mm]	Velocity [mm/yr]
			CGPS@TG Stations (TG)			
SHEE	4.38	15.03 ± 0.70	4.32	18.41 ± 0.57	8.39	0.66 ± 1.51
ABER	4.05	14.97 ± 0.89	7.71	16.02 ± 1.45	9.16	1.66 ± 2.17
BRST	3.32	15.75 ± 0.87	6.73	17.83 ± 1.48	11.39	0.40 ± 2.89
NEWL	3.15	15.93 ± 0.71	5.25	16.94 ± 0.98	11.22	0.97 ± 2.46
LIVE	3.25	14.32 ± 0.80	4.93	16.34 ± 1.01	6.88	2.18 ± 2.10
LOWE	2.18	14.90 ± 0.55	3.43	18.47 ± 0.69	6.03	0.49 ± 2.00
NSTG	5.13	14.70 ± 1.06	9.82	18.64 ± 1.77	14.53	0.75 ± 2.70
PMTG	2.56		4.52		7.37	
			UK Met Office CGPS Stations (MO)			
CAMB	3.24	15.92 ± 0.64	5.37	16.80 ± 0.89	10.29	1.25 ± 2.07
ABYW	2.90	15.80 ± 0.58	5.75	17.77 ± 0.95	12.39	2.20 ± 2.31
HEMS	2.84	15.14 ± 0.84	4.48	19.24 ± 1.09	6.30	1.45 ± 2.40
LERW	3.12	16.28 ± 0.62	5.28	13.59 ± 0.87	8.02	0.83 ± 1.82
DUNK	3.01	16.15 ± 1.07	5.25	17.34 ± 1.55	8.70	2.53 ± 3.37
HURN	2.51		4.68		8.84	
PERS	2.27		3.84		6.05	
			Environment Agency, IESSG and NCL CGPS Stations (OTHER)			
IESG	2.48	14.27 ± 0.40	4.03	17.91 ± 0.53	6.36	-0.77 ± 1.32
BARK	3.86	15.17 ± 0.62	4.30	18.06 ± 0.57	7.36	-0.25 ± 1.41
SUNB	3.46	15.40 ± 0.56	6.48	17.90 ± 0.88	7.86	0.96 ± 1.46
MORP	4.40	16.39 ± 0.70	7.65	14.92 ± 1.05	10.12	-0.36 ± 1.67
			UK based IGS Stations (IGS)			
HERS	3.44	15.64 ± 0.71	4.50	17.27 ± 0.76	9.70	0.26 ± 2.08
NPLD	2.38		3.51		5.77	
Mean[a]:	3.03		4.76		8.03	

[a]excluding ABER, ABYW, NSTG and MORP

for the North, East and height components, respectively. When comparing these with the statistics obtained for the Met Office CGPS stations (excluding ABYW) of 2.8, 4.8 and 8.0 for the North, East and height components, respectively, then it can be argued that the Met Office stations are, in fact, only slightly less noisy. If the average WRMS statistics for the CGPS@TG stations are compared with the overall mean WRMS shown in Table 6.5 then the assumption that CGPS@TG sites are noisier seems further weakened. What these result however do suggest, is that individual CGPS@TG stations are prone to a number of additional effects that possibly lead to a larger WRMS statistic, e.g. seasonal signals and OTL effects.

Ocean Tide Loading Tests

The apparent large day–to–day scatter in the coordinate time series for stations BRST, CAMB and NEWL, all situated in the southwestern section of the CGPS network analysed, prompted the author to carry out several tests on modelling of the OTL effect in GAS in order to identify the source of the problems. As stated above, previous work by several authors concluded that the FES99 model, currently used in this analysis, is in all respects superior to the FES94.1 model as applied previously. Therefore, the problem was assumed to be within GAS and not the FES99 model itself. As stated, OTL values have been obtained by the author from the Ocean Tide Loading provider at the Onsala Space Observatory (Scherneck and Bos, 2001).

Through discussion with Trevor Baker it was suggested that the problem could be to do with the application of the computed OTL corrections within GAS due to a mis–interpretation of the sign conventions for the North and East coordinate components outlined in the IERS Standards (McCarthy, 1992). This and the fact that the author is believed to be the first researcher to attempt applying OTL corrections to the horizontal coordinate components within GAS, would explain as to why this problem has not been identified previously.

Six tests were carried out by the author in which several scenarios were investigated for a small network including BRST, CAMB and NEWL over a timespan of two months. These tests varied in that no OTL corrections were applied to the horizontal coordinate

components (1), no OTL corrections were applied to the North (2) or alternatively the East (3) component, OTL corrections for the horizontal components were applied but with opposite sign (4) and OTL corrections for the North (5) or alternatively the East (6) component were applied but with opposite sign. All tests showed a reduction in the day–to–day scatter of the newly obtained height time series when compared to the scatter of the standard coordinate time series for the common period. Furthermore, for tests 1, 4, 5 and 6, the largest reduction in the day–to–day was observed. This meant that in fact the problem was due to the incorrect application of the corrections for plan components. These findings were confirmed by auto–correlation functions computed for each coordinate time series showing large short–term periodicities if the OTL corrections were applied incorrectly.

These findings suggest that the results for all CGPS stations in this analysis are to a varying degree affected by mis–modelling of the OTL effect. Re–processing of the entire data set to take this into account was considered to be beyond the scope of the author's work, but is given as one of the suggestions for future work.

Strategy Comparison

Based on the standard coordinate time series obtained from the two GPS processing strategies outlined in §6.2.1, it was possible to investigate the effect of the processing strategy on coordinate time series, using data up to 25 September 2001. Due to the change in the reference frame definition, by tightly constraining four IGS stations rather than just one, the daily standard errors of the period prior to the change on 13 September 1998 had to be re–scaled to the level after this break in order to compute corrected weights for the total time span analysed.

The resulting coordinate time series for the nine CGPS stations analysed using Strategy 1 are shown in Figure 6.5. The figure comprises plots of the daily coordinate estimates, including a linear trend (Eq. E.1 in Appendix E) for each coordinate component and station. Furthermore, the station velocities are shown and the associated uncertainties have been computed using Eqs. H.12, H.19 and H.20 in Appendix H. The WRMS statistic (Eq. D.2 in Appendix D) about the best fitting line is shown for each coordinate component

and station. Its magnitude gives a good indication on the precision and quality of the results obtained for each station, as it allows to identify stations with larger day–to–day scatter.

From a first impression, it can be seen that all of the height time series in Figure 6.5 undergo similar periodic variations with approximately yearly periods and varying amplitudes. Some of the time series for the horizontal components also show a periodic signal with annual frequency. The coordinate time series for IESG and SHEE are both about 4.4 years in length and are the longest analysed using Strategy 1. The shortest coordinate time series shown are for LIVE and LOWE with approximately 2.6 years in length. With a WRMS statistic of 2.83, 4.90 and 6.86 mm for the North, East and height components respectively, station IESG seems to be the *cleanest* and the coordinate time series for ABER with WRMS values of 4.97, 9.04 and 9.87 mm for North, East and height components respectively, the *noisiest* over the complete observation period. In §5.3.3 it was shown that ABER was subjected to RF interference from a close by radio transmitter. However, during early 2001, this interference problem was resolved, which is evident from the reduction in the day–to–day scatter shown in Figure 6.5.

Figure 6.6 shows the coordinate time series obtained for the nine CGPS stations analysed using Strategy 2, for data up to 25 September 2001. The figure comprises the plots for the North, East and height coordinate components for each station, a linear trend, the station velocities and associated uncertainties, and the WRMS about the best fitting line. Immediately visible in Figure 6.6, is the fact that the height time series based on Strategy 2, do not show the periodic variations apparent in the vertical component of the results for Strategy 1. Although, the periodic signal in the height component is largely reduced, some variations with annual character remain in the horizontal components of several stations, an indication that these may be attributed to real motions of the CGPS station rather than the *strategy–induced* signals as shown in Figure 6.5. It was mentioned in §6.2.3 that annual signals may be introduced by errors in orbit modelling that have annual modulations due to the orbital periods of the satellites (Scherneck et al., 1998; Dong et al., 2002b; Herring and Springer, 2002).

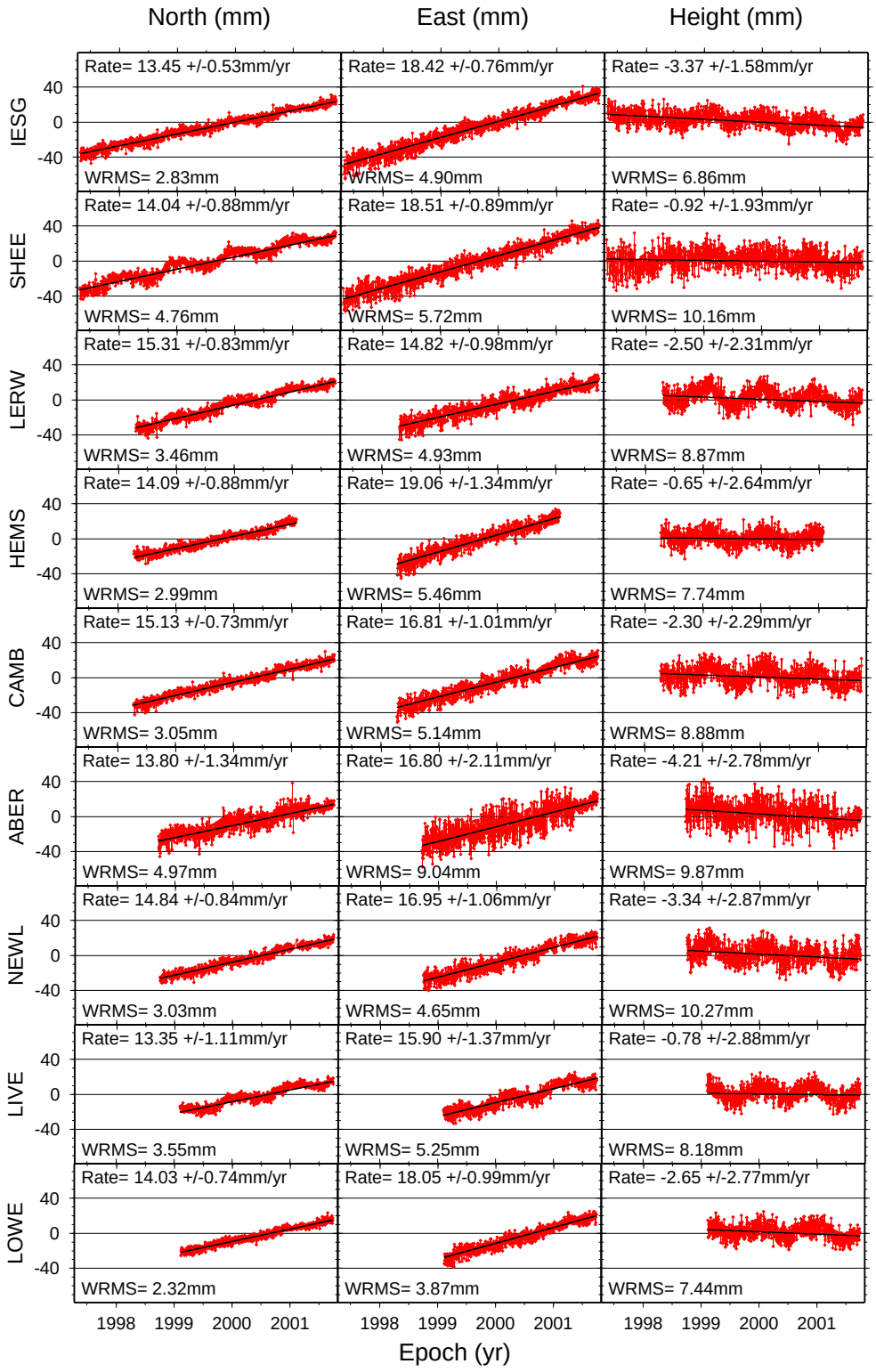

Figure 6.5: Standard ITRS97 coordinate time series for 9 UK CGPS stations, based on Strategy 1 and using data up to 25 September 2001.

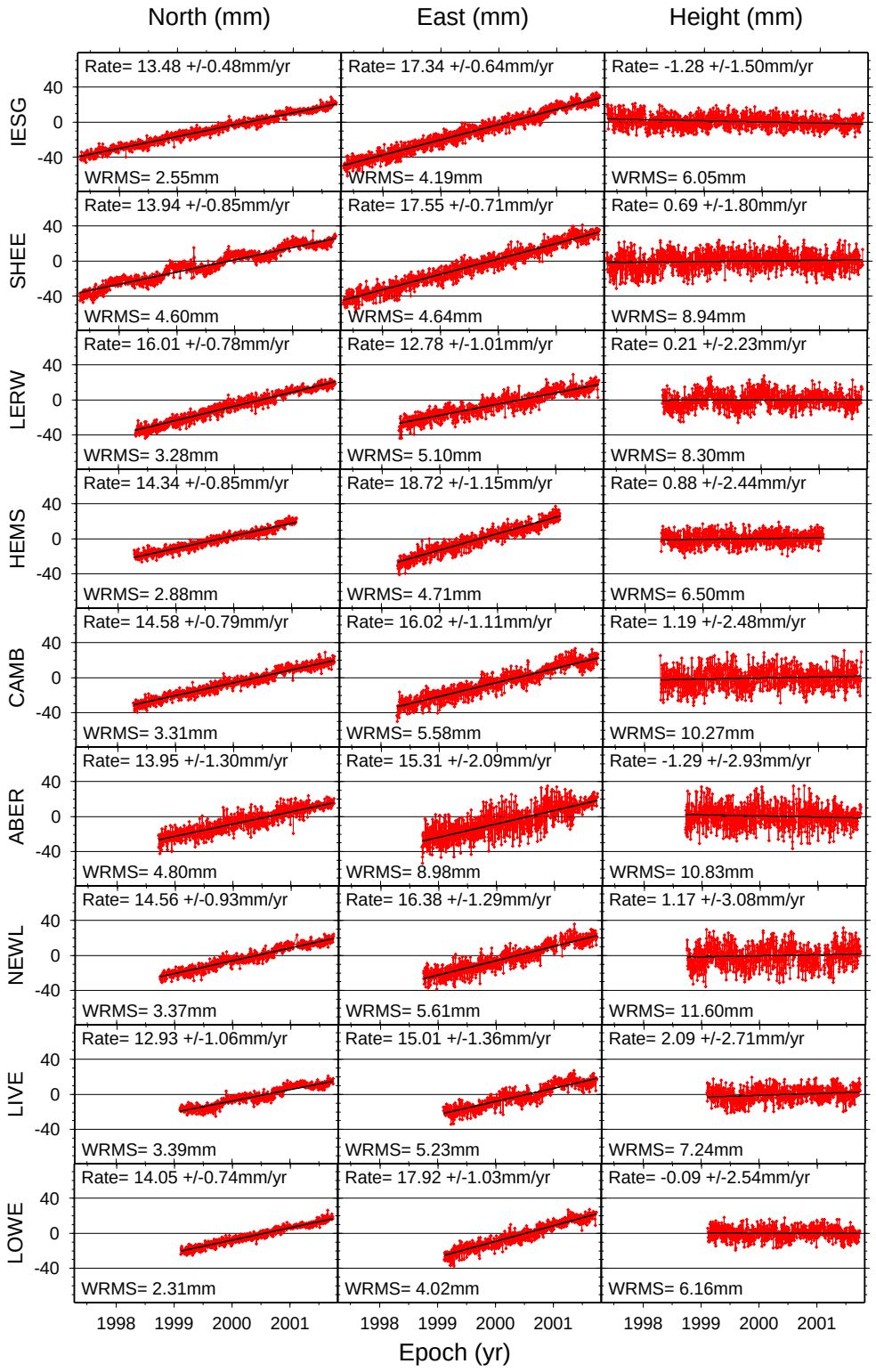

Figure 6.6: Standard ITRS97 coordinate time series for 9 UK CGPS stations, based on Strategy 2 and using data up to 25 September 2001.

Table 6.6: Comparison of the standard ITRS97 height time series, based on Strategies 1 and 2 and using data up to 25 September 2001.

Site	Strategy 1		Strategy 2		Differences	
	WRMS [mm]	Velocity [mm/yr]	WRMS [mm]	Velocity [mm/yr]	WRMS [mm]	Velocity [mm/yr]
IESG	6.86	-3.37 ± 1.58	6.05	-1.28 ± 1.50	-0.81	2.09 ± 2.18
SHEE	10.16	-0.92 ± 1.93	8.94	0.69 ± 1.80	-1.22	1.61 ± 2.64
LERW	8.87	-2.50 ± 2.31	8.30	0.21 ± 2.23	-0.57	2.71 ± 3.21
HEMS	7.74	-0.65 ± 2.64	6.50	0.88 ± 2.44	-1.24	1.53 ± 3.59
CAMB	8.88	-2.30 ± 2.29	10.27	1.19 ± 2.48	1.39	3.49 ± 3.38
ABER	9.87	-4.21 ± 2.78	10.83	-1.29 ± 2.93	0.96	2.92 ± 4.04
NEWL	10.27	-3.34 ± 2.87	11.60	1.17 ± 3.08	1.33	4.51 ± 4.21
LIVE	8.18	-0.78 ± 2.88	7.24	2.09 ± 2.71	-0.94	2.87 ± 3.95
LOWE	7.44	-2.65 ± 2.77	6.16	-0.09 ± 2.54	-1.28	2.56 ± 3.76

The fact that the height time series of the re–analysed CGPS data of Strategy 2 is affected by the annually repeating signal to a far lesser degree, improves the results of the analysis; the WRMS statistics are reduced, station velocities are less affected by annual periods and due to the lower WRMS, the velocity uncertainties are reduced too.

The complete numerical results based on processing Strategies 1 and 2 for the nine CGPS stations are given in Table J.2 in Appendix J. Here, only the results of the comparison of the height component are discussed, and summarized in Table 6.6.

Table 6.6 shows the WRMS statistic, the velocity and associated uncertainties for the vertical coordinate component for Strategies 1 and 2. Also shown are the differences between the two processing strategies. As suggested from the coordinate time series plots, the annual signal in the height time series of the results for Strategy 1 degraded the WRMS statistic for all stations, except CAMB, ABER and NEWL. More importantly, the vertical station velocities were systematically changed by about 2.7 mm/yr from an average of -2.3 mm/yr to an average of 0.4 mm/yr for the two respective strategies.

In order to investigate the effect of periodic variations in the coordinate time series of Strategy 1 on the station velocities and to assess whether the differences in velocities, from Strategies 1 and 2 can be solely attributed to this effect, the author also estimated the *combined* model parameters of a linear plus annual term according to Eq. E.9 in

Appendix E. Furthermore, it has been shown that the *velocity bias* due to such a cyclic signal can be estimated using a *theoretical* sine and cosine model (Eq. F.5) or a more *realistic* Fourier series (Eq. F.8) as detailed in Appendix F. By application of this velocity bias as a correction to the velocity estimate obtained from the linear regression only model, a *corrected* velocity estimate can be obtained. These should in theory be identical to the velocity estimates obtained from the estimation of the combined model. Furthermore, if the differences in the station velocities between Strategies 1 and 2 are solely an artefact of the annually repeating signals, then the corrected velocity estimates and those obtained from the combined model should match the velocity estimates for Strategy 2 much closer.

The obtained amplitudes and phase shifts of the annually repeating signals of the coordinate time series of Strategy 1 are summarized for each coordinate component in Table J.3 in Appendix J. This table also shows the theoretical and realistic estimates of the velocity bias. Using these, it is possible to compute corrected velocity estimates r'_{th} and r'_{re} based on the theoretical and realistic velocity bias, respectively. The velocity estimate of the linear regression plus annual term model r_m, the two corrected velocities and their differences are shown for each coordinate component and station in Table J.4. Important for this investigation is the fact that the differences between r_m and the corrected velocities r'_{th} are on average 0.02 ± 0.20 mm/yr, 0.00 ± 0.11 mm/yr and 0.25 ± 0.33 mm/yr for the North, East and height component respectively. The magnitudes of the average differences of r_m minus r'_{re} are slightly larger with -0.27 ± 0.24 mm/yr, -0.09 ± 0.14 mm/yr and -0.48 ± 0.56 mm/yr for the North, East and height components respectively. This means that although there are slight discrepancies between the two possible methods of dealing with the annual signals in the coordinate time series of Strategy 1, both methods tend to agree to within 0.5 mm/yr. The remaining disagreements may be attributable to the fact that the observed cyclic signals may not strictly be of annual frequency or that they are not really sinusoidal. There may also be the possibility of a semi–annual signal in the coordinate time series, which has not been accounted for in this test. The still relative short observation time span and the large day–to–day scatter in some coordinate time series may also fault the estimation of the annual signals or the velocity bias themselves.

Using these results, it is now possible to compare the height velocity estimates of Strategy 1 and 2 in more detail. The height velocities r_1 and r_2 obtained from a linear

Table 6.7: Comparison of vertical station velocity estimates obtained from the analysis of the standard ITRS97 height time series, based on Strategies 1 and 2. All velocity estimates are given in mm/yr.

Site	Velocity			Corrected Velocity		Difference to Strategy 2			
	r_1	r_2	r_m	r'_{th}	r'_{re}	δr_1	δr_m	$\delta r'_{th}$	$\delta r'_{re}$
IESG	−3.37	−1.28	−3.11	−3.32	−3.11	2.09	1.83	2.04	1.83
SHEE	−0.92	0.69	−0.88	−0.94	−0.88	1.61	1.57	1.63	1.57
LERW	−2.50	0.21	−2.09	−2.45	−1.54	2.71	2.30	2.66	1.75
HEMS	−0.65	0.88	1.37	0.32	0.87	1.53	−0.49	0.56	0.01
CAMB	−2.30	1.19	−2.09	−2.30	−1.73	3.49	3.28	3.49	2.92
ABER	−4.21	−1.29	−2.80	−2.96	−1.66	2.92	1.51	1.67	0.37
NEWL	−3.34	1.17	−2.66	−2.62	−1.83	4.51	3.83	3.79	3.00
LIVE	−0.78	2.09	−0.52	−0.52	0.56	2.87	2.61	2.61	1.53
LOWE	−2.65	−0.09	−2.31	−2.54	−1.45	2.56	2.22	2.45	1.36
Mean:						2.70	2.07	2.32	1.59
S.D.:						0.93	1.23	0.99	0.99

regression fit to the height time series of Strategy 1 and 2 respectively, the height velocities r_m obtained from a linear regression plus annual signal model fit to the height time series of Strategy 1, the corrected height velocities r'_{th} and r'_{re} based on the r_1 and the theoretical and realistic velocity bias respectively are summarized in Table 6.7. Additionally, this table shows the differences between r_2 and all other height velocity estimates.

From Table 6.7 it is clear that the disagreement in the height velocities between Strategies 1 and 2 cannot solely be attributed to the effect of the periodic signal apparent in the height time series of Strategy 1. The different processing strategies themselves cause a change in the obtained height velocities. This is an important finding as it demonstrates the importance of choosing the *right* processing strategy. Based on the differences in Table 6.7, it may be argued that the effect of the periodic signal on the vertical station velocity estimates ranges from 0.4 mm/yr to 1.1 mm/yr, whilst the effect of the processing strategy itself is from 1.6 mm/yr to 2.3 mm/yr.

In order to evaluate whether the amplitudes of the observed annually repeating signals follow a similar pattern to the distortions reported by Panafidina and Malkin (2001) and Malkin and Voinov (2001), the amplitudes of the height component were plotted

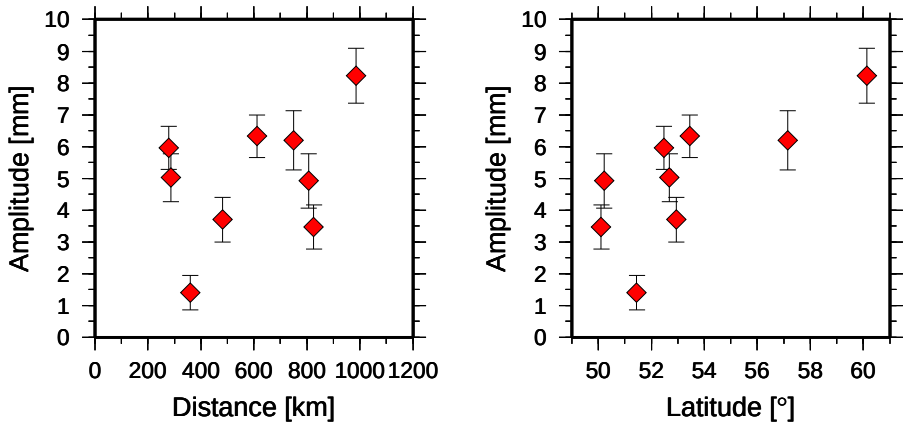

Figure 6.7: Amplitudes of the annual term estimates in the standard ITRS97 height time series for Strategy 1 plotted versus the distance of the station from IGS station KOSG and versus the latitude of the station.

against the distance from IGS station KOSG, i.e. the station constrained to its epochal ITRF97 coordinates during the network processing stage. Figure 6.7 contains plots of the estimated amplitudes and their standard errors for the stations analysed in Strategy 1, plotted against the distance from KOSG and against the latitude of the station.

From Figure 6.7 there seems to be little evidence that the amplitudes of the annually repeating signals in the height time series increase with the distance from KOSG. However, it could be argued that the figure suggests a dependency of the amplitude on latitude, such that the amplitude increases with an increase in latitude. Due to the shortness of some height time series and with only nine stations analysed it is difficult to clearly identify a correlation between the distance from station KOSG and the magnitude in the amplitude. A north–south dependency may however also be suggested by inspection of some of the improved EUREF weekly time series for geokinematics (EPNCB, 2002b). Especially the longer coordinate time series at higher latitude, e.g. HOFN, TRO1 or NYA1, show larger amplitudes in their height time series than those in Central or Southern Europe, e.g. WTZR, GRAZ, ZIMM, or MATE.

Generally, it was reported that the atmospheric pressure loading signal is stronger at higher latitude sites than for stations in mid–latitudes due to more intensive weather systems (van Dam et al., 2002). However, this effect is believed to be reduced for locations

within 500 km of the sea due to the inverted barometer response of the sea surface (Dong et al., 2002b; van Dam et al., 2002). The signal due to soil moisture and snow load shows a similar pattern in that the maximum effect is observed over the large continental areas (Mangiarotti et al., 2001; Dong et al., 2002b).

Although Mangiarotti et al. (2001) found a large annual signal in the DORIS observations for e.g. Ny–Alesund (NYAL and NYA1 CGPS sites), these could not be explained by the climatic contributors only. They concluded that displacements due to the ocean load must play a more significant role than currently assumed. Clearly, the periodic signal observed in the standard ITRS97 coordinate time series for Strategy 1 for LERW cannot be attributed to any of the above loading effects without additional information. Due to the fact that Figure 6.6 does however also indicate an apparent annual component in the height time series for LERW, a contribution from the above loading effects may be suggested.

At this point, investigations into the GPS baseline vectors themselves could be carried out in order to further describe the periodic variations observed, as e.g. in Poutanen et al. (2001). However, this would be beyond the scope of this thesis, especially as no further processing using Strategy 1 has been carried out and the current GPS processing is based on Strategy 2.

Reference Frame Comparison

It is now possible to compare the results obtained for Strategy 2 when using either ITRF97 and ITRF2000 station coordinates and velocities for the European IGS stations. Table 6.8 shows the official ITRF97 and ITRF2000 station velocities for the four European IGS stations KOSG, ONSA, WTZR and VILL used to realize the reference frame in this analysis. Additionally, the differences between both reference frames for each coordinate component and their mean differences are listed.

From Table 6.8 it can be seen that the difference for the two reference frames can reach magnitudes of several millimetres for each station and coordinate component. From the mean differences in this table it can be assumed that the disagreements between the

Table 6.8: ITRF97 and ITRF2000 station velocities for KOSG, ONSA,WTZR and VILL.

Site	ITRF97			ITRF2000			Difference		
	North [mm/yr]	East [mm/yr]	Height [mm/yr]	North [mm/yr]	East [mm/yr]	Height [mm/yr]	North [mm/yr]	East [mm/yr]	Height [mm/yr]
KOSG	14.53	17.03	0.32	15.22	17.77	0.67	0.69	0.74	0.35
ONSA	13.11	17.19	1.54	13.52	17.25	2.59	0.41	0.06	1.05
WTZR	13.36	20.19	−2.21	14.31	20.27	−0.92	0.95	0.08	1.29
VILL	13.76	18.17	0.76	15.70	19.27	−1.36	1.94	1.10	−2.12
Mean:							1.00	0.49	0.14

Table 6.9: Summary of the difference between the standard ITRS97 and the ITRS2000 coordinate time series results of Strategy 2.

	North Component		East Component		Height Component	
	WRMS [mm]	Velocity [mm/yr]	WRMS [mm]	Velocity [mm/yr]	WRMS [mm]	Velocity [mm/yr]
Min:	−0.08	0.13	−0.09	0.51	−0.16	−0.08
Max:	0.06	1.26	0.15	0.86	0.10	0.66
Mean:	0.00	0.81	0.01	0.71	−0.01	0.31
RMS:	0.03	0.85	0.06	0.09	0.06	0.36

station velocity estimates for the standard ITRS97 and ITRS2000 coordinate time series for this analysis should be at the 1, 0.5 and 0.1 mm/yr level for the North, East and height components respectively.

Table 6.9 summarizes the computed differences between the standard ITRS97 and ITRS2000 coordinate time series for the WRMS statistics and the station velocity estimates for each coordinate component obtained by the author. The table shows the minimum, maximum, mean and RMS (Eq. D.1 in Appendix D) of the differences. A good indicator of the fact that the day–to–day scatter of the coordinate time series are independent of the reference frame is that the mean difference for the WRMS is basically zero.

From Table 6.9 it can be concluded that the change from using ITRF97 to using ITRF2000 as the basis for the coordinates of the European IGS stations does have an effect on the station velocity estimates for the UK CGPS stations. As predicted in Table 6.8, the effect seems to be more pronounced in the horizontal components than for the vertical component. Overall it can be concluded that the differences in the velocity estimates

computed for this analysis (Table 6.9) can be explained by the predicted disagreements in the official ITRF station velocities for the four IGS stations.

At this stage it is important to mention that using the non–fiducial GPS processing approach allows the complete coordinate time series to be re–computed in new realizations using the GAS post processing stage (§4.2.3 in Chapter 4) to take advantage of future *improvements* which are still of the order of 1 to 2 mm/yr.

6.3.2 Noise Analysis Comparison

The noise analysis of the coordinate time series obtained for the UK CGPS stations was carried out for both the unfiltered and the filtered improved ITRS2000 coordinate time series. These were not corrected for coordinate offsets, which were then estimated simultaneously with all other parameters during the MLE. The analysis was only based on coordinate time series of stations with observation time spans longer than 2.5 years.

Spectral Analysis

The first step of the noise analysis was to obtain estimates for the spectral indices from the spectral analysis. Figure 6.8 shows the power spectral densities (PSD) for the unfiltered (red) and filtered (blue) residual coordinate time series, i.e. a linear trend and an annual signal have been removed, of SHEE for the North, East and height components. The figure also includes the fitted lines, which have been estimated for frequencies with periods of 14 days or more. The spectral indices (slopes) have been shown for the lines fitted to the spectra of the unfiltered (unflt) and filtered (flt) coordinate time series and are an indication of fractional white noise (Williams, 2003a).

The power spectra for all other CGPS stations analysed by the author can be found on the CD–Rom in directory `/Results/finalukkovw00results/psd_compr5a`. The numerical results for the spectral indices obtained have been compiled in Table K.1 in Appendix K, were they can be compared with those from the MLE (see below).

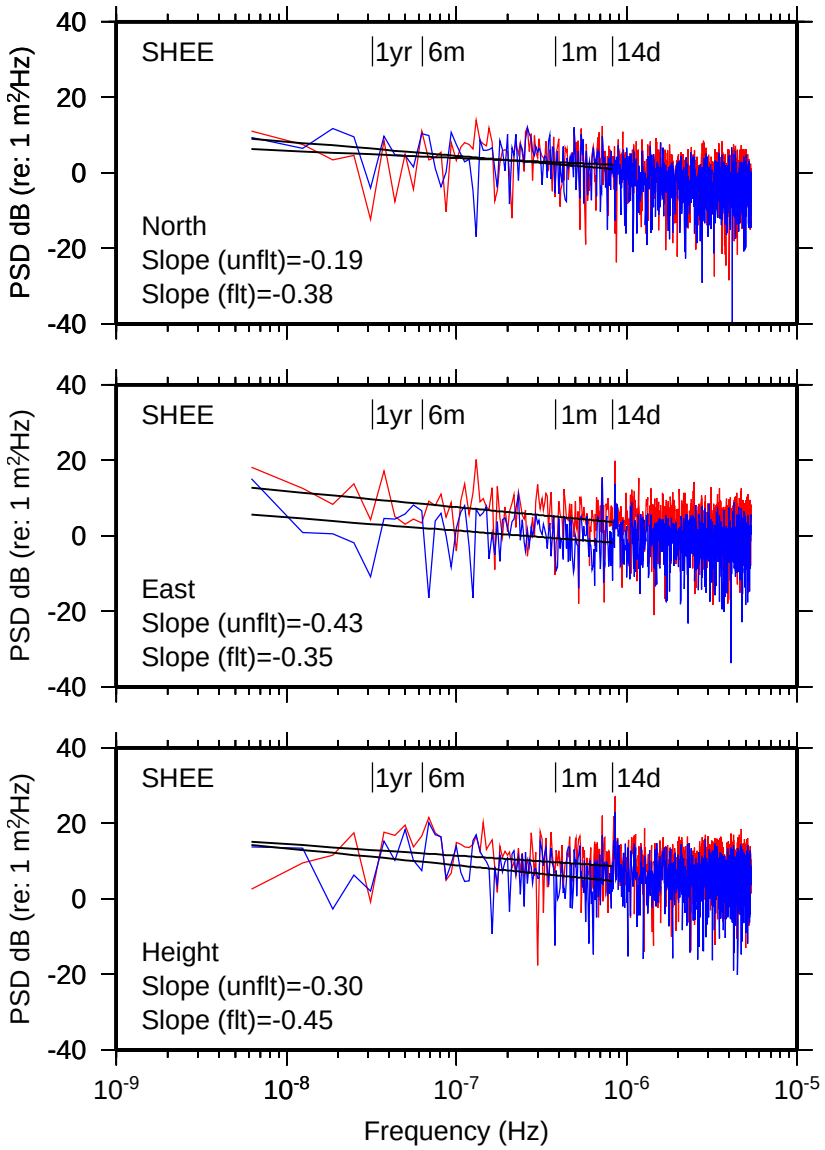

Figure 6.8: Power spectral density (PSD) estimates for the North, East and height components of the unfiltered (red) and filtered (blue) coordinate time series for SHEE. The spectral index (slope) for each PSD has been estimated for frequencies of less than 14 days period. The vertical lines indicate frequencies of 14 days, 1 month, 6 months and 1 year.

MLE with fractional and integer spectral indices

Using the MLE (Eq. H.7 in Appendix H) with fractional and with integer spectral indices, four different noise models can be fitted to the unfiltered and filtered coordinate time series: a WN model, a WN+FN model, a WN+RWN model and a WN+PLN model.

As a result of the MLE, the noise amplitudes according to the different noise models, the parameters for a linear and annual term, and the magnitudes of the coordinate offsets for epochs listed in Table 6.14 have been estimated simultaneously. Using the MLE an estimate of the non–integer spectral index has also been obtained, which will allow for comparison with those obtained from the spectral analysis.

The Λ–statistic (Eq. 6.4) and maximum values of the log–likelihood function for all four models have been tabulated for both the unfiltered and filtered coordinate time series in Tables K.2 and K.3 in Appendix K respectively. From these two tables it can be seen that with the exception of NSTG and the North component for ABER, the Λ–statistic indicates that the alternative hypothesis of a combined white and coloured noise model is to be accepted for both the unfiltered and filtered coordinate time series. As mentioned in §5.3.3, both of these stations are or have been affected by interference or multipath. For NSTG, however, the large data gaps prior to the commencement of continuous operation in May 2001, may however also be considered as reason as to why none of the combined white and coloured noise models are favoured. Furthermore, it can be seen that the maximum–log–likelihood values for the WN+PLN model are largest in all cases followed by those of the WN+FN and the WN+RWN models. In order to identify the best fitting combined white plus coloured noise model among the models tested, the Λ–statistic can be re–computed by taking e.g. the WN+PLN model as null hypothesis and the WN+FN model as alternative hypothesis. Alternatively, a quick overview as to which model is the preferred solution can be obtained by plotting the histogram of the difference in the maximum–log–likelihood of two models for each coordinate component. Figure 6.9 shows the distributions of the differences in the maximum–log–likelihood (MLE) values with respect to the WN+PLN model for each component of the unfiltered coordinate time series. A similar figure (Figure K.1) showing the MLE differences for the filtered coordinate time series is included in Appendix K.

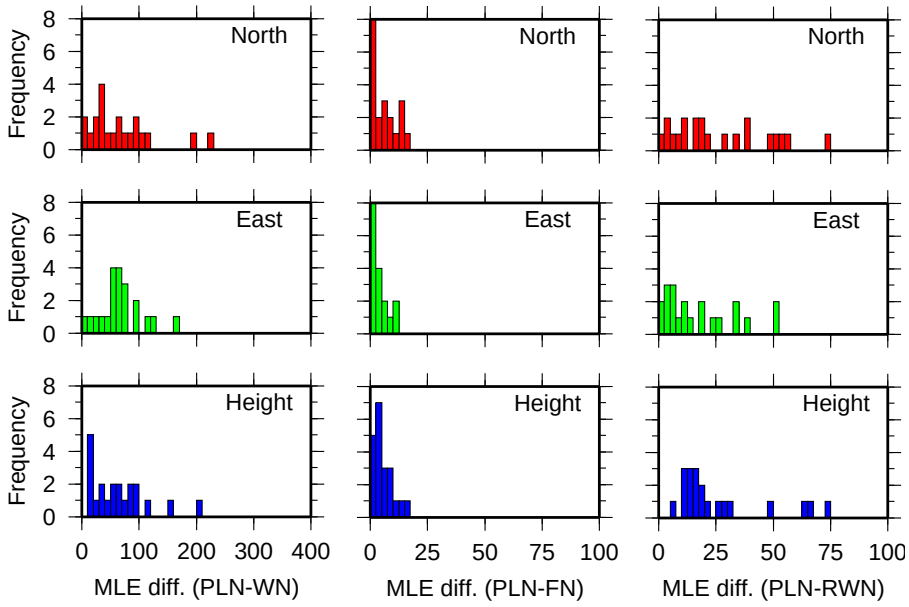

Figure 6.9: Distribution of the differences of the maximum–log–likelihood values (MLE diff.) for the white plus power-law minus the white noise only (PLN-WN), the white plus power–law minus white plus flicker noise (PLN-FN) and the white plus power–law minus the white plus random walk noise (PLN-RWN) models for the coordinate components of the unfiltered improved ITRS2000 coordinate time series. Note the different scale for the PLN-WN MLE differences.

Figure 6.9 indicates that the WN+PLN model best describes the noise characteristics of the coordinate time series for the UK CGPS stations. There are no negative log–likelihood differences, indicating that this model always fits at least as well as the others. From the scale of the abscissa for the PLN-WN MLE differences it can be seen that these are more than 4 times larger than for the PLN-RWN or PLN-FN MLE differences. The importance of Figure 6.9 lies in the fact that although it identifies the WN+PLN model as the best, it also shows that the WN+FN gives similar results, indicating that it may be possible to use this model instead, as the MLE with integer spectral indices is much faster than the MLE with fractional spectral indices. For a Linux PC with a 1.4 GHz processor and 256 Mb RAM, the MLE with fractional spectral indices took approximately 3 to 4 weeks pure processing time for the 25 CGPS station data set as compared to 3 to 4 days when using the MLE with integer spectral indices. From an inspection of Figure K.1 in Appendix K, it

is clear that the differences in the log-likelihood values for the WN+PLN and the WN+FN models are also the smallest for the filtered coordinate time series analysed.

MLE with fractional and integer spectral indices compared

Using the results for the MLE with fractional (WN+PLN) and integer (WN+FN) spectral indices, it is important to compare the noise amplitudes, the station velocities and uncertainties. This can be carried out by plotting the estimated amplitudes for white and flicker noise against the white and power–law noise respectively (see Figure 6.10). Tables K.4 and K.5 (Appendix K) show the estimated noise amplitudes for North, East and height for the unfiltered and filtered improved ITRS2000 coordinate time series. The top row of Figure 6.10 shows the white noise amplitudes a for the WN+FN model plotted against those of the WN+PLN model for both the unfiltered and filtered improved ITRS2000 coordinate time series. From this it appears that a number of white noise amplitudes were estimated to be of magnitude zero in the WN+PLN model. This stems from the fact that when the spectral index κ is in the range $-1 < \kappa < 0$ and is approaching 0, the MLE with fractional spectral indices does not differentiate between fractional white noise and integer white noise, therefore the integer white noise amplitude is set to zero as the power–law noise amplitude accounts for the total noise content. The second row of Figure 6.10 shows the comparison of the flicker b_{-1} and power–law noise b_κ amplitudes for the unfiltered and filtered improved ITRS2000 coordinate time series. In this case, there is a good correlation between the amplitudes from both MLE processes for both data sets. Finally, the bottom row of Figure 6.10 compares the estimated velocity uncertainties σ_r for both unfiltered and filtered improved ITRS2000 coordinate time series, which suggests that the obtained uncertainties are slightly larger for the WN+FN model in both cases. This is good news, if the MLE is to be used with integer (i.e. WN+FN) rather than with fractional (i.e. WN+PLN) spectral indices for logistical reasons, then the velocity uncertainties tend to be slightly pessimistic.

In a similar manner, it is possible to compare the differences between the station velocity estimates for the WN+FN and WN+PLN models as obtained for the unfiltered and filtered improved ITRS2000 coordinate time series. The top row in Figure 6.11 shows the station

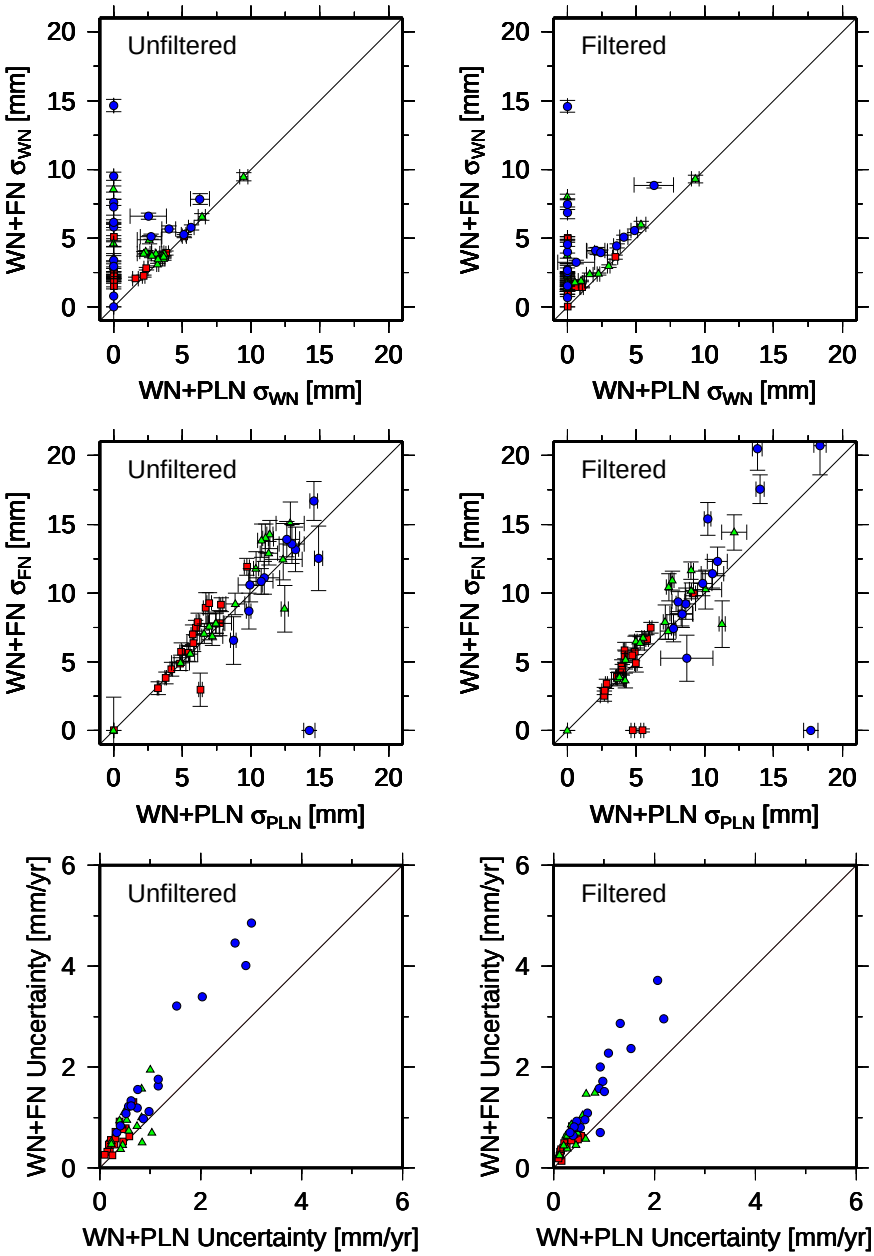

Figure 6.10: White plus flicker (WN+FN) and white plus power–law (WN+PLN) noise model results compared for unfiltered and filtered improved ITRS2000 coordinate time series. Values for the North, East and height components are shown in red (squares), green (triangles) and blue (circles), respectively. Top row compares the white noise a, the middle row the coloured noise b_{-1} and b_κ amplitudes and the bottom row the velocity uncertainties σ_r. 1σ error bars shown for noise amplitudes.

velocities for the North, East and height components for the WN+FN model plotted against the station velocity estimates for the WN+PLN model for both the unfiltered and filtered data. The bottom row shows filtered plotted against the unfiltered station velocity estimates for both noise models investigated. The error bars in all figures show velocity uncertainties from the MLE. From Figure 6.11 it is possible to conclude that there is a good agreement between the computed station velocities for both models, and for the unfiltered and filtered coordinate time series. As expected, the spread for the height velocity estimates is larger than for the North and East components, but still show high correlations. There is however the suggestion that the height velocity estimates for the filtered coordinate time series are slightly larger than for the unfiltered ones.

Figure 6.12 shows the distribution of the differences in the station velocity estimates between the WN+FN and the WN+PLN models for the unfiltered and filtered improved ITRS2000 coordinate time series. Clearly, the velocity estimates for the North and East coordinate components agree to within $\pm 0.5\,\mathrm{mm/yr}$, whereas those for the height component only agree to about $\pm 1\,\mathrm{mm/yr}$. Furthermore, there seems to be no improvement in the differences due to filtering of the coordinate time series. All numerical results for the station velocities obtained for the MLE with fractional (WN+PLN) and integer (WN+FN) spectral indices have been compiled for the unfiltered and filtered coordinate time series in Tables K.6 and K.7 in Appendix K.

Figures 6.13 and 6.14 compare the annual term estimates for the MLE with fractional (WN+PLN) and integer (WN+FN) spectral indices for the unfiltered and filtered improved ITRS2000 coordinate time series. For both, the unfiltered and filtered data, the agreement between the amplitudes and phases obtained from the MLE is excellent. Furthermore, a closer inspection reveals that amplitudes in general have been reduced for the filtered improved ITRS2000 coordinate time series, with the exception of those for which a particular coordinate component has been excluded in the common mode bias computation.

Further results obtained from the MLE with fractional (WN+PLN) and integer (WN+FN) spectral indices, e.g. the magnitudes of the estimated offsets, will not be discussed here any further. However, all numerical results have been tabulated for both

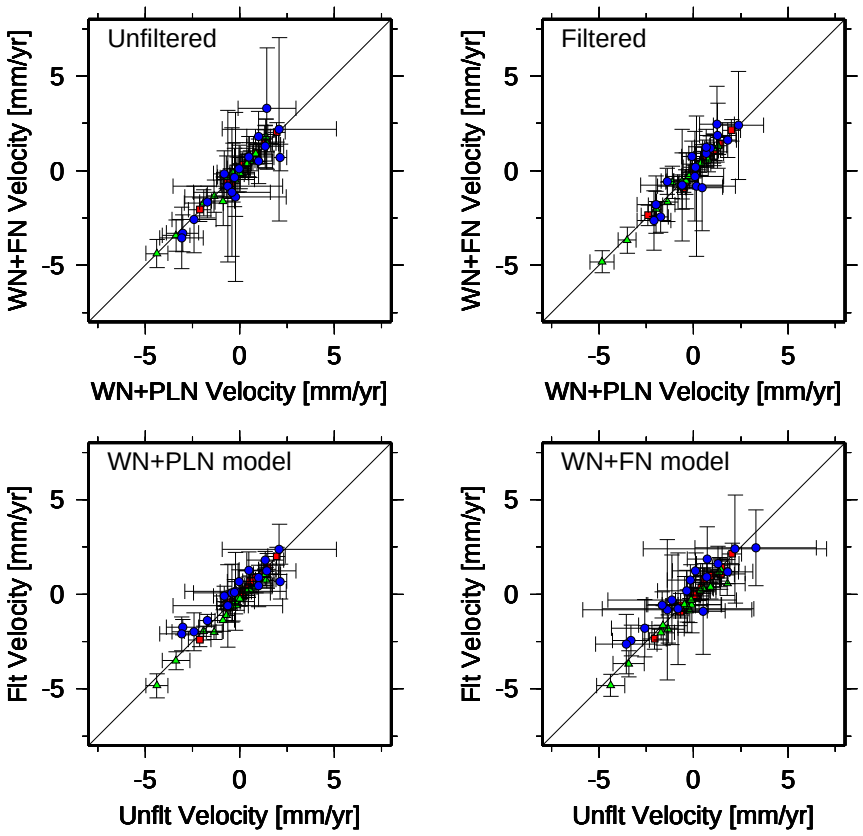

Figure 6.11: Station velocities from white plus flicker (WN+FN) and white plus power–law (WN+PLN) noise models compared for unfiltered (unflt) and filtered (flt) improved ITRS2000 coordinate time series. Values for the North, East and height components are shown in red (squares), green (triangles) and blue (circles) respectively. Uncertainties stem from the MLE model.

the unfiltered and filtered improved ITRS2000 coordinate time series in Tables K.8 to K.11 in Appendix K.

Spectral indices from the power spectrum and MLE with fractional spectral indices compared

It is now possible to compare the spectral indices obtained from the power spectra by fitting a line in the log–log space (Eq. H.5 in Appendix H), denoted as *PSD Spectral Indices*, and those from the MLE with fractional spectral indices (Eq. H.7), denoted as

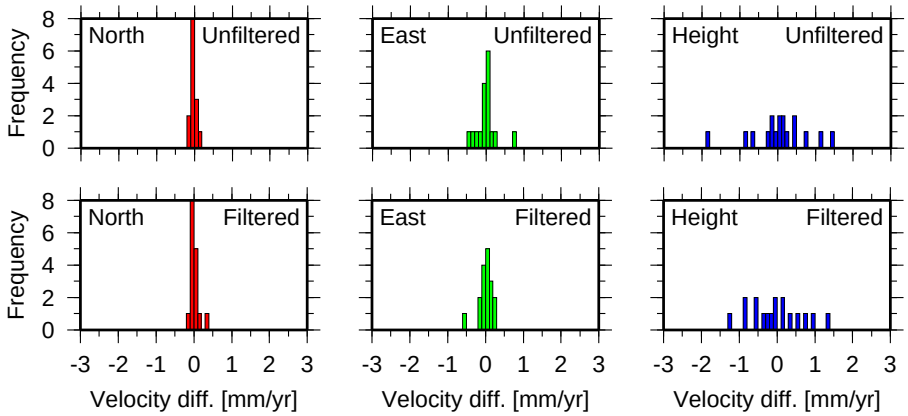

Figure 6.12: Distribution of station velocity differences for MLE with fractional (WN+PLN) minus integer (WN+FN) spectral indices for unfiltered and filtered improved ITRS2000 coordinate time series.

MLE Spectral Indices. In Figure 6.15 the PSD spectral indices are plotted against the MLE spectral indices for the unfiltered and filtered improved ITRS2000 coordinate time series. Clearly visible is the fact that indeed, the PSD spectral indices tend to be smaller (less negative) than the MLE spectral indices, although the PSD derived ones were only estimated for frequencies with periods longer than 14 days in an attempt, to reduce the effect of dominating white noise at the high frequency band.

From Figure 6.15 it is suggested that there is little difference in the spectral indices obtained for the unfiltered and filtered improved ITRS2000 coordinate time series, which can be confirmed when computing the average spectral indices for the values in Table K.1 in Appendix K. These average values and those derived from the least–squares linefit to the log–log power spectra have been compiled in Table 6.10. Furthermore, the table also shows average values for several previous studies (Zhang et al., 1997; Mao et al., 1999; Calais, 1999; Lavallée, 2000; Nikolaidis, 2002).

From Table 6.10 it can be seen that generally the results for this analysis are in good agreement with those of previous studies. Especially the average PSD spectral index for the filtered coordinate time series agree well with those of Zhang et al. (1997). There is also a good agreement between the average for the MLE spectral index and those of Lavallée (2000). The global analyses of Mao et al. (1999) and Nikolaidis (2002) show slightly smaller

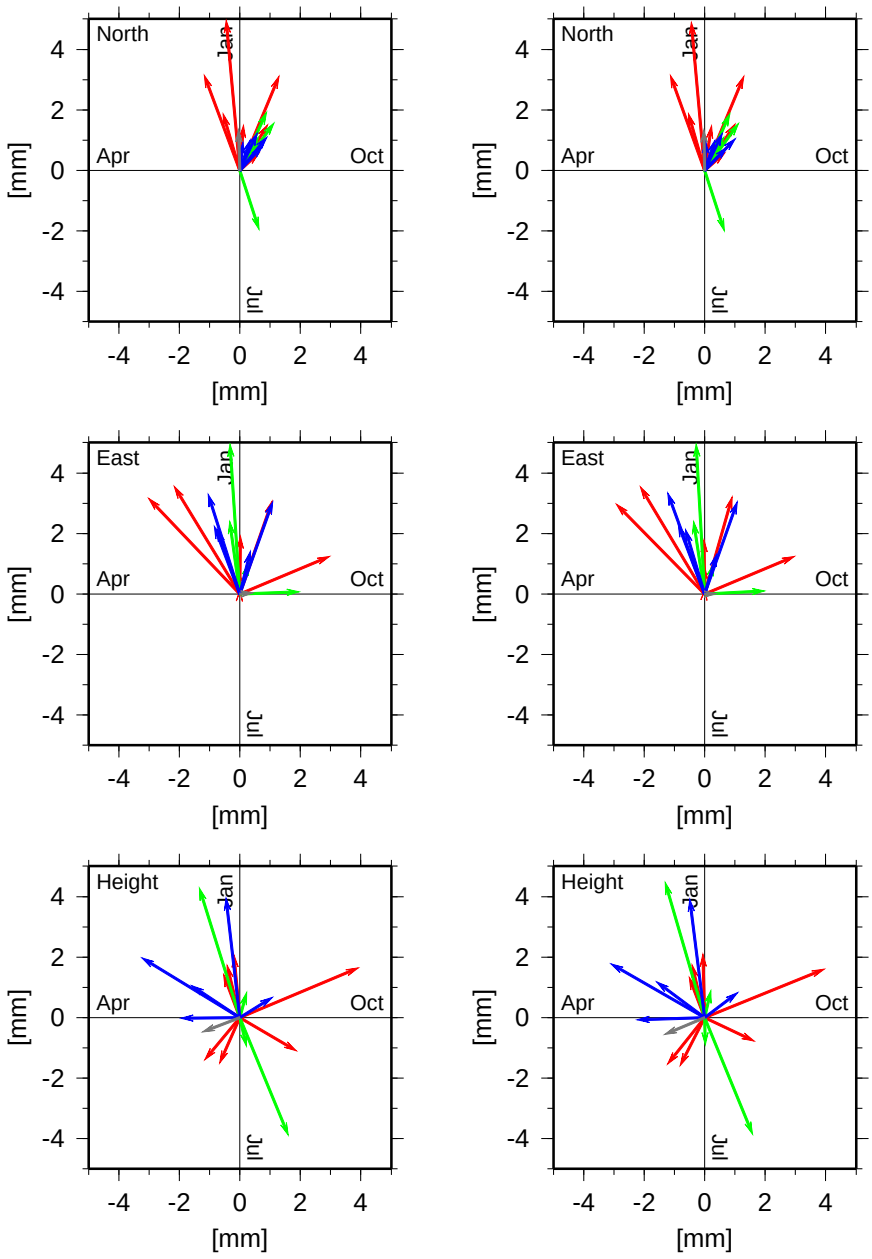

(a) WN+PLN model (b) WN+FN model

Figure 6.13: Annual term estimates from MLE with fractional (WN+PLN) and with integer (WN+FN) spectral indices for the unfiltered improved ITRS2000 coordinate time series for CGPS@TG (red), MO CGPS (green), OTHER CGPS (blue) and IGS (grey) stations. The amplitude is indicated by the vector length and the seasonal maximum by the vector direction, which is measured counter–clock–wise from the vertical axis.

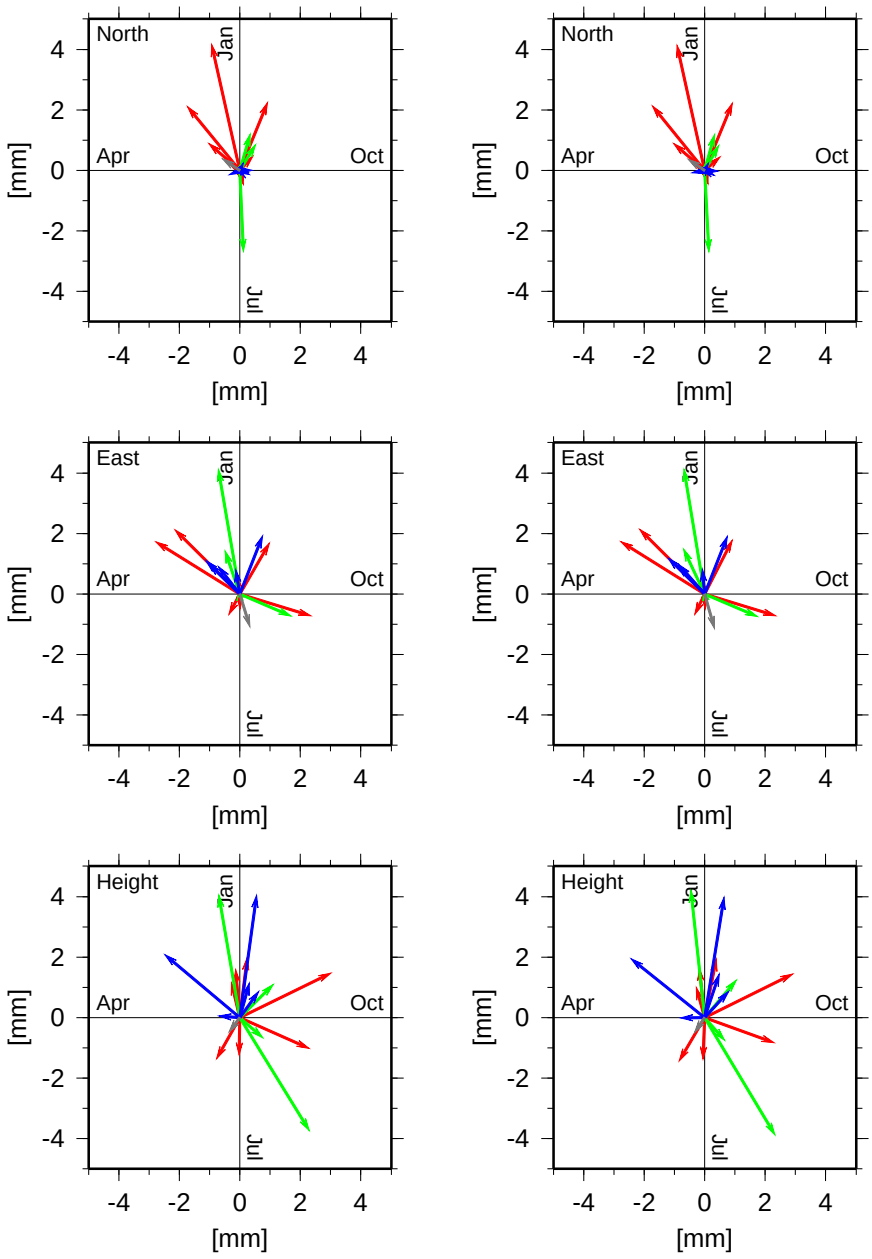

(a) WN+PLN model (b) WN+FN model

Figure 6.14: Annual term estimates from MLE with fractional (WN+PLN) and with integer (WN+FN) spectral indices for the filtered improved ITRS2000 coordinate time series of CGPS@TG (red), MO CGPS (green), OTHER CGPS (blue) and IGS (grey) stations. The amplitude is indicated by the vector length and the seasonal maximum by the vector direction, which is measured counter–clock–wise from the vertical axis.

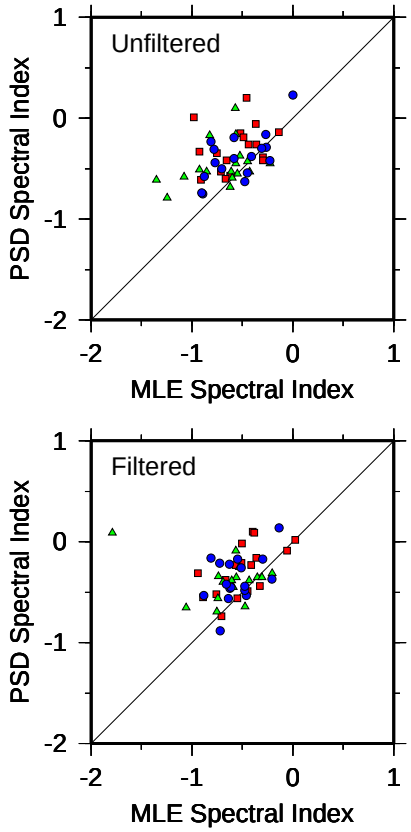

Figure 6.15: Spectral indices obtained from spectral analysis (PSD Spectral Index) and MLE with fractional spectral indices (MLE Spectral Index) compared. The figures show the spectral indices for the North (red squares), East (green triangles) and height (blue circles) components.

spectral inidices than those obtained in this study. The average spectral indices obtained by Calais (1999) for the unfiltered coordinate time series seem smaller than those for the analyses of Zhang et al. (1997); Mao et al. (1999); Lavallée (2000); Nikolaidis (2002). This may be attributed to the fact that Calais (1999) only used frequencies with periods of less than one month. These data also indicate a larger difference between the spectral indices obtained for the unfiltered and filtered coordinate time series compared to the differences obtained by the author. This may be attributed to the fact that the common mode bias in this study was based on a larger number of CGPS stations, whereas in Calais (1999) the common mode bias values were only based on three CGPS stations. As will be shown by the results for the common mode bias tests (§6.3.3), the choice of stations used in the

Table 6.10: Mean spectral indices for this analysis and previous analyses for the unfiltered and filtered North, East and height components (if available). Spectral indices obtained from the MLE with fractional spectral indices are denoted *MLE Spectral Index* and those obtained from the slope of the power spectrum in the log–log space are denoted as *PSD Spectral Index*.

Analysis	Coordinte Time Series	North	East	Height
MLE Spectral Index	unfiltered	−0.6	−0.7	−0.5
	filtered	−0.5	−0.6	−0.6
PSD Spectral Index	unfiltered	−0.3	−0.5	−0.4
	filtered	−0.3	−0.4	−0.4
A[a]	filtered	−0.4	−0.4	−0.4
B[b]	unfiltered	−1.0	−0.7	−1.0
C[c]	unfiltered	−1.8	−1.6	N/A
	filtered	−0.7	−0.5	N/A
D[d]	unfiltered	−0.6	−0.6	−0.6
E[e]	unfiltered	−0.8	−0.7	−0.8

[a]Regional analysis of data from 10 CGPS stations over a 19–month period (Zhang et al., 1997)
[b]Global analysis of data from 23 CGPS stations with 3–years of data (Mao et al., 1999)
[c]Regional analysis of data from 3 CGPS stations with 3–years of data (Calais, 1999)
[d]Global analysis (Joint Kinematic Solution) of IGS station data for a 5–year period (Lavallée, 2000)
[e]Global analysis of GPS data for an 11–years period (Nikolaidis, 2002)

computation of the common mode bias in small networks does affect the degree to which the coordinate time series are filtered.

MLE with integer spectral indices and empirical noise estimation compared

In §6.3.1 it was discussed, how more realistic station velocity uncertainties have been computed for the standard ITRS2000 coordinate time series of this analysis using a set of linear combinations (Eqs. H.12, H.19 and H.20 in Appendix H). However, this approach was criticized by Williams (2003a), who stated that deriving the white and flicker noise magnitudes from the WRMS of a coordinate time series might only be valid if the time series are all of similar lengths and sampling frequency. Furthermore, if two or more power–law noise were present in a coordinate time series, then the RMS would be a combination

of the individual RMS from each noise source. Varying relative RMS contributions from these sources, would also yield the linear combinations in Eq. H.12 in Appendix H invalid.

Of all previously applied methods for estimating the noise amplitudes and the spectral indices of coordinate time series, the MLE has proven to be the most reliable way of obtaining these parameters (Zhang et al., 1997; Mao et al., 1999; Calais, 1999; Williams, 2003a; Williams et al., 2003). However, the algorithm requires large memory capacities and is computationally inefficient (Williams, 2003a). The estimation of the noise amplitudes and spectral indices of the unfiltered and filtered improved ITRS2000 coordinate time series of the UK CGPS stations, took approximately 3 to 4 weeks for all MLE runs. Clearly, with longer coordinate time series and more and more CGPS stations included, daily MLE of the coordinate time series in larger networks is at this stage impossible. Unless drastic changes occur at a specific CGPS station, it can however be assumed that the obtained amplitudes for white and coloured noise do not change by large amounts over time scales of one to two years. It may therefore be suggested that an MLE is carried out at regular, e.g. annual or bi–annual, intervals. During the interim periods, the velocity uncertainties may then be computed using the previously estimated noise amplitudes or using Eqs. H.12 along with H.19 and H.20, i.e. the method by Mao et al. (1999). Alternatively, Williams (2003a) suggested a different approach that has been outlined in Appendix H based on the equivalence of the RMS and the power spectrum of a coordinate time series (Eq. H.13 and H.14 in Appendix H). For comparison, the method by Mao et al. (1999) is denoted as *Method 1*, as it has been in use for the standard coordinate time series, and the method by Williams (2003a) is denoted as *Method 2*.

In order to evaluate both methods for determining the coordinate time series noise characteristics, the noise amplitudes, the station velocity estimates and their associated uncertainties obtained from the MLE and Methods 1 and 2 have been compared. In this comparison, the obtained parameter values from the MLE have been assumed to be the truth to which the results for both other methods have been compared. Figure 6.16 shows the white a and flicker b_{-1} noise amplitudes and velocity uncertainties σ_r obtained for both methods plotted against those obtained from the MLE. From the figure it is clearly visible that the white and flicker noise amplitudes based on Method 2 are more consistent with the MLE than those obtained using Method 1. From the velocity uncertainty comparison,

there is the suggestion that based on Method 2, slightly more pessimistic uncertainties have been obtained than for the MLE.

A direct comparison between the white and flicker noise amplitudes and the uncertainties obtained from Methods 1 and 2 is shown in Figure 6.17. From this figure it is suggested that for both white and flicker noise the magnitudes of their amplitudes are smaller for Method 1, thus resulting in slightly optimistic velocity uncertainties.

It is also possible to compare the obtained white and flicker noise amplitudes for each of the three methods discussed. Figure 6.18 shows the white noise amplitudes a plotted against the flicker noise amplitudes b_{-1} for the MLE with integer spectral indices, and Methods 1 and 2. Generally, it can be seen that the amount of flicker noise is larger than the amount of white noise in nearly all cases. Again, Method 2 seems superior to Method 1 and shows a similar pattern in the distribution of white and flicker noise amplitudes as the results obtained for the MLE. The deficiencies of Method 1 in adequately obtaining the magnitudes of the noise amplitudes for each coordinate time series are clearly visible in the linear relationships. Based on these findings, the author suggests that for future analysis, the computation of the velocity uncertainties should be carried out for both the standard and improved coordinate time series analysis procedures with the Method 2 using Eqs. H.13 and H.14 to estimate the white and flicker noise amplitudes and Eqs. H.19 and H.20 to compute the station velocity uncertainties. All formulas are given in Appendix H.

The numerical results of this comparison have been compiled in Tables K.12, K.13 and K.14 for the unfiltered and in Tables K.15, K.16 and K.17 for the filtered improved ITRS2000 North, East and height time series respectively (Appendix K). At this stage it should be noted that the MLE analysis returned rather large flicker noise amplitudes of up to 45 mm for the height component of stations ABYW, BRST, CAMB, DUNK, HURN, NEWL and PMTG, which have not been shown in Figures 6.16, 6.17 and 6.18. As previously discussed, ABYW seems to be affected by multipath or interference possibly from a radar wind profiler at the site (§5.3.3), whereas BRST, CAMB and NEWL are situated in an area with large OTL effects, of which this analysis discovered a problem with the application of the OTL corrections in GAS (§6.3.1). Part of the large flicker noise amplitude obtained for the height time series for DUNK and PMTG may also be

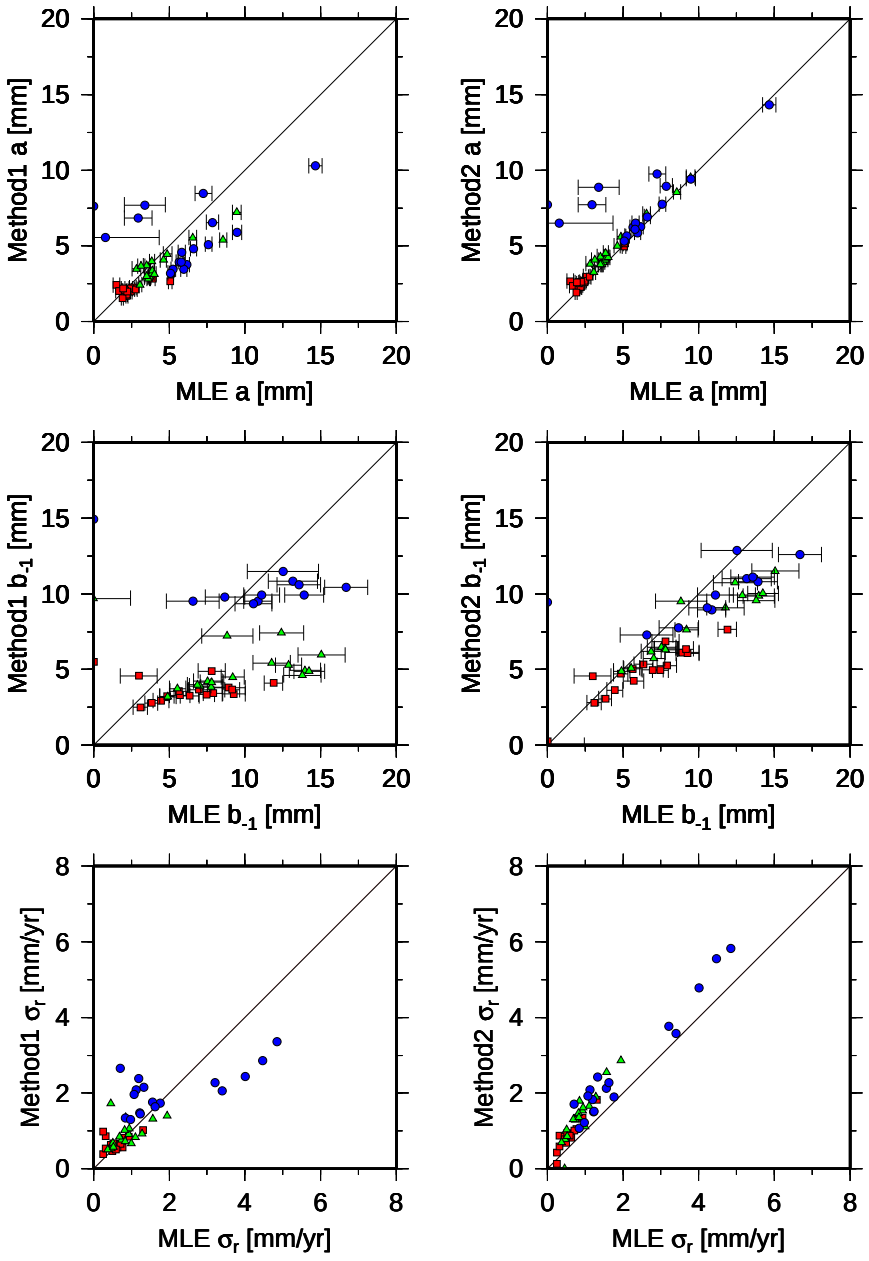

Figure 6.16: Comparison of the white a and flicker b_{-1} noise amplitudes and the station velocity uncertainties σ_r obtained using empirical Methods 1 (Mao et al., 1999) and 2 (Williams, 2003a) with the results obtained from the MLE with integer spectral indices. Values for the North, East and height components are shown in red (squares), green (triangles) and blue (circles) respectively. 1σ error bars have been included were obtained from the MLE.

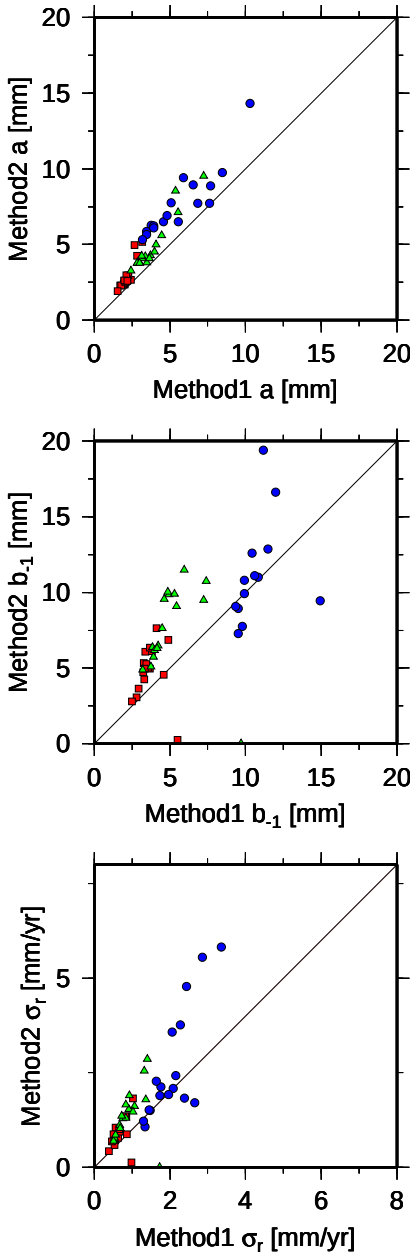

Figure 6.17: Comparison of the white a and flicker b_{-1} noise amplitudes and station velocity uncertainties σ_r obtained for empirical Methods 1 (Mao et al., 1999) and 2 (Williams, 2003a). Values for the North, East and height components are shown in red (squares), green (triangles) and blue (circles) respectively.

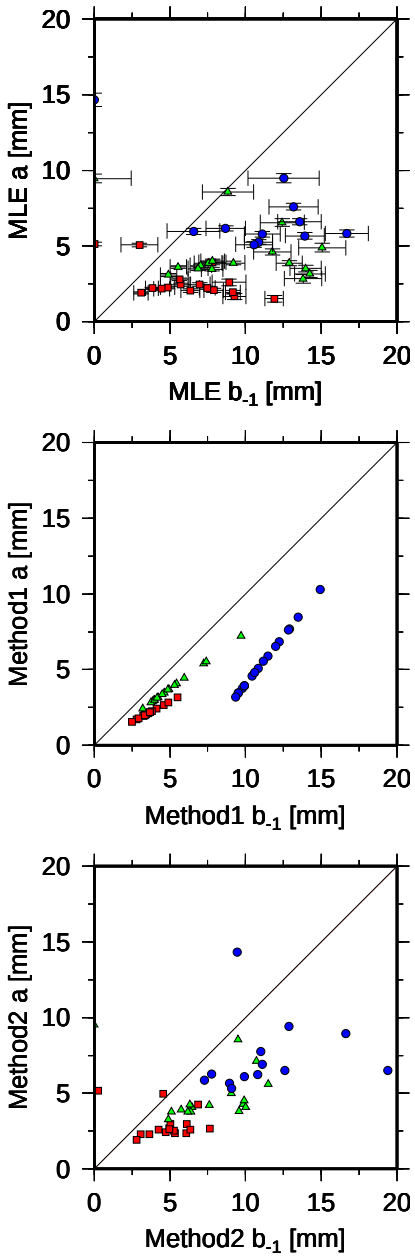

Figure 6.18: Comparison of the white a and flicker noise amplitudes b_{-1} obtained from the MLE with integer spectral indices and empirical Methods 1 (Mao et al., 1999) and 2 (Williams, 2003a). Values for the North, East and Height components are shown in red (squares), green (triangles) and blue (circles) respectively. 1σ error bars have been included were obtained from the MLE.

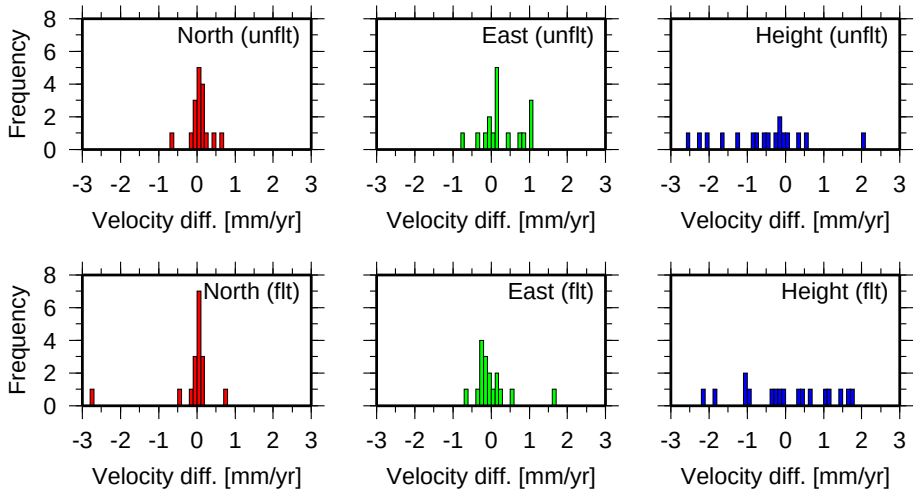

Figure 6.19: Distribution of station velocity differences for the MLE with integer spectral indices (WN+FN) and the North, East and height components of the unfiltered (unflt) and filtered (flt) improved ITRS2000 coordinate time series.

attributed to this problem, as both stations are also situated close to the south west of England. The short observation time span in both cases, approximately 2.5 and 0.8 years for DUNK and PMTG respectively, may however be a more important factor.

Finally, it is possible to compare the estimated velocities obtained from the MLE with those from the improved ITRS2000 coordinate time series analysis. Figure 6.19 shows the differences in the velocities computed by subtracting the station velocities for the unfiltered and filtered improved ITRS2000 coordinate time series from those of the MLE. From this figure it is suggested that the station velocities for both the unfiltered and filtered cases roughly agree to within ± 0.5 and ± 1.0 mm/yr for the North and East components. As expected the agreement for the height component is worse. The velocities obtained from the MLE are overall more negative than those from the analysis of the unfiltered improved ITRS2000 coordinate time series, whereas, for the filtered improved ITRS2000 coordinate time series there seems to be a more equal distribution of the height velocity differences.

Table 6.11 confirms the findings from Figure 6.19. The table shows the mean differences of the station velocity estimates and the associated velocity uncertainties computed by subtracting the velocity estimates obtained from the analysis of the unfiltered and filtered

Table 6.11: Mean differences and standard deviations in the station velocities and associated uncertainties. The station velocity differences have been computed by subtracting those for the unfiltered and filtered improved ITRS2000 coordinate time series from those of the MLE with integer spectral indices. The velocity uncertainty differences were computed by subtracting the uncertainties, σ_{r1} and σ_{r2}, obtained for empirical Methods 1 (Mao et al., 1999) and 2 (Williams, 2003a), respectively, from those of the MLE.

Component	Velocity Difference [mm/yr]	σ_{r1} Difference [mm/yr]	σ_{r2} Difference [mm/yr]
	unfiltered improved ITRS2000 coordinate time series		
North	0.1 ± 0.3	-0.1 ± 0.3	-0.3 ± 0.2
East	0.3 ± 0.5	0.0 ± 0.4	-0.5 ± 0.3
Height	-0.6 ± 1.1	0.0 ± 1.1	-0.6 ± 0.3
	filtered improved ITRS2000 coordinate time series		
North	-0.1 ± 0.7	-0.1 ± 0.3	-0.3 ± 0.2
East	0.0 ± 0.5	0.0 ± 0.4	-0.3 ± 0.2
Height	0.0 ± 1.2	-0.2 ± 0.8	-0.5 ± 0.5

improved ITRS2000 coordinate time series from those obtained from the MLE with integer spectral indices. The mean differences in the velocity uncertainties were computed by subtracting the uncertainties σ_{r1} and σ_{r2} obtained for empirical Methods 1 and 2, respectively, from those of the MLE. The error boundaries for the mean values are the standard deviations for the individual station velocity estimates and their uncertainties. From Table 6.11 it can be seen that except for the unfiltered height component, the mean difference in the velocity estimates is close to zero for both the unfiltered and filtered coordinate time series. The mean vertical velocity difference of -0.6 mm/yr, suggests that the vertical velocity estimates derived from the MLE are generally smaller in magnitudes than those obtained from the unfiltered improved height time series. Table 6.11 also suggests that the mean differences in the velocity uncertainties for those of Method 1 and the MLE is zero with a standard deviation reaching approximately 1 mm/yr for the vertical component. As has already been suggested in Figure 6.16, the mean velocity uncertainty differences for both the unfiltered and filtered improved ITRS2000 coordinate time series for Method 2 in Table 6.11 confirm that the uncertainties derived using this method are slightly more pessimistic than those from the MLE.

6.3.3 Improved Coordinate Time Series

From §6.3.1 it is clear that the standard coordinate time series, which are generated using the automated coordinate time series analysis (§4.6), are a valuable tool in monitoring station performance and detecting changes in the tracking performance of CGPS stations. It was possible to identify stations with poor data quality based on a larger than average WRMS statistic, to identify stations affected by annually repeating signals and to locate large discontinuities in the coordinate time series. It is clear that such coordinate offsets or periodic signals do affect estimated station velocities and hence need to be accounted for, if vertical land movements at the millimetre level are to be measured. The importance of this was recognized by the EUREF Commission, who set up a special project in 2000, with the task to monitor the weekly EPN combined solutions and to analyse the coordinate time series in order to identify and model these effects (Kenyeres et al., 2001; Bruyninx et al., 2002). In a similar way the standard coordinate time series for the network analysed in this research have been re–analysed to produce *improved* coordinate time series.

Annual Signal Estimates

In §6.3.1 the effect on station velocities due to an annually repeating signal was investigated, but in the current automated coordinate time series analysis it is not possible to account for these. In order to obtain improved coordinate time series, those coordinate time series that are affected by periodic variations have to be identified and dealt with appropriately.

Using Eq. E.9 in Appendix E, the parameters describing a periodic signal can be estimated simultaneously with the parameters of a linear trend using least–squares. Using the F–test (Eq. D.5 in Appendix D), it can be investigated whether introducing extra parameters for modelling an annual term improves the overall model when compared to a model only estimating the parameters of a linear trend. The null hypothesis for this test is that there is no improvement and both models are equal, the alternative hypothesis is that the model fitting a linear and annual term is an improvement.

Table 6.12 shows the estimated amplitudes and phases and their statistical uncertainties, based on Eq. E.9 in Appendix E, assuming a linear trend and annual term fitted to the daily coordinates, for each component, for stations with at least 2.5 years of data. Furthermore, it also indicates, whether the null hypothesis for the F–test is to be rejected or accepted at the 95% significance level. The results presented have been grouped according to the categories of the CGPS stations analysed.

Based on the F–test results in Table 6.12, it is suggested that modelling an annual signal simultaneously with a linear trend does improve the functional model for about two-thirds of the stations for the North, East and height components. The largest amplitudes in the North, East and height components have been estimated to be 4.9, 5.2 and 4.2 mm for SHEE, SUNB and BARK respectively. Furthermore, for the North, East and height components, there are two, six and six stations respectively, for which the estimated amplitudes are larger than 3 mm.

It is also possible to compute the mean amplitudes for each CGPS station category. These and their associated standard deviations have been summarized for each coordinate component in Table 6.13. From this table it is suggested that the largest mean amplitude for the North component is shown for the CGPS@TG stations and the smallest for the Met Office CGPS stations. For the mean amplitudes of the East component, the magnitudes are equal, however, their standard deviations differ, showing the smallest value again for the Met Office CGPS stations. For the height component, the largest mean amplitude is shown for the CGPS stations belonging to category OTHER. Interestingly, for the CGPS@TG stations, the mean amplitude for the height component is the smallest and also has the smallest standard deviation.

Table L.4 in Appendix L shows the annual term estimates for the unfiltered and filtered improved ITRS2000 coordinate time series for the North, East, and height coordinate components and the four station categories. Figures L.5 and L.6 in Appendix L show the phase–amplitude diagrams for the North, East and height components of the unfiltered and filtered improved ITRS2000 coordinate time series.

Table 6.12: Annual term estimates for the unfiltered improved ITRS2000 coordinate time series. Stations shorter than 2.5 years have been omitted.

Site	North Component			East Component			Height Component		
	Amplitude [mm]	Phase [days]	F-Test 95%	Amplitude [mm]	Phase [days]	F-Test 95%	Amplitude [mm]	Phase [days]	F-Test 95%
				CGPS@TG Stations (TG)					
SHEE	4.9 ± 0.2	6 ± 2	reject	0.5 ± 0.2	19 ± 18	accept	1.6 ± 0.4	157 ± 10	reject
ABER	1.7 ± 0.2	26 ± 5	reject	3.6 ± 0.4	330 ± 4	reject	1.7 ± 0.5	3 ± 13	reject
BRST	1.3 ± 0.2	364 ± 7	accept	4.8 ± 0.4	37 ± 3	reject	3.2 ± 0.7	244 ± 5	accept
NEWL	1.7 ± 0.2	337 ± 4	reject	2.3 ± 0.3	358 ± 5	reject	1.6 ± 0.6	161 ± 15	reject
LIVE	3.2 ± 0.2	22 ± 2	reject	4.0 ± 0.3	28 ± 3	reject	1.8 ± 0.3	7 ± 9	reject
LOWE	0.9 ± 0.1	309 ± 3	reject	0.7 ± 0.2	2 ± 11	reject	1.9 ± 0.3	16 ± 7	reject
NSTG	3.0 ± 0.4	345 ± 6	reject	2.8 ± 0.8	305 ± 7	accept	3.9 ± 1.2	291 ± 4	accept
				UK Met Office CGPS Stations (MO)					
CAMB	1.3 ± 0.2	342 ± 5	reject	2.6 ± 0.2	19 ± 4	reject	1.4 ± 0.5	104 ± 3	reject
ABYW	1.1 ± 0.1	314 ± 4	reject	2.3 ± 0.3	10 ± 5	reject	3.8 ± 0.6	63 ± 3	reject
HEMS	1.0 ± 0.2	339 ± 7	accept	1.4 ± 0.3	1 ± 9	accept	1.9 ± 0.4	53 ± 6	accept
LERW	1.1 ± 0.1	346 ± 6	reject	3.5 ± 0.2	339 ± 3	reject	3.9 ± 0.4	7 ± 5	reject
DUNK	1.3 ± 0.2	325 ± 5	accept	3.4 ± 0.3	13 ± 4	reject	1.2 ± 0.5	286 ± 5	accept
				Environment Agency, IESSG and NCL CGPS Stations (OTHER)					
IESG	1.2 ± 0.1	331 ± 3	reject	1.3 ± 0.2	341 ± 6	reject	1.3 ± 0.3	317 ± 7	reject
BARK	2.3 ± 0.2	339 ± 3	reject	1.9 ± 0.2	280 ± 0	reject	4.2 ± 0.3	209 ± 3	reject
SUNB	2.3 ± 0.1	198 ± 3	reject	5.2 ± 0.3	4 ± 3	reject	1.0 ± 0.3	223 ± 12	reject
MORP	1.9 ± 0.3	326 ± 5	accept	2.6 ± 0.5	0 ± 9	accept	3.4 ± 0.6	19 ± 8	accept
				UK based IGS Stations (IGS)					
HERS	1.3 ± 0.2	16 ± 6	reject	0.59 ± 0.22	307 ± 10	accept	1.2 ± 0.5	99 ± 3	reject

Table 6.13: Mean annual amplitudes and associated standard deviations for the unfiltered improved ITRS2000 coordinate time series.

Category	North Component		East Component		Height Component	
	Mean [mm]	S.D. [mm]	Mean [mm]	S.D. [mm]	Mean [mm]	S.D [mm]
TG	2.4	1.4	2.7	1.7	2.2	0.9
MO	1.1	0.2	2.7	0.8	2.4	1.3
OTHER	1.9	0.5	2.7	1.7	2.5	1.6
IGS[a]	1.3		0.6		1.2	
Overall	1.9	1.0	2.6	1.4	2.3	1.1

[a]Based on IGS station HERS only

Coordinate Offset Estimation

In order to obtain a list of epochs at which coordinate offsets are to be estimated in the final analysis strategy, the change detection algorithm (CDA) (Eq. G.4 in Appendix G) was used to scan for any unknown discontinuities in the coordinate time series for the UK CGPS stations. As the focus of this research is on the vertical coordinate component, the CDA was only applied to the time series of the residuals obtained after a linear and annual term were removed from the height time series. Tests on the horizontal coordinate components carried out by the author using the potential offset epochs listed in Tables 6.2 and 6.3 for the UK CGPS and IGS stations respectively, revealed offsets with only sub–millimetric magnitudes. Furthermore, with the exception of HERS, no coordinate offsets in the North or East components could be identified in the standard coordinate time series (§6.3.1). Besides detecting unknown coordinate offsets using the CDA, it was hoped that if there were any significant height offsets at the epochs listed in Tables 6.2 and 6.3, then these would be detected by the algorithm.

The application of the CDA highlighted a weakness of the algorithm in that several offsets were identified close to the edges of the coordinate time series for which no plausible cause could be found. Williams (2002) showed a U–shaped distribution of the probability to detect offsets at the edges of synthetic coordinate time series, which had no offsets incorporated. He stated that offsets were often associated with the start and end of coordinate time series because the CDA was searching for a maximum/minimum in a

correlated function, which would naturally find them there (Williams, 2003b). It is therefore believed by the author that the offsets detected at the edges of the coordinate time series for the UK CGPS stations may be artefacts. Hence, these were not included in the following analysis.

The discontinuities in the height time series detected by the CDA and those summarized in Tables 6.2 and 6.3, were further investigated using the t–test (Eq. D.4) and F–test (Eq. D.5) as outlined in Appendix D. It was suspected that offsets in the height time series for the IGS stations and the IESG would affect the height time series for all other CGPS stations in the network. Therefore, offsets associated with the IGS stations and IESG, were also investigated for all other CGPS stations. If the t–test suggested a significant change in the mean, then this offset was included in a station dependent list of offsets. These were then tested by individually estimating each offset magnitude separately, together with the parameters for a linear and annual term (Eq. E.12 in Appendix E), and by estimating all offsets simultaneously. By carrying out the least–squares procedure for each individual offset and then for all offsets in one process, it was hoped to get a better idea of the magnitude of the offsets and their effect on the estimated station velocities and the annual signal parameters, as all estimated parameters are highly correlated. All models obtained in this way were then tested by means of the F–test, to see whether there was a statistically significant improvement in the fitted models including offset parameters when compared to those models only containing a linear and annual term.

Table 6.14 shows the results of the statistical tests carried out on the documented offset epochs of Tables 6.2 and 6.3 and for the detected offsets in the height time series obtained using the CDA. The table shows the station name, the date and MJD for the documented and detected offset epochs. Also shown are the results for the t–test and the F–test, as to whether their null hypotheses can be accepted or have to be rejected. Both statistical tests were carried out at the 95% significance level. The table also indicates whether the cause for the offset is known or unknown. Lastly, the table indicates whether the author decided that the offset magnitude should be estimated at this epoch in the improved coordinate time series analysis, or the noise analysis using the MLE.

Table 6.14: Determined epochs of height offsets for the UK CGPS stations for the period from March 1997 to May 2002.

Site	Documented Offset Epochs				Detected Offset Epochs				Reason	Applied
	Date	MJD	t–Test 95%	F–Test 95%	Date	MJD	t–Test 95%	F–Test 95%		
IESG					31–05–97	50599	reject	reject	unknown	no
					03–11–97	50755	reject	reject	unknown	no
					22–12–97	50804	reject	reject	unknown	no
	09–03–98	50881	reject	reject	07–03–98	50879	reject	reject	known	yes
	02–02–99	51211	reject	reject	25–01–99	51203	reject	reject	known	yes
					20–08–00	51776	reject	accept	unknown	no
					24–02–01	51964	reject	reject	unknown	no
					14–03–02	52347	reject	reject	unknown	no
ABER	02–02–99	51211	accept	accept	no offsets detected				known	yes
	30–04–01	52029	accept	accept					unknown	no
ABYW					21–11–98	51138	reject	reject	unknown	no
	02–02–99	51211	accept	accept					known	yes
					30–12-01	52273	reject	reject	unknown	no
BARK	22–12–97	50804	accept	reject					unknown	no
	09–03–98	50881	reject	reject	07–03–98	50879	reject	reject	known	yes
	02–02–99	51211	reject	reject					known	yes
					28–12–01	52271	reject	reject	unknown	no
BRST	no documeted changes				no offsets detected					
CAMB	02–02–99	51211	reject	reject					known	yes
					04–01–02	52278	reject	reject	unknown	no
DUNK	no documented changes				no offsets detected					
HEMS	02–02–99	51211	reject	accept	no offsets detected				known	yes
HERS	02–02–99	51211	not reasonable						known	no
	21–03–99	51258	reject	reject	19–03–99	51256	reject	reject	known	yes
	08–08–01	52129	reject	reject	06–06–01	52066	reject	reject	known	yes
HURN	no documented changes				no offsets detected					
LERW	02–02–99	51211	reject	reject					known	yes
					04–01–02	52278	reject	reject	unknown	no
LIVE	no documented changes				12–11-99	51494	reject	reject	unknown	no
					24–11–01	52237	reject	reject	unknown	no

continued on next page

continued from previous page

Site	Documented Offset Epochs				Detected Offset Epochs				Reason	Applied
	Date	MJD	t–Test 95%	F–Test 95%	Date	MJD	t–Test 95%	F–Test 95%		
LOWE	no documented changes				29–05–01	52058	reject	reject	unknown	no
MORP					29–05–97	50597	reject	accept	unknown	no
	22–12–97	50804	accept	accept					unknown	no
	09–03–98	50881	reject	accept	07–03–98	50879	reject	accept	known	yes
	03–03–00	51606		accept					known	no
	12–03–02	52345		accept					known	no
	15–04–02	52379		accept					known	no
	20–05–02	52414		accept					known	no
NEWL					22–11–98	51139	reject	reject	unknown	no
	02–02–99	51211	reject	accept					known	yes
					17–01–02	52291	reject	reject	unknown	no
NPLD	no documented changes				28–05–01	52057	reject	accept	unknown	no
NSTG	30–08–98	51055		accept	no offsets detected				known	no
	04–12–99	51516		accept					known	no
	12–02–00	51586		accept					known	no
	09–05–01	52038		accept					known	no
	12–06–01	52073	accept	accept					known	no
	13–03–02	52346	accept	accept					known	no
	05–04–02	52369	accept	accept					known	no
	18–05–02	52412	accept	accept					known	no
PERS	no documented changes				no offsets detected					
PMTG	no documented changes				no offsets detected					
SHEE					26–06–97	50625	reject	reject	unknown	no
					23–20–97	50744	reject	reject	unknown	no
	22–12–97	50804	accept	reject					unknown	no
	09–03–98	50881	reject	reject	18–03–98	50890	reject	reject	known	yes
					11–11–98	51128	reject	reject	unknown	no
	02–02–99	51211	accept	reject					known	yes
					12–05–00	51883	reject	reject	unknown	no
					18–12–01	52261	reject	reject	unknown	no
SUNB	22–12–97	50804	accept	accept					unknown	no
	09–03–98	50881	reject	reject	19–03–98	50891	reject	reject	known	yes
	02–02–99	51211	accept	accept					known	yes
					25–11–01	52238	reject	reject	unknown	no

The first coordinate time series to be investigated was the one for IESG. From Table 6.14 it is possible to see that for both known offset epochs, the null hypotheses of both statistical tests was rejected at the chosen significance level. This means, that there is a statistically significant difference in the mean height coordinate before and after each break and that introducing additional offset parameters for both epochs in the fitted model improves the overall modelling. It is therefore suggested, that the temporary removal of the GPS antenna at station IESG did in fact cause a height offset in the height time series for this station. Also, the reported height offset for ONSA on 2 February 1999 seems to have affected the height time series for station IESG. This clearly indicates that a coordinate offset in a reference frame defining station may propagate into the coordinate time series of a regional network. The CDA applied to the residual height time series of IESG, indicates a number of possible epochs with coordinate offsets. It can be seen that there is a rather good correlation between the suggested epochs, 7 March 1998 and 25 January 1999, and the documented epochs. The other detected epochs cannot be attributed to any known change at the moment and their closeness to the edges of the height time series may suggest an artefact of the CDA. The suggested height discontinuity on 22 December 1997, however, is clearly identifiable in the height time series for IESG in Figure 6.3 in §6.3.1.

Less successful was the application of the CDA to the height time series of ABER, which might be a result of the larger noise level at this site. For both investigated documented offset epochs, the test statistics showed that the null hypotheses was accepted at the 95% significance level, suggesting that no height time series offsets occurred. This also holds true for the height time series of ABYW. A height time series discontinuity could statistically not be confirmed on 2 February 1999. This may be due to the fact that both stations ABER and ABYW have been identified as being affected by interference (§5.3.3). It was however possible, to detect two epochs of possible offsets using the CDA. Again, these could not be positively correlated with any event and it is believed that they are artefacts. Furthermore, modelling them in a least–squares estimation produced large offset magnitudes that seemed unrealistic.

For BARK, three documented epochs have been investigated and the F–test suggests that all three should be included in a least–squares model fit. These include the two discontinuities identified in the height time series for IESG, including the offset on 2 February

1999 for ONSA. The CDA was able to detect a jump on 7 March 1998, which coincides nicely with the levelling of the marker at IESG on 9 March 1998. The other two jumps could not be detected by the CDA, however, a similar epoch as detected for ABYW at the end of 2001 was identified. Neither documented nor detected offset epochs have been obtained for BRST, which is one of the noisier stations in the network and additionally has some larger data gaps in its coordinate time series.

For the height time series for CAMB it can be seen from Table 6.14 that the null hypotheses for the t–test and F–test was rejected at the 95% significance level for both the documented and detected offset epochs. This indicates that the height offset reported for ONSA propagated into the height time series for CAMB. The CDA also detected a change in the height time series for CAMB in early 2002. There were no documented offset epochs for the height time series for DUNK. Furthermore, the CDA did not detect any significant offsets. For the height time series of HEMS, the t–test indicated a statistically significant difference in the mean for a period before and after the 2 February 1999, the F–test accepts the null hypothesis in that an additional parameter in the least–squares estimation does not improve the overall model fit. The CDA could not detect a height offset at this site.

In Figure 6.4 the large and visible coordinate offsets in the coordinate time series for HERS have already been shown. Due to the large coordinate offset on 21 March 1999, it was not possible to successfully estimate the offset for 2 February 1999 or the documented offset for HERS on 21 March 1999. Therefore, the height offset for HERS on 2 February 1999 was not further investigated in this thesis. Both documented offsets for this station have been shown to improve the model fit at the 95% significance level. Both documented offset epochs have also been detected by the CDA. The detected offset epoch on 19 March 1999 coincides well with the large height offset documented for 21 March 1999, the difference in the documented and detected epoch for the offset on 8 August 2001 can be explained by the fact that the CDA identified the last epoch with a height solution prior to the data gap during which the antenna change of the 8 August 2001 actually occurred.

The height time series for HURN is still very short and neither documented nor detected offset epochs were reported. The height discontinuity on 2 February 1999 has also been identified as statistically significant at the 95% significance level for the height time series of LERW and it is suggested that modelling this offset improves the overall model. For this height time series, the CDA also detected a possible offset epoch in early 2002, consistent with CAMB. For both LIVE and LOWE there have been no documented receiver or antenna changes. The CDA identified several epochs, however none of these can be attributed to any particular event.

There are six documented offset epochs for the height time series of MORP. The first two, associated with station IESG and shown as statistically significant at the 95% level for other longer height time series, have not been investigated for this station as they fall into a data gap. The large number of gaps and the large number of documented offset epochs make the estimation of the offset parameters unreliable and it was not possible to carry out the t–test for several offset epochs. Furthermore, the CDA could only detect two epochs for possible discontinuities. The first one is only 25 days into the height time series and is therefore believed to be an artefact of the CDA, however, the second offset, detected for 7 March 1998, coincides well with the documented offset epoch for IESG on the 9 March 1998.

Although the offset on 2 February 1999 for NEWL was identified as statistically significant at the 95% level, it does not improve the model fit of the least–squares estimation. The CDA was able to detect two offset epochs of which one is also in early 2002. For NPLD no changes in equipment have been documented, however the CDA suggests a height discontinuity on 28 May 2001. Modelling this height offset does not significantly improve the the overall model at the 95% significance level. A number of offset epochs have been documented for NSTG. However, similar to the height time series of MORP, the height time series for NSTG contain numerous data gaps and it is therefore very unreliable to estimate all offset parameters from a least–squares fit. Due to the data gaps, it was also not possible to carry out the t–test at several epochs. The CDA could not detect any offset for the height time series of this station. Both PERS and PMTG are still very short, but have been included for completeness.

The last two CGPS stations investigated are SHEE and SUNB. Both have some of the longest height time series in the UK. For SHEE the documented offset epochs on 9 March 1998 and 2 February 1999 have been confirmed by the statistical tests to improve the least–squares model at the 95% significance level, however, only the offset for 9 March 1998 was positively identified by the CDA. For SUNB only the offset on 9 March 1998 was confirmed to be statistically significant. For both other dates, 22 December 1997 and 2 February 1999, the null hypothesis that modelling their associated offset parameters improves the overall model cannot be confirmed. Again, the offset for 9 March 1998 was positively identified by the CDA. For both stations the CDA detected numerous epochs with possible height discontinuities of which one lies close to those identified for ABYW, BARK, CAMB, LERW, and NEWL in late 2001 and early 2002. As stated, it is currently not possible to clearly associate these detected epochs with any particular event. Due to the fact that the height time series only extend until 31 May 2002, these detected offset epochs might still be an artefact of the algorithm.

It can be concluded that estimating the offset on 22 December 1997, apparent in the height time series for IESG shown in Figure 6.3 significantly improves the model fit for three out of five of the height time series affected. However, only for the height time series of IESG itself, are significantly different means before and after this date suggested. Furthermore, the estimation of this offset is highly correlated with the offset for 9 March 1998. The author decided, therefore, that this offset should not be included in the further analysis. The offset associated with the 9 March 1998, was positively identified by the t–test in all five cases, and the inclusion of an offset parameter in the least–squares model significantly improved the overall model for four of the five stations affected. This epoch was therefore included in further investigations for all stations concerned. The height discontinuity associated with ONSA on 2 February 1999, can potentially affect the nine longest height time series analysed. In three height time series, the null hypotheses of the t–test and F–test were accepted at the 95% significance level, in four cases, the null hypotheses of both statistical tests were rejected at this significance level, in one case the null hypothesis for the t–test was rejected and the null hypothesis for the F–test was accepted and for one case the results for the t–test and F–test were in reverse order. This epoch was therefore included in further investigations for all stations concerned.

Based on the offset epochs summarized in Table 6.14, it was possible to estimate the offset magnitudes for each height time series available at the applied epochs using Eq.. E.12 as shown in Appendix E. Offsets in the horizontal coordinate components have only been estimated for HERS. This was carried out for the same epochs as for the height offsets. Estimates of these coordinate offsets for the unfiltered and filtered improved ITRS2000 coordinate time series have been summarized in Table L.5 Appendix L.

As already indicated by the results of the statistical tests shown in Tables 6.14 and L.5 it is possible to estimate a height offset for 9 March 1998 for all five stations operational at this date. As mentioned above, on this day the CGPS antenna was temporarily removed in order to carry out the levelling of the survey marker on the turret of the IESSG building. It is furthermore believed that either in late 1997 or early 1998, initiated by the installation of the Met Office CGPS stations at CAMB, ABYW, and HEMS, an antenna radome was added to the CGPS antenna at IESG. From, Johansson et al. (e.g. 2002), it can be seen that the addition of an antenna radome lowers the antenna phase centre, thus lowering the height estimates for a particular station. Although not documented, there is the possibility that the addition of the radome coincided with the levelling work on 9 March 1998 and that the offset observed is a result of both events at this site. This theory can be supported by the fact that the offset estimated for IESG shown in Table L.5 is negative and the offset estimates for the other stations, which do not have radomes, are all positive.

From Table L.5 it is also clear that it is possible to obtain an estimate of a height offset at the epoch coinciding with the antenna change at ONSA. Confirming that, due to the fact that ONSA is one of four reference frame defining stations in the processing strategy applied, the offset at ONSA has propagated to some degree into the coordinates obtained for a regional network.

Regional Filtering Comparison

In order to quantify the amount of inter–station correlation for the UK CGPS stations analysed in this research, the author has computed the cross–correlations C_{xy} at zero lag between the *residual* coordinate time series of 17 of the 21 stations investigated, omitting the four stations with shortest observation spans. The residual coordinate time series

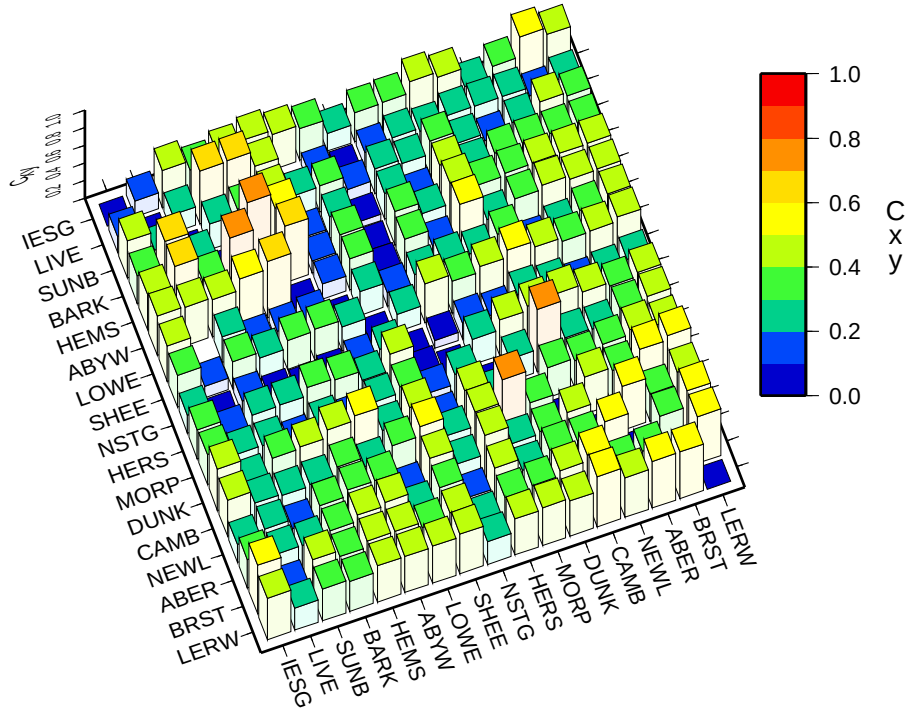

Figure 6.20: Cross–correlations C_{xy} at zero lag of the residual height time series for 17 UK CGPS stations. Note: The computation was based on a common time span between each station pair.

were based on the daily post–fit residuals, i.e. after the removal of a linear trend and the correction for any coordinate offsets according to Tables 6.14 and L.5.

Figure 6.20 shows the cross–correlation C_{xy} of the residual coordinate time series for the height component at zero lag. The respective figures for the horizontal components can be found in Appendix L (Figures L.1 and L.2).

From Figure 6.20 it can be seen that the cross–correlation between most of the residual height time series is in the range of 30 to 60%. Only for the residual height time series of NSTG, LIVE and LOWE, are the indicated cross–correlations at lower levels. From §5.3.3 it may be suggested that the interference or multipath problems observed at NSTG may be the reason for this low cross–correlation with the other sites. There are however no indications, as to why the residual coordinate time series for LIVE and LOWE are less correlated than average. The largest cross–correlations have been computed for the

residual coordinate time series of the CGPS station pairs HEMS–BARK and CAMB–MORP, in the range of 70 to 80%. Furthermore, there is the suggestion that the spatial correlation in the current analysis is not restricted by the network scale itself as the cross–correlation computed for the CGPS station pairs LERW–BRST, LERW–CAMB, and ABER–NEWL is in the range of 50 to 60% although the distances between these stations are the longest in the network.

Figure 6.21 shows the results obtained from the common mode bias tests carried out by the author (as outlined in Table 6.4). The figure includes the time series of daily common mode values, a linear trend (Eq. E.1 in Appendix E), the RMS statistic (Eq. D.1 in Appendix D) and the velocity and its uncertainty computed using Eqs. H.12, H.19 and H.20 in Appendix H, i.e. with a WN+FN model. Unlike the velocity estimates of the standard or improved coordinate time series presented, this velocity estimate is not based on weighted least–squares, as during the common mode bias computation no weights are carried forward (Teferle et al., 2002a).

From a first impression it would seem that the common mode bias is largely unaffected by the data used in the stacking process. Based on the RMS statistic for each test and coordinate component, it is possible, to distinguish between the different tests. For example, it is possible to reduce the RMS for the North and East component by a more rigorous selection of the input data to the stacking process (i.e. tests 5, 7 and 9). There is a slight indication that this may also be the case for the height component. Due to the fact that a linear trend was removed from the North and East components prior to the computation of the common mode bias, it would be expected that the velocity estimated for the bias time series is zero. This largely holds true, however, in all tests a velocity different from zero has been obtained. At this stage it should be noted that there will be a residual velocity due to the fact that the initial trend removed was based on a weighted computation rather than assuming equal weights for the velocity estimate. Table 6.15 summarizes the results of the common mode bias tests carried out in accordance with Table 6.4 for all thirteen tests.

Using all thirteen common mode bias time series, each raw coordinate time series for all UK CGPS stations has been filtered, a linear trend estimated and the RMS statistic of the

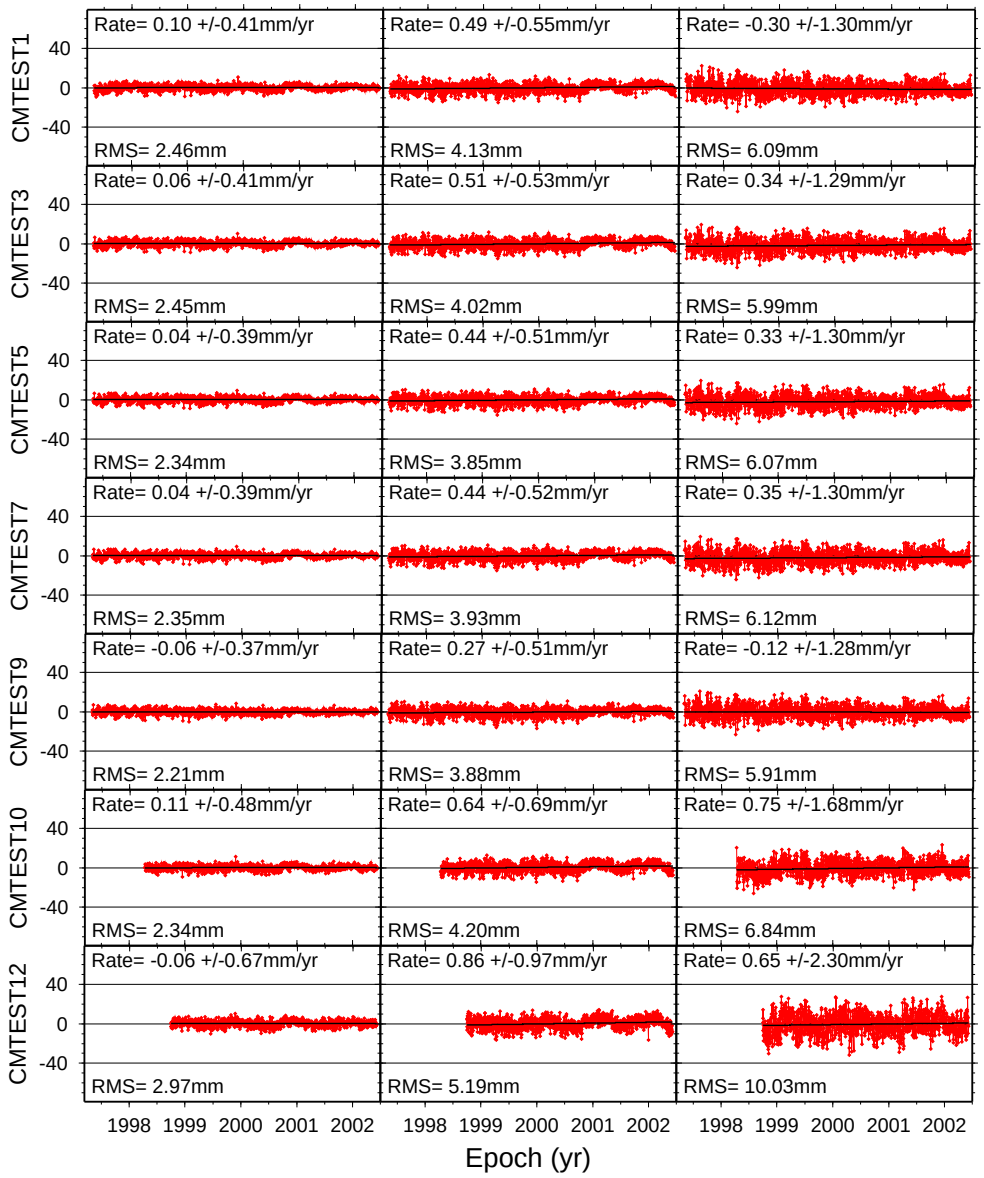

Figure 6.21: Common mode bias time series up to 31 May 2002.

Table 6.15: Results of the common mode bias tests as outlined in Table 6.4 for the UK CGPS network.

Test	North Component		East Component		Height Component	
	RMS [mm]	Velocity [mm/yr]	RMS [mm]	Velocity [mm/yr]	RMS [mm]	Velocity [mm/yr]
1	2.46	0.09 ± 0.41	4.14	0.48 ± 0.55	6.15	-0.12 ± 1.30
2					6.11	-0.15 ± 1.30
3	2.45	0.05 ± 0.40	4.03	0.51 ± 0.53	5.96	-0.09 ± 1.29
4					5.94	-0.14 ± 1.29
5	2.34	0.04 ± 0.39	3.86	0.43 ± 0.51	6.05	-0.05 ± 1.30
6					6.01	-0.12 ± 1.29
7	2.35	0.03 ± 0.39	3.94	0.44 ± 0.52	6.10	-0.02 ± 1.30
8					6.07	-0.12 ± 1.30
9	2.15	-0.04 ± 0.48	3.77	0.25 ± 0.50	5.57	-0.13 ± 1.25
10	2.34	0.11 ± 0.48	4.20	0.64 ± 0.69	6.77	0.25 ± 1.67
11					6.76	-0.05 ± 1.67
12	2.97	-0.06 ± 0.67	5.19	0.86 ± 0.97	9.92	0.18 ± 2.29
13					9.95	-0.35 ± 2.29

post–fit residuals computed. Based on Eq. 6.3 the percentage improvement for each test, station and coordinate component has been computed. Figure 6.22 shows the resulting percentages for the height components for all 21 UK CGPS stations and common mode bias tests 1, 3, 5, 7, 9, 10, and 12, according to Table 6.4. The equivalent figures for the North and East components can be found in Appendix L as Figures L.3 and L.4.

As can be seen from Figure 6.22, for most stations and tests the improvement in the RMS scatter of the height component is better than 20%. It is also possible to clearly identify those stations experiencing GPS signal degradations (i.e. ABER, ABYW, MORP and NSTG) or those containing large data gaps (i.e. BRST and HERS) as there is visibly less improvement due to the site–specific behaviour. When inspecting the outcome of the common mode bias tests, it can be seen that for Tests 1, 3, 5, and 7 the percentages of the improvement in the RMS scatter is generally of similar magnitude. For Test 1 the best station–specific improvements are observed for stations that have been used in the stacking process. This is confirmed by the test results for ABER, ABYW, NSTG and MORP, and by the results of Tests 5 and 7 for BARK and LERW. In both cases, the percentage of improvement dropped as the height components for BARK and LERW

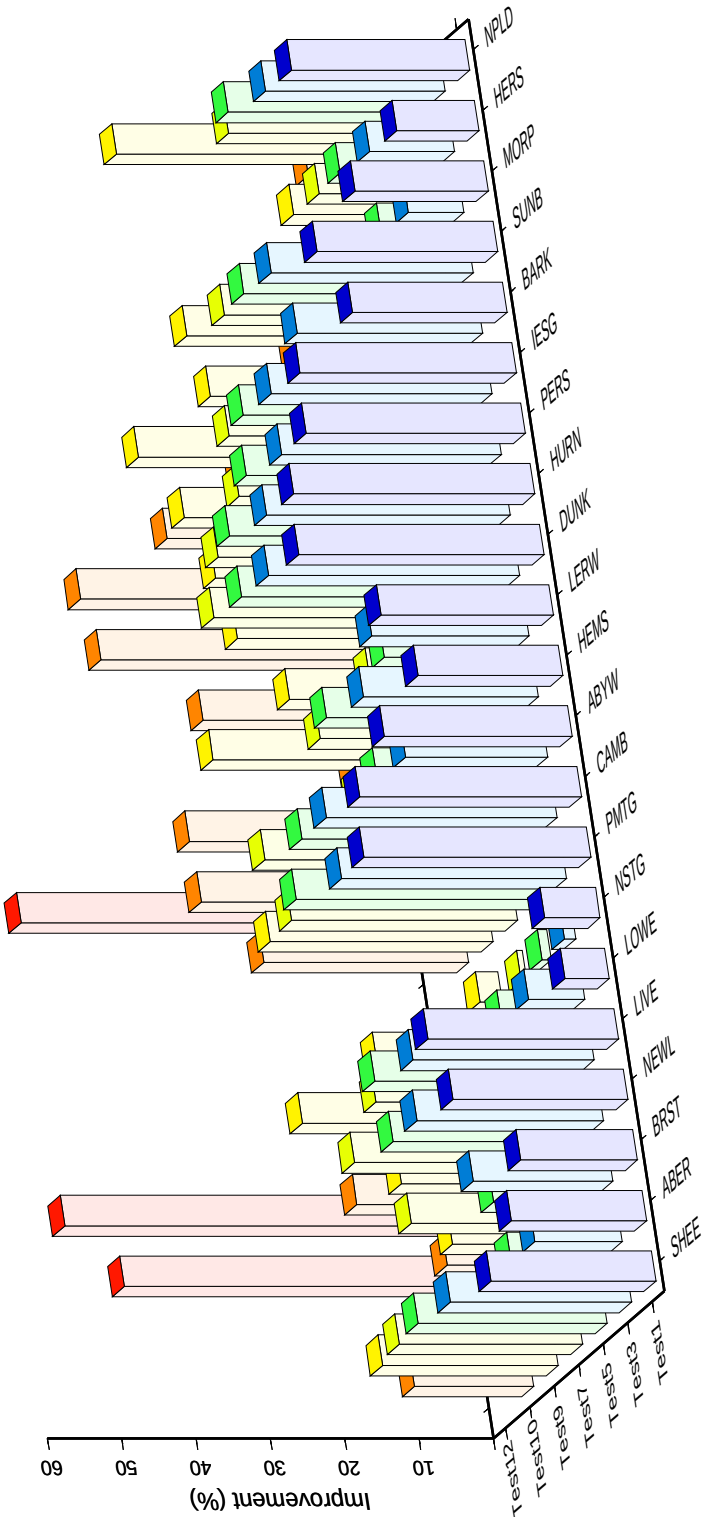

Figure 6.22: Improvement in % of the RMS scatter of the filtered improved ITRS2000 height time series for the 21 UK CGPS stations following common mode bias tests 1, 3, 5, 7, 9, 10 and 12 as outlined in Table 6.4.

were excluded from the stacking process in Test 7. In the bias computation for Test 9 all stations were used, thus the percentage improvements for BARK and LERW increased.

As described, Test 10 was to clarify, whether it would be possible to use a selected sub–set of CGPS stations throughout the UK in order to compute a representative common mode bias for filtering of all stations in the network. As indicated by previous test results, there is a large percentage improvement for stations used in the stacking process such as ABYW, CAMB, DUNK, HURN, LERW, and PERS. Although IESG and HEMS were also applied in the computation of the bias, they show less improvement in Test 10 than for Tests 1 to 9. Interestingly, using Test 10, it was possible to improve the RMS scatter for BRST, NEWL and PMTG, all three situated in the south of England and France, close to the stacking site CAMB. In Test 12, the common mode bias was based only on the input from the three stations in the south westerly part of the CGPS network analysed. All three stations BRST, CAMB and NEWL show an improvement in the RMS scatter of more than 50%. However from Figure 6.22 it is clear that using this estimated bias, it is not possible to improve the other CGPS stations in the network. It can be assumed that the mis–modelling of the OTL effect (§6.3.1) introduced a common systematic bias which dominates the stacking process and hence enables the larger reduction in the RMS scatter for these three stations. For all other stations, however, no or little percentage improvement was achieved.

The numerical results of all tests outlined in Table 6.4 are compiled in tabular format in Tables L.1 and L.2 in Appendix L. Based on the results shown in Table 6.15 and Figure 6.22, Test 5 was selected as the best approach, as it gave the largest improvement for 13 out of 21 CGPS stations. The filtered coordinate time series plot for all of the common mode bias tests can be found on the CD–Rom in directory `/Results/Common_Mode_Bias_Tests`.

Final improved coordinate time series

The final improved coordinate time series have been obtained for the unfiltered and filtered data sets. Figures 6.23 to 6.26 show the unfiltered improved ITRS2000 coordinate time series for the UK CGPS stations analysed by the author. Only stations with observation

time spans of ≥ 2.5 years have been included. For each station and coordinate component, the WRMS statistic (Eq. D.2 in Appendix D) and the station velocity with associated uncertainty are shown. For the horizontal coordinate components the station velocities have been obtained by modelling a linear plus annual term according to Eq. E.9 in Appendix E. No coordinate offset magnitudes were estimated apart from those at HERS. The vertical station velocities were modelled including parameters for coordinate offset magnitudes (Eq. E.12 in Appendix E) at epochs listed in Tables 6.14 and L.5. The velocity uncertainties are based on the findings in §6.3.2 in that the empirical method for obtaining the amplitudes of white and coloured noise discussed in Williams (2003a) seem superior to that in Mao et al. (1999). Therefore, the uncertainties have been computed using Eq. H.13, and H.14 along with Eqs. H.19 and H.20 in Appendix H, (i.e. a WN+FN model).

The filtered improved ITRS2000 coordinate time series are shown in Figures 6.27 to 6.30. These were obtained based on common mode bias Test 5. Test 5 being were SHEE (N, E, H), BRST (N), NEWL (N, E, H), LIVE (H), LOWE (N, E, H), CAMB (N, E, H), HEMS (N, E, H), LERW (N), IESG (N, E, H), BARK (N, E), SUNB (N, H), HERS (N, E, H) and NPLD (N, E, H) were included in the stacking process. They have been modelled in a similar manner as the unfiltered coordinate time series above. These figures do include all stations investigated, as the regional filtering technique can be used to filter coordinate time series shorter than 2.5 years. For those stations, however, no station velocities and uncertainties are shown.

The RMS statistic, station velocities and uncertainties for the unfiltered and filtered improved ITRS2000 coordinate time series have been compiled in Table L.3 in Appendix L. As mentioned above Appendix L also contains Table L.4 and Figures L.5 and L.6, summarizing the annual term estimates for the unfiltered and filtered improved ITRS2000 coordinate time series. The coordinate offset estimates for both the unfiltered and filtered improved ITRS2000 coordinate time series are compared in Table L.5 in Appendix L. The table shows the estimated magnitudes for the coordinate offsets and their uncertainties for epochs listed in Tables 6.14 for the North, East and height components.

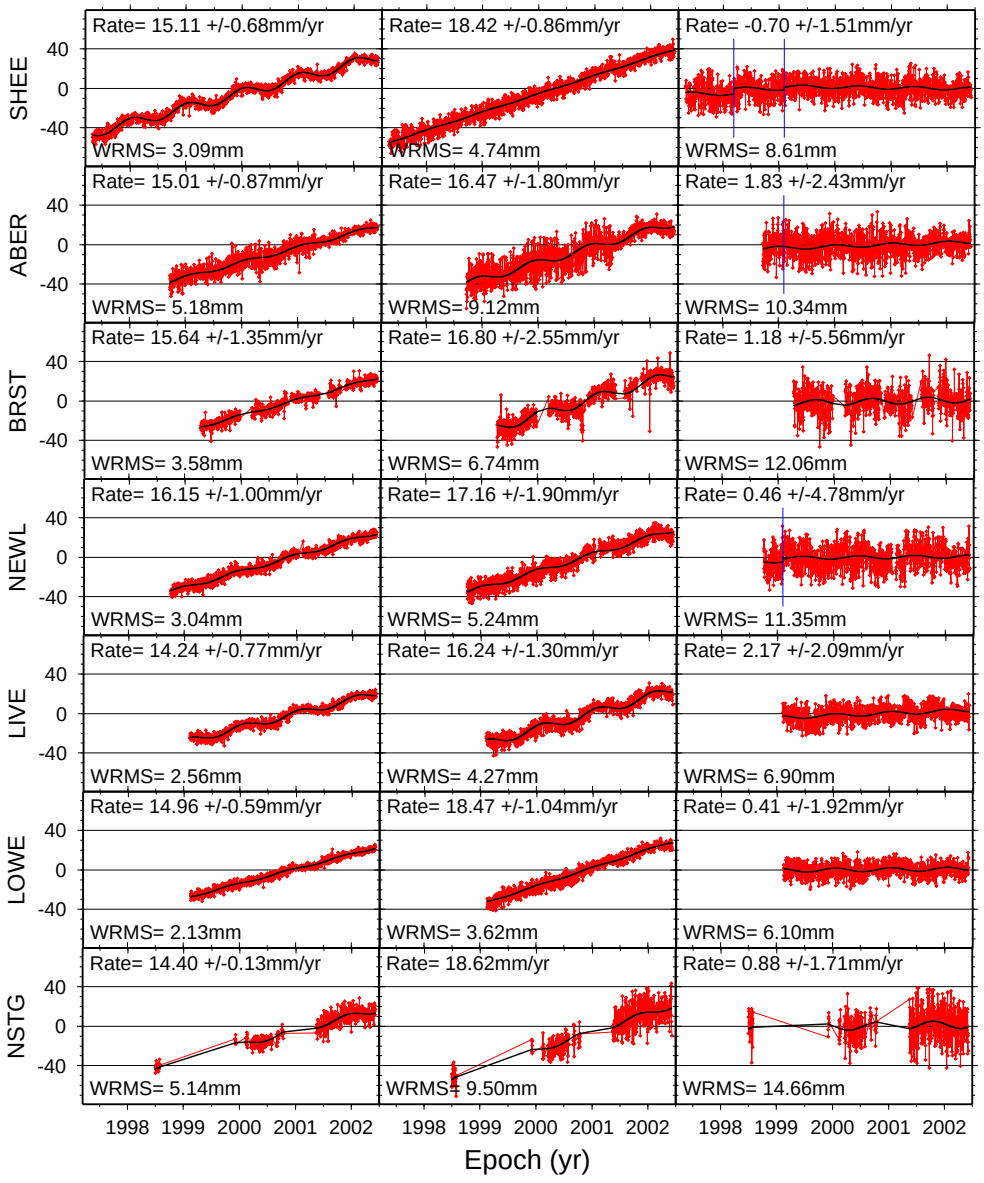

Figure 6.23: Unfiltered improved ITRS2000 coordinate time series for the CGPS@TG stations, based on data analysed up to 31 May 2002. Least–squares model fit is based on a linear and annual term. Vertical lines indicate coordinate offset epochs included in the model.

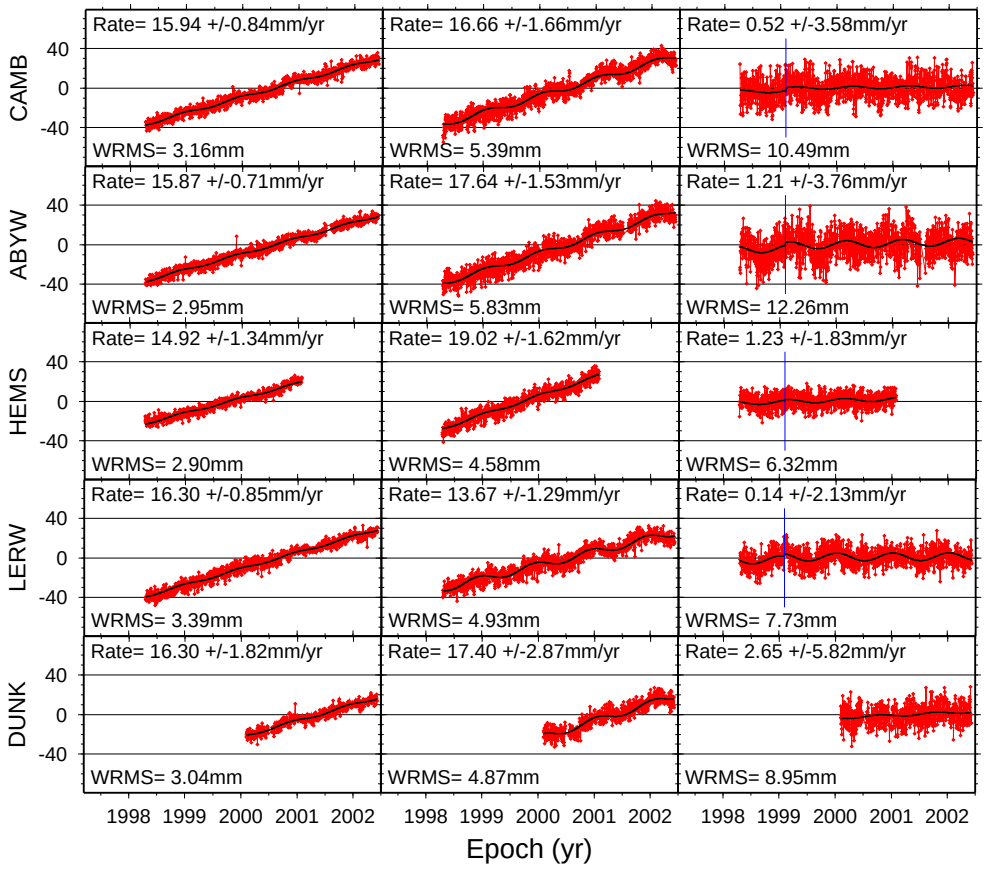

Figure 6.24: Unfiltered improved ITRS2000 coordinate time series for the UK Met Office CGPS stations, based on data analysed up to 31 May 2002. Least–squares model fit is based on a linear and annual term. Vertical lines indicate coordinate offset epochs included in the model.

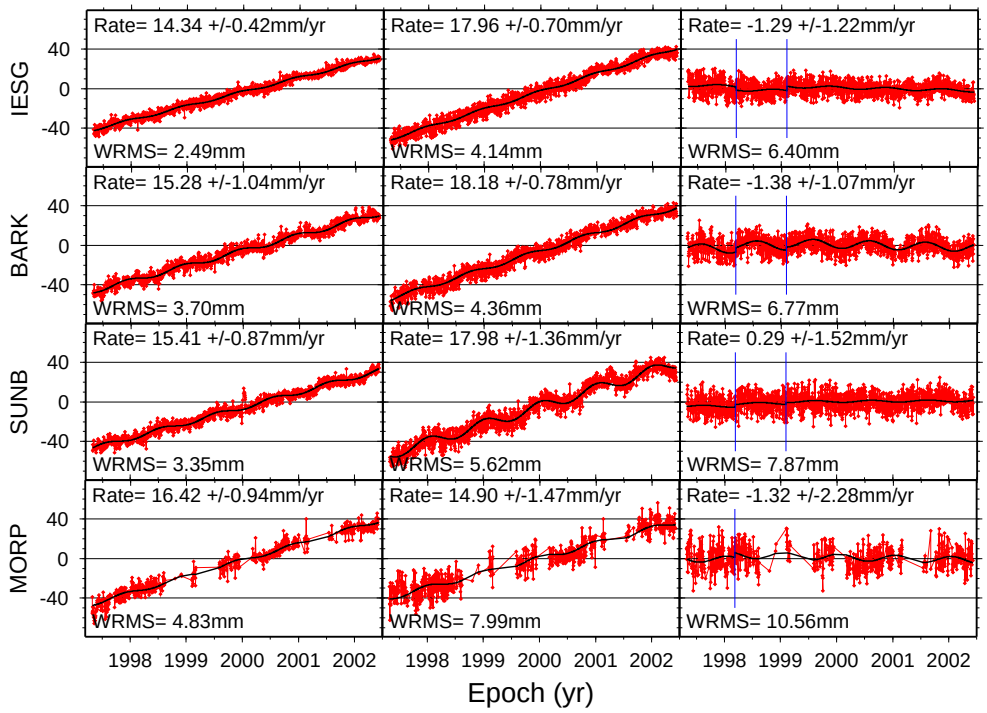

Figure 6.25: Unfiltered improved ITRS2000 coordinate time series for CGPS stations belonging to category *OTHER*, based on data analysed up to 31 May 2002. Least–squares model fit is based on a linear and annual term. Vertical lines indicate coordinate offset epochs included in the model.

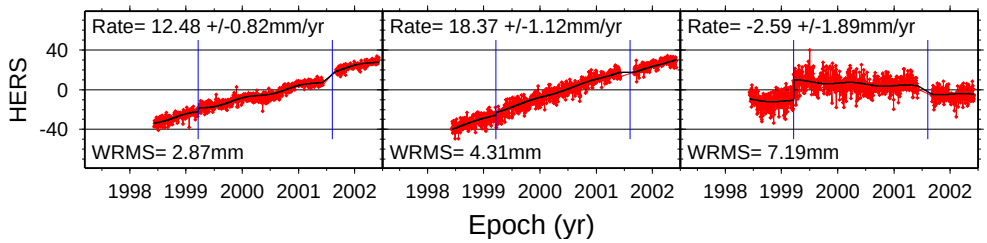

Figure 6.26: Unfiltered improved ITRS2000 coordinate time series for the UK IGS stations, based on data analysed up to 31 May 2002. Least–squares model fit is based on a linear and annual term. Vertical lines indicate coordinate offset epochs included in the model.

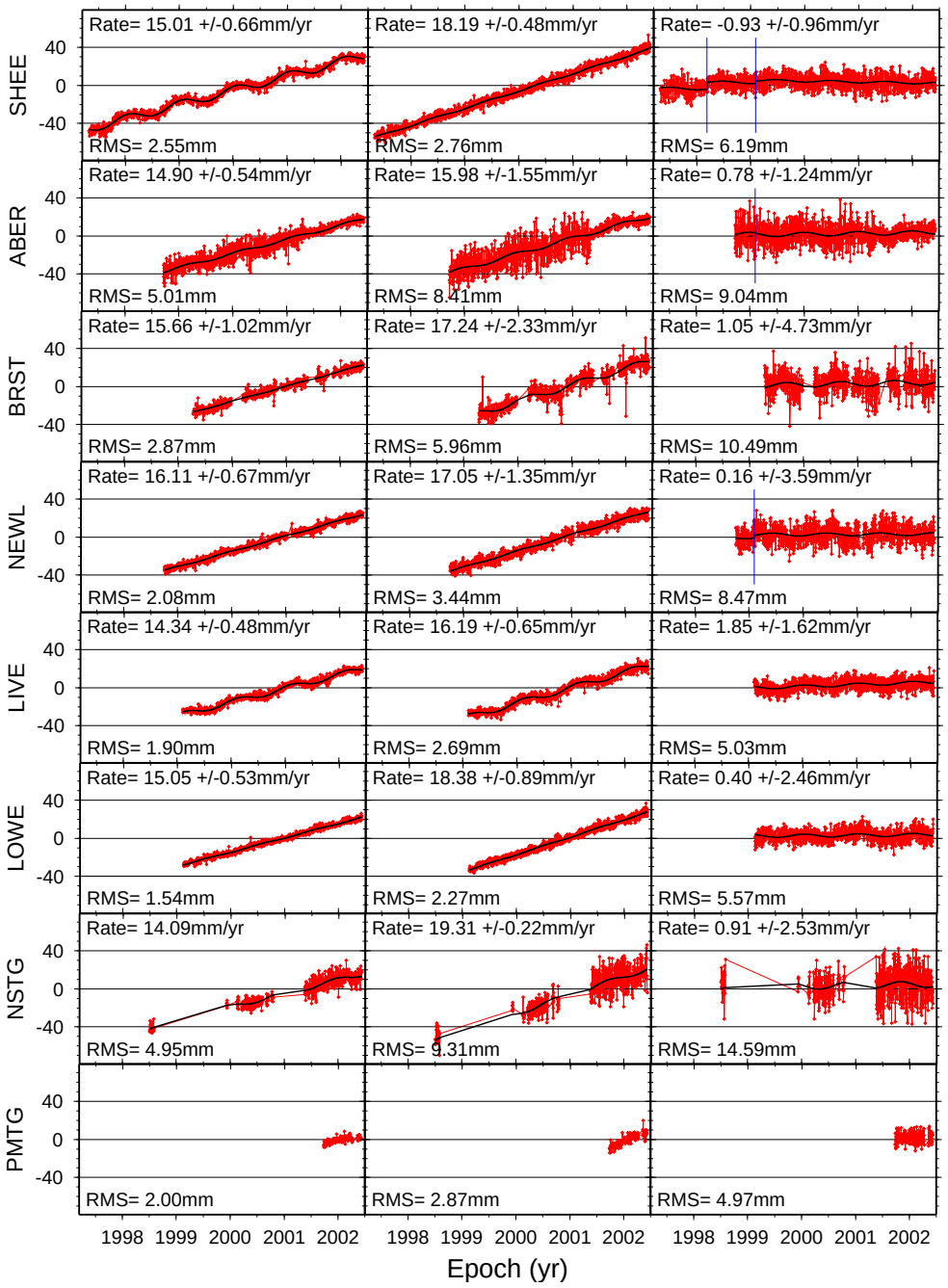

Figure 6.27: Filtered improved ITRS2000 coordinate time series for the CGPS@TG stations, based on data analysed up to 31 May 2002. Least–squares model fit is based on a linear and annual term. Vertical lines indicate coordinate offset epochs included in the model.

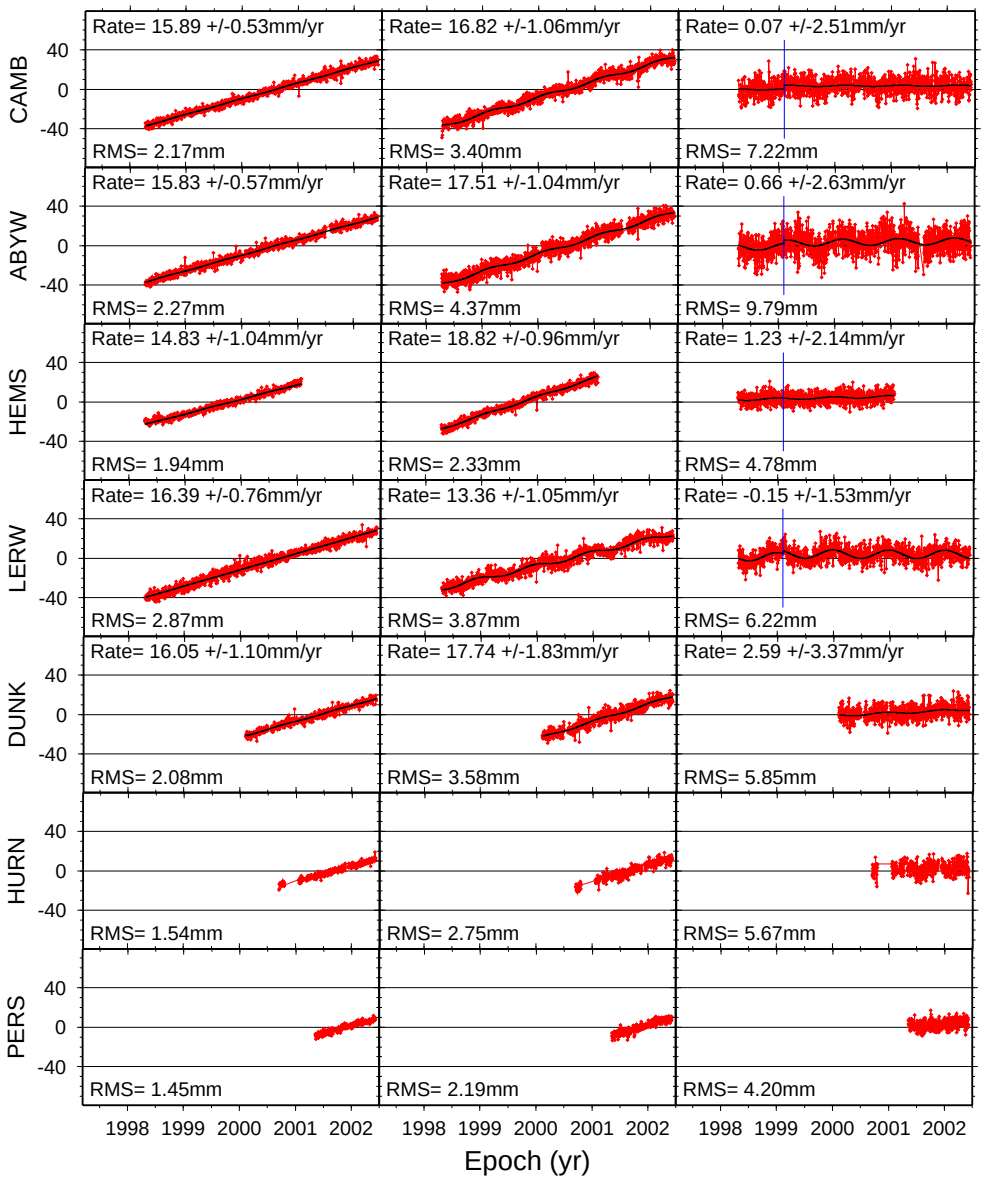

Figure 6.28: Filtered improved ITRS2000 coordinate time series for the UK Met Office CGPS stations, based on data analysed up to 31 May 2002. Least–squares model fit is based on a linear and annual term. Vertical lines indicate coordinate offset epochs included in the model.

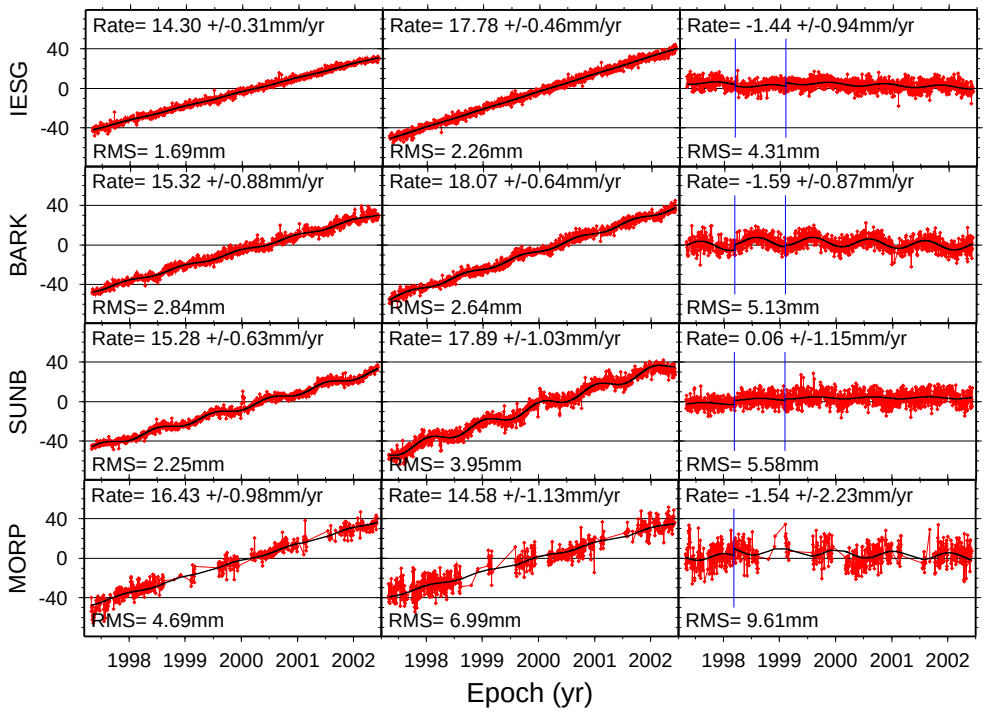

Figure 6.29: Filtered improved ITRS2000 coordinate time series for CGPS stations belonging to category *OTHER*, based on data analysed up to 31 May 2002. Least–squares model fit is based on a linear and annual term. Vertical lines indicate coordinate offset epochs included in the model.

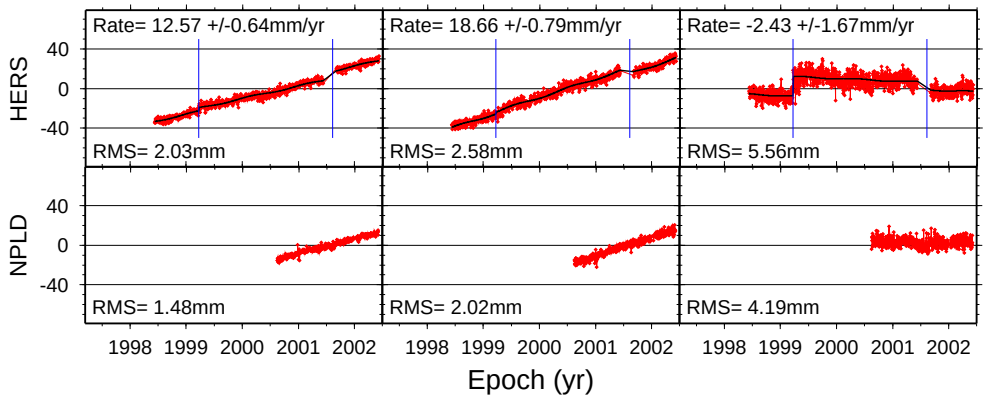

Figure 6.30: Filtered improved ITRS2000 coordinate time series for the UK IGS stations, based on data analysed up to 31 May 2002. Least–squares model fit is based on a linear and annual term. Vertical lines indicate coordinate offset epochs included in the model.

6.4 Summary

In this chapter the analysis of the CGPS coordinate time series for the UK CGPS stations has been discussed. Standard and improved coordinate time series have been introduced.

Using the standard coordinate time series, it was possible to investigate the effect of the GPS processing strategy on the coordinate time series. Furthermore, the differences for two global realizations of the ITRS: ITRF97 and ITRF2000, have been investigated for this network. Based on this it is clear that it is currently not possible to determine absolute vertical station velocities with the required accuracy for monitoring vertical land movements using GPS.

Results for the standard coordinate time series have been improved by the careful identification of coordinate offsets and the inclusion of an annual term in the station velocity estimation using least–squares. The improved coordinate time series have then been used to obtain a set of filtered improved ITRS2000 coordinate time series.

Using MLE a complete model has been fitted to the coordinate time series, estimating all model parameters simultaneously. These MLE derived model parameters obtained for the unfiltered and filtered improved ITRS2000 coordinate time series have been compared with parameters obtained from a simpler analysis. Based on this, the author has arrived at a series of vertical station velocities and uncertainties which can now be used for interpretation of vertical land movements in the UK and comparison with station velocities obtained from absolute gravimetry, GIA models and other GPS analyses.

Chapter 7

The Dual–CGPS Station Concept

7.1 Introduction

In Chapter 3, European Commission COST Action 40, *the European sea–level observing system (EOSS)* was introduced. EOSS working group 1, which was concerned with height reference systems and fixing of TGBMs, recommended the monitoring of vertical land movements at tide gauge sites with CGPS stations established on stable ground within 500 m of the tide gauge itself, in order to enable frequent (at least once a year) high–precision levelling between the tide gauge contact point, the TGBM and the CGPS station survey marker. This requirement may sometimes prove to be difficult to fulfill, as tide gauges are conveniently situated for observing tidal cycles in port or harbour environments, which can be far from optimal for CGPS installations and observations. Large ships moored at the quayside may temporarily inflict large signal obstructions, while activities at the vessel may create hazardous conditions, in which a GPS antenna located at the quayside can potentially be damaged. Additionally, as has been reported in §5.3.3 and in Teferle et al. (2002a), GPS observations in harbours may be affected by radio frequency (RF) interference or multipath effects.

Plag et al. (2000) suggested that in the case where the CGPS station cannot be established on stable ground within 500 m of the tide gauge, a *dual–CGPS station concept* should be employed with a second CGPS station established directly adjacent to or

physically coupled with the tide gauge, in order to guarantee sufficient monitoring of the tide gauge movement relative to the CGPS station on stable ground. Clearly, a problem setting up this second CGPS station can arise if there are large obstructions or possible GPS signal interference close to the tide gauge.

Bevis et al. (2001) agreed that this dual–CGPS station concept is very attractive as the CGPS station at the tide gauge would be expected to be affected by a combination of crustal motion and local vertical land movements, whereas the CGPS station sited on *stable ground* or bedrock would only be subjected to crustal motion. Hence, this would allow for a separation of the underlying geophysical motions from the local vertical land movements in the vicinity of the tide gauge and help in the validation of any vertical station velocity estimates. Bevis et al. (2001) went further, to say that the real benefit of the dual–CGPS station concept would be if the CGPS observations were analysed using kinematic as well as static GPS processing techniques, as this would allow for the identification of short–term relative motion due to thermoelastic or other effects at the tide gauge. However Bevis et al. (2001) questioned whether it was feasible to have two CGPS stations at each tide gauge, in terms of cost. Therefore, Bevis et al. (2001) recommended to always place the CGPS station as close as possible or on the tide gauge and if funding allows for a second CGPS station, this should then be situated on bedrock.

In the UK, the approach has been to establish a single CGPS@TG station at a number of tide gauges, as close as possible or on the tide gauge itself, and then to form dual–CGPS station pairs if there is a second CGPS station founded on solid rock, and within 20km of the tide gauge. In this way, it has been possible to test the dual–CGPS station concept at Newlyn and Lowestoft tide gauges. At this point it should be noted that the author has not attempted to carry out kinematic GPS processing for either of the dual–CGPS station pairs investigated. Such an analysis would have been difficult over the 20km baseline and beyond the scope of this thesis.

Systematic effects introduced by the applied GPS processing strategy, e.g. mis–modelled atmospheric delays or different reference frame constraints, create temporal or spatial correlations within a regional CGPS network. Besides this, loading effects due to surface or atmospheric mass redistribution induce annual vertical crustal motions that have been

shown to be detectable by CGPS measurements (van Dam et al., 1994, 2001). The spatial extent of these long–wavelength loading effects is comparable to the extent of national or regional CGPS networks and hence, can contribute to the spatial correlations contained in the CGPS coordinate time series of such networks. Using the regional filtering technique (§6.2.5), it was shown how common systematic effects can be reduced and the day–to–day scatter in coordinate time series improved. The dual–CGPS station concept is based on a similar approach in that systematic effects common to both stations, i.e. spatial correlations, can be removed. This is true even more so than for a regional network, as it is assumed that the CGPS stations are only separated by a few kilometres, in which case their coordinate time series are normally highly correlated.

An initial evaluation of the dual–CGPS station analysis for the coordinate time series of two dual–CGPS station pairs in the UK has already been described by the author in Teferle et al. (2001, 2002b). These papers discussed the dual–CGPS station analysis in comparison to the more commonly known single baseline analysis, and investigated whether the dual–CGPS station concept improved results when annually repeating signals were apparent in synthetic coordinate time series. Plag and Kristiansen (2001) also showed initial results realized at the tide gauge at Andenes, Norway. In this case, the baseline between a CGPS station installed on bedrock and the CGPS@TG station is 7 km and had been observed since December 2000. After performing a dual–CGPS station analysis and a single baseline analysis on these data, their initial results showed that if the integer ambiguities were resolved at the GPS processing stage, the coordinate difference time series and the baseline time series were almost identical.

Plag and Kristiansen (2001) used coordinate time series obtained from daily solutions of the precise point positioning technique (Zumberge et al., 1997). Using this method, each station is determined on its own and not in a network, therefore GPS measurements from close by stations do not affect the coordinate determination. In the case of double–differencing, it is generally accepted that the inclusion of baselines of >100 km and baselines of a few kilometres in one network adjustment may lead to problems related to the tropospheric delay estimates. Therefore, in global or regional network analyses, the mixing of medium or long baselines with very short ones is usually avoided. If it can be shown by the author that using the currently implemented GPS processing strategy,

the dual–CGPS station analysis delivers equivalent results to the single baseline analysis, where the short baselines are about 20km, this would be of great importance in several ways. Firstly, it would confirm the high quality of the results obtained by the author using the currently implemented GPS processing strategy (§4.5 and §6.3.1). Secondly, it would suggest that reliable relative vertical station velocity estimates can be obtained from a dual–CGPS station analysis, even if the absolute vertical station velocity estimates are biased due to the global reference frame or periodic signals. The last point is even more important when considering the potential number of tide gauges for which there is an existing IGS or EUREF CGPS station on stable ground, within a few kilometers of the tide gauge. The results of a global survey to establish the number of CGPS stations at or close to tide gauges have been presented by Wöppelmann et al. (2002).

This Chapter introduces the concepts and methodology of the dual–CGPS station analysis. The single baseline analysis, as the most accurate method of investigating relative motions between two CGPS stations, is revisited. Using synthetic coordinate time series for the dual–CGPS stations, the effect of annual signals on absolute station velocity estimates is demonstrated. By analyzing these synthetic coordinate time series according to the dual–CGPS station concept, the concept's ability to monitor relative station motions even under the influence of periodic signals is highlighted. Finally, the author has also investigated the feasibility of using an adaptive filtering technique to the analysis of the coordinate time series of dual–CGPS station pairs.

7.2 Concepts and Methodology

This section briefly introduces the concepts of dual–CGPS station and single baseline analysis, the generation of synthetic coordinate time series and the optimisation of an adaptive filtering technique, for this specific application.

7.2.1 Dual–CGPS Station Analysis

In this analysis, data of four UK CGPS stations were used to form two station pairs according to the dual–CGPS concept. As funding was only available to establish a single

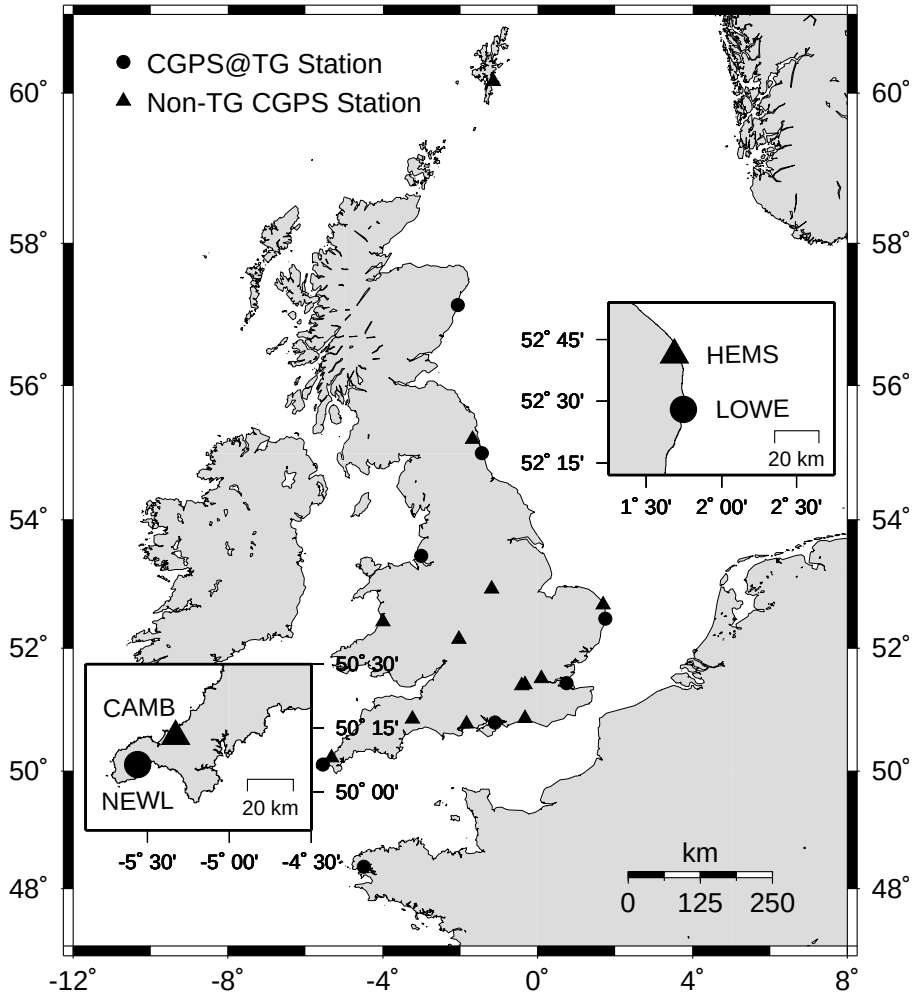

Figure 7.1: The dual–CGPS station pairs

CGPS station at a tide gauge, the GPS antennas were placed as close as possible to the tide gauges at Newlyn (NEWL) and Lowestoft (LOWE) (§5.2). Fortunately, both CGPS@TG stations were close (approximately 20 km) to already existing CGPS stations at Camborne (CAMB) and Hemsby (HEMS). As both of these stations are believed to be well founded and are located in an open environment (§5.2), it was hoped that they would prove to be useful for monitoring vertical land movements and could be considered as *stable*. The UK CGPS network used for the evaluation of the dual–CGPS station concept is shown in Figure 7.1.

At the time of writing, the dual–CGPS station pairs NEWL–CAMB and LOWE–HEMS had a common observation time span of 3.7 and 2.0 years respectively. Unfortunately, the

CGPS site at Hemsby was abandoned in early 2001 (§5.2) and hence, the available time span for the dual–CGPS station analysis for HEMS–LOWE is limited.

Within the dual–CGPS station concept, the coordinate time series of the individual CGPS stations are derived by GPS processing in a *network context*, rather than as a single baseline between the station pair. Once a series of daily network solutions at times t with $t = 1, \ldots, N$, have been obtained for each station, these coordinate time series are differenced such that

$$\mathbf{X}_{AB}(t) = \mathbf{X}_A(t) - \mathbf{X}_B(t) \tag{7.1}$$

with $\mathbf{X}_A(t)$ and $\mathbf{X}_B(t)$ being the coordinates for stations A and B. The coordinate difference time series, as a series of daily coordinate differences $\mathbf{X}_{AB}$, can then be subjected to further analysis and relative station velocities and uncertainties estimated for all components.

7.2.2 Single Baseline Analysis

In contrast to the dual–CGPS station concept discussed above, the single baseline analysis uses the relative coordinate vector between two CGPS stations and is thus independent of constraints due to the global reference frame. Furthermore, it can be argued that if the CGPS stations investigated are close to each other, systematic effects would be common to the GPS signals received at both stations and would cancel during GPS processing. This has the effect that the day–to–day scatter of baseline time series can be smaller than the day–to–day scatter of conventional CGPS coordinate time series. One of the first reported single baseline analyses was carried out across the Hayward fault, California, between 1991 and 1994, using 2.5 years of CGPS data over an eight kilometre baseline (King et al., 1995). A reduction of almost 10 times in the day–to–day scatter of a baseline time series compared to the globally–referenced coordinate time series of two CGPS stations 50 m apart was recently reported by Johnson and Agnew (2000).

In order to be able to assess the results of the dual–CGPS station analysis, the CGPS data of the two CGPS station pairs has also been processed as two single baselines, from CAMB to NEWL and from HEMS to LOWE. Due to the fact that the CGPS stations are

separated by about 20 km, a similar magnitude of reduction in the day–to–day scatter of the baseline time series as in Johnson and Agnew (2000) was not expected. Systematic effects, e.g. tropospheric delay, cannot be assumed to be equal at both stations over such a distance and hence need to be mitigated. Tests on modelling the tropospheric delay by the author showed that the best results for the baseline time series were achieved, using the same strategy as for the automated GPS processing outlined in §4.4. For the single baseline analysis, however, the coordinates for CAMB and HEMS had to be fixed. The tight constraints were necessary as the data from the two stations in the single baseline analysis does not contain enough information to allow the decorrelation of the tropospheric delay estimates. An initial single baseline analysis of the two station pairs in which the coordinates were not fixed, showed a large day–to–day scatter (Teferle et al., 2001).

7.2.3 Synthetic Coordinate Time Series Generation

As mentioned in §6.2.3, Blewitt and Lavallée (2000, 2002) described how annually repeating signals in coordinate time series can bias least–squares velocity estimates. Loading effects, reference frame biases or effects due to the GPS processing strategy, show as periodic signals predominantly in the vertical coordinate component.

Due to the common characteristics of these systematic effects on neighbouring CGPS stations, the dual–CGPS station concept is expected to remove large quantities of these biases. In order to evaluate this over longer time scales than those actually observed at CGPS@TGS stations in the UK, the author generated synthetic coordinate time series with *similar* statistical characteristics to the observed coordinate time series. These synthetic data were based on the RMS statistics of the observed coordinate time series for the individual CGPS stations, the periods and amplitudes of their cyclic signals, especially in the height component, and the apparent improvement of the coordinate difference time series when compared to the coordinate time series. The percentage of improvement and computed cross–correlation coefficients were used as initial values for the amount of spatial correlation assumed between the coordinate time series of the dual–CGPS station pairs.

After numerous test runs were carried out, in which the input parameters were varied in order to reproduce the coordinate time series of the individual CGPS stations, the synthetic coordinate time series were generated using the following equation

$$y_i = x_0 + rt_i + a\cos\left(\frac{2\pi t_i}{365.24219} - \psi\right) + \epsilon_c(t_i) + \epsilon_i(t_i) \tag{7.2}$$

with y_i being the daily synthetic coordinate value at time t_i in days, x_0 and r the initial position and velocity of a linear trend, and a and ψ the amplitude in millimetres and phase shift in units of days of an annually repeating signal in the form of a sinusoid. The random errors $\epsilon_c(t_i)$ and $\epsilon_i(t_i)$ reflect an error component common to both coordinate time series of a station pair and an error component attributed to each individual coordinate time series.

Figure 7.2 compares the observed and synthetic height and height difference time series for NEWL and CAMB for a time span of 2.5 years. The observed height time series for NEWL and CAMB were obtained from Strategy 1 (§6.2.1) and the annually repeating signals had amplitudes of approximately 6 to 8 mm. The figure also includes the RMS statistics (Eq. D.1 in Appendix D) on which the generation of the synthetic height time series was based.

7.2.4 Adaptive Filter Optimization

Adaptive filters based on a least–mean–squares (LMS) algorithm have recently been applied to GPS observations in order to mitigate multipath effects or to investigate plate–tectonic motion signals (Ge et al., 2000; Dodson et al., 2001a; Meng, 2002). In particular, Ge et al. (2000) suggested the use of this filtering method to analyse the CGPS coordinate time series of two neighbouring stations of the Southern California Integrated GPS Network (SCIGN), where they were able to decompose the observed time series into tectonic signal and measurement noise. Furthermore, Ge et al. (2000) successfully applied the adaptive filter to single baseline time series of a five CGPS station network in Taiwan in order to derive fault slip rates.

The general structure of the adaptive filter used in this study, has been denoted in the literature as linear transversal or Wiener filter, e.g. Farhang-Boroujeny (1999); Haykin

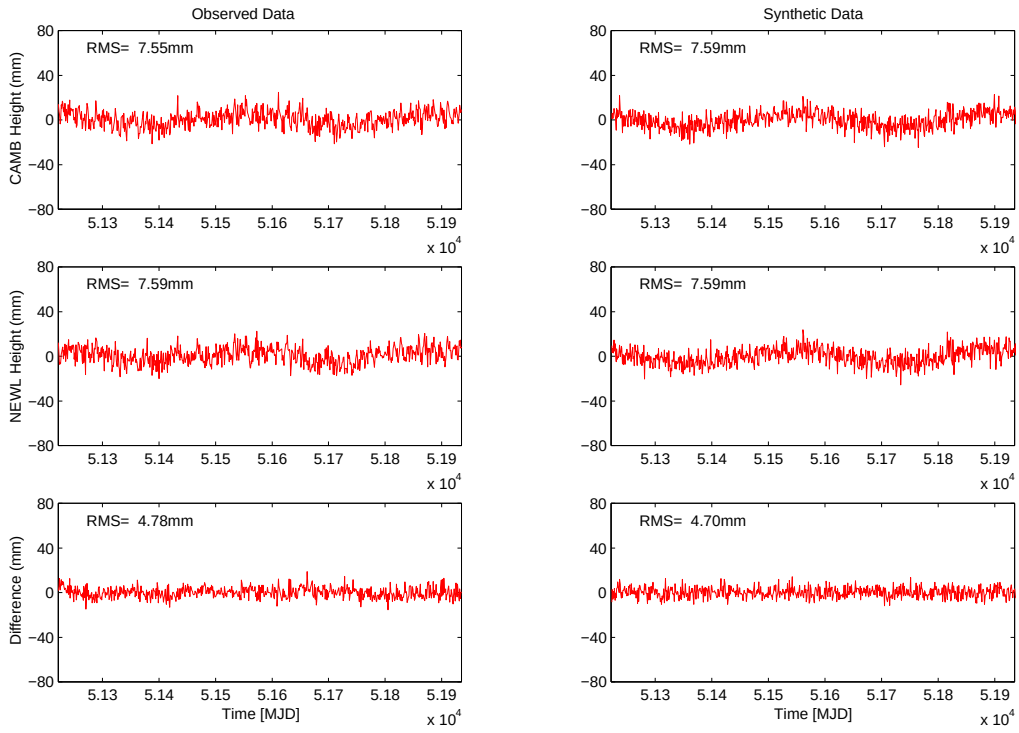

Figure 7.2: Observed and synthetic height and height difference time series compared for dual–CGPS station pair NEWL–CAMB over a common time span of 2.5 years.

(2002), and its formalism (Eqs. I.1 and I.2) are discussed in Appendix I. For the adaptation of the filter coefficients to the input signals, the filter uses the least–mean–squares (LMS) algorithm (Eq. I.8 in Appendix I).

The two main parameters determining the filter characteristics are the *filterlength* M and the *step size parameter* μ (Appendix I). In the investigations detailed in Ge et al. (2000), M was set to 1, 5, and 11 for filtering the kinematic position time series of two consecutive days, the plan coordinate time series of two or more stations and synthetic time series respectively. Ge et al. (2000), however, did not indicate their choice of μ. For the application of the adaptive filter to common signal processing problems, μ was suggested to be between 0.01 and 0.1 (Embree, 1995). Based on the *minimum description length (MDL)* (Eq. I.12 in Appendix I) it is possible to derive the optimum value for M for a specific sample sequence. This, however, requires a MLE in which the optimal filterlength is determined by minimizing the MDL. Although it was assumed to be of great

importance to optimize the adaptive filter for this specific application, the author felt that the MLE at this stage would have been beyond the scope of this research. Instead, the author derived a quick empirical method for finding a *good* set of M and μ to create a highly effective filter that can be applied to the coordinate time series of a dual–CGPS station pair. However, it is strongly suggested that a validation of this empirical method using the MLE is carried out if adaptive filtering is to be used in the long term.

A criterion for testing the effectiveness of the adaptive filter was described by Dodson et al. (2001a). Both reference and desired input sequences, $\{x(n)\}$ and $\{d(n)\}$ respectively, with $n = 0, \ldots, N$, can be decomposed into a signal and noise component. S and S' denoting the signal components and R and R' denoting the noise components of the desired and reference input sequences respectively. If S and S' are correlated signals and R and R' are uncorrelated random noise, then the error sequence $\{e(n)\}$ will be an estimate of S, precisely the correlated or coherent part of $\{d(n)\}$ and $\{x(n)\}$. On the other hand, the filter output sequence $\{y(n)\}$ will be an estimate of R, the uncorrelated or incoherent part, stripped of the common signal S. A similar common part S' and uncorrelated part R' can then be obtained from the adaptive filter by exchanging the input sequences $\{x(n)\}$ and $\{d(n)\}$. Thus the forward and reversed direction filter process can be defined.

To verify this, two uncorrelated white noise sequences with an amplitude of 8 mm where added to two synthetic coordinate time series containing a common linear trend and a common periodic signal. The adaptive filter was then applied in forward direction with $\{d(n)\}$ and $\{x(n)\}$ as desired and reference input sequences and in reversed direction with $\{d(n)\}$ and $\{x(n)\}$ swapped.

The result of this test on the ability of the adaptive filter to separate the correlated or coherent and uncorrelated or incoherent part of two input sequences is shown in Figure 7.3. The figure comprises graphs for the input sequences $\{d(n)\}$ and $\{x(n)\}$ in forward (*Column A*) and in reversed direction (*Column B*) and the four output sequences $\{y(n)\}$, $\{y'(n)\}$, $\{e(n)\}$, and $\{e'(n)\}$. As expected, the filtered sequences $\{y(n)\}$ and $\{y'(n)\}$ show an estimate for the uncorrelated white noise time series of R and R' respectively and the error sequences $\{e(n)\}$ and $\{e'(n)\}$ show an estimate for the correlated or coherent signals S and S'.

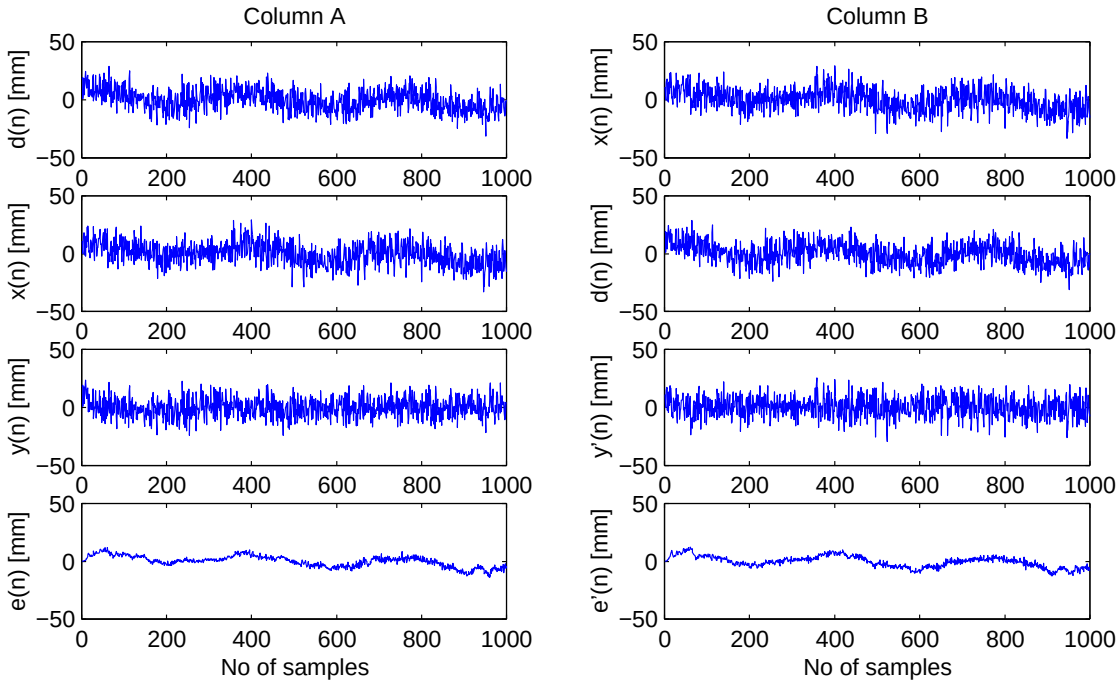

Figure 7.3: Adaptive filter correlation test results. The filter was applied in forward (Column A) and reversed (Column B) input direction by swapping the two input sequences $\{d(n)\}$ and $\{x(n)\}$ of two synthetic time series. The time series contained a common linear trend, a common annually repeating signal and two uncorrelated random noise sequences.

These properties can be used to test the effectiveness and correctness of the adaptive filter (Dodson et al., 2001a), as e.g. the two error sequences $\{e(n)\}$ and $\{e'(n)\}$ should be very similar and hence highly correlated. This assumption is validated for the case, where the adaptive filter is to be used to estimate the signal of two coordinate time series as the average of $\{e(n)\}$ and $\{e'(n)\}$. On the other hand, $\{y(n)\}$ and $\{y'(n)\}$ are estimates of the individually added random noise components and hence, should be uncorrelated. Furthermore, the correlated and uncorrelated components should have been separated by the filter so that $\{e(n)\}$ and $\{y(n)\}$ are not correlated. This also applies to $\{e'(n)\}$ and $\{y'(n)\}$ of the reversed direction filter process. The relationship between the output sequences of the forward and reversed direction filter process expressed by their cross–

correlation coefficients can therefore be summarized by (Dodson et al., 2001a; Meng, 2002)

$$\begin{array}{rll} r_{ee'} = & E[\{e(n)\}\{e'(n-k)\}] = P_k & \forall\, k,n \\ r_{ey} = & E[\{e(n)\}\{y(n-k)\}] = 0 & \forall\, k,n \\ r_{ey'} = & E[\{e(n)\}\{y'(n-k)\}] = 0 & \forall\, k,n \\ r_{e'y} = & E[\{e'(n)\}\{y(n-k)\}] = 0 & \forall\, k,n \\ r_{e'y'} = & E[\{e'(n)\}\{y'(n-k)\}] = 0 & \forall\, k,n \\ r_{yy'} = & E[\{y(n)\}\{y'(n-k)\}] = 0 & \forall\, k,n \end{array} \tag{7.3}$$

with $E[]$ being the statistical expectation operator, P_k the cross–correlation function with $n, k = 0, \ldots, N-1$.

The results of the adaptive filter are dependent on the initial filter parameters, filter-length M and step size parameter μ, as outlined above. Hence, it might be possible to use Eq. 7.3 in order to obtain station–specific values for M and μ that enable a good separation of the coherent and incoherent signals in the coordinate time series of a dual–CGPS station pair.

Intuitively, during effective operation of the adaptive filter the cross–correlation function $r_{ee'}$ should in the best case, approach unity. Similarly, the other cross–correlation functions r_{ey}, $r_{ey'}$, $r_{e'y}$, $r_{e'y'}$ and $r_{yy'}$ should always be close to 0. By definition, these cross–correlation functions can be computed from the filtered and error sequences of the forward and reversed direction filter processes as

$$r_{ee'}(k) = \sum_{n=0}^{N} e(n)e'(n-k), \qquad 0 \le k \le N-1 \tag{7.4}$$

$$r_{ey}(k) = \sum_{n=0}^{N} e(n)y(n-k), \qquad 0 \le k \le N-1 \tag{7.5}$$

The RMS of the difference in the error sequences of the forward and reversed direction filter process can be defined as

$$RMS_a = \sqrt{\frac{1}{N}\sum_{n=0}^{N}(e(n) - e'(n))^2} \tag{7.6}$$

Furthermore, from the above defined cross–correlations it is possible to derive an expression denoted by the author as *separation*. Supposed the adaptive filter effectively separates

coherent and incoherent components in $\{x(n)\}$ and $\{d(n)\}$, then the separation is defined by the cross–correlations in Eqs. 7.4 and 7.5 at zero lag as

$$1 - \frac{r_{ey}(0)}{r_{ee'}(0)} \tag{7.7}$$

Intuitively, for an effectively operating adaptive filter, the correlation and the separation should approach 1, and RMS_a should be small.

Numerous tests carried out by the author showed that the application of the correlation (Eq. 7.4), the separation (Eq. 7.7) and the RMS_a (Eq. 7.6) to finding an empirically optimized combination of M and μ for the adaptive filter, did not lead to satisfactory results. This approach tended to suggest larger M and smaller μ than necessary, i.e. the filter output sequences were too smooth and the filter itself had required longer to adapt its filter coefficients to changes in the input sequences.

In order to correct for this, the author derived an additional parameter in support of the selection of M and μ. This approach was based on the regional filtering technique introduced in §6.2.5. Here it was shown how, by using the common mode bias, systematic effects common to the UK CGPS stations were removed. In this case, an altered bias estimation was carried out in that only data of the dual–CGPS station pair were used. For the general case with input sequences $\{x(n)\}$ and $\{d(n)\}$ the *two–station common mode bias* ϵ can be written as

$$\epsilon(n) = \frac{x(n) + d(n)}{2} \qquad 0 \leq n \leq N \tag{7.8}$$

From experience with the regional filtering technique, it can be assumed that the two–station common mode bias provides an independent estimate of the coherent signal component of $\{x(n)\}$ and $\{d(n)\}$. Subtracting $\{e(n)\}$ and $\{e'(n)\}$ of the forward and reversed direction filter process from the common mode sequence $\{\epsilon(n)\}$, allows the computation of the RMS statistic for the two difference sequences so that

$$RMS_{cm} = \sqrt{\frac{1}{N}\sum_{n=0}^{N}(\epsilon(n) - e(n))^2} \tag{7.9}$$

$$RMS_{cm'} = \sqrt{\frac{1}{N}\sum_{n=0}^{N}(\epsilon(n) - e'(n))^2} \tag{7.10}$$

and their average as

$$RMS_b = \frac{1}{2}(RMS_{cm} + RMS_{cm'}) \tag{7.11}$$

If the two–station common mode bias is a good estimate for the common signal part as assumed, then RMS_{cm} and $RMS_{cm'}$ should be small. As the common mode bias is computed at each sample epoch, it is independent of the common mode estimates before and after. The adaptive filter however, computes its filter output based on a series of filter coefficients, hence its similarity to a moving average process with length M. The differences between the common mode sequence $\{\epsilon(n)\}$ and the error sequences $\{e(n)\}$ and $\{e'(n)\}$ are therefore smaller if a shorter M is chosen. Thus, the author believes that using RMS_b together with the correlation (Eq. 7.4), the separation (Eq. 7.7) and RMS_a (Eq. 7.6) should lead to the selection of a combination of M and μ specific to the input sequences, i.e. the two coordinate time series of a dual–CGPS station pair.

By variation of M and μ in numerous filter processes, the author computed matrices of values for Eqs. 7.4, 7.7, 7.6 and 7.11 to try to identify an area for which M and μ enable *empirically optimized* filtering results.

Figure 7.4 shows the results achieved for the adaptive filter tests using M in the range of 1 to 31 and μ from 1×10^{-6} to 6×10^{-4} for the synthetic coordinate time series described above. The area in the lower right corners show no results as in these areas μ crossed the upper limit (Eq. I.9 in Appendix I) and the filter may become unstable.

The correlation matrix in Figure 7.4 shows the cross–correlation coefficient of $\{e(n)\}$ and $\{e'(n)\}$ according to Eq. 7.4. It demonstrates that a cross–correlation of the error sequences of over 80% is obtainable for $M > 10$ with an area of maximum cross–correlation for $\mu < 1 \times 10^{-4}$. The separation matrix in Figure 7.4 shows the values computed using Eq. 7.7. As described above, it should give an indication of the range for M and μ to be used to achieve a good separation of the coherent and incoherent signal components. The separation matrix indicates that for the synthetic coordinate time series a good separation > 0.8 can be achieved for most of the tested filter parameter combinations. The RMS_a matrix in Figure 7.4 shows the RMS_a values derived according to Eq. 7.6. The figure indicates that the largest RMS statistics of > 3 mm can be found for the area with $M < 10$

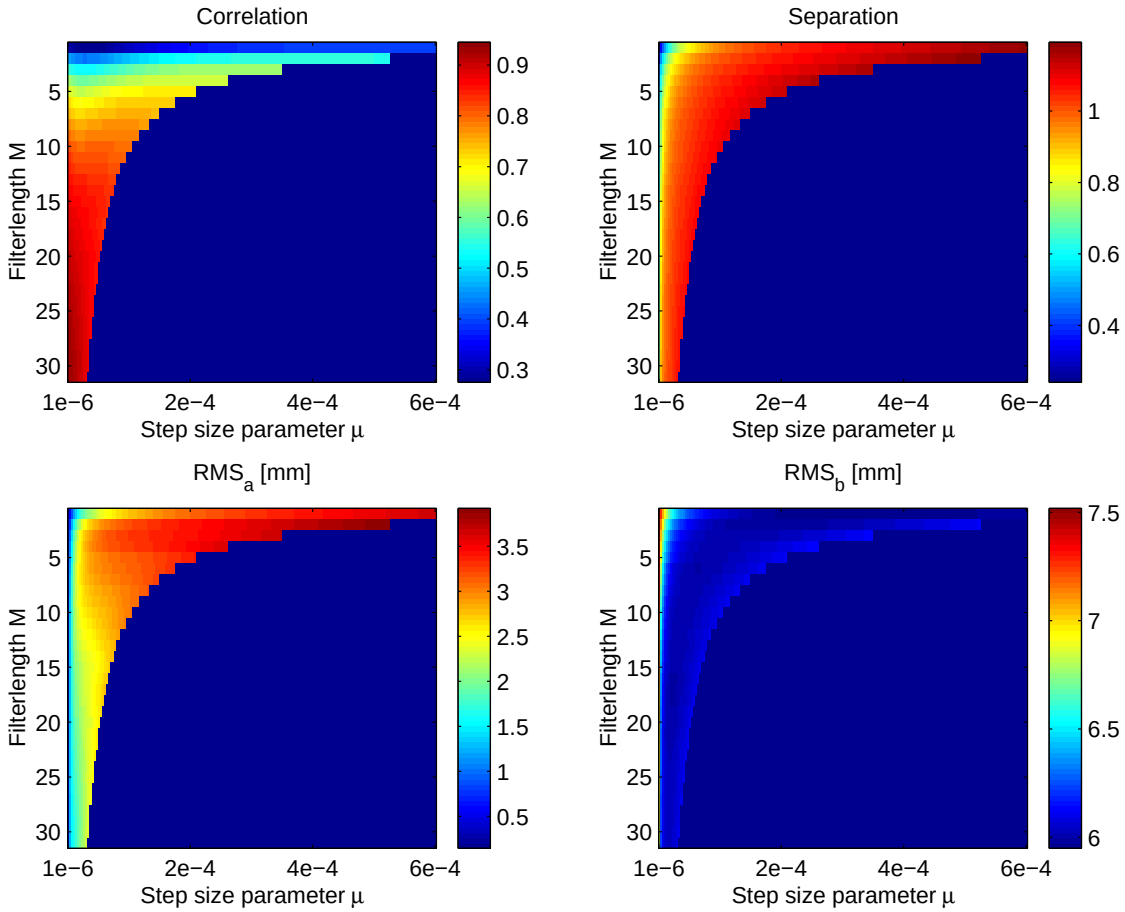

Figure 7.4: Adaptive filter parameter search results for synthetic data.

and $\mu > 5 \times 10^{-5}$, and that the RMS value reduces for larger M and smaller μ. Finally, the RMS_b matrix in Figure 7.4 presents the average RMS statistics computed using Eq. 7.11. For most areas, a $RMS_b < 6.5\,\text{mm}$ is indicated. Only for $M < 5$ and $\mu < 5 \times 10^{-5}$ were larger magnitudes computed.

A quick validation of the empirical optimization can be obtained in two ways for the case of synthetic coordinate time series. Firstly, as the coherent and incoherent signal sequences, $\{S(n)\}$ and $\{R(n)\}$, of the synthetic coordinate time series are known, it is

possible to compute the RMS statistic for the differences between these and the error $\{e(n)\}$ and filtered $\{y(n)\}$ sequences obtained from the filter such that

$$RMS_{S-e} = \sqrt{\frac{1}{N}\sum_{n=0}^{N}(S(n) - e(n))^2} \tag{7.12}$$

$$RMS_{R-y} = \sqrt{\frac{1}{N}\sum_{n=0}^{N}(R(n) - y(n))^2} \tag{7.13}$$

For an effective adaptive filter it is intuitive that both RMS statistics in Eqs. 7.12 and 7.13 should be small or close to zero.

The effectiveness of the adaptive filter using the LMS algorithm can also be evaluated in the frequency–domain. Plotting the power spectra of the input sequences $\{x(n)\}$ and $\{d(n)\}$ enables the identification of common characteristics in both filter inputs, while the power spectra of the filter output sequences $\{e(n)\}$ and $\{y(n)\}$, indicate whether the filter was able to separate these common characteristics from the other features in $\{x(n)\}$ and $\{d(n)\}$. Therefore, the author computed the power spectra (Eq. H.2 in Appendix H) for the filter input and output sequences.

Table 7.1 summarizes the results for Combinations 1 to 12 of M and μ sampled in order to represent a good range of possible filter outcomes.

As can be seen from Table 7.1, this empirical optimization method, identifies a number of combinations with very similar outcomes, hence not clearly defining one optimal combination of M and μ. However, Combination 5, with $M = 25$ and $\mu = 1 \times 10^{-5}$, can be suggested as the most favourable filter parameters for this set of synthetic coordinate time series. The cross–correlation coefficient $r_{ee'}(0)$ of 87% is among the largest, indicating that $\{e(n)\}$ and $\{e'(n)\}$ are highly correlated. Also the difference between $r_{ee'}(0)$ and $r_{ey}(0)$ is among the largest of the combinations, leading to a good decomposition of the filter input signals into coherent and incoherent components. Although, the RMS_a values of Combinations 3 and 5 are equally the smallest of all combinations, the RMS_b is slightly less for Combination 5. Furthermore, both RMS_{S-e} and RMS_{R-y} of Combination 5 indicate that $\{e(n)\}$ and $\{y(n)\}$ better fit the initially generated sequences $\{S(n)\}$ and $\{R(n)\}$ respectively.

Table 7.1: Adaptive filter parameter combination test results for filterlength M and step size parameter μ. $r_{ee'(0)}$ and $r_{ey}(0)$ are the cross–correlation coefficients defined by Eqs. 7.4 and 7.5 at zero lag. RMS_a and RMS_b are computed according to Eqs. 7.6 and 7.11. RMS_{S-e} and RMS_{R-y} are computed using Eqs. 7.12 and 7.13.

Combination	M	μ [$\times 10^{-5}$]	$r_{ee'}(0)$ [%]	$r_{ey}(0)$ [%]	RMS_a [mm]	RMS_b [mm]	RMS_{S-e} [mm]	RMS_{R-y} [mm]
1	5	1	65	13	1.98	6.47	3.45	3.44
2	10	1	77	9	2.31	6.20	2.83	2.82
3	15	1	84	6	2.21	6.07	2.60	2.58
4	20	1	86	4	2.23	6.00	2.50	2.49
5	25	1	87	3	2.21	6.01	2.41	2.41
6	30	1	87	2	2.30	5.99	2.46	2.47
7	5	5	66	0	3.04	6.03	3.05	3.05
8	10	5	78	-2	2.99	6.01	2.67	2.68
9	15	5	83	-5	2.78	6.04	2.63	2.65
10	20	5	84	-6	2.89	6.08	2.71	2.74
11	25	5	83	-8	3.05	6.15	2.79	2.83
11	5	9	69	-3	3.17	6.01	3.04	3.04
12	10	9	77	-6	3.19	6.08	2.81	2.82

Figure 7.5 shows the power spectra of the reference, the desired, the filtered and the error sequence for combination 5 of M and μ, based on the synthetic coordinate time series discussed above. From Figure 7.5 it can be seen that in both power spectra plots of the filter inputs, there is a *well defined* peak at the annual frequency of approximately $3.2 * 10^{-8}$ Hz. At lower frequencies, both power spectra show a typical white noise spectrum. As expected, the power spectral density of $\{y(n)\}$ shows less power at the annual frequency, the common component, and resembles features of the power spectrum of $\{d(n)\}$. Although, the common component seems to have not been removed completely, there is a reduction from approximately 30 dB to less than 25 dB. The peak at the annual frequency of the power spectrum of the error sequence is with approximately 28 dB at similar power to the powers of both input sequences. Furthermore, the power spectral density plot for $\{e(n)\}$ seems to contain some coloured noise (Appendix H), which was introduced by the filtering process.

The introduction of coloured noise into the error sequence by the filtering process is an important finding that needs to be considered when the adaptive filter is to be applied to the observed coordinate time series in §7.3.4.

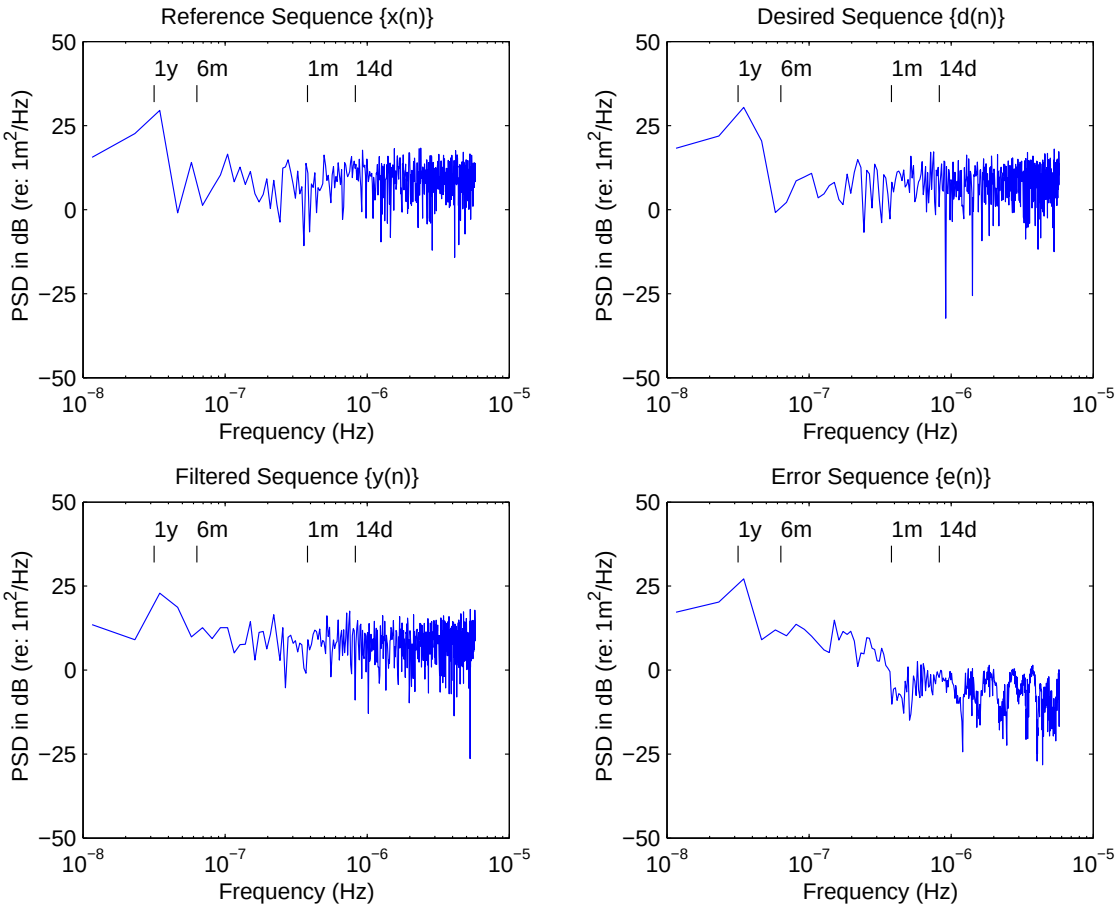

Figure 7.5: Power spectra of the adaptive filter analysis for the reference, desired, filtered and error sequences of the synthetic coordinate time series using $M = 25$ and $\mu = 1 \times 10^{-5}$. Periods of 14 days (14d), one month (1m), six months (6m) and one year (1y) are indicated.

Although the correlation matrix in Figure 7.4 shows the highest cross–correlation and the RMS_a matrix the smallest RMS values for $M > 10$, and the tests suggested that combination 5, with $M = 25$ and $\mu = 1 \times 10^{-5}$, were the most favourable filter parameters for the synthetic coordinate time series, tests by the author showed that the filter tends to *over–filter* the synthetic coordinate time series in those areas. This is due to the fact that for large M, more samples of the input sequence $\{x(n)\}$ are used to compute the filtered sequence $\{y(n)\}$, which has an averaging effect and thus short–term variations may be reduced. Similarly, an increasingly smaller μ makes it difficult for the filter to

adapt to changes in both input sequences and may therefore, not separate the coherent and incoherent components reliably.

7.3 Results

After the dual–CGPS station analysis, the single baseline analysis and the adaptive filter optimization have been discussed in the previous section, it is now possible to present the results obtained for each method for the dual–CGPS station pairs NEWL–CAMB and LOWE–HEMS. Furthermore, the effect of the GPS processing strategy (§6.2.1) and the reference frame(§6.2.2) on the resulting coordinate difference time series is investigated. It is also possible to compare the dual–CGPS station analysis results with those of the single baseline and adaptive filter analysis.

7.3.1 Dual–CGPS Station Analysis

As described in §7.2.1 the dual–CGPS station analysis is carried out by differencing the coordinate time series of two CGPS stations. For the dual–CGPS station pair NEWL–CAMB the analysis results are shown in Figure 7.6. The figure shows the observed ITRS2000 coordinate time series for both stations and the coordinate difference time series for the common period from September 1998 to May 2002. Additionally, Figure 7.6 shows a linear trend model with its rate and uncertainty of which the latter was computed using Eq. H.13 and H.14 along with Eq. H.19 and H.20, i.e. the empirical method given by Williams (2003a). As the coordinate time series for both CGPS stations have been reduced to daily solutions present at both stations, the station velocities and uncertainties differ from those in Chapter 6.

When comparing the coordinate time series for the dual–CGPS station pair NEWL–CAMB, similarities in trend or other signals, especially the annually repeating character of both height time series, can be considered as common systematic features or errors. The dual–CGPS station analysis should difference away those common signals. The day–to–day scatter of the coordinate difference time series should be reduced and the coordinate difference time series itself should be free of common systematic errors. This assumption is

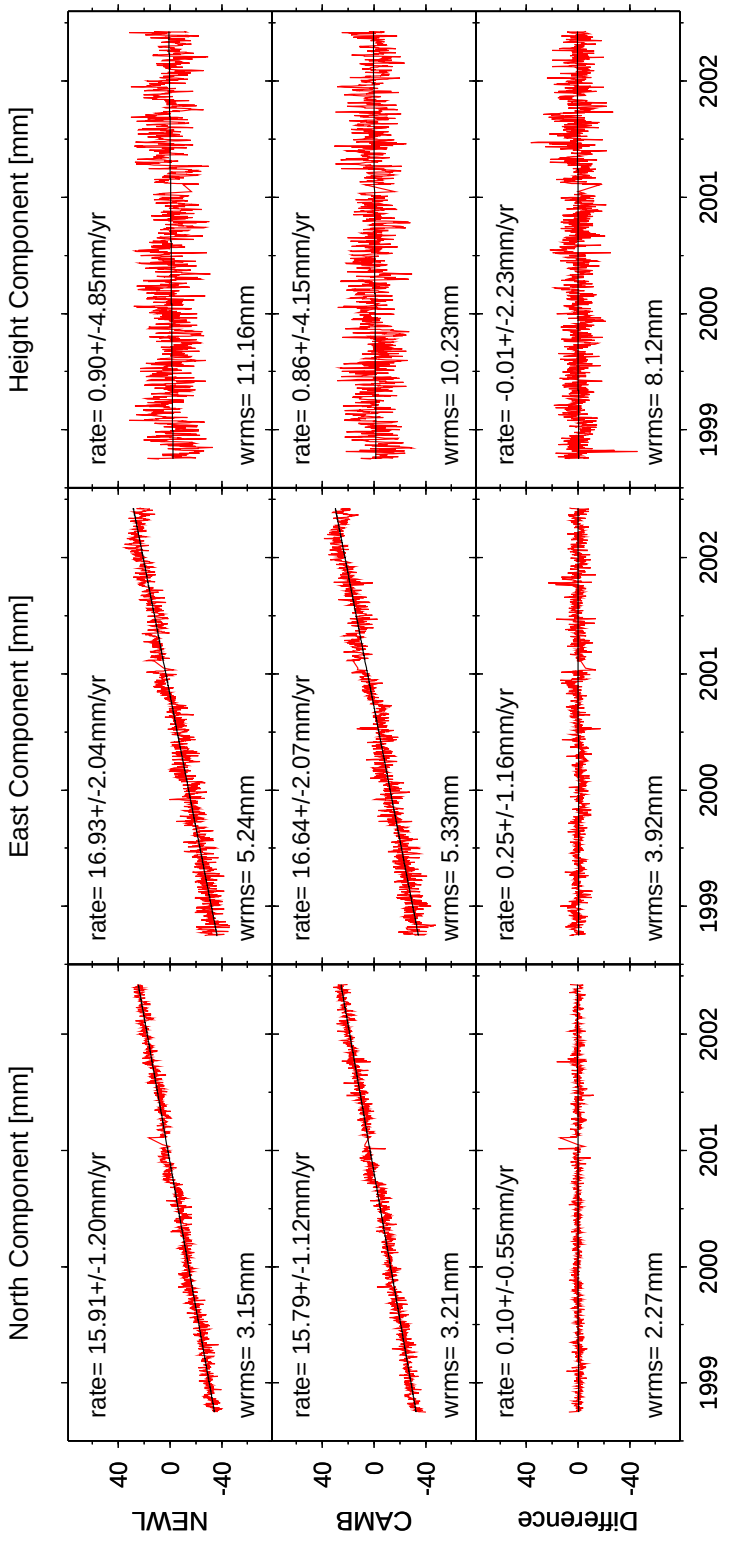

Figure 7.6: Dual–CGPS station analysis of observed ITRS2000 coordinate time series for station pair NEWL–CAMB over a common time span of 3.7 years.

validated when comparing the *cleaner* coordinate difference time series with the coordinate time series for the individual CGPS stations. Furthermore, this is quantified by comparing the WRMS statistic (Eq. D.2 in Appendix D) for the coordinate time series with the WRMS statistic for the coordinate difference time series.

Figure 7.7 shows the observed ITRS2000 coordinate time series and the coordinate difference time series for the dual–CGPS station pair LOWE–HEMS for the common period from February 1999 to January 2001. Due to the fact that this period is shorter than the recommended minimum observation time span of 2.5 years (Blewitt and Lavallée, 2002), no station velocities are shown in this figure. However, the relative velocities of the coordinate difference time series are given.

The results of the dual–CGPS station analyses have been summarized in Table 7.2. The table shows the WRMS statistic for all coordinate and coordinate difference time series, the station velocities and associated uncertainties computed using Eq. H.13 and H.14 along with Eq. H.19 and H.20 for station pair NEWL–CAMB and both coordinate difference time series. As mentioned, the reduction in the day–to–day scatter in the coordinate difference time series is an indicator of the correlation in the coordinate time series of each station pair. The amount of correlation can easily be estimated by computing the cross–correlation coefficients between the coordinate time series (see §6.2.5). Table 7.2 shows the cross–correlation coefficients of the coordinate time series computed over the common observation spans for each station pair, and with a linear trend removed. Furthermore, the table shows the percentage of the improvement of the WRMS statistics denoted as WRMS improvement.

From Table 7.2 it can be seen that the WRMS statistic for the height components of stations NEWL and CAMB are both larger than 10 mm. This has already been discussed in §6.3.1 and is due to the wrong application of the OTL corrections in GAS. This is also the reason for the larger uncertainties associated with the station velocities obtained for these stations. The effects of mis–modelling the OTL effect are not apparent in the coordinate time series for station pair LOWE–HEMS. This can be explained by the fact that the effect is less pronounced on England's east coast than in the south west. From the station velocities it can be seen that the difference in the velocities of the individual coordinate

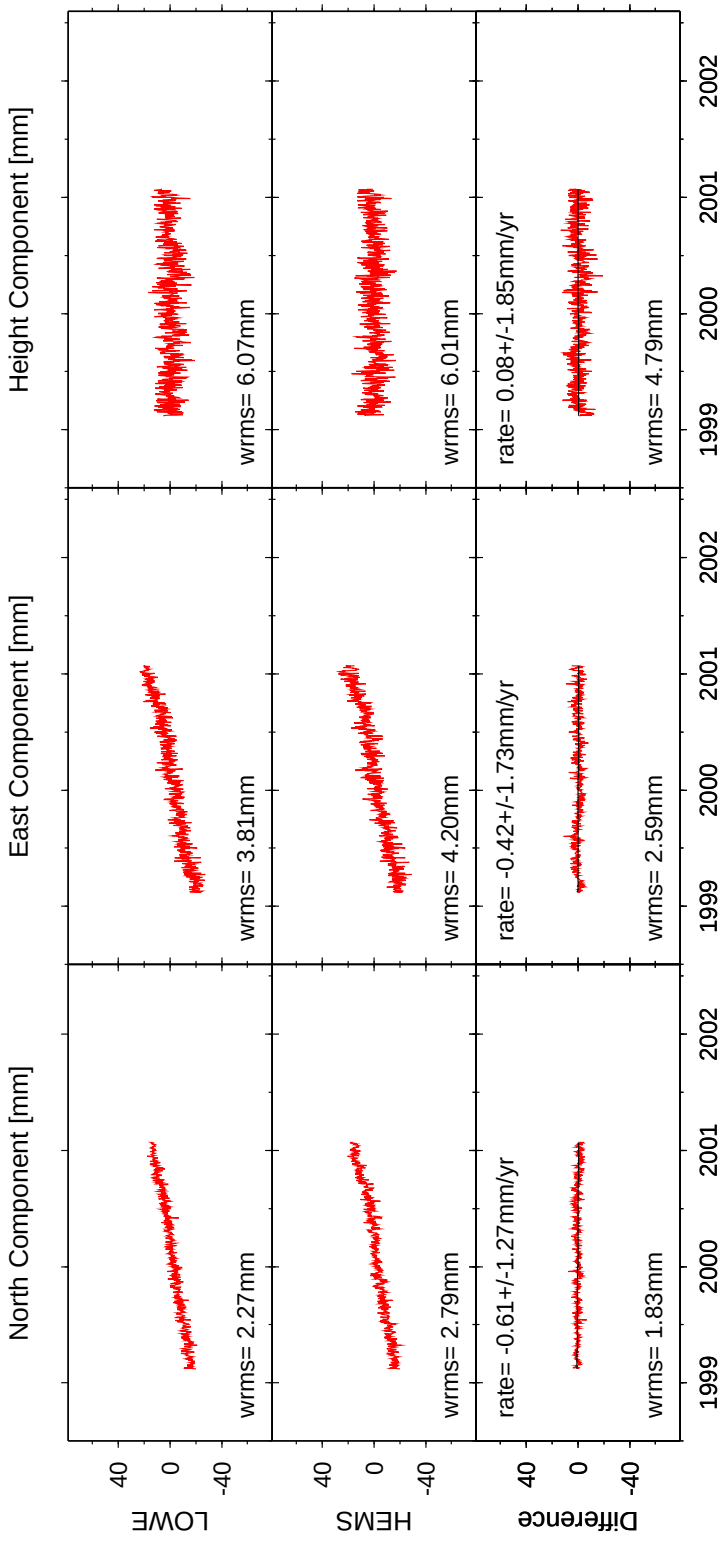

Figure 7.7: Dual–CGPS station analysis of observed ITRS2000 coordinate time series for station pair LOWE–HEMS over a common time span of 2.0 years.

Table 7.2: Results of the dual–CGPS station analysis for station pairs NEWL–CAMB and LOWE–HEMS based on observed ITRS2000 coordinate time series over time spans of 3.7 and 2.0 years respectively. The cross–correlation coefficients have been computed between the coordinate components of both station pairs. The WRMS improvement is the average percentage by which the WRMS statistic was reduced.

Site	Component	WRMS [mm]	Velocity [mm/yr]	Correlation Coefficient [%]	WRMS Improvement [%]
NEWL	North	3.15	15.91 ± 1.20	76	
	East	5.24	16.93 ± 2.04	73	
	Height	11.16	0.90 ± 4.85	73	
CAMB	North	3.21	15.79 ± 1.12		
	East	5.33	16.64 ± 2.07		
	Height	10.23	0.86 ± 4.15		
NEWL–CAMB	North	2.27	0.10 ± 0.55		28
	East	3.92	0.25 ± 1.16		26
	Height	8.12	-0.01 ± 2.23		24
LOWE	North	2.27		78	
	East	3.81		82	
	Height	6.07		71	
HEMS	North	2.79			
	East	4.20			
	Height	6.01			
LOWE–HEMS	North	1.83	-0.61 ± 1.13		26
	East	2.59	-0.42 ± 1.73		35
	Height	4.79	0.08 ± 1.85		21

time series for station pair NEWL–CAMB is effectively equal to the velocity estimate from the coordinate difference time series. However, the large uncertainties indicate that none of the station velocities are statistically significant at this stage. From the cross–correlation coefficients it can be seen that the coordinate time series of both station pairs are correlated by more than 70%. This indicates that although the OTL effect has not been correctly modelled, the overall modelling errors introduced are similar for both stations in each station pair, and that by using the dual–CGPS station analysis it was possible to reduce this error to a large degree. The WRMS improvement is indicated to be on average 26% and 27% for station pairs NEWL–CAMB and LOWE–HEMS respectively. Both the cross–correlation coefficients and the WRMS improvements suggest that if the individual coordinate time series are correlated with approximately 75%, a reduction in the day–to–day scatter of the coordinate difference time series of about 25% may be expected.

In order to demonstrate the independence of the coordinate difference time series from reference frame biases, the author carried out a dual–CGPS station analysis of both the ITRS97 and ITRS2000 coordinate time series for both station pairs. The coordinate difference time series for the two reference frames have then been compared by differencing the coordinate difference time series and computing the RMS statistic (Eq. D.1 in Appendix D). From Figures M.1 and M.2 in Appendix M it can be seen that this RMS statistic is in all cases sub–millimetric, with a maximum value of <0.2 mm. These test results confirm that the coordinate difference time series obtained from the dual–CGPS station analysis of both station pairs are independent of the reference frame for the individual coordinate time series and that reference frame biases are removed successfully by this analysis.

In a similar manner, it was possible to test the independence of the coordinate difference time series to the different GPS processing strategies; Strategies 1 and 2 outlined in §6.3.1. As a reminder, in Strategy 1, the coordinates of KOSG were tightly constrained at the network processing stage, while in Strategy 2, the non–fiducial approach was carried out and no stations were constrained. Besides this, the OTL model was updated and modelling of OTL was also carried out for the horizontal coordinates, which highlighted the problem with the application of the OTL corrections in GAS (see §6.3.1).

Figures M.3 and M.4 in Appendix M show the coordinate difference time series obtained for both processing strategies. Again the RMS statistic was computed for the coordinate difference time series of two dual–CGPS station analyses. With RMS values of 0.6, 1.1 and 2.0 mm and 0.4, 0.7 and 1.3 mm for the North, East and height components of station pairs NEWL–CAMB and LOWE–HEMS, respectively, the difference between the two processing strategies seems to be greater than the difference between the two reference frames. Although the author believes that a large amount of the systematic effect due to the mis–modelling of the OTL effect has been cancelled out in the dual–CGPS station analysis of the coordinate time series for Strategy 2, it is difficult to draw final conclusions about the effect of this at this stage. However, the fact that the RMS values for station pair LOWE–HEMS are also larger when compared to those of the reference frame test, and that the OTL effect is less pronounced at these sites, suggests that the apparent differences, although small, are due to the change in the processing strategy.

7.3.2 Dual–CGPS Analysis and Single Baseline Analyses Compared

In §7.2.2 the single baseline analysis was discussed. For both station pairs investigated, NEWL–CAMB and LOWE–HEMS, the single baseline analysis has been carried out with coordinates of CAMB and HEMS fixed, respectively. In this manner, baseline time series were obtained for each coordinate component, which can now be compared to the coordinate difference time series obtained from the dual–CGPS station analysis.

Figure 7.8 shows the coordinate difference and the single baseline time series for the North, East and height components for station pair NEWL–CAMB. The baseline time series is basically the variation of the coordinates of NEWL with respect to CAMB. By differencing these two time series, the difference between the results of the dual–CGPS station and single baseline analyses have been obtained. These difference time series are shown in the bottom row. As an indication of the scatter in all time series plots shown in Figure 7.8, the RMS statistic computed using Eq. D.1 in Appendix D is also given.

When comparing the single baseline time series with the coordinate difference time series, it is immediately visible that both seem to be very similar in their features and day–to–day scatter. This is confirmed by the RMS statistics for both the coordinate difference and single baseline time series, with RMS values being equal in the North and slightly smaller for the baseline time series in the East and vertical components. The agreement between the coordinate difference and single baseline time series can be quantified by the RMS statistics for their difference time series, which range from about 1.6 to 4.3 mm for all coordinate components. Additionally, cross–correlation coefficients can be computed between the coordinate difference and single baseline time series shown in Figure 7.8. With 72, 80 and 83% for the North, East and height components respectively, it can be concluded that the results from the dual–CGPS and single baseline analysis are highly correlated and in good agreement.

Figure 7.9 shows the coordinate difference, the single baseline and their difference time series for station pair LOWE–HEMS. Again the RMS statistics for all time series are shown in the figure. For this station pair the RMS statistics for the coordinate difference and single baseline time series indicate even more so that the results from the different analyses

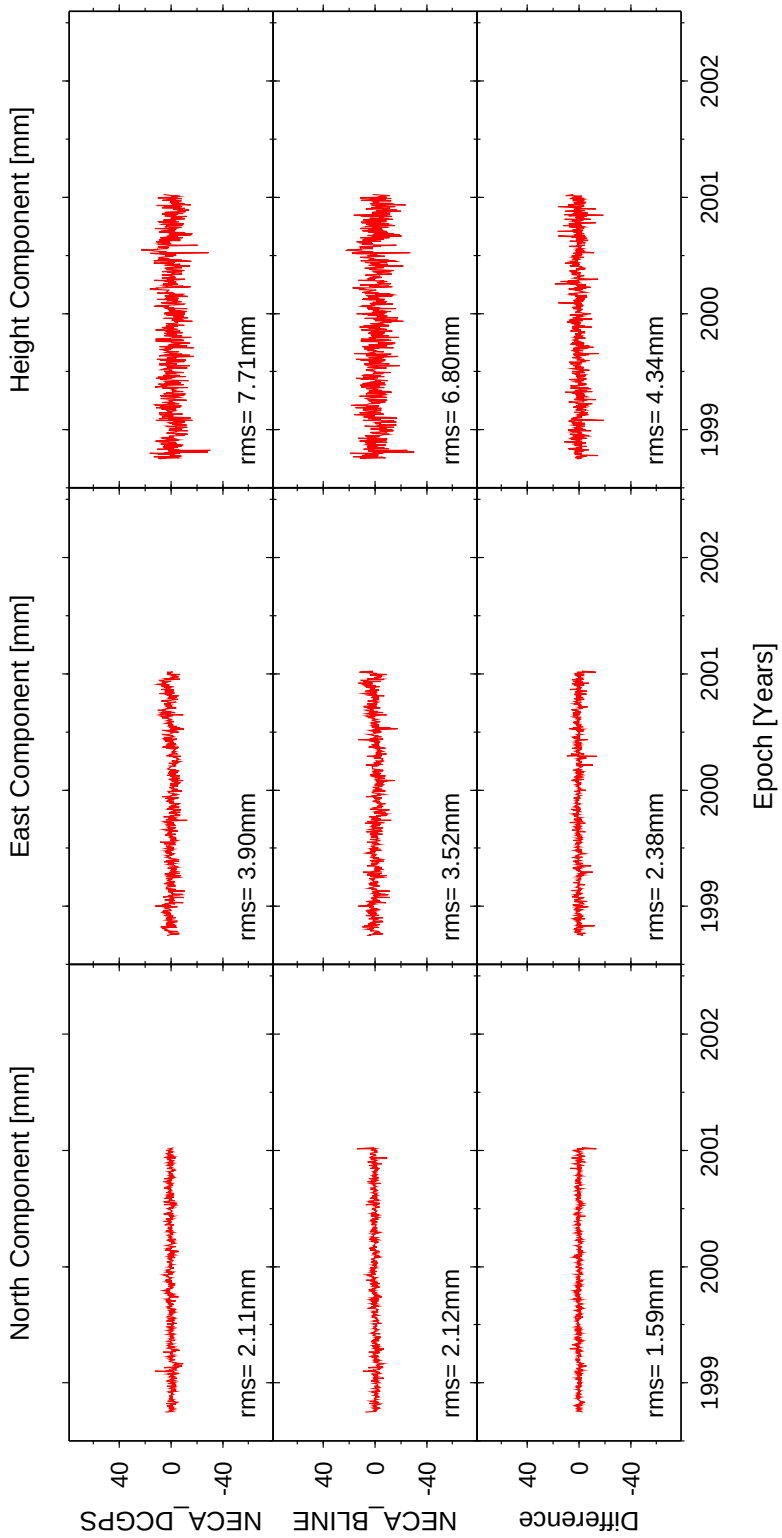

Figure 7.8: Dual–CGPS station and single baseline analyses compared for station pair NEWL–CAMB over a common time span of 2.3 years. NECA_DCGPS and NECA_BLINE denote the coordinate difference and baseline time series respectively.

are very similar. It must, however, be noted that the RMS statistic of the difference time series for the North component does not indicate an agreement as high as for station pair NEWL–CAMB. In fact, the cross–correlation coefficient between the coordinate difference and single baseline time series for the North component only indicates a correlation of 50%, rather than the 85 and 71% for the East and vertical components respectively.

These results are very encouraging, especially when considering that the resulting time series were derived using completely different processing strategies. They further underline that possible effects due to reference frame constraints or the applied processing strategy can to a large degree be reduced by the dual–CGPS station analysis.

7.3.3 Synthetic Coordinate Time Series Analysis

As outlined in §7.2.3, synthetic coordinate time series with a length of 6 years were generated using input parameters derived from the observed coordinate time series of both dual–CGPS station pairs. The synthetic coordinate time series were then analysed according to the dual–CGPS station concept. In a further step, the velocities were estimated at daily intervals for a time span of 1 to 6 years. Figure 7.10 shows the least–squares velocity estimates for the synthetic height time series of the individual CGPS stations and the height difference time series, with time series 1 and 2 being representative of the synthetic height time series of CAMB and NEWL, respectively. For demonstrational purposes, linear trends were omitted when generating these synthetic coordinate time series, hence the *true* relative vertical station velocity is 0.

Cyclic variations are clearly visible in the absolute vertical station velocity estimates for time series 1 and 2. These graphs confirm the recommendation of Blewitt and Lavallée (2000, 2002) to only analyse CGPS coordinate time series that contain annually repeating signals with a minimum observation length of 2.5 years and to only use data time spans of integer–plus–half years thereafter, as the velocity bias is minimal at those times. The figure also demonstrates that in a case similar to the dual–CGPS station pair NEWL–CAMB, vertical station velocity estimates will still be subjected to a bias due to the annual signal, even after 6 years of observations. The relative vertical station velocity estimates based on the coordinate difference time series however, do not show any periodic variations.

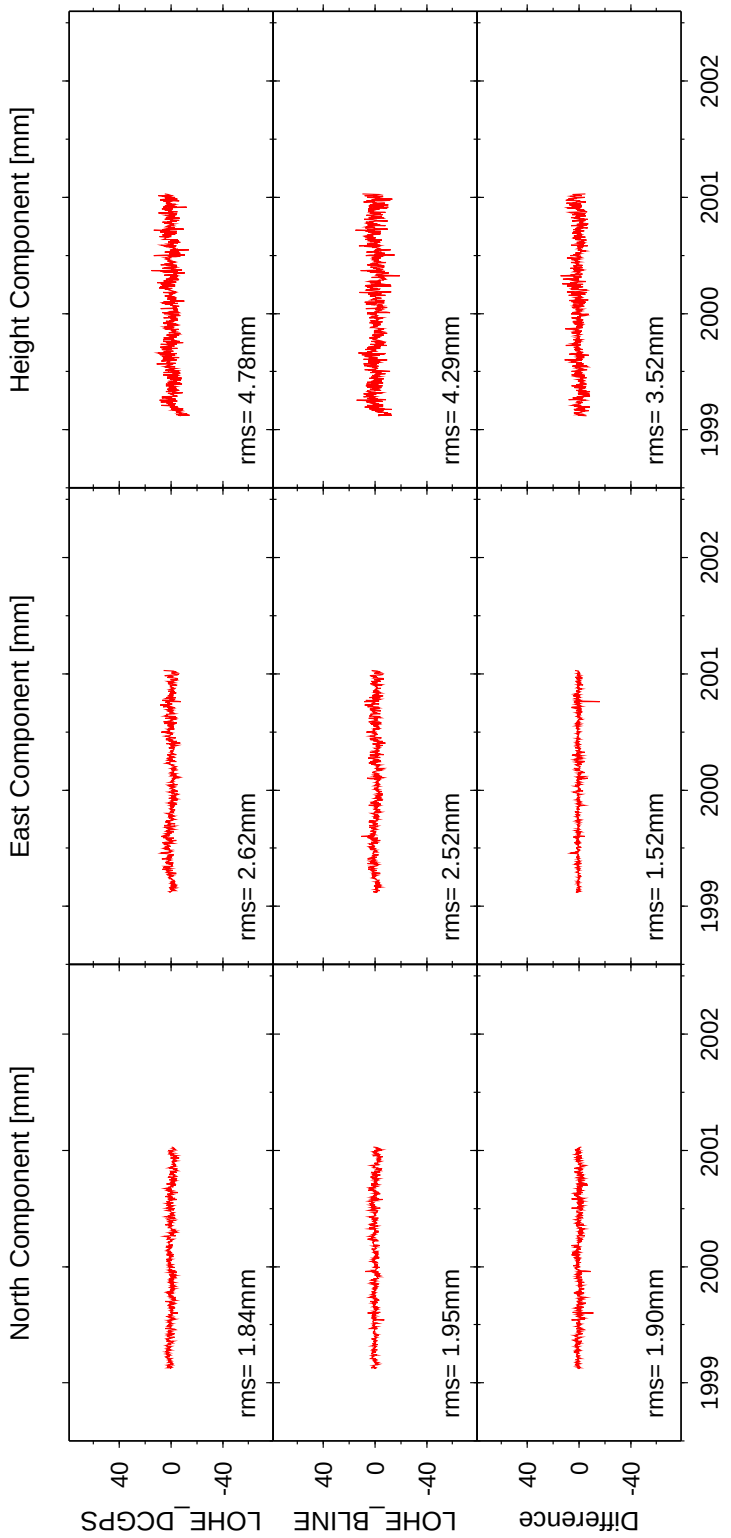

Figure 7.9: Dual–CGPS station and single baseline analyses compared for station pair LOWE–HEMS over a common time span of 1.9 years. LOHE_DCGPS and LOHE_BLINE denote the coordinate difference and baseline time series respectively.

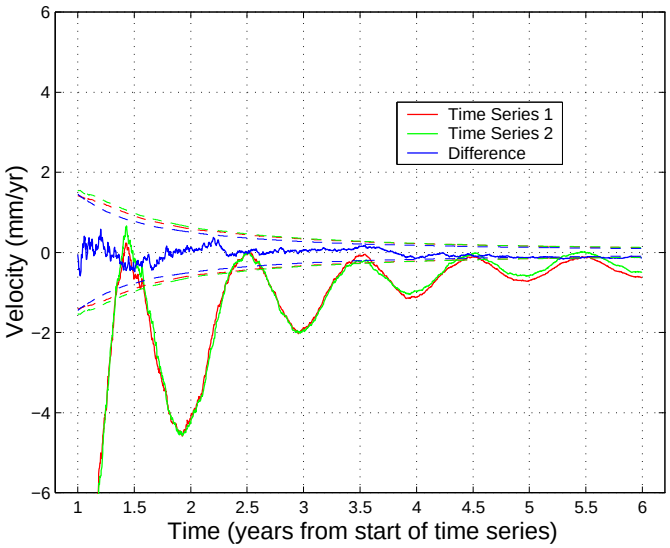

Figure 7.10: Least–squares velocity estimates of two synthetic coordinate time series and their coordinate difference time series for 1 to 6 years. Dashed lines show the velocity uncertainties according to a white noise only model.

Furthermore, in this case, the *true* relative vertical station velocity is obtained after only 2.5 years.

Additionally, Figure 7.10 shows velocity uncertainty estimates as dashed lines according to the standard white noise model. This model does not account for the velocity bias introduced by the periodic variations in the synthetic coordinate time series. As can be seen from the figure, the uncertainty estimates for the velocities of time series 1 and 2 are too optimistic if an annual signal is present and it has not been modelled in the least–squares fit. Hence, the velocity bias due to the annually repeating signal should be included when estimating these uncertainties. However, for the relative vertical station velocity estimates the computed uncertainties based on a white noise only model quantify the errors reliably.

7.3.4 Adaptive Filtering

In this section, a set of empirically optimized filter parameters, i.e. the filterlength M and the step size parameter μ of an adaptive filter using the LMS algorithm are presented. The

empirical method has been applied to the coordinate time series of the two dual–CGPS station pairs NEWL–CAMB and LOWE–HEMS according to §7.2.4.

The practical application of the adaptive filter to the dual–CGPS station concept is carried out by using the individual coordinate time series as reference and desired sequences $\{x(n)\}$ and $\{d(n)\}$. This is done for each coordinate component and for the forward and reversed direction filter process.

Filter Parameters for the dual–CGPS stations

In the first step of the adaptive filter analysis, a combination of empirically optimized M and μ have to be determined for each coordinate component and each dual–CGPS station pair. This has been carried out using the method outlined in §7.2.4. Due to the problems related to the OTL modelling in the ITRS2000 coordinate time series obtained using the non–fiducial GPS processing strategy (Strategy 2 §6.2.1), the filter parameter tests were based on the ITRS97 coordinate time series from Strategy 1.

Figures 7.11, 7.13, and 7.15 show the resulting correlation, separation, RMS_a and RMS_b matrices for the North, East and height components for station pair NEWL–CAMB, and Figures 7.12, 7.14, and 7.16 for station pair LOWE–HEMS, respectively.

In each figure, M was varied between 1 and 31, and μ between 1×10^{-6} and 6×10^{-4} in order to find a combination specific for each coordinate component of each dual–CGPS station pair. When comparing the results for the combinations of M and μ in the figures for NEWL–CAMB with those of LOWE–HEMS, the different upper limits for μ (Eq. I.9 in Appendix I) largely define the number of combinations of M and μ available for comparisons without being in danger of the LMS algorithm becoming unstable. As can be seen from Eq. I.9, the upper limit for μ is largely dependent on the power of a coordinate time series.

From a first impression of Figures 7.11 to 7.16, it can be said that the correlation (Eq. 7.4) matrices show the highest cross–correlation coefficients for $\{e(n)\}$ and $\{e'(n)\}$ for μ generally smaller than 1×10^{-4}. Furthermore, M has got to be larger than 5 in order for the cross–correlation coefficients to approach 1.

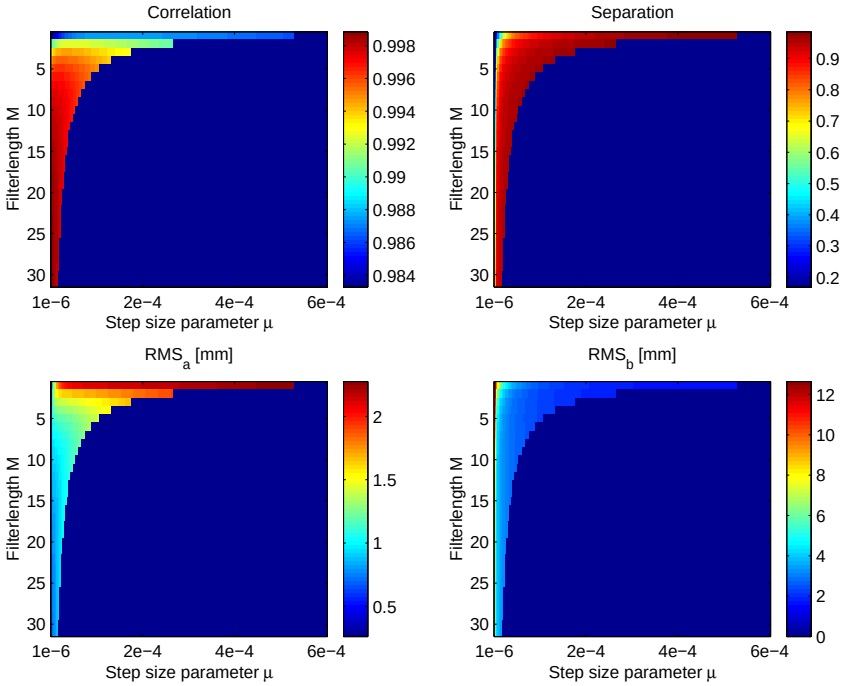

Figure 7.11: Adaptive filter parameter search results for the NEWL–CAMB North component.

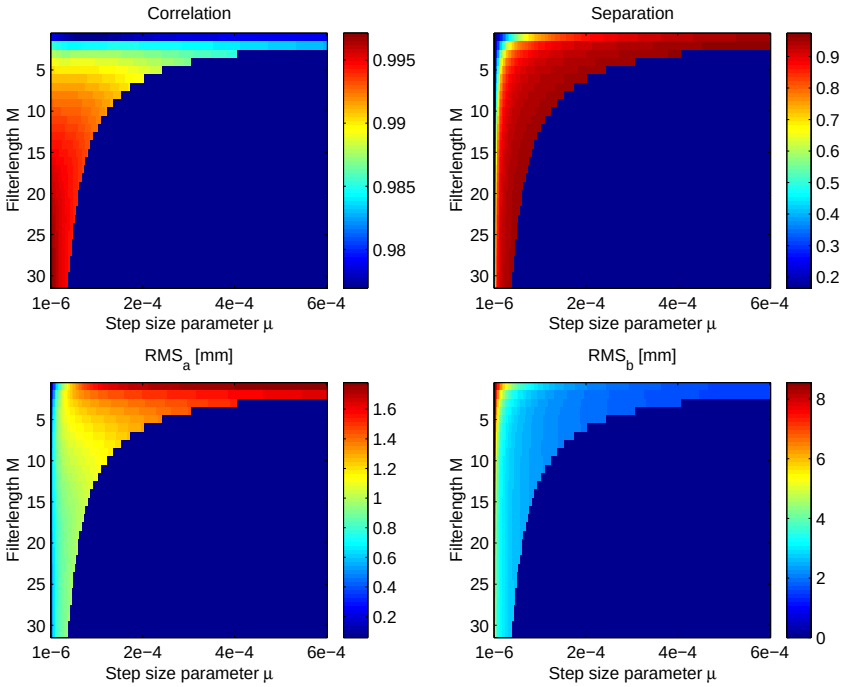

Figure 7.12: Adaptive filter parameter search results for the LOWE–HEMS North component.

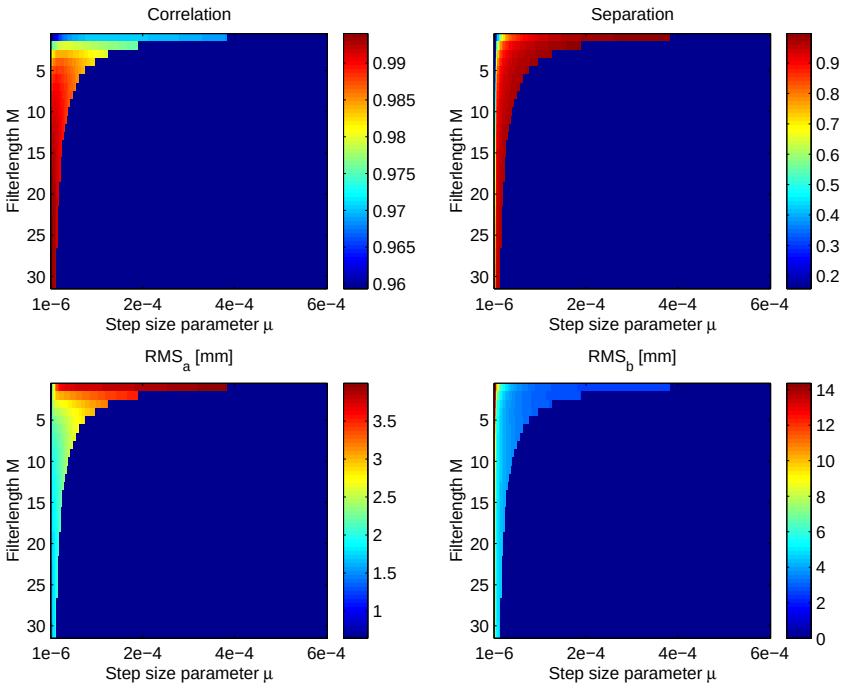

Figure 7.13: Adaptive filter parameter search results for the NEWL–CAMB East component.

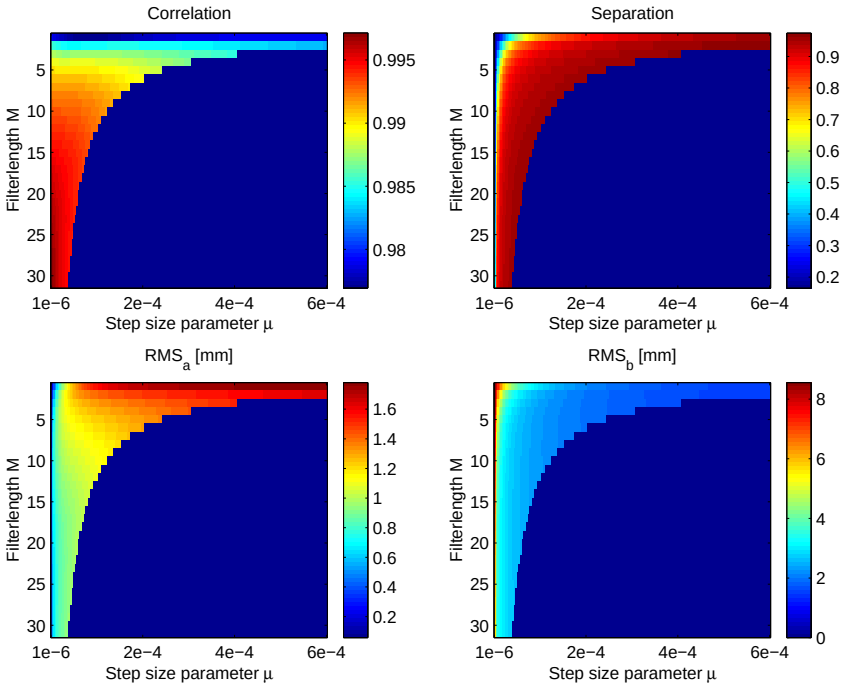

Figure 7.14: Adaptive filter parameter search results for the LOWE–HEMS East component.

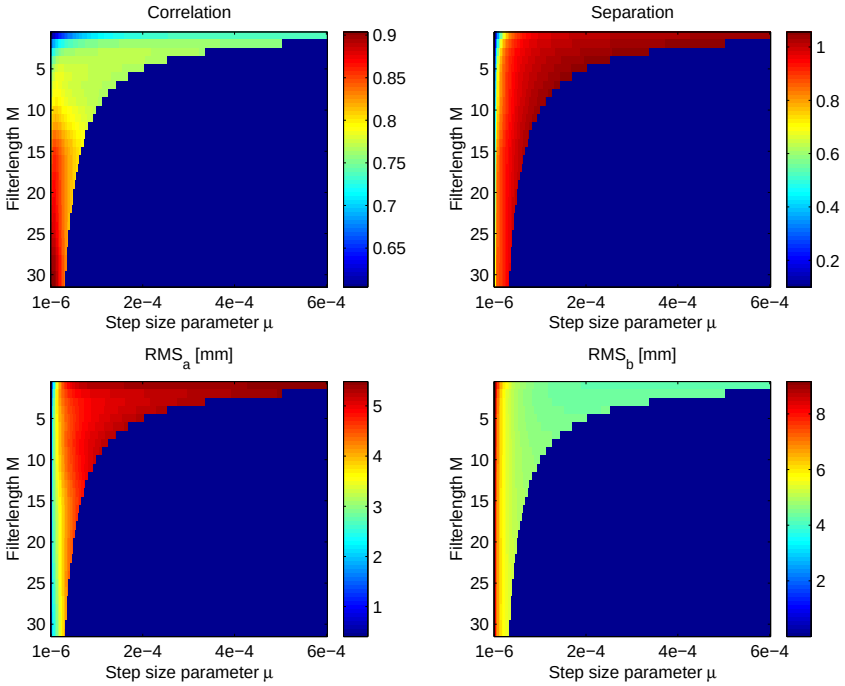

Figure 7.15: Adaptive filter parameter search results for the NEWL–CAMB height component.

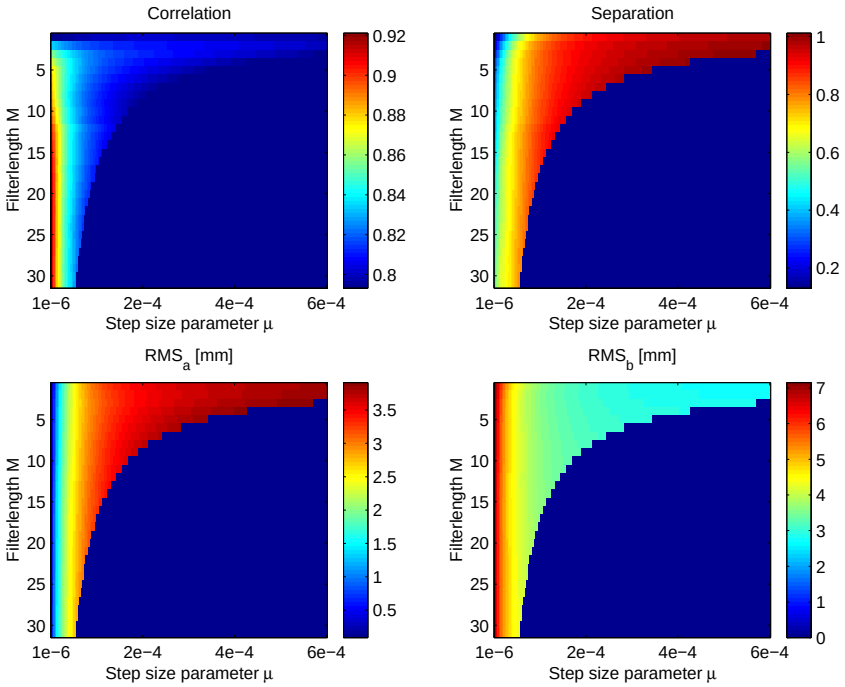

Figure 7.16: Adaptive filter parameter search results for the LOWE–HEMS height component.

The largest values in the separation matrices (Eq. 7.7) of Figures 7.11 to 7.16, can be found along the upper limit for μ for all M for the North and East coordinate components. For the height components, the pattern seems to be different, as the largest separation values are found for smaller M and in areas of larger μ. Due to this, the areas showing better separation are better defined for height rather than for the plan components. However this may be an artefact of the annual variations in the ITRS97 height time series of Strategy 1 (§6.3.1).

When comparing the RMS_a (Eq. 7.6) matrices in Figures 7.11 to 7.16, it is clear that the RMS_a values are generally smaller for the plan components than for the height component. However, with the exception of the height component of station pair LOWE–HEMS, the RMS_a statistics indicate smaller magnitudes for smaller μ and larger M. The RMS_b matrices in Figures 7.11 to 7.16 show the RMS_a statistics of the difference between the error sequences and the two–station common mode bias time series. In general, the pattern of the RMS_b values show smaller magnitudes for smaller M and larger μ. This effect is more pronounced for the height components of both dual–CGPS station pairs. It is now possible to describe the results for the different coordinate components of the two station pairs in more detail.

From the correlation matrix of the North components shown in Figures 7.11 and 7.12, it can be seen that $\{e(n)\}$ and $\{e'(n)\}$ show a very high cross–correlation throughout the investigated combinations of M and μ. In fact, for $M > 5$ correlations reach above 99.5%. The separation matrices in these figures show that the best possible separation between coherent and incoherent time series components can be achieved independently of M by using a μ close to its upper limits. The RMS_a values reduce quickly in the range of $1 \leq M \leq 5$ to values around 1 mm and below. The RMS_b values, are small throughout both plots, however, they tend to be smallest at shorter filterlenghts and larger step sizes.

A similar scenario can be found in Figures 7.13 and 7.14, showing the results for the East component of both station pairs. Again, the highest cross–correlation of the error sequences can be found for $M > 5$ and the best separation of the input signal components can be achieved independently of M by selecting μ close to its upper limits. In order to keep the RMS_a values around 2 mm, $M > 5$ and $\mu < 2.5 \times 10^{-5}$ would be preferable for

the case of station pair NEWL–CAMB, whereas for station pair LOWE–HEMS, all RMS_a values are smaller than 1 mm. However, again the RMS_b values tend to be smallest for shorter M and larger μ.

The results for the height components shown in Figures 7.15 and 7.16 give a slightly different pattern for the matrices. It can be assumed that this is due to the presence of the annually repeating signal in these height time series. Hence, in order to achieve a high correlation, μ should be selected as small as possible. The separation matrix shows magnitudes larger than 80% from approximately $\mu > 0.5 \times 10^{-4}$ and follows the upper limits. For both station pairs, the maximum RMS_a and RMS_b values are approximately 8 mm. Their distribution indicates a pattern of minimum values at opposite sides of the selected search area.

For a sample of some combinations of M and μ the results have been tabulated for each coordinate component of the dual–CGPS station pair NEWL–CAMB. Tables 7.3 to 7.5 show the cross–correlation coefficients $r_{ee'}(0)$ (Eq. 7.4) of the error sequences of the forward and reversed direction filter process at zero lag and the cross–correlation coefficients $r_{ey}(0)$ (Eq. 7.5) of the error and filtered sequences at zero lag. The tables also show the RMS_a and RMS_b statistics (Eqs. 7.6 and 7.11) and the ratios RMS_a/RMS_b for each coordinate component.

According to Figure 7.11, M should be chosen to be at least 5 and μ should be close to its upper limit. Table 7.3 presents three possible choices of M with μ approaching the upper limit. It seems that a combination of $M = 7$ and $\mu = 7.5 \times 10^{-5}$ gives good filter results for the North component. A larger M seems unnecessary in this case as $r_{ee'}$ and r_{ey} do not improve anymore. With RMS_a and RMS_b statistics of 1.28 and 2.49 mm respectively, their ratio is only at 0.5.

From Figure 7.13 it can be seen that the scenario for the East component is very similar. Hence, from Table 7.4 it can be seen that a combination of $M = 7$ and $\mu = 5.4 \times 10^{-5}$ is a good choice for this component. For the East component $r_{ee'}(0)$ is only 98%, which is slightly less than for the North component, possibly due to the larger day–to–day scatter in the East time series. The RMS_a and RMS_b statistics with 2.66 and 3.48 mm respectively,

Table 7.3: Adaptive filter parameter combinations tested for the North component of dual–CGPS station pair NEWL–CAMB.

M	μ [$\times 10^{-4}$]	$r_{ee'}(0)$[a] [%]	$r_{ey}(0)$[b] [%]	RMS_a[c] [mm]	RMS_b[d] [mm]	$RMSRatio$
5	0.20	100	9	1.18	3.36	0.4
5	0.30	100	7	1.20	3.05	0.4
5	0.60	100	5	1.28	2.60	0.5
5	0.76	100	4	1.33	2.47	0.5
5	1.06	99	3	1.42	2.30	0.6
7	0.20	100	7	1.06	3.28	0.3
7	0.30	100	5	1.09	3.01	0.4
7	0.54	100	4	1.19	2.67	0.4
7	0.60	100	4	1.21	2.61	0.5
7	0.75	100	3	1.28	2.49	0.5
9	0.20	100	6	0.99	3.25	0.3
9	0.30	100	5	1.04	3.01	0.3
9	0.42	100	4	1.10	2.82	0.4
9	0.59	100	3	1.19	2.64	0.5

[a]Cross–correlation coefficient of the forward and reversed direction error sequences (Eq. 7.4)

[b]Cross–correlation coefficient of the error and filtered sequences (Eq. 7.5)

[c]RMS statistic of the difference in the forward and reversed direction error sequences (Eq. 7.6)

[d]Average RMS statistic of the difference in the two–station common mode bias and error sequences of the forward and reversed direction filter process (Eq. 7.11)

approach similar magnitudes as their ratio is 0.8. They are also larger than for the North component.

Table 7.5 summarizes the results for the height component. As seen in Figure 7.15, the situation for the height component is different than for the plan components. The day–to–day scatter is larger and the height time series contain an annually repeating signal common to both stations. Both features contribute to the fact that the correlation coefficients $r_{ee'}(0)$ are lower and generally only reach about 80%. This also causes the RMS_a and RMS_b values to be generally larger and only have minimum values of 3.54 and 4.59 mm respectively, for the combinations shown in this table. For the height component it is therefore possible to find combinations of M and μ, which have an RMS ratio of 1. Using $M = 15$ and $\mu = 6.7 \times 10^{-5}$ from Table 7.5, it is possible to keep both RMS statistics below 5 mm and their ratio at 1.

Table 7.4: Adaptive filter parameter combinations tested for the East component of dual–CGPS station pair NEWL–CAMB

M	μ [$\times 10^{-4}$]	$r_{ee'}(0)$[a] [%]	$r_{ey}(0)$[b] [%]	RMS_a[c] [mm]	RMS_b[d] [mm]	$RMSRatio$
5	0.20	99	4	2.38	4.28	0.6
5	0.30	99	2	2.47	3.93	0.6
5	0.60	98	0	2.75	3.38	0.8
5	0.76	98	0	2.88	3.23	0.9
7	0.20	99	3	2.24	4.26	0.5
7	0.30	99	2	2.36	3.93	0.6
7	0.54	98	0	2.66	3.48	0.8
9	0.20	99	2	2.19	4.26	0.5
9	0.30	99	1	2.34	3.94	0.6
9	0.42	99	1	2.52	3.69	0.7

[a]Cross–correlation coefficient of the forward and reversed direction filter error sequences (Eq. 7.4)
[b]Cross–correlation coefficient of the error and filtered output sequences (Eq. 7.5)
[c]RMS statistic of the difference in the forward and reversed direction filter error sequences (Eq. 7.6)
[d]Average RMS statistic of the difference in the two–station common mode bias and error sequences of the forward and reversed direction filter process (Eq. 7.11)

As seen in Figures 7.12 to 7.16, the situation for the dual–CGPS station pair LOWE–HEMS is similar to that of station pair NEWL–CAMB. Therefore, the selection of the filter parameters is not described in detail. For completeness, Tables M.1 to M.3 are given in Appendix M to summarize the combination of filter parameters tested for the North, East and height components of station pair LOWE–HEMS respectively. Table 7.6 summarizes the selected filter parameter combinations for the coordinate components of both dual–CGPS station pairs investigated.

Effect of the filter parameters on velocity estimates

After an appropriate M and μ were identified to fit a specific coordinate component of either dual–CGPS station pair, the author investigated what effect a slightly different combination of filter parameters might have on the estimated velocities for error sequences $\{e(n)\}$ and $\{e'(n)\}$ and filtered sequences $\{y(n)\}$ and $\{y'(n)\}$. As both error sequences contain the coherent signal components of the desired and reference sequences $\{d(n)\}$

Table 7.5: Adaptive filter parameter combinations tested for the height component of dual–CGPS station pair NEWL–CAMB

M	μ [$\times 10^{-4}$]	$r_{ee'}(0)$[a] [%]	$r_{ey}(0)$[b] [%]	RMS_a[c] [mm]	RMS_b[d] [mm]	$RMSRatio$
7	0.20	78	10	3.90	5.75	0.7
7	0.30	77	6	4.27	5.35	0.8
7	0.54	76	1	4.73	4.89	1.0
7	0.60	76	0	4.80	4.82	1.0
7	0.75	76	-1	4.93	4.71	1.0
7	1.20	76	-4	5.17	4.59	1.1
7	1.44	75	-5	5.27	4.58	1.2
9	0.20	78	10	3.86	5.75	0.7
9	0.30	78	6	4.24	5.35	0.8
9	0.42	77	3	4.54	5.08	0.9
9	0.59	77	-0	4.79	4.86	1.0
9	0.60	77	-0	4.81	4.85	1.0
9	1.12	76	-4	5.21	4.67	1.1
11	0.20	80	9	3.79	5.71	0.7
11	0.30	79	5	4.18	5.34	0.8
11	0.60	77	-1	4.77	4.88	1.0
11	0.92	76	-4	5.09	4.74	1.1
13	0.20	82	8	3.68	5.70	0.6
13	0.30	81	5	4.06	5.34	0.8
13	0.60	78	-2	4.70	4.90	1.0
13	0.77	78	-4	4.92	4.81	1.0
15	0.20	83	7	3.57	5.69	0.6
15	0.30	82	4	3.95	5.34	0.7
15	0.60	79	-2	4.65	4.92	0.9
15	0.67	79	-3	4.75	4.88	1.0
16	0.20	84	7	3.54	5.70	0.6
16	0.30	82	4	3.94	5.35	0.7
16	0.60	79	-2	4.65	4.93	0.9
16	0.63	79	-2	4.70	4.92	1.0

[a] Cross–correlation coefficient of the forward and reversed direction filter error sequences (Eq. 7.4)

[b] Cross–correlation coefficient of the error and filtered output sequences (Eq. 7.5)

[c] RMS statistic of the difference in the forward and reversed direction filter error sequences (Eq. 7.6)

[d] Average RMS statistic of the difference in the two–station common mode bias and error sequences of the forward and reversed direction filter process (Eq. 7.11)

Table 7.6: Selected adaptive filter parameter combinations of M and μ for dual–CGPS station pairs NEWL–CAMB and and LOWE–HEMS

Dual–CGPS Station Pair	Components	M	μ [$\times 10^{-4}$]
NEWL–CAMB	North	7	0.75
	East	7	0.54
	Height	15	0.67
LOWE–HEMS	North	7	1.74
	East	7	1.09
	Height	13	1.31

and $\{x(n)\}$ respectively, i.e. the two coordinate time series of a specific component and station pair, they contain the common station movements due to regional and global geophysical phenomena, e.g. glacial isostatic adjustment or plate motions and common noise characteristics due to the processing strategy. The velocity estimates of $\{y(n)\}$ and $\{y'(n)\}$ contain the incoherent signal components, and should only show possible station specific features, e.g. local trends, local periodic variations or noise due to local environmental effects.

Depending on the filter parameters, the adaptive filter process requires an initial period until the LMS algorithm has converged. Due to this delay, the velocity estimates for all of the following sequences have been based on time spans without the first 30 elements.

Three different tests were carried out in order to estimate the effect of the applied filter parameters on the velocity estimates of the error and filtered sequences. In Test 1, the velocity estimates were computed using the optimized μ as shown in Table 7.6 for a specific coordinate component and station pair with M varied from 2 to 30. In Test 2, M was held constant at the optimized value and μ was varied from 0.1×10^{-4} to 2×10^{-4} including the value for μ in Table 7.6. In Test 3, both filter parameters were varied, however, μ was kept at the upper limit (Eq. I.9 in Appendix I) for a specific M, while M was varied from 2 to 30.

For the dual–CGPS station pair NEWL–CAMB, the results of the three velocity tests are shown in Figure 7.17. The figure shows the velocity estimates for the forward and reversed direction error sequences for each component of the ITRS2000 coordinate time series. For ease of comparison, the estimated velocities were reduced by the first velocity

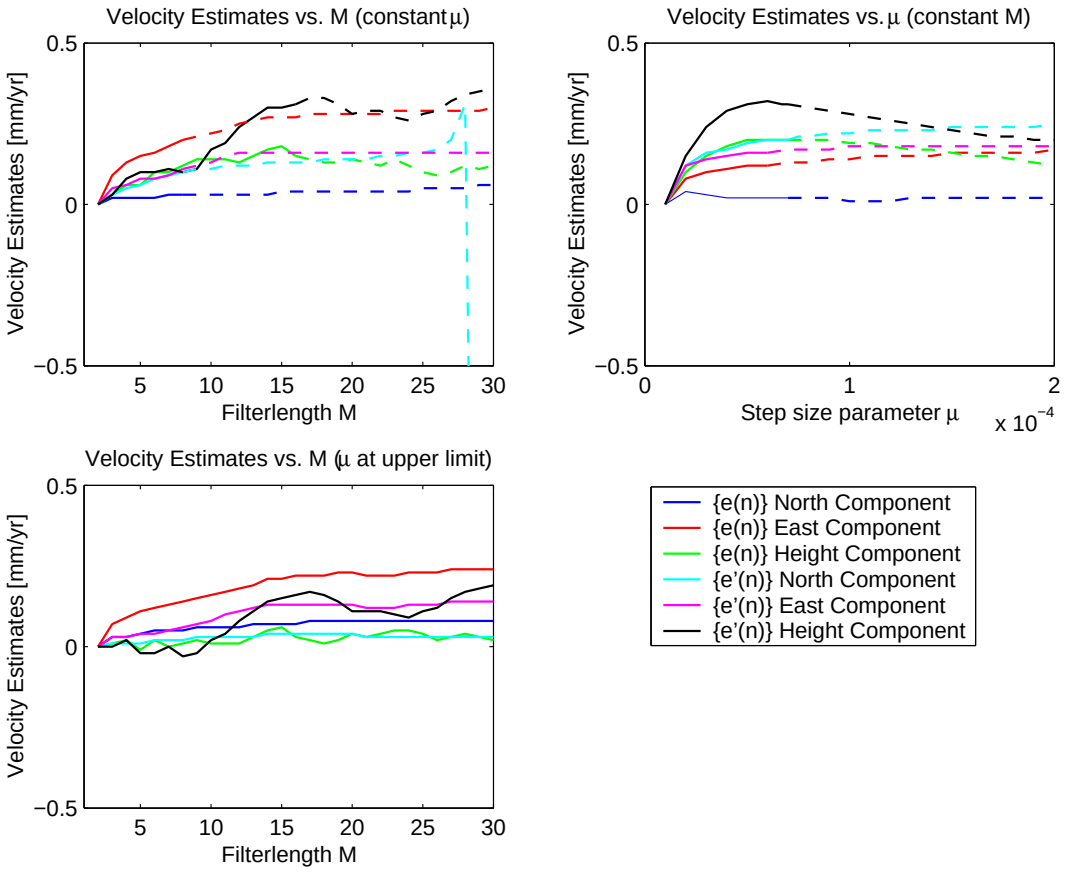

Figure 7.17: Adaptive filter velocity test results for dual–CGPS station pair NEWL–CAMB. Velocity estimates computed for error sequences $\{e(n)\}$ and $\{e'(n)\}$ for varying M and μ. Solid lines indicate that μ is below the upper limit (Eq. I.9 in Appendix I) for a specific M, while dashed lines indicate a μ larger than the upper limit.

estimate for each coordinate component in each test. Solid lines for the velocity estimates indicate that the applied μ is below the upper limit, while dashed lines indicate a μ larger than the upper limit. In this region, it cannot be guaranteed that the LMS algorithm remains stable, however, for the purpose of these tests, velocity estimates are also shown for larger μ. For ease of representation, the velocity estimates of the forward and reversed direction filtered sequences have not been included in Figure 7.17, as these are very small and remained constant within the test boundaries.

From Figure 7.17 it can be seen that for Tests 1 and 2 the curves of the velocity estimates follow a similar pattern for both plan components of both error sequences. In general, after

an initial phase, the velocity estimates seem to flatten and approach a constant value. For the North component of the reversed direction error sequence, however, the adaptive filter becomes unstable within the test boundaries of Test 1 as indicated by the irregular drop in the series of velocity estimates. The velocity estimates of the error sequences of the height components, do not seem to settle within the test boundaries of Test 1, however, the total variation in the velocities remains below 0.25 mm/yr. The resulting velocity estimates of the error sequences of the height component in Test 2 seem somehow more stable than those for Test 1. Similar to the case of the plan components, they also seem to approach a constant value. The results for Test 3 are shown in the lower row of Figure 7.17. Due to the fact that μ is chosen to be at its upper limit for a specific M, there are no dashed lines in this plot. As for the velocity estimates for the plan components of Test 1 and 2, the velocity estimates of Test 3, also seem to approach a constant value, a possible indication of their independency to a chosen M after an initial period. For the height component, the velocity estimates do not seem to settle within the test boundaries and show an oscillating pattern, believed to be due to the annual signal in the observed coordinate time series. This suggests that a periodic signal in the filter input sequences does not only affect velocity estimates of the individual coordinate time series, it also affects the filter error sequences and their velocity estimates. Overall it can be concluded that the effect on the velocity estimates of choosing a slightly different combination of M and μ when filtering the coordinate time series of dual–CGPS station pair NEWL–CAMB is less than the bias introduced by periodic signals, but can reach 0.25 mm/yr.

Although the common observation period of dual–CGPS station pair LOWE–HEMS is only 2.0 years, the above velocity tests were also carried out for the coordinate time series of these stations. The results can be seen in Figure M.5 in Appendix M. From this figure it can be concluded that the variations in the velocity estimates remain within 0.25 mm/yr for the plan components while for the height component they vary by approximately 0.5 mm/yr. This larger variability in the velocity estimates than for station pair NEWL-CAMB, can be attributed to the shorter observation span for station pair LOWE–HEMS.

Filtering of the dual–CGPS station pairs

Once an empirically derived set of parameter combinations for the adaptive filter were selected for each coordinate component and both dual–CGPS station pairs, the ITRS2000 coordinate time series were filtered in a forward and reversed direction. The observed coordinate time series of stations NEWL and CAMB, and the filtered and error sequences obtained from the forward direction adaptive filter analysis are shown in Figure 7.18. The figure also shows the RMS statistic (Eq. D.1 in Appendix D) and the velocity estimates and their associated uncertainties computed using the empirical method by Williams (2003a) based on the assumption of white and flicker noise (i.e. Eqs. H.13 and H.14 along with Eqs. H.19 and H.20 in Appendix H). From this figure it can be seen that by using the coordinate time series of NEWL as desired sequence and those of CAMB as reference sequence, the sum of the velocity estimates of the filtered and error sequences approximately equals the velocity estimates of the desired sequence. This also holds true for the reversed direction filter results for dual–CGPS station pair NEWL–CAMB shown in Figure M.6 in Appendix M.

As indicated previously, the filtered sequence describes the incoherent component between the coordinate time series of the two stations, whereas the error sequence describes the coherent or common part. In Figure 7.18 common features of the coordinate time series can be clearly identified in the error sequence, whereas the filtered sequence seems to contain only noise. The error sequence for the plan components also contains an estimate of the tectonic motion due to the fact that both stations are situated on the Eurasian plate. Obviously, the error sequence for the height component does not show a large secular trend, it does however, give a good representation of the common features of the height time series of NEWL and CAMB. An additional fact to be noted is that as with the dual–CGPS station analysis, the RMS statistics for the filtered and error sequences show a reduced day–to–day scatter.

Figure 7.19 shows the forward direction filter results for the observed ITRS2000 coordinate time series for dual–CGPS station pair LOWE–HEMS. Due to the shortness of the coordinate time series for this station pair, no station velocities and uncertainties are

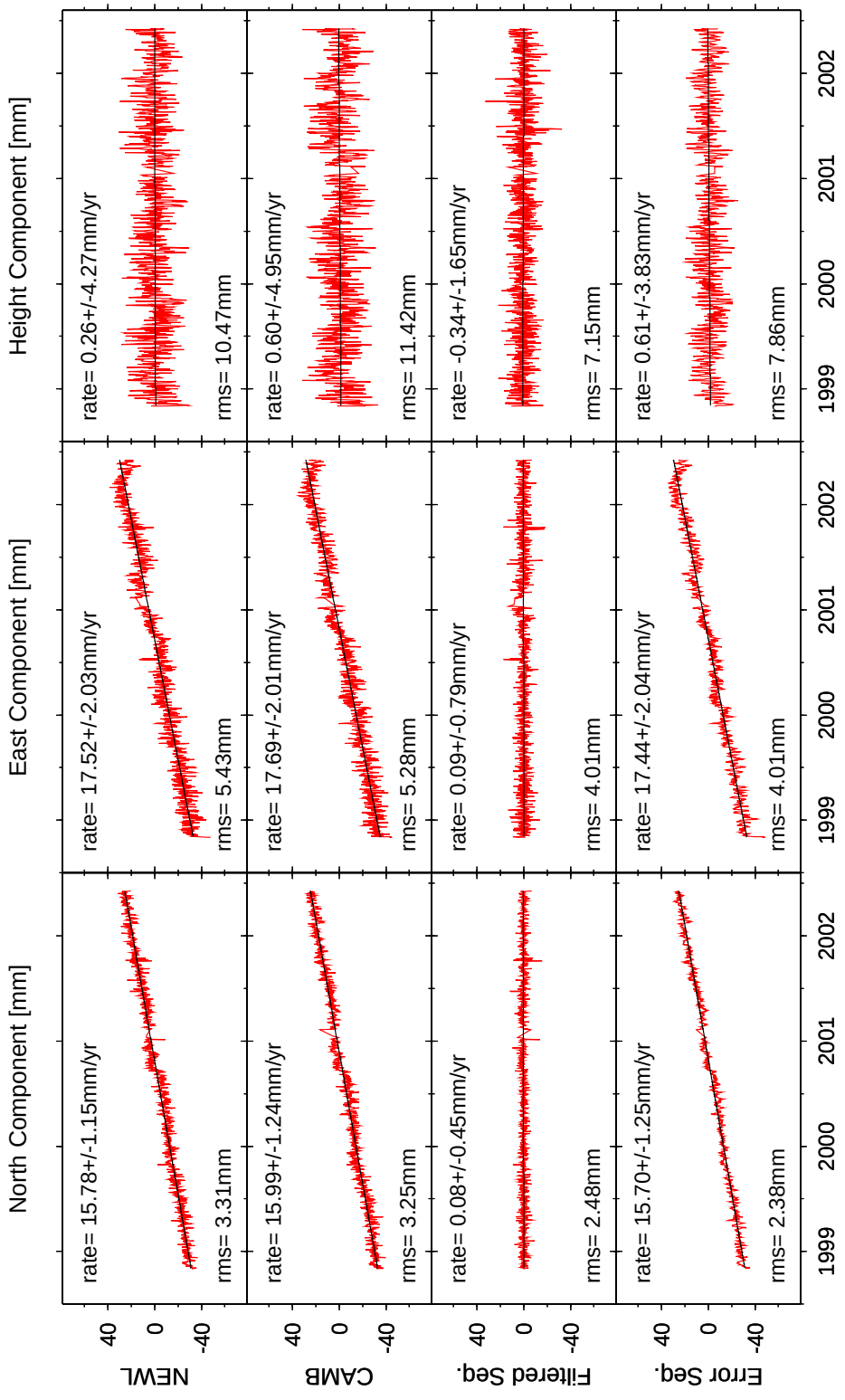

Figure 7.18: Forward direction adaptive filter analysis of observed ITRS2000 coordinate time series for dual–CGPS station pair NEWL–CAMB over a common time span of 3.7 years.

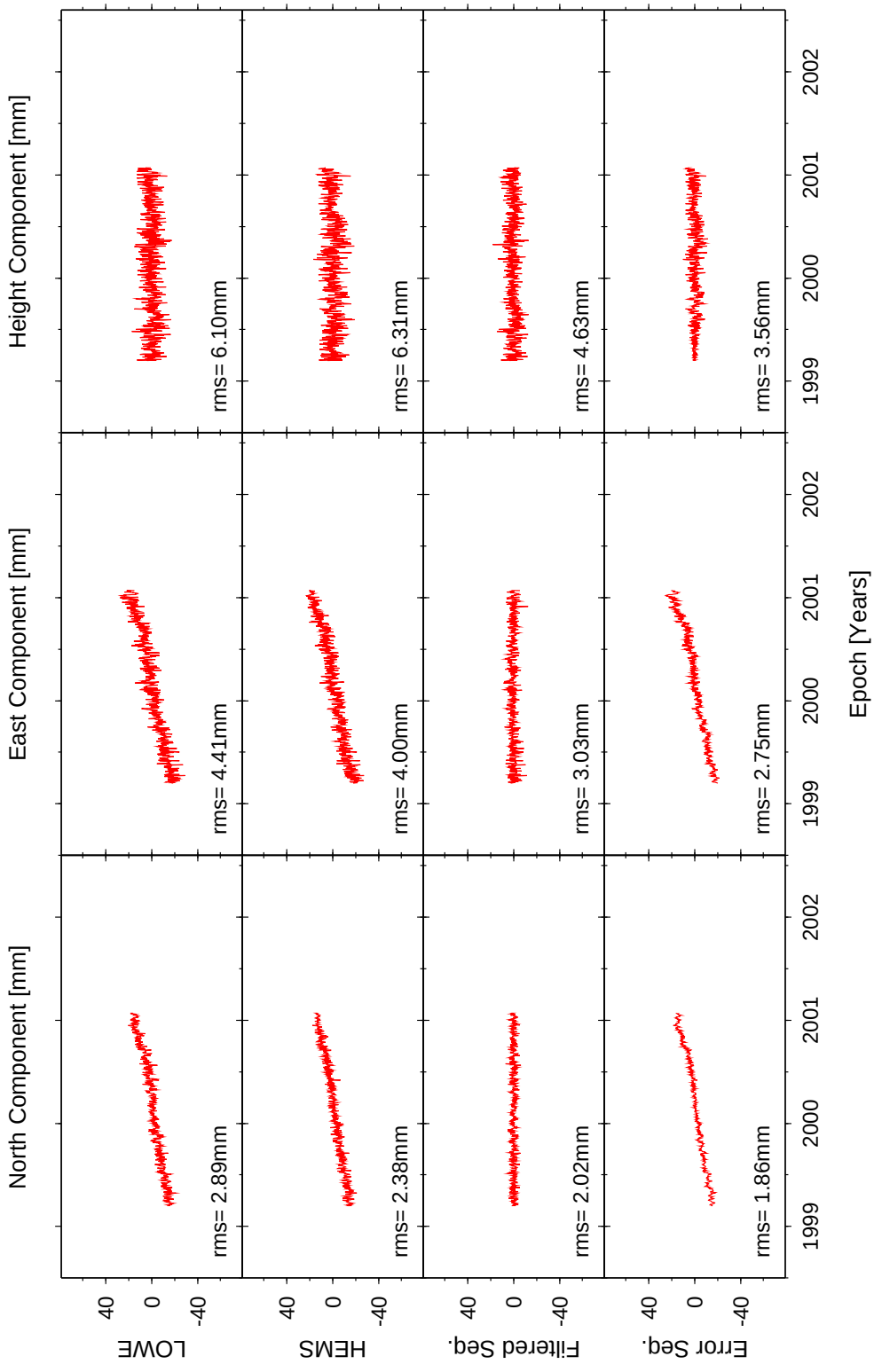

Figure 7.19: Forward direction adaptive filter analysis of observed ITRS2000 coordinate time series for dual–CGPS station pair LOWE–HEMS over a common time span of 2.0 years.

given and the figure only includes the RMS statistics. The reversed direction filter results for this station pair LOWE–HEMS are shown in Figure M.7 in Appendix M.

From Figure 7.19 it can be seen that in all cases the RMS statistics of the filter output sequences are less than the reference and desired sequences. Again, the filtered sequence gives a good representation of the desired sequence, i.e. the coordinate time series of LOWE. From the inspection of the error sequence it is clear that also for this case, the adaptive filter was able to successfully separate the common and incoherent signal components of the coordinate time series of LOWE and HEMS.

As has been shown in §7.2.4, the investigation of the adaptive filtering technique can be extended to the frequency domain by the use of the periodogram (Eq. H.2 in Appendix H). The author has computed the power spectra of all filter input and output sequences for both dual–CGPS station pairs for the forward and reversed direction adaptive filter analysis. The resulting power spectra can be found on the CD–Rom in directory `/Results/AdaptiveFiltering`. As an example, the power spectra for the height component of the forward direction adaptive filter analysis for station pair NEWL–CAMB are shown in Figure 7.20. The figure shows the power spectra of the reference (CAMB), the desired (NEWL), the filtered and error sequences. Also included are power–law noise estimates based on the estimated white and flicker noise content (Eq. H.13 and H.14 in Appendix H) of each sequence. Also indicated in Figure 7.20 are the frequencies of 14 days (14d), one month (1m), six months (6m), and one year (1y).

From Figure 7.20 it can be seen that all sequences typically show a white noise dominated high frequency range which changes into non–white, i.e. flicker noise, behaviour at lower frequencies. Besides the peak at the annual frequency of 3.2×10^{-8} Hz, visible in all spectra, the input and error sequences feature a peak at approximately 13.6 days ($\approx 8.5 \times 10^{-7}$ Hz). This peak is consistent with the known lunar tide period of 13.63 days (Bellanger et al., 2002) and may be a further indicator of a problem in the OTL modelling in GAS. However, Figure 7.20 successfully demonstrates that the adaptive filter does separate the incoherent and coherent signal components, as there is no indication of a 13.6 days period in the filtered sequence. Although, the coloured noise introduced by the adaptive filter is not necessarily flicker noise, it is clear that the line showing the

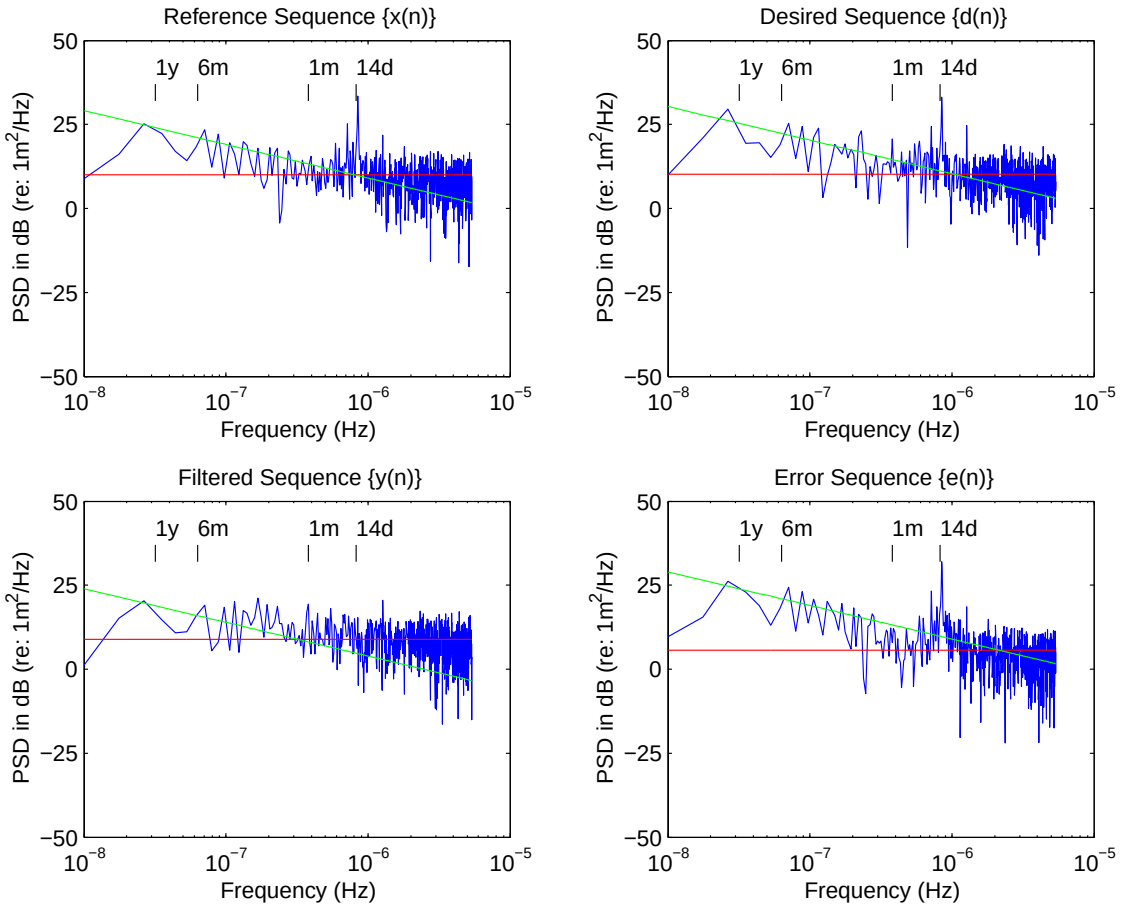

Figure 7.20: Power spectra of the forward direction adaptive filter analysis for the reference (CAMB), desired (NEWL), filtered and error sequences of the height component of dual–CGPS station pair NEWL–CAMB. The horizontal (red) and sloped (green) lines show the theoretical white and flicker noise, respectively, at the levels determined from each sequence.

theoretical power–law noise is a better approximation of the power spectra in the lower frequency range than the classical white noise model.

7.3.5 Dual–CGPS Station Adaptive Filter Analyses Compared

In §7.2.4 the similarity of the two–station common mode bias time series and the error sequences of the forward and reversed direction adaptive filter analysis were used to derive an empirically optimized combination of filter parameters. Besides this similarity of the coherent signal component with a two–station common mode bias time series, it is also possible to show that the filtered sequence, i.e. the incoherent signal component, shows features of the coordinate difference time series obtained from a dual–CGPS station analysis. This section, therefore, investigates to what degree the error and filtered sequences of the forward and reversed direction adaptive filter analysis are comparable to the two–station common mode bias and coordinate difference time series respectively.

As mentioned in §7.2.4, the filterlength M determines the number of filter coefficients and thus, the number of input samples multiplied and summed to form one sample of the filtered sequence. Therefore, the shorter M, the more the filtered sequence will resemble the coordinate difference time series. To carry out this comparison, Figure 7.21 shows the coordinate difference time series obtained in §7.3.1 for dual–CGPS station pair NEWL–CAMB reduced to the time span used in the adaptive filter analysis. The figure also includes the filtered sequences of the forward direction filter for each coordinate component. Based on these time series, the difference was computed by subtracting the filtered sequences from the coordinate difference time series. Additionally, as a measure of the day–to–day scatter, the RMS statistic (Eq. D.1 in Appendix D) is shown for each sequence.

From an initial impression of Figure 7.21, it is clear that the day–to–day scatter in each of the coordinate components are of similar magnitudes for the different analysis methods, with the scatter in the filtered sequences being slightly smaller. A closer inspection also confirms the similarity in the time series of both analysis methods, as common features are clearly distinguishable. For the North component, the RMS statistic of the difference between the two time series is slightly larger than the RMS values for the time series from

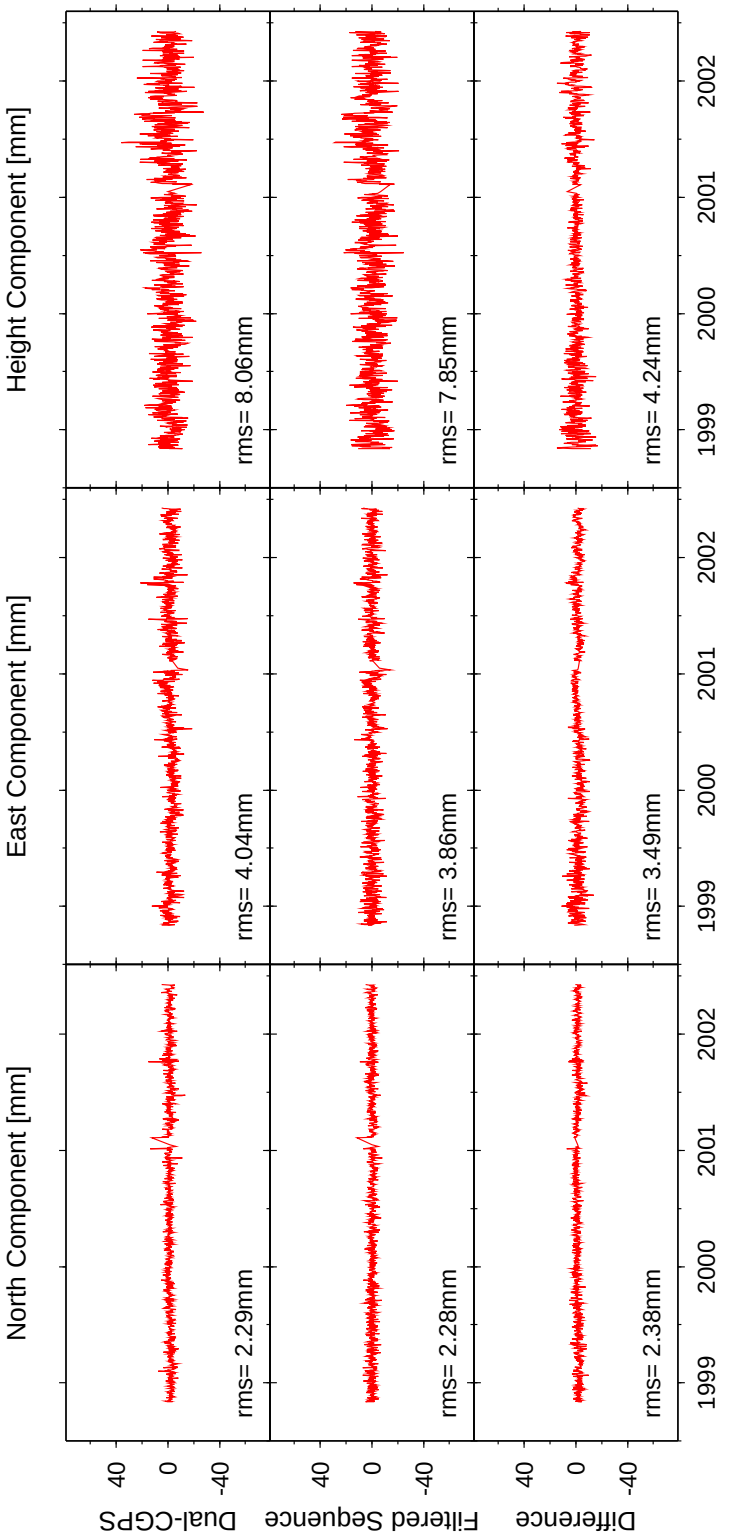

Figure 7.21: Dual–CGPS station and adaptive filter analyses compared for the observed ITRS2000 coordinate time series of station pair NEWL–CAMB over a common time span of 3.7 years. Dual–CGPS denotes the coordinate difference time series from the dual–CGPS station analysis and the filtered sequence is obtained from the forward direction adaptive filter analysis.

the dual–CGPS station analysis and the filtered sequence from the adaptive filter analysis. This would indicate that there is no correlation between the results of the two methods for this coordinate component. However, for the East and height components, the RMS statistics of the difference between the two time series are smaller than those of the initial analyses, which is a clear indication of the comparability of the methods.

By reversing the sign of the dual–CGPS station analysis, i.e. by subtracting the coordinate time series for NEWL from CAMB, the coordinate difference time series can be compared to the filtered sequence of the reversed direction filter. Figure 7.22 shows the coordinate difference time series for CAMB–NEWL, the filtered sequences of the reversed direction filter and the difference time series obtained by subtracting the adaptive filter results from the dual–CGPS station results.

From Figure 7.22 it can be seen again that the time series from the different analysis methods show common features and similar magnitudes in their day–to–day scatter. The magnitudes of the RMS values indicate that for all three coordinate components the RMS values of the difference between the two time series are smaller than those for the initial time series. Again, an indicator for the comparability of the analysis results of both methods.

The comparison has also been carried out for the dual–CGPS station pair LOWE–HEMS. Figures M.8 and M.9 in Appendix M show the coordinate difference time series, the filtered sequences and the difference for both the forward and reversed direction adaptive filter analysis. Again the figures contain the RMS statistics which show that the magnitudes of day–to–day scatter in each coordinate component are similar for both analysis methods. For all coordinate components and process directions, the difference between the time series show a smaller day–to–day scatter than the initial time series. Giving an indication of the correlation between the results of both analysis methods.

Besides the comparison of the filtered sequences of the adaptive filter analysis with the coordinate difference time series of the dual–CGPS station analysis, it is also possible to investigate the error sequences and the two–station common mode bias time series (Eq. 7.8) for each coordinate component. Figure 7.23 shows the two–station common mode bias time series from the dual–CGPS station analysis, the error sequences of the

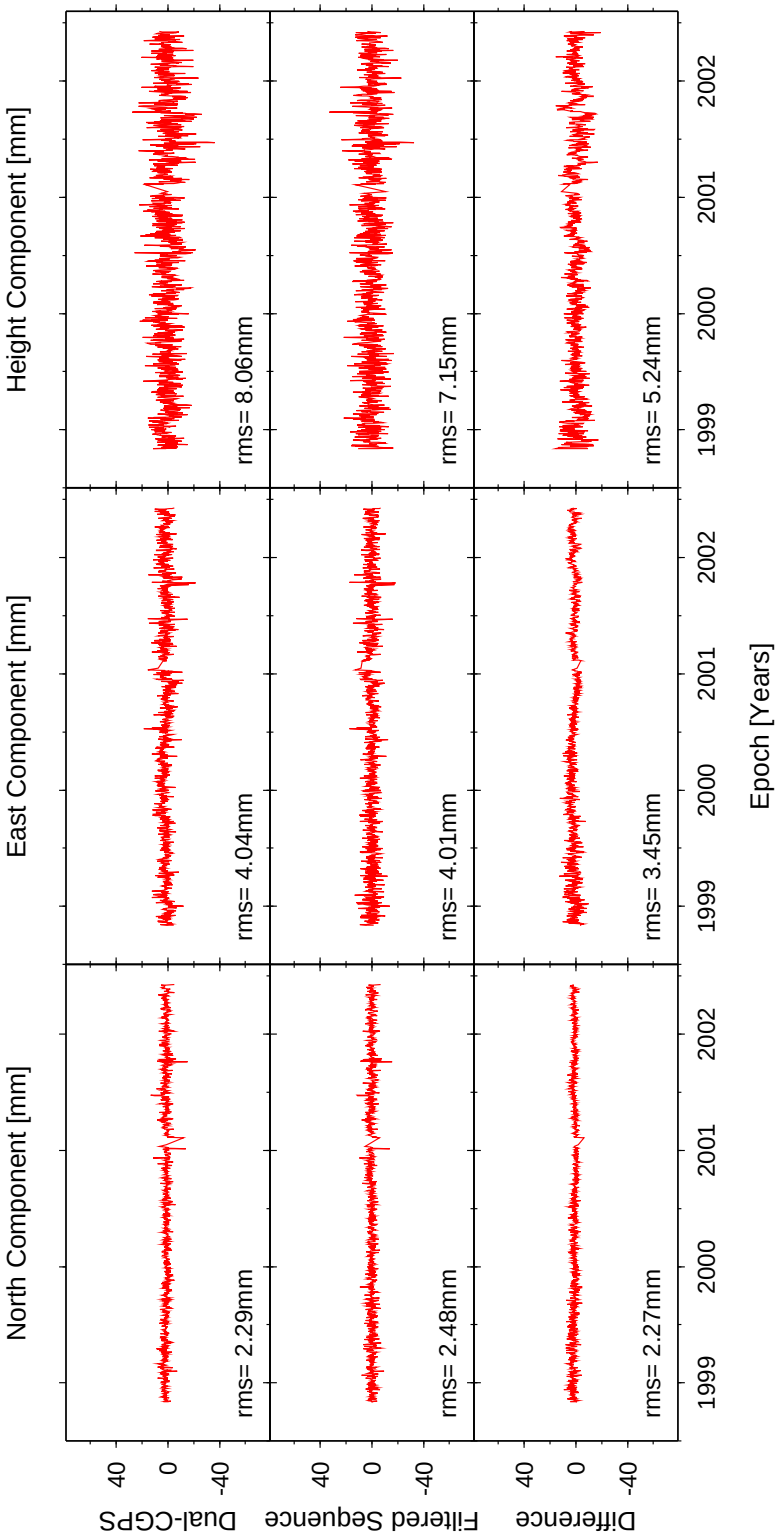

Figure 7.22: Dual–CGPS station and adaptive filter analyses compared for the observed ITRS2000 coordinate time series of station pair CAMB–NEWL over a common time span of 3.7 years. Dual–CGPS denotes the coordinate difference time series from the dual–CGPS station analysis and the filtered sequence is obtained from the reversed direction adaptive filter analysis.

forward direction adaptive filter analysis and the difference between the two time series for each coordinate component of the ITRS2000 coordinate time series of dual–CGPS station pair NEWL–CAMB. The figure also contains the RMS statistic for each time series. The similarity between the two–station common mode bias time series and the error sequences are clearly visible in their common variations and secular trend. The correlation between these time series is further highlighted by the significantly reduced RMS statistics for the difference between the two time series.

This similarity in the two–station common mode bias time series and the error sequences of the forward direction adaptive filter analysis is also expected for the error sequences of the reversed direction filter process. Figure 7.24 shows the two–station common mode bias, the error sequences of the reversed direction adaptive filter analysis and the difference between the two time series for each coordinate component of the observed ITRS2000 coordinate time series of dual–CGPS station pair NEWL–CAMB. Again, the RMS statistics are included in the figure. From Figure 7.24 it is clear that the error sequences of the reversed direction adaptive filter analysis resemble the secular trend of the two–station common mode bias time series.

These investigations into the comparability of the two–station common mode bias time series and the error sequences of the forward and reversed direction adaptive filter analysis have also been carried out for dual–CGPS station pair LOWE–HEMS. Figures M.10 and M.11 in Appendix M show the results for the comparison using the sequences of the forward and reversed direction adaptive filter analysis. For station pair LOWE–HEMS, the equivalence in the time series is also confirmed.

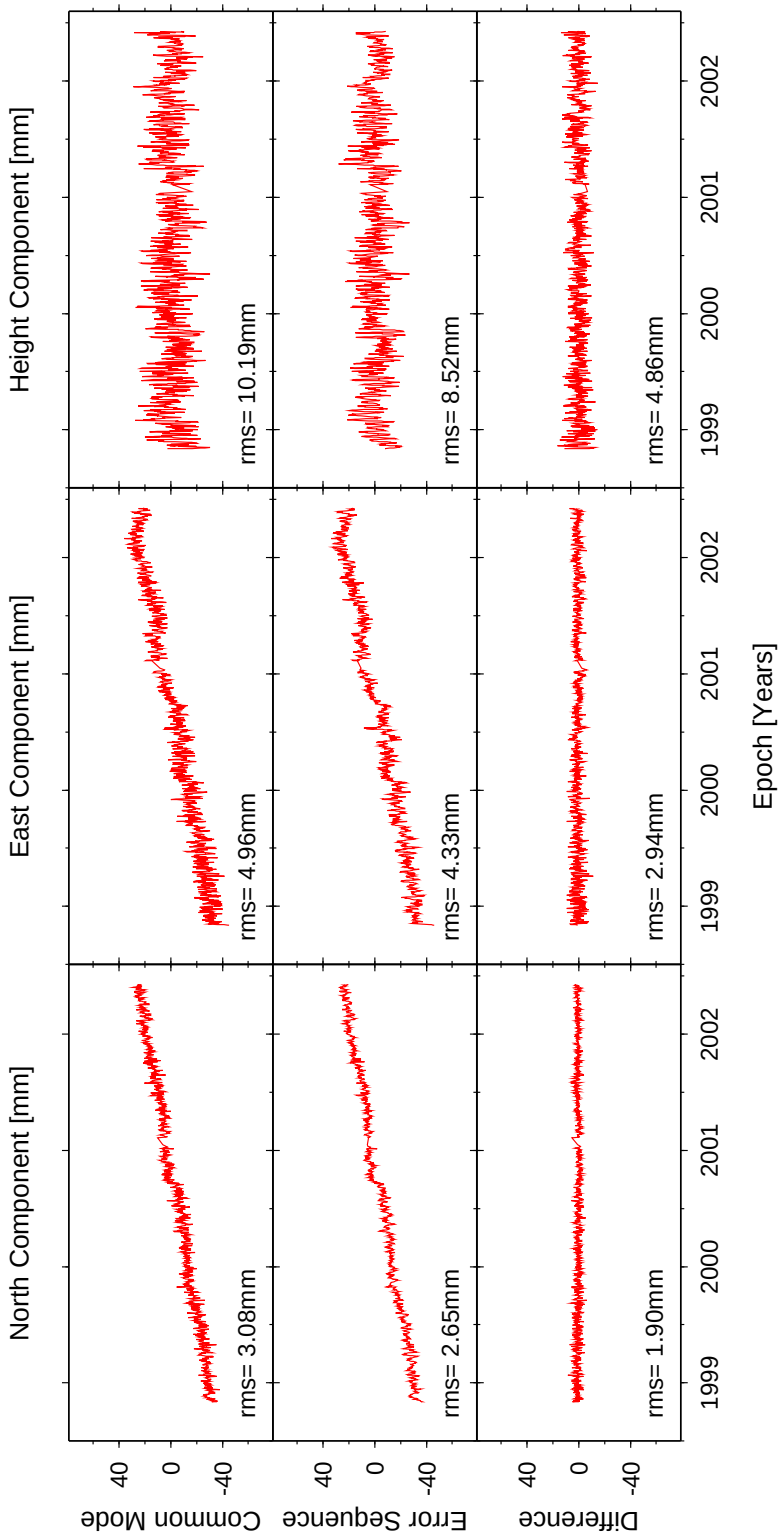

Figure 7.23: Two–station common mode bias time series and error sequences of the forward direction adaptive filter analysis for the observed ITRS2000 coordinate time series of the dual–CGPS station pair NEWL–CAMB compared over a common time span of 3.7 years. Common mode denotes the two–station common mode bias time series computed using Eq. 7.8 and error sequence denotes the coherent signal components of the two input sequences to the the adaptive filter.

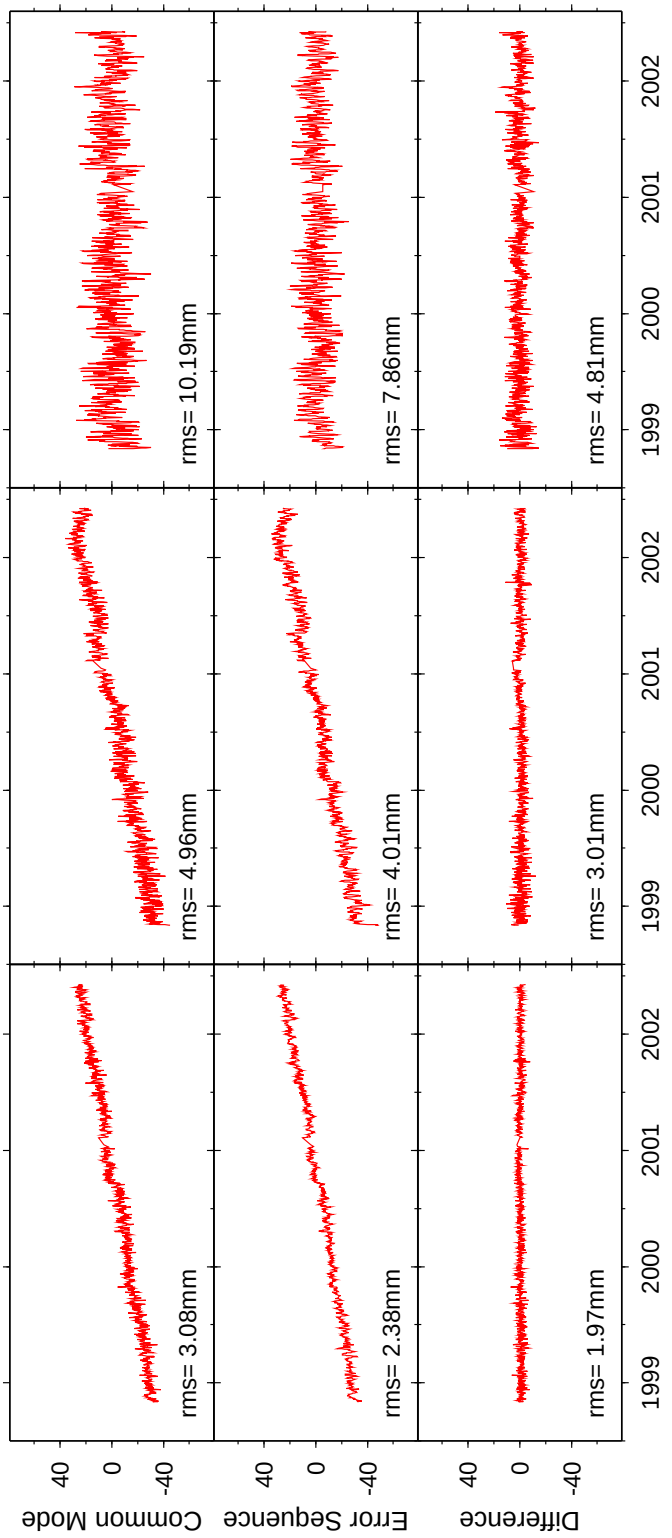

Figure 7.24: Two–station common mode bias time series and error sequences of the reversed direction adaptive filter analysis for the observed ITRS2000 coordinate time series of the dual–CGPS station pair NEWL–CAMB compared over a common time span of 3.7 years. Common mode denotes the two–station common mode bias time series computed using Eq. 7.8 and error sequence denotes the coherent signal components of the two input sequences to the adaptive filter.

7.4 Summary

Two dual–CGPS station pairs have been analysed according to the recently proposed dual–CGPS station concept. It was possible to show that for the two station pairs, approximately 20 km apart, common systematic features are removed from the resulting coordinate difference time series. This is supported by the fact that the coordinate difference time series show reduced WRMS values when compared to the coordinate time series of the individual CGPS stations. It was also possible to prove that the coordinate difference time series are independent of the reference frame of the initial coordinate time series and to a large degree, independent of small changes in the GPS processing strategy.

The coordinate difference time series derived from the dual–CGPS station analysis showed a similar day–to–day scatter as the single baseline time series, with the latter being slightly better. This finding has important consequences for the GPS processing strategies applied in large networks using either the current strategy in this research or precise point positioning (Zumberge et al., 1997). A second processing stage in which neighbouring CGPS stations are connected to regional or global CGPS stations by single baseline analysis is not required.

The analysis of synthetic data clearly demonstrated that when coordinate time series contain annually repeating signals, a bias due to this seasonal feature should be included in the uncertainty estimation if the annual signal has not been modelled and the time series is not at integer–plus–half years in length. However, the dual–CGPS station analysis shows that relative vertical station velocities quickly approach reliable values, even if the vertical station velocity estimates for the individual stations are affected by periodic variations.

Using an adaptive filtering technique it was possible to analyse the coordinate time series of both dual–CGPS station pairs. It was shown that the filter parameters can be empirically optimized for each coordinate component and each station pair, and that periodic signals in the input sequences do affect the choice of the filter parameters. The adaptive filter analysis is capable of successfully separating the incoherent and coherent signal components of the input sequences into the filtered and error sequences. From a comparison of these sequences with coordinate difference time series and the two–station

common mode bias time series, it can be concluded that velocity estimates obtained for the filtered output sequences are affected by the day–to–day scatter, the filter parameters and possible periodic signals in the input sequences. The latter can introduce the largest variations, whereas the selection of the filter parameters can introduce a velocity bias of up to 0.25 mm/yr.

The dual–CGPS station concept supports the investigations into vertical land movements by enabling a range of methods to be applied for analysis. This allows a comprehensive and qualitative description of the station motions observed. For the dual–CGPS station pairs analysed by the author, it can be concluded that both stations at tide gauge and inland locations are of similar quality over the observation timespan. At present their relative station motions seem to be insignificant, suggesting that both CGPS@TG stations are well founded and are not experiencing any local vertical land movements in addition to the underlying geophysical crustal motion.

Chapter 8

The UK CGPS Results Compared

8.1 Introduction

This Chapter discusses further the results obtained in Chapters 6 and 7 for the analysis of the UK CGPS network and the dual–CGPS station concept respectively. Firstly, the coordinate time series and vertical station velocity estimates of the UK based IGS stations and the EUREF station BRST are compared to several alternative solutions available to the author. This comparison allows a qualitative description of the results of this analysis. Secondly, absolute and relative vertical station velocity estimates are discussed and compared to vertical land movement estimates from alternative evidence, as described in Chapter 2. An *alignment procedure* is investigated in order to remove a constant reference frame bias from the vertical station velocity estimates obtained in Chapter 6. These estimates are then compared with those based on MSL trends and predicted vertical crustal movements from two GIA models.

8.2 CGPS station results compared

As described in Chapter 5, HERS is an important IGS tracking station as it is co–located with a SLR system and was, up to 2000, the only CGPS station contributing to the IGS in the UK. Since then data from HERS have been routinely included in the EUREF and

IGS analyses and it is one of 83 core sites used for IGS reference frame determinations (Heflin, 2003). Figures B.2, B.3 and B.4 in Appendix B show the coordinate time series for HERS from the improved EUREF weekly time series for geokinematics, the IGS global analysis carried out at JPL and the global SOPAC analysis respectively.

Recently, all CGPS data archived at SOPAC have been re–analysed in a uniform manner for the period from January 1991 to present (Scharber, 2002). In this re–analysis linear station velocities, coordinate offsets and seasonal signals were simultaneously estimated using a MLE with WN+FN model as described in Appendix H (see also Nikolaidis (2002)). The author has obtained the unfiltered daily ITRS2000 coordinate solutions for the SOPAC re–analysis in the form of a North, East and Up coordinate time series file from the SOPAC/CSRC Public FTP Archive at `ftp://garner.ucsd.edu/pub/timeseries`. Using this file, it is possible to carry out a more comprehensive comparison of the coordinate time series for HERS than by comparing Figures B.2, B.3 and B.4 in Appendix B with Figures 6.4 or 6.26 in Chapter 6 or simply comparing station velocity estimates.

Table 8.1: RMS and station velocities for HERS from the JPL and SOPAC coordinate time series analyses for the observation time span from 1991 to 2002.

Component	JPL Analysis		SOPAC Analysis	
	RMS [mm]	Velocity [mm/yr]	RMS [mm]	Velocity [mm/yr]
Latitude	4.0	15.6 ± 0.1	2.5	15.9 ± 0.1
Longitude	5.6	17.0 ± 0.1	5.0	16.6 ± 0.2
Height	10.5	-0.1 ± 0.1	8.0	-1.4 ± 0.3

As can be seen from the RMS values in Table 8.1, the day–to–day scatter in the coordinate time series for the SOPAC analysis is slightly smaller than for the JPL analysis. The station velocity estimates for HERS do not agree for the two analyses, and the uncertainties of the SOPAC analysis seem to be slightly more pessimistic. Perhaps of most interest is the fact that there is a 1.3 mm/yr difference in the vertical station velocity estimates.

Using the unfiltered SOPAC North, East and Up coordinate time series for HERS as a reference, the author evaluated the unfiltered improved ITRS2000 height time series for HERS (see §6.3.3), denoted as the IESSG analysis in Figure 8.1. This shows the ITRS2000

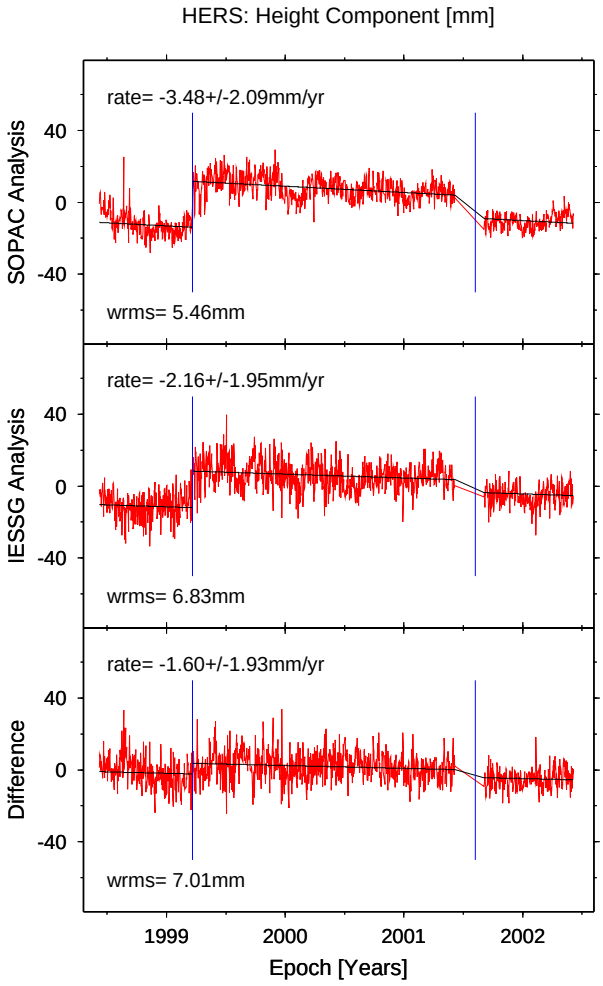

Figure 8.1: ITRS2000 height time series for HERS compared for the SOPAC and IESSG analyses. Both data sets have been reduced to a common observation time span.

height time series for the SOPAC and IESSG analyses for the common time span from May 1998 to May 2002. The figure also includes the height difference time series. The graphs also contain the best fitting model consisting of a linear trend plus two height offsets estimated at the two epochs shown in Table 6.14 in §6.3.3. For each model fit the WRMS statistic (Eq. D.2 in Appendix D) and the vertical station velocity estimate and its associated uncertainty are stated. The velocity uncertainties have been computed using the empirical method developed by Williams (2003a) using Eqs. H.13 and H.14 along with Eqs. H.19 and H.20 in Appendix H.

The day–to–day scatter and WRMS statistic of both height time series indicate that the SOPAC analysis is slightly less noisy than the IESSG analysis. The large day–to–day scatter in the height difference time series suggest that there is little correlation in the two height time series, thus there is no significant improvement in the WRMS statistic. Although, the vertical station velocity estimates of both analyses agree to within their given uncertainties, there is a difference in the rate of 1.3 mm/yr. An explanation for this difference can most probably be found in the fact that the SOPAC height time series were derived from a global network solution, whereas the IESSG height time series were derived from a regional network solution with ONSA, KOSG, VILL and WTZR as fiducial stations (see §6.2.1 and §6.2.2). Interestingly though, the difference between the vertical station velocity estimates for the IESSG and SOPAC analyses for 1998 to 2002 is the same magnitude and sign as the difference between the JPL and SOPAC analyses for 1991 to 2002.

Table 8.2: Vertical station velocity estimates for IGS stations WTZR, KOSG, ONSA and VILL for the official ITRF2000 and the SOPAC analyses compared.

Site	ITRF2000 [mm/yr]	SOPAC Analysis [mm/yr]	Difference [mm/yr]
WTZR	−0.9	−0.6	−0.3
KOSG	0.7	−0.6	1.3
ONSA	2.6	0.7	1.9
VILL	−1.4	−1.3	−0.1

Table 8.2 shows the vertical station velocity estimates for the four European IGS stations defining the reference frame in the IESSG analysis, based on the published ITRF2000 values and the SOPAC analysis. Also listed are the differences in the velocity estimates between both solutions. From this table it can be seen that the differences in the absolute vertical station velocity estimates vary between -0.3 to 1.9 mm/yr. Clearly, such discrepancies will affect the estimated vertical station velocities for a regional network solution. A rough estimate of the relative vertical station velocity for HERS with respect to ONSA, KOSG, WTZR and VILL can be obtained by subtracting the average vertical station velocity estimate of +0.25 mm/yr for the ITRF2000 solution shown in Table 8.2 from the velocity estimate for the IESSG analysis shown in Figure 8.1. This results in a relative vertical station velocity for HERS in the IESSG analysis of -2.4 mm/yr. A

similar reduction of the absolute vertical station velocity for HERS can be carried out for the SOPAC analysis, thus producing a relative vertical station velocity of -3.0 mm/yr. Although, this method is arguably not exact, using the relative vertical station velocity in both analyses reduces the difference in the velocity estimates from 1.3 to 0.6 mm/yr.

Immediately visible in Figure 8.1 are the height offsets on 21 March 1999 and 8 August 2001 as discussed in §6.2.4. A closer inspection of Figure 8.1 indicates that both analyses differ significantly in the estimated magnitudes of the height offsets at those epochs. Table 8.3 shows the offset estimates for the height time series for the SOPAC and IESSG analysis and for the height difference time series.

Table 8.3: Offset estimates for the height time series of the SOPAC and IESSG analyses and the height difference time series.

Epoch	SOPAC Analysis [mm]	IESSG Analysis [mm]	Difference [mm]
21 March 1999	25.6 ± 0.5	20.4 ± 1.1	6.0 ± 0.4
8 August 2001	-12.2 ± 0.5	-6.7 ± 1.1	-4.1 ± 0.5

As can be seen from this table, the estimated height offsets can differ by up to 6 mm in magnitude. Without detailed information on the SOPAC analysis it is difficult to interpret these differences. However, tests by the author showed that even by artificially adjusting the offset magnitudes in the height time series of the IESSG analysis to those of the SOPAC analysis, the velocity estimates do not change by a large amount.

A similar comparison of the height time series for HERS can be carried out with the I3 analysis by Panafidina and Malkin (2001). In this analysis the weekly EUREF solutions computed by the Bundesamt für Kartographie und Geodäsie, Germany, were de–constrained to result in a series of weekly non–fiducial solutions nearly free of distortions caused by tight constraints (Malkin and Voinov, 2000). Then these free network solutions were transformed to ITRF2000 with a 7–parameter Helmert transformation.

Figure 8.2 shows the I3 weekly ITRS2000 height time series for HERS obtained from Zivony Malkin superimposed onto the daily height time series of this analysis (IESSG Analysis) for the time span between 21 March 1999 and 8 August 2001. Also included are the estimates of the vertical station velocity and associated uncertainties for the I3

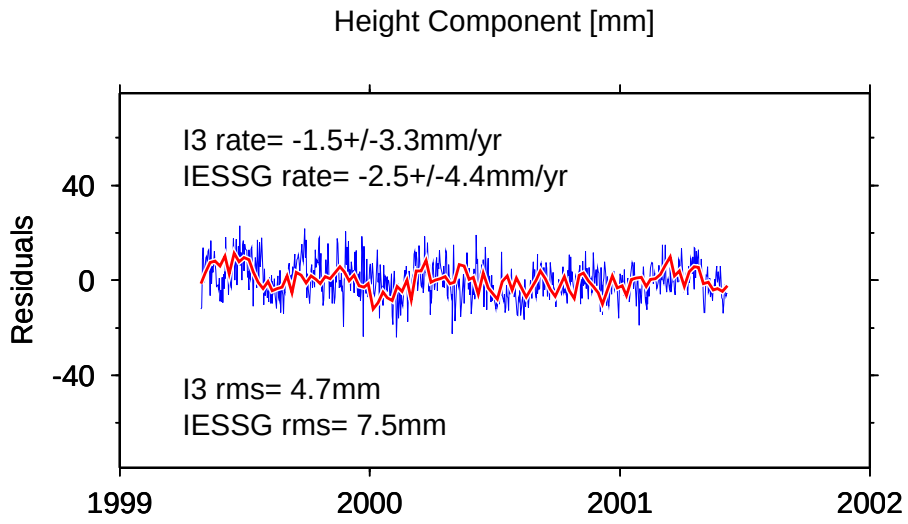

Figure 8.2: Daily and weekly ITRS2000 height time series for HERS. The series of daily position estimates is formed from the solutions of the IESSG analysis and those of the weekly position estimates is formed from the I3 analysis ((Panafidina and Malkin, 2001)).

and IESSG analyses. The velocity uncertainties have been computed using the empirical method by Williams (2003a) with Eqs. H.13 and H.14 along with Eqs. H.19 and H.20 (see Appendix H). As a measure of spread in the height time series, the RMS statistics (Eq. D.1 in Appendix D) for each series are also shown in Figure 8.2. Clearly visible in this figure is the much smoother line for the weekly than for the daily height time series, which is also indicated by the RMS statistics. Due to the limited timespan between the two coordinate offsets in the height time series for HERS, the vertical station velocity estimates shown in this figure are not accurate in an absolute sense. Of much more importance, however, is the fact that the estimates agree to within 1 mm/yr.

Unfortunately, for the remaining two UK based IGS tracking stations, i.e. NPLD and MORP, their height time series results cannot be compared in such detail. Figures B.5 and B.6 in Appendix B show the weekly EUREF and daily JPL coordinate time series for NPLD. Although Figure B.6 gives station velocity estimates, the author did not attempt to estimate station velocities for NPLD as the coordinate time series were still less than 2.5 years in length. It is however possible to compare the WRMS statistic (Eq. D.2 in Appendix D) obtained from Figures 6.4 (see §6.3.1) and B.6. With WRMS values of 2.4,

3.5 and 5.8 mm for the North, East and height components for the IESSG analysis, the results are very promising when compared to WRMS values of 2.6, 2.8 and 5.9 mm for the North, East and height components for the JPL analysis.

As mentioned in Chapter 5, MORP has only recently become an official IGS tracking station. Hence, there are currently no official coordinate time series available for comparison with the results obtained from this analysis.

In an attempt to obtain more comparisons, the author included the CGPS@TG station BRST in France in the IESSG analysis. BRST is regularly included in the EUREF analysis and the improved EUREF weekly time series for geokinematics for BRST is shown in Figure B.1 in Appendix B. There are no station velocity estimates available for this site for this analysis. It is however possible to obtain coordinates and station velocity estimates from the ITRF2000 EUREF densification (see `http://lareg.ensg.ign.fr`).

Table 8.4 compares the vertical station velocity estimates from the official ITRF2000 EUREF densification with those of the unfiltered improved ITRS2000 height time series, denoted as IESSG analysis.

Table 8.4: Absolute vertical station velocity estimates for BRST for the ITRF2000 EUREF densification and the IESSG analysis. All values are in mm/yr.

Site	ITRF2000 EUREF Densification	IESSG Analysis
BRST	−3.4	1.2

Immediately noticeable is the large discrepancy between the estimates. However, it must be noted that the ITRF2000 EUREF densification was based on GPS measurements up to 2000. For BRST this means that the official ITRF2000 station velocity estimates were based on less than 2 years of data, whereas for the IESSG analysis, data were used up to the end of May 2002.

In order to better understand the reliability of absolute vertical station velocity estimates, comparisons between different solutions are necessary. From the comparisons shown for HERS and BRST, it is clear that there may be large discrepancies between the height time series and their velocity estimates for different analyses. Also, estimated coordinate

offsets may vary by large amounts between different analyses. For the height time series of HERS it was shown that by a more detailed investigation and by focusing on relative rather than absolute velocity estimates, the disagreement in the vertical station velocity estimates was reduced. As longer coordinate time series for BRST, MORP and NPLD will be available in the future, similar comparisons are recommended. Furthermore, it is intended to submit data from several UK CGPS stations to EUREF in the hope that this will allow further investigations. Of great importance, however, will be the comparisons possible for those UK CGPS stations re–analysed through the IGS TIGA PP and ESEAS, as both projects will focus primarily on the vertical coordinate component.

8.3 Absolute vertical station velocity estimates

Figure 8.3 shows the ITRS2000 vertical station velocity estimates obtained for the 17 CGPS stations analysed in Chapter 6. The vertical station velocity estimates have been obtained from the unfiltered and filtered improved ITRS2000 coordinate time series analysed using the improved analysis strategy (ImpA) and the MLE (Eq. H.7 in Appendix H) with fractional and integer spectral indices, i.e. the white plus power–law (WN+PLN) and the white plus flicker (WN+FN) noise models respectively. The velocity uncertainties obtained from the MLE stem from the variance–covariance matrix of the estimation which attempts to model both the white and coloured noise components in the coordinate time series. The figure also includes the velocity uncertainties computed for the improved analysis strategy using the empirical method developed by Williams (2003a) (Eqs. H.13 and H.14 along with Eqs. H.19 and H.20 in Appendix H) in order to account for temporal correlations in the coordinate time series and arrive at more realistic uncertainties.

From a first impression of Figure 8.3 it is apparent that the vertical station velocity estimates from the six coordinate time series analyses show significant variations, of up to 2 mm/yr for several stations. The figure suggests that seven of the stations are rising, four are subsiding, and six are not moving, however, the velocity uncertainties shown in this figure confirm that these estimates are not yet statistically significant. For stations BRST, NEWL, CAMB and DUNK, the velocity uncertainties are larger than those of

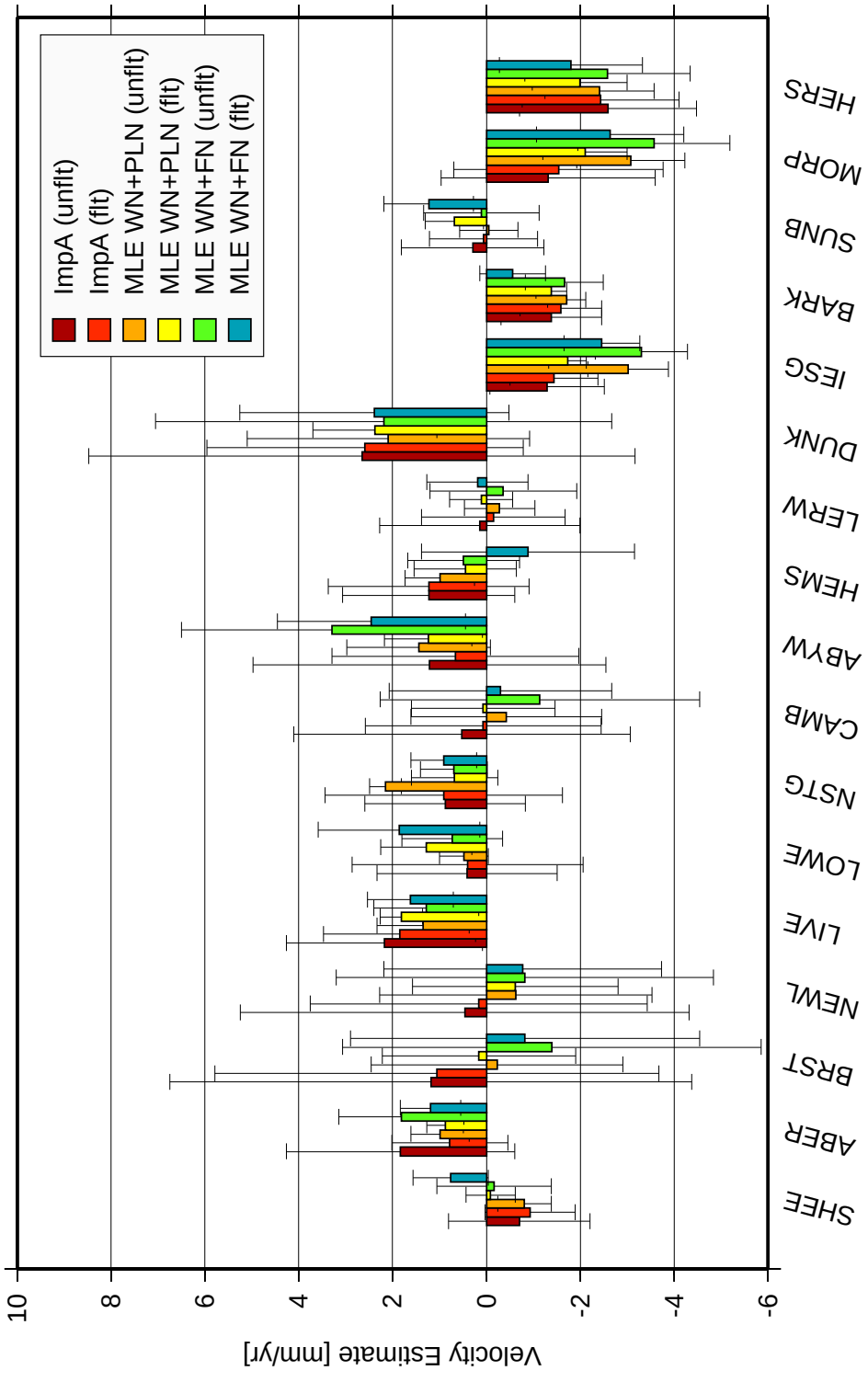

Figure 8.3: Absolute vertical station velocity estimates and uncertainties for the unfiltered and filtered improved ITRS2000 coordinate time series. The estimates shown are those obtained by the improved analysis strategy (ImpA) and the maximum likelihood estimation (MLE) with fractional and integer spectral indices assuming a white plus power–law (WN+PLN) and a white plus flicker (WN+FN) noise model respectively.

the other stations, which can be attributed to the problem in modelling the OTL effect, as discussed in Chapter 6. Although these results expose the current limits of GPS for monitoring vertical land movements at the 1 mm/yr level, for some stations there seems to be a consistent uplift or subsidence for all six coordinate time series analyses, were none or only one or two of the velocity uncertainties cross the zero velocity line. The stations that fall into this category are LIVE, IESG, HERS, BARK and MORP.

For LIVE, there is a strong suggestion that the station is rising. This GPS derived uplift at LIVE is contrary of the vertical land movement rates obtained from geological information (Shennan and Horton, 2002) as shown in Table 2.2. However, the MSL trend for Liverpool and the assumption of an absolute sea level rise of 1.5 mm/yr, together with the predicted crustal movements from both GIA models (Peltier, 2001a; Scherneck et al., 2002a) in Table 2.2 agree with the suggested uplift in the vertical station velocity estimates.

For IESG and HERS the vertical station velocity estimates and uncertainties in Figure 8.3 suggest subsidence. In Shennan and Horton (2002) subsidence of 0.9 mm/yr is indicated for Central England. With the CGPS antenna at IESG being situated on the top of a two–storey building, it could be argued that the observed subsidence may partly be due to settlement of the building. For HERS, according to most evidence in Table 2.2, Southeast England may be undergoing vertical land movements between -0.2 and -0.9 mm/yr, which would support the vertical station velocities obtained.

ABER is close to the areas in Central Scotland predicted to be undergoing uplift due to GIA. Shennan and Horton (2002) showed uplift for North East Scotland based on geological sea level indicators, and the vertical station velocity estimates obtained for ABER support this theory.

For BARK there is a suggestion of subsidence. With BARK being situated on top of the Barking Barrier with its foundations reaching to Upper Chalk (Booth, 2000), the indicated subsidence at BARK may be due to real vertical crustal movements. The vertical land movement estimates from the geological information collected in and around the Thames Estuary paint a complex picture of subsidence and uplift. Differential crustal movements within the estuary, the inner estuary generally revealing less submergence than the mid–

estuary, possible neo–tectonic phenomena and a possible reduction in the tidal range may all contribute to the observed crustal motion (Shennan, 1989).

The vertical station velocity estimates of approximately -2 mm/yr for MORP are contrary to the crustal movement predictions by the GIA models shown in Table 2.2. This is interesting, as it is assumed that the monumentation at MORP is very stable and tightly connected to bedrock. The observed vertical station velocity estimates may therefore be an indication of an additional effect, e.g. subsidence due to mining activities, at this station.

The numerical values for all vertical station velocity estimates shown in Figure 8.3 have for convenience been summarized in Table N.1 in Appendix N. Here it should be noted that these vertical station velocities are indicative of the station movements in the ITRS2000, and are only absolute for the reference frame realized through the four IGS stations constrained in the analysis.

8.4 Relative vertical station velocity estimates

This section compares the velocity estimates for the coordinate difference time series obtained from dual–CGPS station analyses with relative vertical station velocities derived from the difference between two vertical station velocity estimates in the various analyses discussed in Chapter 6. Although this is strictly speaking without reducing all coordinate time series to exactly the same common epochs not valid, the comparison should give an indication of the agreement between all vertical station velocity estimates.

8.4.1 Dual–CGPS station pairs

The two dual–CGPS station pairs NEWL–CAMB and LOWE–HEMS were discussed in Chapter 7. Table 8.5 compares the results from these dual–CGPS station analyses with relative vertical station velocity estimates computed from the unfiltered standard, and the unfiltered and filtered improved, ITRS2000 coordinate time series. The vertical station velocity estimates for the standard analysis are shown for completeness and should not be used for any further interpretation. Furthermore, the reader should be reminded that

both the dual–CGPS station and the standard analysis do not explicitly model periodic signals and coordinate offsets. However, the dual–CGPS station analysis has been shown to successfully deal with common systematic effects such as common periodic signals and common coordinate offsets.

Table 8.5: Comparison of dual–CGPS station analysis results for NEWL–CAMB and LOWE–HEMS with relative vertical station velocity estimates of the standard analysis, improved analysis and MLE with a WN+PLN and WN+FN model. All values are in mm/yr.

	Dual–CGPS Station Analysis	Standard Analysis	Improved Analysis		Maximum Likelihood Estimation (WN+PLN)		(WN+FN)	
Site	(unflt)	(unflt)	(unflt)	(flt)	(unflt)	(flt)	(unflt)	(flt)
NEWL	0.9	1.0	0.5	0.2	−0.6	−0.6	−0.8	−0.8
CAMB	0.9	1.3	0.5	0.1	−0.4	0.1	−1.1	−0.3
Difference	0.0[a]	−0.3	−0.1	0.1	−0.2	−0.7	0.3	−0.5
LOWE		0.5	0.4	0.4	0.5	1.3	0.7	1.9
HEMS		1.5	1.2	1.2	1.0	0.4	0.5	−0.9
Difference	0.1[b]	−1.0	−0.8	−0.8	−0.5	0.8	0.2	2.8

[a]This value is the velocity estimate for the coordinate difference time series and not the difference of the vertical station velocity estimates.

[b]This value is the velocity estimate for the coordinate difference time series and not the difference of the vertical station velocity estimates. No individual vertical station velocity estimates for the dual–CGPS station pair of LOWE–HEMS are shown as the common observation time span is less than the recommended 2.5 years.

For both dual–CGPS station pairs NEWL–CAMB and LOWE–HEMS, Table 8.5 indicates good agreement between the different analysis strategies. For NEWL–CAMB the differences vary between -0.7 and 0.3 mm/yr and for LOWE–HEMS between -1.0 and 2.8 mm/yr. The larger variation in the relative vertical station velocity estimates of LOWE–HEMS is assumed to be due to the shorter observation time spans of these CGPS stations.

8.4.2 Cross–Channel vertical station velocity estimates

One interest of the author was to obtain precise estimates of the relative vertical station velocity estimates between CGPS@TG stations NEWL, in the Southwest of England, and BRST in France. As has been mentioned above, due to mis–modelling of the OTL effect, the absolute vertical station velocity estimates may be biased and the associated uncertainties are unusually large for this analysis. It was also shown that the GPS data quality of BRST is compromised when compared to other stations in this analysis.

Although NEWL and BRST are approximately 200 km apart, the author has carried out a dual–CGPS station analysis between these sites. Furthermore, from the additional evidence of vertical land movements presented in Table 2.2 in Chapter 2, it is possible to compute relative vertical land movement estimates based on the MSL trends of both tide gauges (Eq. 2.1 in Chapter 2), the predicted vertical crustal movements from the GIA models by Peltier (2001a) and Scherneck et al. (2002a), and the relative vertical land movement estimates based on geological information from Woodworth et al. (1999) and Shennan and Horton (2002). These can then be compared with the relative vertical station velocity estimates obtained by the author. Table 8.6 summarizes all computed estimates of the relative vertical land movement between NEWL and BRST.

Table 8.6: Cross–channel vertical station velocity estimates for NEWL–BRST based on a dual–CGPS station analysis, relative vertical station velocity estimates and alternative evidence. All values are given in mm/yr.

Site	Dual–CGPS Station Analysis	Improved Analysis		MLE[a] (WN+PLN)		MLE[a] (WN+FN)		Alternative Evidence			
		(unflt)	(flt)	(unflt)	(flt)	(unflt)	(flt)	MSL[b]	GIA[c]	GIA[d]	Geo[e]
NEWL	0.3	0.5	0.2	−0.6	−0.6	−0.8	−0.8	−0.2	−0.3	−0.4	−1.1
BRST	0.9	1.2	1.1	−0.2	0.2	−1.4	−0.8	0.5	−0.3	−0.5	−0.2
Diff.	0.4[f]	0.7	0.9	0.4	0.8	−0.6	0.0	0.7	0.0	0.9	0.9

[a] Maximum Likelihood Estimation

[b] -(MSL-1.5)

[c] Peltier (2001a)

[d] Scherneck et al. (2002a)

[e] Woodworth et al. (1999); Shennan and Horton (2002)

[f] This value is the velocity estimate of the coordinate difference time series and not the difference of the vertical station velocity estimates.

From Table 8.6 it can be seen that most relative vertical land movement estimates are positive. It is possible to compute an average rate of approximately 0.5 mm/yr, suggesting uplift of BRST with respect to NEWL or subsidence of NEWL with respect to BRST. It should be mentioned at this stage that the vertical land and crustal movement estimates shown in Table 2.2 for geological data and GIA models respectively, suggest subsidence for Southwest England.

With respect to the disagreement of the vertical station velocity estimates for BRST from the official ITRF2000 EUREF densification and this analysis (Table 8.4 in §8.2), it will be interesting to see whether this relative motion between both CGPS@TG stations can be confirmed by the IGS TIGA PP (§3.2.4) and ESEAS (§3.2.3) analyses.

8.4.3 Station pair NSTG–MORP

Potentially important for monitoring vertical land movements in North East England and at the tide gauge in North Shields is the fact that using the CGPS@TG station NSTG and CGPS station MORP, another dual–CGPS station pair can be formed and analysed. Although, much effort was involved in the establishing the monumentation for the CGPS site at Morpeth (see Chapter 5 and Blewitt et al. (1997)) the coordinate time series for MORP are of lesser quality than for other stations analysed (see Figure 6.3).

In §5.3.3 the quality of the GPS observations at NSTG were investigated and it was demonstrated that, at this site, the quality is also compromised. With these problems and with a distance of approximately 28 km between NSTG and MORP, it cannot be expected that the results of a dual–CGPS station analysis for these sites would be of similar quality as for the station pairs NEWL–CAMB and LOWE–HEMS. In fact, the cross–correlation coefficient between the detrended height time series is only 0.13 (see Figure 6.20 in Chapter 6), demonstrating the uncorrelated site–specific effects at both stations.

Table 8.7 shows the results from a dual–CGPS station analysis and the relative vertical station velocity estimates for NSTG and MORP for the unfiltered standard, and the unfiltered and filtered improved, ITRS2000 coordinate time series.

Table 8.7: Comparison of dual–CGPS station analysis results for NSTG–MORP with relative vertical station velocity estimates from the standard analysis, improved analysis and Maximum Likelihood Estimation with a WN+PLN and a WN+FN model. All values are in mm/yr.

	Dual–CGPS Station Analysis	Standard Analysis	Improved Analysis		Maximum Likelihood Estimation (WN+PLN)		(WN+FN)	
Site	(unflt)	(unflt)	(unflt)	(flt)	(unflt)	(flt)	(unflt)	(flt)
NSTG	3.0	0.8	0.9	0.9	2.1	0.7	0.7	0.9
MORP	1.8	−0.4	−1.3	−1.5	−3.1	−2.1	−3.6	−2.6
Difference	−0.4[a]	1.1	2.2	2.5	5.2	2.8	4.3	3.5

[a]This value is the velocity estimate for the coordinate difference time series and not the difference of the vertical station velocity estimates

As can be seen from Table 8.7 the computed relative vertical station velocity estimates vary by large amounts. It should be pointed out that the individual vertical station velocity estimates of the dual–CGPS station analysis and the standard coordinate time series were obtained without modelling an annual signal or coordinate offsets. However, as has been shown in Chapter 7, the dual–CGPS station analysis successfully removes common periodic effects. The vertical station velocity estimates for the standard analysis strategy are only included for completeness. The six other analyses included parameters for the coordinate offset magnitudes and annual signals when estimating the vertical station velocities. A large portion of the disagreement in the velocity estimates for MORP between the standard and the other analyses can be attributed to the coordinate offset on 9 March 1998. This offset was estimated to be approximately 5 and 7 mm for the unfiltered and filtered improved ITRS2000 coordinate time series analysed using the improved analysis strategy. From the MLE with the WN+PLN and WN+FN model, the offset magnitudes were estimated to be 10 and 11 mm for the unfiltered, and 8 and 9 mm for the filtered, improved ITRS2000 coordinate time series respectively (see Tables L.5 in Appendix L, and K.10 and K.11 in K).

These results show once more the difficulty of deriving vertical station velocity estimates at the 1 mm/yr level from GPS coordinate time series. It is however believed that the poor agreement in the analyses for this particular station pair is due to the poor quality of the GPS data at both stations, i.e. the frequent and long data gaps prior to becoming

continuously operating and the mentioned signal problems which affect both stations in different ways.

It is therefore important to further investigate the problems at NSTG in order to improve the data for this site. As has been discussed in §5.3.3 in Chapter 5, the problems at MORP seem to have been solved in late 2002.

8.5 Vertical station velocity estimates compared with alternative evidence for vertical land movements

In Chapter 2 alternative evidence for vertical land movements at UK tide gauge sites were discussed and were summarized in Table 2.2. In an attempt to compare these with the vertical station velocity estimates obtained by the author, estimates based on the alternative evidence have been plotted together with estimates from the various analyses in Figures 8.4 to 8.10. All figures show the vertical station velocity estimates from the unfiltered and filtered improved ITRS2000 coordinate time series, analysed using the improved analysis strategy and the MLE with a WN+PLN and WN+FN model. In each of the figures, these estimates are compared to vertical land movement estimates from either MSL trends, AG measurements, geological information or predicted crustal movements from two GIA models. The comparisons have been carried out for seven CGPS@TG stations, namely Brest (BRST), Newlyn (NEWL), Sheerness (SHEE), Lowestoft (LOWE), Liverpool (LIVE), North Shields (NSTG) and Aberdeen (ABER), and the CGPS station LERW, which is approximately 5 km from the tide gauge in Lerwick. The numerical values for all comparisons have been summarized in Table N.1 in Appendix N.

Figure 8.4 compares the vertical station velocity estimates obtained by the author with those computed by subtracting an absolute sea level change of 1.5 mm/yr from the MSL trends of Table 2.1, and taking the negative of it. Although the individual velocity estimates for each station vary largely, the vertical land movements for Brest, Newlyn, Sheerness and Aberdeen are within the spread of the GPS estimates. However, for Lowestoft, Liverpool, North Shields and Lerwick, this is not the case. The discrepancies at these sites may be due to the fact the vertical station velocity estimates are based on

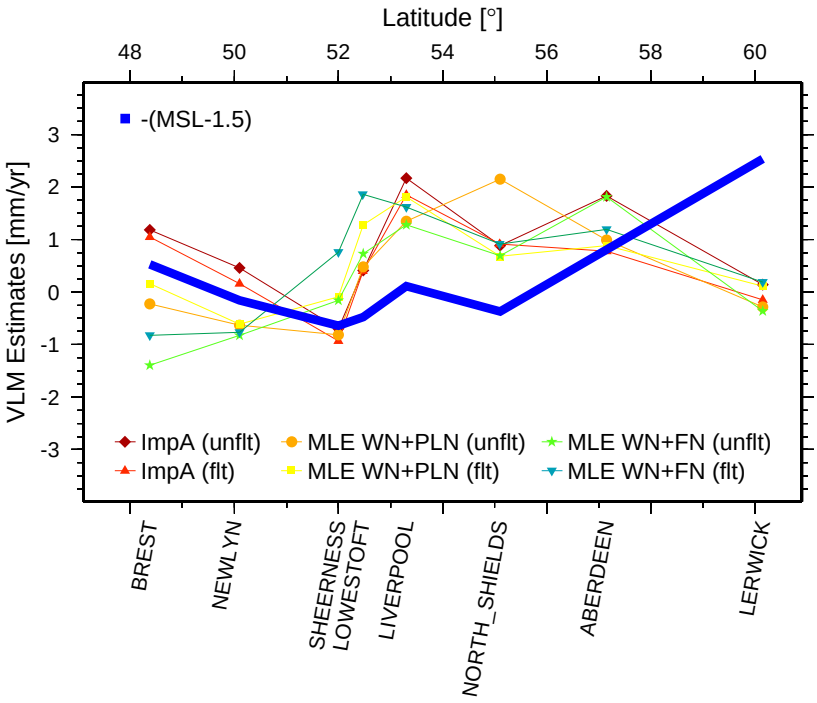

Figure 8.4: Vertical station velocity estimates compared with vertical land movements computed from MSL trends

less than five years of observations while the MSL trends used to compute the vertical land movement estimates are based on much longer observation spans. Furthermore, the assumed absolute change in sea level of 1.5 mm/yr may not be correct for every site. Especially at Lerwick anomalous real sea level changes have been reported due to the near shelf edge (Baker, 2003a).

Considering Brest it may be said that the vertical station velocity estimates for Brest from the MLE with a WN+FN model seem biased. From Tables K.4 and K.5 in Appendix K it can be seen that the flicker noise amplitudes for this analysis were estimated to be 44.3±2.6 mm/yr and 36.8±2.3 mm/yr for the unfiltered and filtered coordinate time series respectively. Clearly, these large noise amplitudes can be attributed to the mis–modelling of the OTL effect. Also shown in these tables are the noise amplitudes for the MLE with a WN+PLN model, which are of similar magnitude. Based on these, the author believes that in the case of Brest, forcing the MLE to use an integer spectral index (assuming flicker noise), rather than letting the MLE select a fractional spectral index (no assumption on the character of coloured noise), may have caused the vertical station

velocity estimates to be biased. This argument may also be supported by the better agreement of the velocity estimates from the MLE with a WN+PLN model with those from the improved analysis or the MSL trends. Also the uplift of Brest with respect to Newlyn or subsidence of Newlyn with respect to Brest indicated by four of the six analyses shown in Figure 8.4, which was also discussed in §8.4.2, supports the author's view.

The vertical station velocity estimate for North Shields based on the MLE using a WN+PLN model seems to be an outlier, when compared to the other five velocity estimates for this station. As has been shown in §5.3.3, the GPS observations at this site are degraded by either RF interference or multipath. From Table K.1 in Appendix K it is shown that the spectral indices of the unfiltered and filtered height time series for North Shields are close to zero, which is an indication of a white noise only process. This is confirmed by the noise amplitudes for the unfiltered and filtered coordinate time series obtained from the MLE with a WN+PLN and WN+FN model in Tables K.4 and K.5 in Appendix K. In these tables the differences between the two MLE analyses are highlighted. For the MLE with a WN+PLN model the integer white noise component is zero and all noise (including the white component) is described by the variable power–law noise. For the MLE with a WN+FN model all noise is attributed to the integer white noise and none to flicker noise. It is clear that these findings do not explain the large vertical station velocity estimate shown in Figure 8.4 obtained for the unfiltered height time series using the MLE with a WN+PLN model. The only remaining factor, however, that might be responsible for this outlier, is the fact that there are large data gaps in the coordinate time series for North Shields. It has to be stated that without further investigations, it is not possible to make any conclusions with respect to the velocity outlier at this stage.

Figure 8.5 shows the vertical station velocity estimates obtained by the author along with those obtained from several absolute gravimetry (AG) campaigns ((Williams et al., 2001)) as detailed in Table 2.2. The vertical land movement estimate derived from the AG measurements in Newlyn is higher than all of the estimates based on GPS, whereas the agreement at Aberdeen and Lerwick is much closer, with the AG estimates being slightly larger at Aberdeen and slightly lower at Lerwick than the GPS estimates. It can be said that both GPS and AG estimates for Aberdeen and Lerwick agree to within the uncertainties shown for the AG estimates in Table 2.2. The amount of fluctuations in

the estimates of vertical crustal movements from AG measurements can be underlined by plotting previous AG estimates for Aberdeen and Newlyn together with the current data shown in Figure 8.5.

Figure 8.6 shows the vertical station velocity estimates obtained by the author along with those from the previous and current estimates obtained from the AG measurements. The solid line indicates the current AG estimates for Newlyn, Aberdeen and Lerwick (as shown in Figure 8.5), whereas the dashed line shows the previous estimates. Both curves agree to within their uncertainties, however it is clear from Figure 8.6 that the previous vertical crustal movement estimates seem to fit the GPS estimates better. Especially between Aberdeen and Lerwick the slope between the GPS estimates seem to match the slope between AG estimates.

At this stage it should be mentioned that the author is aware of similar AG measurements being carried out at Brest, however, he was not able to obtain any estimates of vertical crustal movements during this work.

The vertical station velocity estimates obtained by the author have also been compared to the vertical land movements inferred from geological information published by Woodworth et al. (1999) for Brest and by Shennan and Horton (2002) for all other locations. These have been shown in Table 2.2 in Chapter 2. Figure 8.7 shows the vertical station velocity estimates along with vertical land movements from the geological evidence. From this figure it is clear that the GPS estimates are systematically offset from those inferred from geological data.

From a closer inspection of Figure 8.7 is can be argued that there is an overall trend of uplift between Newlyn and Aberdeen, and Sheerness and Aberdeen, which is consistent between the GPS estimates and the vertical land movements inferred from the geological data. Similarly, it can be argued that there is uplift between Newlyn and Brest visible for both sets of estimates.

Figures 8.8 and 8.9 compare the vertical station velocity estimates obtained by the author with the predicted vertical crustal movements from two GIA models. Both GIA models were introduced in Chapter 2 and their details have been described in Peltier

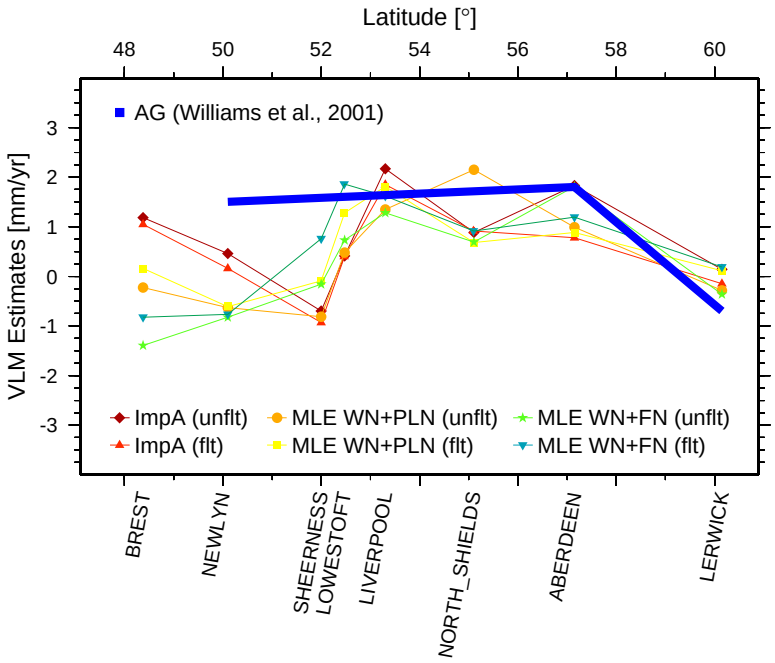

Figure 8.5: Vertical station velocity estimates compared with vertical crustal movements from absolute gravimetry (AG) measurements.

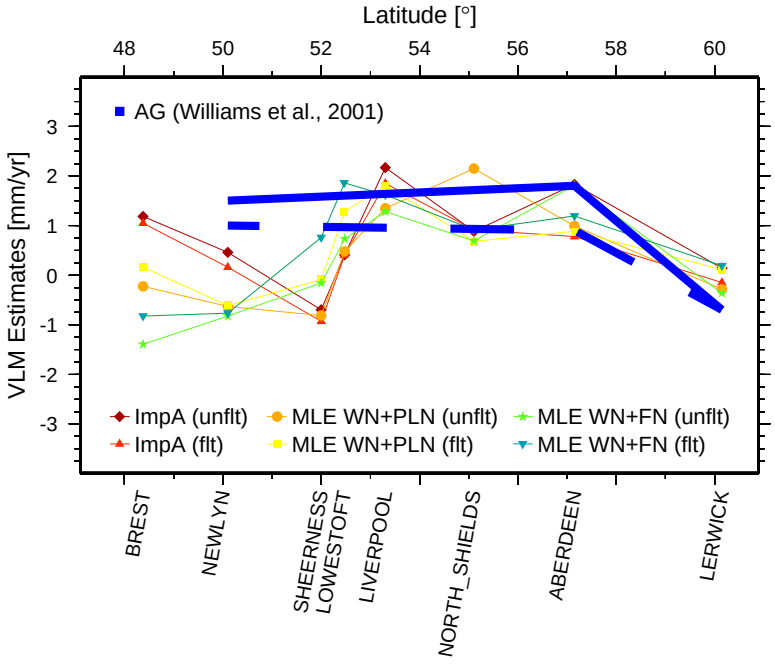

Figure 8.6: Vertical station velocity estimates compared with current and previous vertical crustal movement estimates from AG measurements. The solid line indicates the current AG estimates and the dashed line previous AG estimates.

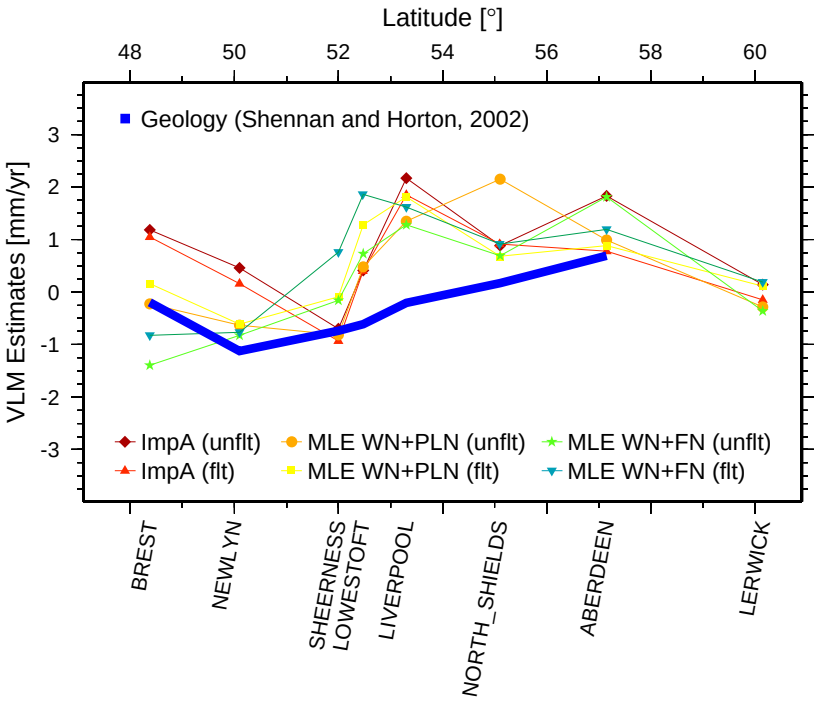

Figure 8.7: Vertical station velocity estimates compared with vertical land movements from geological information.

(2001a) and Scherneck et al. (2002a) respectively. The numerical values of the predicted vertical crustal movements are shown for the eight CGPS stations in Table 2.2 in Chapter 2. Both figures show an interesting pattern in their GIA model predicted crustal movements. From Figure 8.8 it can be seen that the GIA model used in Peltier (2001a) is giving slightly lower estimates than the GPS estimates. Interestingly, the curve for the predicted vertical crustal movements of the second GIA model (Scherneck et al., 2002a) seems to follow the pattern of the GPS estimates much closer. However, the reader should be reminded that the author obtained the predicted crustal movements for this model from Figure A.1 in Appendix A and these have to be assumed to be approximate.

Recently, Nerem and Mitchum (2002) demonstrated that estimates of vertical land movements can also be obtained from satellite altimetry and tide gauge sea level differences for open ocean or island sites with continuous records covering the entire satellite altimetry mission period. Although their estimates of vertical land movements are inconclusive at this stage, Nerem and Mitchum (2002) stated that the results reported should be regarded as validation targets for future solutions. Furthermore, the reference frame used

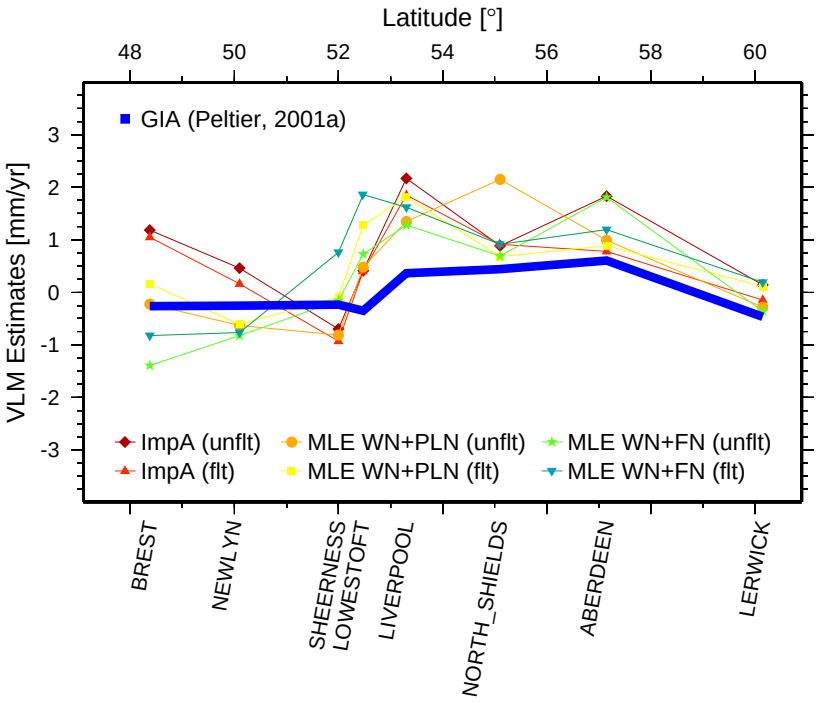

Figure 8.8: Vertical station velocity estimates compared with predicted vertical crustal movements from a GIA model (Peltier, 2001a).

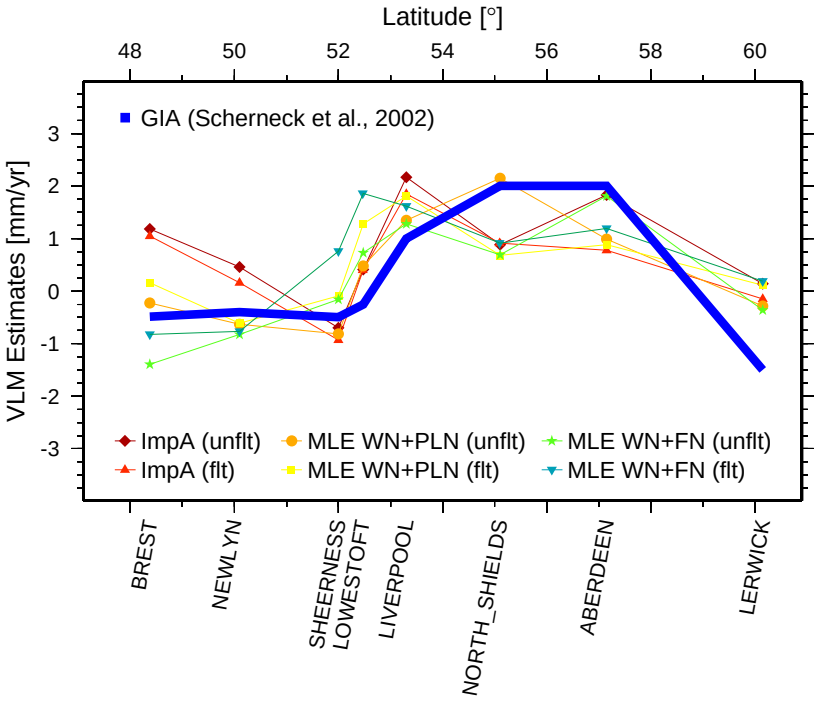

Figure 8.9: Vertical station velocity estimates compared with predicted vertical crustal movements from a GIA model (Scherneck et al., 2002a).

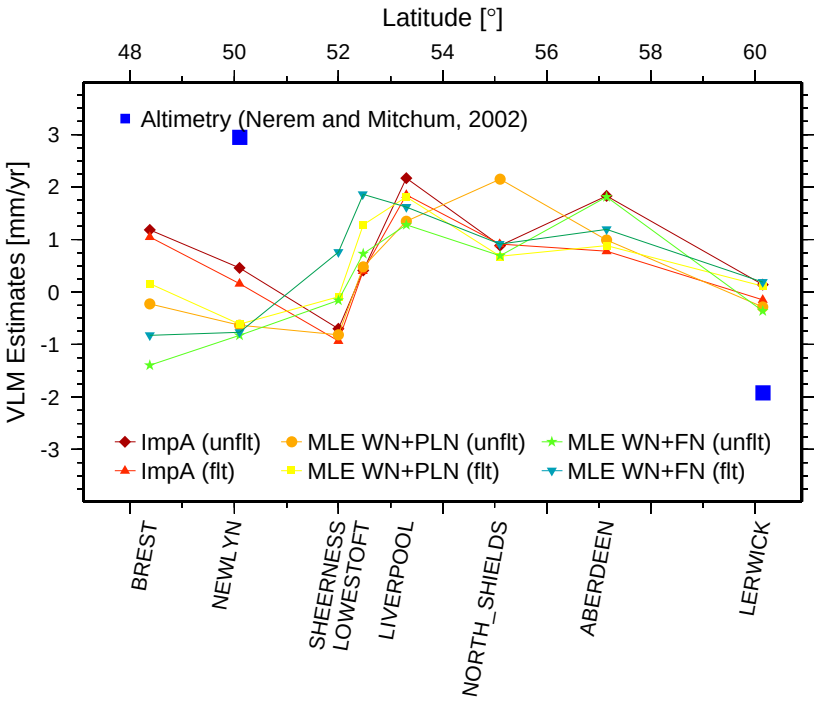

Figure 8.10: Vertical station velocity estimates compared with vertical land movements from satellite altimetry (Nerem and Mitchum, 2002).

for satellite altimetry measurements is not the ITRF, as used by the GPS, strictly speaking making a direct comparison of vertical land movement estimates derived from these space geodetic techniques impossible. The comparison carried out here is therefore included for completeness only.

Figure 8.10 shows the vertical land movement estimates for Newlyn and Lerwick from the analysis of satellite altimetry observations compared to the vertical station velocity estimates obtained by the author. From this figure it can be seen that there is a discrepancy of approximately 3 mm/yr at Newlyn and 2 mm/yr at Lerwick between the GPS and satellite altimetry estimates. Interestingly, the satellite altimetry estimate for Lerwick agrees better with the GIA models in Figures 8.8 and 8.9 than it does with the estimates computed from the MSL trends in Figure 8.4 from the tide gauge.

For ease of comparison of the vertical station velocity estimates obtained by the author with the alternative evidence for vertical land and crustal movements, all numerical values have been summarized in Table N.1 inAppendix N.

8.6 Aligned vertical station velocity estimates

Estimates of vertical land movements derived from AG measurements and geological information are independent of the reference frame used by the GPS. The comparisons in Figures 8.5 and 8.7, especially, suggest that it might be possible to use this characteristic to reduce or possibly even remove reference frame dependent biases from vertical station velocity estimates inferred from GPS coordinate time series. If it is assumed that for a regional network analysis a reference frame bias manifests itself as a constant offset in the vertical station velocity estimates, then a simple procedure can be derived to normalize the GPS velocity estimates to those obtained from a reference frame independent method. Logically, the procedure requires at least one station for which vertical station velocity estimates and vertical land/crustal movement estimates are available. In a first step, all relative vertical station velocity estimates are computed with respect to a reference station. This step already removes a constant reference frame bias as it is differenced away. In a second step, the relative vertical station velocity estimates are aligned to the vertical land/crustal movement estimates for the reference station by adding its vertical land movement estimate.

There are a number of assumptions connected to this *alignment procedure* that may give rise to problems. Differencing of vertical station velocity estimates removes a constant bias, but does not remove biases associated with the estimation of the vertical station velocity in different GPS coordinate time series. Therefore, the success of this procedure is dependent on the quality of the initial coordinate time series, the parameter model and the observation time span. Errors in the vertical land movement estimates from AG measurements or geological information depend even more on the quality of observations as fewer are used to derive those land movement estimates. It is therefore recommended that this alignment procedure is viewed as an approximate method and is carried out for as many station combinations as possible in order to be able to compare the aligned vertical station velocity estimates.

Based on Figures 8.5, 8.6 and 8.7 in the previous section it is proposed that the *alignment procedure* should be tested at Aberdeen and Lerwick using the vertical land movement estimates from the AG measurements, and at Newlyn, Liverpool and Aberdeen

using the vertical land movement estimates derived from the geological evidence. Figures 8.11 and 8.12 show the vertical station velocity estimates aligned to the vertical land movement estimates inferred from the AG measurements at Lerwick and Aberdeen respectively. In both figures the previous estimates for Newlyn and Aberdeen were used along with the current estimate for Lerwick. Here it should be noted that, the alignment procedure has not been carried out with respect to Newlyn due to the larger discrepancies between the GPS estimates and AG estimates at this site.

From Figures 8.11 and 8.12 it is noticeable that the spread in the aligned vertical station velocity estimates increases with the distance from the reference station for which the alignment was computed. This spread is obviously depending on the agreement between the vertical station velocity estimates for the reference station. Therefore, due to the better agreement of the vertical station velocity estimates at Lerwick, the spread in the aligned vertical station velocities is less than that for Aberdeen. The numerical values for both alignment procedures shown in Figures 8.11 and 8.12 can be viewed in Tables N.2 and N.3 in Appendix N respectively.

From the vertical land movement estimates based on geological information discussed in Woodworth et al. (1999), it can be seen that the velocity uncertainties were smallest for Aberdeen, Liverpool and Newlyn. However, these uncertainties were the statistical uncertainties and may have been largely underestimated (Woodworth et al., 1999). The recent study by Shennan and Horton (2002) stated no uncertainties for Aberdeen, 0.03 mm/yr for Liverpool and 0.21 mm/yr for Newlyn (see Table 2.2 in Chapter 2). Although the velocity uncertainty for Liverpool compares well with the one in Woodworth et al. (1999), the uncertainty for Newlyn is more pessimistic than in the previous analysis. Additionally, from Figure 8.3 it can be seen that the agreement in the vertical station velocity estimates for these stations are approximately at the 1 mm/yr level, although those of Newlyn may be affected by the mis–modelling of the OTL effect. The author therefore decided to align the vertical station velocity estimates to the vertical land movements of these three stations inferred from geological data. Figures 8.13, 8.14 and 8.15 show the aligned vertical station velocity estimates for the eight CGPS stations using Aberdeen, Liverpool and Newlyn as reference stations. For convenience, the computed values are summarized in Tables N.4, N.5 and N.6 in Appendix N.

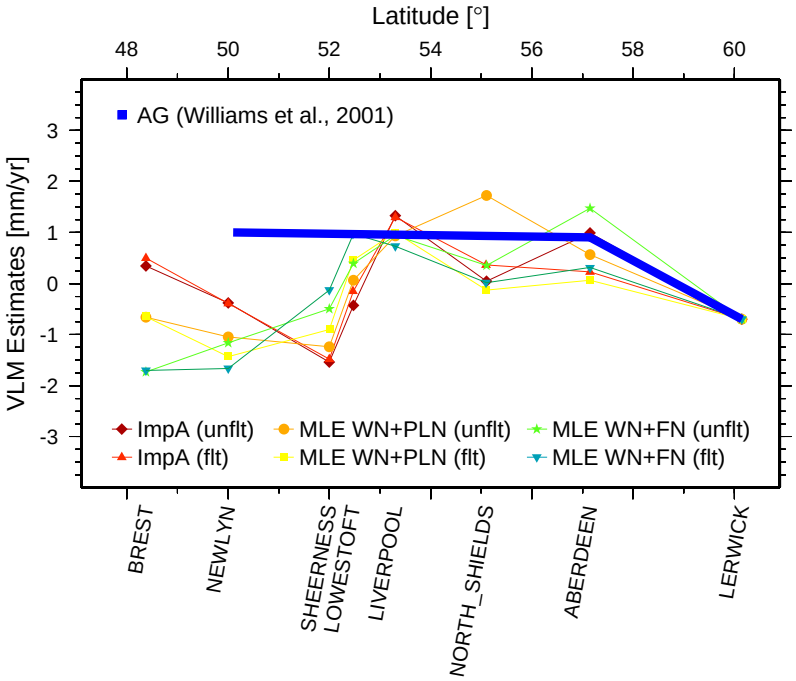

Figure 8.11: AG–aligned vertical station velocity estimates referred to Lerwick.

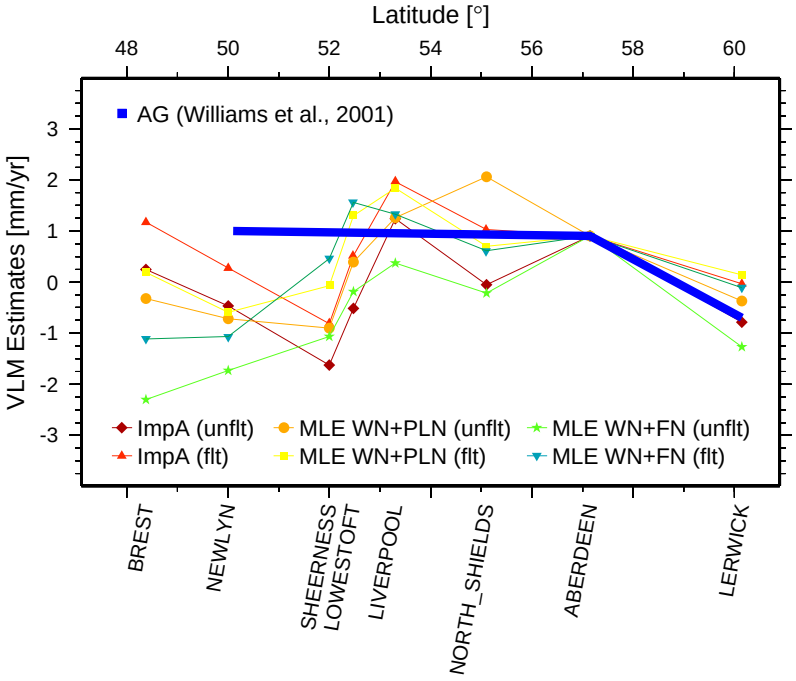

Figure 8.12: AG–aligned vertical station velocity estimates referred to Aberdeen.

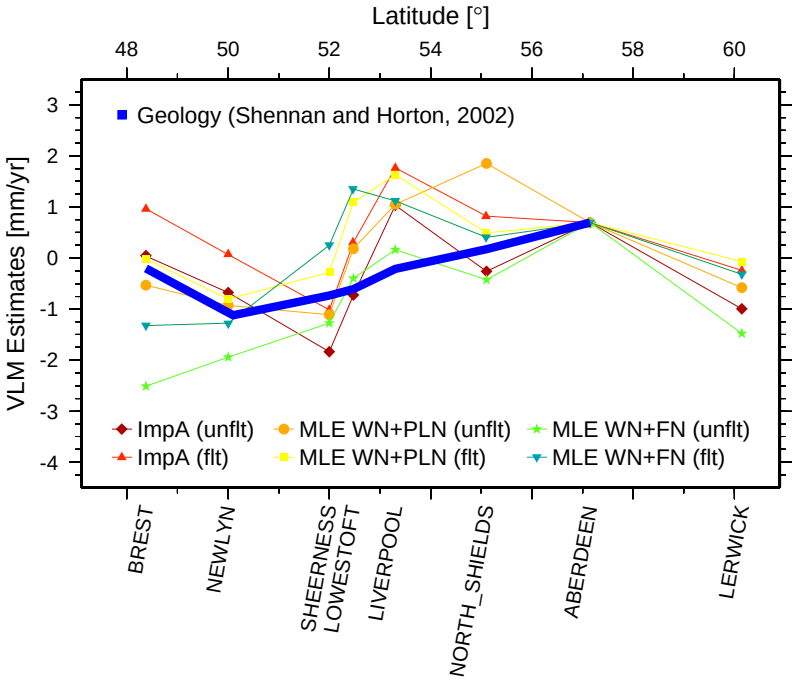

Figure 8.13: Geology–aligned vertical station velocity estimates referred to Aberdeen.

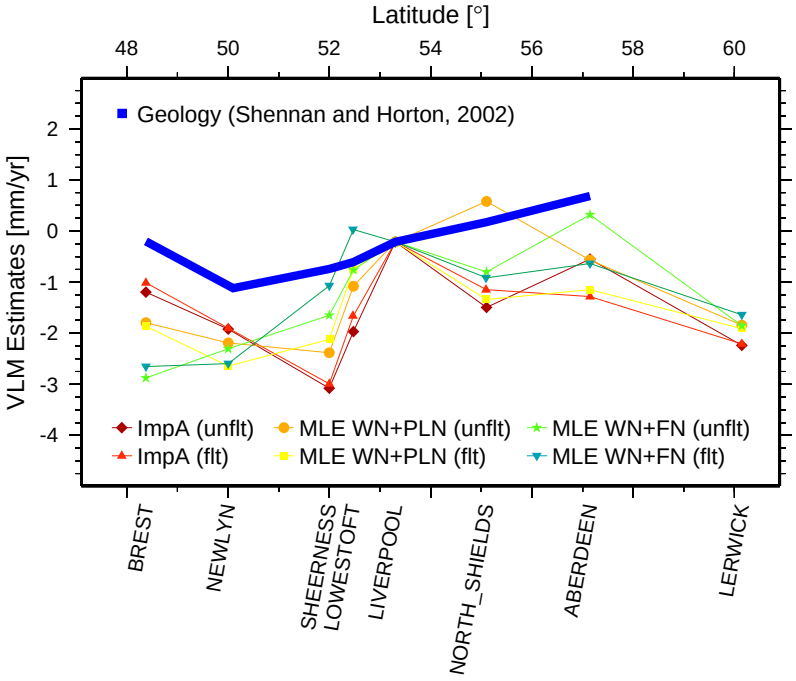

Figure 8.14: Geology–aligned vertical station velocity estimates referred to Liverpool.

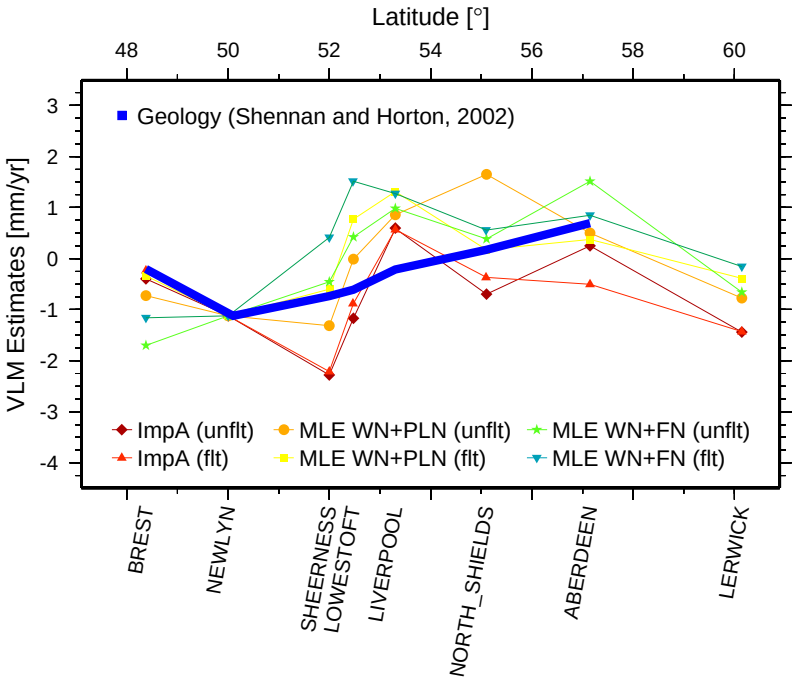

Figure 8.15: Geology–aligned vertical station velocity estimates referred to Newlyn.

From Figure 8.13 it can be seen that the result is similar to that shown in Figure 8.12, both showing the alignment computed with reference to Aberdeen. If the alignment procedure is carried out using the vertical land movement estimates from geological information for Liverpool and Newlyn, the spread of the aligned vertical station velocity estimates is reduced. However, from Figure 8.14 it seems that the vertical station velocity estimates are systematically lower than those for the geological data, whereas, similar to Figure 8.13, Figure 8.15 reveals a more homogeneous picture of the aligned vertical station velocity estimates in relation to the vertical land movements from the geological evidence. Woodworth et al. (1999) stated that there are significant deficiencies in the geological data for Southwest England, in that there were simply not enough geological sea level index points available, with available sites spread over a wide area, and possibly subjected to geomorphological complications. Although, Woodworth et al. (1999) applied a vertical land movement estimate of -1.4 mm/yr for Southwest England, the *real* value may only be small as -0.7 mm/yr. As shown in Table 2.2 in Chapter 2, the value of -1.2 mm/yr applied in this analysis lies between these. To the contrary, the vertical land movement estimates based on geological evidence for Northeast Scotland are fairly

well established with the estimates from Shennan (1989) and Shennan and Woodworth (1992) agreeing on approximately 0.5 mm/yr, and those recently published on 0.7 mm/yr, of uplift. Furthermore, the predicted vertical crustal movements from the GIA model (Peltier, 2001a) and the AG measurements (Williams et al., 2001) are of similar magnitudes and agree to within 0.3 mm/yr (see Table N.1 in Appendix N). This is a strong argument to carry out the further discussion of the vertical station velocity estimates based on the geology–aligned estimates referred to Aberdeen.

It is possible to compute the RMS (Eq. D.1 in Appendix D) of the fit of the aligned vertical station velocity estimates to those of the geological evidence using Newlyn, Liverpool and Aberdeen. This computation reveals that the best RMS fit is obtained by the unfiltered improved ITRS2000 coordinate time series analysed using the improved analysis strategy, i.e. ImpA(unflt).

Based on the geology–aligned vertical station velocity estimates referred to Aberdeen new estimates have been obtained for all other CGPS stations analysed by the author. Figure 8.16 shows the geology–aligned vertical station velocity estimates for all 17 stations referred to Aberdeen. The figure does not contain any uncertainties as the procedure can only be regarded as approximate.

From Figure 8.16 it can be seen that the alignment procedure has a subtle effect on all estimates. Whereas in Figure 8.3, showing the absolute vertical station velocity estimates, it was suggested that seven of the stations are rising, four are subsiding and six are not moving, Figure 8.16 now suggests that six of the stations are rising, eight are subsiding and three are not moving. Although, these estimates are only approximate, the use of the geology–aligned vertical station velocity estimates may be giving a better indication of the real station motions.

8.6.1 Correlation with MSL trends

Using the geology–aligned vertical station velocity estimates referred to Aberdeen from the improved analysis strategy for the unfiltered improved ITRS2000 coordinate time series, it is possible to investigate their correlation with the MSL trends at the tide gauge sites.

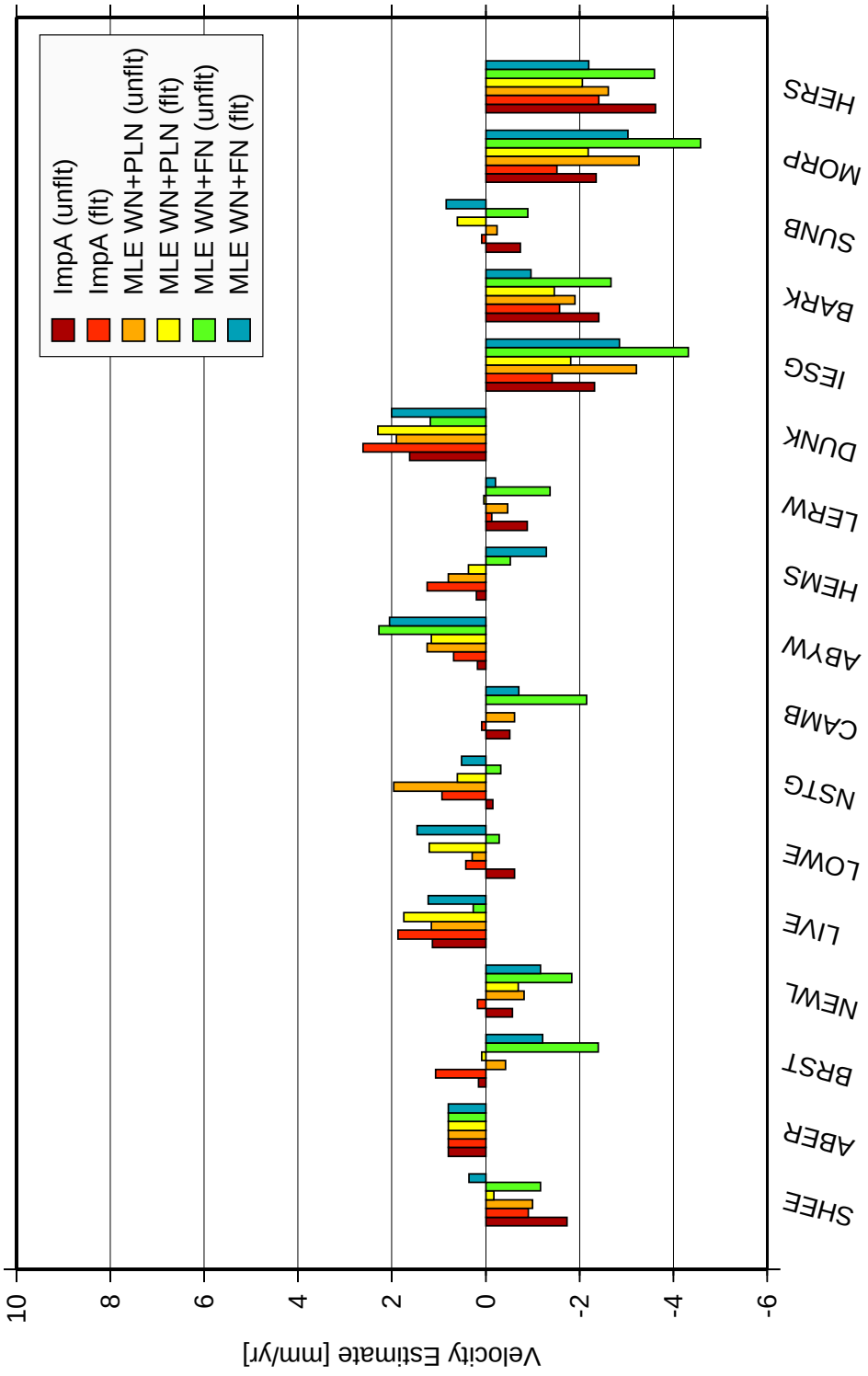

Figure 8.16: Geology–aligned vertical station velocity estimates referred to Aberdeen for the unfiltered and filtered improved ITRS2000 coordinate time series. The estimates shown are those obtained by the improved analysis strategy (ImpA) and the maximum likelihood estimation (MLE) with fractional and integer spectral indices assuming a white plus power–law (WN+PLN) and a white plus flicker (WN+FN) noise model respectively.

Figure 8.17 shows the MSL trends for the eight tide gauge sites, i.e. Aberdeen (ABER), Brest (BRST), Lerwick (LERW), Liverpool (LIVE), Lowestoft (LOWE), Newlyn (NEWL), North Shields (NSTG), and Sheerness (SHEE) against the negative of the vertical station velocity estimates which have been aligned to the uplift rate of Aberdeen based on geological evidence. The uncertainties included for the MSL trends are the statistical uncertainties. The figure uses the 4–character CGPS station code for identification of the site. At this stage the reader should be reminded that apart from CGPS station LERW, all other stations are CGPS@TG stations.

From a first impression of Figure 8.17 it is again suggested that Lerwick is an outlier. Already in Figure 8.4 it was visible that the relative MSL trend for this site was exceptionally low, as indicated by the large vertical land movement estimate computed in Table 2.2 in Chapter 2, when compared to all other estimates. All other evidence of vertical land movements for Lerwick suggest that the predicted subsidence due to GIA is confirmed. Unfortunately, none of the AG or CGPS measurements are actually from the pier on which the tide gauge is located. It should therefore be noted that one of the next CGPS stations to be established as part of the UK tide gauge monitoring project will be located directly adjacent to the tide gauge on the pier in Lerwick.

Besides Lerwick, the results for Sheerness and Liverpool seem next furthest from the dashed line which implies a rise in absolute sea level of 1 mm/yr. With both tide gauges having some of the longest MSL records in the UK (see Table 2.1 in Chapter 2) a problem with the vertical station velocity estimate representing the long–term sea level trends must be assumed. A global sea level rise of 1 mm/yr would indicate that the vertical station velocity estimates for Liverpool are currently too large and for Sheerness too small. The remaining CGPS@TG stations lie within ± 0.3 mm/yr of a suggested absolute sea level rise of 1 mm/yr. Again, with the exception of Lowestoft, the tide gauges have some of the longest MSL records in the world and can be regarded as some of the best records currently available.

For completeness, the author has included the comparisons of the relative MSL trends for the eight tide gauges with the negative of the estimates of the geology–aligned vertical station velocities referred to Aberdeen for all six analysis results, i.e. the improved analysis

strategy, and the MLE with a WN+PLN and a WN+FN model, of the unfiltered and filtered improved ITRS2000 coordinate time series as Figure N.1 in Appendix N.

In order to compare the geology–aligned vertical station velocity estimates referred to Aberdeen with the predicted vertical crustal movements from both GIA models investigated, the author has also included Figure 8.18 showing the GPS estimates plotted against the predicted values for the GIA models in Peltier (2001a) and Scherneck et al. (2002a).

Figure 8.18 indicates variable agreement between the geology–aligned vertical station velocity estimates and the vertical crustal movements predicted due to GIA. In general it seems that at the current stage for most stations the magnitudes of the geology–aligned vertical station velocity estimates are either underestimated or the magnitudes of the crustal movements inferred from both GIA predictions are overestimated. For LIVE there is close agreement between both GIA models and the vertical station velocity estimates from the author's analysis. For SHEE, LOWE and NEWL both models agree with each other. However, as already indicated in Figures 8.13 to 8.15, the geology–aligned vertical station velocity estimate for SHEE seems to be too small, which is confirmed in Figure 8.18.

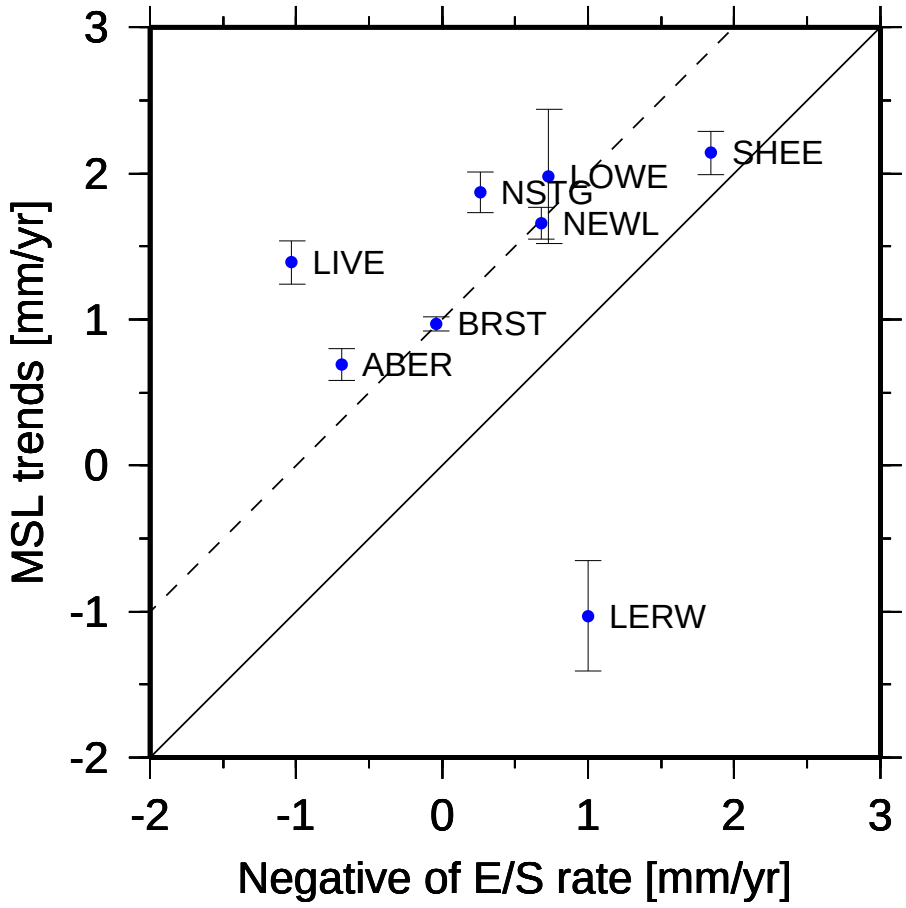

Figure 8.17: Relative MSL trends for eight tide gauges compared with the negative of the vertical station velocity estimates (emergence/submergence rates), which have been aligned to the geological uplift rate for Aberdeen. Data points aligned along the solid line would imply relative MSL trends equivalent to the *geology–aligned* vertical station velocity estimates; points aligned along the dashed line would imply an absolute sea level rise of 1 mm/yr.

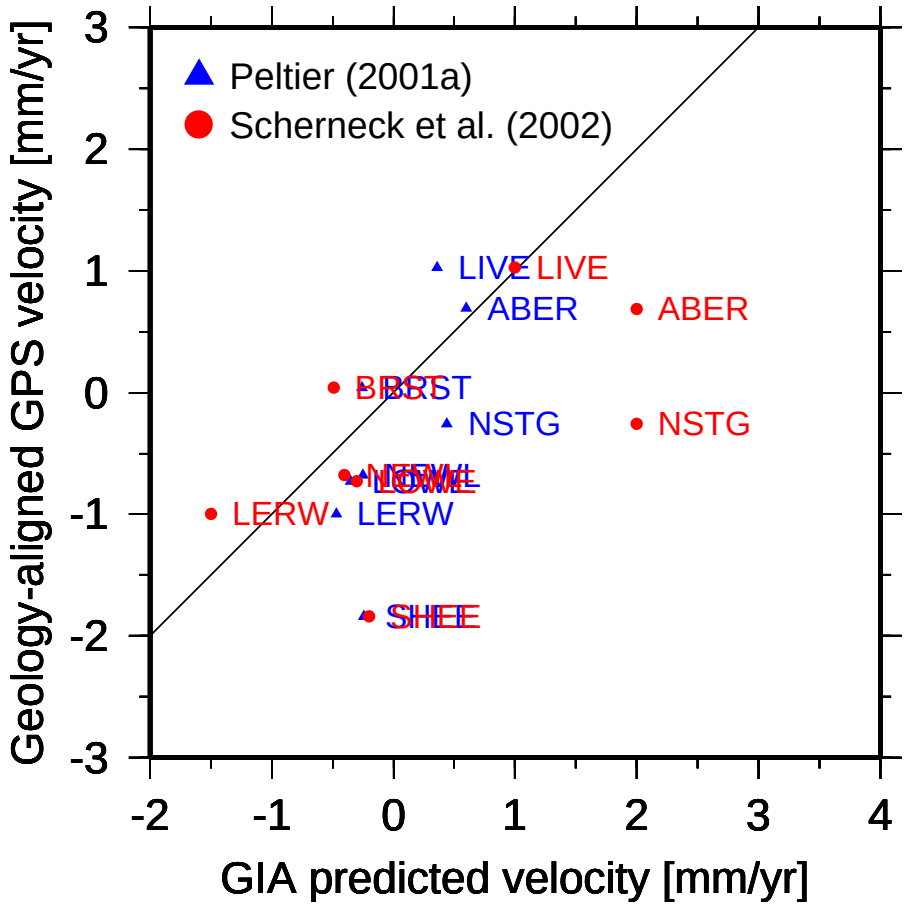

Figure 8.18: Geology–aligned vertical station velocity estimates referred to Aberdeen compared with predicted vertical crustal movements from the GIA models for eight CGPS stations. The GIA predicted vertical crustal movements are the precise values of Peltier (2001a) (blue triangles) and the approximate values from Figure 2 in Scherneck et al. (2002a) (red circles).

8.7 Summary

In this Chapter the vertical station velocity estimates obtained by the author have been discussed in detail. In particular the estimates from the improved analysis strategy, and the MLE with a WN+PLN and WN+FN model, of the unfiltered and filtered improved ITRS2000 coordinate time series have been investigated. The daily height time series for HERS was compared with the daily height time series from the SOPAC analysis and the weekly height time series (I3 analysis) described in Panafidina and Malkin (2001). It was shown that it is difficult to compare absolute vertical station velocity estimates from different analyses without detailed knowledge of the applied processing parameters, e.g. coordinate offsets. It was possible to show good agreement of the vertical station velocity estimates for HERS for the SOPAC analysis and the analysis by the author. Large disagreements in the vertical station velocity estimates for BRST between the ITRF2000 EUREF densification and this analysis were detected. They have been attributed to the shorter time span analysed for inclusion in the official ITRF2000 analysis.

Variations of up to 2 mm/yr are evident in the different absolute vertical station velocity estimates obtained for each of the 17 CGPS stations in the different coordinate time series analysis strategies discussed. It is suggested that seven of the stations are undergoing uplift, four are subsiding and six are not moving, however, only at seven sites the vertical station velocity estimates can be regarded as significant.

For dual–CGPS station pairs NEWL–CAMB and LOWE–HEMS the vertical station velocity estimates for the coordinate difference time series have been compared to the relative vertical station velocity estimates obtained from all coordinate time series analysis strategies. For station pair NEWL–CAMB, excellent agreement was indicated. For station pair LOWE–HEMS, the agreement was slightly worse. The relative vertical station velocity estimates between NEWL and BRST have been compared with those from a dual–CGPS station analysis, evidence of vertical land movements computed from the MSL trends at both tide gauge sites and predicted vertical crustal movements from two GIA models. There was good agreement between the different estimates for the cross–channel vertical land movements and a subsidence of NEWL relative to BRST was computed to be on average 0.5 mm/yr. The analysis of stations MORP and NSTG revealed large

disagreements between a dual–CGPS station analysis and the relative vertical station velocity estimates. There was no improvement in the day–to–day scatter for the coordinate difference time series obtained from the dual–CGPS station analysis, as the height time series are largely uncorrelated due to the quality of the GPS observations being site–dependent.

The vertical station velocity estimates have been compared with alternative evidence for vertical land/crustal movements at eight tide gauges of which seven are CGPS@TG stations. Alternative vertical land movement estimates were obtained from MSL trends, AG measurements and geological information, whereas vertical crustal movement predictions were from two GIA models. There is some reasonable agreement between the different estimates for vertical land and crustal movements for the British Isles. Possible outliers have been identified for the relative MSL trend for Lerwick and the AG measurements for Newlyn.

Aligned vertical station velocity estimates have been computed for eight CGPS stations using the vertical land movement estimates from the AG measurements and geological information. The alignment procedure was carried out for the AG measurements at Lerwick and Aberdeen and for the geological data at Aberdeen, Liverpool and Newlyn. From the geology–aligned vertical station velocity estimates referred to Aberdeen for all 17 CGPS stations it was suggested that six of the stations are rising, eight are subsiding and three are not moving.

Based on the RMS of the fit of the aligned vertical station velocity estimates to the vertical land movements from the geological information, the velocity estimates from the improved analysis strategy using the unfiltered improved ITRS2000 coordinate time series were selected for further investigations and compared to the MSL trends for the eight tide gauges. The geology–aligned vertical station velocity estimates referred to Aberdeen were also compared to the predicted vertical crustal movements for two GIA models. These comparisons suggest that five of the eight stations fit the assumption of an absolute sea level rise of approximately 1 mm/yr. However, the agreement between the geology–aligned vertical station velocity estimates referred to Aberdeen and the GIA predictions of vertical crustal movements were not as good.

Chapter 9

Conclusions and Suggestions for Future Work

Tide gauge MSL records are contaminated by vertical land movements at tide gauge sites. Therefore, in order to arrive at realistic estimates of changes in absolute sea level, these records must be corrected for the observed changes in land level. However, due to the variety of geophysical, geological or engineering type processes which may cause uplift or subsidence at one site, it is often difficult to analyse this complex pattern of vertical land movements.

The Earth's crust is periodically deformed with periods from several hours to several years due to global mass–redistribution in the atmosphere, continents and oceans. Furthermore, episodic mass–redistributions cause additional loading effects. Current realizations of the ITRS do not model these movements in their station motion model, introducing biases in the reference frame. Additionally, these effects are not accounted for in the computation of precise satellite orbits, which causes orbits to be biased. Both effects bias regional GPS network analyses, degrading their accuracy and their ability to determine vertical station velocities.

Errors in tropospheric delay estimates and antenna phase centre models cause scale biases in the estimation of the reference frame and satellite orbits, and in regional network analyses. Especially, the combination of mis–modelling the antenna phase centre variations

both of the receiver and satellite antennas, and the change in the GPS satellite constellation, can introduce long–term changes in the GPS scale, at the level of up to 3 mm/yr. These errors further prohibit the estimation of absolute vertical station velocities using GPS.

In this thesis the author has investigated strategies for the long–term monitoring of vertical land movements at the 1 mm/yr level at tide gauge sites in the UK. The objective was to arrive at possible observation, processing and analysis strategies in order to achieve these stringent accuracy requirements. The author has investigated the dual–CGPS station concept in particular and demonstrated its performance in dealing with systematic biases common to both stations. Two processing strategies have been investigated and several methods for the analysis of coordinate time series have been discussed and compared. The author has also suggested mechanisms for monitoring and quality–checking the complete analysis process, i.e. from the RINEX format observation files to reporting of results.

With current GPS techniques and accuracy levels of reference frames, satellite orbits, and mitigation of biases and errors, the author concludes that a combination of different estimates from several independent techniques is required to arrive at realistic estimates of vertical land movements. In this context, this Chapter presents the specific conclusions of the author's research and gives suggestions for further work.

9.1 Conclusions

The author's conclusions are separated into eight specific sections relating to the research that has been carried out in order to improve the current estimates of vertical station velocities and their uncertainties for the 21 CGPS stations in the UK and France, and their interpretation in terms of vertical land movements in the UK.

Automated processing and analysis using GAS (see Chapter 4)

The author has further developed automated GPS processing and analysis already in place at the IESSG. These automated scripts allow the GPS processing on a daily basis with no user intervention. Furthermore, it is possible to carry out the standard coordinate time series analysis in an automated manner, from which the standard ITRS97 and ITRS2000 coordinate time series have been obtained. Further analysis of the coordinate time series was based on a comprehensive set of Matlab© scripts developed by the author and the `cats_MLE` C programs developed by Simon Williams.

UK CGPS station data quality (see Chapter 5)

The UK CGPS station network has been introduced and detailed analysis of the quality of the GPS observations archived in RINEX format observation files was carried out. This analysis highlighted the mixed quality of the GPS data collected at the UK CGPS stations. A set of parameters was identified which allows quality–checking of raw GPS data using TEQC. A second analysis investigated the σ_0 of the residuals of the ionospherically free observable after detection and removal of cycle slips. This analysis allows the identification of stations for which automated detection and removal of cycle slips is difficult or not possible. Based on this information it is possible to draw conclusions about the quality of the raw data from a particular site. Station statistics detailing the actual number of available daily RINEX data, actual number of sessions from RINEX data, total number of days cleaned, and the total number of sessions cleaned, were provided.

From Figure 5.7 showing the values of mean σ_0 of the residuals of the ionospherically free observable plotted against the length of the baseline from IESG to each CGPS station, it was not possible to identify correlation, in the magnitude of the σ_0 does not depend on the baseline length. There was however a slight suggestion that as a group, the CGPS@TG stations are noisier than the CGPS stations at Met Office sites.

Following the results of the two quality–checks, special site investigations at ABER, ABYW, MORP and NSTG were carried out. For ABER it was concluded that the degraded quality of the GPS observations for this site was due to RF interference from a

faulty radio transmitter near the GPS antenna. No definite conclusions have been drawn for ABYW. The quality inspections revealed a seasonal signal in the quality parameters at a slightly raised level. At this stage it is believed that the signal degradation may be due to multipath or interference from a wind profiler close by. The degradation of the GPS observations at MORP showed itself through problems of the receiver tracking signals of low elevation satellites. This was initially believed to be due to the proximity of the antenna to the ground. The recent introduction of a line amplifier, however, improving the signal–to–noise ratio at the receiver, has improved the quality of the GPS observations dramatically. Unfortunately, this improvement is not visible in this analysis as only data up to 31 May 2002 was used. It was also not possible to draw any conclusions for NSTG as to the source of the degradation in the GPS observations. EGPS observations in December 1999 do not reveal any identifiable problems in the data. However, data collected from February 2000 onwards is degraded, showing the worst quality of all stations analysed by the author. During tests in 2002, the antenna, the antenna cable and the receiver were changed, but an improvement was only partially possible during the receiver change. The full range of the signal degradation as observed since February 2000, was not explained. Since the return of the CGPS receiver the quality of the data have degraded again. Strong multipath must be assumed at this site, possibly due to changes at the site between 9 December 1999 and 12 February 2000.

Estimates of vertical station velocities

Two processing strategies, i.e. Strategy 1 and 2, have been applied by the author during his research. In Strategy 1 the ITRF97 coordinates of KOSG were tightly constrained during the GPS processing stage, and the standard ITRS97 coordinate time series based on Strategy 1 were obtained for nine CGPS stations. In Strategy 2 no constraints were applied, i.e. a non–fiducial approach, and the standard ITRS97 and ITRS2000 coordinate time series based on Strategy 2 were obtained for 21 CGPS stations in the UK and France.

From the analysis of the standard ITRS2000 coordinate time series (Strategy 2) it can be seen that the average WRMS statistics for the North, East and height components, are 3, 5, and 8 mm respectively. These estimates exclude data of the coordinate time

series for ABER, ABYW, MORP and NSTG as these were shown to be affected by signal degradations. CAMB, BRST and NEWL show larger WRMS statistics for the height components than other stations, which is due to mis–modelling of the OTL effect in the GPS processing. The suggestion that CGPS@TG stations are noisier than Met Office CGPS stations was not confirmed. The results however do suggest that individual CGPS@TG stations are prone to a number of additional effects that possibly lead to larger WRMS statistics.

The two processing strategies showed significant differences when their standard ITRS97 coordinate time series were compared for nine CGPS stations up to 25 September 2001. The most pronounced effect was the introduction of a large annual signal with amplitudes between 1.5 and 8 mm in the height time series for Strategy 1. In six out of nine cases, the WRMS statistic was reduced for the height time series of Strategy 2, with ABER, CAMB, and NEWL showing worse WRMS values. The disagreement in the vertical station velocity estimates based on a linear trend model for the two strategies varies between 1.5 and 4.5 mm/yr, with estimates for Strategy 2 being less negative than estimates for Strategy 1.

From a comparison of the vertical station velocity estimates for Strategy 1 (obtained from a least–squares model including a linear and annual term and from a model only including the linear term, but corrected for the annual signal using the theoretical and realistic velocity bias) with the vertical station velocity estimates for Strategy 2, it is evident that both the periodic signal and the GPS processing strategy itself affect the velocity estimates. It may be argued that the effect of the periodic signal on the vertical station velocity estimates ranges from 0.4 to 1.1 mm/yr, whilst the effect of the processing strategy itself was from 1.6 to 2.3 mm/yr.

It was not possible to identify a positive correlation between the magnitude of the amplitudes for the periodic signal in the standard ITRS97 coordinate time series for Strategy 1 with the distance from KOSG. It could however be argued that there is a latitude–dependency in the magnitude of the amplitudes, with stations further north showing larger amplitudes.

From a comparison of the the station velocity estimates for the standard ITRS97 with the standard ITRS2000 coordinate time series it was shown that the effect of the reference frame only being based on four IGS stations (KOSG, ONSA, VILL and WTZR), is in the order of approximately 1 mm/yr in the horizontal components and approximately 0.7 mm/yr in the vertical component.

Estimates of vertical station velocities and their uncertainties

The MLE analysis of the unfiltered and filtered improved ITRS2000 coordinate time series showed that a white plus power–law noise (WN+PLN) model best describes the noise characteristics of the coordinate time series for the UK CGPS stations. Although, the WN+PLN model was identified as the best, the results for the white plus flicker noise (WN+FN) model were very similar, indicating that this model is a good compromise, in case there are time restrictions on the analysis. The white noise only (WN) and the white plus random walk noise (WN+RWN) models did not fit the data as well as the WN+PLN and WN+FN models.

The estimated noise amplitudes for the unfiltered and filtered improved ITRS2000 coordinate time series from the MLE with a WN+PLN and a WN+FN model show a good correlation, although some classical white noise amplitudes were set to zero for the WN+PLN model when the total noise content was estimated to be fractional white noise. The velocity uncertainties obtained from the analysis showed that the uncertainties from the MLE with the WN+FN model are slightly larger than those for the WN+PLN model. However, there was good agreement between the station velocity estimates from the MLE using both noise models. For the unfiltered and filtered improved ITRS2000 coordinate time series the agreement in the station velocity estimates for the horizontal and vertical coordinate components is within ± 0.5 and ± 1 mm/yr, respectively. Furthermore, there is good agreement in the amplitudes and phases of the annual signal terms between the two noise models, with amplitudes for the filtered improved ITRS2000 coordinate time series being slightly smaller than those for the unfiltered improved ITRS2000 coordinate time series.

A comparison of spectral indices obtained by fitting a line to the power spectra of the unfiltered and filtered improved ITRS2000 coordinate time series, with those obtained from the MLE with a WN+PLN model, showed that the latter were slightly larger (more negative). With average spectral indices for the unfiltered and filtered improved ITRS2000 coordinate time series of -0.5 and -0.6 from the MLE with a WN+PLN model and -0.4 and -0.4 from the power spectra respectively, these compare well with those from other regional or global analyses.

The comparison of the white and flicker noise amplitudes, and the velocity uncertainties obtained for the empirical methods by Mao et al. (1999) and Williams (2003a) with those from the MLE with a WN+FN model showed positive correlation in all cases. The agreement between the empirical method by Williams (2003a) and the MLE was better for all three parameters compared. Furthermore, there was a suggestion of slightly more pessimistic uncertainties for the empirical method by Williams (2003a) when compared to those from the MLE, and slightly more optimistic uncertainties for the empirical method by Mao et al. (1999) when compared to those from the MLE.

The direct comparison of the noise amplitudes and the velocity uncertainties between the empirical methods by Mao et al. (1999) and Williams (2003a) confirmed these findings in that both the computed white and flicker noise amplitudes were larger for the method by Williams (2003a), thus giving slightly more pessimistic velocity uncertainties.

The comparison of the white and flicker noise amplitudes from the MLE with a WN+FN model and both empirical methods revealed that in all three cases the computed flicker noise amplitudes were larger than the white noise amplitudes. This comparison demonstrated the inability of the empirical method by Mao et al. (1999) to appropriately compute both noise amplitudes due to their linear dependency on the WRMS statistic.

The differences in the station velocity estimates for the unfiltered and filtered improved ITRS2000 coordinate time series from the MLE with a WN+FN model, and those from the improved coordinate time series analysis, roughly agree to within ± 0.5 mm/yr for the plan components. For the height component the mean difference in the velocity estimates was computed to be -0.6$\pm$1.1 and 0.0$\pm$1.2 for the unfiltered and filtered improved ITRS2000 height time series respectively. This suggests that for the unfiltered improved ITRS2000

height time series the velocity estimates from the MLE are in general more negative than those from the improved coordinate time series analysis.

From the improved coordinate time series analysis it is suggested that including an annual signal term does improve the functional model for two–thirds of the stations for the North, East and height components of the unfiltered improved ITRS2000 coordinate time series. The largest amplitudes for the North, East and height components were estimated to be 5, 5 and 4 mm for SHEE, SUNB, and BARK respectively. Furthermore, for the North, East and height components, there were two, six and six stations respectively, for which the estimated amplitudes were larger than 3 mm. For the filtered improved ITRS2000 coordinate time series the largest amplitudes for the North, East and height coordinate components were estimated to be 4 mm for SHEE, SUNB, and BARK. Furthermore, for the North, East and height components of the filtered improved ITRS2000 coordinate time series, there were one, two and five stations respectively, for which the estimated amplitudes were larger than 3 mm.

The coordinate offset analysis showed that the offset associated with the 9 March 1998, was positively identified by the t–test for all stations affected, i.e. IESG, BARK, MORP, SHEE and SUNB. Furthermore, the inclusion of an offset parameter in the least–squares model significantly improved the overall model for IESG, BARK, SHEE and SUNB. The change detection algorithm was able to detect this coordinate offset to within ± 2 days for IESG, BARK and MORP, and to within ± 10 days for SHEE and SUNB.

The coordinate offset associated with the introduction of a radome at ONSA on 2 February 1999, was positively identified by the t–test for stations IESG, BARK, CAMB, HEMS, LERW, and NEWL, but was not identified for ABER, ABYW, SHEE and SUNB. The inclusion of an offset parameter at this date improved the overall model according to the F–test for IESG, BARK, CAMB, LERW, and SHEE, but did not improve the overall model for ABER, ABYW, HEMS, NEWL, and SUNB. The change detection algorithm was able to detect this coordinate offset to within ± 8 days for IESG. However, for no other stations could the change detection algorithm identify a corresponding epoch.

From the coordinate offset analysis it was concluded that discontinuities in the coordinate time series of fiducial stations used to define the reference frame of regional CGPS networks, can propagate into the coordinate time series of stations in those networks.

Correlations and common mode biases

The cross–correlation analysis between the unfiltered, detrended, coordinate offsets corrected, ITRS2000 coordinate time series revealed cross–correlations between 30 to 60% for the height components for most station pairs. For NSTG, LIVE, and LOWE, the cross–correlations were indicated to be at lower levels, which in the case for NSTG can be attributed to the signal degradation at this site, but cannot be explained for LIVE and LOWE. The largest cross–correlations were computed for the height components of CGPS station pairs HEMS–BARK and CAMB–MORP to be within 70 to 80%. The 21 UK CGPS station data set does not indicate a dependency of the cross–correlation coefficients for the height component on the baseline length, as the cross–correlation coefficients for some of the longest baselines, e.g. CGPS station pairs LERW–BRST, LERW–CAMB and ABER–NEWL, were computed to be in the range of 50 to 60%.

The common mode bias analysis showed the best overall improvement in the day–to–day scatter of the improved ITRS2000 coordinate time series when all CGPS stations except for ABER, ABYW, BARK (height component), BRST (East and height components), DUNK (East component), LERW (East and height components), LIVE (North and East components), MORP, NSTG, SHEE (North component) and SUNB (East component) were included in the stacking process.

Dual–CGPS station analysis

The dual–CGPS station pairs NEWL–CAMB and LOWE–HEMS were analysed over their common time spans of 3.7 and 2.0 years respectively. The analysis showed that for the two station pairs, approximately 20 km apart, common systematic features are removed from the resulting coordinate difference time series. This is supported by the fact that the coordinate difference time series showed reduced WRMS values, i.e. on average 26 and

27% better for NEWL–CAMB and LOWE–HEMS respectively. The dual–CGPS station analysis of both pairs showed that if the individual coordinate time series are correlated with approximately 75%, a reduction in the day–to–day scatter of the coordinate difference time series of about 25% may be expected.

The comparison of the coordinate difference time series of a dual–CGPS station analysis for the standard ITRS97 and ITRS2000 coordinate time series for station pairs NEWL–CAMB and LOWE–HEMS revealed that the coordinate difference time series are independent of the reference frame. The agreement was in all cases sub–millimetric, with a maximum value of 0.2 mm.

The comparison of the coordinate difference time series of the dual–CGPS station analysis with the baseline time series of a single baseline analysis shows that both analyses are highly comparable. The RMS statistics of the difference time series computed between both analyses range from 2 to 4 mm for all three coordinate components and both station pairs. The cross–correlation coefficients between the coordinate difference time series and single baseline time series show on average 72, 80 and 83% for the North, East and height components respectively. This finding has important consequences for the GPS processing strategies applied in large networks using either the current strategy in this research or precise point positioning, as a second processing stage, in which neighbouring CGPS stations are connected to regional or global CGPS stations by single baseline analysis, is not required.

Using synthetic coordinate time series it was possible to show that when coordinate time series contain annually repeating signals, a bias due to this seasonal periodicity should be included in the uncertainty estimation if the annual signal has not been modelled and the time series is not at integer–plus–half years in length. However, the dual–CGPS station analysis of the synthetic coordinate time series showed that relative vertical station velocity estimates quickly approach reliable values, even if the vertical station velocity estimates for the individual stations are affected by periodic variations.

An empirical method for optimizing the filter parameters of an adaptive filter was demonstrated. Using this method it was possible to obtain filterlength M and step size parameter μ specific to the North, East and height components of dual–CGPS station

pairs NEWL–CAMB and LOWE–HEMS. However, the choice of the filter parameters did affect the velocity estimates obtained for the error sequence by as much as 0.25 mm/yr and 0.5 mm/yr for the coordinate components of dual–CGPS station pairs NEWL–CAMB and LOWE–HEMS.

Using the optimized filter parameters the adaptive filter analysis was shown to be capable of successfully separating the incoherent and coherent signal components of the input sequences into filtered and error sequences for both dual–CGPS station pairs. It was shown that the error sequences for the plan components contain an estimate of the tectonic motion due to the fact that both stations are situated on the Eurasian plate. The error sequences for the height component do not show a large secular trend, but do give a good representation of the common features of height time series for both dual–CGPS station pairs.

It was demonstrated that the error sequences of the forward and reversed direction adaptive filter analysis showed similarities to the two–station common mode bias and that the filtered sequences of the forward and reversed direction adaptive filter analysis showed similarities to the coordinate difference time series of a dual–CGPS station analysis.

In summary, the dual–CGPS station concept has been demonstrated to allow a comprehensive and qualitative description of the station motions observed, even for shorter (< 2.5 years) observation time spans, through a multitude of possible analysis methods. It was shown that at present the relative station motions for the dual–CGPS station pairs NEWL–CAMB and LOWE–HEMS seem to be insignificant, suggesting that both CGPS@TG stations are well founded and are not experiencing any local vertical land movements in addition to the underlying geophysical crustal motion.

Comparisons with other GPS analyses

Using the height time series for HERS it was demonstrated that care must be taken when comparing coordinate time series results with results from other analyses. Based on the JPL and SOPAC analyses, the level of agreement between different analysis centres was shown to be at the 1 to 2 mm/yr level for this station. The direct comparison of the

HERS height time series from the SOPAC analysis and from the IESSG analysis, showed a slightly larger day–to–day scatter in the IESSG analysis and a difference in the vertical station velocity estimate for HERS of 1.3 mm/yr. However, this was reduced to 0.6 mm/yr by investigating relative station velocity estimates.

The comparison of the weekly I3 coordinate time series and the daily ITRS2000 coordinate time series from the IESSG analysis showed an agreement of 1 mm/yr in the vertical station velocity estimates for a common time period. However, it was highlighted that it is difficult to compare vertical station velocity estimates for different analyses without detailed knowledge of the processing strategy.

Final vertical station velocities

The absolute vertical station velocity estimates for the six different coordinate time series analyses obtained by the author show significant variations of up to 2 mm/yr for several stations.

The author's results suggest that ABER, LIVE, LOWE, NSTG, ABYW, HEMS, and DUNK are rising, IESG, BARK, MORP and HERS are subsiding, and SHEE, BRST, NEWL, CAMB, LERW, and SUNB are not moving, within the ITRS2000 realization used for this analysis. The velocity uncertainties shown, however demonstrated that none of the velocity estimates are statistically significant at this stage.

Comparison of vertical station velocity estimates with other evidence

The absolute vertical station velocity estimates obtained by the author have been compared to estimates of vertical land movements from MSL trends, AG measurements, geological data, and satellite altimetry measurements, and with predicted vertical crustal movements from two GIA models. Some reasonable agreement was shown between the different estimates from this analysis and the alternative evidence. Although, comparisons with the evidence from geology, the AG measurements, and one GIA model suggested that the absolute vertical station velocity estimates were systematically offset from the other evidence.

An alignment procedure was demonstrated using vertical land movement estimates from the AG measurements or geological information. The procedure was carried out for the AG measurements at Lerwick and Aberdeen and for the geological data at Aberdeen, Liverpool and Newlyn.

From the geology–aligned vertical station velocity estimates referred to Aberdeen for 17 CGPS stations the author's results suggest that ABER, LIVE, LOWE, NSTG, ABYW and DUNK are rising, SHEE, NEWL, CAMB, LERW, IESG, BARK, MORP, and HERS are subsiding, and BRST, HEMS, and SUNB are not moving.

A comparison of the negative of the geology–aligned vertical station velocity estimates with the MSL trends showed a positive correlation. The correlation suggested that ABER, BRST, NSTG, NEWL and LOWE show a change in absolute sea level of approximately $+1\,\mathrm{mm/yr}$.

The comparison of the geology–aligned vertical station velocity estimates with the GIA predicted vertical crustal movements showed a positive correlation. However, the agreement was not as good as for the correlation between the negative of the geology–aligned vertical station velocity estimates and the MSL trends.

Nevertheless, the need for an alignment procedure to remove systematic biases in regional GPS network analyses has been demonstrated, which strengthens the argument by the author that highly accurate vertical station velocity estimates can currently only be obtained from the analysis of different estimates from several independent techniques.

9.2 Suggestions for Future Work

Based on the findings by the author through his work, some suggestions for future work are detailed below.

CGPS data and processing

Special site investigations at NSTG and ABYW are required in order to identify the source of the observed signal degradation. The abrupt increase in the RMS MP1 and MP2 values for ABER in 2002 also needs to be investigated. Along with these investigations, a critical review of the data quality of the GPS observations from all other stations should be carried out in order to improve our understanding of the problems associated with each station and allow easier identification of the source of potential problems. As the determination of the vertical coordinate component is the most difficult in the first place, it cannot be expected that high quality long–term estimates of vertical land movements can be obtained from poor sites.

A similar investigation into the data quality of the stations in the Ordnance Survey active GPS network should be carried out in order to qualify potential stations to be included in the analysis of vertical land movements in the UK. A denser network would enable a clearer picture of the regional differences in the observed vertical land movements and would help in identifying unrealistic estimates. It must however be stated that this will also increase the need for more stringent documentation of changes to the equipment and the local environment of the antenna.

Due to the mis–modelling of the ocean tide loading effect discussed in Chapter 6, it is necessary that the complete UK CGPS data set is re–processed and re–analysed. In any re–processing it will be worth considering the benefits which may be gained from other improvements such as the inclusion of absolute antenna phase centre models and the use of elevation–dependent weighting. Although these will require modifications to GAS, the former should only be used if there are new IGS products available in which these absolute antenna phase centre models were used.

Any increase in the number of CGPS stations analysed potentially increases the number of dual–CGPS station pairs that can be formed. Hence, an investigation into forming further dual–CGPS station pairs throughout the UK is recommended. Furthermore, observations from dual–CGPS station pairs should also be processed in a kinematic fashion, if feasible.

The analysis of episodic and quasi–continuous GPS observations should be carried out and it should be evaluated, how results for these can be improved by using daily common mode bias estimates from the analysis of the continuous GPS observations.

Coordinate time series analysis

In order to further evaluate the quality of the coordinate time series obtained using GAS it is recommended that parallel GPS processing is carried out with other GPS software packages. This can be carried out at the IESSG using the Bernese GPS software. It may however also be possible to carry out comparisons for those CGPS@TG stations submitted to the IGS TIGA PP and ESEAS projects once coordinate time series are available.

It is suggested that the empirical optimization of the filter parameters of the adaptive filter demonstrated by the author is further investigated and compared to the strictly optimal parameter estimates obtained from the MLE in combination with the minimum description length (see Eq. I.12 in Appendix I).

The author has obtained atmospheric loading corrections for the UK 21 CGPS station network analysed. An investigation is suggested into whether the loading signals can be detected and whether these corrections improve the current height time series.

Similar investigations are proposed for GPS stations located along the east coast of England with respect to the predicted loading effects due to storm surge events. As these events normally only last for 24 to 48 hours, data from episodic and quasi–continuous GPS stations could also be included.

Improvements in GAS

The author has identified several issues within GAS that require attention if it is to be used for GPS processing in the future. A complete overhaul is recommended focusing on the compilation using Lahey FORTRAN in order to better utilize the processing capabilities at the IESSG using several high power Linux workstations. Furthermore, it should be investigated how the number of simultaneously processed baselines using the current

processing strategy can be increased. The inclusion of additional stations will require the division into more sub–networks. Therefore a network of sixty UK CGPS stations would require, assuming the current processing strategy, 19 sub–networks, which is clearly not efficient.

The currently developed and tested absolute receiver and satellite antenna phase centre models will become the IGS recommended antenna phase centre models to be applied by the user community. The inclusion of these will require modifications to GAS. At this stage the author suggests to modify GAS in such a way that future antenna phase centre models can be read directly from the new ANTEX (IGSCB, 2003) format files. This would remove the need to re–compile GAS each time a new antenna phase centre model has been included.

A further way of improving the estimates in the vertical coordinate component is by better de–correlation of height and tropospheric delay estimates based on the inclusion of low–elevation satellite data in the GPS processing. This however requires elevation–dependent weighting and the estimation of troposphere gradients to be implemented in GAS.

Improvements in processing scripts

Changes to the automated daily processing script are recommended with respect to improving station times file entries in order to allow episodic and quasi–continuous GPS stations to be automatically included in the daily automated processing. The possibility of combining the station times file with the content reports created for the processing data archive should be investigated. The use of a database system, e.g. mySQL on Linux workstations, to store station statistics should be evaluated.

Improvements in analysis scripts

The automated coordinate time series analysis requires updating in order to include the recently obtained `cats_MLE` C programs, which will allow the modelling of annual, semi–annual and other periodic signals and the inclusion of offsets in the coordinate time

series. This would also allow the use of the empirical method by Williams (2003a) for the computation of station velocity uncertainties.

Scripts to carry out the MLE with fractional spectral indices on an annual basis for the complete CGPS network should be developed. Intermediate estimates of noise amplitudes should be obtained from the empirical method by Williams (2003a).

Further improvements to the outlier detection and removal algorithm are necessary as can be seen for the coordinate time series of BRST and MORP. In particular an iterative process is suggested, possibly also modelling annual and semi–annual terms to closely match the data.

The author suggests station–dependent summary plots for each coordinate component showing the de–meaned raw, de–meaned cleaned (outliers removed) and residual coordinate time series. The figure showing the de–meaned cleaned coordinate time series should include the model fitted to the data (partially already available through the automated coordinate time series analysis). Furthermore, this summary plot should show the power spectrum and the auto–correlation function for the residual coordinate time series. Additionally, a special frame should be included showing daily or monthly estimates of current and previous parameter estimates, e.g. for velocities, amplitudes and phases of periodic signals, and coordinate offset magnitudes. Besides the associated uncertainties, this will allow a better assessment of the stability of all estimated parameters.

Future Global Navigation Satellite Systems

In years 2000 and 2001 five Block IIR satellites were set *healthy* and have significantly enhanced GPS system performance and availability (Marquis, 2001). Furthermore, an effort is underway to bring modernized functionality to Block IIR satellites built several years ago and placed in storage until needed for launch. It has been reported that three new signals and increased L–band power will significantly improve navigation performance for users worldwide.

By the year of 2008 the European Satellite Navigation System Galileo is expected to achieve full operational capability (Ochieng et al., 2001). The system will offer global

coverage and will support transport navigation requirements and many other applications requiring spatial and/or temporal information. It is intended that Galileo will be compatible with GPS/GLONASS and interoperable with space– and ground–based augmentation systems. The combined use of Galileo with these other systems could lead to significant benefits due to enhanced navigation performance.

In both these cases the author believes that to a certain degree it is currently questionable whether improvements with respect to precise monitoring of vertical land movements can be expected in the immediate future. Yes, benefits will arise from the increased numbers of satellites allowing a better geometrical distribution and so forth. Such systems will however bring other difficulties that require investigations and solutions.

References

Agnew, D. C., 1992. The time-domain behaviour of power-law noises. Geophysical Research Letters 19 (4), 333–336.

Altamimi, Z., Angermann, D., Argus, D. F., Blewitt, G., Boucher, C., Chao, B. F., Drewes, H., Eanes, R., Feissl, M., Ferland, R., Herring, T. A., Holt, W. E., Johansson, J. M., Larson, K. M., Ma, C., Manning, J., Meertens, C., Nothnagel, A., Pavlis, E., Petit, G., Ray, J., Ries, J., Scherneck, H. G., Sillard, P., Watkins, M. M., 2001. The terrestrial reference frame and the dynamic Earth. EOS Transactions, American Geophysical Union 82 (25), 273–279.

Altamimi, Z., Boucher, C., 1999. Recent results of the International Terrestrial Reference Frame. In: Communications Research Laboratory (Ed.), International Workshop on Geodetic Measurements by the collocation of Space Techniques on Earth. Communications Research Laboratory, Koganei, Tokyo, Japan, pp. 15–21.

Altamimi, Z., Sillard, P., Boucher, C., 2002. ITRF2000: A new release of the International Terrestrial Reference Frame for Earth science applications. Journal of Geophysical Research 107 (B10), 2214, doi:10.1029/2001JB000561.

Angermann, D., Drewes, H., Gerstl, M., Kaniuth, K., Kelm, R., Müller, H., Seemüller, W., Tesmer, V., 2001. Realization of the International Terrestrial Reference Frame by DGFI Analysis Center. EOS Transactions, American Geophysical Union 82 (47), Fall Meet. Suppl.

Angermann, D., Kaniuth, K., Müller, H., Tesmer, V., 2002. Contribution of individual space techniques to the realization of vertical reference systems. In: Drewes, H., Dodson,

A. H., Fortes, L. P. S., Sánchez, L., Sandoval, P. (Eds.), Vertical Reference Systems. Vol. 124 of International Association of Geodesy Symposia. Springer-Verlag, Berlin Heidelberg, pp. 91–96.

Araújo, I., Pugh, D., Collins, M., 2001. An intensive analysis of trends in sea level variability at Newlyn. In: Book of Extended Abstracts, Final Workshop of COST Action 40, Sea Level in Europe: Observation, Interpretation and Exploitation, Dubrovnik, Croatia, 19-21 September 2001. Hydrographic Institute of the Republic of Croatia, Split, pp. 93–96.

Argus, D. F., Peltier, W. R., Watkins, M. M., 1999. Glacial isostatic adjustment observed using very long baseline interferometry and satellite laser ranging geodesy. Journal of Geophysical Research 104 (B12), 29077–29093.

Árnadóttir, T., Geirsson, H., Bergsson, B. H., Völksen, C., 2000. The Icelandic continuous GPS network - ISGPS, March 18, 1999 - February 20, 2000. Tech. rep., Icelandic Meteorological Office Department of Geophysics, Reykjavik.

Ashkenazi, V., (Co-ordinator) 1995. The use of GPS to monitor changes in absolute sea level: concept validation and first epoch measurements at selected tide gauges on the Atlantic Coast of Europe. Final rep., The Institute of Engineering Surveying and Space Geodesy, University of Nottingham, Nottingham.

Ashkenazi, V., Beamson, G. A., Bingley, R. M., Dodson, A. H., Baker, T. F., 1994. The determination of tide gauge heights using GPS. POL Internal Report 75, The Proudman Oceanographic Laboratory, Birkenhead.

Ashkenazi, V., Bingley, R. M., Booth, S. J., Greenaway, R. G., Nursey, K., Bedlington, D., Ellison, R. A., Arthurton, R. S., 1998. Monitoring long term vertical land movements in the Thames Estuary and Greater London. In: FIG Commission 5 (Ed.), XXI FIG International Congress: Developing the Profession in a Developing World, 19-25 July 1998, Brighton, UK. FIG Commission 5, pp. 176–188.

Ashkenazi, V., Bingley, R. M., Dodson, A. H., Penna, N. T., Baker, T. F., 1997. The determination of tide gauge heights using GPS (Second Report). POL Internal Report 125, The Proudman Oceanographic Laboratory, Birkenhead.

Ashkenazi, V., Bingley, R. M., Whitmore, G. M., Baker, T. F., 1993. Monitoring changes in mean sea level to millimeters using GPS. Geophysical Research Letters 20 (18), 1951–1954.

Baker, H. C., 1998. GPS water vapour estimation for meteorological applications. Ph.D. thesis, University of Nottingham.

Baker, R., 2000. Some useful statistical tables [online]. Available at: `<http://duke.usask.ca/~rbaker/Tables.html>`[3 October 2002].

Baker, T. F., 1984. Tidal deformations of the Earth. Sci. Prog., Oxf. 69, 197–233.

Baker, T. F., 1993. Absolute sea level measurements, climate change and vertical crsutal movements. Global and Planetary Change 8, 149–159.

Baker, T. F., `(tfb@pol.ac.uk)` 2003a. Re: EGS 2003 abstract. 10 January. Email to: Norman Teferle (`norman.teferle@nottingham.ac.uk`).

Baker, T. F., `(tfb@pol.ac.uk)` 2003b. Re: Storm surge loading. 25 April. Email to: Norman Teferle (`norman.teferle@nottingham.ac.uk`).

Baker, T. F., Bos, M. S., 2003. Validating Earth and ocean tide models using tidal gravity measurements. Geophysical Journal International 152, 468–485.

Baker, T. F., Curtis, D. J., Dodson, A. H., 1995. Ocean tide loading and GPS. GPS World 6 (3), 54–59.

Baker, T. F., Woodworth, P. L., Blewitt, G., Boucher, C., Wöppelmann, G., 1997. A European network for sea level and coastal land level monitoring. Journal of Marine Systems 13 (1-4), 163–171.

Basseville, M., Nikiforov, I. V., 1993. Detection of abrupt changes: Theory and Application. Information and system science series. Prentice Hall, Englewood Cliffs, New Jersey, USA.

Beamson, G. A., 1995. Precise height determination of tide gauges using GPS. Ph.D. thesis, University of Nottingham.

Becker, M., Zerbini, S., Baker, T. F., Bürki, B., Galanis, J., Garate, J., Georgiev, I., Kahle, H. G., Kotzev, V., Lobazov, V., Marson, I., Negusini, M., Richter, B., Veis, G., Yuzefovich, P., 2002. Assessment of height variations by GPS at Mediterranean and Black Sea coast tide gauges from SELF projects. Global and Planetary Change 34 (1-2), 5–35.

Bellanger, E., Blanter, E. M., LeMouël, J. L., Shnirman, M. G., 2002. Estimation of the 13.63-day lunar tide effect on the length of day. Journal of Geophysical Research 107 (B5), ETG4/1–4/6.

Bennike, O., Björck, S., Lambeck, K., 2002. Estimates of South Greenland late-glacial ice limits from a new relative sea level curve. Earth and Planetary Science Letters 197, 171–186.

Beutler, G., 1996a. Development of the IGS. IGS Annual Report 1994, IGS Central Bureau, Jet Propulsion Laboratory, California Institute of Technology, Pasadena, California.

Beutler, G., 1996b. GPS satellite orbits. In: Teunissen, P. J. G., Kleusberg, A. (Eds.), GPS for Geodesy, 2nd Edition. Springer-Verlag, Berlin Heidelberg, pp. 43–110.

Bevis, M., Bock, Y., Fang, P., Reilinger, R., Herring, T. A., Stowell, J., Smally, R., 1997. Blending old and new approaches to regional GPS geodesy. EOS Transactions, American Geophysical Union 78 (6), 64–66.

Bevis, M., Scherer, W., Merrifield, M., 2001. Technical issues and recommendations related to the installation of continuous GPS stations at tide gauges [online]. Available at: `<http://imina.seast.hawaii.edu/cgps_tg/introduction/index.html>` [1 October 2001].

Bevis, M., Scherer, W., Merrifield, M., 2002. Technical issues and recommendations related to the installation of continuous GPS stations at tide gauges. Marine Geodesy 25 (1), 87–99.

BGS, 1979. Geological Map of the United Kingdom South.

Bingley, R. M., Dodson, A. H., Penna, N. T., Teferle, F. N., 2000a. The determination of tide gauge heights using GPS & the University of Nottingham's contribution to MAFF Final R&D Project FD0305. Final Report NERC R&D Contract F3CR07-G1-02-05, The Institute of Engineering Surveying and Space Geodesy, University of Nottingham, Nottingham.

Bingley, R. M., Dodson, A. H., Penna, N. T., Teferle, F. N., Baker, T. F., 2001a. Monitoring the vertical land movement component of changes in mean sea level using GPS: Results from tide gauges in the UK. Journal of Geospatial Engineering 3 (1), 9–20.

Bingley, R. M., Dodson, A. H., Penna, N. T., Teferle, F. N., Booth, S. J., 2000b. Using a combination of continuous and episodic GPS data to separate crustal movements and sea level changes at tide gauges in the UK. In: Real Instituto y Observatorio de la Armada en San Fernando (Ed.), Extended Abstracts Book of the 10th General Assembly of the WEGENER Project (WEGENER 2000), San Fernando, Spain, 18-20 September 2000. Ministerio de Defensa.

Bingley, R. M., Dodson, A. H., Teferle, F. N., 2001b. GPS monitoring of changes in ground level for flood and coastal defence. In: Proceedings of the 36th DEFRA Conference of River and Coastal Engineers, Keele Universty, 20-22 June 2001. DEFRA Flood Management Division, London, pp. 03.5.1–03.5.12.

Blewitt, G., Bock, Y., Kouba, J., 1994. Constraining the IGS polyhedron by distributed processing. In: Zumberge, J. F., Liu, R. (Eds.), IGS Workshop Proceedings: Densification of the IERS Terrestrial Reference Frame through Regional GPS Networks, 30 November - 2 December, 1994. IGS Central Bureau, Jet Propulsion Laboratory, California Institute of Technology, Pasadena, California, pp. 21–37.

Blewitt, G., Clarke, P. J., 2003. Inversion of Earth's changing shape to weigh sea level in static equilibrium with surface mass redistribution. Journal of Geophysical Research , DOI:10.1029/2002JB002290 (in press).

Blewitt, G., Davies, P., Gregorius, T. L. H., Kawar, R., Sanli, U., 1997. Sustainable geodetic monitoring of the natural environment using the IGS. In: Neilan, R. E., Van Scoy, P. A., Woodworth, P. L. (Eds.), Methods for monitoring Sea Level: GPS

and Tide Gauge Benchmark Monitoring and Altimeter Calibration. Jet Propulsion Laboratory, California Institute of Technology, Pasadena, California, pp. 69–83.

Blewitt, G., Heflin, M. B., Webb, F. H., Lindqwister, U. J., Malla, R. P., 1992. Global coordinates with centimeter accuracy in the International Terrestrial Reference Frame using GPS. Geophysical Research Letters 19 (9), 853–856.

Blewitt, G., Lavallée, D., 2000. Effect of annually repeating signals on geodetic velocity estimates. In: Real Instituto y Observatorio de la Armada en San Fernando (Ed.), Extended Abstracts Book of the 10th General Assembly of the WEGENER Project (WEGENER 2000), San Fernando, Spain, 18-20 September 2000. Ministerio de Defensa.

Blewitt, G., Lavallée, D., 2002. Effect of annual signals on geodetic velocity. Journal of Geophysical Research 107 (B7), ETG9–1/9–11, DOI:10.1029/2001JB000570.

Blewitt, G., Lavallée, D., Clarke, P. J., Nurutdinov, K., 2001. A new global mode of Earth deformation: Seasonal cycle detected. Science 294, 2342–2345.

Bock, Y., 1996. Reference systems. In: Teunissen, P. J. G., Kleusberg, A. (Eds.), GPS for Geodesy, 2nd Edition. Springer-Verlag, Berlin Heidelberg, pp. 1–43.

Bock, Y., Nikolaidis, R. M., de Jonge, P. J., Bevis, M., 2000. Instantaneous geodetic positioning at medium distances with the global positioning system. Journal of Geophysical Research 105 (B12), 28223–28253.

Bock, Y., Wdowinski, S., Fang, P., Zhang, J., Williams, S. D. P., Johnson, H. O., Behr, J., Genrich, J., Dean, J., Van Domselaar, M., Agnew, D. C., Wyatt, F., Stark, K., Oral, B., Hudnut, K., King, R., Herring, T. A., Dinardo, S., Young, W., Jackson, D., Gurtner, W., 1997. Southern California Permanent GPS Geodetic Array: Continuous measurements of regional crustal deformation between the 1993 Landers and 1994 Northridge earthquakes. Journal of Geophysical Research 102 (B8), 18013–18033.

Booth, S. J., 2000. Monitoring long term vertical land movements in the Thames Estuary and Greater London. Ph.D. thesis, University of Nottingham.

Borza, T., Fejes, I., 1999. GPS interference in Hungary. In: 5th International Seminar on GPS in Central Europe, 5-7 May 1999, Penc, Hungary. Vol. 5(46) of Reports on Geodesy. p. 215.

Bos, M. S., Baker, T. F., Røthing, K., Plag, H. P., 2002. Testing ocean tide models in the Nordic seas with tidal gravity observations. Geophysical Journal International 150 (3), 687–694.

Boucher, C., Altamimi, Z., 1996. International Terrestrial Reference Frame. GPS World 7, 71–74.

Boucher, C., Altamimi, Z., Duhem, L., 1993. ITRF92 and its associated velocity field. IERS Technical Note 15, International Earth Rotation Service, Observatoire de Paris.

Boucher, C., Altamimi, Z., Duhem, L., 1994. Results and analysis of the ITRF93. IERS Technical Note 18, International Earth Rotation Service, Observatoire de Paris.

Boucher, C., Altamimi, Z., Feissl, M., Sillard, P., 1996. Results and analysis of the ITRF94. IERS Technical Note 20, International Earth Rotation Service, Observatoire de Paris.

Boucher, C., Altamimi, Z., Sillard, P., 1998. Results and analysis of the ITRF96. IERS Technical Note 24, International Earth Rotation Service, Observatoire de Paris.

Boucher, C., Altamimi, Z., Sillard, P., 1999. The 1997 international reference frame (ITRF97). IERS Technical Note 27, International Earth Rotation Service, Observatoire de Paris.

Boy, J. P., Hinderer, J., Florsch, N., 2003. A comparison of tidal ocean loading models using superconducting gravimeter data. Journal of Geophysical Research 108 (B4), 2193, doi:10.1029/2002JB002050.

Braitenberg, C., Nagy, I., Negusini, M., Romangnoli, C., Zadro, M., Zerbini, S., 2001. Geodetic measurements at the northern border of the Adria plate. Journal of Geodynamics 32 (1-2), 267–286.

Braun, J. J., Stephens, B., Ruud, O., Meertens, C. M., 1997. The effect of antenna covers on GPS baseline solutions [online]. Available at: `<http://www.unavco.ucar.edu/`

`science_tech/dev_test/publications/dome_report/domeX5Freport-1.html>` [Accessed 18 September 2002].

Brown, I., 2001. The UKCIP02 climate change scenarios: Context and application. In: Proceedings of the 36th DEFRA Conference of River and Coastal Engineers, Keele University, 20-22 June, 2001. DEFRA Flood Management Division, London, pp. 3.2.1–3.2.9.

Bruyninx, C., Becker, M., Stangl, G., 2001. Regional densification of the IGS in Europe using the EUREF Permanent GPS Network (EPN). Physics and Chemistry of the Earth 26 (6-8), 531–538.

Bruyninx, C., Kenyeres, A., Takacs, B., 2002. EPN data an product analysis for improved velocity estimation: First results. In: Ádám, J., Schwarz, K. P. (Eds.), Vistas for Geodesy in the New Millennium. Vol. 125 of International Association of Geodesy Symposia. Springer-Verlag, Berlin Heidelberg, pp. 47–52.

Butch, F., 1997. GPS and GLONASS radio interference in Germany. In: Institute of Navigation (Ed.), Proc. of the 10th International Technical Meeting of the Satellite Division of the Institute of Navigation, ION GPS-97, 16-19 September 1997, Kansas City. Institute of Navigation, Washington D. C., pp. 1427–1437.

Butch, F., 2002. Radio frequency interference and GPS. GPS World 13 (10), 40–50.

Calais, E., 1999. Continuous GPS measurements across the Western Alps, 19961998. Geophysical Journal International 138 (1), 221–230.

Carter, W. E., 1994. Report of the Surrey Workshop of the IAPSO tide gauge bench mark fixing committee. NOAA Technical Report NOSOES0006, Institute of Oceanographic Sciences, Deacon Laboratory, Surrey, UK.

Carter, W. E., Aubrey, D. G., Baker, T. F., Boucher, C., LeProvost, C., Pugh, D., Peltier, W. R., Zumberge, M., Rapp, R. H., Schutz, R. E., Emery, K. O., Enfield, D. B., 1989. Geodetic fixing of tide gauge bench marks. Technical Report WHOI-89-31, Woods Hole Oceanographic Institution, Woods Hole, Massachusetts.

Chang, C. C., Ashkenazi, V., Bingley, R. M., Dodson, A. H., 1996. The effect of fixing or improving satellite orbits on high accuracy GPS. In: Proceedings of the 1996 International Conference on GPS. Taipei, Taiwan, p. 14.

Chatfield, C., 1996. The Analysis of Time Series: An Introduction, 5th Edition. Chapman and Hall/CRC, Boca Raton.

Chen, J. L., Wilson, C. R., Eanes, R. J., Nerem, R. S., 1999. Geophysical interpretation of observed geocenter variations. Journal of Geophysical Research 104 (B2), 2683–2690.

Chen, X., Langley, R. B., Dragert, H., 1996. Investigation of annual variations in the WCDA GPS solutions. In: Institute of Navigation (Ed.), Proc. of the 9th International Technical Meeting of the Satellite Division of the Institute of Navigation ION GPS-96, Kansas City, 17-20 September 1996. Institute of Navigation, Washington D. C., pp. 1809–1818.

Clarke, P. J., (`peter.clarke@newcastle.ac.uk`) 2003. Re: reprint on North Shields. 11 March. Email to: Geoffrey Blewitt (`gblewitt@unr.edu`).

Clynch, J. R., Parker, A. A., Adler, R. W., Vincent, W. R., McGill, P., Badger, G., 2003. The hunt for RFI unjamming a coast harbor. GPS World 14 (1), 16–22.

Craymer, M., Piraszewski, M., 2002. ITRF and IGS reference frames. In: Canadian Geodetic Reference System Committee. Ottawa, Canada, 13-15 May 2002, p. 24.

Crétaux, J. F., Soudarin, L., Davidson, F. J. M., Gennero, M.-C., Bergé-Nguyen, M., Cazenave, A., 2002. Seasonal and interannual geocenter motion from SLR and DORIS measurements: Comparison with surface loading. Journal of Geophysical Research 107 (B12), 2374, doi:10.1029/2002JB001820.

Cross, P. A., 1992. Advanced least squares applied to position-fixing. Tech. Rep. Working Paper No. 6, University of East London, Department of Land Surveying.

Curtis, D. J., 1996. Ocean tide loading for geodetic applications. Ph.D. thesis, University of Nottingham.

Davies, P., Blewitt, G., 2000. Methodology for global geodetic time series estimation: A new tool for geodynamics. Journal of Geophysical Research 105 (B5), 11083–11100.

Davis, A., Marshak, A., Wiscombe, W., Cahalan, R., 1994. Multifractal characterizations of nonstationarity and intermittency in geophysical fields: Observed, retrieved, or simulated. Journal of Geophysical Research 99 (D4), 8055–8072.

Davis, J. L., Mitrovica, J. X., Scherneck, H. G., Fan, H., 1999. Investigations of Fennoscandian glacial isostatic adjustment using modern sea level records. Journal of Geophysical Research 104 (B2), 2733–2747.

Deakin, R., Burgess, K., Samuels, P., Sayers, P., Chatterton, J., 2001. A national economic appraisal of the impacts flooding and coastal erosion considering the potential impacts of climate change. In: Proceedings of the 36th DEFRA Conference of River and Coastal Engineers, Keele Universty, 20-22 June 2001. DEFRA Flood Management Division, London, pp. 4.2.1–4.2.11.

Dixon, T. H., 1991. An introduction to the Global Positioning System and some geological applications. Reviews of Geophysics 29 (2), 249–276.

Dixon, T. H., Mao, A., 1997. A GPS estimate of relative motion between North and South America. Geophysical Research Letters 24 (5), 535–538.

Dixon, T. H., Miller, M., Farina, F., Wang, H., Johnson, D., 2000. Present-day motion of the Sierra Nevada block and some tectonic implications for the Basin and Range province, North American Cordillera. Tectonics 19 (1), 1–24.

Dodson, A. H., Bingley, R. M., Penna, N. T., Aquino, M. H. O., 2000. A national network of continuously operating GPS receivers for the UK. In: Schwarz, K. P. (Ed.), Geodesy Beyond 2000 – The Challanges of the First Decade. International Association of Geodesy Symposia. Springer-Verlag, Berlin Heidelberg, pp. 367–372.

Dodson, A. H., Curtis, D. J., Baker, T. F., 1999. Ocean tide loading effects on height. In: Proc. of the FIG Commission 5 Seminar Geodesy and Surveying in the Future, Importance of Heights, 15-17 March 1999, Gävle, Sweden. FIG Commission 5, pp. 261–272.

Dodson, A. H., Meng, X., Roberts, G. W., 2001a. Adaptive method for multipath mitigation and its applications for structural deflection monitoring. In: International

Symposium on Kinematic System in Geodesy, Geomatics and Navigation (KIS 2001), June 5-8, 2001, Banff, Alberta, Canada. Department of Geomatics Engineering, University of Calgary, Calgary.

Dodson, A. H., Moore, T., Aquino, M. H. O., Waugh, S. J., 2001b. Ionospheric scintillation monitoring in Northern Europe. In: Institute of Navigation (Ed.), Proc. of the 14th International Technical Meeting of the Satellite Division of the Institute of Navigation ION GPS 2001, 11-14 September 2001, Salt Lake City, Utah. Institute of Navigation, Washington D. C., pp. 2490–2499.

Dodson, A. H., Shardlow, P. J., Hubbard, L. C. M., Elgered, G., Jarlemark, P. O. J., 1996. Wet tropospheric effects on precise relative GPS height determination. Journal of Geodesy 70 (4), 188–202.

Dong, D., Fang, P., Bock, Y., Cheng, M. K., Miyazaki, S., 2002b. Anatomy of apparent seasonal variations from GPS derived site position time series. Journal of Geophysical Research 107 (B4).

Dong, D., Yunck, T. P., Heflin, M. B., 2003. Origin of the International Terrestrial Reference Frame. Journal of Geophysical Research 108 (B4), 2200, doi:10.1029/2002JB002035.

Dong, X., Woodworth, P. L., Moore, P., Bingley, R. M., 2002a. Absolute calibration of the TOPEX/POSEIDON altimeters using UK tide gauges, GPS and precise, local geoid-differences. Marine Geodesy 25 (3), 189–204.

Douglas, B. C., Kearney, M. S., Leatherman, S. P. (Eds.), 2001. Sea Level Rise History and Consequences. Vol. 75 of International Geophysics Series. Academic Press, San Diego.

Douglas, B. C., Peltier, W. R., 2002. The puzzle of global sea-level rise. Physics Today 55 (3), 35–40.

Dragert, H., James, T. S., Lambert, A., 2000. Ocean loading corrections for continuous GPS: A case study at the Canadian coastal site Holberg. Geophysical Research Letters 27 (14), 2045–2048.

Dziewonski, A. M., Anderson, D. L., 1981. Preliminary Reference Earth Model. Phys. Earth Planet. Inter. 25, 297–356.

Emardson, T. R., Johansson, J. M., Elgered, G., 2000. The systematic behaviour of water vapor estimates using four years of GPS observations. IEEE Transactions on Geoscience and Remote Sensing 38 (1), 324–329.

Embree, P. M., 1995. C Algorithms for Real Time DSP. Prentice Hall PTR, New Jersey.

EPNCB, 2002a. EUREF permanent network tracking network - temporary excluded stations [online]. Available at: `<http://www.epncb.oma.be/excluded.html#BRST>` [Accessed 12 August 2002].

EPNCB, 2002b. EUREF time series for geokinematics [online]. Available at: `<http://www.epncb.oma.be/series_sp.html>` [Accessed 9 September 2002].

Estey, L. H., Meertens, C. M., 1999. TEQC: The multi-purpose toolkit for GPS/GLONASS data. GPS Solutions 3 (1), 42–49.

Farhang-Boroujeny, B., 1999. Adaptive Filters Theory and Applications. John Wiley and Sons, Chichester, England.

Feigl, K. L., Agnew, D. C., Bock, Y., Dong, D., Donnellan, A., Hager, B. H., Herring, T. A., Jackson, D. D., Jordan, T. H., King, R. W., Larsen, S., Larson, K. M., Murray, M. H., Shen, Z., Webb, F. H., 1993. Space geodetic measurements of crustal deformation in Central and Southern California, 1984-1992. Journal of Geophysical Research 98 (B12), 21677–21712.

Ferland, R., 2001. Apparent geocenter variations from IGS analysis. EOS Transactions, American Geophysical Union 82 (47), Fall Meet. Suppl.

Ferland, R., 2002. Reference Frame Working Group Technical Report. In: IGS Central Bureau (Ed.), IGS Technical Report 2000. Jet Propulsion Laboratory, California Institute of Technology, Pasadena, California, pp. 61–70.

Firth, C. R., Stewart, I. S., 2000. Postglacial tectonics of the Scottish glacio-isostatic uplift centre. Quaternary Science Reviews 19 (14-15), 1469–1493.

Flather, R. A., 2001. Statistics of extreme sea levels and their changes with time. In: Book of Extended Abstracts, Final Workshop of COST Action 40, Sea Level in Europe: Observation, Interpretation and Exploitation, Dubrovnik, Croatia, 19-21 September 2001. Hydrographic Institute of the Republic of Croatia, Split, pp. 66–67.

Flather, R. A., Baker, T. F., Woodworth, P. L., Vassie, J. M., Blackman, D. L., 2001. Integrated effects of climate change on coastal extreme sea levels. In: Proceedings of the 36th DEFRA Conference of River and Coastal Engineers, Keele University, 20-22 June 2001. DEFRA Flood Management Division, London, pp. 3.4.1–3.4.12.

Flather, R. A., Williams, J., 2000. Climate change effects on storm surges: methodologies and results. In: Climate Scenarios for Water-Related and Coastal Impacts, Proceedings of the EU Concerted Action Initiative ECLAT-2, Workshop 3. Climatic Research Unit, Norwich, KNMI Netherlands, p. 140.

Forrester, W. D., 1983. Canadian Tidal Manual. Department of Fisheries and Ocean, Ottawa.

Forssell, B., Olsen, T. B., 2003. Jamming GPS susceptibility of some civil GPS receivers. GPS World 14 (1), 54–58.

Ge, L., Chen, H. Y., Han, S., Rizos, C., 2000. Adaptive filtering of continuous GPS results. Journal of Geodesy 74 (7-8), 572–580.

GLOSS, 2002. The Global Sea Level Observing System (GLOSS) [online]. <http://www.nbi.ac.uk/psmsl/programmes/gloss.info.html> [22 July 2002].

Gregory, J. M., 2001. Climate change - state of the art of global and regional modelling. In: Proceedings of the 36th DEFRA Conference of River and Coastal Engineers, Keele University, 20-22 June 2001. DEFRA Flood Management Division, London, pp. 3.1.1–3.1.9.

Gurtner, W., Mader, G. L., 1990. RINEX: The receiver independent exchange format version 2. CSTG GPS Bulletin 3 (3).

Haddrell, T., Khawaja, H., 1998. Effects and mitigation of land based interferers on fixed site GPS installations - A manufacturers experience. In: Institute of Navigation

(Ed.), Proc. of the 11th International Technical Meeting of the Satellite Devision of the Institute of Navigation, ION GPS-98, 15-18 September 1998, Nashville. Institute of Navigation, Washington D. C., pp. 851–861.

Harvey, N., Belperio, A., Bourman, R., Mitchell, W., 2002. Geologic, isostatic and anthropogenic signals affecting sea level records at tide gauge sites in southern Australia. Global and Planetary Change 32 (1), 1–11.

Haykin, S., 2002. Adaptive Filter Theory, 4th Edition. Prentice Hall, Upper Saddle River, New Jersey.

Heflin, M. B., 2003. [IGSMAIL-4281]: IGS reference site candidates [online], 28 February. Available at: <http://igscb.jpl.nasa.gov/mail/igsmail/2003/msg00059.html> [Accessed 28 February 2003].

Heflin, M. B., Argus, D. F., Jefferson, D. C., Webb, F. H., Zumberge, J. F., 2002. Comparison of a GPS-defined global reference frame with ITRF2000. GPS Solutions 6 (1-2), 72–75.

Heflin, M. B., Bertiger, W. I., Blewitt, G., Freedman, A., Hurst, K., Lichten, S., Lindqwister, U. J., Vigue, Y., Webb, F. H., Yunck, T., Zumberge, J. F., 1992. Global geodesy using GPS without fiducial sites. Geophysical Research Letters 19 (2), 131–134.

Heki, K., 2001. Seasonal modulation of interseismic strain buildup in Northeastern Japan driven by snow loads. Science 293, 89–92.

Herring, T. A., 1999. Geodetic applications of GPS. Proceedings of the IEEE 87 (1), 92–110.

Herring, T. A., 2001. Vertical reference frame for sea level monitoring. EOS Transactions, American Geophysical Union 82 (47), Fall Meet. Suppl.

Herring, T. A., 2002. Stability of global geodetic results [online]. Available at: <http://bowie.mit.edu/~tah/Herr_egs02.pdf> [Accessed 10 January 2003], presented at the 27th EGS General Assembly, Nice, France, 21-26 April 2002.

Herring, T. A., 2003. High precision realization and applications of GPS [online]. Available at: <http://bowie.mit.edu/~tah/ION2003.pdf> [Accessed 3 March 2003], presented

at the New England Section of the Institute of Navigation 28th Meeting, 5 February 2003.

Herring, T. A., Hager, B. H., Meade, B., Zubovich, A. V., 2002. Contemporary horizontal and vertical deformation of the Tien Shan. Available at: `<http://bowie.mit.edu/~tah/APSG02/APSG_Herr.pdf>` [Accessed 3 March 2003], presented at the Asia-Pacific Space Geodynamics Program (APSG-2002), Irkutsk, Russia, 5-10 August 2002.

Herring, T. A., Springer, T., 2002. Current state of IGS analysis: Quality assessment. In: IGS Central Bureau (Ed.), IGS Technical Report 2000. Jet Propulsion Laboratory, California Institute of Technology, Pasadena, California, pp. 51–59.

Hofmann-Wellenhof, B., Lichtenegger, H., Collins, J., 1993. Global Positioning System: theory and practice, 2nd Edition. Springer-Verlag, Wien.

Hosking, J. R. M., 1981. Fractional differencing. Biometrika 68 (1), 165–176.

Houghton, J. T., Ding, Y., Griggs, D. J., Noguer, M., van der Linden, P. J., Dai, X., Maskell, K., Johnson, C. A., 2001. Climate Change 2001: The Scientific Basis - Contribution of Working Group 1 to the Third Assessment Report of the Intergovernmental Panel on Climate Change. Cambridge University Press, Cambridge.

Howarth, R. B., Monahan, P. A., 1996. Economics, ethics, and climate policy: framing the debate. Global and Planetary Change 11 (4), 187–199.

Hubbard, L. C. M., 1995. Atmospheric water vapour effects on GPS measurements. Ph.d. thesis, University of Nottingham.

Hudnut, K. W., Shen, Z., Murray, M. H., McClusky, S., King, R., Herring, T. A., Hager, B. H., Feng, Y., Fang, P., Donnellan, A., Bock, Y., 1996. Co-seismic displacements of the 1994 Northridge, California, earthquake. Bulltetin of the Seismological Society of America 86 (1B), S19–S36.

Hugentobler, U., Schaer, S., Fridez, P. (Eds.), 2001. Bernese GPS Software Version 4.2. Astronomical Institute University of Berne, Berne, Switzerland.

Hulme, M., Jenkins, G. J., Lu, X., Turnpenny, J. M., Mitchel, T. D., Jones, R. G., Lowe, J. A., Murphy, J. M., Hassell, D., Boorman, P., McDonald, R., Hill, S., 2002.

Climate change scenarios for the United Kingdom. The UKCIP02 Scientific Report, Tyndall Centre for Climate Research, School of Environmental Sciences, University of East Anglia, Norwich.

Hurst, K. J., 2000. SCIGN Analysis 2.0.0 [online]. Available at: `<http://milhouse.jpl.nasa.gov/scign/analysis/description_2.0.0.html>` [Accessed 29 November 2001].

Hurst, K. J., 2001. SCIGN Analysis 3.0.0 [online]. Available at: `<http://milhouse.jpl.nasa.gov/scign/analysis/description_3.0.0.html>` [Accessed 14 October 2002].

Hurst, K. J., Argus, D. F., Donnellan, A., Heflin, M. B., Jefferson, D. C., Lyzenga, G. A., Parker, J. W., Smith, M., Webb, F. H., Zumberge, J. F., 2000. The coseismic geodetic signature of the 1999 Hector Mine earthquake. Geophysical Research Letters 27 (17), 2733–2736.

IGSCB, 2000. SINEX - Solution (Software/Technique) INdependent EXchange Format Version 1.0 (June 30 1996) [online]. Available at: `<ftp://igscb.jpl.nasa.gov/igscb/data/format/sinex.txt>` [Accessed 29 May 2000].

IGSCB, 2003. ANTEX - ANTenna independent EXchange Format Version 1.0 (22 January) [online]. Available at: `<ftp://igscb.jpl.nasa.gov/igscb/station/general/pcv_proposed/antex10.txt>` [Accessed 27 March 2003].

Ineichen, D., Gurtner, W., Springer, T., Engelhardt, G., Luthardt, J., Ihde, J., 1999. EUVN97 Combined GPS solution. In: Mitteilungen des Bundesamtes für Kartographie und Geodäsie. EUREF Publication No. 7/II. Vol. 7. Frankfurt am Main, pp. 23–46.

Ingle, V. K., Proakis, J. G., 2000. Digital Signal Processing using Matlab. BookWare Companion Series. Brooks/Cole, Pacific Grove.

Jaksic, J., 2001. Running interference - multipath detection for GPS monitoring sites. GPS World 12 (2), 32–36.

Jaldehag, R. T. K., Johansson, J. M., Davis, J. L., Elósegui, P., 1996. Geodesy using swedish permanent GPS network: Effects of snow accumulation on estimates of site positions. Geophysical Research Letters 23 (13), 1601–1604.

Johansson, J. M., Davis, J. L., Scherneck, H. G., Milne, G. A., Vermeer, M., Mitrovica, J. X., Bennett, R. A., Jonsson, B., Elgered, G., Elósegui, P., Koivula, H., Poutanen, M., Rönnäng, B. O., Shapiro, I. I., 2002. Continuous GPS measurements of postglacial adjustment in Fennoscandia 1. Geodetic Results. Journal of Geophysical Research 107 (B8), ETG 3/1–3/27.

Johnson, H. O., Agnew, D. C., 1995. Monument motion and measurements of crustal velocities. Geophysical Research Letters 22 (21), 2905–2908.

Johnson, H. O., Agnew, D. C., 15 February 2000 2000. Correlated noise in geodetic time series. Final Technical Report 1434-HQ-97-GR-03155, Institute of Geophysics and Planetary Physics, University of California.

Johnson, H. O., Wyatt, F., 1994. Geodetic network design for fault-mechanics studies. manuscripta geodetica 19, 309–323.

Johnson, M., Erlandson, R., 1995. GNSS receiver interference: Susceptibility and civil aviation impact. In: Institute of Navigation (Ed.), Proc. of the 8th International Technical Meeting of the Satellite Division of the Institute of Navigation, ION GPS-95, 12-15 September 1995, Palm Springs. Institute of Navigation, Washington D. C., pp. 781–791.

Johnston, P. J., Lambeck, K., 2000. Automatic inference of ice models from postglacial sea level observations: Theory and apllication to the British Isles. Journal of Geophysical Research 105 (B6), 13179–13194.

Kaniuth, K., Stuber, K., 2002. The impact of antenna radomes on height estimates in regional GPS networks. In: Drewes, H., Dodson, A. H., Fortes, L. P. S., Sánchez, L., Sandoval, P. (Eds.), Vertical Reference Systems. Vol. 124 of International Association of Geodesy Symposia. Springer-Verlag, Berlin Heidelberg, pp. 101–106.

Kaplan, E. D. (Ed.), 1996. Understanding GPS: principles and applications. Artech House Inc., Norwood.

Kearney, M. S., 2001. Late holocene sea level variations. In: Douglas, B. C., Kearney, M. S., Leatherman, S. P. (Eds.), Sea Level Rise History and Consequences. Vol. 75 of International Geophysics Series. Academic Press, San Diego, pp. 13–36.

Kendall, M., Stuart, A., 1979. The Advanced Theory of Statistics, Vol 2, Inference and Relationship. Charles Griffin, London.

Kenyeres, A., (Kenyeres@sgo.fomi.hu) 2002. Offsets in EUREF standard time series. 24 September. Email to: Norman Teferle norman.teferle@nottingham.ac.uk.

Kenyeres, A., Bosy, J., Brockmann, E., Bruyninx, C., Caporali, A., Hefty, J., Jivall, L., Kosters, A., Poutanen, M., Fernandes, R., Stangl, G., 2001. EPN Special Project on "Time series analysis ..." preliminary results and future prospects. In: Proceedings of EUREF Symposium. Dubrovnik, Croatia, May 2001.

Keshner, M. S., 1982. 1/f noise. Proceedings of the IEEE 70 (3), 212–218.

Kierulf, H. P., Kristiansen, O., Plag, H. P., 2001. Can GPS determine geocentric vertical crustal motion at the 1 mm/yr accuracy level ? In: Book of Extended Abstracts, Final Workshop of COST Action 40, Sea Level in Europe: Observation, Interpretation and Exploitation, Dubrovnik, Croatia, 19-21 September 2001. Hydrographic Institute of the Republic of Croatia, Split, pp. 31–34.

King, M., 2002. MORP site information form [online], 20 December. Available at: <ftp://igscb.jpl.nasa.gov/igscb/station/log/morp_20021219.log> [Accessed 30 April 2003].

King, M., 2003. [IGSMAIL-4222]: Addition of LNA to MORP [online], 13 January. Available at: <http://igscb.jpl.nasa.gov/mail/igsmail/2003/msg00000.html> [Accessed 13 January 2003].

King, N. E., Svarc, J. L., Fogleman, E. B., Gross, W. K., Clark, K. W., Hamilton, G. D., Stiffler, C. H., Sutton, J. M., 1995. Continuous GPS observations across the Hayward fault, California, 1991-1994. Journal of Geophysical Research 100 (B10), 20271–20283.

King, R. W., Bock, Y., 2000. Documentation for the GAMIT GPS Software Version 10.03. Massachusetts Institute of Tehnology, Massachusetts.

Kleijer, F., 2002. Time series analysis of the daily solutions of the AGRS.NL reference stations. In: Drewes, H., Dodson, A. H., Fortes, L. P. S., Sánchez, L., Sandoval, P.

(Eds.), Vertical Reference Systems. Vol. 124 of International Association of Geodesy Symposia. Springer-Verlag, Berlin Heidelberg, pp. 60–65.

Kreyszig, E., 1970. Introductory Mathematical Statistics Priciples and Methods. John Wiley and Sons, New York.

Kuhn, M., Bosch, W., Kaniuth, R., 2001. Sea level variations in the North Atlantic. In: IAG 2001 Scientific Assembly Vistas for Geodesy in the New Millennium. Budapest, Hungary, 2-7 September, 2001, p. 6.

Lambeck, K., 1993. Glacial rebound of the British Isles II: A high-resolution, high-precision model. Geophysical Journal International 115, 960–990.

Lambeck, K., 1997. Sea-level change along the French Atlantic and Channel coasts since the time of the Last Glacial Maximum. Palaeogeography Palaeoclimatology Palaeoecology 129 (1-2), 1–22.

Lambeck, K., 1998. On the choice of timescale in glacial rebound modelling: mantle viscosity estimates and the radiocarbon timescale. Geophysical Journal International 134 (2), 647–651.

Lambeck, K., Chappell, J., 2001. Sea level change through the last glacial cycle. Science 292 (5517), 679–686.

Lambeck, K., Smither, C., Ekman, M., 1998b. Tests of glacial rebound models for Fennoscandinavia based on instrumented sea- and lake-level records. Geophysical Journal International 135 (2), 375–387.

Lambeck, K., Smither, C., Johnston, P. J., 1998a. Sea-level change, glacial rebound and mantle viscosity for Northern Europe. Geophysical Journal International 134 (1), 102–144.

Lambert, A., Courtier, N., Sasagawa, G. S., Klopping, F., Winester, D., James, T. S., Liard, J. O., 2001. New constraints on Laurentide postglacial rebound from absolute gravity measurements. Geophysical Research Letters 28 (10), 2109–2112.

Langbein, J., Johnson, H. O., 1997. Correlated errors in geodetic time series: Implications for time-dependent deformation. Journal of Geophysical Research 102 (B1), 591–603.

Langley, R. B., 1996. Propagation of GPS signals. In: Teunissen, P. J. G., Kleusberg, A. (Eds.), GPS for Geodesy, 2nd Edition. Springer-Verlag, Berlin Heidelberg, pp. 111–150.

Larson, K. M., Agnew, D. C., 1991. Application of the Global Positioning System to crustal deformation measurement 1: Precision and accuracy. Journal of Geophysical Research 96 (B10), 16547–16565.

Larson, K. M., Webb, F. H., Agnew, D. C., 1991. Application of the global positioning system to crustal deformation measurement 2: The influence of errors in orbit determination networks. Journal of Geophysical Research 96 (B10), 16567–16584.

Lavallée, D. A., 2000. Tectonic plate motions from global GPS measurements. Ph.d. thesis, University of Newcastle.

Le Provost, C., Genco, M. L., Lyard, F., Vincent, P., Canceil, P., 1994. Spectroscopy of the world ocean tides from a finite element hydrodynamic model. Journal of Geophysical Research 99 (C12), 24777–24797.

Leatherman, S. P., 2001. Social and economic costs of sea level rise. In: Douglas, B. C., Kearney, M. S., Leatherman, S. P. (Eds.), Sea Level Rise History and Consequences. International Geophysics Series. Academic Press, San Diego, pp. 181–223.

Lefèvre, F., Le Provost, C., Lyard, F. H., Schrama, E. J. O., 2001. FES98 and FES99: Two new versions of the FES' global tide finite element solutions [online]. Available at: <http://www.joss.ucar.edu/joss_psg/meetings/TOPEX2000/lefevre.f.html> [Accessed 7 November 2001], presented at the Joint TOPEX/POSEIDON and Jason-1 Science Working Team Meeting, Miami Beach, 15-17 November 2000.

Leick, A., 1995. GPS satellite surveying, 2nd Edition. Wiley, New York.

Li, J., Miyashita, K., Kato, T., Miyazaki, S., 2000. GPS time series modeling by autoregressive moving average method: Application to the crustal deformation in central Japan. Earth Planets Space 52, 155–162.

Lowe, J. A., Gregory, J. M., Flather, R. A., 2002. Changes in the occurrence of storm surges around the United Kingdom under a future climate scenario using a dynamic

storm surge model driven by the Hadley Centre climate models. Climate Dynamics 18 (3-4), 179–188.

Mader, G. L., Czopek, F. M., 2001. Calibrating the L1 and L2 phase centers of a Block II antenna. In: Proc. of the 14th International Technical Meeting of the Satellite Division of the Institute of Navigation ION GPS 2001, 11-14 September 2001, Salt Lake City, Utah. Institute of Navigation, Washington D. C., pp. 1979–1984.

Mader, G. L., MacKay, J. R., 1996. Calibration of GPS antennas. In: Neilan, R. E., Van Scoy, P. A., Zumberge, J. F. (Eds.), 1996 Analysis Centre Workshop, 19-21 March 1996, Silver Spring. IGS Central Bureau, Jet Propulsion Laboratory, California Institute of Technology, Pasadena, California, pp. 81–105.

Maillard, D., 2000. EUREF Mail 0487 Problem in BRST, 30 March. Available at: `<ftp://ftp.epncb.oma.be/pub/mail/eurefmail.0487>` [Accessed 13 September 2002].

Malkin, Z. M., Voinov, A. V., 2000. Preliminary results of processing EUREF observations using non-fiducial strategy. In: IGS Network Workshop 2000. Oslo, Norway, 12-15 July, 2000.

Malkin, Z. M., Voinov, A. V., 2001. Preliminary results of processing EUREF network observations using a non-fiducial strategy. Physics and Chemistry of the Earth 26 (6-8), 579–583.

Mandelbrot, B. B., 1982. The fractal geometry of nature. W H Freeman, New York.

Mangiarotti, S., Cazenave, A., Soudarin, L., Crétaux, J. F., 2001. Annual vertical crustal motions predicted from surface mass redistribution and observed by space geodesy. Journal of Geophysical Research 106 (B3), 4277–4292.

Mao, A., Harrison, C. G. A., Dixon, T. H., 1999. Noise in GPS coordinate time series. Journal of Geophysical Research 104 (B2), 2797–2818.

Mareyen, M., Becker, M., 2000. On the removal of a priori restrictions from GPS network solutions in a SINEX format. Allgemeine Vermessungs-Nachrichten 107 (11/12), 405–411.

Marotta, A. M., Sabadini, R., 2002. Tectonic versus glacial isostatic deformation in Europe. Geophysical Research Letters 29 (10), 73–1–73–4.

Marquis, W., 2001. M is for modernization. GPS World 12 (9), 36–42.

McCarthy, D. D., 1992. IERS Standards (1992). IERS Technical Note 13, Central Bureau of IERS, Observatoire de Paris.

McCarthy, D. D., 1996. IERS Conventions (1996). IERS Technical Note 21, Central Bureau of IERS, Observatoire de Paris.

McCarthy, D. D., 2000. IERS Conventions 2000. Tech. rep., International Earth Rotation Service.

Meng, X., 2002. Real-time deformation monitoring of bridges using GPS/accelerometers. Ph.D. thesis, University of Nottingham.

Menke, W., 1989. Geophysical Data Analysis: Discrete Inverse Theory, 2nd Edition. International Geophysics Series. Academic Press, Inc., San Diego.

Merrifield, M., Kilonsky, B., Nakahara, S., 1999. Interannual sea level changes in the tropical Pacific associated with ENSO. Geophysical Research Letters 26 (21), 3317–3320.

Met Office, 2002. The NERC MST radar facility at Aberystwyth [online]. Available at: `<http://www.metoffice.org.uk/>` [Accessed 14 September 2002].

Milne, G. A., 2002. Recent advances in predicting glaciation-induced sea level changes and their impact on model applications. In: Mitrovica, J. X., Vermeersen, B. L. A. (Eds.), Ice sheets sea level and the dynamic Earth. Vol. 29 of Geodynamics Series. American Geophysical Union, Washington D.C., pp. 157–176.

Milne, G. A., Davies, J. L., Mitrovica, J. X., Scherneck, H. G., Johansson, J. M., Vermeer, M., Koivula, H., 2001. Space-geodetic constraints on glacial isostatic adjustment in Fennoscandia. Science 291 (23 March 2001), 2381–2385.

Milne, G. A., Mitrovica, J. X., 1998. The influence of a time-dependent ocean-continent geometry on predictions of post-glacial sea level change in Australia and New Zealand. Geophysical Research Letters 25 (6), 793–796.

Milne, G. A., Mitrovica, J. X., Davis, J. L., 1999. Near-field hydro-isostasy: the implementation of a revised sea-level equation. Geophysical Journal International 139 (2), 464–482.

Mitrovica, J. X., Davis, J. L., 1995. Present-day post-glacial sea level change far from the Late Pleistocene ice sheets: Implications for recent analyses of tide gauge records. Geophysical Research Letters 22 (18), 2529–2532.

Mitrovica, J. X., Milne, G. A., Davis, J. L., 2001. Glacial isostatic adjustment on a rotating Earth. Geophysical Journal International 147 (3), 562–578.

Mitrovica, J. X., Peltier, W. R., 1989. Pleistocene deglaciation and the global gravity field. Journal of Geophysical Research 94 (B10), 13651–13671.

Miyazaki, S., Tsuji, H., Hatanaka, Y., Abe, Y., Yoshimura, A., Kamada, K., Kobayashi, K., Morishita, H., IImura, Y., 1996. Establishment of the nationwide GPS array (GRAPES) and its initial results on crustal deformation of Japan.

Neilan, R. E., Van Scoy, P. A., Woodworth, P. L. (Eds.), 1997. Methods for monitoring sea level: GPS and tide gauge benchmark monitoring and altimeter calibration. Jet Propulsion Laboratory, California Institute of Technology, Pasadena, California.

Nerem, R. S., Mitchum, G. T., 2002. Estimates of vertical crustal motion derived from differences of TOPEX/POSEIDON and tide gauge sea level measurements. Geophysical Research Letters 29 (19), 40/1–40/4.

Nerem, R. S., Van Dam, T. M., Schenewerk, M. S., 1997. A GPS network for monitoring absolute sea level in the Chesapeake Bay: BAYONET. In: Neilan, R. E., Van Scoy, P. A., Woodworth, P. L. (Eds.), Methods for monitoring Sea Level: GPS and Tide Gauge Benchmark Monitoring and Altimeter Calibration. Jet Propulsion Laboratory, California Institute of Technology, Pasadena, California, pp. 107–117.

Nicholls, R. J., Small, C., 2002. Improved estimates of coastal population and exposure to hazards released. EOS Transactions, American Geophysical Union 83 (28), 301,305.

Nicolon, P., 2000a. EUREF Mail 0503 BRST station problem, 25 April. Available at: <ftp://ftp.epncb.oma.be/pub/mail/eurefmail.0503> [13 September 2002].

Nicolon, P., 2000b. EUREF Mail 0508 BRST station problem, 28 April. Available at: <ftp://ftp.epncb.oma.be/pub/mail/eurefmail.0508> [13 September 2002].

Nicolon, P., 2000c. EUREF Mail 0509 problem in BRST again, 1 May. Available at: <ftp://ftp.epncb.oma.be/pub/mail/eurefmail.0509> [13 September 2002].

Nicolon, P., 2001. EUREF Mail 0914 BRST problems, 28 May. Available at: <ftp://ftp.epncb.oma.be/pub/mail/eurefmail.0914> [13 September 2002].

Nicolon, P., 2002. BRST site information form [online]. Available at: <ftp://ftp.epncb.oma.be/pub/station/log/brst0201.log> [Accessed 17 April 2002].

Niell, A. E., 1996. Global mapping functions for the atmospheric delay at radio wavelenghts. Journal of Geophysical Research 101 (B2), 3227–3246.

Nikolaidis, R. M., 2002. Observation of geodetic and seismic deformation with the Global Positioning System. Ph.d. thesis, University of California.

Nisner, P., Owen, J., 1995. Practical measurements of radio frequency interference to GPS receivers and an assessment of interference levels by flight trials in the European regions. In: of Navigation, I. (Ed.), Proc. of the 8th International Technical Meeting of the Satellite Division of the Institute of Navigation, ION GPS-95, 12-15 September 1995, Palm Springs. Institute of Navigation, Washington D. C., pp. 1373–1382.

Ochieng, W. Y., Sauer, K., Cross, P. A., Sheridan, K. F., Iliffe, J., Lannelongue, S., Ammour, N., Petit, K., 2001. Potential performance levels of a combined Galileo/GPS navigation system. The Journal of Navigation 54 (2), 185–197.

Pagiatakis, S. D., 1999. Stochastic significance of peaks in the least-squares spectrum. Journal of Geodesy 73 (2), 67–78.

Panafidina, N. A., Malkin, Z. M., 2001. On computation of a homogeneous coordinate time series for the EPN network. In: IAG Scientific Assembly 2001 - Vistas for Geodesy in the New Millennium. Budapest, Hungary, 2-7 September 2001.

Park, K. D., Nerem, R. S., Davis, J. L., Schenewerk, M. S., Milne, G. A., Mitrovica, J. X., 2002. Investigation of glacial isostatic adjustment in the Northeast U. S. using GPS measurements. Geophysical Research Letters 29 (11), 4/1–4/4.

Pavlis, E. C., 2002. Dynamical determination of origin and scale in the Earth system from Satellite Laser Ranging. In: Ádám, J., Schwarz, K. P. (Eds.), International Association of Geodesy Symposia - "Vistas for Geodesy in the New Millennium". Vol. 125. Springer-Verlag, Berlin Heidelberg, pp. 36–41.

Peltier, W. R., 1998. Postglacial variations in the level of the sea: Implications for climate dynamics and solid-Earth geophysics. Reviews of Geophysics 36 (4), 603–689.

Peltier, W. R., 1999. Global sea level rise and glacial isostatic adjustment. Global and Planetary Change 20 (2-3), 93–123.

Peltier, W. R., 2001a. ICE-4G (VM2) glacial isostatic adjustment corrections. In: Douglas, B. C., Kearney, M. S., Leatherman, S. P. (Eds.), Sea Level Rise History and Consequences. Vol. 75 of International Geophysics Series. Academic Press, San Diego.

Peltier, W. R., 2001b. Global glacial isostatic adjustment and modern instrumental records of relative sea level history. In: Douglas, B. C., Kearney, M. S., Leatherman, S. P. (Eds.), Sea Level Rise History and Consequences. Vol. 75 of International Geophysics Series. Academic Press, San Diego, pp. 65–95.

Peltier, W. R., Jiang, X., 1996. Mantle viscosity from the simultaneous inversion of multiple data sets pertaining to postglacial rebound. Geophysical Research Letters 23 (5), 503–506.

Peltier, W. R., Shennan, I., Drummond, R., Horton, B., 2002. On the postglacial isostatic adjustment of the British Isles and the shallow viscoelastic structure of the Earth. Geophysical Journal International 148 (3), 443–475.

Penna, N. T., 1997. Monitoring land movement at UK tide gauge sites using GPS. Ph.D. thesis, University of Nottingham.

Plag, H. P., 1998. Sea level and ice sheets: What can tide gauges tell us? In: Plag, H. P. (Ed.), Book of Extended Abstracts for the 9th General Assembly of the Working group of European Geoscientists for the Establishment of Networks for Earth-science Research - WEGENER98. Norwegian Mapping Authority, Hønefoss, Norway, pp. 86–89.

Plag, H. P., Ambrosius, B., Baker, T. F., Beutler, G., Bianco, G., Blewitt, G., Boucher, C., Davis, J. L., Degnan, J. J., Johansson, J. M., Kahle, H.-G., Kumkova, I., Marson, I., Mueller, S., Pavlis, E. C., Pearlman, M. R., Richter, B., Spakman, W., Tatevian, S. K., Tomasi, P., Wilson, P., Zerbini, S., 1998a. Scientific objectives of current and future WEGENER activities. Tectonophysics 294, 177–223.

Plag, H. P., Axe, P., Knudsen, P., Richter, B., Verstraeten, J. E., 2000. European sea-level observing systems (EOSS) Status and future Developements. European Commission Publication EUR 19682, European cooperation in the field of scientific and technical research (COST) Action 40.

Plag, H. P., Kristiansen, O., 2001. First experience with the "two-GPS-receiver" concept proposed by eoss for tide gauge collocation. In: Book of Extended Abstracts, Final Workshop of COST Action 40, Sea Level in Europe: Observation, Interpretation and Exploitation, Dubrovnik, Croatia, 19-21 September 2001. Hydrographic Institute of the Republic of Croatia, Split, pp. 35–39.

Plag, H. P., Tatevian, S., Zilberstein, O., 1998b. Crustal motion and sea level changes along the Arctic Coast (CRUSLAC). In: Book of Extended Abstracts for the 9th General Assembly of the Working group of European Geoscientists for the Establishment of Networks for Earth-science Research - WEGENER98. Norwegian Mapping Authority, Hønefoss, Norway, pp. 98–103.

Plag, H. P., Tsimplis, M. N., 1999. Temporal variability of the seasonal sea-level cycle in the North Sea and Baltic Sea in relation to climate variability. Global and Planetary Change 20 (2-3), 173–203.

Poutanen, M., Koivula, H., Ollikainen, M., 2001. On the periodicity of GPS time series. In: Proceedings of the IAG 2001 Scientific Assembly "Vistas for Geodesy in the New Millennium". Budapest, Hungary, 2-7 September, 2001, p. 4.

Poutanen, M., Vermeer, M., Mäkinen, J., 1996. The permanent tide in GPS positioning. Journal of Geodesy 70 (8), 499–504.

Press, W. H., Flannery, B. P., Teukolsky, S. A., Vetterling, W. T., 1992. Numerical Recipes in FORTRAN, 2nd Edition. Cambridge University Press, New York.

Price, D., McInally, G., Sokmener, B., 2001. Predicted implications of climate change to future levels of protection offered by fluvial and coastal flood alleviation schemes in Scotland. In: Proceedings of the 36th DEFRA Conference of River and Coastal Engineers, Keele University, 20-22 June 2001. DEFRA Flood Management Division, London, pp. 4.3.1–4.3.14.

PSMSL, 2002a. The Permanent Service for Mean Sea Level (PSMSL)[online]. Available at: <http://www.nbi.ac.uk/psmsl/whatispsmsl.html> [22 July 2002].

PSMSL, 2002b. Table of MSL secular trends derived from PSMSL RLR data [online]. Available at: <http://www.nbi.ac.uk/psmsl/datainfo/rlr.trends> [22 July 2002].

Pugh, D. T., 1987. Tides, Surges and Mean Sea Level. John Wiley and Sons, Chichester.

Rabbel, W., Zschau, J., 1985. Static deformations and gravity changes at the Earth's surface due to atmospheric loading. Journal of Geophysics 56, 81–99.

Ries, J. C., Chambers, D. P., Choi, K., Eanes, R. J., 2001. Effect of ITRF2000 on TOPEX/POSEIDON orbit determination and mean sea level. EOS Transactions, American Geophysical Union 82 (74), Fall Meet. Suppl.

Rissanen, J., 1978. Modeling by shortest data description. Automatica 14, 465–471.

Rius, A., Juan, J. M., Hernandez-Pajares, M., Madrigal, A. M., 1995. Measuring geocentric radial coordinates with a non-fiducial GPS network. Bulletin Geodesique 69, 320–328.

Rosenblatt, B., 1993. Learning the Korn shell. O'Reilly and Associates, Sebastopol, CA.

Rothacher, M., 2002. Estimation of station heights with GPS. In: Drewes, H., Dodson, A. H., Fortes, L. P. S., Sánchez, L., Sandoval, P. (Eds.), Vertical Reference Systems. Vol. 124 of International Association of Geodesy Symposia. Springer-Verlag, Berlin Heidelberg, pp. 81–90.

Rothacher, M., 2003. [IGSMAIL-4324]: Test set of absolute antenna PCVs [online], 28 March. Available at: <http://igscb.jpl.nasa.gov/mail/igsmail/2003/msg00102.html> [Accessed 28 March 2003].

Rothacher, M., Mader, G. L., 1996. Combination of antenna phase centre offsets and variations, Antenna Calibration Set, 30th June 1996.

Rothacher, M., Mader, G. L., 2002. Receiver and satellite antenna phase center offsets and variations. In: IGS Network, Data and Analysis Center Workshop 2002. IGS, Ottawa, Canada, p. 12.

Rothacher, M., Schaer, S., Mervart, L., Beutler, G., 1995. Determination of antenna phase centre variations using GPS data. In: Gendt, G., Dick, G. (Eds.), Proceedings of 1995 IGS Workshop: Special Topics and New Directions. GeoForschungsZentrum, Potsdam.

Saastamoinen, J. H., 1973. Contributions to the theory of atmospheric refraction. Bulletin Geodesique (105, 106, and 107), 279–298, 383–397, 13–34.

Sagiya, T., Yoshimura, A., Iwata, E., Abe, K., Kimura, I., Uemura, K., Tada, T., 1995. Establishment of permanent GPS observation network and crustal deformation monitoring in the Southern Kanto and Tokai areas.

Samuels, P., Burgess, K., 2001. National appraisal of assests at risk from flooding and coastal erosion. Final report, Halcrow Group Ltd, HR Wallingford, John Chatterton Associates.

Sang, J., Kubik, K., 1997. Analysis of interfered GPS signals. In: Institute of Navigation (Ed.), Proc. of the 10th International Technical Meeting of the Satellite Division of the Institute of Navigation, ION GPS-97, 16-19 September 1997, Kansas City. Institute of Navigation, Washington D. C., pp. 1467–1472.

Sanli, D. U., Blewitt, G., 2001. Geocentric sea level trend using GPS and >100-year tide gauge record on a postglacial rebound nodal line. Journal of Geophysical Research 106 (B1), 713–719.

Santerre, R., 1991. Impact of GPS satellite sky distribution. manuscripta geodaetica 16, 28–53.

Scargle, J. D., 1982. Studies in astronomical time series analysis. II. Statistical aspects of spectral analysis of unevenly spaced data. The Astrophysical Journal, The American Astronomical Society 263, 835–853.

Scharber, M., 2002. [IGSMAIL-4089]: ITRF 1997 and 2000 SOPAC reruns [online], 25 September. Available at: <http://igscb.jpl.nasa.gov/mail/igsmail/2002/msg00427.html> [Accessed 26 September 2002].

Schenewerk, M. S., Van Dam, T. M., Nerem, R. S., 1999. Gauging the tides: Monitoring subsidence around Chesapeake Bay. GPS World 10 (5), 34–41.

Scherneck, H. G., Bos, M. S., 2001. Ocean tide loading provider [online]. Available at: <http://www.oso.chalmers.se/~loading> [Accessed 10 October 2001].

Scherneck, H. G., Haas, R., Bos, M. S., 2002a. Station motion model. In: Campbell, J., Haas, R., Nothnagel, A. (Eds.), TMR Networks - Measurement of Vertical Crustal Motion in Europe by VLBI. Geodetic Institute, University of Bonn, Bonn, pp. 30–50.

Scherneck, H. G., Johansson, J. M., Elgered, G., Davis, J. L., Jonsson, B., Hedling, G., Koivula, H., Ollikainen, M., Poutanen, M., Vermeer, M., Mitrovica, J. X., Milne, G. A., 2002b. BIFROST: Observing the three-dimensional deformation of Fennoscandia. In: Mitrovica, J. X., Vermeersen, B. L. A. (Eds.), Ice Sheets Sea Level and the Dynamic Earth. Vol. 29 of Geodynamics Series. American Geophysical Union, Washington, D.C., pp. 69–93.

Scherneck, H. G., Johansson, J. M., Mitrovica, J. X., Davies, J. L., 1998. The BIFROST project: GPS determined 3-D displacement rates in Fennoscandia from 800 days of continuous observations in the SWEPOS network. Tectonophysics 294 (3-4), 305–321.

Scherneck, H. G., Johansson, J. M., Webb, F. H., 2000. Ocean loading tides in GPS and rapid variations of the frame origin. In: Schwarz, K. P. (Ed.), Geodesy Beyond 2000 - The Challenges of the First Decade. Vol. 121 of International Association of Geodesy Symposia. Springer-Verlag, Berlin Heidelberg, pp. 32–40.

Schöne, T., 2001. [IGSMAIL-3370]: Call for participation for the GPS tide gauge benchmark monitoring pilot project [online], 28 April. Available at: <http://igscb.jpl.nasa.gov/mail/igsmail/2001/msg00215.html> [Accessed 28 April 2001].

Schupler, B. R., Clark, T. A., 1991. How different antennas affect the GPS observable. GPS World 2 (11-12), 32–36.

Schupler, B. R., Clark, T. A., 2001. Characterizing the behavior of geodetic GPS antennas. GPS World 12 (2), 48–55.

Seeber, G., 1993. Satellite Geodesy: foundations, methods and applications. W. de Gruyter, Berlin.

Shardlow, P. J., 1994. Propagation effects on precise GPS heighting. Ph.d. thesis, University of Nottingham.

Shemar, S., 2001. NPLD site information form [online]. Available at: <ftp://igscb.jpl.nasa.gov/igscb/station/log/npld0109.log> [17 April 2002].

Shennan, I., 1989. Holocene crustal movements and sea-level changes in Great Britain. Journal of Quaternary Science 4, 77–89.

Shennan, I., Horton, B., 2002. Holocene land- and sea-level changes in Great Britain. Journal of Quaternary Science 17 (5-6), 511–526, doi: 10.1002/jqs.710.

Shennan, I., Lambeck, K., Horton, B., Innes, J., Lloyd, J., McArthur, J., Purcell, T., Rutherford, M., 2000. Late Devensian and Holocene records of relative sea-level changes in northwest Scotland and their implications for glacio-hydro-isostatic modelling. Quaternary Science Reviews 19 (11), 1103–1135.

Shennan, I., Peltier, W. R., Drummond, R., Horton, B., 2002. Global to local scale parameters determining relative sea-level changes and the post-glacial isostatic adjustment of Great Britain. Quaternary Science Reviews 21 (1-3), 397–408.

Shennan, I., Woodworth, P. L., 1992. A comparison of late Holocene and twentieth-century sea-level trends from the UK and North Sea region. Geophysical Journal International 109, 96–105.

Sillard, P., Altamimi, Z., Boucher, C., 1998. The ITRF96 realization and its associated velocity field. Geophysical Research Letters 25 (17), 3223–3226.

Sillard, P., Boucher, C., 2001. A review of algebraic constraints in terrestrial reference frame definition. Journal of Geodesy 75 (2/3), 63–73.

Stewart, M. P., Ffoulkes-Jones, G. H., Ochieng, W. Y., Shardlow, P. J., Penna, N. T., Bingley, R. M., 2002. GAS: GPS Analysis Software User Manual. Version 2.4. IESSG, University of Nottingham, Nottingham.

Sutherland, J., Wolf, J., 2001. Coastal defence vulnerability 2075. In: Proceedings of the 36th DEFRA Conference of River and Coastal Engineers, Keele University, 20-22 June 2001. DEFRA Flood Management Division, London, pp. 3.6.1–3.6.12.

Takacs, B., Bruyninx, C., 2001. Quality checking the raw data of the EUREF permanent network [online]. In: Proceedings of the EUREF Symposium, Dubrovnik, Croatia, May 16-18, 2001. Available at: `<http://www.epncb.oma.be/papers/euref01/EPNCB_qc1.pdf>` [Accessed 5 May 2002].

Tamisiea, M. E., Mitrovica, J. X., Milne, G. A., Davis, J. L., 2001. Global geoid and sea level changes due to present-day ice mass fluctuations. Journal of Geophysical Research 106 (B12), 30849–30863.

Teferle, F. N., 2000. Continuous GPS measurements at UK tide gauge sites, 1997-2000. In: Proc. of the 13th International Technical Meeting of the Satellite Division of the Institute of Navigation ION GPS 2000, 19-22 September 2000, Salt Lake City, Utah. Institute of Navigation, Washington D. C., pp. 17–27.

Teferle, F. N., Bingley, R. M., Dodson, A. H., Baker, T. F., 2002b. Application of the dual-CGPS concept to monitoring vertical land movements at tide gauges. Physics and Chemistry of the Earth 27 (32-34), 1401–1406.

Teferle, F. N., Bingley, R. M., Dodson, A. H., Baker, T. F., Williams, S. D. P., 2001. Evaluation of the dual-CGPS concept to monitoring vertical land movements at tide gauges. In: Book of Extended Abstracts, Final Workshop of COST Action 40, Sea Level in Europe: Observation, Interpretation and Exploitation, Dubrovnik, Croatia, 19-21 September 2001. Hydrographic Institute of the Republic of Croatia, Split, pp. 40–43.

Teferle, F. N., Bingley, R. M., Dodson, A. H., Penna, N. T., Baker, T. F., 2002a. Using GPS to separate crustal movements and sea level changes at tide gauges in the UK. In: Drewes, H., Dodson, A. H., Fortes, L. P. S., Sánchez, L., Sandoval, P. (Eds.),

Vertical Reference Systems. Vol. 124 of International Association of Geodesy Symposia. Springer-Verlag, Heidelberg Berlin, pp. 264–269.

Thompson, K. R., 1980. An analysis of British monthly mean sea level. Geophysical Journal of the Royal Astronomical Society 63, 57–73.

Torge, W., 2001. Geodesy, 3rd Edition. Walter de Gruyter, Berlin.

van Dam, T., Plag, H. P., Francis, O., Gegout, P., 2002. GGFC Special Bureau for Loading: Current status and plans [online]. Position paper, GGFC Special Bureau for Loading, Available at: `<http://www.sbl.statkart.no/aboutloading/pos_paper_final.pdf>` [Accessed 10 April 2003].

van Dam, T., Wahr, J., 1987. Displacements of the Earth's gravity surface due to atmospheric loading effects on gravity and baseline measurements. Journal of Geophysical Research 92 (B2), 1281–1286.

van Dam, T., Wahr, J., Chao, Y., Leuliette, E., 1997. Predictions of crustal deformation and of geoid and sea-level variability caused by oceanic and atmospheric loading. Geophysical Journal International 129 (3), 507–517.

van Dam, T. M., Blewitt, G., Heflin, M. B., 1994. Atmospheric pressure loading effects on Global Positioning System coordinate determinations. Journal of Geophysical Research 99 (B12), 23939–23950.

van Dam, T. M., Wahr, J., Milly, P. C. D., Shmakin, A. B., Blewitt, G., Lavallée, D., Larson, K. M., 2001. Crustal displacements due to continental water loading. Geophysical Research Letters 28 (4), 651–654.

Vanìček, P., Krakiwsky, E., 1986. Geodesy The Concepts, 2nd Edition. North-Holland, Amsterdam.

Vespe, F., Rutigliano, P., Ferraro, C., Nardi, A., 2002. Vertical motions from geodetic and geological data: a critical discussion of the results. In: Drewes, H., Dodson, A. H., Fortes, L. P. S., Sánchez, L., Sandoval, P. (Eds.), Vertical Reference Systems. Vol. 124 of International Association of Geodesy Symposia. Springer-Verlag, Berlin Heidelberg, pp. 66–71.

Wall, L., Christiansen, T., Schwartz, R. l., 1996. Programming Perl, 2nd Edition. O'Reilly and Associates, Cambridge, MA.

Wdowinski, S., Bock, Y., Zhang, J., Fang, P., Genrich, J., 1997. Southern California Permanent GPS Geodetic Array: Spatial filtering of daily positions for estimating coseismic and postseismic displacements induced by the 1992 Landers earthquake. Journal of Geophysical Research 102 (B8), 18057–18070.

Weber, R., 2001. [IGSMAIL-3605]: Towards ITRF2000 [online], 20 November. Available at: `<http://igscb.jpl.nasa.gov/mail/igsmail/2001/msg00450.html>` [Accessed 4 April 2002].

Wessel, P., Smith, W. H. F., 1995. A new version of Generic Mapping Tools released. EOS: Transactions American Geophysical Union 76.

Wessel, P., Smith, W. H. F., 1998. New, improved version of Generic Mapping Tools released. EOS Transactions, American Geophysical Union 79 (47), 579.

Williams, S. D. P., 2002. Offsets in geodetic time series. Journal of Geophysical Research (in press).

Williams, S. D. P., 2003a. The effect of coloured noise on the uncertainties of rates estimated from geodetic time series. Journal of Geodesy 76 (9-10), 483–494, doi:10.1007/s00190–002–0283–4.

Williams, S. D. P., (`sdwil@pol.ac.uk`) 2003b. Re: offset section. 31 January. Email to: Norman Teferle (`norman.teferle@nottingham.ac.uk`).

Williams, S. D. P., Baker, T. F., Jeffries, G., 2001. Absolute gravity measurements at UK tide gauges. Geophysical Research Letters 28 (12), 2317–2320.

Williams, S. D. P., Nikolaidis, R. M., Bock, Y., Fang, P., Miller, M., Johnson, D., 2003. MLE error analysis of global and regional continuous GPS time series. Journal of Geophysical Research (in press).

Willis, P., Morel, L., 2002. Present mean sea level indetermination coming from ITRF reference frame uncertainties on TOPEX/POSEIDON orbits [online]. Available at:

<http://www-aviso.cls.fr/documents/swt/posters2001/willis.pdf> [Accessed 9 September 2002].

Wood, R., 2000. HERS site information form [online]. Available at: <ftp://igscb.jpl.nasa.gov/igscb/station/log/hers0109.log> [Accessed 17 April 2002].

Woodworth, P. L., 1997. The need for GPS to provide information on vertical land movements at tide gauges with long records. In: Neilan, R. E., Van Scoy, P. A., Woodworth, P. L. (Eds.), Methods for Monitoring Sea Level: GPS and Tide Gauge Benchmark Monitoring and Altimeter Calibration. Jet Propulsion Laboratory, California Institute of Technology, Pasadena, California, pp. 57–63.

Woodworth, P. L., 1999. High waters at Liverpool since 1768: the UK's longest sea level record. Geophysical Research Letters 26 (11), 1589–1592.

Woodworth, P. L., Tsimplis, M. N., Flather, R. A., Shennan, I., 1999. A review of the trends observed in British Isles mean sea level data measured by tide gauges. Geophysical Journal International 136, 651–670.

Wöppelmann, G., Boucher, C., Bevis, M., Bruyninx, C., Woodworth, P. L., 2002. An inventory of collocated and nearly-collocated CGPS stations and tide gauges [online]. <http://www.sonel.org/stations/cgps/surv_update.html> [10 September 2002].

Wübbena, G., Menge, F., Schmitz, M., Seeber, G., Voelksen, C., 1998. A new approach for field calibration of absolute antenna phase center variations. In: Proc. of the 11th International Technical Meeting of the Satellite Division of the Institute of Navigation ION GPS98, 15-18 September 1998, Nashville. Institute of Navigation, Washington D. C., pp. 1205–1214.

Wübbena, G., Schmitz, M., Menge, F., Böder, V., Seeber, G., 2000. Automated absolute field calibration of GPS antennas in real-time. In: Proc. of the 13th International Technical Meeting of the Satellite Division of the Institute of Navigation ION GPS 2000, 19-22 September 2000, Salt Lake City, Utah. Institute of Navigation, Washington D. C., pp. 2512–2522.

Zerbini, S., 1994. SELF SEa Level Fluctuations: geophysical interpretation and environmental impact. Prochure, Commission of the European Communities Directorate - General XII Science, Research and Development.

Zerbini, S., 1996. SELF II: SEa Level Fluctuations in the Mediterrranean: interactions with climate processes and vertical crustal movements. Prochure, European Commission, Directorate General XII, Science, Research and Development.

Zerbini, S., 1997. The SELF II Project. In: Neilan, R. E., Van Scoy, P. A., Woodworth, P. L. (Eds.), Methods for monitoring sea level: GPS and tide gauge benchmark monitoring and altimeter calibration. Jet Propulsion Laboratory, California Institute of Technology, Pasadena, California, pp. 93–95.

Zerbini, S., Plag, H. P., Baker, T. F., Becker, M., Billiris, H., Bürki, B., Kahle, H. G., Marson, I., Pezzoli, L., Richter, B., Romangnoli, C., Sztobyrn, M., Tomasi, P., Tsimplis, M. N., Veis, G., Verrone, G., 1996. Sea level in the Mediterranean: a first step towards separating crustal movements and absolute sea-level variations. Global and Planetary Change 14 (1996), 1–48.

Zerbini, S., Richter, B., Negusini, M., Romangnoli, C., Simon, D., Domenichini, F., Schwahn, W., 2001. Height and gravity variations by continuous GPS, gravity and environmental parameter observations in the southern Po Plain, near Bologna, Italy. Earth and Planetary Science Letters 192 (3), 267–279.

Zhang, J., Bock, Y., Johnson, H. O., Fang, P., Williams, S. D. P., Genrich, J., Wdowinski, S., Behr, J., 1997. Southern California Permanent GPS Geodetic Array: Error analysis of daily position estimates and site velocities. Journal of Geophysical Research 102 (B8), 18035–18055.

Zumberge, J. F., Heflin, M. B., Jefferson, D. C., Watkins, M. M., Webb, F. H., 1997. Precise point positioning for the efficient and robust analysis of GPS data from large networks. Journal of Geophysical Research 102 (B3), 5005–5017.

Appendix A

Geophysical and Geological Evidence for Vertical Land/Crustal Movements

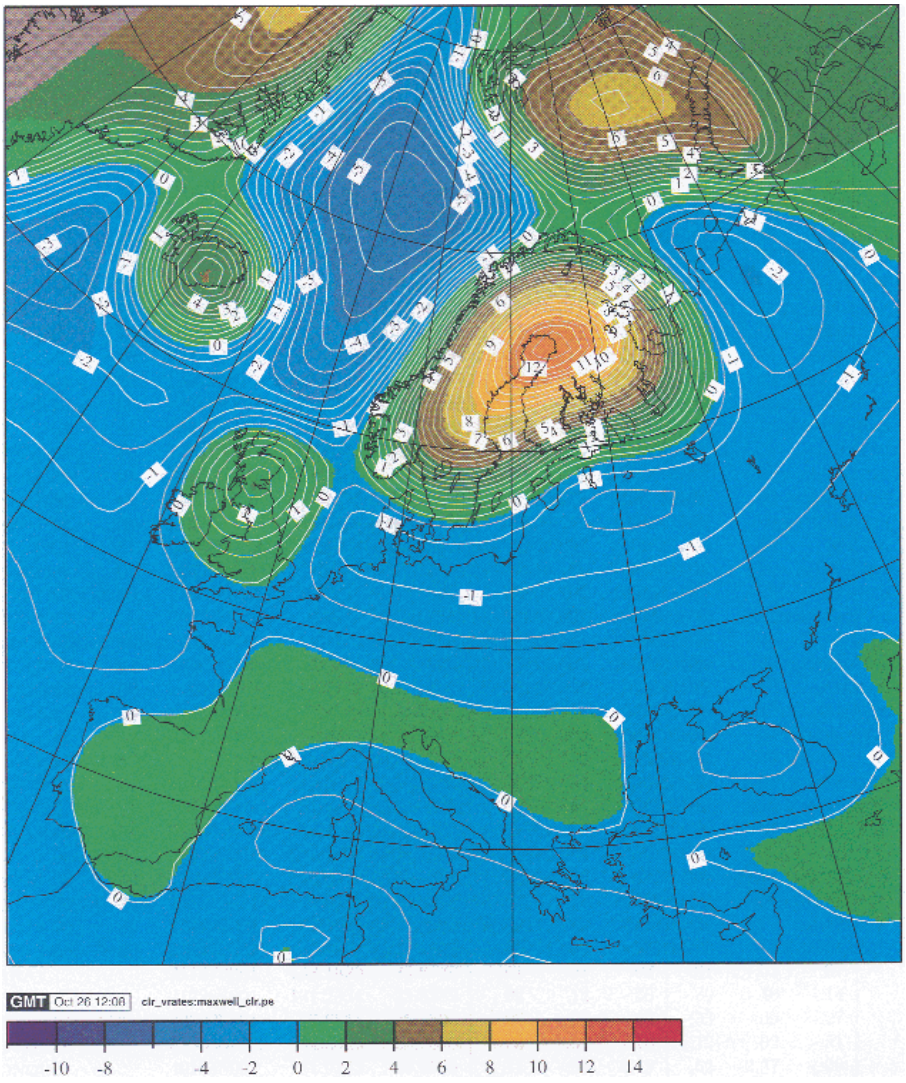

Figure A.1: Predicted vertical crustal movements in mm/yr for Europe due to glacial isostatic adjustment (GIA) process. Figure reproduced from (Scherneck et al., 2002a)

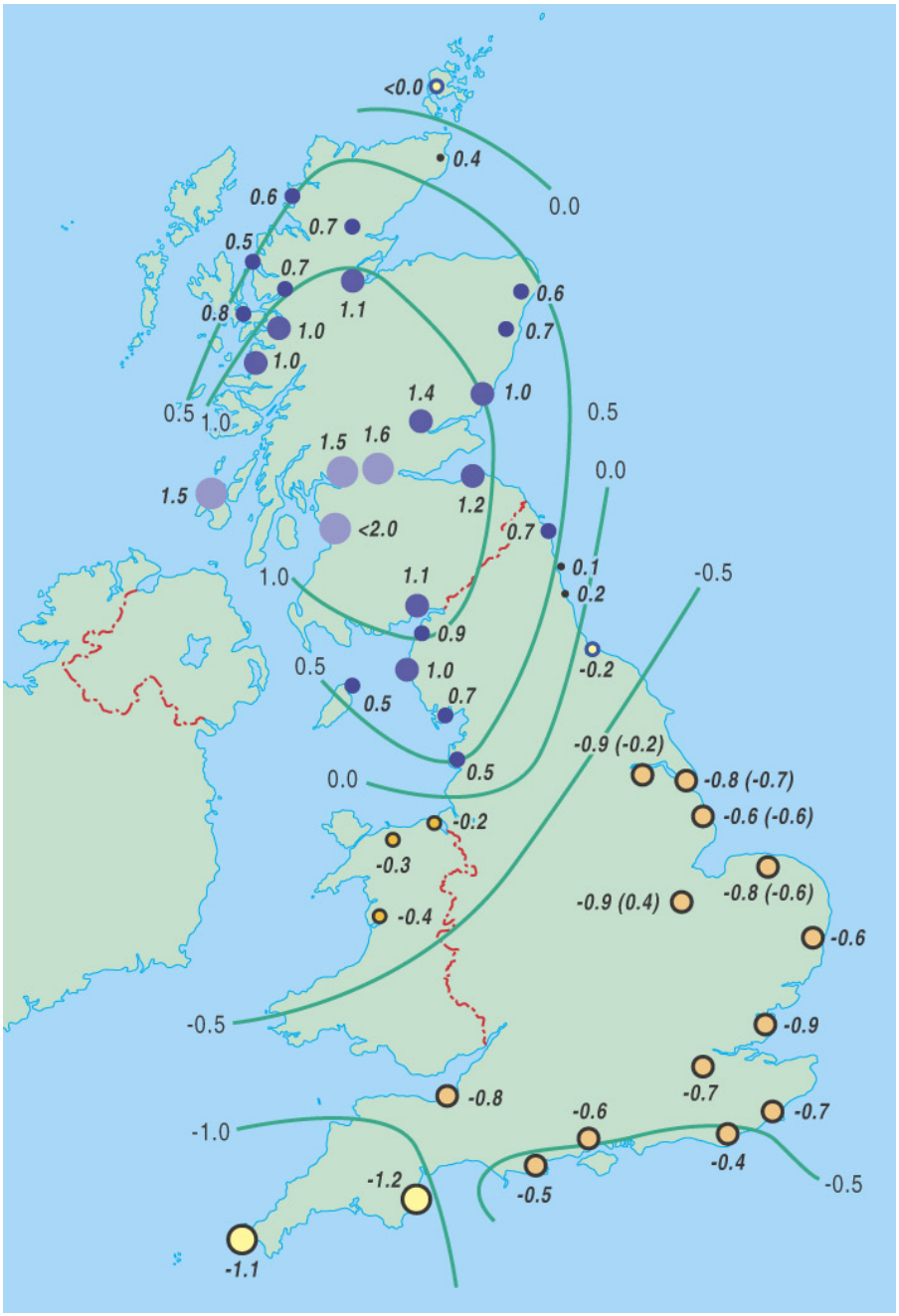

Figure A.2: Estimated rates of current vertical land movements in mm/yr for the UK based on geological information. Figure reproduced from Shennan and Horton (2002).

Appendix B

Existing Coordinate Time Series

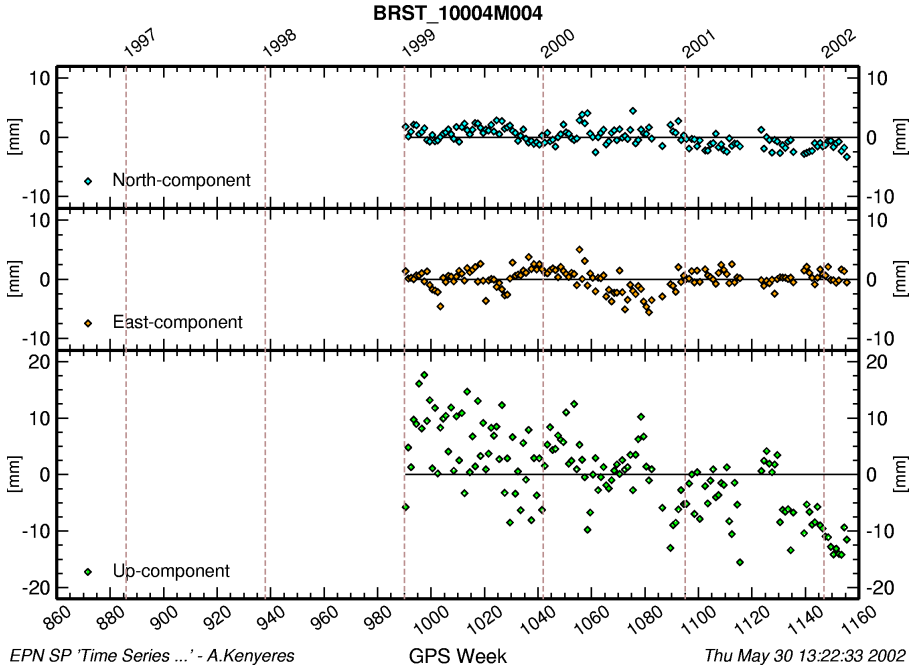

Figure B.1: Improved EUREF weekly ITRS97 coordinate time series for geokinematics for BRST up to end of May 2002 obtained from the EPN website: `http://www.epncb.oma.be/series_sp.html`. The North and East coordinate components have their associated Nuvel–1A NNR station velocities removed.

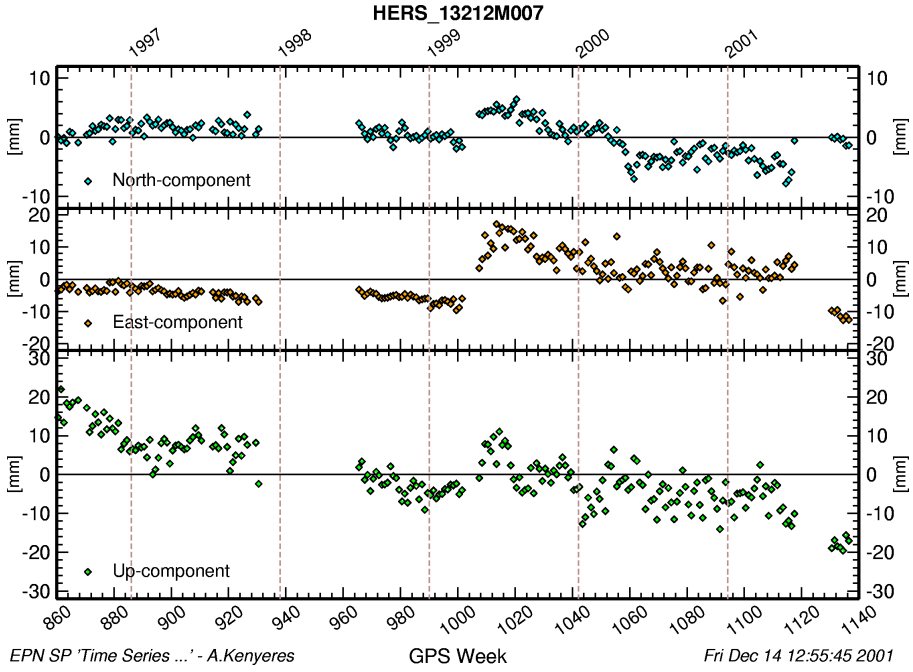

Figure B.2: Improved EUREF weekly ITRS97 coordinate time series for geokinematics for HERS up to end of May 2002 obtained from the EPN website: `http://www.epncb.oma.be/series_sp.html`. The North and East coordinate components have their associated Nuvel–1A NNR station velocities removed.

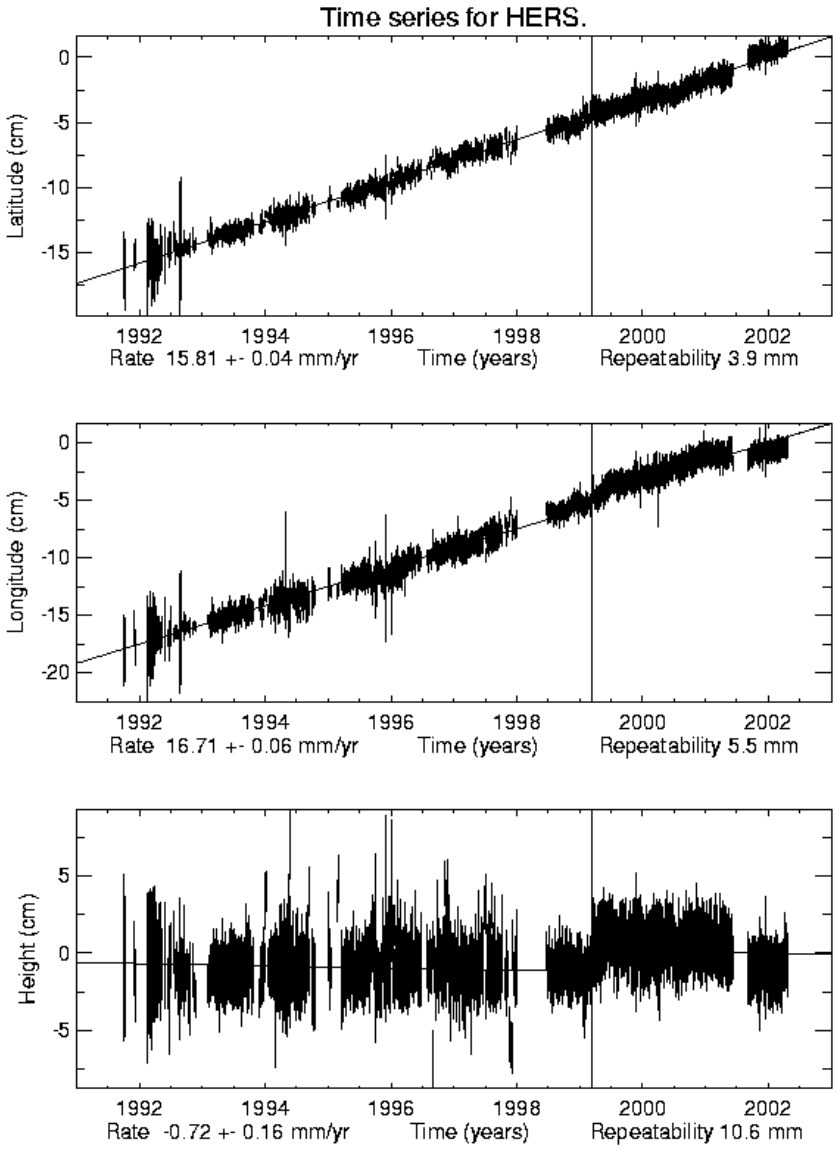

Figure B.3: JPL daily ITRS2000 coordinate time series for HERS up to April 2002 obtained from the JPL GPS time series website: `http://sideshow.jpl.nasa.gov/mbh/series.html`.

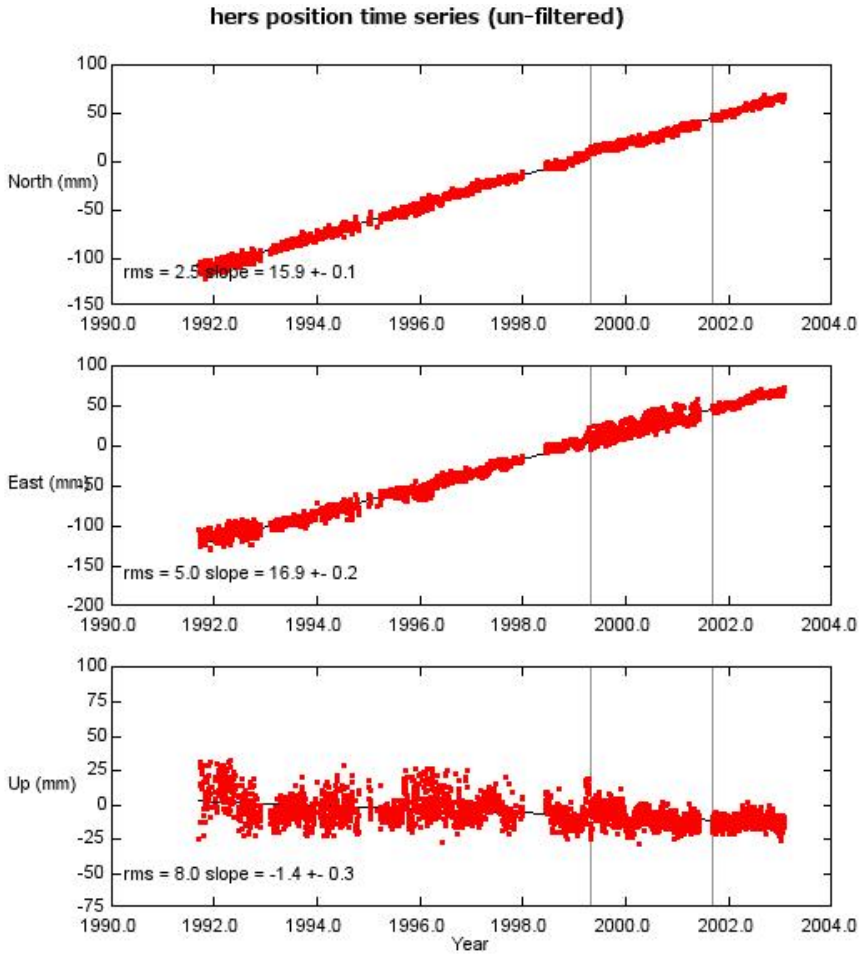

Figure B.4: SOPAC daily ITRS2000 coordinate time series for HERS up to January 2003 obtained from the SOPAC website: `http://sopac.ucsd.edu`.

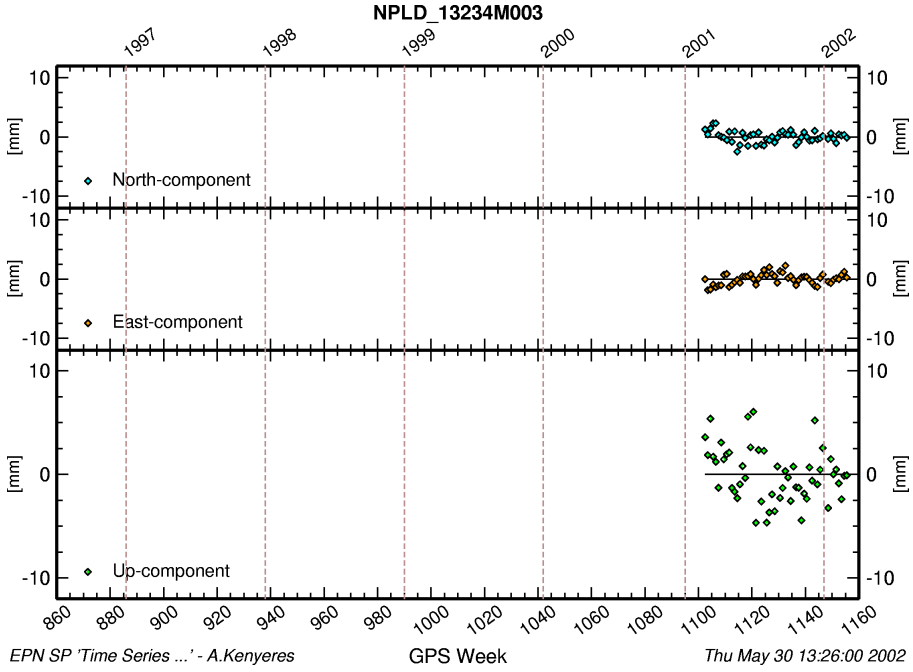

Figure B.5: Improved EUREF weekly ITRS97 coordinate time series for station NPLD up to end of May 2002 obtained from the EPN website: `http://www.epncb.oma.be/series_sp.html`. The North and East coordinate components have their associated Nuvel–1A NNR station velocities removed.

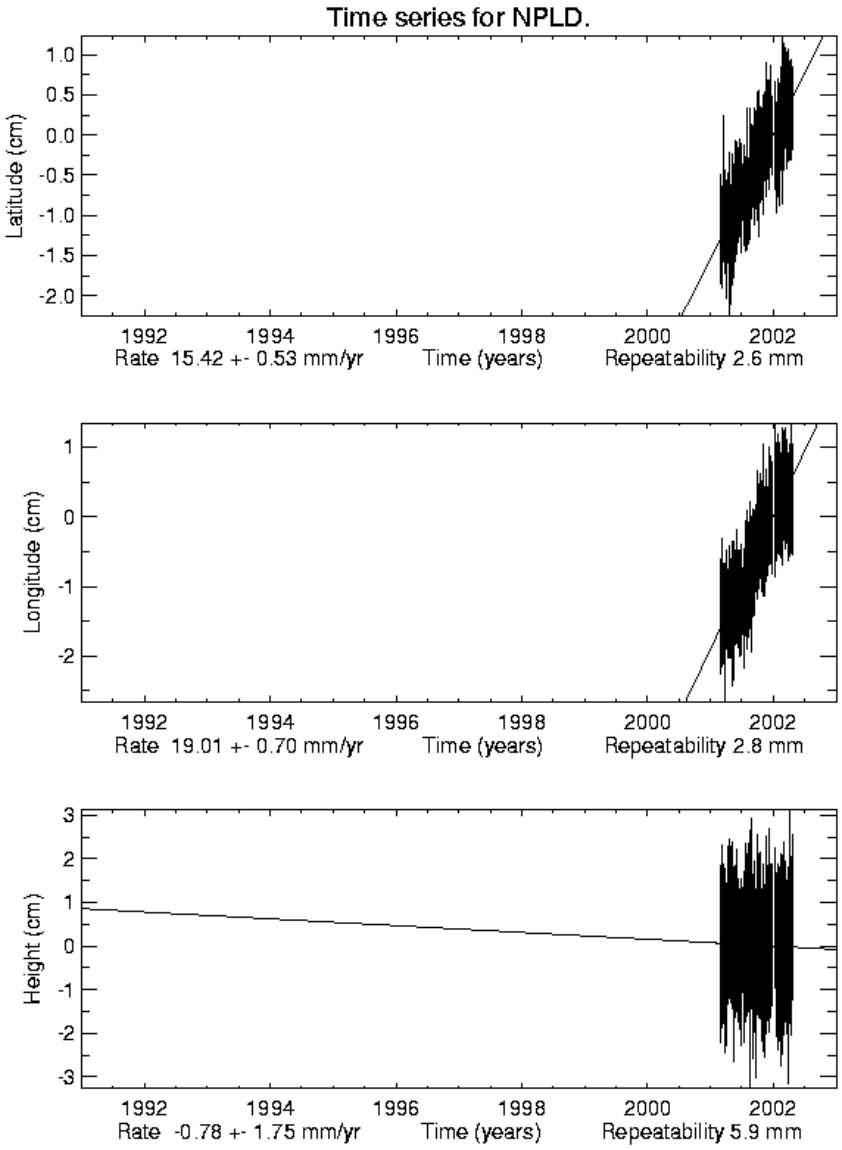

Figure B.6: JPL daily ITRS2000 coordinate time series for NPLD up to March 2002 obtained from the JPL GPS time series website: `http://sideshow.jpl.nasa.gov/mbh/series.html`.

Appendix C

Daily TEQC Summary Plots

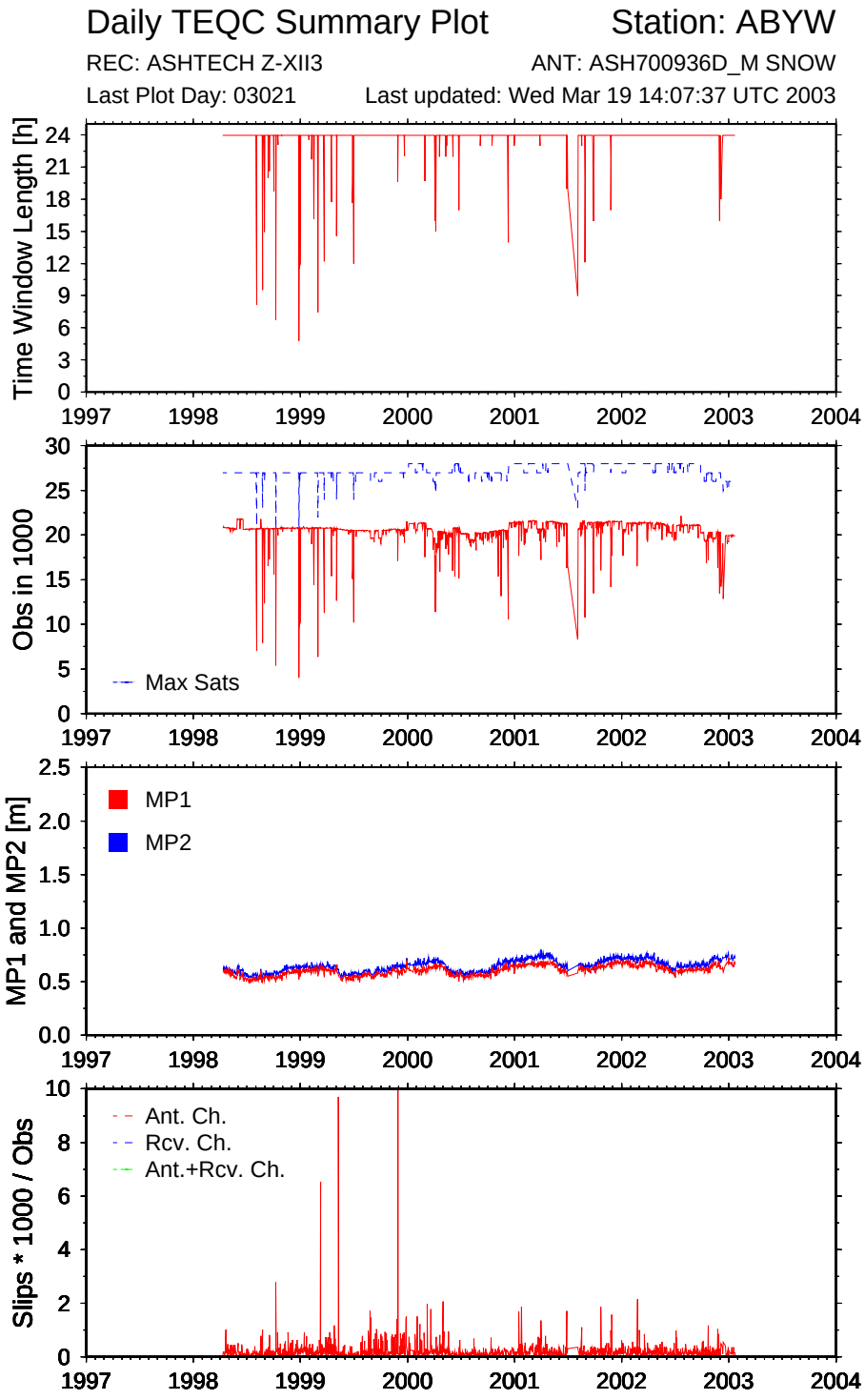

Figure C.1: Daily TEQC Summary Plot for ABYW

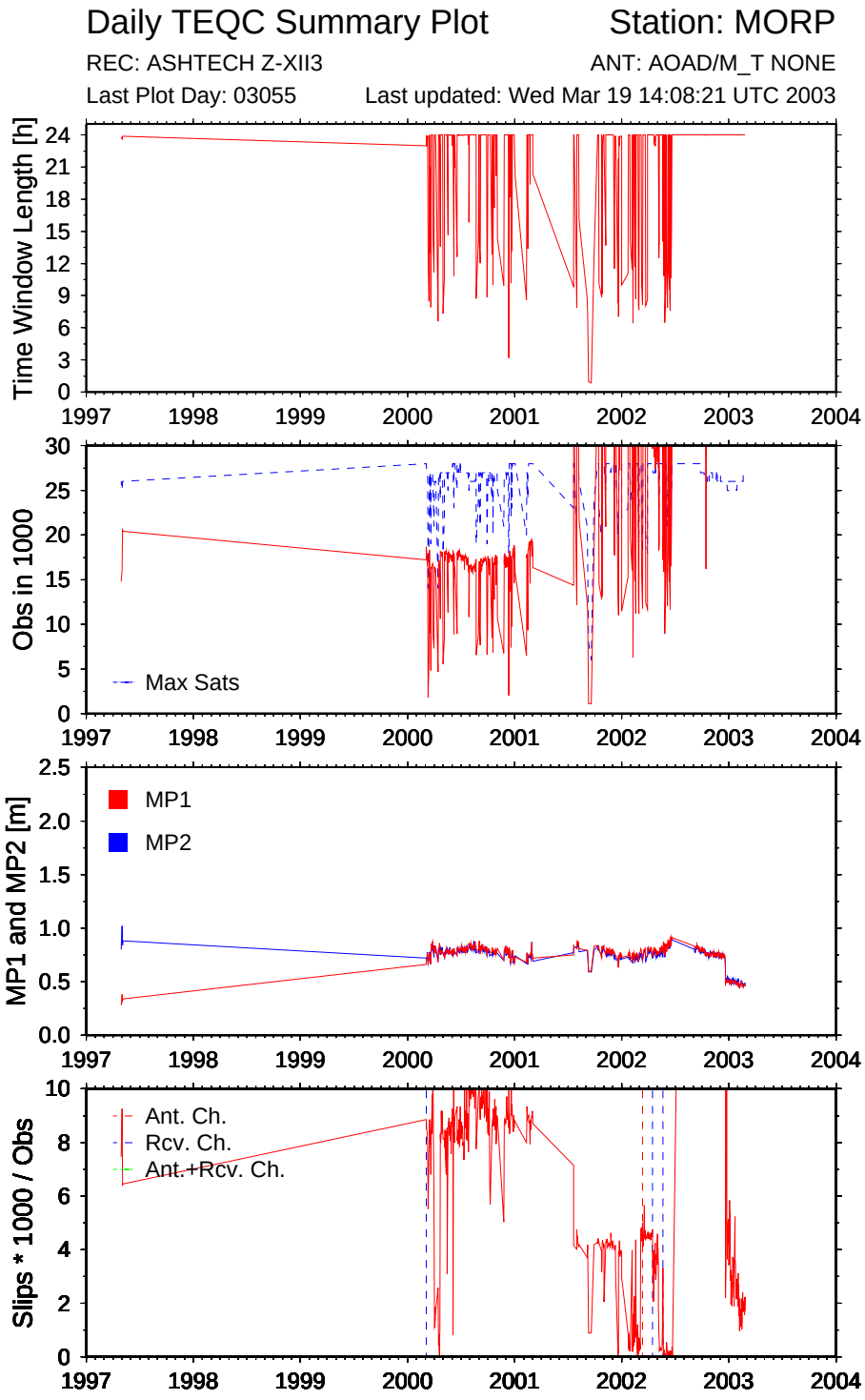

Figure C.2: Daily TEQC Summary Plot for MORP

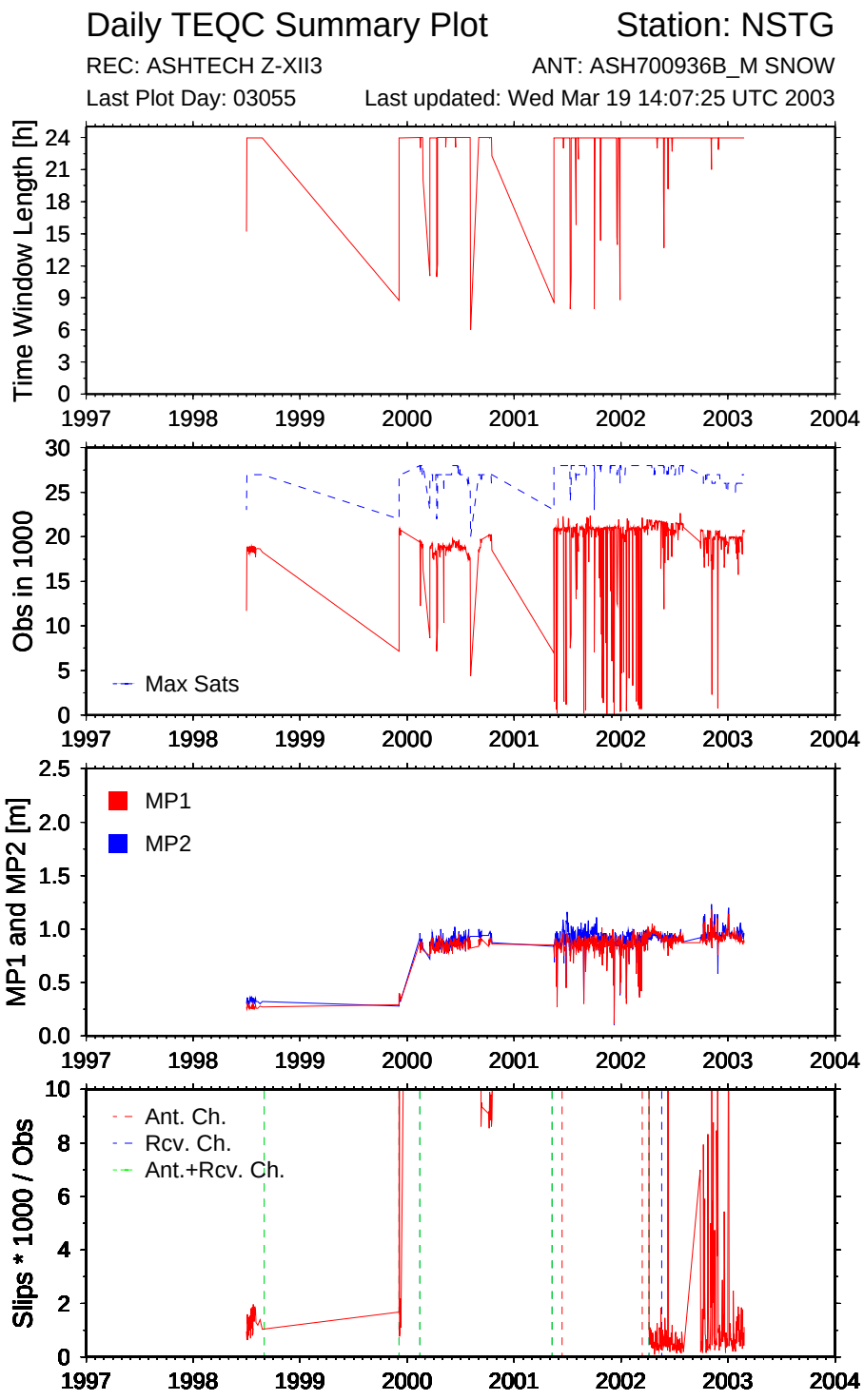

Figure C.3: Daily TEQC Summary Plot for NSTG

Appendix D

Residual Quality Measures and Hypothesis Testing

It is important to asses the quality of coordinate time series as this may point to problems in the observational data or in the least–squares adjustment process. Often a series of position estimates y_i with $i = 1, \ldots, N$ are evaluated by their residuals v_i, which can be computed by subtracting a model value, e.g. the mean or a linear trend, from the individual estimates. The Root Mean Square (RMS) statistic for N independent residuals v_i is defined by

$$RMS = \sqrt{\sum_{i=1}^{N} \frac{v_i^2}{N}} \tag{D.1}$$

Standard errors σ_i are obtained from the variance–covariance matrix of the least–squares estimation for each coordinate component. These formal errors can be used as weights in the following interpretations and the Weighted RMS (WRMS) can be defined as (Dixon, 1991; Larson and Agnew, 1991)

$$WRMS = \sqrt{\frac{\left(\frac{N}{N-u}\right) \sum_{i=1}^{N} \frac{v_i^2}{\sigma_i^2}}{\sum_{i=1}^{N} \frac{1}{\sigma_i^2}}} \tag{D.2}$$

were u denotes the number of unknowns. As a measure for the correctness of the formal errors the reduced χ^2 statistic can be used and is defined such that

$$\chi^2 = \frac{1}{N-u} \sum_{i=1}^{N} \frac{v_i^2}{\sigma_i^2} \tag{D.3}$$

Values of reduced $\chi^2 \sim 1$ indicate a good fit of data to model and suggest that formal error estimates are reasonable. Reduced $\chi^2 < 1$ suggest that errors are overestimated and a reduced $\chi^2 > 1$ suggest either that errors are underestimated or that a given model poorly fits the data (Dixon et al., 2000).

In this research residuals have been computed for several model fits to the coordinate time series. The models, the computation of the residuals v_i and the associated number of unknowns u have been summarized in Table D.1. The models presented in Table D.1 for the computation of the residuals can be expanded to account for the case of combined estimation of offset magnitudes and periodic signals in coordinate time series.

Table D.1: Models, residuals and number of unknowns used for computing RMS, WRMS and reduced χ^2 statistics in this thesis with μ denoting the mean or weighted mean, x_0 and r the initial coordinate and rate of change of the position at time t_i, o_i a value of 0 or 1, x_{off} a linear offset and p and q the sine and cosine amplitudes of a periodic signal

Model	Residuals v_i	u
mean	$v_i = y_i - \mu$	1
linear trend	$v_i = y_i - (x_0 + rt_i)$	2
linear trend plus offset	$v_i = y_i - (x_0 + rt_i + o_i x_{off})$	3
linear trend plus periodic signal	$v_i = y_i - (x_0 + rt_i + p\sin(2\pi f t_i) + q\cos(2\pi f t_i))$	4
linear trend plus offset and periodic signal	$v_i = y_i - (x_0 + rt_i + o_i x_{off} + p\sin(2\pi f t_i) + q\cos(2\pi f t_i))$	5

Hypothesis Testing

The theory of hypothesis testing is well documented in statistical literature and examples for the tests described below can been found e.g. in Kreyszig (1970); Menke (1989); Cross (1992) and Press et al. (1992).

The Student's t–test allows the comparison of the means of two normally distributed random variables and can be used to assess whether there has been a coordinate shift at a certain epoch in a coordinate time series. The computed means for a period before and after the specific epoch may vary due to random fluctuations in the coordinate time series rather than a significant offset in the coordinates. Therefore, this test can be applied to determine, whether or not the means μ_1 and μ_2, before and after an event at a specific

epoch are significantly different. The test is carried out by comparing the Student's t test value to a critical value c distributed following the Student's t–distribution with ν degrees of freedom and significance level α (Kreyszig, 1970). When the two populations with n_1 and n_2 numbers of independent samples are thought to have the same variance, but possibly different means, then the Student's t is computed as follows (Kreyszig, 1970)

$$t = \sqrt{\frac{n_1 n_2 (n_1 + n_2 - 2)}{n_1 + n_2}} \frac{\mu_1 - \mu_2}{\sqrt{(n_1 - 1)\sigma_1^2 + (n_2 - 1)\sigma_2^2}} \tag{D.4}$$

with σ_1^2 and σ_2^2 being the variances for each sample. The null hypothesis that there is no significant difference in the two means, i.e. $H_0 : \mu_1 = \mu_2$ can then be tested against the alternative hypothesis $H_A : \mu_1 \neq \mu_2$, i.e. the means are significantly different. This alternative hypothesis is two–sided, as it accounts for the cases $\mu_1 > \mu_2$ and $\mu_1 < \mu_2$. Therefore, the probabilities $P(t \leq c_1) = \alpha/2$ and $P(t \leq c_2) = 1 - \alpha/2$ must be evaluated with the critical values c_1 and c_2 being obtained from the theoretical t–distribution with $\nu = n_1 + n_2 - 2$ degrees of freedom (Kreyszig, 1970; Baker, 2000). If $c_1 \leq t \leq c_2$ is not true, then the null hypothesis is rejected at the significance level α, alternatively, if $c_1 \leq t \leq c_2$ holds true, the null hypothesis is accepted.

The F–test for error improvement significance allows the comparison of variances of two normal distributions. Using this test, it is possible to compare two different models, of which one is more complicated than the other, for describing an over–determined least–squares problem, e.g. a series of daily coordinate solutions derived from CGPS observations.

In almost every case, a more complicated model will fit the coordinate time series better than a less complicated one, but the question is whether the fit is significantly better, i.e. the improvement is too large to be accounted for by random fluctuations (Menke, 1989). It is clear that the ratio of the two estimated variances σ_1 and σ_2 for the two models is an indicator for the model fit. If one model fits the data about as well as the other, then the ratio σ_1/σ_2 is about unity. If the more complicated model fits the coordinate time series better, then this ratio will be greater than unity. However, if it is only slightly greater than unity, then the difference in the fit might be entirely due to random fluctuations in

the coordinate time series and may not be significant. Using the theoretical distribution of the ratio of two variances, it is possible to compute a critical value c at which the ratio indicates a significant difference. The test therefore determines whether or not ratios greater than or equal to the observed ratio occur less than a certain significance level α. If they do, then there is a $1-\alpha$ probability that the more complicated model fits the coordinate time series significantly better.

The F–test is carried using the reduced χ^2 quantity which is related to the variance and has been introduced above. This quantity is chosen because it has a χ^2 distribution with ν degrees of freedom. The ratio of the χ_1^2 and χ_2^2 for model 1 and model 2 respectively, is then given by

$$F = \chi_1^2/\chi_2^2 \tag{D.5}$$

which follows the F distribution with ν_1 and ν_2 degrees of freedom, i.e. $F \sim F_{\nu_1,\nu_2}$ (Kreyszig, 1970).

The null hypothesis is that both models fit the coordinate time series at about the same level, i.e. $H_0 : \sigma_1^2 = \sigma_2^2$. This can then be tested against the alternative hypothesis that the variance estimated from model 1 is larger than the variance estimated from model 2, i.e. $H_A : \sigma_1^2 > \sigma_2^2$. The probability $P(F \leq c) = 1-\alpha$ can be evaluated by e.g. setting $\alpha = 5\%$ and obtaining c from tabulated values of the F distribution with ν_1 and ν_2 degrees of freedom (Kreyszig, 1970; Baker, 2000). If the F for the two least–squares models is greater than this critical value, then it is reasonable to assume that the improvement in error by using model 2 is not a result of random fluctuations in the coordinate time series but of a significant difference between the models. The null hypothesis can therefore be *rejected* at the $1-\alpha$ significance level. Alternatively, the null hypothesis is *accepted* at significance level α.

Appendix E

Coordinate Time Series – Model Parameter Estimation

The evolution of station positions in time has traditionally been modelled by fitting a straight line to a series of coordinate solutions obtained from geodetic observations. For the estimation of *station velocities*, i.e. the rate of change in the station coordinates, the basic form of the linear regression problem can be expressed as a series of N sample points y_i at times t_i with $i = 1, \ldots, N$ such that

$$y_i = x_0 + rt_i + \epsilon_x(t_i) \tag{E.1}$$

with x_0 and r being the initial position and velocity respectively, and $\epsilon_x(t_i)$ being the error term (Zhang et al., 1997). Eq. E.1 can be re–written in matrix form as

$$\mathbf{y}(t) = \mathbf{A}\mathbf{x}(t) + \epsilon(t) \tag{E.2}$$

with $\mathbf{A}$ being the design matrix in the form of

$$\mathbf{A} = \begin{bmatrix} 1 & t_1 \\ 1 & t_2 \\ \vdots & \vdots \\ 1 & t_N \end{bmatrix}, \tag{E.3}$$

$\mathbf{x}$ being the vector of the unknown parameters

$$\mathbf{x} = (x_0, r)^T \tag{E.4}$$

and $\mathbf{y}$ being the vector of observations

$$\mathbf{y} = (y_1, \ldots, y_N)^T. \tag{E.5}$$

In the simplest case of one *known* offset x_{off} at time t_{off} (where $t_1 < t_{off} < t_N$) in the coordinate time series, Eq. E.1 now becomes (Williams, 2002):

$$y_i = x_0 + rt_i + o_i x_{off} + \epsilon_x(t_i) \tag{E.6}$$

where

$$o_i = \begin{cases} 1 & t_i \geq t_{off} \\ 0 & t_i < t_{off} \end{cases} \tag{E.7}$$

In matrix form this can be written as

$$\begin{aligned} \mathbf{y} &= (y_1, \ldots, y_N)^T \\ \mathbf{A} &= \begin{bmatrix} 1 & t_1 & o_1 \\ 1 & t_2 & o_2 \\ \vdots & \vdots & \vdots \\ 1 & t_{N-1} & o_{N-1} \\ 1 & t_N & o_N \end{bmatrix} \\ \mathbf{x} &= (x_0, r, x_{off})^T \end{aligned} \tag{E.8}$$

For any additional offset, Eq. E.6 requires an additional term, leading to an extra column in matrix $\mathbf{A}$ and an extra parameter for this second offset in the vector of the unknown parameters $\mathbf{x}$.

A sine or cosine curve, representing a periodic signal in the coordinate time series can be estimated in a similar manner as shown for offsets using a least–squares fit. Assuming a simple model consisting of a linear trend with an additional periodic signal, Eq. E.1 can be expanded to account for a repeating signal in the form

$$y_i = x_0 + rt_i + p\sin(2\pi f t_i) + q\cos(2\pi f t_i) + \epsilon_x(t_i) \tag{E.9}$$

with f being the fundamental frequency and the parameters p and q being related to the amplitude a and phase shift ϕ by:

$$a = \sqrt{p^2 + q^2} \qquad \phi = atan\left(\frac{p}{q}\right) \tag{E.10}$$

In matrix form this can be written as

$$\begin{aligned} \mathbf{y} &= (y_1, \ldots, y_N)^T \\ \mathbf{A} &= \begin{bmatrix} 1 & t_1 & \sin 2\pi f t_1 & \cos 2\pi f t_1 \\ 1 & t_2 & \sin 2\pi f t_2 & \cos 2\pi f t_2 \\ \vdots & \vdots & \vdots & \vdots \\ 1 & t_{N-1} & \sin 2\pi f t_{N-1} & \cos 2\pi f t_{N-1} \\ 1 & t_N & \sin 2\pi f t_N & \cos 2\pi f t_N \end{bmatrix} \\ \mathbf{x} &= (x_0, r, p, q)^T. \end{aligned} \tag{E.11}$$

Additional periodic variations, e.g. a semi–annual signal, can be modelled in a simillar manner as shown in Eq. E.9. Based on Eq. E.1, Eq. E.6 and E.9, it is possible to build a parameter model of the coordinate time series estimating a linear plus annual term and an offset magnitude at a given epoch such that:

$$y_i = x_0 + r t_i + o_i x_{off} + p \sin(2\pi f t_i) + q \cos(2\pi f t_i) + \epsilon_x(t_i). \tag{E.12}$$

In matrix form this can be written as

$$\begin{aligned} \mathbf{y} &= (y_1, \ldots, y_N)^T \\ \mathbf{A} &= \begin{bmatrix} 1 & t_1 & o_1 & \sin 2\pi f t_1 & \cos 2\pi f t_1 \\ 1 & t_2 & o_2 & \sin 2\pi f t_2 & \cos 2\pi f t_2 \\ \vdots & \vdots & \vdots & \vdots & \vdots \\ 1 & t_{N-1} & o_{N-1} & \sin 2\pi f t_{N-1} & \cos 2\pi f t_{N-1} \\ 1 & t_N & o_N & \sin 2\pi f t_N & \cos 2\pi f t_N \end{bmatrix} \\ \mathbf{x} &= (x_0, r, o, p, q)^T. \end{aligned} \tag{E.13}$$

In case of uncorrelated white noise, the variance–covariance matrix $\mathbf{C}$ of the observations is defined by the individual variances σ_i^2, of the daily coordinate estimates giving

$$\mathbf{C} = \begin{bmatrix} \sigma_1^2 & 0 & 0 & \ldots & 0 \\ 0 & \sigma_2^2 & 0 & \ldots & 0 \\ 0 & 0 & \sigma_3^2 & \ldots & 0 \\ \vdots & \vdots & \vdots & \ddots & \vdots \\ 0 & 0 & 0 & \ldots & \sigma_N^2 \end{bmatrix} \tag{E.14}$$

The weighted least–squares estimates for the best fitting parameter model is then obtained by

$$\hat{\mathbf{x}} = (\mathbf{A}^T \mathbf{C}^{-1} \mathbf{A})^{-1} \mathbf{A}^T \mathbf{C}^{-1} \mathbf{y} \tag{E.15}$$

and the variance–covariance matrix $\hat{\mathbf{C}}_x$ of the estimated parameters with

$$\mathbf{C}_{\hat{x}} = (\mathbf{A}^T \mathbf{C}^{-1} \mathbf{A})^{-1} \tag{E.16}$$

The post–fit residuals can then be computed using

$$\hat{\mathbf{v}} = \mathbf{y} - \mathbf{A}\hat{\mathbf{x}} \tag{E.17}$$

Appendix F

Coordinate Time Series – Periodic Signals

Below is a summary of some equations derived in Lavallée (2000) and Blewitt and Lavallée (2002) to describe the effect of periodic signals in coordinate time series on station velocity estimates. Previously, it was assumed that this velocity bias is minimal at full integer years of the observation time span, however this has been shown to be incorrect. The following describes how the velocity bias can be estimated for a theoretical sine and cosine signal or for a *realistic* estimate of this bias including higher harmonics of the fundamental frequency based on a Fourier series expansion.

A periodic signal y at time t_i with $i = 1, \ldots, n$ can be described by

$$y_i = a\cos(2\pi f t_i - \phi) + \epsilon_x(t_i) \tag{F.1}$$

with a being the amplitude at fundamental frequency f with a phase shift ϕ and an arbitrary term $\epsilon_x(t_i)$ accounting for any kind of noise. Equivalently, this equation can be expanded into form

$$y_i = p\sin(2\pi f t_i) + q\cos(2\pi f t_i) + \epsilon_x(t_i) \tag{F.2}$$

with the parameters p and q being related to the amplitude a and phase shift ϕ by:

$$a = \sqrt{p^2 + q^2} \qquad \phi = atan\left(\frac{p}{q}\right) \tag{F.3}$$

Based on Eq. F.1 or F.2, it is therefore possible, to include the estimation of the parameters describing an annual sinusoidal signal beside the term for the initial position x_0 and velocity r in the least–squares estimation process in the form, e.g. for Eq. F.2

$$y_i = x_0 + rt_i + p\sin(2\pi f t_i) + q\cos(2\pi f t_i) + \epsilon_x(t_i) \tag{F.4}$$

According to Blewitt and Lavallée (2002), the velocity bias $\hat{r}_b(T)$ due to a sinusoidal signal can be expressed as

$$\hat{r}_b(T) = \frac{6a}{\pi f T^2}\left[\cos\pi f T - \frac{\sin\pi f T}{\pi f T}\right]\sin(\pi f T - \phi) \tag{F.5}$$

with T being the total time span of the data. This velocity bias is a zero–crossing oscillatory function of T, which approaches zero for large T, and for arbitrary phase shift ϕ the velocity bias is zero when T satisfies (Blewitt and Lavallée, 2002):

$$0 = \cos\pi f T - \frac{\sin\pi f T}{\pi f T} \tag{F.6}$$

Apart from the trivial case $T = 0$, there is no analytical solution to this equation, however, based on a numerical solution, it can be shown that for positive data spans T, this equation is zero near integer–plus–half $(m + 1/2)$ cycles. These nodes, when the velocity bias is zero near integer–plus–half cycles, can clearly be seen in Figure F.1. This figure shows the theoretical velocity bias (Eq. F.5) for f=1/yr and $a = 1$ mm using example values of phase shift $\phi = 0, \pi$ for a pure ±cosine and $\phi = \pm\pi/2$ for a pure ±sine signal.

Furthermore, Lavallée (2000) derived the velocity bias as a root mean square (RMS) quantity, averaged over all possible phase shifts in order to quantify the magnitude of the bias. The RMS of the theoretical velocity bias is therefore

$$\sigma_b = \frac{6a}{\sqrt{2}\pi f T^2}\left|\cos\pi f T - \frac{\sin\pi f T}{\pi f T}\right| \tag{F.7}$$

with $||$ implying the absolute value.

Any repeating time series discretely sampled at intervals Δt can be expanded as a Fourier series (Chatfield, 1996). Blewitt and Lavallée (2002) derive equations for the velocity bias and the RMS velocity bias described by the Fourier parameters a_k and ϕ_k, with $k = 1, \ldots, 1/(2f\Delta t)$ of a *realistic* periodic signal. This limit for k is given by the

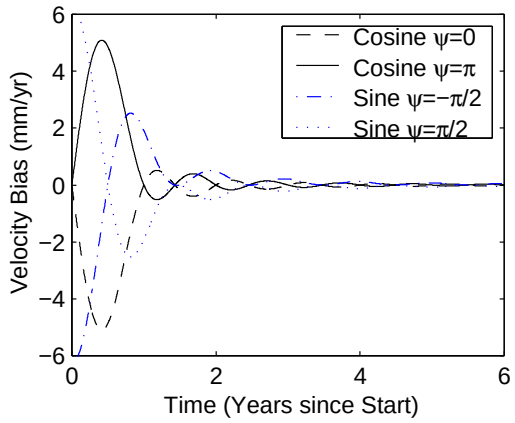

Figure F.1: Theoretical velocity bias for pure sine and cosine signals

highest frequency that can be examined, i.e. the *Nyquist* frequency $1/(2\Delta t)$ (Chatfield, 1996) and the fact that there are $1/(f\Delta t)$ samples within the fundamental period. To compute the velocity bias of a realistic repeating signal, the frequency in Eq. F.5 has to be replaced by each harmonic of the fundamental frequency and each contribution has to be summed up. Therefore the velocity bias for a realistic repeating signal over an arbitrary time span T is given as (Blewitt and Lavallée, 2002):

$$\hat{r}_b(T) = \sum_{k=1}^{1/(2f\Delta t)} \frac{6a_k}{\pi k f T^2} \left[\cos \pi k f T - \frac{\sin \pi k f T}{\pi k f T}\right] \sin(\pi k f T - \phi_k) \tag{F.8}$$

The derivation of the RMS velocity bias is then based on the assumption that types of physical processes that might give rise to annual signals can be described as a power–law process (Agnew, 1992). The power spectrum of such processes are approximately proportional to $f^{-\kappa}$, where κ is the spectral index. Using $a_k = a_1 k^{-\kappa/2}$, Blewitt and Lavallée (2002) expressed the RMS velocity bias for a realistic repeating signal as

$$\sigma_b(T) = \frac{6a_1}{\sqrt{2}\pi f T^2} \left(\sum_{k=1}^{1/(2f\Delta t)} \frac{1}{k^{2+\kappa}} \left[\cos \pi k f T - \frac{\sin \pi k f T}{\pi k f T}\right]^2 \right)^{1/2} \tag{F.9}$$

For an annually repeating signal observed in a coordinate time series of daily position samples, using the fundamental frequency $f = 1$, the maximum Fourier component $k = 183$ (for a year of 366 days), the amplitude a_1 for the annual variation and T specified in years, it is possible to compute the velocity bias according to Eq. F.9 for different spectral indexes κ. Figure F.2 shows this RMS velocity bias for spectral indexes κ of 0.5, 1 and 2.

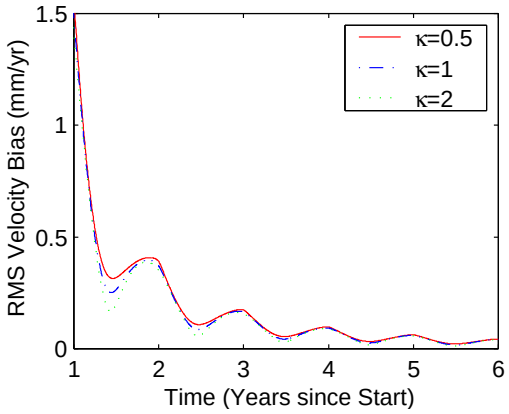

Figure F.2: Realistic velocity bias for time series with different spectral indexes κ

Further investigations into the formal error due to the estimation of the additional sine and cosine amplitudes or Fourier amplitudes of higher harmonics by Blewitt and Lavallée (2002) showed that for periods below 2.5 cycles this error becomes unstable as the estimated parameters are highly correlated. However, for data spans thereafter, the formal error of the estimation reduces rapidly and becomes negligible. Furthermore, they stated the gain to be made from the estimation of the annually repeating signal would rapidly decrease for data spans of 4.5 years or more. For data spans of integer–plus–half years, the estimation of the annual signal is not necessary, as the remaining dominant bias would be due to the smaller semi–annual signals. Also, at these *zero–bias* data spans it is not possible to improve the precision of estimated velocities, because any error in the sine and cosine term at these data spans has no consequence on the estimate of the velocity (Blewitt and Lavallée, 2002). To account for the effect of the periodic variations in the coordinate time series, the associated velocity bias can also be added in quadrature to the velocity uncertainties obtained from the trend analysis.

Appendix G

Coordinate Time Series – Change Detection Algorithm

The change detection algorithm (CDA) is a simple method for estimating the time of changes in time series. It was initially described by Basseville and Nikiforov (1993) and adopted for the application to GPS coordinate time series by Williams (2002).

If y_i is a sequence of $i = 1, \ldots, N$ random observations with a standard deviation σ_y, and there exists an unknown change in time $t_1 \leq t_{off} \leq t_N$ such that before t_{off}, the mean is equal to μ_0 and after the change the mean is equal to μ_1 and $\mu_0 \neq \mu_1$, then the estimated change time $\hat{t}_{off}$ can be found by maximizing the function

$$f(l) = l(N-1)(\mu_0 - \mu_1)^2 \tag{G.1}$$

that is

$$\hat{t}_{off} = \max_{1 \leq l \leq N} \left[l(N-l)(\mu_0 - \mu_1)^2 \right] \tag{G.2}$$

with

$$\mu_0 = \tfrac{1}{l} \textstyle\sum_{i=1}^{l} y_i \quad \text{and} \quad \mu_1 = \tfrac{1}{N-l} \textstyle\sum_{i=l+1}^{N} y_i. \tag{G.3}$$

Williams (2002) modified Eq. G.1 in order to simplify any statistical computations and obtained in equivalence

$$f(l) = \left| \sqrt{\frac{l(N-l)}{N}} \, \frac{(\mu_0 - \mu_1)}{\sigma_y} \right| \tag{G.4}$$

so that

$$\hat{t}_{off} = \max_{1 \leq l \leq N} \left| \sqrt{\frac{l(N-l)}{N}} \, \frac{(\mu_0 - \mu_1)}{\sigma_y} \right| \tag{G.5}$$

with $|\ |$ indicating the absolute value. Clearly, if the coordinate time series contains no offset, then $\mu_0 = \mu_1$ and $f(l) = 0$. If an offset occurs, then the change time t_{off} is at the j^{th} epoch and the theoretical shape of f becomes

$$\begin{aligned} f(l) &= \sqrt{\tfrac{l(N-j)^2}{N(N-l)}} \tfrac{\Delta y}{\sigma_y} \quad l < j \\ f(l) &= \sqrt{\tfrac{(N-l)}{Nl}} \tfrac{j\Delta y}{\sigma_y} \quad l \geq j \end{aligned} \tag{G.6}$$

with $\Delta y = \mu_0 - \mu_1$ being the offset size. Dividing Δy by σ_y gives a normalized offset, which means that results can be stated independently of the noise in the coordinate time series.

Appendix H

Coordinate Time Series – Noise Analysis

Power–law noise

Agnew (1992) investigated the behaviour of one–dimensional stochastic processes in the time–domain and concluded that a wide variety of geophysical phenomena can be approximated by a power–law dependence on frequency such that its power spectrum can be described as

$$P_y(f) = P_0 \left(\frac{f}{f_0} \right)^{\kappa} \tag{H.1}$$

with f being the spatial or temporal frequency, P_0 and f_0 being normalizing constants, and κ being the spectral index. For many geophysical phenomena the index κ would fall in the range -3 to -1 with the integer cases ($\kappa = -1$) and ($\kappa = -2$) being flicker and random walk noise respectively (Agnew, 1992). Classical white noise can be shown to have a spectral index $\kappa = 0$. Generally, processes in the range of -3 $< \kappa <$ -1 have been termed as *fractional Brownian motion* and those in the range -1 $< \kappa <$ 1 as *fractional white noise* (Mandelbrot, 1982; Davis et al., 1994). Throughout this thesis, the term *coloured noise* is used to refer to power–law processes other than classical white noise.

Spectral Analysis

The periodogram by Scargle (1982) can be computed for an arbitrarily, at times t_j, sampled data set y_j with $j = 1, \ldots, N$ and frequency f such that

$$\mathbf{P}_y(f) = \frac{1}{2}\left\{ \frac{\left[\sum_j y_j \cos 2\pi f(t_j - \tau)\right]^2}{\sum_j \cos^2 2\pi f(t_j - \tau)} + \frac{\left[\sum_j y_j \sin 2\pi f(t_j - \tau)\right]^2}{\sum_j \sin^2 2\pi f(t_j - \tau)} \right\} \tag{H.2}$$

where τ is defined by

$$\tan(4\pi f\tau) = \frac{\sum_j \sin 2\pi f t_j}{\sum_j \cos 2\pi f t_j} \tag{H.3}$$

The constant τ is an offset that makes the power spectrum independent of a constant time shift that may be applied to all y_j. The lowest and highest frequencies that can be examined are the inverse of the data span $(1/T)$ and the *Nyquist* frequency $(1/(2\Delta t))$ respectively. For evenly sampled data the periodogram is evaluated at intervals of $1/T$ giving $N/2$ frequencies. For uneven sampling, the meaning of the Nyquist frequency is more complicated but the *mean* Nyquist frequency $N/(2T)$ can be used to compute an upper sampling boundary which then determines the number of independent frequencies analysed (Press et al., 1992).

After the power spectrum $\mathbf{P}_y(f)$ (Eq. H.2) has been estimated, the noise power can be transformed to dB as

$$\mathbf{P}(\mathbf{f}) = 10 \log_{10}\left(\frac{2\mathbf{P}_y(f)}{f_s}\right) \tag{H.4}$$

with f_s being the sampling frequency with period of one day. An estimate of the spectral index κ of a power–law process (Eq. H.1) can be determined by fitting a line to the power spectrum in the log–log space (Eq. H.4) such that

$$\kappa = \frac{\mathbf{P}(\mathbf{f})}{10 \log_{10} \mathbf{f}} \tag{H.5}$$

Maximum Likelihood Estimation

The maximum likelihood estimator (MLE) determines the best fitting noise model to the post–fit residuals $\hat{\mathbf{v}}$ by maximizing the log–likelihood probability function (Langbein and Johnson, 1997; Zhang et al., 1997; Mao et al., 1999; Williams, 2003a):

$$\mathrm{lik}\,(\hat{\mathbf{v}}, \mathbf{C}) = \frac{1}{(2\pi)^{N/2}(\det \mathbf{C})^{1/2}} \exp(-\frac{1}{2}\,\hat{\mathbf{v}}^T \mathbf{C}^{-1} \hat{\mathbf{v}}) \tag{H.6}$$

or by applying natural logarithms to both sides

$$\ln\left[\,\mathrm{lik}\,(\hat{\mathbf{v}}, \mathbf{C})\right] = -\frac{N}{2}\ln(2\pi) - \frac{1}{2}\ln(\det \mathbf{C}) - \frac{1}{2}\,\hat{\mathbf{v}}^T \mathbf{C}^{-1} \hat{\mathbf{v}} \tag{H.7}$$

using a fully populated covariance matrix for observations,

$$\mathbf{C} = a^2\mathbf{I} + b_\kappa^2 \mathbf{J}_\kappa \tag{H.8}$$

described by a combination of white and power–law noise with amplitudes a and b_κ respectively. The identity matrix $\mathbf{I}$ is the covariance matrix of the white noise, resembling the time–independence of this noise process. $\mathbf{J}_\kappa$, the covariance matrix of the power–law noise is computed by means of fractional differencing (Hosking, 1981; Johnson and Wyatt, 1994; Williams, 2003a) such that

$$\mathbf{J}_\kappa = \mathbf{T}\mathbf{T}^T \tag{H.9}$$

where $\mathbf{T}$ is a transformation matrix obtained from

$$\mathbf{T} = \Delta T^{-\kappa/4} \begin{bmatrix} \psi_0 & 0 & 0 & \dots & 0 \\ \psi_1 & \psi_0 & 0 & \dots & 0 \\ \psi_2 & \psi_1 & \psi_0 & \dots & 0 \\ \vdots & \vdots & \vdots & \ddots & 0 \\ \psi_N & \psi_{N-1} & \psi_{N-2} & \dots & \psi_0 \end{bmatrix} \tag{H.10}$$

with sampling interval ΔT and with

$$\psi_N = \frac{-\frac{\kappa}{2}(1-\frac{\kappa}{2})\dots(N-1-\frac{\kappa}{2})}{N!} = \frac{\Gamma(N-\frac{\kappa}{2})}{N!\Gamma(-\frac{\kappa}{2})} \tag{H.11}$$

and Γ being the Gamma Function.

Mao Method

Mao et al. (1999) and Dixon et al. (2000) stated that they observed a strong linear correlation between the WRMS of their coordinate time series from 33 globally distributed CGPS stations and the estimated noise amplitudes for white and flicker noise. Based on this, they give following linear equations:

$$\begin{aligned} a(N) &= 0.613\,\mathrm{WRMS}(N) + 0.259 \\ a(E) &= 0.767\,\mathrm{WRMS}(E) - 0.183 \\ a(H) &= 0.843\,\mathrm{WRMS}(H) - 1.772 \\ b_{-1}(N) &= 1.139\,\mathrm{WRMS}(N) + 0.117 \\ b_{-1}(E) &= 1.041\,\mathrm{WRMS}(E) - 0.342 \\ b_{-1}(H) &= 0.668\,\mathrm{WRMS}(H) + 5.394 \end{aligned} \tag{H.12}$$

where a is the white and b_{-1} the flicker noise amplitude for the (N)orth, (E)ast and (H)eight components.

Williams Method

Williams (2003a) showed that for a linear combination of white and coloured noise of spectral index κ, with amplitudes a and b_κ respectively, and equally spaced data that

$$\mathbf{RMS} = \sqrt{a^2 + cb_\kappa^2} \tag{H.13}$$

where

$$\begin{aligned} c &= \frac{1}{sf}\frac{D_\kappa}{f_s^{\frac{\kappa}{2}+1}(\kappa+1)}\left[\left(\frac{f_s}{2}\right)^{\kappa+1} - \left(\frac{1}{T}\right)^{\kappa+1}\right] && \kappa \neq -1 \\ c &= \frac{D_{-1}}{\sqrt{f_s}}\left[\log\left(\frac{f_s}{2}\right) - \log\left(\frac{1}{T}\right)\right] && \kappa = -1. \end{aligned} \tag{H.14}$$

and

$$D_\kappa = 2(2\pi)^\kappa (24 \times 60 \times 60 \times 365.249)^{\kappa/2}$$

f_s is the sampling frequency in Hz and T the total time span in years. The scaling factor sf for $\kappa < -1$ is given by

$$sf = 0.5718\kappa^2 + 1.0826\kappa + 1.5838$$

and for $\kappa \geq -1$ is given by

$$sf = -0.0681\kappa + 1.0$$

This is required as using $f_s/2$ and $1/T$ in Eq. H.14 limits the bandwidth of the computed variance. In order to account for contributing noise outside this interval, factor c requires re–scaling with sf. If the white noise amplitude a has been estimated, e.g. by computing the RMS of the differences between samples (assuming even sampling) and dividing it by $\sqrt{2}$ and the RMS of the coordinate time series has been computed, then the noise amplitude for any given κ can be estimated using Eq. H.13.

Velocity Uncertainty

The equations describing the effect of power–law noise on the station velocity uncertainties were originally derived in Zhang et al. (1997). For classical white noise ($\kappa = 0$), it can be shown for n equally spaced data such that $t_i = (i-1)\Delta T$ and $T = (n-1)\Delta T$ with T being the total observation span in years and ΔT the interval, that the velocity uncertainty $\sigma^2_{\hat{r}}$ can be computed from

$$\sigma^2_{\hat{r}} = \frac{a^2}{\Delta T^2}\frac{12}{n^3 - n} = \frac{a^2}{T^2}\frac{12(n-1)}{n(n+1)}; \quad n \geq 2 \tag{H.15}$$

For large n, Eq. H.15 can be further reduced to

$$\sigma^2_{\hat{r}} = \frac{12a^2}{nT^2} \tag{H.16}$$

For flicker noise ($\kappa = -1$), the equation for the velocity uncertainty $\sigma^2_{\hat{r}}$ can be calculated following (Zhang et al., 1997) as

$$\sigma^2_{\hat{r}} \approx \frac{9b^2_{-1}}{16\Delta T^2(n^2-1)} \tag{H.17}$$

and for random walk noise ($\kappa = -2$), the velocity uncertainty $\sigma^2_{\hat{r}}$ can be evaluated from

$$\sigma^2_{\hat{r}} = \frac{b^2_{-2}}{(n-1)\Delta T} = \frac{b^2_{-2}}{T}; \quad n \geq 2 \tag{H.18}$$

From these it can be seen that $\sigma^2_{\hat{r}} \propto 1/n^3$ for white noise, $\sigma^2_{\hat{r}} \propto 1/n^2$ for flicker noise and $\sigma^2_{\hat{r}} \propto 1/n$ for random walk noise. Thus, the assumed combination of noise greatly affects the resulting velocity uncertainty (Williams, 2003a).

With a, b_{-1} and b_{-2} being the white, flicker and random walk noise amplitudes respectively, g being the number of observations in one year, T the total time span in years,

Mao et al. (1999) presented Eq. H.16, H.17 and H.18 in slightly altered but equivalent form:

$$\sigma_{\hat{r}}^2 \cong \frac{12a^2}{gT^3} \tag{H.19}$$

$$\sigma_{\hat{r}}^2 \cong \frac{1.78b_{-1}^2}{g^{0.22}T^2} \tag{H.20}$$

$$\sigma_{\hat{r}}^2 \cong \frac{b_{-2}^2}{gT} \tag{H.21}$$

For the case of non–integer coloured noise ($-3 \leq \kappa \leq 0$), Williams (2003a) derived a general formula for the variance of the station velocity $\sigma_{\hat{r}}^2$ such that

$$\sigma_{\hat{r}}^2 \approx b_\kappa^2 \alpha \Delta T^\beta n^\gamma \tag{H.22}$$

where

$$\beta = -\frac{\kappa}{2} - 2 \qquad \gamma \approx -3 - \kappa \tag{H.23}$$

and α is a polynomial of degree N such that

$$\alpha = P(1)\kappa^N + P(2)\kappa^{N-1} + \ldots + P(N)\kappa + P(N+1) \tag{H.24}$$

where the $N+1$ coefficients have been determined as

$$P = \begin{bmatrix} -0.0237 \\ -0.3881 \\ -2.6610 \\ -9.8529 \\ -21.0922 \\ -25.1638 \\ -11.4275 \\ 10.7839 \\ 20.3377 \\ 11.9942 \end{bmatrix}. \tag{H.25}$$

Furthermore, Williams (2003a) gives a corrected form for γ if κ is close to -1 or < -2.0, the γ in Eq. H.23 must be replaced by

$$\gamma \approx -3 - \kappa + 7.7435e^{-10}\kappa^{17} - \frac{0.0144}{0.27\sqrt{2\pi}} \exp\left[-\frac{1}{2}\left(\frac{\kappa + 1.025}{0.27}\right)^2\right]. \tag{H.26}$$

This ensures that the simple approximation of γ in Eq. H.23 is within 5% of the true value for $n >> 100$ for all κ.

Appendix I

Adaptive Filtering using the Least–Mean–Squares (LMS) Algorithm

This appendix introduces the reader to the basic theory of adaptive filtering. A detailed introduction can be found in, e.g. Farhang-Boroujeny (1999) or Haykin (2002). For a more application oriented approach, literature by Embree (1995) and Ingle and Proakis (2000) are recommended.

The most widely used adaptive filtering algorithm in practice is the least–mean–squares (LMS) algorithm which was first proposed in the 1960s (Farhang-Boroujeny, 1999). Its wide spectrum of applications from such diverse fields as speech analysis, seismic, acoustic and radar signal processing can be attributed to its simplicity and robustness to signal statistics. The adaptive filter basically involves two processes: a filtering process to produce an impulse response, e.g. using a linear transversal filter, and an adaptive process for the control of the adjustable parameters used in the filtering process (Ge et al., 2000).

The structure of the linear transversal filter is shown in Figure I.1. It involves a combination of three basic operations: storage, multiplication, and addition (Haykin, 2002).

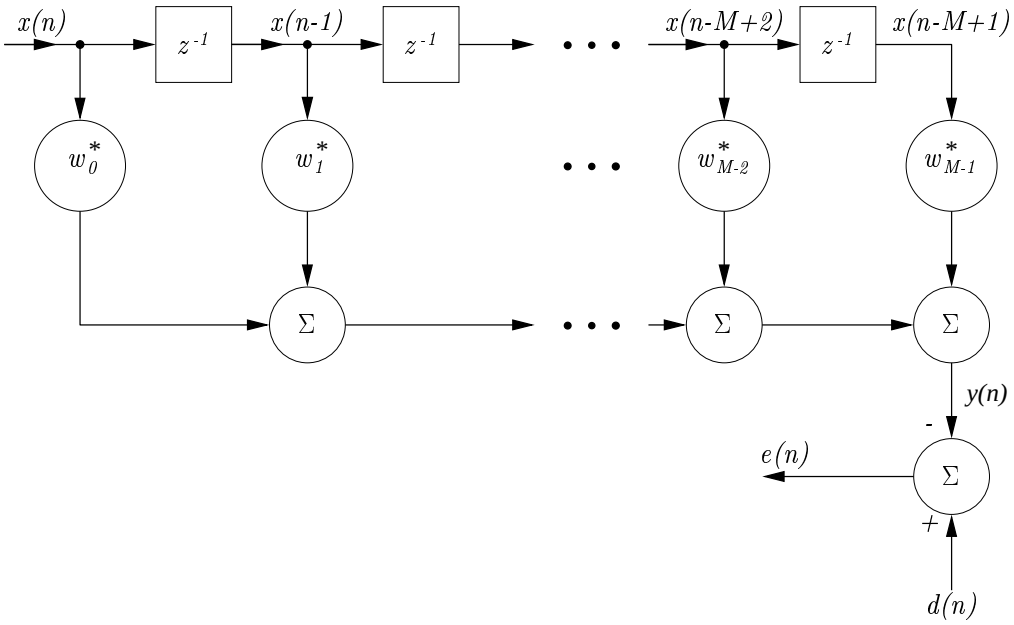

Figure I.1: Structure of the linear transversal filter (Haykin, 2002).

- $M-1$ one–sample delays shown as blocks and labeled as z^{-1} carry out the storage. The points at which these one–sample delays are accessed are termed tap points. The tap inputs are denoted by $x(n), x(n-1), \ldots, x(n-M+1)$. Thus, with $x(n)$ viewed as current input value to the filter, the remaining $M-1$ tap inputs, $x(n-1), \ldots, x(n-M+1)$ represent past values of the input sequence $\{x(n)\}$.

- The scalar inner products of tap inputs $x(n), x(n-1), \ldots, x(n-M+1)$ and the tap weights $w_0, w_1, \ldots, w_{M-1}$, respectively, are formed by using a corresponding set of multipliers. The circles labeled $w_0^*, \ldots, w_{M-1}^*$ represent the inner products of the multiplication process.

- The addition is carried out at the adders in order to produce the output sequence $\{y(n)\}$ for the filter. By subtracting the filtered sequence $\{y(n)\}$ from the desired sequence $\{d(n)\}$ at the last adder, the error sequence $\{e(n)\}$ is produced.

Hence, the impulse response of the transversal filter (as shown in Figure I.1) is defined by the finite set of tap weights $w_0, \ldots, w_{M-1}$, with M denoted as the *filterlength*. Using the LMS algorithm, it is these tap weights or *filter coefficients* that are constantly adjusted to

changes of the input sequences $\{x(n)\}$ and $\{d(n)\}$. The structure of the linear transversal filter can therefore be described as (Ingle and Proakis, 2000)

$$y(n) = \sum_{k=0}^{M-1} w(k)x(n-k), \quad n = 0, \ldots, N \tag{I.1}$$

with N being the number of samples. The filter output sequence $\{y(n)\}$ can then be compared to the desired sequence $\{d(n)\}$, and the error sequence $\{e(n)\}$ can be formed by taking the difference between $d(n)$ and $y(n)$ so that

$$e(n) = d(n) - y(n), \quad n = 0, \ldots, N \tag{I.2}$$

By recursively updating the filter tap weights $w(0), \ldots, w(M-1)$, the error sequence $\{e(n)\}$ can be minimized by minimizing the sum of the squared errors. Thus we have for the mean–squared error or MSE ($\mathcal{E}$)

$$\begin{aligned} \mathcal{E} &= \sum_{n=0}^{N} e^2(n) = \sum_{n=0}^{N} \left[d(n) - \sum_{k=0}^{M-1} w(k)x(n-k) \right]^2 \\ &= \sum_{n=0}^{N} d^2(n) - 2\sum_{k=0}^{M-1} w(k)r_{dx}(k) + \sum_{k=0}^{M-1}\sum_{l=0}^{M-1} w(k)w(l)r_{xx}(k-l) \end{aligned} \tag{I.3}$$

where by definition (Ingle and Proakis, 2000),

$$r_{dx}(k) = \sum_{n=0}^{N} d(n)x(n-k), \quad 0 \le k \le M-1 \tag{I.4}$$

$$r_{xx}(k) = \sum_{n=0}^{N} x(n)x(n+k), \quad 0 \le k \le M-1 \tag{I.5}$$

with $\{r_{dx}(k)\}$ being the cross–correlation sequence between the desired sequence $\{d(n)\}$ and the reference sequence $\{x(n)\}$ and $\{r_{xx}(k)\}$ being the auto–correlation sequence of $\{x(n)\}$.

The MSE ($\mathcal{E}$) is a quadratic function of the filter coefficients and its minimization can therefore be achieved by differentiating $\mathcal{E}$ with respect to each of the filter coefficients $\{w_k\}$ and setting the partial derivates equal to 0. Thus (Ingle and Proakis, 2000)

$$\frac{\partial \mathcal{E}}{\partial w(m)} = 0, \quad 0 \le m \le M-1 \tag{I.6}$$

and, hence

$$\sum_{k=0}^{M-1} w(k)r_{xx}(k-m) = r_{dx}(m), \quad 0 \le m \le M-1 \tag{I.7}$$

Equation I.7 specifies the set of linear equations used to derive the optimal filter coefficients. By computing the auto–correlation sequence $\{r_{xx}(k)\}$ of the reference signal and the cross–correlation sequence $\{r_{dx}(k)\}$ between the desired and reference sequences $\{d(n)\}$ and $\{x(n)\}$ respectively, the linear equations of Eq. I.7 can be solved directly.

The LMS algorithm however, does not solve this set of linear equations to compute the optimal filter coefficient explicitly. It finds the minimum $\mathcal{E}$ and thus yields the set of optimum filter coefficients using a recursive gradient method, which is also called *steepest descent method* (Ingle and Proakis, 2000). Hence, the LMS algorithm updates the filter coefficients after the arrival of each input sample $x(n)$ and the computation of the error sample $e(n) = d(n) - y(n)$ using

$$w_n(k) = w_{n-1}(k) + \mu e(n)x(n-k), \quad 0 \leq k \leq M-1 \text{ and } 0 \leq n \leq N-1 \tag{I.8}$$

where μ is the *step size parameter*. $x(n-k)$ on the right hand side of the equation, is the sample of the input sequence located at the kth element of the filter coefficient vector at time n and $e(n)x(n-k)$ is an estimate of the negative of the gradient for the kth filter coefficient. The complete second term, $\mu e(n)x(n-k)$ on the right hand side of Eq. I.8 represents the correction that is applied to the current estimate of the filter coefficients $w_{n-1}(k)$.

When the sequences of $\{x(n)\}$ and $\{d(n)\}$ are jointly stationary, the LMS algorithm converges to an optimum set of filter coefficients as in Eq. I.7. The rate of convergence is controlled by the step size parameter μ and hence needs to be selected appropriately. If it is too small, the filter coefficients will adapt only very slowly and might not react to changes of the input signals. If μ is chosen too large, the system will adapt to noise in the signals and may not converge to the optimal solution (e.g. Haykin, 2002; Ingle and Proakis, 2000; Dodson et al., 2001a). A commonly used range for μ to be stable can be specified as (Ge et al., 2000)

$$0 < \mu < \frac{1}{10MP_x} \tag{I.9}$$

where P_x is the power of the reference sequence $\{x(n)\}$, which can be approximated by

$$P_x \approx \frac{1}{N+1}\sum_{n=0}^{N-1} x^2(n) = \frac{r_{xx}(0)}{N+1} \tag{I.10}$$

with $r_{xx}(0)$ being the auto–correlation function for the reference sequence at zero lag.

A method to describe the convergence of the LMS algorithm is to require that the MSE is a constant (Haykin, 2002)

$$\mathcal{E}(n) = E[|e(n)|^2] \rightarrow \text{constant as } n \rightarrow \infty \tag{I.11}$$

where $|e(n)|$ and $\mathcal{E}(n)$ are the absolute value of the estimation error and the MSE at iteration n. The evolution of $\mathcal{E}(n)$ can be plotted against n and is termed the *learning curve* of the LMS algorithm. Hence, the learning curve can be used as an independent way to monitor the stability of the algorithm.

When the representation of a stochastic process by a linear model is used in analysis, the parameters of the model are estimated by processing a given sequence of finite length. Unless some prior information is assumed, the estimation procedure should include a criterion for selecting the model order, i.e. the filterlength M. Using the adaptive filter, M should be chosen so that the filter best models features of a set of input sequences. The adoption of a larger than necessary M, will lead to *over–filtering* of the input sequences and important features may be lost. The *minimum description length (MDL)* described by Rissanen (1978) stated that the best statistical model for a given data set is the one that provides the shortest description length for the data (Haykin, 2002). In mathematical terms, this model is defined by

$$\mathbf{MDL}(M) = -L(\hat{\theta}_M) + \frac{1}{2} M \ln N \tag{I.12}$$

where $L(\hat{\theta}_M)$ is the logarithm of the maximum likelihood estimates of the filter parameters and N the sample size of the input sequence. The first term in this equation tends to decrease rapidly with increasing M, while the second term increases linearly with increasing M. Therefore, there is a value of M which minimizes the MDL and the optimum filterlength can be obtained (Haykin, 2002; Ge et al., 2000).

Appendix J

Standard Coordinate Time Series Results

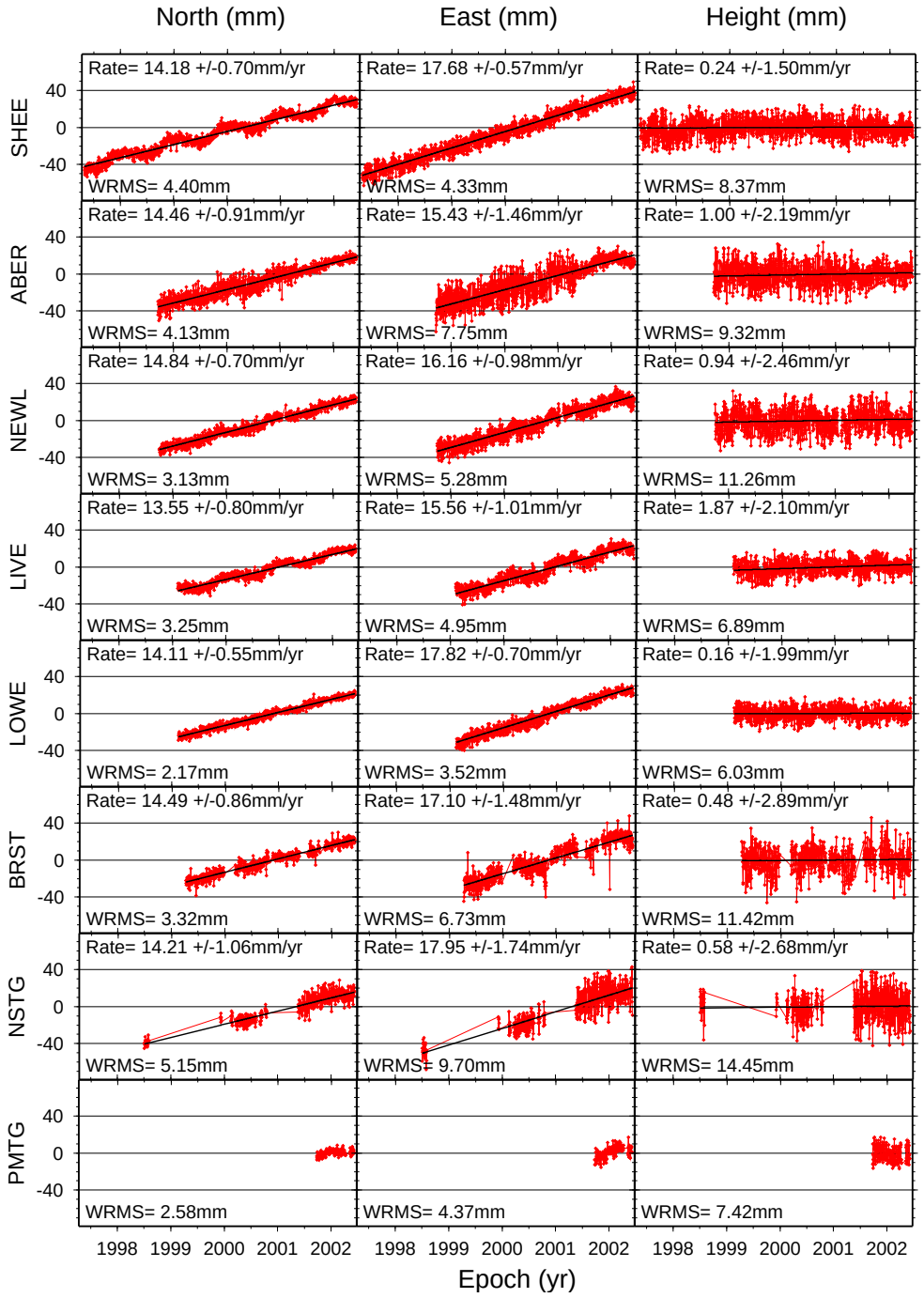

Figure J.1: Standard ITRS97 coordinate time series for CGPS@TG stations, based on Strategy 2 and using data up to 31 May 2002.

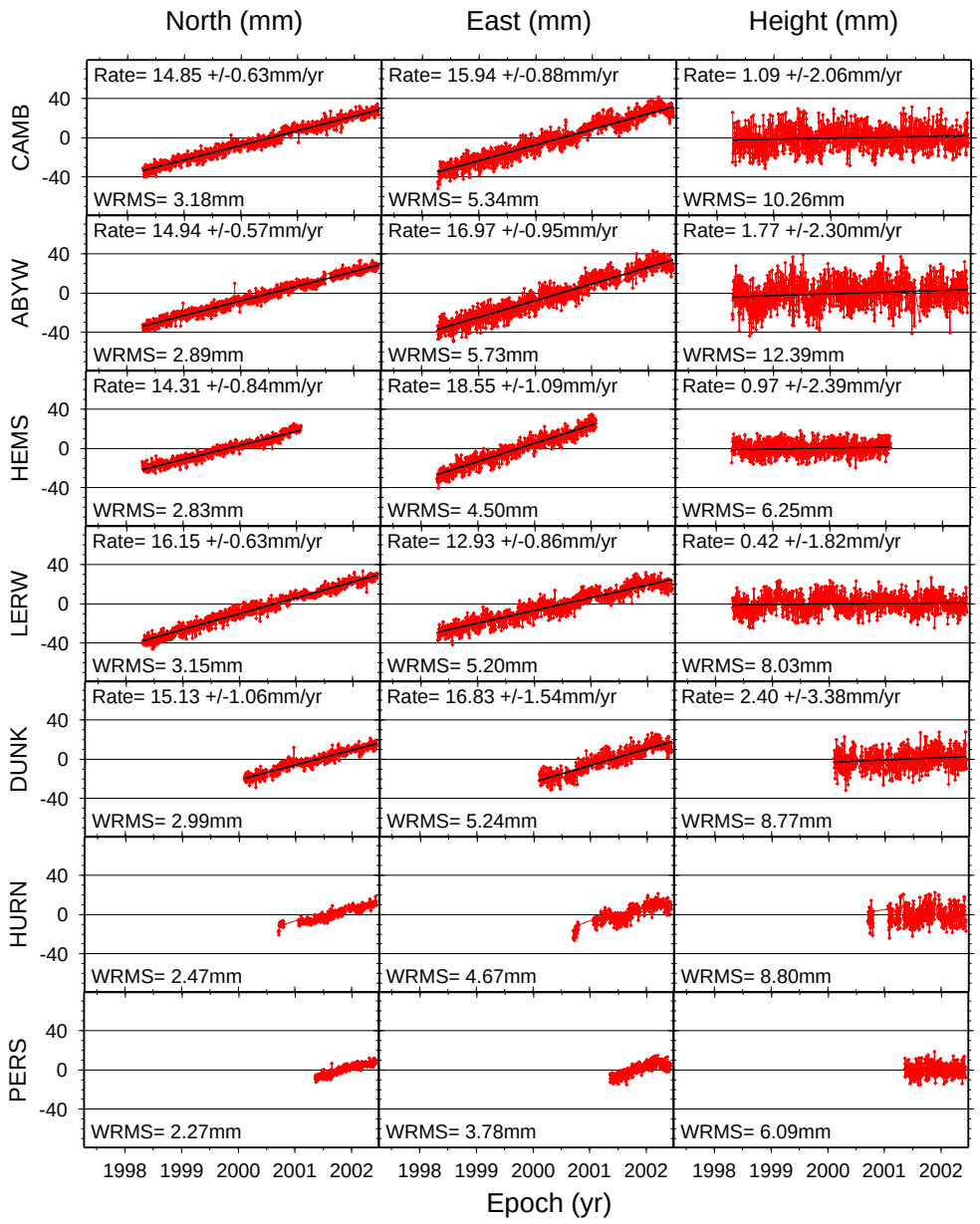

Figure J.2: Standard ITRS97 coordinate time series for the UK Met Office CGPS stations, based on Strategy 2 and using data up to 31 May 2002.

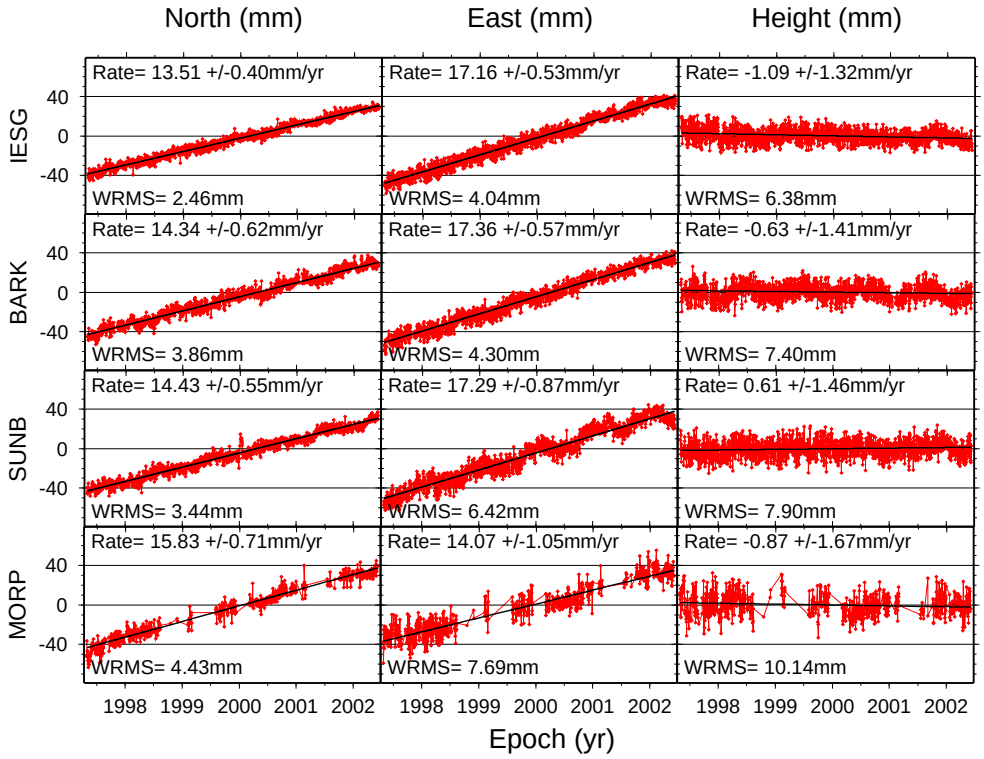

Figure J.3: Standard ITRS97 coordinate time series for CGPS stations belonging to category *OTHER*, based on Strategy 2 and using data up to 31 May 2002.

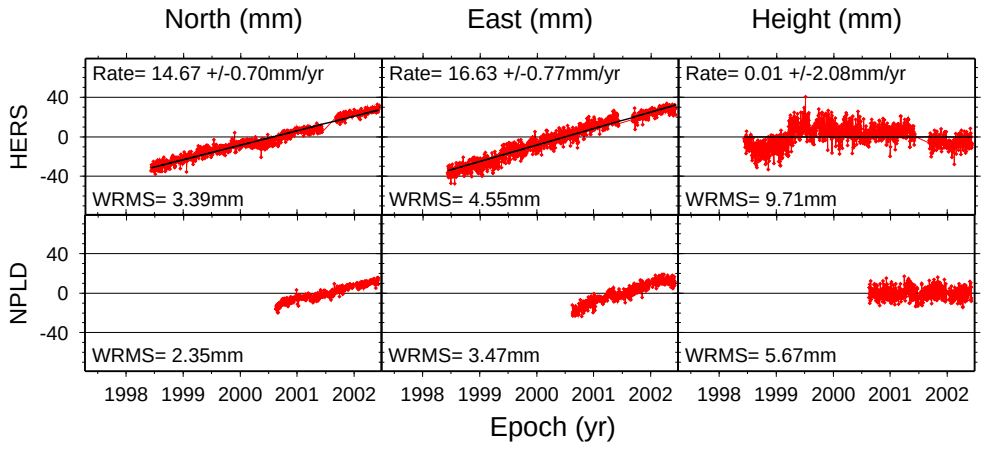

Figure J.4: Standard ITRS97 coordinate time series for the UK based IGS stations, based on Strategy 2 and using data up to 31 May 2002.

Table J.1: Summary of the standard ITRS97 coordinate time series results, based on Strategy 2 and using data up to 31 May 2002.

Site	North Component		East Component		Height Component	
	WRMS [mm]	Velocity [mm/yr]	WRMS [mm]	Velocity [mm/yr]	WRMS [mm]	Velocity [mm/yr]
			CGPS@TG Stations (TG)			
SHEE	4.40	14.18 ± 0.70	4.33	17.68 ± 0.57	8.37	0.24 ± 1.51
ABER	4.13	14.46 ± 0.91	7.75	15.43 ± 1.46	9.32	1.00 ± 2.19
BRST	3.32	14.49 ± 0.87	6.73	17.10 ± 1.48	11.42	0.48 ± 2.89
NEWL	3.13	14.84 ± 0.70	5.28	16.16 ± 0.98	11.26	0.94 ± 2.46
LIVE	3.25	13.55 ± 0.80	4.95	15.56 ± 1.02	6.89	1.87 ± 2.10
LOWE	2.17	14.11 ± 0.55	3.52	17.82 ± 0.71	6.03	0.16 ± 1.99
NSTG	5.15	14.21 ± 1.07	9.70	17.95 ± 1.74	14.45	0.58 ± 2.69
PMTG	2.58		4.37		7.42	
			UK Met Office CGPS Stations (MO)			
CAMB	3.18	14.85 ± 0.63	5.34	15.94 ± 0.88	10.26	1.09 ± 2.06
ABYW	2.89	14.94 ± 0.57	5.73	16.97 ± 0.95	12.39	1.77 ± 2.31
HEMS	2.83	14.31 ± 0.84	4.50	18.55 ± 1.09	6.25	0.97 ± 2.39
LERW	3.15	16.15 ± 0.63	5.20	12.93 ± 0.86	8.03	0.42 ± 1.82
DUNK	2.99	15.13 ± 1.06	5.24	16.83 ± 1.54	8.77	2.40 ± 3.39
HURN	2.47		4.67		8.80	
PERS	2.27		3.78		6.09	
			Environment Agency, IESSG and NCL CGPS Stations (OTHER)			
IESG	2.46	13.51 ± 0.40	4.04	17.16 ± 0.53	6.38	-1.09 ± 1.32
BARK	3.86	14.34 ± 0.62	4.30	17.36 ± 0.57	7.40	-0.63 ± 1.42
SUNB	3.44	14.43 ± 0.55	6.42	17.29 ± 0.87	7.90	0.61 ± 1.46
MORP	4.43	15.83 ± 0.71	7.69	14.07 ± 1.05	10.14	-0.87 ± 1.67
			UK based IGS Stations (IGS)			
HERS	3.39	14.67 ± 0.70	4.55	16.63 ± 0.77	9.71	0.01 ± 2.08
NPLD	2.35		3.47		5.67	
Mean:	3.23		5.31		8.71	

Table J.2: Comparison of the standard ITRS97 coordinate time series based on Strategies 1 and 2 compared and using data up to 25 September 2001. Station velocities have been obtained from a best fitting trend model. Velocity uncertainties account for coloured noise and have been estimated using Eqs. H.12, H.19 and H.20 (using a WN+FN model) in Appendix H.

Site	North Component		East Component		Height Component	
	WRMS [mm]	Velocity [mm/yr]	WRMS [mm]	Velocity [mm/yr]	WRMS [mm]	Velocity [mm/yr]
	Strategy 1 (Station constraints at the network processing stage)					
IESG	2.83	13.45 ± 0.53	4.90	18.42 ± 0.76	6.86	-3.37 ± 1.58
SHEE	4.76	14.04 ± 0.88	5.72	18.51 ± 0.89	10.16	-0.92 ± 1.93
LERW	3.46	15.31 ± 0.83	4.93	14.82 ± 0.98	8.87	-2.50 ± 2.31
HEMS	2.99	14.09 ± 0.88	5.46	19.06 ± 1.34	7.74	-0.65 ± 2.64
CAMB	3.05	15.13 ± 0.73	5.14	16.81 ± 1.01	8.88	-2.30 ± 2.29
ABER	4.97	13.80 ± 1.34	9.04	16.80 ± 2.11	9.87	-4.21 ± 2.78
NEWL	3.03	14.84 ± 0.84	4.65	16.95 ± 1.06	10.27	-3.34 ± 2.87
LIVE	3.55	13.35 ± 1.11	5.25	15.90 ± 1.37	8.18	-0.78 ± 2.88
LOWE	2.32	14.03 ± 0.74	3.87	18.05 ± 0.99	7.44	-2.65 ± 2.77
	Strategy 2 (No station constraints at the network processing stage)					
IESG	2.55	13.48 ± 0.48	4.19	17.34 ± 0.64	6.05	-1.28 ± 1.50
SHEE	4.60	13.94 ± 0.85	4.64	17.55 ± 0.71	8.94	0.69 ± 1.80
LERW	3.28	16.01 ± 0.78	5.10	12.78 ± 1.01	8.30	0.21 ± 2.23
HEMS	2.88	14.34 ± 0.85	4.71	18.72 ± 1.15	6.50	0.88 ± 2.44
CAMB	3.31	14.58 ± 0.79	5.58	16.02 ± 1.11	10.27	1.19 ± 2.48
ABER	4.80	13.95 ± 1.30	8.98	15.31 ± 2.09	10.83	-1.29 ± 2.93
NEWL	3.37	14.56 ± 0.93	5.61	16.38 ± 1.29	11.60	1.17 ± 3.08
LIVE	3.39	12.93 ± 1.06	5.23	15.01 ± 1.36	7.24	2.09 ± 2.71
LOWE	2.31	14.05 ± 0.74	4.02	17.92 ± 1.03	6.16	-0.09 ± 2.54
			Differences			
IESG	-0.28	0.03 ± 0.72	-0.71	-1.08 ± 0.99	-0.81	2.09 ± 2.18
SHEE	-0.16	-0.10 ± 1.22	-1.08	-0.96 ± 1.14	-1.22	1.61 ± 2.64
LERW	-0.18	0.70 ± 1.14	0.17	-2.04 ± 1.41	-0.57	2.71 ± 3.21
HEMS	-0.11	0.25 ± 1.22	-0.75	-0.34 ± 1.77	-1.24	1.53 ± 3.59
CAMB	0.26	-0.55 ± 1.08	0.44	-0.79 ± 1.50	1.39	3.49 ± 3.38
ABER	-0.17	0.15 ± 1.87	-0.06	-1.49 ± 2.97	0.96	2.92 ± 4.04
NEWL	0.34	-0.28 ± 1.25	0.96	-0.57 ± 1.67	1.33	4.51 ± 4.21
LIVE	-0.16	-0.42 ± 1.53	-0.02	-0.89 ± 1.93	-0.94	2.87 ± 3.95
LOWE	-0.01	0.02 ± 1.05	0.15	-0.13 ± 1.43	-1.28	2.56 ± 3.76

Table J.3: Annual term estimates and the theoretical and realistic velocity bias for the standard ITRS97 coordinate time series based on Strategy 1 and using data up to 25 September 2001.

Site	Timespan	North Component				East Component				Height Component			
	T	a[a]	ϕ [b]	$\hat{r}_{th}(T)$[c]	$\hat{r}_{re}(T)$[d]	a	ϕ	$\hat{r}_{th}(T)$	$\hat{r}_{re}(T)$	a	ϕ	$\hat{r}_{th}(T)$	$\hat{r}_{re}(T)$
	[years]	[mm]	[days]	[mm/yr]	[mm/yr]	[mm]	[days]	[mm/yr]	[mm/yr]	[mm]	[days]	[mm/yr]	[mm/yr]
IESG	4.41	1.5	113.9	−0.02	−0.10	0.3	14.0	0.01	0.00	3.7	113.9	−0.05	−0.26
SHEE	4.41	5.0	81.4	−0.01	−0.35	0.4	275.5	0.00	0.03	1.4	31.4	0.02	−0.04
LERW	3.44	2.8	98.8	−0.01	−0.33	1.3	65.1	0.01	−0.13	8.2	100.6	−0.05	−0.96
HEMS	2.80	1.2	107.5	−0.16	−0.28	0.8	73.2	−0.15	−0.23	5.0	79.1	−0.97	−1.52
CAMB	3.47	1.4	111.0	0.00	−0.15	1.9	42.4	0.00	−0.15	4.9	94.2	0.00	−0.57
ABER	3.02	3.0	86.6	−0.62	−1.20	1.0	125.0	−0.19	−0.39	6.2	108.1	−1.25	−2.55
NEWL	2.99	1.6	110.4	−0.32	−0.66	1.1	8.7	−0.04	−0.14	3.5	103.5	−0.72	−1.51
LIVE	2.64	3.8	74.4	−0.37	−0.95	3.9	23.8	−0.57	−0.74	6.3	100.0	−0.26	−1.34
LOWE	2.62	1.0	138.4	0.06	−0.09	1.0	352.9	−0.11	−0.04	6.0	104.1	−0.11	−1.20
Mean:	3.31	2.4	102.5	−0.16	−0.46	1.3	109.0	−0.12	−0.20	5.0	92.8	−0.38	−1.11
S.D.:	0.69	1.4	19.6	0.23	0.40	1.1	123.2	0.19	0.24	2.0	25.0	0.48	0.76

[a] Amplitude

[b] Phase shift

[c] Theoretical velocity bias (sine and cosine)

[d] Realistic velocity bias (Fourier Series)

Table J.4: Comparison of station velocity estimates for the standard ITRS97 coordinate time series based on Strategy 1, modelled using a linear and annual term, with those obtained from a linear term only model corrected for the effect of an annual cyclic variation.

Site	North Component					East Component					Height Component				
	Velocity	Corrected Velocity		Difference		Velocity	Corrected Velocity		Difference		Velocity	Corrected Velocity		Difference	
	r_m [mm/yr]	r'_{th} [mm/yr]	r'_{re} [mm/yr]	$\delta r'_{th}$ [mm/yr]	$\delta r'_{re}$ [mm/yr]	r_m [mm/yr]	r'_{th} [mm/yr]	r'_{re} [mm/yr]	$\delta r'_{th}$ [mm/yr]	$\delta r'_{re}$ [mm/yr]	r_m [mm/yr]	r'_{th} [mm/yr]	r'_{re} [mm/yr]	$\delta r'_{th}$ [mm/yr]	$\delta r'_{re}$ [mm/yr]
IESG	13.58	13.47	13.55	0.11	0.03	18.45	18.41	18.42	0.04	0.03	−3.11	−3.32	−3.11	0.21	0.00
SHEE	14.25	14.05	14.39	0.20	−0.14	18.50	18.51	18.48	−0.01	0.02	−0.88	−0.94	−0.88	0.06	0.00
LERW	15.48	15.32	15.64	0.16	−0.16	14.93	14.81	14.95	0.12	−0.02	−2.09	−2.45	−1.54	0.36	−0.55
HEMS	13.79	14.25	14.37	−0.46	−0.58	19.00	19.21	19.29	−0.21	−0.29	1.37	0.32	0.87	1.05	0.50
CAMB	15.18	15.13	15.28	0.05	−0.10	16.94	16.81	16.96	0.13	−0.02	−2.09	−2.30	−1.73	0.21	−0.36
ABER	14.59	14.42	15.00	0.17	−0.41	17.00	16.99	17.19	0.01	−0.19	−2.80	−2.96	−1.66	0.16	−1.14
NEWL	15.16	15.16	15.50	0.00	−0.34	17.03	16.99	17.09	0.04	−0.06	−2.66	−2.62	−1.83	−0.04	−0.83
LIVE	13.63	13.72	14.30	−0.09	−0.67	16.33	16.47	16.64	−0.14	−0.31	−0.52	−0.52	0.56	0.00	−1.08
LOWE	14.05	13.97	14.12	0.08	−0.07	18.14	18.16	18.09	−0.02	0.05	−2.31	−2.54	−1.45	0.23	−0.86
Mean:				0.02	−0.27				0.00	−0.09				0.25	−0.48
S.D.:				0.20	0.24				0.11	0.14				0.33	0.56

Appendix K

Noise Analysis Results

Table K.1: Spectral indices obtained from the MLE with fractional spectral indices and from the slope of the power spectra in the log–log space for the North, East and height components, for the unfiltered and filtered improved ITRS2000 coordinate time series.

Site	Spectral Indices from MLE analysis						Spectral Indices from PSD analysis					
	North		East		Height		North		East		Height	
	unflt	flt	unflt	flt	unflt	flt	unflt	flt	unflt	flt	unflt	flt
						CGPS@TG Stations (TG)						
SHEE	−0.5	−0.7	−0.4	−0.3	−0.3	−0.6	−0.2	−0.4	−0.4	−0.4	−0.3	−0.5
ABER	−0.1	−0.1	−0.2	−0.2	−0.3	−0.2	−0.1	−0.1	−0.5	−0.3	−0.3	−0.4
BRST	−0.5	−0.4	−0.6	−0.6	−0.8	−0.7	0.2	0.1	−0.2	−0.4	−0.3	−0.2
NEWL	−0.5	−0.5	−0.6	−0.7	−0.9	−0.9	−0.2	−0.2	−0.6	−0.3	−0.6	−0.5
LIVE	−0.4	−0.3	−1.2	−0.7	−0.9	−0.5	−0.3	−0.4	−0.8	−0.6	−0.7	−0.4
LOWE	−0.3	−0.5	−1.3	−0.6	−0.4	−0.7	−0.4	−0.5	−0.6	−0.5	−0.5	−0.9
NSTG	−1.0	0.0	−0.6	−1.8	0.0	−0.1	0.0	0.0	0.1	0.1	0.2	0.1
						UK Met Office CGPS Stations (MO)						
CAMB	−0.4	−0.4	−0.5	−0.6	−0.8	−0.8	−0.3	−0.2	−0.6	−0.5	−0.4	−0.2
ABYW	−0.4	−0.4	−0.4	−0.3	−0.6	−0.5	−0.1	0.1	−0.5	−0.4	−0.4	−0.5
HEMS	−0.7	−0.7	−0.6	−0.4	−0.2	−0.5	−0.5	−0.7	−0.5	−0.4	−0.4	−0.2
LERW	−0.7	−0.4	−0.9	−1.1	−0.5	−0.6	−0.6	−0.2	−0.5	−0.7	−0.6	−0.6
DUNK	−0.6	−0.5	−0.6	−0.5	−0.8	−0.6	−0.6	0.0	−0.5	−0.3	−0.2	−0.2
						Environment Agency, IESSG and NCL CGPS Stations (OTHER)						
IESG	−0.3	−0.5	−1.1	−0.5	−0.9	−0.5	−0.4	−0.6	−0.6	−0.6	−0.8	−0.5
BARK	−0.8	−0.9	−0.5	−0.6	−0.3	−0.3	−0.4	−0.3	−0.4	−0.4	−0.2	−0.2
SUNB	−0.7	−0.8	−0.6	−0.7	−0.4	−0.7	−0.4	−0.5	−0.7	−0.7	−0.4	−0.4
MORP	−0.9	−0.9	−0.9	−0.7	−0.7	−0.5	−0.6	−0.6	−0.5	−0.4	−0.5	−0.3
						UK based IGS Stations (IGS)						
HERS	−0.9	−0.6	−0.8	−0.6	−0.6	−0.6	−0.3	−0.2	−0.2	−0.1	−0.2	−0.5

Table K.2: Log–likelihood tests for the four noise models: white noise only (WN), white plus flicker noise (WN+FN), white plus random walk noise (WN+RWN) and white plus power–law noise (WN+PLN). Λ–statistic computed with respect to white noise only model. MLE was applied to unfiltered improved ITRS2000 coordinate time series with time spans > 2.5 years.

Site	Component	Log–Likelihood				Λ–Statistic		
		WN	WN+FN	WN+RWN	WN+PLN	WN+FN	WN+RWN (versus WN)	WN+PLN
				CGPS@TG Stations (TG)				
SHEE	North	7526.96	7609.83	7566.00	7621.75	0.00	0.00	0.00
SHEE	East	6796.17	6855.11	6833.91	6861.08	0.00	0.00	0.00
SHEE	Height	5760.79	5787.73	5769.98	5798.29	0.00	0.00	0.00
ABER	North	4730.78	4731.86	4730.78	4735.70	0.34	1.00	0.01
ABER	East	4036.99	4049.70	4045.83	4052.40	0.00	0.00	0.00
ABER	Height	3885.39	3895.91	3887.82	3903.68	0.00	0.09	0.00
BRST	North	3721.06	3743.16	3722.41	3756.27	0.00	0.26	0.00
BRST	East	3163.62	3219.71	3204.05	3222.54	0.00	0.00	0.00
BRST	Height	2645.61	2728.53	2685.18	2732.85	0.00	0.00	0.00
NEWL	North	5614.05	5681.47	5640.96	5694.06	0.00	0.00	0.00
NEWL	East	4924.22	5041.26	4997.97	5048.90	0.00	0.00	0.00
NEWL	Height	3925.76	4124.53	4064.52	4127.15	0.00	0.00	0.00
LIVE	North	5389.24	5422.71	5407.78	5427.88	0.00	0.00	0.00
LIVE	East	4791.73	4861.82	4858.74	4862.38	0.00	0.00	0.00
LIVE	Height	4214.44	4273.05	4266.33	4273.13	0.00	0.00	0.00
LOWE	North	5522.18	5539.28	5526.70	5545.81	0.00	0.01	0.00
LOWE	East	4919.13	4977.55	4976.56	4978.46	0.00	0.00	0.00
LOWE	Height	4295.58	4337.46	4324.03	4340.91	0.00	0.00	0.00
NSTG	North	2099.61	2099.61	2099.61	2099.61	1.00	1.00	1.00
NSTG	East	1766.47	1766.47	1766.47	1766.47	1.00	1.00	1.00
NSTG	Height	1528.32	1528.32	1528.32	1544.02	1.00	1.00	0.00
				UK Met Office CGPS Stations (MO)				
CAMB	North	6358.65	6404.56	6372.88	6420.43	0.00	0.00	0.00
CAMB	East	5589.86	5692.72	5652.69	5703.99	0.00	0.00	0.00
CAMB	Height	4602.19	4748.29	4632.78	4756.13	0.00	0.00	0.00
ABYW	North	6335.60	6361.11	6336.25	6375.34	0.00	0.52	0.00
ABYW	East	5361.03	5417.31	5394.71	5427.73	0.00	0.00	0.00
ABYW	Height	4291.17	4388.81	4337.28	4402.65	0.00	0.00	0.00
HEMS	North	4390.57	4480.85	4462.77	4482.25	0.00	0.00	0.00
HEMS	East	3942.58	3972.63	3962.91	3974.17	0.00	0.00	0.00
HEMS	Height	3612.62	3616.98	3612.89	3622.96	0.01	0.76	0.00
LERW	North	6193.07	6269.22	6254.54	6271.21	0.00	0.00	0.00
LERW	East	5647.55	5741.47	5728.37	5741.81	0.00	0.00	0.00

continued on next page

continued from previous page

Site	Component	Log–Likelihood				Λ–Statistic		
		WN	WN+FN	WN+RWN	WN+PLN	WN+FN	WN+RWN (versus WN)	WN+PLN
LERW	Height	4994.21	5073.51	5048.88	5080.02	0.00	0.00	0.00
DUNK	North	3352.01	3408.83	3376.95	3415.31	0.00	0.00	0.00
DUNK	East	2991.99	3057.10	3028.10	3062.46	0.00	0.00	0.00
DUNK	Height	2524.84	2597.06	2527.39	2600.00	0.00	0.08	0.00
		Environment Agency, IESSG and NCL CGPS Stations (OTHER)						
IESG	North	8196.17	8225.71	8204.59	8233.61	0.00	0.00	0.00
IESG	East	7301.50	7367.47	7361.55	7367.55	0.00	0.00	0.00
IESG	Height	6514.94	6605.31	6592.27	6605.46	0.00	0.00	0.00
BARK	North	6764.08	6977.70	6911.33	6985.79	0.00	0.00	0.00
BARK	East	6510.31	6559.61	6540.75	6563.28	0.00	0.00	0.00
BARK	Height	5789.38	5808.80	5795.71	5816.44	0.00	0.00	0.00
SUNB	North	7435.34	7627.13	7581.67	7631.93	0.00	0.00	0.00
SUNB	East	6540.84	6700.15	6666.09	6704.75	0.00	0.00	0.00
SUNB	Height	5950.04	6008.56	5989.58	6015.40	0.00	0.00	0.00
MORP	North	3196.08	3240.90	3230.30	3240.98	0.00	0.00	0.00
MORP	East	2780.74	2829.05	2819.80	2829.13	0.00	0.00	0.00
MORP	Height	2553.49	2608.62	2595.93	2609.36	0.00	0.00	0.00
		UK based IGS Stations (IGS)						
HERS	North	5872.83	5989.20	5978.67	5989.30	0.00	0.00	0.00
HERS	East	5343.35	5404.93	5394.22	5405.28	0.00	0.00	0.00
HERS	Height	4658.27	4723.52	4706.50	4726.19	0.00	0.00	0.00

Table K.3: Log–likelihood tests for the four noise models: white noise only (WN), white plus flicker noise (WN+FN), white plus random walk noise (WN+RWN) and white plus power–law noise (WN+PLN). Λ–statistic computed with respect to white noise only model. MLE was applied to filtered improved ITRS2000 coordinate time series with time spans > 2.5 years.

Site	Component	Log–Likelihood				Λ–Statistic		
		WN	WN+FN	WN+RWN	WN+PLN	WN+FN	WN+RWN (versus WN)	WN+PLN
				CGPS@TG Stations (TG)				
SHEE	North	7855.42	8040.68	7991.71	8047.45	0.00	0.00	0.00
SHEE	East	7719.16	7751.53	7738.34	7761.63	0.00	0.00	0.00
SHEE	Height	6327.59	6362.98	6352.59	6364.46	0.00	0.00	0.00
ABER	North	4768.39	4768.39	4768.39	4769.18	1.00	1.00	0.45
ABER	East	4132.06	4140.03	4134.98	4144.36	0.00	0.05	0.00
ABER	Height	4042.64	4045.55	4044.38	4046.37	0.05	0.18	0.02
BRST	North	3908.35	3917.68	3908.48	3931.82	0.00	0.88	0.00
BRST	East	3263.11	3331.61	3310.78	3334.23	0.00	0.00	0.00
BRST	Height	2764.66	2839.40	2780.55	2844.95	0.00	0.00	0.00
NEWL	North	6099.87	6160.01	6118.50	6173.76	0.00	0.00	0.00
NEWL	East	5451.68	5600.20	5541.61	5608.04	0.00	0.00	0.00
NEWL	Height	4298.39	4509.73	4450.69	4512.19	0.00	0.00	0.00
LIVE	North	5736.11	5754.85	5746.18	5757.91	0.00	0.00	0.00
LIVE	East	5328.45	5356.60	5348.76	5357.17	0.00	0.00	0.00
LIVE	Height	4586.94	4640.76	4626.88	4645.93	0.00	0.00	0.00
LOWE	North	5898.45	5946.88	5922.59	5955.34	0.00	0.00	0.00
LOWE	East	5442.71	5528.07	5486.72	5536.05	0.00	0.00	0.00
LOWE	Height	4396.52	4546.66	4499.02	4552.54	0.00	0.00	0.00
NSTG	North	2120.15	2120.15	2120.15	2135.95	1.00	1.00	0.00
NSTG	East	1775.67	1775.67	1775.67	1775.67	1.00	1.00	1.00
NSTG	Height	1530.74	1530.74	1530.74	1532.51	1.00	1.00	0.17
				UK Met Office CGPS Stations (MO)				
CAMB	North	6904.41	6922.99	6904.96	6941.78	0.00	0.58	0.00
CAMB	East	6247.60	6331.44	6270.50	6348.38	0.00	0.00	0.00
CAMB	Height	5145.17	5311.37	5240.23	5317.14	0.00	0.00	0.00
ABYW	North	6707.12	6747.77	6722.36	6760.01	0.00	0.00	0.00
ABYW	East	5765.37	5781.96	5768.72	5799.33	0.00	0.03	0.00
ABYW	Height	4605.54	4667.81	4643.25	4681.58	0.00	0.00	0.00
HEMS	North	4781.65	4930.26	4905.01	4932.70	0.00	0.00	0.00
HEMS	East	4601.10	4632.89	4616.14	4643.20	0.00	0.00	0.00
HEMS	Height	3889.82	3921.16	3889.82	3934.07	0.00	1.00	0.00
LERW	North	6426.64	6494.10	6478.49	6503.20	0.00	0.00	0.00
LERW	East	5992.11	6117.52	6106.70	6117.57	0.00	0.00	0.00
LERW	Height	5304.98	5370.49	5354.25	5372.57	0.00	0.00	0.00

continued on next page

continued from previous page

Site	Component	Log–Likelihood				Λ–Statistic		
		WN	WN+FN	WN+RWN	WN+PLN	WN+FN	WN+RWN (versus WN)	WN+PLN
DUNK	North	3632.89	3657.83	3633.00	3667.68	0.00	0.90	0.00
DUNK	East	3218.61	3247.77	3220.99	3256.45	0.00	0.09	0.00
DUNK	Height	2844.05	2879.73	2844.40	2888.36	0.00	0.71	0.00
		Environment Agency, IESSG and NCL CGPS Stations (OTHER)						
IESG	North	8807.57	8871.69	8850.98	8875.45	0.00	0.00	0.00
IESG	East	8290.58	8369.70	8351.37	8376.42	0.00	0.00	0.00
IESG	Height	7147.19	7243.67	7211.85	7251.03	0.00	0.00	0.00
BARK	North	7192.08	7517.37	7436.48	7518.13	0.00	0.00	0.00
BARK	East	7312.14	7431.03	7383.75	7440.90	0.00	0.00	0.00
BARK	Height	6241.27	6267.32	6254.36	6275.59	0.00	0.00	0.00
SUNB	North	8101.14	8379.36	8328.78	8382.17	0.00	0.00	0.00
SUNB	East	7121.81	7346.42	7307.22	7348.74	0.00	0.00	0.00
SUNB	Height	6524.65	6612.63	6590.91	6615.04	0.00	0.00	0.00
MORP	North	3154.73	3210.29	3198.28	3210.42	0.00	0.00	0.00
MORP	East	2835.40	2864.37	2856.63	2865.24	0.00	0.00	0.00
MORP	Height	2580.61	2638.36	2619.35	2641.31	0.00	0.00	0.00
		UK based IGS Stations (IGS)						
HERS	North	6317.26	6441.27	6413.91	6446.78	0.00	0.00	0.00
HERS	East	5995.55	6097.19	6061.80	6101.99	0.00	0.00	0.00
HERS	Height	4995.25	5105.33	5080.31	5108.97	0.00	0.00	0.00

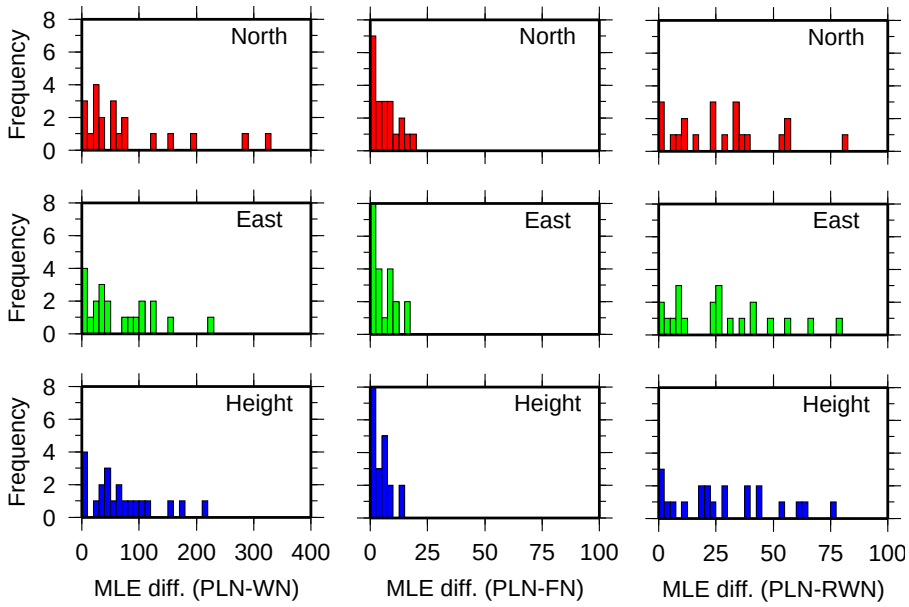

Figure K.1: Distribution of the differences of the maximum log–likelihood values (MLE diff.) for the white plus power-law minus the white noise only (PLN-WN), the white plus power–law minus white plus flicker noise (PLN-FN) and the white plus power–law minus the white plus random walk noise (PLN-RWN) models for the coordinate components of the filtered improved ITRS2000 coordinate time series. Mind the different scale for the PLN-WH MLE differences.

Table K.4: Noise amplitudes from the MLE with white plus power–law noise (WN+PLN) and white plus flicker noise (WN+FN) models for the unfiltered improved ITRS2000 coordinate time series. a denotes the white and b the coloured noise amplitudes.

Site	MLE with fractional spectral indices (WN+PLN)						MLE with integer spectral indices (WN+FN)					
	North Component		East Component		Height Component		North Component		East Component		Height Component	
	a [mm]	b [mm]	a [mm]	b [mm]	a [mm]	b [mm]	a [mm]	b [mm]	a [mm]	b [mm]	a [mm]	b [mm]
						CGPS@TG Stations (TG)						
SHEE	0.0 ± 0.0	6.0 ± 0.1	2.3 ± 0.4	7.4 ± 0.5	0.0 ± 0.0	13.2 ± 0.2	2.2 ± 0.1	7.5 ± 0.5	4.0 ± 0.1	7.8 ± 0.8	7.6 ± 0.2	13.2 ± 1.6
ABER	0.0 ± 0.0	6.3 ± 0.1	0.0 ± 0.0	12.5 ± 0.3	0.0 ± 0.0	14.9 ± 0.3	5.1 ± 0.1	3.0 ± 1.2	8.6 ± 0.2	8.8 ± 1.7	9.5 ± 0.3	12.5 ± 2.4
BRST	0.0 ± 0.0	6.7 ± 0.2	2.6 ± 0.9	12.8 ± 1.0	0.0 ± 0.0	34.1 ± 0.8	2.6 ± 0.2	8.9 ± 1.1	4.9 ± 0.3	15.1 ± 1.6	3.4 ± 1.3	44.3 ± 2.6
NEWL	0.0 ± 0.0	6.1 ± 0.1	0.0 ± 0.0	11.4 ± 0.2	0.0 ± 0.0	35.1 ± 0.7	2.1 ± 0.1	7.9 ± 0.6	3.2 ± 0.2	14.3 ± 1.0	0.0 ± 0.0	42.1 ± 0.8
LIVE	0.0 ± 0.0	4.2 ± 0.1	3.6 ± 0.1	7.2 ± 0.8	5.6 ± 0.2	11.0 ± 1.1	2.2 ± 0.1	4.5 ± 0.5	3.5 ± 0.1	6.9 ± 0.7	5.8 ± 0.2	11.1 ± 1.2
LOWE	0.0 ± 0.0	3.2 ± 0.1	3.2 ± 0.1	4.9 ± 0.7	2.7 ± 0.8	9.9 ± 0.9	1.9 ± 0.1	3.1 ± 0.5	3.1 ± 0.1	4.9 ± 0.6	5.1 ± 0.2	10.6 ± 1.2
NSTG	5.1 ± 0.2	0.0 ± 0.0	9.5 ± 0.3	0.0 ± 0.0	0.0 ± 0.0	14.2 ± 0.4	5.1 ± 0.1	0.0 ± 0.0	9.5 ± 0.3	0.0 ± 2.4	14.7 ± 0.4	0.0 ± 0.0
						UK Met Office CGPS Stations (MO)						
CAMB	0.0 ± 0.0	5.8 ± 0.1	0.0 ± 0.0	11.0 ± 0.2	0.0 ± 0.0	29.2 ± 0.5	2.4 ± 0.1	7.0 ± 0.7	3.5 ± 0.2	14.0 ± 1.0	3.0 ± 0.9	38.5 ± 1.8
ABYW	0.0 ± 0.0	4.9 ± 0.1	0.0 ± 0.0	10.4 ± 0.2	0.0 ± 0.0	26.6 ± 0.5	2.4 ± 0.1	5.7 ± 0.7	4.6 ± 0.2	11.8 ± 1.2	7.3 ± 0.6	35.7 ± 2.4
HEMS	1.6 ± 0.2	5.8 ± 0.5	3.1 ± 0.3	7.0 ± 0.7	0.0 ± 0.0	8.7 ± 0.2	2.0 ± 0.1	6.4 ± 0.6	3.9 ± 0.1	7.5 ± 0.9	6.0 ± 0.2	6.6 ± 1.7
LERW	2.4 ± 0.2	5.4 ± 0.5	3.7 ± 0.2	8.8 ± 0.7	0.0 ± 0.0	14.6 ± 0.3	2.8 ± 0.1	5.6 ± 0.6	3.9 ± 0.1	9.2 ± 0.8	5.8 ± 0.2	16.7 ± 1.4
DUNK	0.0 ± 0.0	6.9 ± 0.2	0.0 ± 0.0	10.8 ± 0.3	0.0 ± 0.0	26.5 ± 0.7	1.7 ± 0.2	9.3 ± 0.8	2.8 ± 0.3	13.8 ± 1.2	0.8 ± 3.6	34.9 ± 2.1
						Environment Agency, IESSG and NCL CGPS Stations (OTHER)						
IESG	0.0 ± 0.0	3.8 ± 0.1	3.7 ± 0.1	5.6 ± 0.6	5.1 ± 0.2	10.7 ± 0.9	2.2 ± 0.1	3.8 ± 0.4	3.6 ± 0.1	5.6 ± 0.5	5.3 ± 0.1	10.9 ± 0.9
BARK	0.0 ± 0.0	9.7 ± 0.2	2.8 ± 0.3	6.6 ± 0.5	0.0 ± 0.0	9.8 ± 0.2	1.5 ± 0.2	11.9 ± 0.6	3.7 ± 0.1	7.0 ± 0.7	6.2 ± 0.2	8.7 ± 1.3
SUNB	0.0 ± 0.0	7.8 ± 0.1	2.2 ± 0.5	11.3 ± 0.6	2.5 ± 1.3	13.0 ± 0.9	1.9 ± 0.1	9.2 ± 0.5	3.9 ± 0.2	12.9 ± 0.9	6.6 ± 0.2	13.6 ± 1.4
MORP	3.8 ± 0.2	7.7 ± 0.9	6.4 ± 0.3	12.3 ± 1.4	6.3 ± 0.7	19.7 ± 1.7	3.9 ± 0.2	7.8 ± 0.9	6.6 ± 0.3	12.4 ± 1.5	7.8 ± 0.4	21.2 ± 2.1
						UK based IGS Stations (IGS)						
HERS	2.2 ± 0.1	4.8 ± 0.4	3.2 ± 0.1	7.4 ± 0.6	4.0 ± 0.5	12.6 ± 1.0	2.2 ± 0.1	4.8 ± 0.5	3.5 ± 0.1	7.8 ± 0.7	5.7 ± 0.2	13.9 ± 1.3

Table K.5: Noise amplitudes from the MLE with white plus power–law noise (WN+PLN) and white plus flicker noise (WN+FN) models for the filtered improved ITRS2000 coordinate time series. a denotes the white and b the coloured noise amplitudes.

Site	MLE with fractional spectral indices (WN+PLN)						MLE with integer spectral indices (WN+FN)					
	North Component		East Component		Height Component		North Component		East Component		Height Component	
	a [mm]	b [mm]	a [mm]	b [mm]	a [mm]	b [mm]	a [mm]	b [mm]	a [mm]	b [mm]	a [mm]	b [mm]
						CGPS@TG Stations (TG)						
SHEE	0.0 ± 0.0	6.1 ± 0.1	0.0 ± 0.0	4.2 ± 0.1	4.9 ± 0.2	8.4 ± 0.8	1.4 ± 0.1	7.5 ± 0.4	2.5 ± 0.1	3.6 ± 0.5	5.5 ± 0.1	8.5 ± 1.0
ABER	0.0 ± 0.0	5.5 ± 0.1	0.0 ± 0.0	11.2 ± 0.2	6.3 ± 1.4	8.7 ± 1.9	5.0 ± 0.1	0.0 ± 0.1	8.0 ± 0.2	7.7 ± 1.7	8.9 ± 0.2	5.3 ± 1.7
BRST	0.0 ± 0.0	4.9 ± 0.1	2.2 ± 0.7	12.1 ± 0.9	0.0 ± 0.0	27.6 ± 0.7	2.4 ± 0.2	5.7 ± 1.1	4.1 ± 0.3	14.4 ± 1.3	4.0 ± 0.9	36.8 ± 2.3
NEWL	0.0 ± 0.0	4.2 ± 0.1	0.0 ± 0.0	9.0 ± 0.2	0.0 ± 0.0	26.3 ± 0.5	1.4 ± 0.1	5.4 ± 0.5	1.3 ± 0.2	11.6 ± 0.6	0.7 ± 2.5	31.0 ± 1.4
LIVE	0.9 ± 0.3	2.7 ± 0.3	2.3 ± 0.1	3.6 ± 0.4	2.0 ± 0.7	8.6 ± 0.7	1.7 ± 0.1	2.5 ± 0.4	2.4 ± 0.1	3.7 ± 0.5	4.1 ± 0.2	9.2 ± 1.1
LOWE	0.0 ± 0.0	2.8 ± 0.1	0.0 ± 0.0	5.0 ± 0.1	0.0 ± 0.0	14.0 ± 0.3	1.2 ± 0.1	3.4 ± 0.3	1.4 ± 0.1	6.5 ± 0.5	2.5 ± 0.3	17.6 ± 1.0
NSTG	0.0 ± 0.0	4.8 ± 0.1	9.3 ± 0.3	0.0 ± 0.0	0.0 ± 0.0	17.7 ± 0.5	4.9 ± 0.1	0.0 ± 0.0	9.3 ± 0.3	0.0 ± 0.0	14.6 ± 0.4	0.0 ± 0.0
						UK Met Office CGPS Stations (MO)						
CAMB	0.0 ± 0.0	3.6 ± 0.1	0.0 ± 0.0	7.6 ± 0.1	0.0 ± 0.0	21.2 ± 0.4	1.9 ± 0.1	3.9 ± 0.6	1.8 ± 0.2	10.9 ± 0.7	1.5 ± 0.8	27.0 ± 1.2
ABYW	0.0 ± 0.0	3.9 ± 0.1	0.0 ± 0.0	7.1 ± 0.1	0.0 ± 0.0	18.3 ± 0.3	1.8 ± 0.1	4.6 ± 0.5	3.7 ± 0.2	7.9 ± 1.3	7.5 ± 0.4	21.6 ± 2.3
HEMS	0.0 ± 0.0	4.7 ± 0.1	0.0 ± 0.0	4.2 ± 0.1	0.0 ± 0.0	10.2 ± 0.2	1.0 ± 0.1	5.4 ± 0.4	1.8 ± 0.1	5.1 ± 0.7	2.7 ± 0.3	15.4 ± 1.2
LERW	0.0 ± 0.0	5.0 ± 0.1	3.0 ± 0.1	7.3 ± 0.6	4.1 ± 0.3	10.5 ± 0.8	2.4 ± 0.1	4.9 ± 0.6	3.0 ± 0.1	7.2 ± 0.6	5.1 ± 0.2	11.4 ± 1.1
DUNK	0.0 ± 0.0	4.2 ± 0.1	0.0 ± 0.0	7.4 ± 0.2	0.0 ± 0.0	13.8 ± 0.4	1.4 ± 0.1	5.8 ± 0.6	2.3 ± 0.2	10.4 ± 1.0	2.7 ± 0.5	20.5 ± 1.5
						Environment Agency, IESSG and NCL CGPS Stations (OTHER)						
IESG	1.1 ± 0.1	2.7 ± 0.2	1.0 ± 0.2	3.8 ± 0.3	0.6 ± 1.3	8.1 ± 0.5	1.4 ± 0.0	2.9 ± 0.3	1.9 ± 0.1	3.9 ± 0.4	3.3 ± 0.1	9.4 ± 0.7
BARK	0.0 ± 0.0	9.2 ± 0.2	0.0 ± 0.0	5.5 ± 0.1	0.0 ± 0.0	7.7 ± 0.1	0.0 ± 0.0	10.0 ± 0.2	1.7 ± 0.1	6.7 ± 0.5	4.5 ± 0.1	7.4 ± 1.0
SUNB	0.0 ± 0.0	5.8 ± 0.1	1.6 ± 0.2	9.0 ± 0.5	3.6 ± 0.3	9.8 ± 0.7	1.0 ± 0.1	6.6 ± 0.3	2.4 ± 0.1	10.2 ± 0.6	4.4 ± 0.1	10.7 ± 0.9
MORP	3.5 ± 0.2	8.3 ± 0.8	5.4 ± 0.3	10.0 ± 1.2	0.0 ± 0.0	18.4 ± 0.5	3.6 ± 0.2	8.5 ± 0.9	6.0 ± 0.2	10.2 ± 1.4	6.8 ± 0.4	20.7 ± 2.1
						UK based IGS Stations (IGS)						
HERS	0.6 ± 0.3	4.0 ± 0.3	0.6 ± 0.5	5.3 ± 0.3	2.4 ± 0.5	10.9 ± 0.7	1.4 ± 0.1	4.4 ± 0.4	1.8 ± 0.1	6.3 ± 0.5	3.9 ± 0.2	12.3 ± 1.0

Table K.6: Station velocity estimates from MLE with white plus power–law noise (WN+PLN) and white plus flicker noise (WN+FN) models for the unfiltered improved ITRS2000 coordinate time series.

Site	MLE with fractional spectral indices (WN+PLN)			MLE with integer spectral indices (WN+FN)		
	North Component [mm/yr]	East Component [mm/yr]	Height Component [mm/yr]	North Component [mm/yr]	East Component [mm/yr]	Height Component [mm/yr]
			CGPS@TG Stations (TG)			
SHEE	15.16 ± 0.19	18.56 ± 0.23	-0.81 ± 0.57	15.29 ± 0.48	18.52 ± 0.52	-0.16 ± 1.22
ABER	14.99 ± 0.20	16.65 ± 0.43	0.99 ± 0.62	15.05 ± 0.32	16.66 ± 0.85	1.81 ± 1.33
BRST	15.54 ± 0.39	17.62 ± 0.83	-0.23 ± 2.68	15.57 ± 0.92	17.90 ± 1.57	-1.39 ± 4.46
NEWL	16.30 ± 0.30	17.12 ± 0.61	-0.63 ± 2.90	16.43 ± 0.71	16.38 ± 1.29	-0.82 ± 4.02
LIVE	14.31 ± 0.19	16.09 ± 1.03	1.35 ± 0.98	14.31 ± 0.45	16.29 ± 0.69	1.28 ± 1.12
LOWE	14.98 ± 0.14	18.86 ± 0.84	0.48 ± 0.52	14.99 ± 0.32	18.90 ± 0.51	0.73 ± 1.07
NSTG	14.29 ± 0.25	19.45 ± 0.46	2.15 ± 0.34	14.29 ± 0.25	19.45 ± 0.46	0.69 ± 0.71
			UK Met Office CGPS Stations (MO)			
CAMB	15.91 ± 0.22	17.30 ± 0.48	-0.42 ± 2.03	15.91 ± 0.56	17.67 ± 1.10	-1.14 ± 3.40
ABYW	15.87 ± 0.17	17.86 ± 0.39	1.44 ± 1.53	15.92 ± 0.46	17.79 ± 0.94	3.29 ± 3.21
HEMS	14.51 ± 0.51	19.38 ± 0.54	0.99 ± 0.74	14.32 ± 0.78	19.79 ± 0.95	0.49 ± 1.19
LERW	16.43 ± 0.28	13.61 ± 0.58	-0.28 ± 0.75	16.45 ± 0.45	13.61 ± 0.74	-0.36 ± 1.56
DUNK	16.39 ± 0.66	17.77 ± 1.01	2.09 ± 3.01	16.43 ± 1.30	17.53 ± 1.95	2.19 ± 4.86
			Environment Agency, IESSG and NCL CGPS Stations (OTHER)			
IESG	14.34 ± 0.09	17.89 ± 0.42	-3.02 ± 0.86	14.36 ± 0.25	17.91 ± 0.37	-3.30 ± 0.98
BARK	15.46 ± 0.44	18.39 ± 0.23	-1.71 ± 0.41	15.43 ± 0.76	18.37 ± 0.47	-1.66 ± 0.83
SUNB	15.40 ± 0.31	18.02 ± 0.43	-0.05 ± 0.62	15.41 ± 0.59	17.88 ± 0.83	0.11 ± 1.23
MORP	16.95 ± 0.46	14.63 ± 0.74	-3.08 ± 1.15	17.03 ± 0.52	14.57 ± 0.83	-3.57 ± 1.62
			UK based IGS Stations (IGS)			
HERS	12.88 ± 0.59	19.33 ± 0.83	-2.41 ± 1.16	12.94 ± 0.62	19.37 ± 1.00	-2.58 ± 1.76

Table K.7: Station velocity estimates from MLE with white plus power–law noise (WN+PLN) and white plus flicker noise (WN+FN) models for the filtered improved ITRS2000 coordinate time series.

Site	MLE with fractional spectral indices (WN+PLN)			MLE with integer spectral indices (WN+FN)		
	North Component [mm/yr]	East Component [mm/yr]	Height Component [mm/yr]	North Component [mm/yr]	East Component [mm/yr]	Height Component [mm/yr]
			CGPS@TG Stations (TG)			
SHEE	15.08 ± 0.24	18.22 ± 0.11	-0.09 ± 0.53	15.13 ± 0.48	18.28 ± 0.25	0.76 ± 0.80
ABER	14.90 ± 0.15	16.00 ± 0.38	0.88 ± 0.39	14.90 ± 0.13	16.16 ± 0.75	1.19 ± 0.64
BRST	15.69 ± 0.27	17.39 ± 0.82	0.16 ± 2.06	15.79 ± 0.60	17.44 ± 1.49	-0.82 ± 3.72
NEWL	16.12 ± 0.20	16.62 ± 0.57	-0.61 ± 2.19	16.03 ± 0.49	16.35 ± 1.04	-0.77 ± 2.96
LIVE	14.31 ± 0.12	16.04 ± 0.27	1.81 ± 0.45	14.24 ± 0.26	15.97 ± 0.38	1.62 ± 0.92
LOWE	15.01 ± 0.15	18.38 ± 0.30	1.28 ± 0.97	14.96 ± 0.34	18.38 ± 0.64	1.86 ± 1.72
NSTG	14.47 ± 0.11	19.31 ± 0.45	0.68 ± 0.92	14.09 ± 0.24	19.31 ± 0.45	0.91 ± 0.70
			UK Met Office CGPS Stations (MO)			
CAMB	15.91 ± 0.13	16.89 ± 0.35	0.07 ± 1.53	15.94 ± 0.31	17.39 ± 0.86	-0.30 ± 2.37
ABYW	15.87 ± 0.14	17.40 ± 0.24	1.24 ± 0.93	15.96 ± 0.37	17.13 ± 0.63	2.45 ± 2.00
HEMS	14.57 ± 0.41	18.76 ± 0.27	0.45 ± 1.09	14.39 ± 0.66	18.57 ± 0.64	-0.89 ± 2.27
LERW	16.40 ± 0.19	13.17 ± 0.64	0.11 ± 0.67	16.40 ± 0.39	13.18 ± 0.58	0.19 ± 1.08
DUNK	16.08 ± 0.35	17.61 ± 0.64	2.38 ± 1.32	16.09 ± 0.82	17.46 ± 1.47	2.39 ± 2.87
			Environment Agency, IESSG and NCL CGPS Stations (OTHER)			
IESG	14.31 ± 0.09	17.74 ± 0.12	-1.73 ± 0.40	14.30 ± 0.19	17.67 ± 0.25	-2.46 ± 0.81
BARK	15.37 ± 0.54	18.13 ± 0.20	-1.38 ± 0.33	15.36 ± 0.64	18.20 ± 0.44	-0.56 ± 0.70
SUNB	15.32 ± 0.26	17.76 ± 0.40	0.68 ± 0.62	15.33 ± 0.42	17.71 ± 0.65	1.23 ± 0.95
MORP	17.01 ± 0.48	14.49 ± 0.47	-2.10 ± 0.90	17.13 ± 0.56	14.32 ± 0.69	-2.64 ± 1.57
			UK based IGS Stations (IGS)			
HERS	12.59 ± 0.35	19.05 ± 0.46	-1.99 ± 1.01	12.63 ± 0.55	19.18 ± 0.77	-1.80 ± 1.52

Table K.8: Annual term estimates from MLE with white plus power–law noise (WN+PLN) and white plus flicker noise (WN+FN) models for the unfiltered improved ITRS2000 coordinate time series.

Site	MLE with fractional spectral indices (WN+PLN)						MLE with integer spectral indices (WN+FN)					
	North Component		East Component		Height Component		North Component		East Component		Height Component	
	a [mm]	ϕ [days]	a [mm]	ϕ [days]	a [mm]	ϕ [days]	a [mm]	ϕ [days]	a [mm]	ϕ [days]	a [mm]	ϕ [days]
						CGPS@TG Stations (TG)						
SHEE	5.0 ± 0.4	5 ± 3	0.2 ± 0.5	362 ± 114	1.6 ± 0.8	158 ± 19	4.9 ± 0.6	5 ± 5	0.2 ± 0.7	358 ± 132	1.8 ± 1.2	155 ± 27
ABER	1.9 ± 0.4	17 ± 8	3.2 ± 0.8	346 ± 10	2.1 ± 1.0	5 ± 20	1.9 ± 0.4	16 ± 9	3.3 ± 1.0	349 ± 12	2.1 ± 1.4	2 ± 27
BRST	1.5 ± 0.6	361 ± 15	4.4 ± 1.1	44 ± 11	2.2 ± 3.2	243 ± 62	1.5 ± 0.9	356 ± 25	4.2 ± 1.6	45 ± 16	1.8 ± 4.5	248 ± 106
NEWL	1.8 ± 0.5	333 ± 11	1.9 ± 0.9	365 ± 19	1.8 ± 3.2	142 ± 73	1.8 ± 0.8	331 ± 17	1.8 ± 1.4	1 ± 31	2.0 ± 4.1	143 ± 85
LIVE	3.3 ± 0.3	21 ± 4	4.2 ± 0.9	32 ± 9	1.8 ± 1.1	14 ± 26	3.3 ± 0.5	20 ± 6	4.1 ± 0.7	31 ± 7	1.8 ± 1.2	14 ± 27
LOWE	0.9 ± 0.2	317 ± 11	0.9 ± 0.6	5 ± 31	1.5 ± 0.8	21 ± 20	0.9 ± 0.3	315 ± 15	0.9 ± 0.5	364 ± 26	1.4 ± 1.1	21 ± 32
NSTG	3.4 ± 0.5	342 ± 6	3.2 ± 0.9	297 ± 11	4.3 ± 1.3	297 ± 13	3.4 ± 0.4	342 ± 4	3.2 ± 0.9	297 ± 11	4.3 ± 1.3	296 ± 13
						UK Met Office CGPS Stations (MO)						
CAMB	1.3 ± 0.4	340 ± 12	2.3 ± 0.8	19 ± 14	1.9 ± 2.3	92 ± 49	1.4 ± 0.6	339 ± 19	2.2 ± 1.3	17 ± 23	2.2 ± 3.5	93 ± 64
ABYW	1.1 ± 0.3	322 ± 12	2.4 ± 0.7	21 ± 12	3.8 ± 1.9	59 ± 21	1.1 ± 0.5	320 ± 20	2.5 ± 1.1	21 ± 18	3.6 ± 3.3	61 ± 38
HEMS	0.9 ± 0.6	359 ± 25	1.5 ± 0.6	351 ± 18	1.9 ± 0.7	57 ± 14	1.0 ± 0.7	363 ± 30	1.4 ± 0.9	348 ± 26	2.0 ± 0.9	54 ± 18
LERW	1.1 ± 0.4	346 ± 17	3.2 ± 0.8	345 ± 10	4.0 ± 1.0	7 ± 10	1.1 ± 0.5	346 ± 21	3.2 ± 0.9	345 ± 11	3.9 ± 1.5	7 ± 16
DUNK	1.4 ± 0.7	326 ± 20	3.5 ± 1.1	18 ± 12	1.3 ± 2.9	306 ± 95	1.5 ± 1.1	321 ± 32	3.6 ± 1.7	20 ± 19	1.4 ± 4.2	312 ± 127
						Environment Agency, IESSG and NCL CGPS Stations (OTHER)						
IESG	1.3 ± 0.2	336 ± 7	1.1 ± 0.5	349 ± 20	0.9 ± 0.9	350 ± 42	1.3 ± 0.3	335 ± 11	1.1 ± 0.5	348 ± 19	0.9 ± 0.9	352 ± 42
BARK	2.1 ± 0.7	340 ± 14	2.0 ± 0.4	276 ± 9	4.2 ± 0.6	205 ± 6	2.0 ± 1.0	341 ± 20	2.0 ± 0.6	277 ± 13	4.2 ± 0.8	205 ± 8
SUNB	2.1 ± 0.5	201 ± 11	5.0 ± 0.8	4 ± 6	1.0 ± 0.8	196 ± 34	2.1 ± 0.8	201 ± 15	5.0 ± 1.1	3 ± 9	0.9 ± 1.2	184 ± 53
MORP	1.9 ± 0.8	329 ± 16	2.4 ± 1.2	8 ± 21	4.5 ± 1.7	18 ± 16	1.9 ± 0.8	329 ± 17	2.4 ± 1.3	9 ± 21	4.7 ± 2.1	16 ± 18
						UK based IGS Stations (IGS)						
HERS	1.4 ± 0.5	2 ± 14	0.4 ± 0.7	280 ± 63	1.3 ± 1.0	113 ± 31	1.3 ± 0.5	1 ± 15	0.4 ± 0.8	276 ± 80	1.4 ± 1.4	114 ± 39

Table K.9: Annual term estimates from MLE with white plus power–law noise (WN+PLN) and white plus flicker noise (WN+FN) models for the filtered improved ITRS2000 coordinate time series.

Site	MLE with fractional spectral indices (WN+PLN)						MLE with integer spectral indices (WN+FN)					
	North Component		East Component		Height Component		North Component		East Component		Height Component	
	a [mm]	ϕ [days]	a [mm]	ϕ [days]	a [mm]	ϕ [days]	a [mm]	ϕ [days]	a [mm]	ϕ [days]	a [mm]	ϕ [days]
						CGPS@TG Stations (TG)						
SHEE	4.3 ± 0.4	13 ± 4	0.8 ± 0.2	154 ± 13	1.2 ± 0.6	182 ± 20	4.2 ± 0.6	12.6 ± 6.0	0.7 ± 0.3	156 ± 18	1.4 ± 0.8	180 ± 23
ABER	1.3 ± 0.3	50 ± 10	2.0 ± 0.7	335 ± 15	2.0 ± 0.7	358 ± 14	1.3 ± 0.3	50 ± 9	2.0 ± 0.9	338 ± 18	2.0 ± 0.7	354 ± 15
BRST	0.4 ± 0.4	57 ± 38	3.3 ± 1.1	59 ± 14	2.5 ± 2.5	250 ± 43	0.4 ± 0.6	60 ± 63	3.3 ± 1.5	59 ± 20	2.4 ± 3.8	254 ± 66
NEWL	0.6 ± 0.3	322 ± 20	0.6 ± 0.7	9 ± 50	1.6 ± 2.4	153 ± 63	0.7 ± 0.5	316 ± 32	0.5 ± 1.1	12 ± 89	1.7 ± 3.0	152 ± 74
LIVE	2.7 ± 0.2	40 ± 3	3.0 ± 0.3	46 ± 5	1.6 ± 0.7	5 ± 17	2.7 ± 0.3	40 ± 4	3.0 ± 0.4	46 ± 5	1.6 ± 1.0	6 ± 24
LOWE	0.5 ± 0.2	197 ± 18	0.5 ± 0.4	184 ± 33	1.2 ± 1.2	14 ± 42	0.5 ± 0.3	197 ± 31	0.5 ± 0.7	185 ± 56	1.0 ± 1.8	16 ± 71
NSTG	2.4 ± 0.4	343 ± 7	2.5 ± 0.9	257 ± 15	3.4 ± 1.7	300 ± 21	2.4 ± 0.5	343 ± 8	2.5 ± 0.9	257 ± 15	3.2 ± 1.3	301 ± 17
						UK Met Office CGPS Stations (MO)						
CAMB	0.3 ± 0.2	340 ± 34	1.4 ± 0.6	46 ± 16	0.7 ± 1.7	87 ± 103	0.3 ± 0.4	337 ± 54	1.3 ± 1.0	42 ± 31	0.8 ± 2.4	92 ± 126
ABYW	0.3 ± 0.3	250 ± 32	1.6 ± 0.5	46 ± 12	3.2 ± 1.2	51 ± 16	0.3 ± 0.4	247 ± 51	1.7 ± 0.7	46 ± 18	3.1 ± 2.0	52 ± 26
HEMS	0.4 ± 0.4	114 ± 50	0.8 ± 0.3	10 ± 17	1.2 ± 0.9	350 ± 32	0.4 ± 0.6	102 ± 60	0.8 ± 0.6	5 ± 28	1.5 ± 1.8	346 ± 47
LERW	0.1 ± 0.3	57 ± 125	2.1 ± 0.7	344 ± 14	4.1 ± 0.8	357 ± 8	0.1 ± 0.5	66 ± 150	2.1 ± 0.7	343 ± 13	4.0 ± 1.1	356 ± 11
DUNK	0.4 ± 0.4	274 ± 41	1.2 ± 0.7	38 ± 25	1.1 ± 1.4	329 ± 53	0.4 ± 0.7	271 ± 66	1.3 ± 1.3	44 ± 40	1.2 ± 2.5	322 ± 86
						Environment Agency, IESSG and NCL CGPS Stations (OTHER)						
IESG	0.3 ± 0.2	349 ± 21	0.2 ± 0.2	1 ± 55	1.5 ± 0.5	319 ± 13	0.4 ± 0.2	351 ± 29	0.2 ± 0.3	12 ± 72	1.6 ± 0.8	324 ± 20
BARK	1.2 ± 0.7	349 ± 24	1.8 ± 0.4	250 ± 8	4.4 ± 0.4	215 ± 4	1.2 ± 0.8	349 ± 27	1.9 ± 0.6	251 ± 12	4.5 ± 0.7	214 ± 6
SUNB	2.7 ± 0.4	185 ± 6	4.2 ± 0.6	10 ± 6	1.0 ± 0.7	232 ± 28	2.7 ± 0.5	186 ± 8	4.2 ± 0.8	10 ± 8	1.0 ± 0.9	225 ± 37
MORP	1.0 ± 0.8	333 ± 33	1.5 ± 0.9	19 ± 26	4.1 ± 1.5	10 ± 15	1.0 ± 0.8	335 ± 36	1.6 ± 1.1	25 ± 27	4.2 ± 2.0	6 ± 19
						UK IGS Stations (IGS)						
HERS	0.7 ± 0.3	57 ± 18	1.1 ± 0.4	200 ± 15	0.6 ± 0.9	145 ± 61	0.7 ± 0.4	57 ± 27	1.2 ± 0.6	199 ± 22	0.6 ± 1.2	148 ± 85

Table K.10: Coordinate offset estimates from MLE with white plus power–law noise (WN+PLN) and white plus flicker noise (WN+FN) models for the unfiltered improved ITRS2000 coordinate time series.

Site	Date	MLE with fractional spectral indices (WN+PLN)			MLE with integer spectral indices (WN+FN)		
		North Component [mm]	East Component [mm]	Height Component [mm]	North Component [mm]	East Component [mm]	Height Component [mm]
SHEE	9 Mar 1998			6.5 ± 1.5			6.6 ± 2.6
SHEE	2 Feb 1999			2.3 ± 1.6			-0.5 ± 2.7
ABER	2 Feb 1999			0.7 ± 2.0			0.4 ± 2.8
NEWL	2 Feb 1999			2.3 ± 5.4			1.3 ± 6.3
CAMB	2 Feb 1999			2.9 ± 4.4			2.1 ± 5.9
ABYW	2 Feb 1999			1.6 ± 3.7			-2.3 ± 5.9
HEMS	2 Feb 1999			0.7 ± 1.2			1.6 ± 1.7
LERW	2 Feb 1999			3.6 ± 1.9			3.4 ± 3.0
IESG	9 Mar 1998			1.0 ± 1.9			1.6 ± 2.1
IESG	2 Feb 1999			4.8 ± 1.9			4.8 ± 2.1
BARK	9 Mar 1998			5.6 ± 1.1			6.1 ± 1.8
BARK	2 Feb 1999			2.9 ± 1.1			2.4 ± 1.8
SUNB	9 Mar 1998			3.3 ± 1.6			3.3 ± 2.6
SUNB	2 Feb 1999			1.4 ± 1.7			-0.8 ± 2.7
MORP	9 Mar 1998			10.1 ± 3.6			11.2 ± 4.3
HERS	21 Mar 1999	3.4 ± 0.9	-0.7 ± 1.4	19.5 ± 2.0	3.4 ± 1.0	-1.5 ± 1.5	18.6 ± 2.7
HERS	8 Aug 2001	7.0 ± 1.1	-5.6 ± 1.6	-6.7 ± 2.3	6.9 ± 1.2	-5.4 ± 1.9	-5.9 ± 3.4

Table K.11: Coordinate offset estimates from MLE with white plus power–law noise (WN+PLN) and white plus flicker noise (WN+FN) models for the filtered improved ITRS2000 coordinate time series.

Site	Date	MLE with fractional spectral indices (WN+PLN)			MLE with integer spectral indices (WN+FN)		
		North Component [mm]	East Component [mm]	Height Component [mm]	North Component [mm]	East Component [mm]	Height Component [mm]
SHEE	9 Mar 1999			6.6 ± 1.3			5.5 ± 1.7
SHEE	2 Feb 1999			0.7 ± 1.4			-0.9 ± 1.8
ABER	2 Feb 1999			-1.0 ± 1.4			-0.9 ± 1.6
NEWL	2 Feb 1999			2.5 ± 4.1			2.0 ± 4.7
CAMB	2 Feb 1999			3.4 ± 3.2			3.5 ± 4.1
ABYW	2 Feb 1999			1.7 ± 2.4			-1.2 ± 3.9
HEMS	2 Feb 1999			1.4 ± 1.7			3.7 ± 2.7
LERW	2 Feb 1999			3.0 ± 1.6			3.4 ± 2.1
IESG	9 Mar 1999			-0.9 ± 1.0			0.3 ± 1.7
IESG	2 Feb 1999			4.2 ± 1.1			4.7 ± 1.7
BARK	9 Mar 1999			5.5 ± 0.9			3.6 ± 1.5
BARK	2 Feb 1999			2.4 ± 0.9			1.7 ± 1.5
SUNB	9 Mar 1999			3.1 ± 1.5			1.9 ± 2.0
SUNB	2 Feb 1999			-0.2 ± 1.6			-1.6 ± 2.0
MORP	9 Mar 1999			8.2 ± 3.0			9.1 ± 4.1
HERS	21 Mar 1999	3.5 ± 0.6	0.3 ± 0.8	18.9 ± 1.7	3.6 ± 0.8	-0.7 ± 1.1	18.3 ± 2.2
HERS	8 Aug 2001	7.5 ± 0.7	-6.1 ± 0.9	-7.9 ± 2.0	7.5 ± 1.0	-5.6 ± 1.5	-7.8 ± 2.9

Table K.12: White a and flicker b_{-1} noise amplitudes, velocity estimates and their uncertainties σ_r compared for the MLE with white plus flicker noise (WN+FN) model and the empirical Methods 1 (Mao et al., 1999) and 2 (Williams, 2003a) for the unfiltered improved ITRS2000 North time series.

Site	MLE (Integer Spectral Indices)			Method 1[a]		Method 2[b]		Velocity	σ_r[c]	σ_r[d]
	a [mm]	b_{-1} [mm]	Velocity [mm/yr]	a [mm]	b_{-1} [mm]	a [mm]	b_{-1} [mm]	[mm/yr]		
					CGPS@TG Stations (TG)					
SHEE	2.2 ± 0.1	7.5 ± 0.5	15.29 ± 0.48	2.0	3.3	2.6	5.0	15.11	0.46	0.68
ABER	5.1 ± 0.1	3.0 ± 1.2	15.05 ± 0.32	2.7	4.6	5.0	4.6	15.01	0.86	0.87
BRST	2.6 ± 0.2	8.9 ± 1.1	15.57 ± 0.92	2.2	3.8	3.0	6.1	15.64	0.84	1.35
NEWL	2.1 ± 0.1	7.9 ± 0.6	16.43 ± 0.71	2.0	3.4	2.5	5.3	16.15	0.65	1.00
LIVE	2.2 ± 0.1	4.5 ± 0.5	14.31 ± 0.45	1.8	2.9	2.3	3.6	14.24	0.62	0.77
LOWE	1.9 ± 0.1	3.1 ± 0.5	14.99 ± 0.32	1.5	2.5	1.9	2.8	14.96	0.53	0.59
NSTG	5.1 ± 0.1	0.0 ± 0.0	14.29 ± 0.25	3.2	5.5	5.1	0.3	14.40	0.98	0.13
					UK Met Office CGPS Stations (MO)					
CAMB	2.4 ± 0.1	7.0 ± 0.7	15.91 ± 0.56	2.2	3.7	2.7	5.0	15.94	0.61	0.84
ABYW	2.4 ± 0.1	5.7 ± 0.7	15.92 ± 0.46	2.0	3.3	2.6	4.2	15.87	0.55	0.71
HEMS	2.0 ± 0.1	6.4 ± 0.6	14.32 ± 0.78	2.0	3.3	2.3	5.3	14.92	0.82	1.34
LERW	2.8 ± 0.1	5.6 ± 0.6	16.45 ± 0.45	2.1	3.6	2.9	5.0	16.30	0.60	0.85
DUNK	1.7 ± 0.2	9.3 ± 0.8	16.43 ± 1.30	2.0	3.4	2.4	6.1	16.30	1.02	1.82
					Environment Office, IESSG and NCL CGPS Stations (OTHER)					
IESG	2.2 ± 0.1	3.8 ± 0.4	14.36 ± 0.25	1.7	2.8	2.3	3.1	14.34	0.38	0.42
BARK	1.5 ± 0.2	11.9 ± 0.6	15.43 ± 0.76	2.4	4.1	2.7	7.6	15.28	0.56	1.04
SUNB	1.9 ± 0.1	9.2 ± 0.5	15.41 ± 0.59	2.2	3.7	2.6	6.4	15.41	0.50	0.87
MORP	3.9 ± 0.2	7.8 ± 0.9	17.03 ± 0.52	2.8	4.9	4.3	6.8	16.42	0.67	0.94
					UK based IGS Stations (IGS)					
HERS	2.2 ± 0.1	4.8 ± 0.5	12.94 ± 0.62	1.9	3.2	2.4	4.7	12.48	0.56	0.82

[a] Computed using Eq. H.12 (Mao et al., 1999)

[b] Computed using Eq. H.13 and H.14 (Williams, 2003a)

[c] Uncertainty according to Method 1 using Eqs. H.19 and H.20

[d] Uncertainty according to Method 2 using Eqs. H.19 and H.20

Table K.13: White a and flicker b_{-1} noise amplitudes, velocity estimates and their uncertainties σ_r compared for the MLE with white plus flicker noise (WN+FN) model and the empirical Methods 1 (Mao et al., 1999) and 2 (Williams, 2003a) for the unfiltered improved ITRS2000 East time series.

Site	MLE (Integer Spectral Indices)			Method 1[a]		Method 2[b]		Velocity	σ_r[c]	σ_r[d]
	a [mm]	b_{-1} [mm]	Velocity [mm/yr]	a [mm]	b_{-1} [mm]	a [mm]	b_{-1} [mm]		[mm/yr]	
					CGPS@TG Stations (TG)					
SHEE	4.0 ± 0.1	7.8 ± 0.8	18.52 ± 0.52	3.1	4.2	4.2	6.3	18.42	0.57	0.86
ABER	8.6 ± 0.2	8.8 ± 1.7	16.66 ± 0.85	5.4	7.2	8.6	9.5	16.47	1.36	1.80
BRST	4.9 ± 0.3	15.1 ± 1.6	17.90 ± 1.57	4.5	6.0	5.6	11.5	16.80	1.32	2.55
NEWL	3.2 ± 0.2	14.3 ± 1.0	16.38 ± 1.29	3.7	4.9	4.1	10.0	17.16	0.93	1.90
LIVE	3.5 ± 0.1	6.9 ± 0.7	16.29 ± 0.69	3.0	4.0	3.8	6.2	16.24	0.84	1.30
LOWE	3.1 ± 0.1	4.9 ± 0.6	18.90 ± 0.51	2.4	3.2	3.3	4.9	18.47	0.68	1.04
NSTG	9.5 ± 0.3	0.0 ± 2.4	19.45 ± 0.46	7.2	9.7	9.5	0.0	18.62	1.73	0.00
					UK Met Office CGPS Stations (MO)					
CAMB	3.5 ± 0.2	14.0 ± 1.0	17.67 ± 1.10	3.7	4.9	4.3	9.9	16.66	0.83	1.66
ABYW	4.6 ± 0.2	11.8 ± 1.2	17.79 ± 0.94	4.1	5.4	5.0	9.1	17.64	0.92	1.53
HEMS	3.9 ± 0.1	7.5 ± 0.9	19.79 ± 0.95	3.2	4.2	4.1	6.5	19.02	1.06	1.62
LERW	3.9 ± 0.1	9.2 ± 0.8	13.61 ± 0.74	3.4	4.5	4.2	7.6	13.67	0.76	1.29
DUNK	2.8 ± 0.3	13.8 ± 1.2	17.53 ± 1.95	3.5	4.6	3.8	9.6	17.40	1.40	2.87
					Environment Office, IESSG and NCL CGPS Stations (OTHER)					
IESG	3.6 ± 0.1	5.6 ± 0.5	17.91 ± 0.37	2.8	3.7	3.8	5.1	17.96	0.51	0.70
BARK	3.7 ± 0.1	7.0 ± 0.7	18.37 ± 0.47	3.0	3.9	3.9	5.7	18.18	0.54	0.78
SUNB	3.9 ± 0.2	12.9 ± 0.9	17.88 ± 0.83	4.0	5.3	4.5	9.9	17.98	0.73	1.36
MORP	6.6 ± 0.3	12.4 ± 1.5	14.57 ± 0.83	5.5	7.4	7.1	10.7	14.90	1.02	1.47
					UK based IGS Stations (IGS)					
HERS	3.5 ± 0.1	7.8 ± 0.7	19.37 ± 1.00	2.9	3.8	3.8	6.4	18.37	0.67	1.12

[a] Computed using Eq. H.12 (Mao et al., 1999)

[b] Computed using Eq. H.13 and H.14 (Williams, 2003a)

[c] Uncertainty according to Method 1 using Eqs. H.19 and H.20

[d] Uncertainty according to Method 2 using Eqs. H.19 and H.20

Table K.14: White a and flicker b_{-1} noise amplitudes, velocity estimates and their uncertainties σ_r compared for the MLE with white plus flicker noise (WN+FN) model and the empirical Methods 1 (Mao et al., 1999) and 2 (Williams, 2003a) for the unfiltered improved ITRS2000 height time series.

Site	MLE (Integer Spectral Indices)			Method 1[a]		Method 2[b]		Velocity	σ_r[c]	σ_r[d]
	a [mm]	b_{-1} [mm]	Velocity [mm/yr]	a [mm]	b_{-1} [mm]	a [mm]	b_{-1} [mm]	[mm/yr]		
				CGPS@TG Stations (TG)						
SHEE	7.6 ± 0.2	13.2 ± 1.6	-0.16 ± 1.22	5.1	10.8	7.8	11.0	-0.70	1.48	1.51
ABER	9.5 ± 0.3	12.5 ± 2.4	1.81 ± 1.33	5.9	11.5	9.4	12.9	1.83	2.16	2.43
BRST	3.4 ± 1.3	44.3 ± 2.6	-1.39 ± 4.46	7.7	12.9	8.9	25.2	1.18	2.86	5.56
NEWL	0.0 ± 0.0	42.1 ± 0.8	-0.82 ± 4.02	7.6	12.8	7.7	25.2	0.46	2.44	4.78
LIVE	5.8 ± 0.2	11.1 ± 1.2	1.28 ± 1.12	3.9	9.9	6.1	9.9	2.17	2.08	2.09
LOWE	5.1 ± 0.2	10.6 ± 1.2	0.73 ± 1.07	3.2	9.3	5.3	9.1	0.41	1.97	1.92
NSTG	14.7 ± 0.4	0.0 ± 0.0	0.69 ± 0.71	10.3	15.0	14.3	9.5	0.88	2.66	1.71
				UK Met Office CGPS Stations (MO)						
CAMB	3.0 ± 0.9	38.5 ± 1.8	-1.14 ± 3.40	6.9	12.2	7.7	21.3	0.52	2.06	3.58
ABYW	7.3 ± 0.6	35.7 ± 2.4	3.29 ± 3.21	8.5	13.5	9.7	22.4	1.21	2.27	3.76
HEMS	6.0 ± 0.2	6.6 ± 1.7	0.49 ± 1.19	3.4	9.5	5.9	7.3	1.23	2.38	1.83
LERW	5.8 ± 0.2	16.7 ± 1.4	-0.36 ± 1.56	4.6	10.4	6.5	12.6	0.14	1.76	2.13
DUNK	0.8 ± 3.6	34.9 ± 2.1	2.19 ± 4.86	5.5	11.2	6.5	19.4	2.65	3.36	5.82
				Environment Office, IESSG and NCL CGPS Stations (OTHER)						
IESG	5.3 ± 0.1	10.9 ± 0.9	-3.30 ± 0.98	3.4	9.5	5.6	8.9	-1.29	1.30	1.22
BARK	6.2 ± 0.2	8.7 ± 1.3	-1.66 ± 0.83	3.8	9.8	6.3	7.8	-1.38	1.34	1.07
SUNB	6.6 ± 0.2	13.6 ± 1.4	0.11 ± 1.23	4.8	10.6	6.9	11.1	0.29	1.45	1.52
MORP	7.8 ± 0.4	21.2 ± 2.1	-3.57 ± 1.62	6.6	12.0	9.0	16.6	-1.32	1.64	2.28
				UK based IGS Stations (IGS)						
HERS	5.7 ± 0.2	13.9 ± 1.3	-2.58 ± 1.76	3.9	9.9	6.2	10.8	-2.59	1.73	1.89

[a] Computed using Eq. H.12 (Mao et al., 1999)

[b] Computed using Eq. H.13 and H.14 (Williams, 2003a)

[c] Uncertainty according to Method 1 using Eqs. H.19 and H.20

[d] Uncertainty according to Method 2 using Eqs. H.20 and H.20

Table K.15: White a and flicker b_{-1} noise amplitudes, velocity estimates and their uncertainties σ_r compared for the MLE with white plus flicker noise (WN+FN) model and the empirical Methods 1 (Mao et al., 1999) and 2 (Williams, 2003a) for the filtered improved ITRS2000 North time series.

Site	MLE (Integer Spectral Indices)			Method 1[a]		Method 2[b]		Velocity	σ_r[c]	σ_r[d]
	a [mm]	b_{-1} [mm]	Velocity [mm/yr]	a [mm]	b_{-1} [mm]	a [mm]	b_{-1} [mm]	[mm/yr]		
				CGPS@TG Stations (TG)						
SHEE	1.4 ± 0.1	7.5 ± 0.4	15.13 ± 0.48	1.8	3.0	2.0	4.8	15.01	0.41	0.66
ABER	5.0 ± 0.1	0.0 ± 0.1	14.90 ± 0.13	3.3	5.8	4.9	2.8	14.90	1.10	0.54
BRST	2.4 ± 0.2	5.7 ± 1.1	15.79 ± 0.60	2.0	3.4	2.4	4.6	15.66	0.75	1.02
NEWL	1.4 ± 0.1	5.4 ± 0.5	16.03 ± 0.49	1.5	2.5	1.7	3.5	16.11	0.47	0.67
LIVE	1.7 ± 0.1	2.5 ± 0.4	14.24 ± 0.26	1.4	2.3	1.8	2.3	14.34	0.48	0.48
LOWE	1.2 ± 0.1	3.4 ± 0.3	14.96 ± 0.34	1.2	1.9	1.3	2.5	15.05	0.40	0.53
NSTG	4.9 ± 0.1	0.0 ± 0.0	14.09 ± 0.24	3.3	5.8	5.0	0.0	14.09	1.02	0.00
				UK Met Office CGPS Stations (MO)						
CAMB	1.9 ± 0.1	3.9 ± 0.6	15.94 ± 0.31	1.6	2.6	1.9	3.1	15.89	0.44	0.53
ABYW	1.8 ± 0.1	4.6 ± 0.5	15.96 ± 0.37	1.7	2.7	2.0	3.4	15.83	0.45	0.57
HEMS	1.0 ± 0.1	5.4 ± 0.4	14.39 ± 0.66	1.5	2.3	1.4	4.1	14.83	0.58	1.04
LERW	2.4 ± 0.1	4.9 ± 0.6	16.40 ± 0.39	2.0	3.4	2.5	4.5	16.39	0.57	0.76
DUNK	1.4 ± 0.1	5.8 ± 0.6	16.09 ± 0.82	1.5	2.5	1.7	3.7	16.05	0.75	1.10
				Environment Office, IESSG and NCL CGPS Stations (OTHER)						
IESG	1.4 ± 0.0	2.9 ± 0.3	14.30 ± 0.19	1.3	2.0	1.5	2.3	14.30	0.28	0.31
BARK	0.0 ± 0.0	10.0 ± 0.2	15.36 ± 0.64	2.0	3.4	1.8	6.4	15.32	0.46	0.88
SUNB	1.0 ± 0.1	6.6 ± 0.3	15.33 ± 0.42	1.6	2.7	1.6	4.6	15.28	0.37	0.63
MORP	3.6 ± 0.2	8.5 ± 0.9	17.13 ± 0.56	3.1	5.5	4.0	7.1	16.43	0.75	0.98
				UK based IGS Stations (IGS)						
HERS	1.4 ± 0.1	4.4 ± 0.4	12.63 ± 0.55	1.5	2.4	1.6	3.7	15.42	0.55	1.11

[a] Computed using Eq. H.12 (Mao et al., 1999)

[b] Computed using Eq. H.13 and H.14 (Williams, 2003a)

[c] Uncertainty according to Method 1 using Eqs. H.19 and H.20

[d] Uncertainty according to Method 2 using Eqs. H.19 and H.20

Table K.16: White a and flicker b_{-1} noise amplitudes, velocity estimates and their uncertainties σ_r compared for the MLE with white plus flicker noise (WN+FN) model and the empirical Methods 1 (Mao et al., 1999) and 2 (Williams, 2003a) for the filtered improved ITRS2000 East time series.

Site	MLE (Integer Spectral Indices)			Method 1[a]		Method 2[b]		Velocity	σ_r[c]	σ_r[d]
	a [mm]	b_{-1} [mm]	Velocity [mm/yr]	a [mm]	b_{-1} [mm]	a [mm]	b_{-1} [mm]	[mm/yr]		
					CGPS@TG Stations (TG)					
SHEE	2.5 ± 0.1	3.6 ± 0.5	18.28 ± 0.25	1.9	2.5	2.5	3.5	18.19	0.35	0.48
ABER	8.0 ± 0.2	7.7 ± 1.7	16.16 ± 0.75	6.3	8.4	8.0	8.2	15.98	1.59	1.55
BRST	4.1 ± 0.3	14.4 ± 1.3	17.44 ± 1.49	4.4	5.9	4.9	10.5	17.24	1.30	2.33
NEWL	1.3 ± 0.2	11.6 ± 0.6	16.35 ± 1.04	2.5	3.2	2.5	7.1	17.05	0.62	1.35
LIVE	2.4 ± 0.1	3.7 ± 0.5	15.97 ± 0.38	1.9	2.5	2.5	3.1	16.19	0.52	0.65
LOWE	1.4 ± 0.1	6.5 ± 0.5	18.38 ± 0.64	1.6	2.0	1.8	4.2	18.38	0.43	0.89
NSTG	9.3 ± 0.3	0.0 ± 0.0	19.31 ± 0.45	7.0	9.4	9.3	0.2	19.31	1.67	0.22
					UK Met Office CGPS Stations (MO)					
CAMB	1.8 ± 0.2	10.9 ± 0.7	17.39 ± 0.86	2.4	3.2	2.7	6.3	16.82	0.54	1.06
ABYW	3.7 ± 0.2	7.9 ± 1.3	17.13 ± 0.63	3.2	4.2	3.9	6.2	17.51	0.71	1.04
HEMS	1.8 ± 0.1	5.1 ± 0.7	18.57 ± 0.64	1.6	2.1	2.0	3.8	18.82	0.52	0.96
LERW	3.0 ± 0.1	7.2 ± 0.6	13.18 ± 0.58	2.8	3.7	3.3	6.2	13.36	0.63	1.05
DUNK	2.3 ± 0.2	10.4 ± 1.0	17.46 ± 1.47	2.6	3.4	3.0	6.1	17.74	1.02	1.83
					Environment Office, IESSG and NCL CGPS Stations (OTHER)					
IESG	1.9 ± 0.1	3.9 ± 0.4	17.67 ± 0.25	1.6	2.0	2.0	3.4	17.78	0.28	0.46
BARK	1.7 ± 0.1	6.7 ± 0.5	18.20 ± 0.44	1.8	2.4	2.1	4.7	18.07	0.33	0.64
SUNB	2.4 ± 0.1	10.2 ± 0.6	17.71 ± 0.65	2.9	3.8	3.0	7.5	17.89	0.52	1.03
MORP	6.0 ± 0.2	10.2 ± 1.4	14.32 ± 0.69	5.2	6.9	6.4	8.3	14.58	0.95	1.13
					UK based IGS Stations (IGS)					
HERS	1.8 ± 0.1	6.3 ± 0.5	19.18 ± 0.77	1.8	2.4	2.1	4.5	17.50	0.52	1.24

[a] Computed using Eq. H.12 (Mao et al., 1999)

[b] Computed using Eq. H.13 and H.14 (Williams, 2003a)

[c] Uncertainty according to Method 1 using Eqs. H.19 and H.20

[d] Uncertainty according to Method 2 using Eqs. H.19 and H.20

Table K.17: White a and flicker b_{-1} noise amplitudes, velocity estimates and their uncertainties σ_r compared for the MLE with white plus flicker noise (WN+FN) model and the empirical Methods 1 (Mao et al., 1999) and 2 (Williams, 2003a) for the filtered improved ITRS2000 height time series.

Site	MLE (Integer Spectral Indices)			Method 1[a]		Method 2[b]		Velocity	σ_r[c]	σ_r[d]
	a [mm]	b_{-1} [mm]	Velocity [mm/yr]	a [mm]	b_{-1} [mm]	a [mm]	b_{-1} [mm]	[mm/yr]		
CGPS@TG Stations (TG)										
SHEE	5.5 ± 0.1	8.5 ± 1.0	0.76 ± 0.80	3.4	9.5	5.7	7.0	-0.93	1.30	0.96
ABER	8.9 ± 0.2	5.3 ± 1.7	1.19 ± 0.64	5.9	11.4	8.8	6.5	0.78	2.15	1.24
BRST	4.0 ± 0.9	36.8 ± 2.3	-0.82 ± 3.72	7.1	12.4	7.9	21.4	1.05	2.75	4.73
NEWL	0.7 ± 2.5	31.0 ± 1.4	-0.77 ± 2.96	5.4	11.1	5.7	18.9	0.16	2.10	3.59
LIVE	4.1 ± 0.2	9.2 ± 1.1	1.62 ± 0.92	2.5	8.8	4.4	7.7	1.85	1.83	1.62
LOWE	2.5 ± 0.3	17.6 ± 1.0	1.86 ± 1.72	2.9	9.1	4.1	11.6	0.40	1.93	2.46
NSTG	14.6 ± 0.4	0.0 ± 0.0	0.91 ± 0.70	10.5	15.1	13.8	14.1	0.91	2.70	2.53
UK Met Office CGPS Stations (MO)										
CAMB	1.5 ± 0.8	27.0 ± 1.2	-0.30 ± 2.37	4.3	10.2	5.3	14.9	0.07	1.72	2.51
ABYW	7.5 ± 0.4	21.6 ± 2.3	2.45 ± 2.00	6.5	11.9	8.3	15.6	0.66	2.01	2.63
HEMS	2.7 ± 0.3	15.4 ± 1.2	-0.89 ± 2.27	2.3	8.6	3.9	8.6	1.23	2.14	2.14
LERW	5.1 ± 0.2	11.4 ± 1.1	0.19 ± 1.08	3.5	9.6	5.4	9.1	-0.15	1.61	1.53
DUNK	2.7 ± 0.5	20.5 ± 1.5	2.39 ± 2.87	3.2	9.3	4.6	11.2	2.59	2.79	3.37
Environment Office, IESSG and NCL CGPS Stations (OTHER)										
IESG	3.3 ± 0.1	9.4 ± 0.7	-2.46 ± 0.81	1.9	8.3	3.6	6.8	-1.44	1.13	0.94
BARK	4.5 ± 0.1	7.4 ± 1.0	-0.56 ± 0.70	2.6	8.8	4.7	6.3	-1.59	1.21	0.87
SUNB	4.4 ± 0.1	10.7 ± 0.9	1.23 ± 0.95	2.9	9.1	4.8	8.4	0.06	1.25	1.15
MORP	6.8 ± 0.4	20.7 ± 2.1	-2.64 ± 1.57	6.3	11.8	7.9	16.3	-1.54	1.62	2.23
UK based IGS Stations (IGS)										
HERS	3.9 ± 0.2	12.3 ± 1.0	-1.80 ± 1.52	2.9	9.1	4.6	9.6	-2.43	1.59	1.67

[a] Computed using Eq. H.12 (Mao et al., 1999)

[b] Computed using Eq. H.13 and H.14 (Williams, 2003a)

[c] Uncertainty according to Method 1 using Eqs. H.19 and H.20

[d] Uncertainty according to Method 2 using Eqs. H.20 and H.20

Appendix L

Improved Coordinate Time Series Results

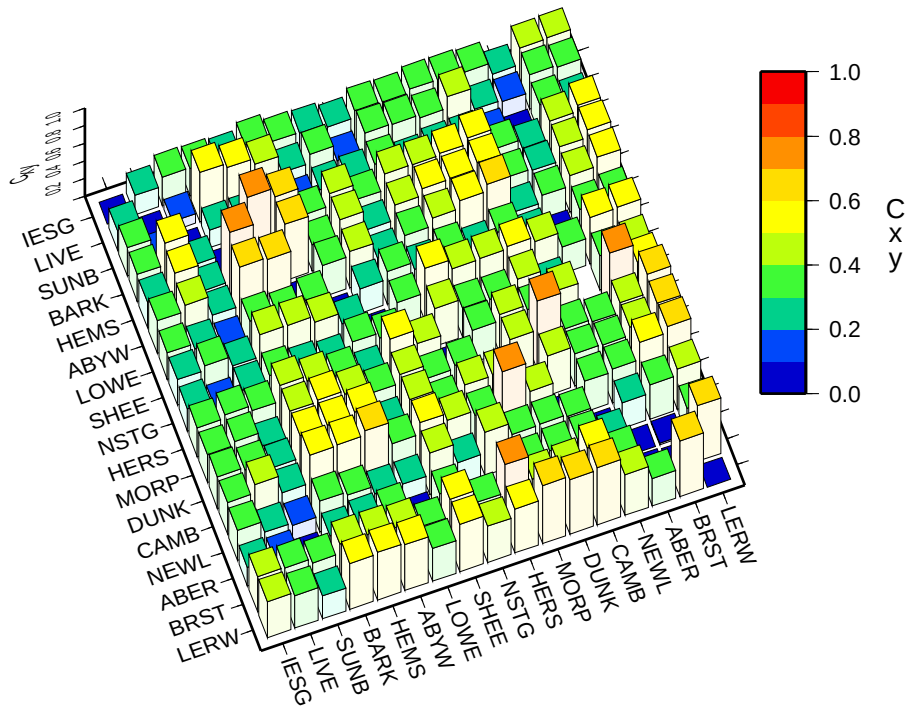

Figure L.1: Cross–correlations C_{xy} at zero lag of the residual ITRS2000 coordinate time series for the North components of 17 UK CGPS stations. Note: The computation was based on a common time span between each station pair.

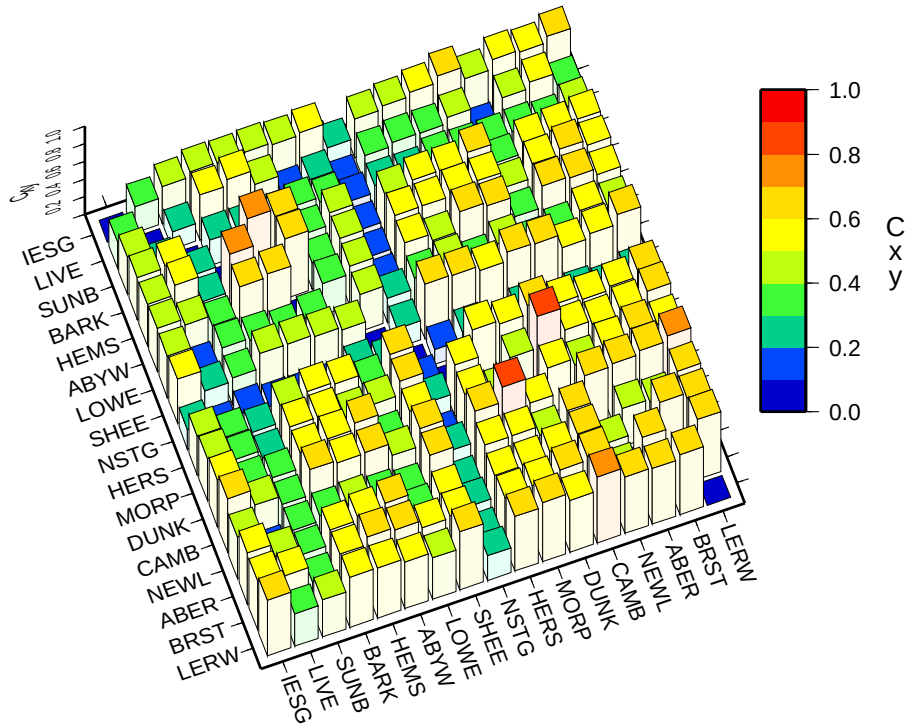

Figure L.2: Cross–correlations C_{xy} at zero lag of the residual ITRS2000 coordinate time series for the East components of 17 UK CGPS stations. Note: The computation was based on a common time span between each station pair.

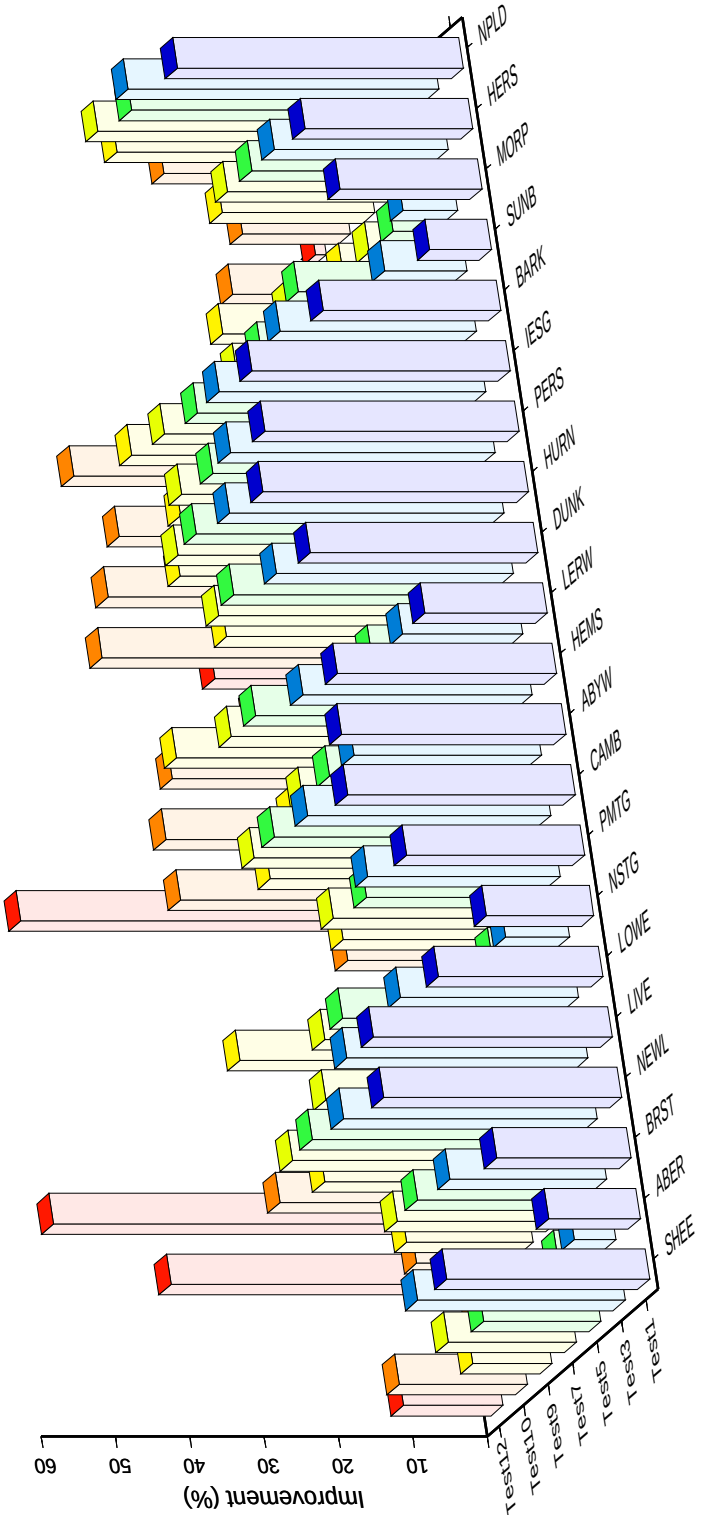

Figure L.3: Improvement in % of the RMS scatter of the filtered improved ITRS2000 North time series for 21 UK CGPS stations following common mode bias tests 1, 3, 5, 7, 9, 10 and 12 as outlined in Table 6.4.

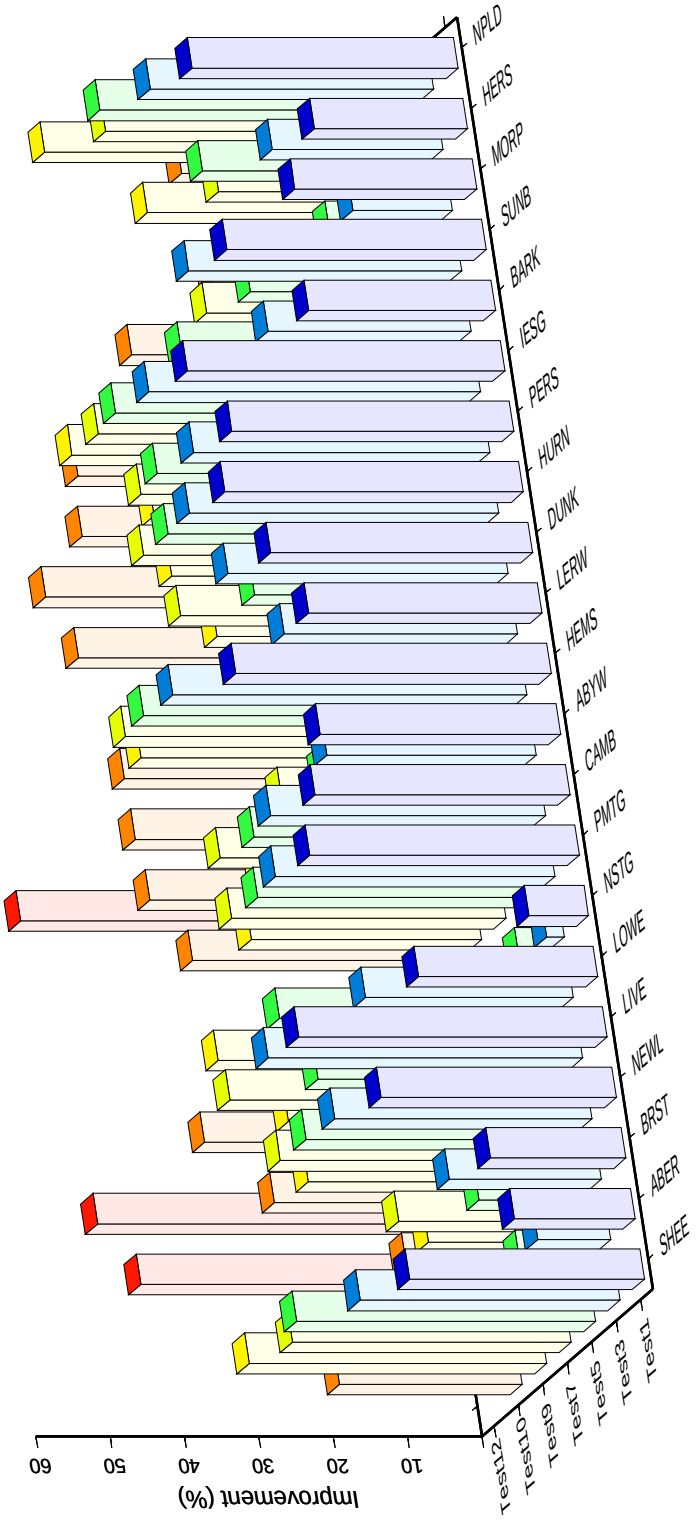

Figure L.4: Improvement in % of the RMS scatter of the filtered improved ITRS2000 East time series for 21 UK CGPS stations following common mode bias tests 1, 3, 5, 7, 9, 10 and 12 as outlined in Table 6.4.

Table L.1: Improvement in % of the RMS scatter for common mode bias tests 1 to 8.

Site	Test 1			Test 2	Test 3			Test 4	Test 5			Test 6	Test 7			Test 8
	N [%]	E [%]	H [%]	H [%]	N [%]	E [%]	H [%]	H [%]	N [%]	E [%]	H [%]	H [%]	N [%]	E [%]	H [%]	H [%]
SHEE	27.3	31.6	22.2	23.3	27.9	35.0	24.4	25.2	15.8	40.3	25.4	26.8	17.3	37.5	24.6	25.8
ABER	12.4	16.2	18.2	18.7	5.6	9.8	11.7	12.1	4.5	9.0	11.6	12.1	5.2	9.7	11.0	11.5
BRST	18.1	18.2	15.7	15.5	21.1	20.4	18.8	18.5	22.2	13.2	12.8	12.5	21.6	20.7	20.6	20.3
NEWL	32.0	31.7	23.5	23.2	34.1	34.6	25.1	24.8	35.1	35.2	25.0	24.6	34.5	35.4	26.9	26.7
LIVE	32.2	41.5	25.7	26.3	32.5	42.3	24.4	25.4	22.0	32.3	26.3	27.1	28.7	40.9	22.8	23.8
LOWE	22.2	24.1	6.0	6.3	24.0	28.0	7.6	8.3	28.5	36.3	7.9	9.1	27.6	30.2	6.5	7.4
NSTG	14.5	8.0	7.5	7.6	8.6	2.4	1.5	1.6	7.1	2.8	1.3	1.3	7.7	2.4	0.7	0.7
PMTG	23.9	36.3	30.5	30.6	25.9	37.6	30.2	30.5	22.8	36.7	33.1	33.1	23.9	36.9	30.4	30.4
CAMB	30.6	34.3	29.8	29.6	32.7	37.0	31.0	31.0	33.9	35.9	31.0	31.0	33.3	37.2	32.7	32.8
ABYW	30.2	32.3	25.3	25.5	25.2	28.2	19.1	19.5	25.2	25.3	19.7	20.1	25.6	27.7	19.0	19.3
HEMS	29.5	42.5	19.5	19.3	30.8	47.6	23.5	23.2	33.9	48.3	25.2	25.1	33.9	47.4	22.8	22.9
LERW	16.5	31.4	23.2	24.3	16.2	31.4	21.2	22.5	17.1	23.2	16.2	17.7	17.1	30.9	14.9	16.3
DUNK	30.6	35.2	33.0	33.3	31.9	37.7	33.8	34.0	34.4	30.9	34.2	34.4	33.1	37.5	34.6	34.9
HURN	35.7	40.2	32.4	33.3	36.9	41.7	32.8	33.7	38.2	41.2	34.5	35.7	37.3	41.2	32.8	33.9
PERS	34.2	38.0	29.5	30.0	35.6	39.8	29.5	30.3	34.7	41.4	31.0	32.1	35.6	40.4	28.7	30.0
IESG	34.7	42.7	29.1	28.8	35.8	44.6	29.7	29.5	35.5	45.8	30.2	30.0	36.6	44.8	28.8	28.3
BARK	23.9	25.1	20.8	21.5	26.4	27.3	24.9	25.5	25.6	35.7	17.5	18.7	25.6	30.6	17.5	18.3
SUNB	8.3	34.9	24.3	24.6	11.1	36.7	27.2	27.3	19.4	25.2	27.6	28.3	17.5	27.7	26.9	27.4
MORP	19.1	24.5	18.0	18.8	7.4	13.4	7.5	7.8	5.4	13.3	7.8	8.2	5.4	13.8	6.5	6.9
HERS	22.6	20.6	11.1	9.9	23.4	23.0	11.4	10.6	23.1	29.1	12.1	11.5	23.1	23.6	11.6	10.4
NPLD	38.5	35.8	24.0	25.4	41.8	38.2	24.2	26.1	38.1	41.6	25.9	28.2	39.3	37.6	22.6	24.5
Average:	25.6	30.7	22.3	22.6	25.5	31.3	21.9	22.3	24.9	30.6	21.7	22.3	25.2	31.2	21.1	21.6

Table L.2: Improvement in % of the RMS scatter for common mode bias tests 9 to 13.

Site	Test 9			Test 10			Test 11	Test 12			Test 13
	N [%]	E [%]	H [%]	N [%]	E [%]	H [%]	H [%]	N [%]	E [%]	H [%]	H [%]
SHEE	10.7	40.0	23.6	17.3	24.6	16.1	15.9	13.4	−2.1	−16.6	−17.3
ABER	3.9	7.7	11.8	5.4	10.0	12.4	12.4	−3.7	1.2	−13.7	−13.8
BRST	17.0	13.4	11.7	12.4	13.2	9.2	9.2	42.2	45.5	49.3	49.2
NEWL	26.8	28.3	17.3	29.6	29.6	20.1	20.1	56.7	50.1	56.1	56.2
LIVE	19.7	29.7	29.4	22.0	37.7	17.5	17.4	7.0	15.2	−39.5	−39.6
LOWE	35.7	38.0	18.1	18.6	11.1	−10.5	−10.5	−16.7	−20.8	−67.0	−68.0
NSTG	5.0	2.7	3.0	7.7	0.2	−1.2	−1.1	−0.4	−5.7	−17.0	−16.9
PMTG	19.3	31.0	30.0	15.4	35.6	27.6	27.4	−10.0	−2.2	−29.6	−29.2
CAMB	27.9	28.5	23.6	36.7	40.1	34.7	34.7	54.8	54.2	55.7	55.7
ABYW	23.6	23.8	17.7	37.4	40.8	35.0	34.9	4.3	10.8	3.0	3.0
HEMS	38.0	42.1	33.9	35.3	41.0	11.6	11.6	13.2	8.6	−55.0	−55.3
LERW	13.9	21.0	22.4	22.8	36.2	30.7	30.6	−8.4	0.4	−24.2	−23.9
DUNK	28.8	29.4	28.1	42.2	44.7	43.2	43.1	23.8	22.3	10.4	10.3
HURN	33.7	34.2	29.8	40.2	47.9	44.7	44.7	−0.8	3.6	−9.5	−9.8
PERS	32.4	35.3	32.8	37.4	41.7	31.8	31.6	−14.0	−7.8	−42.3	−42.0
IESG	37.7	45.1	37.7	42.3	41.0	20.6	20.6	1.9	−4.6	−44.0	−44.5
BARK	15.7	32.4	26.8	11.7	16.3	6.0	5.9	−0.2	−16.7	−27.3	−28.7
SUNB	23.0	21.6	28.7	6.1	31.3	10.9	11.0	−7.5	15.7	−24.8	−25.7
MORP	5.6	12.3	10.8	17.1	18.9	8.9	9.2	8.2	7.0	−23.8	−23.4
HERS	20.6	29.9	11.8	14.6	15.2	3.3	2.9	1.4	−17.8	−21.0	−22.7
NPLD	33.5	42.5	34.4	23.8	20.8	5.3	5.5	−10.9	−19.4	−66.0	−66.5
Average:	22.5	28.0	23.0	23.6	28.5	18.0	18.0	7.3	6.6	−16.5	−16.8

Table L.3: Station velocity estimates for unfiltered and filtered improved ITRS2000 coordinate time series. Velocity uncertainties have been obtained using the empirical method by Williams (2003a), i.e. Eqs. H.13 and H.14 along with Eqs. H.19 and H.20 in Appendix H (i.e. a WN+FN model).

Site	Unfiltered Coordinate Time Series						Filtered Coordinate Time Series					
	North Component		East Component		Height Component		North Component		East Component		Height Component	
	RMS [mm]	Velocity [mm/yr]	RMS [mm]	Velocity [mm/yr]	RMS [mm]	Velocity [mm/yr]	RMS [mm]	Velocity [mm/yr]	RMS [mm]	Velocity [mm/yr]	RMS [mm]	Velocity [mm/yr]
CGPS@TG Stations (TG)												
SHEE	2.83	15.11 ± 0.68	4.31	18.42 ± 0.86	8.14	-0.70 ± 1.51	2.55	15.01 ± 0.66	2.76	18.19 ± 0.48	6.19	-0.93 ± 0.96
ABER	3.91	15.01 ± 0.87	7.26	16.47 ± 1.80	9.10	1.83 ± 2.43	5.01	14.90 ± 0.54	8.41	15.98 ± 1.55	9.04	0.78 ± 1.24
BRST	3.22	15.64 ± 1.35	6.05	16.80 ± 2.55	11.23	1.18 ± 5.56	2.87	15.66 ± 1.02	5.96	17.24 ± 2.33	10.49	1.05 ± 4.73
NEWL	2.90	16.15 ± 1.00	5.01	17.16 ± 1.90	11.14	0.46 ± 4.78	2.08	16.11 ± 0.67	3.44	17.05 ± 1.35	8.47	0.16 ± 3.59
LIVE	2.47	14.24 ± 0.77	4.16	16.24 ± 1.30	6.77	2.17 ± 2.09	1.90	14.34 ± 0.48	2.69	16.19 ± 0.65	5.03	1.85 ± 1.62
LOWE	2.08	14.96 ± 0.59	3.40	18.47 ± 1.04	5.90	0.41 ± 1.92	1.54	15.05 ± 0.53	2.27	18.38 ± 0.89	5.57	0.40 ± 2.46
NSTG	4.73	14.40 ± 0.13	9.64	18.62 ± 0.00	14.31	0.88 ± 1.71	4.95	14.09 ± 0.00	9.31	19.31 ± 0.22	14.59	0.91 ± 2.53
UK Met Office CGPS Stations (MO)												
CAMB	3.10	15.94 ± 0.84	5.07	16.66 ± 1.66	10.22	0.52 ± 3.58	2.17	15.89 ± 0.53	3.40	16.82 ± 1.06	7.22	0.07 ± 2.51
ABYW	2.78	15.87 ± 0.71	5.55	17.64 ± 1.53	12.12	1.21 ± 3.76	2.27	15.83 ± 0.57	4.37	17.51 ± 1.04	9.79	0.66 ± 2.63
HEMS	2.76	14.92 ± 1.34	4.38	19.02 ± 1.62	6.18	1.23 ± 1.83	1.94	14.83 ± 1.04	2.33	18.82 ± 0.96	4.78	1.23 ± 2.14
LERW	3.03	16.30 ± 0.85	4.64	13.67 ± 1.29	7.53	0.14 ± 2.13	2.87	16.39 ± 0.76	3.87	13.36 ± 1.05	6.22	-0.15 ± 1.53
DUNK	2.86	16.30 ± 1.82	4.77	17.40 ± 2.87	8.67	2.65 ± 5.82	2.08	16.05 ± 1.10	3.58	17.74 ± 1.83	5.85	2.59 ± 3.37
Environment Agency, IESSG and NCL CGPS Stations (OTHER)												
IESG	2.33	14.34 ± 0.42	3.92	17.96 ± 0.70	6.18	-1.29 ± 1.22	1.69	14.30 ± 0.31	2.26	17.78 ± 0.46	4.31	-1.44 ± 0.94
BARK	3.50	15.28 ± 1.04	4.08	18.18 ± 0.78	6.56	-1.38 ± 1.07	2.84	15.32 ± 0.88	2.64	18.07 ± 0.64	5.13	-1.59 ± 0.87
SUNB	3.10	15.41 ± 0.87	5.41	17.98 ± 1.36	7.79	0.29 ± 1.52	2.25	15.28 ± 0.63	3.95	17.89 ± 1.03	5.58	0.06 ± 1.15
MORP	4.19	16.42 ± 0.94	7.45	14.90 ± 1.47	9.88	-1.32 ± 2.28	4.69	16.43 ± 0.98	6.99	14.58 ± 1.13	9.61	-1.54 ± 2.23
UK based IGS Stations (IGS)												
HERS	2.73	12.48 ± 0.82	4.02	18.37 ± 1.12	6.77	-2.59 ± 1.89	2.03	12.57 ± 0.64	2.58	18.66 ± 0.79	5.56	-2.43 ± 1.67

Table L.4: Annual term estimates for the unfiltered and filtered improved ITRS2000 coordinate time series.

Site	Unfiltered coordinate time series						Filtered coordinate time series					
	North Component		East Component		Height Component		North Component		East Component		Height Component	
	a [mm]	ϕ [days]	a [mm]	ϕ [days]	a [mm]	ϕ [days]	a [mm]	ϕ [days]	a [mm]	ϕ [days]	a [mm]	ϕ [days]
						CGPS@TG Stations (TG)						
SHEE	4.9 ± 0.2	6 ± 2	0.5 ± 0.2	19 ± 18	1.6 ± 0.4	157 ± 10	4.3 ± 0.1	13 ± 1	0.8 ± 0.1	152 ± 7	1.1 ± 0.3	181 ± 11
ABER	1.7 ± 0.2	26 ± 5	3.6 ± 0.4	330 ± 4	1.7 ± 0.5	3 ± 13	1.3 ± 0.3	50 ± 9	1.9 ± 0.5	334 ± 10	2.0 ± 0.5	359 ± 11
BRST	1.3 ± 0.2	364 ± 7	4.8 ± 0.4	37 ± 3	3.2 ± 0.7	244 ± 5	0.4 ± 0.2	53 ± 19	3.2 ± 0.4	61 ± 5	2.7 ± 0.7	247 ± 12
NEWL	1.7 ± 0.2	337 ± 4	2.3 ± 0.3	358 ± 5	1.6 ± 0.6	161 ± 15	0.6 ± 0.1	325 ± 7	0.7 ± 0.2	6 ± 11	1.5 ± 0.5	152 ± 14
LIVE	3.2 ± 0.2	22 ± 2	4.0 ± 0.3	28 ± 3	1.8 ± 0.3	7 ± 9	2.7 ± 0.1	40 ± 2	2.9 ± 0.2	47 ± 2	1.5 ± 0.3	2 ± 8
LOWE	0.9 ± 0.1	309 ± 3	0.7 ± 0.2	2 ± 11	1.9 ± 0.3	16 ± 7	0.5 ± 0.1	197 ± 7	0.5 ± 0.1	182 ± 11	1.6 ± 0.3	12 ± 8
NSTG	3.0 ± 0.4	345 ± 6	2.8 ± 0.8	305 ± 7	3.9 ± 1.2	291 ± 4	2.4 ± 0.5	343 ± 8	2.5 ± 0.9	257 ± 15	3.2 ± 1.3	301 ± 17
						UK Met Office CGPS Stations (MO)						
CAMB	1.3 ± 0.2	342 ± 5	2.6 ± 0.2	19 ± 4	1.4 ± 0.5	104 ± 3	0.3 ± 0.1	342 ± 17	1.5 ± 0.2	51 ± 5	0.6 ± 0.4	67 ± 26
ABYW	1.1 ± 0.1	314 ± 4	2.3 ± 0.3	10 ± 5	3.8 ± 0.6	63 ± 3	0.3 ± 0.1	250 ± 16	1.5 ± 0.2	46 ± 6	3.3 ± 0.5	49 ± 7
HEMS	1.0 ± 0.2	339 ± 7	1.4 ± 0.3	1 ± 9	1.9 ± 0.4	53 ± 6	0.3 ± 0.1	165 ± 18	0.9 ± 0.2	15 ± 7	1.0 ± 0.3	352 ± 14
LERW	1.1 ± 0.1	346 ± 6	3.5 ± 0.2	339 ± 3	3.9 ± 0.4	7 ± 5	0.1 ± 0.2	55 ± 60	2.0 ± 0.2	341 ± 4	4.2 ± 0.3	359 ± 3
DUNK	1.3 ± 0.2	325 ± 5	3.4 ± 0.3	13 ± 4	1.2 ± 0.5	286 ± 5	0.4 ± 0.2	280 ± 17	1.0 ± 0.3	38 ± 11	1.0 ± 0.4	335 ± 17
						Environment Agency, IESSG, NCL CGPS Stations (OTHER)						
IESG	1.2 ± 0.1	331 ± 3	1.3 ± 0.2	341 ± 6	1.3 ± 0.3	317 ± 7	0.3 ± 0.1	347 ± 10	0.2 ± 0.1	357 ± 26	1.6 ± 0.2	316 ± 5
BARK	2.3 ± 0.2	339 ± 3	1.9 ± 0.2	280 ± 0	4.2 ± 0.3	209 ± 3	1.3 ± 0.1	347 ± 4	1.8 ± 0.1	250 ± 3	4.3 ± 0.3	215 ± 2
SUNB	2.3 ± 0.1	198 ± 3	5.2 ± 0.3	4 ± 3	1.0 ± 0.3	223 ± 12	2.6 ± 0.1	184 ± 2	4.2 ± 0.2	10 ± 2	1.0 ± 0.3	238 ± 11
MORP	1.9 ± 0.3	326 ± 5	2.6 ± 0.5	0 ± 9	3.4 ± 0.6	19 ± 8	1.1 ± 0.3	328 ± 12	1.3 ± 0.5	12 ± 16	3.8 ± 0.7	11 ± 7
						UK based IGS Stations (IGS)						
HERS	1.3 ± 0.2	16 ± 6	0.6 ± 0.2	307 ± 10	1.2 ± 0.5	99 ± 3	0.7 ± 0.1	56 ± 7	1.0 ± 0.1	201 ± 6	0.6 ± 0.3	131 ± 22

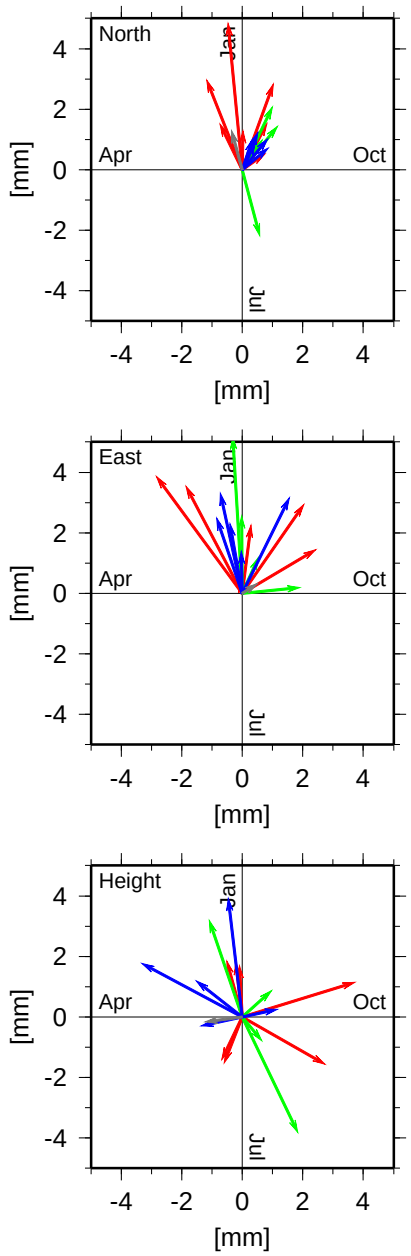

Figure L.5: Annual term estimates for the unfiltered improved ITRS2000 coordinate time series for CGPS@TG (red), MO CGPS (green), OTHER CGPS (blue) and IGS (grey) stations. The amplitude is indicated by the vector length and the seasonal maximum by the vector direction, which is measured counter–clock–wise from the vertical axis.

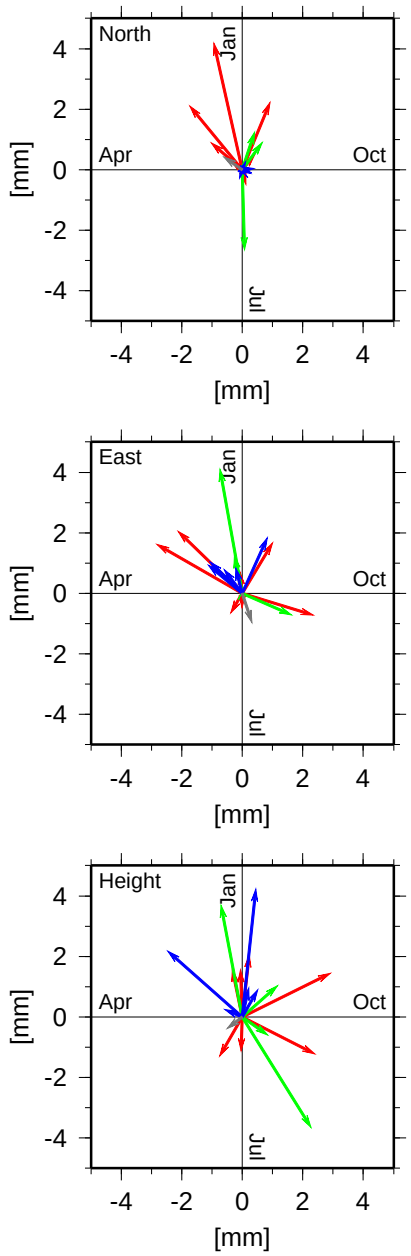

Figure L.6: Annual term estimates for the filtered improved ITRS2000 coordinate time series for CGPS@TG (red), MO CGPS (green), OTHER CGPS (blue) and IGS (grey) stations. The amplitude is indicated by the vector length and the seasonal maximum by the vector direction, which is measured counter–clock–wise from the vertical axis.

Table L.5: Coordinate offset estimates for the unfiltered and filtered improved ITRS2000 coordinate time series.

Site	Date	Unfiltered Coordinate Time Series			Filtered Coordinate Time Series		
		North Component [mm]	East Component [mm]	Height Component [mm]	North Component [mm]	East Component [mm]	Height Component [mm]
SHEE	9 Mar 1998			5.6 ± 0.9			7.4 ± 1.7
SHEE	2 Feb 1999			2.8 ± 0.8			2.6 ± 1.8
ABER	2 Feb 1999			-0.4 ± 1.5			-0.9 ± 1.6
NEWL	2 Feb 1999			3.2 ± 1.6			2.8 ± 4.7
CAMB	2 Feb 1999			3.0 ± 1.0			3.4 ± 4.1
ABYW	2 Feb 1999			2.9 ± 1.2			3.5 ± 3.9
HEMS	2 Feb 1999			0.5 ± 0.8			-0.1 ± 2.7
LERW	2 Feb 1999			2.8 ± 0.8			2.8 ± 2.1
IESG	9 Mar 1998			-3.3 ± 0.6			-1.3 ± 1.7
IESG	2 Feb 1999			4.4 ± 0.6			3.9 ± 1.7
BARK	9 Mar 1998			3.4 ± 0.8			5.3 ± 1.5
BARK	2 Feb 1999			2.9 ± 0.7			1.6 ± 1.5
SUNB	9 Mar 1998			2.5 ± 0.8			4.2 ± 2.0
SUNB	2 Feb 1999			1.6 ± 0.8			1.4 ± 2.0
MORP	9 Mar 1998			4.9 ± 1.3			7.0 ± 4.1
HERS	21 Mar 1999	3.6 ± 0.4	2.7 ± 0.5	20.8 ± 1.1	3.4 ± 0.8	1.6 ± 1.1	19.7 ± 2.2
HERS	8 Aug 2001	8.0 ± 0.4	-5.6 ± 0.5	-6.0 ± 1.1	7.6 ± 1.0	-5.8 ± 1.5	-7.4 ± 2.9

Appendix M

Dual–CGPS Station Analysis Results

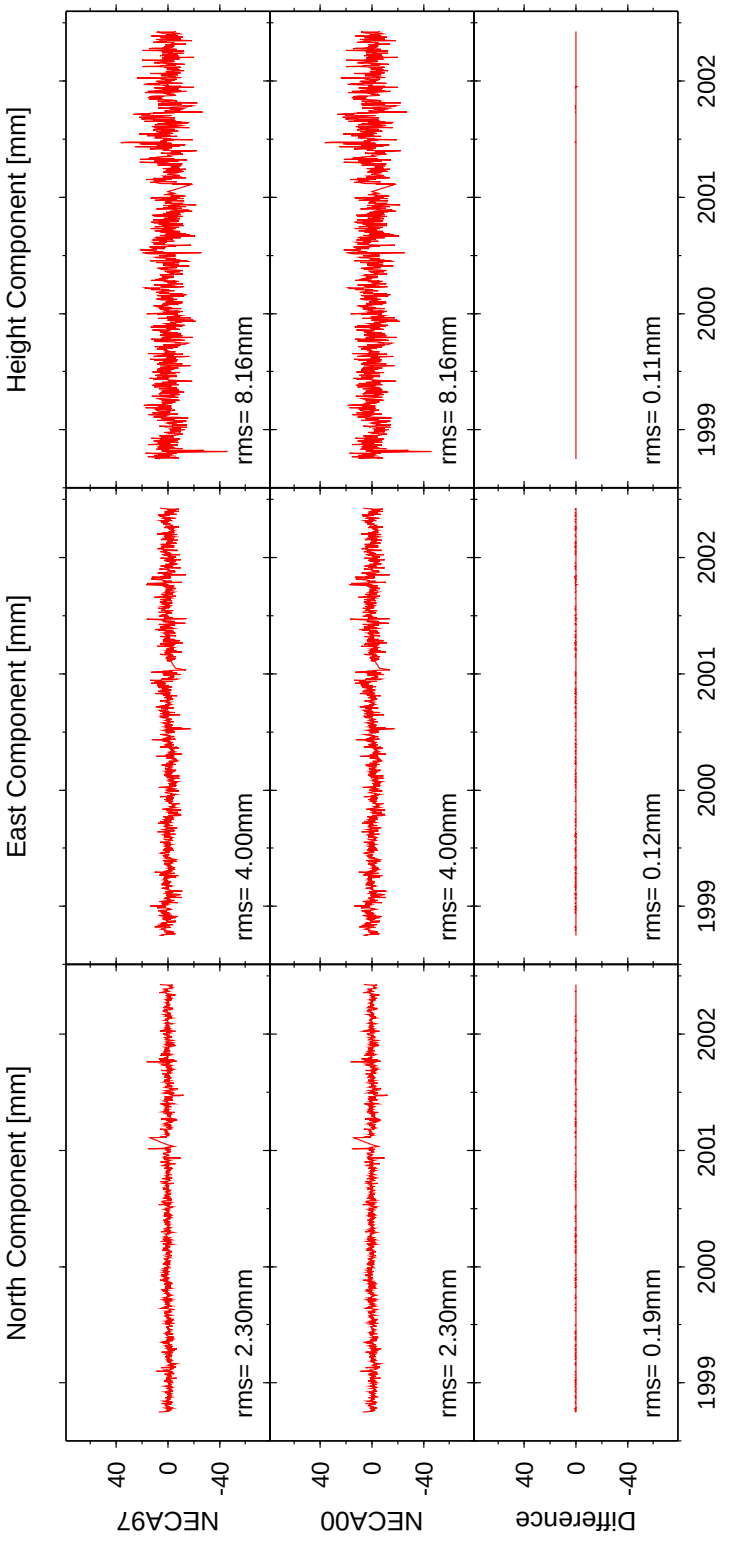

Figure M.1: Dual–CGPS station analysis reference frame comparison of the ITRF97 and ITRS2000 coordinate time series for station pair NEWL-CAMB over a common time span of 3.7 years. NECA97 and NECA00 denote the coordinate difference time series obtained from a dual–CGPS station analysis of the ITRS97 and ITRS2000 coordinate time series, respectively.

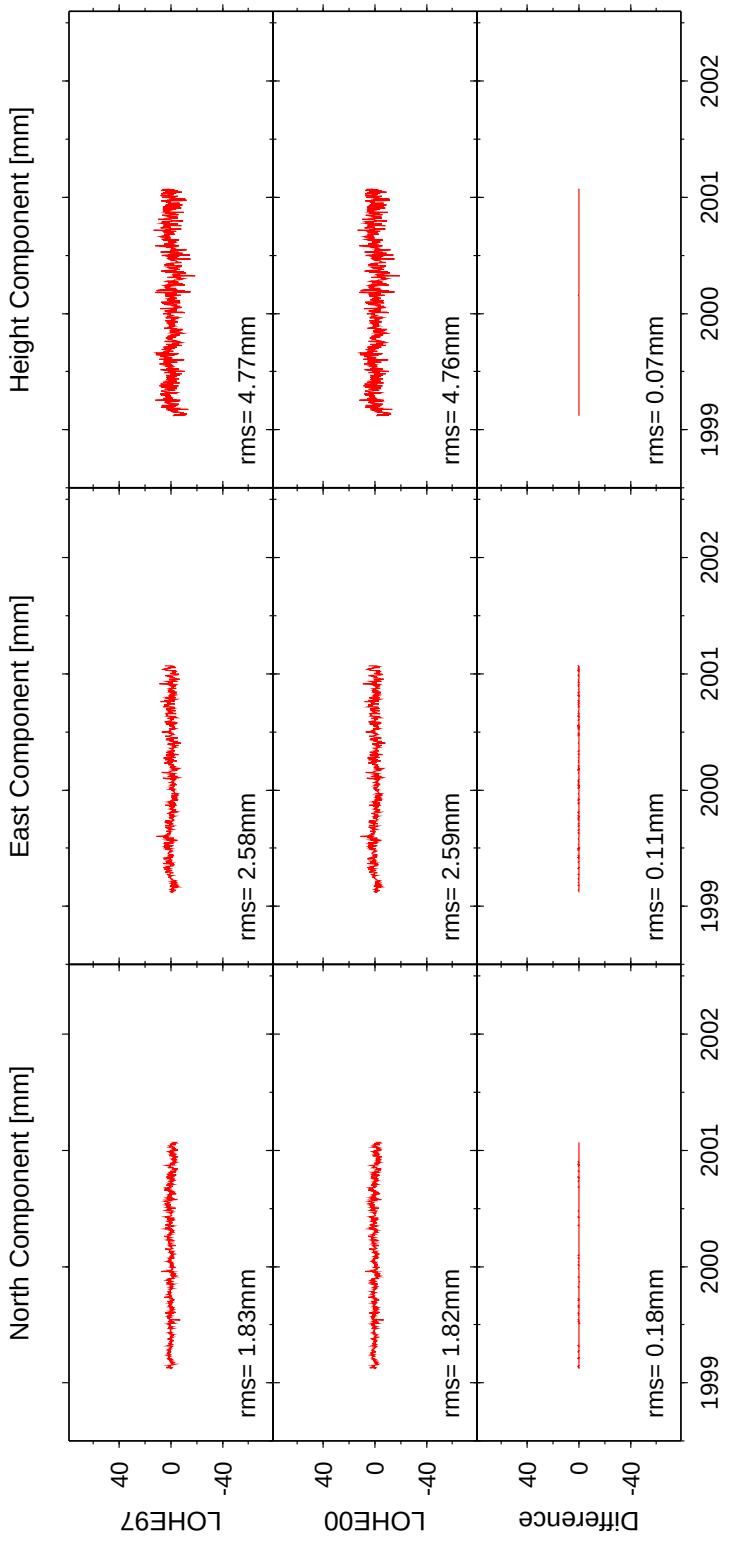

Figure M.2: Dual–CGPS station analysis reference frame comparison of the ITRS97 and ITRS2000 coordinate time series for station pair LOWE–HEMS over a common time span of 2.0 years. LOHE97 and LOHE00 denote the coordinate difference time series obtained from a dual–CGPS station analysis of the ITRS97 and ITRS2000 coordinate time series, respectively.

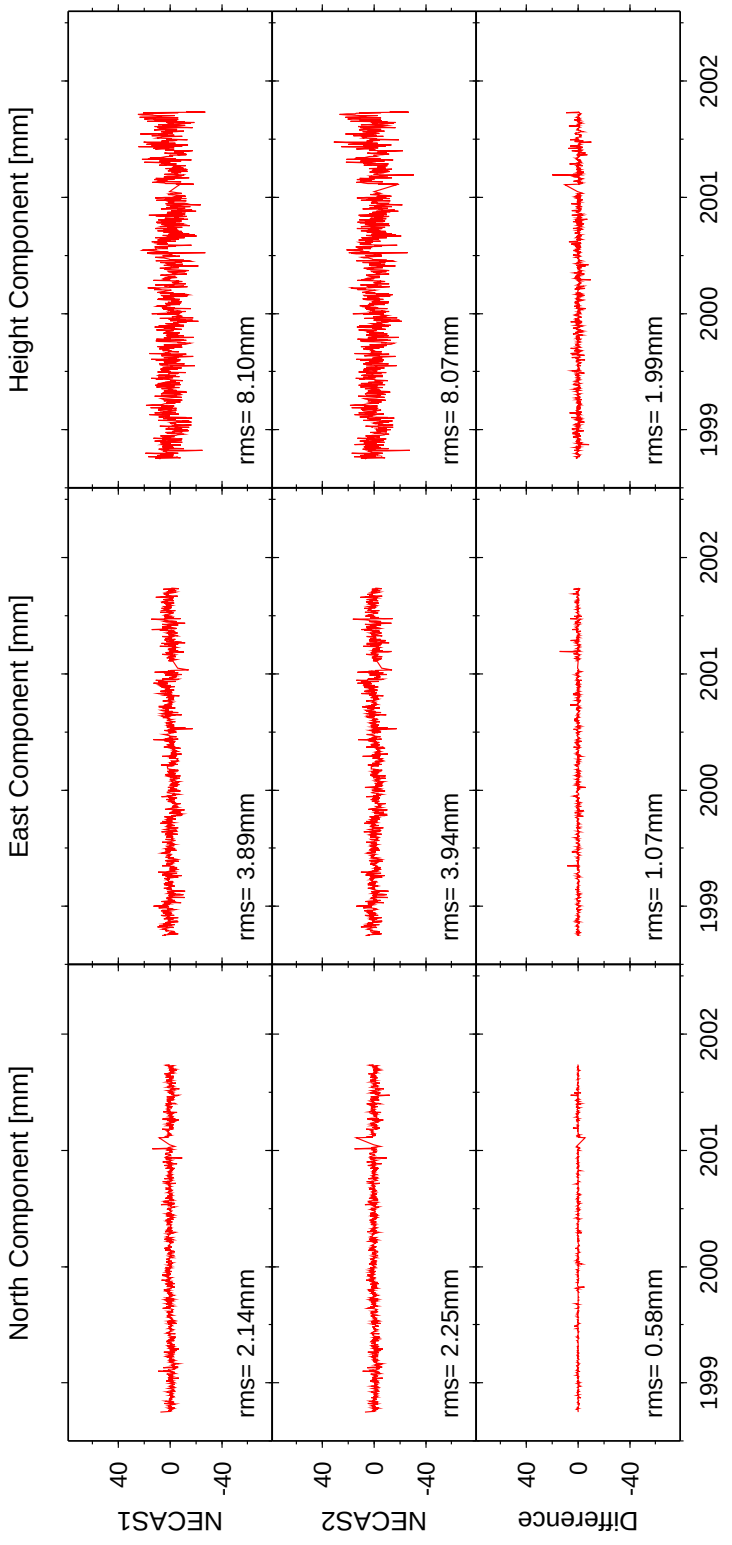

Figure M.3: Dual–CGPS station analysis of the coordinate time series obtained for Strategies 1 and 2 (§6.2.1) for station pair NEWL–CAMB over a common time span of 3.7 years. NECAS1 and NECAS2 denote the coordinate difference time series obtained from a dual–CGPS analysis of the coordinate time series obtained for Strategies 1 and 2 respectively.

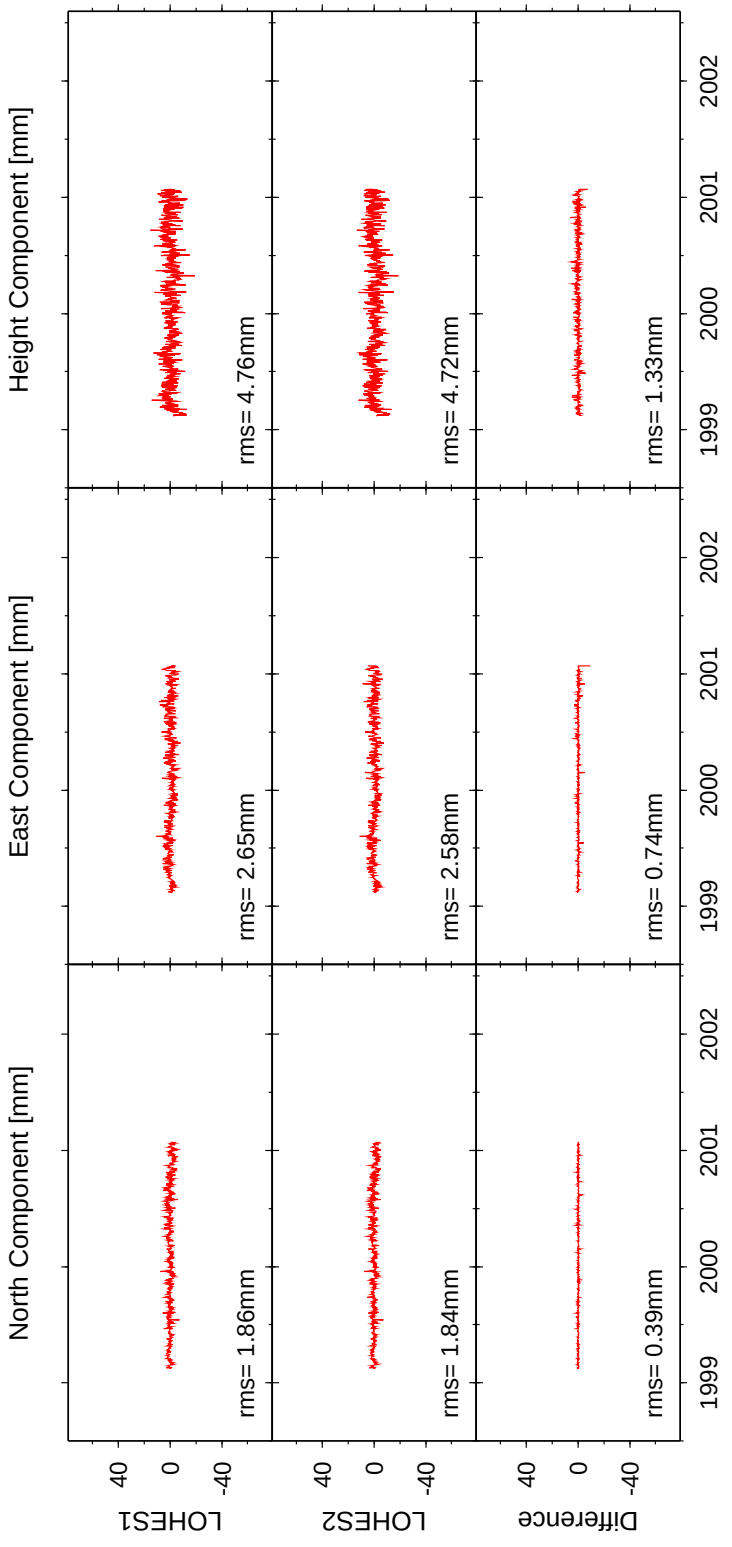

Figure M.4: Dual–CGPS station analysis of the coordinate time series obtained for Strategies 1 and 2 (§6.2.1) for station pair LOWE–HEMS over a common time span of 2.0 years. LOHES1 and LOHES2 denote the coordinate difference time series obtained from a dual–CGPS analysis of the coordinate time series obtained for Strategies 1 and 2 respectively.

Table M.1: Adaptive filter parameter combinations tested for the North component of dual–CGPS station pair LOWE–HEMS

M	μ [$\times 10^{-4}$]	$r_{ee'}(0)$[a] [%]	$r_{ey}(0)$[b] [%]	RMS_a[c] [mm]	RMS_b[d] [mm]	$RMSRatio$
5	0.20	99	25	0.99	3.48	0.3
5	0.30	99	16	1.08	3.09	0.3
5	0.60	99	9	1.17	2.59	0.5
5	1.20	99	6	1.25	2.22	0.6
5	1.52	99	5	1.28	2.10	0.6
5	2.40	99	4	1.36	1.89	0.7
5	2.43	99	4	1.36	1.88	0.7
7	0.20	99	17	0.97	3.25	0.3
7	0.30	99	12	1.04	2.94	0.4
7	0.60	99	7	1.12	2.54	0.4
7	1.09	99	5	1.18	2.25	0.5
7	1.20	99	5	1.19	2.21	0.5
7	1.74	99	4	1.25	2.04	0.6
9	0.20	99	13	0.95	3.14	0.3
9	0.30	99	9	1.00	2.88	0.3
9	0.60	99	6	1.07	2.53	0.4
9	0.85	99	5	1.10	2.36	0.5
9	1.20	99	4	1.15	2.21	0.5
9	1.35	99	4	1.17	2.16	0.5

[a] Cross–correlation coefficient of the forward and reversed direction filter error sequences (Eq. 7.4)

[b] Cross–correlation coefficient of the error and filtered output sequences (Eq. 7.5)

[c] RMS statistic of the difference in the forward and reversed direction filter error sequences (Eq. 7.6)

[d] Average RMS statistic of the difference in the two–station common mode bias and error sequences of the forward and reversed direction filter process (Eq. 7.11)

Table M.2: Adaptive filter parameter combinations tested for the East component of dual–CGPS station pair LOWE–HEMS

M	μ [$\times 10^{-4}$]	$r_{ee'}(0)$[a] [%]	$r_{ey}(0)$[b] [%]	RMS_a[c] [mm]	RMS_b[d] [mm]	$RMSRatio$
5	0.20	99	17	1.65	4.43	0.4
5	0.30	99	13	1.73	4.02	0.4
5	0.60	98	9	1.86	3.32	0.5
5	1.20	98	6	2.10	2.82	0.7
5	1.52	98	5	2.21	2.64	0.8
7	0.20	99	13	1.57	4.31	0.4
7	0.30	99	10	1.63	3.96	0.4
7	0.60	99	8	1.79	3.39	0.5
7	1.09	98	5	2.03	2.91	0.7
9	0.20	99	11	1.51	4.26	0.4
9	0.30	99	9	1.57	3.95	0.4
9	0.60	99	7	1.76	3.40	0.6
9	0.85	98	6	1.91	3.13	0.6

[a]Cross–correlation coefficient of the forward and reversed direction filter error sequences (Eq. 7.4)

[b]Cross–correlation coefficient of the error and filtered output sequences (Eq. 7.5)

[c]RMS statistic of the difference in the forward and reversed direction filter error sequences (Eq. 7.6)

[d]Average RMS statistic of the difference in the two–station common mode bias and error sequences of the forward and reversed direction filter process (Eq. 7.11)

Table M.3: Adaptive filter parameter combinations tested for the height component of dual–CGPS station pair LOWE–HEMS

M	μ [$\times 10^{-4}$]	$r_{ee'}(0)$[a] [%]	$r_{ey}(0)$[b] [%]	RMS_a[c] [mm]	RMS_b[d] [mm]	$RMSRatio$
7	0.20	86	40	1.51	5.34	0.3
7	0.30	85	34	1.91	4.88	0.4
7	0.60	82	22	2.63	4.10	0.6
7	1.09	81	12	3.19	3.54	0.9
7	1.20	81	11	3.27	3.47	0.9
7	1.74	80	6	3.54	3.24	1.1
7	2.40	79	2	3.75	3.11	1.2
7	2.44	79	2	3.76	3.11	1.2
9	0.20	86	39	1.54	5.33	0.3
9	0.30	85	33	1.94	4.87	0.4
9	0.60	82	22	2.66	4.10	0.6
9	0.85	81	16	3.00	3.76	0.8
9	1.20	80	10	3.31	3.49	1.0
9	1.35	80	8	3.41	3.41	1.0
11	0.20	86	37	1.58	5.29	0.3
11	0.30	85	32	1.98	4.85	0.4
11	0.60	82	21	2.69	4.10	0.7
11	1.20	80	9	3.35	3.50	1.0
11	1.55	80	5	3.56	3.34	1.1
13	0.20	87	35	1.63	5.24	0.3
13	0.30	85	30	2.02	4.82	0.4
13	0.60	83	19	2.72	4.09	0.7
13	1.20	80	7	3.39	3.51	1.0
13	1.31	80	6	3.47	3.46	1.0
15	0.20	87	34	1.66	5.24	0.3
15	0.30	85	29	2.03	4.83	0.4
15	0.60	82	19	2.73	4.10	0.7
15	1.14	80	8	3.37	3.57	0.9

[a] Cross–correlation coefficient of the forward and reversed direction filter error sequences (Eq. 7.4)

[b] Cross–correlation coefficient of the error and filtered output sequences (Eq. 7.5)

[c] RMS statistic of the difference in the forward and reversed direction filter error sequences (Eq. 7.6)

[d] Average RMS statistic of the difference in the two–station common mode bias and error sequences of the forward and reversed direction filter process (Eq. 7.11)

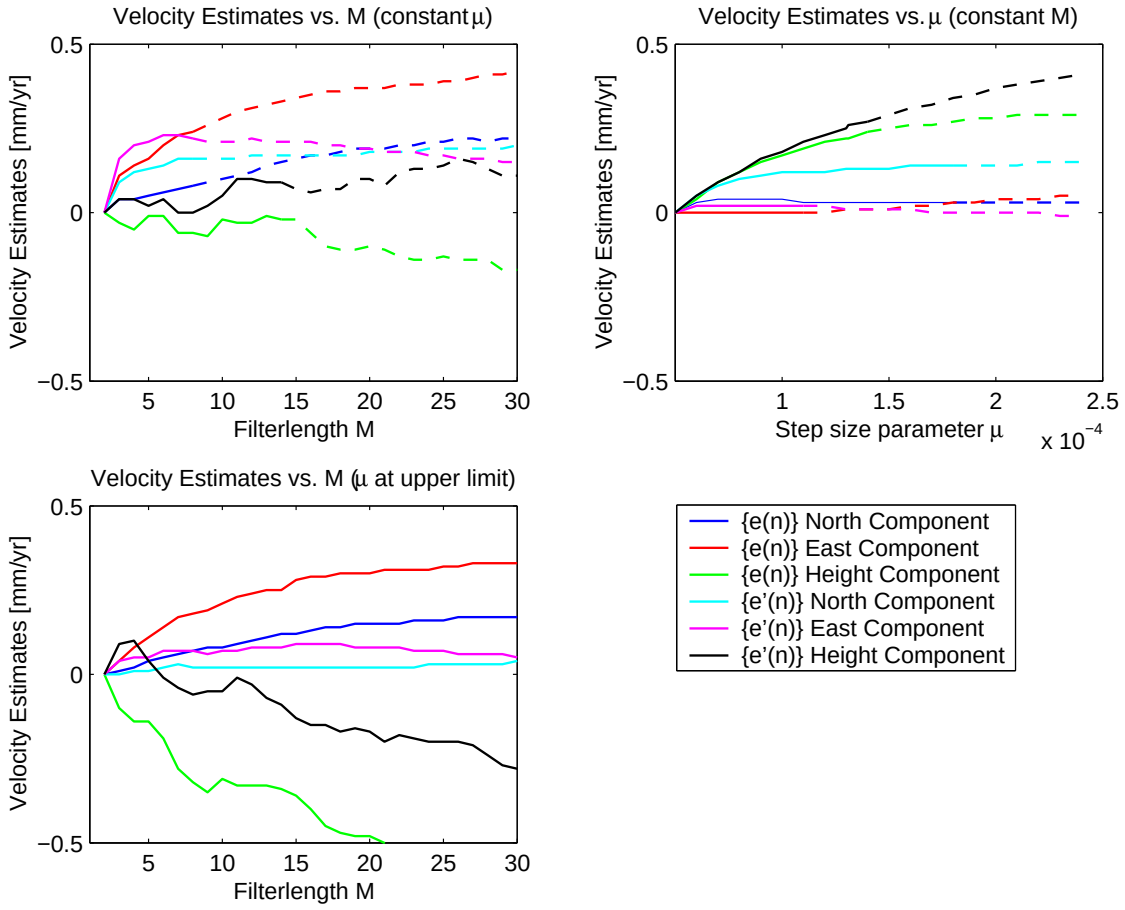

Figure M.5: Adaptive filter velocity test results for dual–CGPS station pair LOWE–HEMS. Velocity estimates computed for error sequences $\{e(n)\}$ and $\{e'(n)\}$ for varying M and μ. Solid lines indicate that μ is below the upper limit (Eq. I.9 in Appendix I) for a specific M, while dashed lines indicate a μ larger than the upper limit.

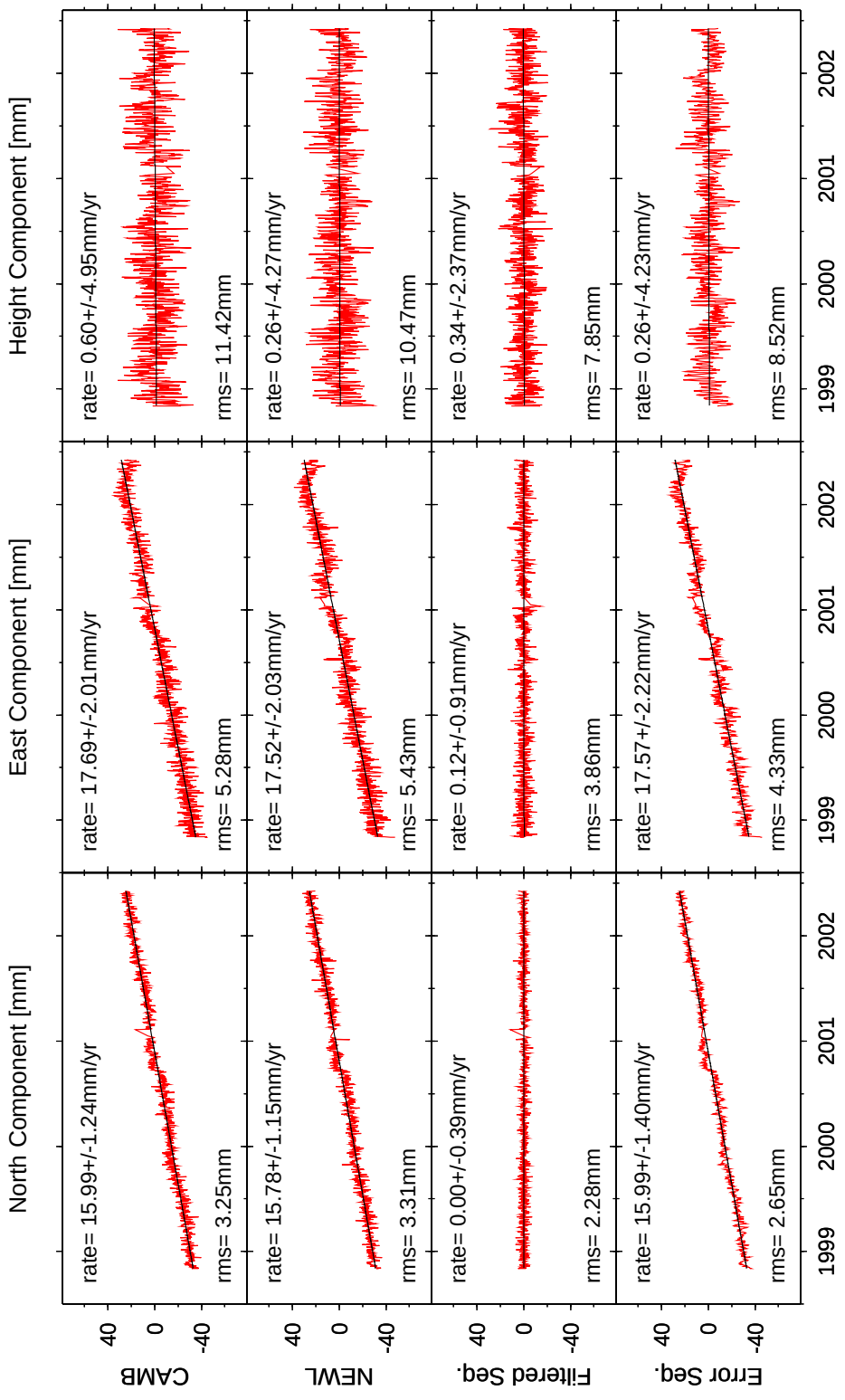

Figure M.6: Reversed direction adaptive filter analysis of observed ITRS2000 coordinate time series for dual–CGPS station pair NEWL–CAMB over a common time span of 3.7 years.

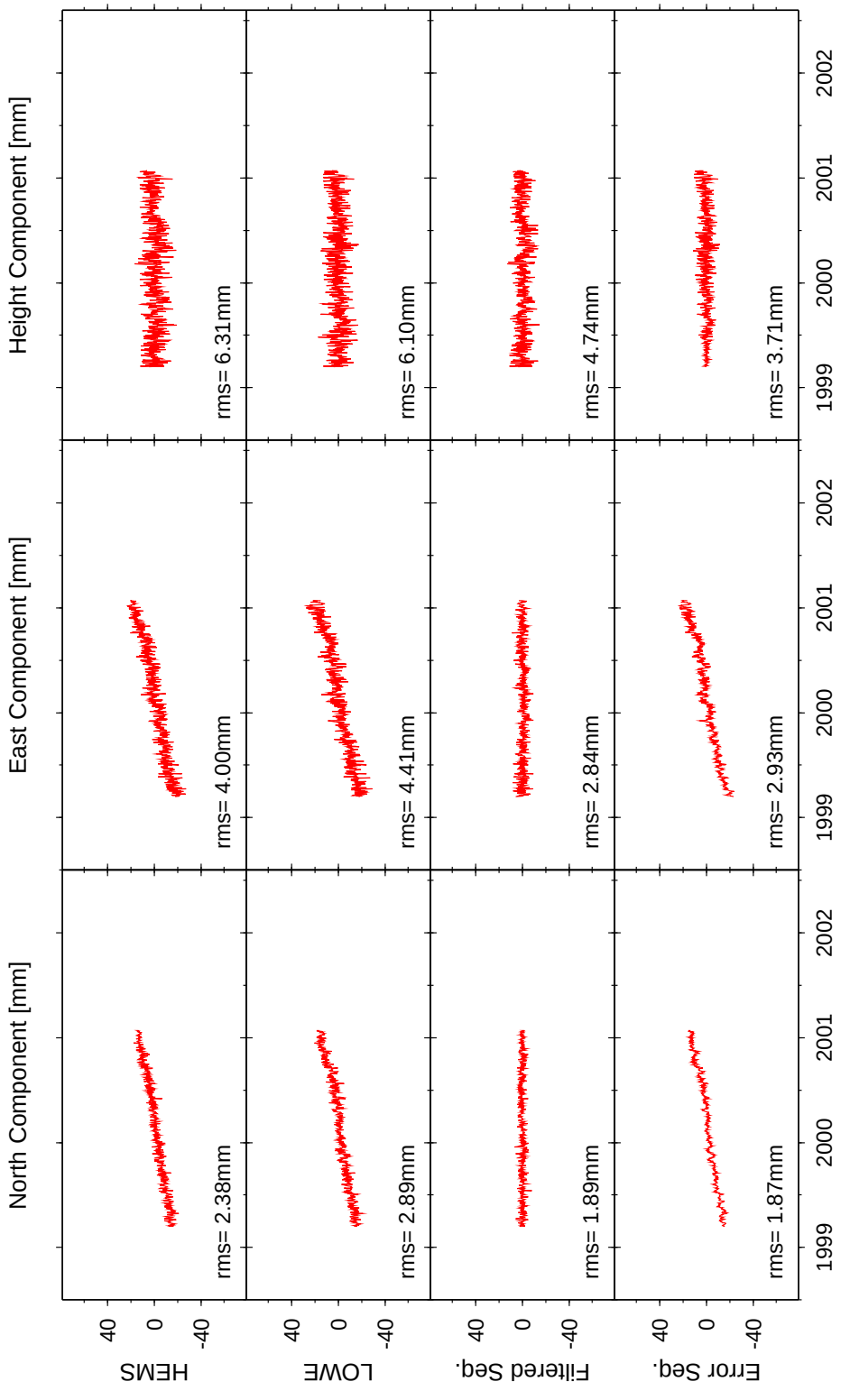

Figure M.7: Reversed direction adaptive filter analysis of observed ITRS2000 coordinate time series for dual–CGPS station pair LOWE–HEMS over a common time span of 2.0 years.

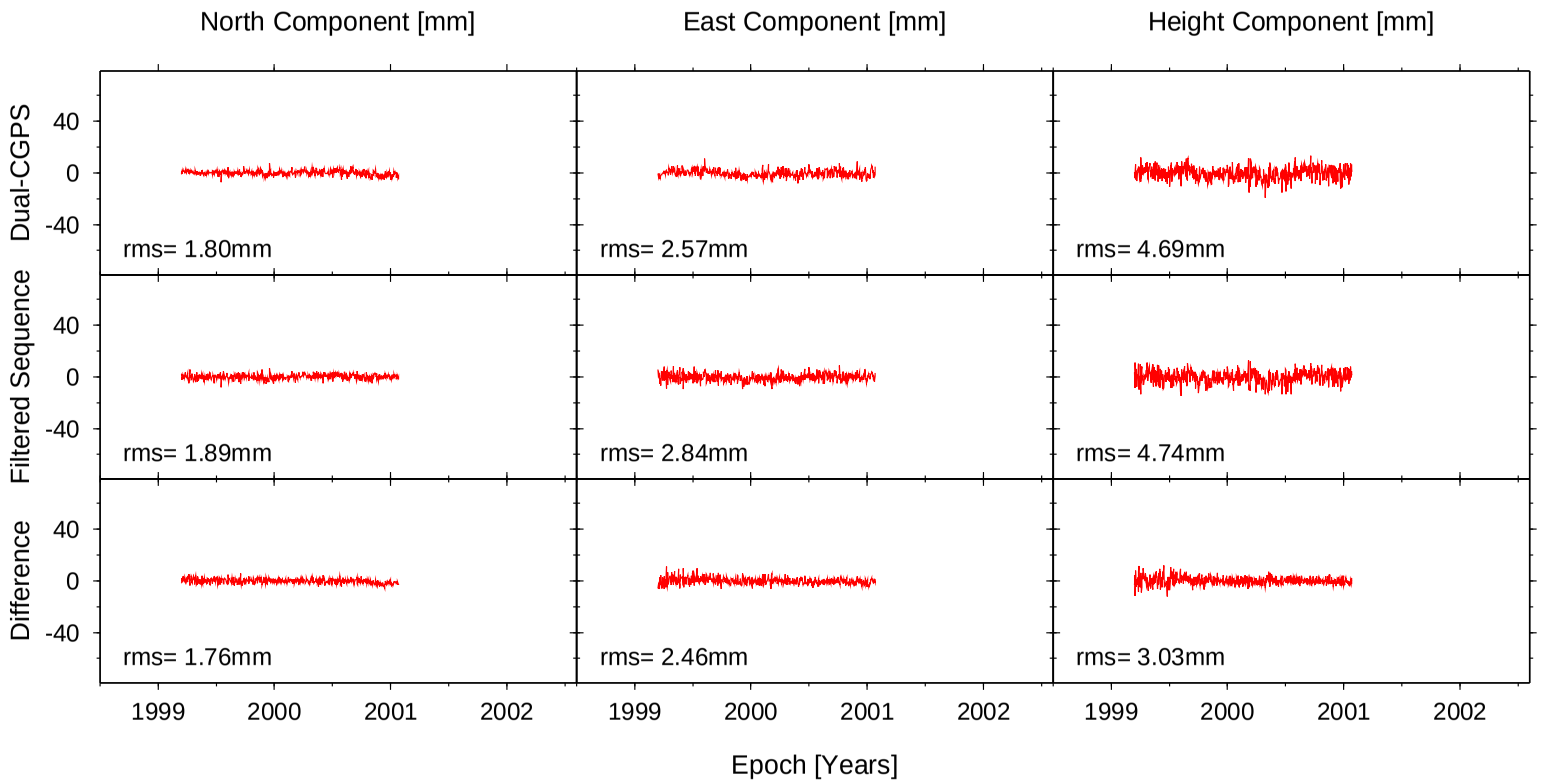

Figure M.8: Dual–CGPS station and adaptive filter analyses compared for the observed ITRS2000 coordinate time series of station pair LOWE–HEMS over a common time span of 2.0 years. Dual–CGPS denotes the coordinate difference time series from the dual–CGPS station analysis and the filtered sequence is obtained from the forward direction adaptive filter analysis.

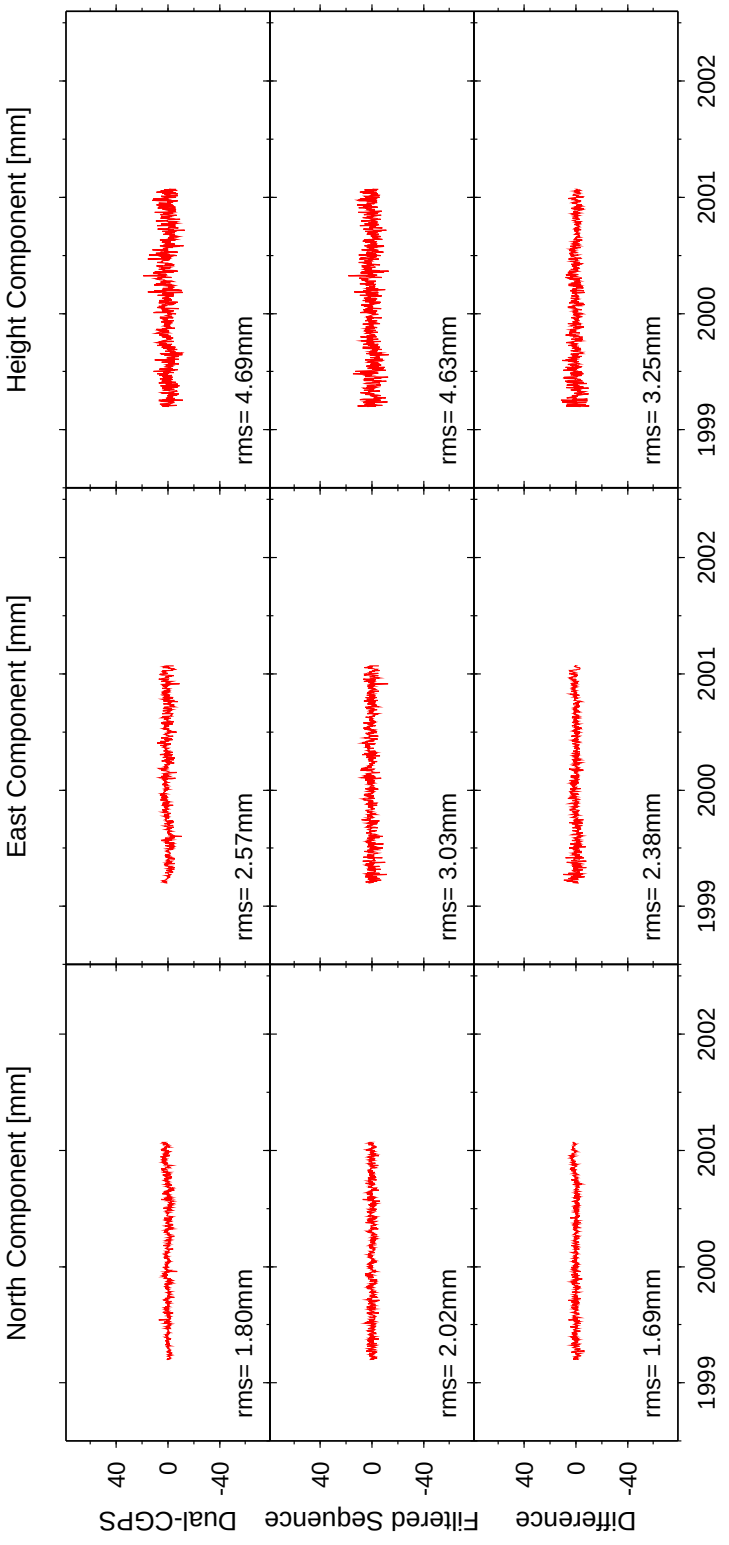

Figure M.9: Dual–CGPS station and adaptive filter analyses compared for the observed ITRS2000 coordinate time series of station pair HEMS–LOWE over a common time span of 2.0 years. Dual–CGPS denotes the coordinate difference time series from the dual–CGPS station analysis and the filtered sequence is obtained from the forward direction adaptive filter analysis.

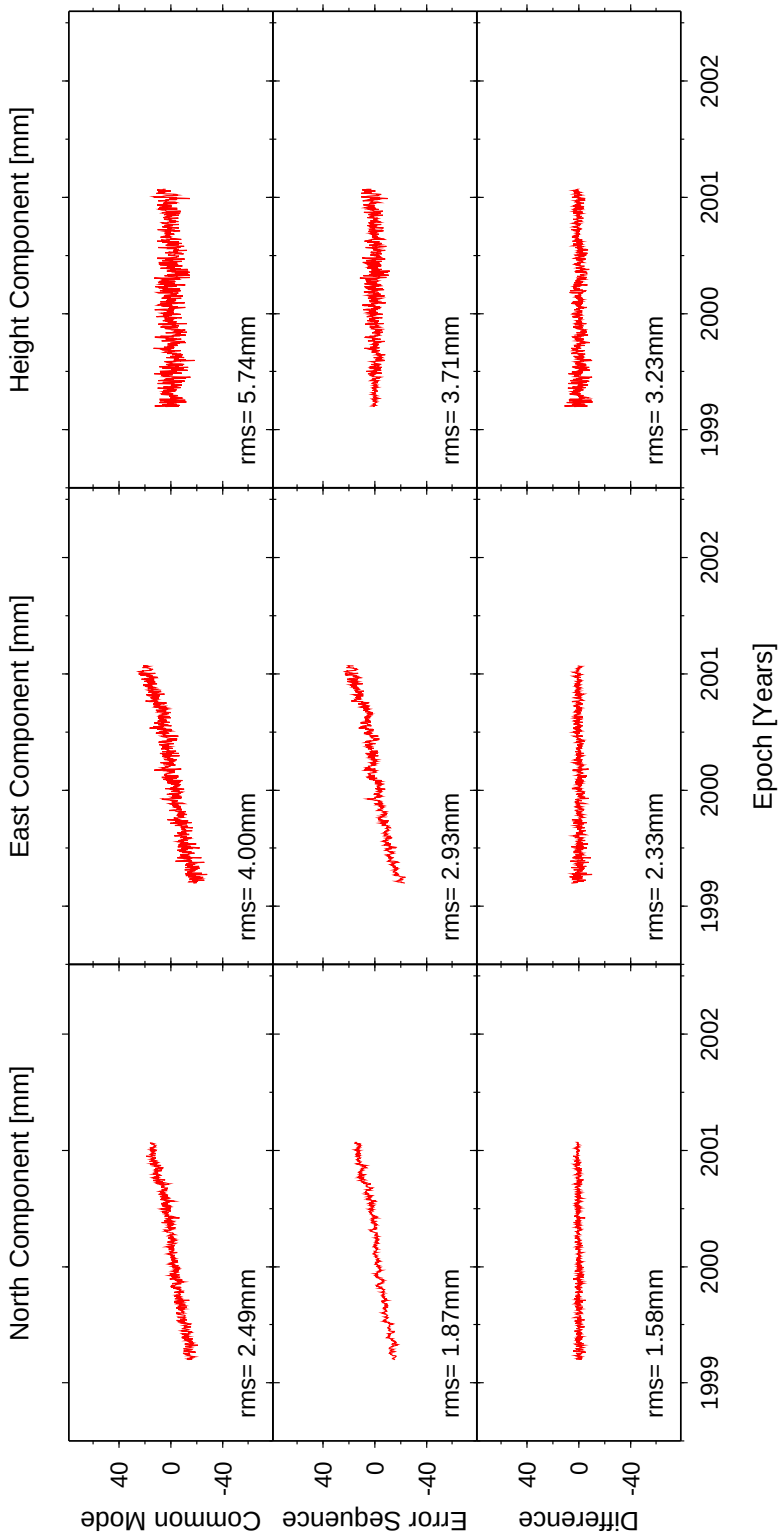

Figure M.10: Two–station common mode bias time series and error sequences of the forward direction adaptive filter analysis for the observed ITRS2000 coordinate time series of the dual–CGPS station pair LOWE–HEMS compared over a common time span of 2.0 years. Common mode denotes the two–station common mode bias time series computed using Eq. 7.8 and error sequence denotes the coherent signal components of the two input sequences to the adaptive filter.

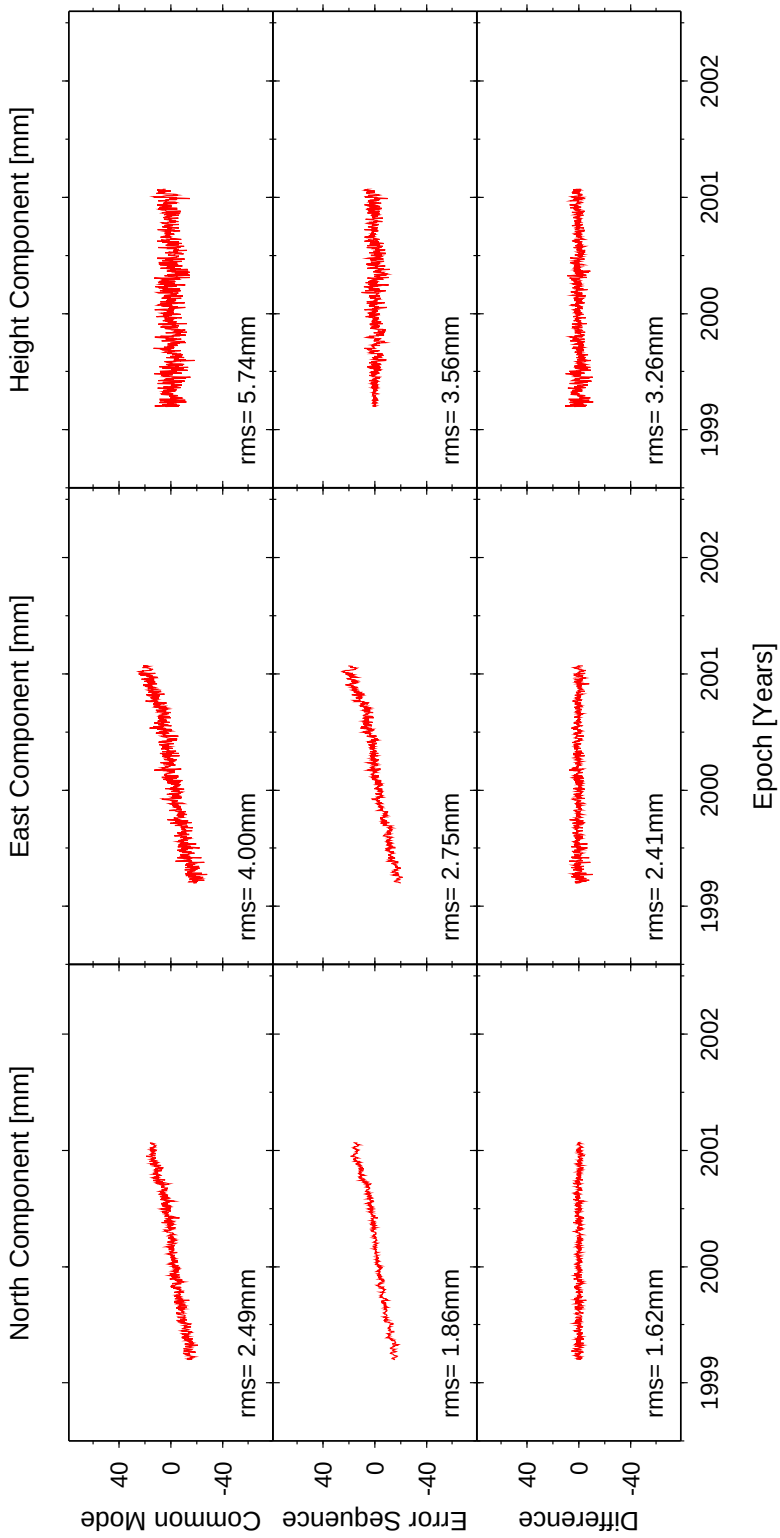

Figure M.11: Two–station common mode bias time series and error sequences of the reversed direction adaptive filter analysis for the observed ITRS2000 coordinate time series of the dual–CGPS station pair LOWE–HEMS compared over a common time span of 2.0 years. Common mode denotes the two–station common mode bias time series computed using Eq. 7.8 and error sequence denotes the coherent signal components of the two input sequences to the the adaptive filter.

Appendix N

Comparison Results

Table N.1: Absolute vertical station velocity estimates obtained from coordinate time series analyses compared with alternative evidence for vertical land/crustal movements for eight CGPS stations. The vertical station velocity estimates have been computed for the unfiltered (unflt) and filtered (flt) improved ITRS2000 coordinate time series (§6.3.3), using the improved coordinate time series analysis strategy and the MLE with fractional and integer spectral indices, i.e. with a white plus power–law noise (WN+PLN) and a white plus flicker noise (WN+FN) model respectively. The alternative estimates of vertical land movements stem from the MSL trends combined with an estimate of absolute sea level rise of 1.5 mm/yr, absolute gravimetry (AG) measurements, geological information, predicted crustal movements from two GIA models and vertical land movement estimates from satellite altimetry. All estimates of vertical land/crustal movements are given in mm/yr.

		Absolute vertical station velocity estimates						Vertical land/crustal movements from alternative evidence						
		Improved Analysis		MLE (WN+PLN)		MLE (WN+FN)		Computed	AG[a]		Geology[b]	GIA[c]	GIA[d]	Altimetry[e]
Site	Latitude	(unflt)	(flt)	(unflt)	(flt)	(unflt)	(flt)	-(MSL-1.5)				Signal	Signal	
LERW	60.15	0.1	−0.2	−0.3	0.1	−0.4	0.2	2.5	−0.7			−0.5	−1.5	−1.9
ABER	57.15	1.8	0.8	1.0	0.9	1.8	1.2	0.8	1.8	(0.9)	0.7	0.6	2.0	
NSTG	55.10	0.9	0.9	2.1	0.7	0.7	0.9	−0.4			0.2	0.4	2.0	
LIVE	53.30	2.2	1.9	1.4	1.8	1.3	1.6	0.1			−0.2	0.4	1.0	
LOWE	52.47	0.4	0.4	0.5	1.3	0.7	1.9	−0.5			−0.6	−0.4	−0.3	
SHEE	52	−0.7	−0.9	−0.8	−0.1	−0.2	0.8	−0.6			−0.7	−0.2	−0.3	
NEWL	50	0.5	0.2	−0.6	−0.6	−0.8	−0.8	−0.2	1.5	(1.0)	−1.1	−0.3	−0.4	2.9
BRST	48.38	1.2	1.1	−0.2	0.2	−1.4	−0.8	0.5			−0.2	−0.3	−0.5	

[a] Absolute gravimetry from Williams et al. (2001) updated with latest results. Values in parenthesis are previous estimates.

[b] Geological information (Woodworth et al., 1999; Shennan and Horton, 2002)

[c] GIA model with precise values for tide gauge sites (Peltier, 2001a)

[d] GIA model with approximate values from Figure 2 in Scherneck et al. (2002a)

[e] Satellite altimetry (Nerem and Mitchum, 2002)

Table N.2: AG–aligned vertical station velocity estimates referred to Lerwick. All velocity estimates are in mm/yr.

		Improved Analysis		MLE (WN+PLN)		MLE (WN+FN)	
Site	Latitude	(unflt)	(flt)	(unflt)	(flt)	(unflt)	(flt)
LERW	60.15	−0.7	−0.7	−0.7	−0.7	−0.7	−0.7
ABER	57.15	1.0	0.2	0.6	0.1	1.5	0.3
NSTG	55.10	0.0	0.4	1.7	−0.1	0.3	0.0
LIVE	53.30	1.3	1.3	0.9	1.0	0.9	0.7
LOWE	52.47	−0.4	−0.2	0.1	0.5	0.4	1.0
SHEE	52.00	−1.5	−1.5	−1.2	−0.9	−0.5	−0.1
NEWL	50.00	−0.4	−0.4	−1.1	−1.4	−1.2	−1.7
BRST	48.38	0.3	0.5	−0.7	−0.7	−1.7	−1.7

Table N.3: AG–aligned vertical station velocity estimates referred to Aberdeen. All velocity estimates are in mm/yr.

		Improved Analysis		MLE (WN+PLN)		MLE (WN+FN)	
Site	Latitude	(unflt)	(flt)	(unflt)	(flt)	(unflt)	(flt)
LERW	60.15	−0.8	0.0	−0.4	0.1	−1.3	−0.1
ABER	57.15	0.9	0.9	0.9	0.9	0.9	0.9
NSTG	55.10	−0.1	1.0	2.1	0.7	−0.2	0.6
LIVE	53.30	1.2	2.0	1.3	1.8	0.4	1.3
LOWE	52.47	−0.5	0.5	0.4	1.3	−0.2	1.6
SHEE	52.00	−1.6	−0.8	−0.9	−0.1	−1.1	0.5
NEWL	50.00	−0.5	0.3	−0.7	−0.6	−1.7	−1.1
BRST	48.38	0.3	1.2	−0.3	0.2	−2.3	−1.1

Table N.4: Geology–aligned vertical station velocity estimates referred to Aberdeen. All velocity estimates are in mm/yr.

		Improved Analysis		MLE (WN+PLN)		MLE (WN+FN)	
Site	Latitude	(unflt)	(flt)	(unflt)	(flt)	(unflt)	(flt)
LERW	60.15	−1.0	−0.2	−0.6	−0.1	−1.5	−0.3
ABER	57.15	0.7	0.7	0.7	0.7	0.7	0.7
NSTG	55.10	−0.3	0.8	1.8	0.5	−0.4	0.4
LIVE	53.30	1.0	1.8	1.1	1.6	0.2	1.1
LOWE	52.47	−0.7	0.3	0.2	1.1	−0.4	1.4
SHEE	52.00	−1.8	−1.0	−1.1	−0.3	−1.3	0.3
NEWL	50.00	−0.7	0.1	−0.9	−0.8	−1.9	−1.3
BRST	48.38	0.0	1.0	−0.5	0.0	−2.5	−1.3

Table N.5: Geology–aligned vertical station velocity estimates referred to Liverpool. All velocity estimates are in mm/yr.

		Improved Analysis		MLE (WN+PLN)		MLE (WN+FN)	
Site	Latitude	(unflt)	(flt)	(unflt)	(flt)	(unflt)	(flt)
LERW	60.15	−2.2	−2.2	−1.8	−1.9	−1.9	−1.6
ABER	57.15	−0.6	−1.3	−0.6	−1.1	0.3	−0.6
NSTG	55.10	−1.5	−1.2	0.6	−1.3	−0.8	−0.9
LIVE	53.30	−0.2	−0.2	−0.2	−0.2	−0.2	−0.2
LOWE	52.47	−2.0	−1.7	−1.1	−0.7	−0.8	0.0
SHEE	52.00	−3.1	−3.0	−2.4	−2.1	−1.7	−1.1
NEWL	50.00	−1.9	−1.9	−2.2	−2.6	−2.3	−2.6
BRST	48.38	−1.2	−1.0	−1.8	−1.9	−2.9	−2.6

Table N.6: Geology–aligned vertical station velocity estimates referred to Newlyn. All velocity estimates in mm/yr.

		Improved Analysis		MLE (WN+PLN)		MLE (WN+FN)	
Site	Latitude	(unflt)	(flt)	(unflt)	(flt)	(unflt)	(flt)
LERW	60.15	−1.4	−1.4	−0.8	−0.4	−0.7	−0.2
ABER	57.15	0.3	−0.5	0.5	0.4	1.5	0.8
NSTG	55.10	−0.7	−0.4	1.7	0.2	0.4	0.6
LIVE	53.30	0.6	0.6	0.9	1.3	1.0	1.3
LOWE	52.47	−1.2	−0.9	0.0	0.8	0.4	1.5
SHEE	52.00	−2.3	−2.2	−1.3	−0.6	−0.5	0.4
NEWL	50.00	−1.1	−1.1	−1.1	−1.1	−1.1	−1.1
BRST	48.38	−0.4	−0.2	−0.7	−0.3	−1.7	−1.2

Table N.7: Geology–aligned vertical station velocity estimates referred to Aberdeen for 17 UK CGPS stations analysed. All velocity estimates are in mm/yr.

Site	Latitude	Improved Analysis (unflt)	Improved Analysis (flt)	MLE (WN+PLN) (unflt)	MLE (WN+PLN) (flt)	MLE (WN+FN) (unflt)	MLE (WN+FN) (flt)
				CGPS@TG Stations (TG)			
SHEE	52.00	−1.8	−1.0	−1.1	−0.3	−1.3	0.3
ABER	57.15	0.7	0.7	0.7	0.7	0.7	0.7
BRST	48.38	0.0	1.0	−0.5	0.0	−2.5	−1.3
NEWL	50.10	−0.7	0.1	−0.9	−0.8	−1.9	−1.3
LIVE	53.30	1.0	1.8	1.1	1.6	0.2	1.1
LOWE	52.47	−0.7	0.3	0.2	1.1	−0.4	1.4
NSTG	55.10	−0.3	0.8	1.8	0.5	−0.4	0.4
				UK Met Office CGPS Stations (MO)			
CAMB	50.22	−0.6	0.0	−0.7	−0.1	−2.3	−0.8
ABYW	52.42	0.1	0.6	1.1	1.1	2.2	1.9
HEMS	52.67	0.1	1.1	0.7	0.3	−0.6	−1.4
LERW	60.15	−1.0	−0.2	−0.6	−0.1	−1.5	−0.3
DUNK	50.86	1.5	2.5	1.8	2.2	1.1	1.9
				Environment Agency, IESSG and NCL CGPS Stations (OTHER)			
IESG	52.94	−2.4	−1.5	−3.3	−1.9	−4.4	−3.0
BARK	51.52	−2.5	−1.7	−2.0	−1.6	−2.8	−1.1
SUNB	51.40	−0.9	0.0	−0.3	0.5	−1.0	0.7
MORP	55.21	−2.5	−1.6	−3.4	−2.3	−4.7	−3.1
				UK based IGS Stations (IGS)			
HERS	50.87	−3.7	−2.5	−2.7	−2.2	−3.7	−2.3

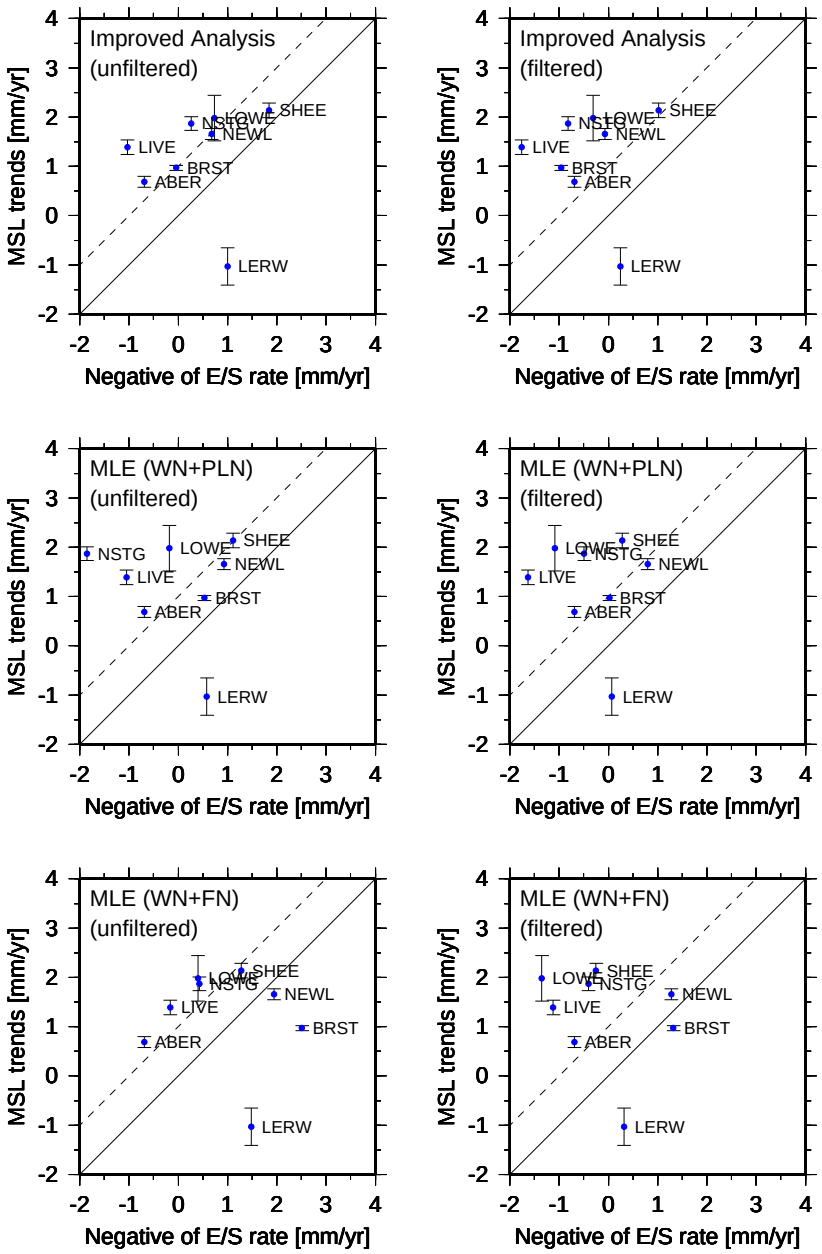

Figure N.1: Relative MSL trends for the eight tide gauges compared with the negative of geology–aligned vertical station velocity estimates (emergence/submergence rates) referred to Aberdeen for all six coordinate time series analyses; the improved analysis, and the MLE using a WN+PLN and a WN+FN model, of the unfiltered and filtered improved ITRS2000 coordinate time series. Data points aligned along the solid line would imply relative MSL trends equivalent to the geology–aligned vertical station velocity estimates; points aligned along the dashed line would imply an absolute sea level rise of 1 mm/yr.